Harald Friedrich

Scattering Theory

Second Edition

Springer

Scattering Theory

Harald Friedrich

Scattering Theory

Second Edition

Springer

Harald Friedrich
Physik Department T30
TU München
Garching, Germany

ISBN 978-3-662-48524-8 ISBN 978-3-662-48526-2 (eBook)
DOI 10.1007/978-3-662-48526-2

Library of Congress Control Number: 2015955829

Springer Heidelberg New York Dordrecht London

Printed on acid-free paper

Springer is part of Springer Science+Business Media (www.springer.com)

Preface to the Second Edition

The production of this second edition of *Scattering Theory* has provided the opportunity to accommodate several corrections and updates. One particular advance that is worth drawing attention to, is the modified effective-range expansion for potentials with an attractive inverse-cube behaviour at large distances. This result, derived by Tim-Oliver Müller, was at the verge of publication when the first edition of *Scattering Theory* came out in 2013. The result published by Müller in *Phys. Rev. Lett.* **110**, 260401 (2013) appears as Eq. (4.129) in Chap. 4.

I repeat my thanks to all mentioned in the preface to the first edition and would like to add thanks to Dr. Thorsten Schneider, Ute Heuser and Birgit Münch from Springer-Verlag for their efficient cooperation and assistance.

Garching, Germany
October 2015

Harald Friedrich

Preface to the First Edition

This book presents a modern and concise coverage of "scattering theory", a topic with a long history dating back to the first half of the twentieth century. It is motivated by the observation that most important books on the subject were written several decades ago, from the first edition of *Theory of Atomic Collisions* by Mott and Massey (Clarendon Press, Oxford, 1933), over *Scattering Theory* by John R. Taylor (John Wiley & Sons, Hoboken (NJ), 1972), to the second edition of *Scattering Theory of Waves and Particles* by Roger G. Newton (Springer-Verlag, New York, 1982). Several such classics have been reprinted in recent years, but new original publications are rare.[1]

The need for a fresh look at scattering theory follows from the fact that experimental advances have shifted and broadened the scope of applications where concepts from scattering theory are used. Beyond traditional scattering experiments, which continue to be performed with increasing refinement and precision, a deeper understanding of scattering theory has become important in other contexts as well. One example is provided by the field of ultracold atoms and molecules, which has been experiencing enormous growth in recent years, largely triggered by the successful realization of Bose–Einstein condensates of dilute atomic gases in 1995. A sound comprehension of the physics of weakly bound states just below the continuum threshold and low-energy scattering states just above threshold is important for understanding the phenomena observed in this ultracold regime.

The book starts with a chapter on the classical theory describing the scattering of a projectile particle from a target particle. This is helpful, because important concepts such as cross sections can already be explained in this context. Furthermore, the relation between classical mechanics and quantum mechanics and the behaviour of quantum systems in the "semiclassical" or "anticlassical" limits are subjects of lasting interest.

The second chapter contains a detailed formulation of the quantum mechanical description of elastic scattering by a conservative potential. Particular attention is

[1] One new book has just been published: *Scattering Theory of Molecules, Atoms and Nuclei* (World Scientific, Singapore, 2013) by L. Felipe Canto and Mahir S. Hussein.

given to the influence of the large-distance behaviour of the interaction potential, which is often well known in realistic situations. The concept of channels, which are related to internal degrees of freedom of the projectile and/or the target, is introduced for the example of internal orbital angular momenta and spins.

The third chapter generalizes this ansatz to arbitrary internal excitations, which enables the description of inelastic scattering via the appropriate coupled-channel equations. This chapter contains the theory of Feshbach resonances, as opposed to single-channel shape resonances, and an account of multichannel quantum-defect theory, which is a powerful tool for describing Coulombic systems with attractive interactions falling off as $1/r$ for large values of the projectile-target separation r.

Chapter 4 addresses some special topics which are particularly relevant for current research involving cold atoms and molecules. Section 4.1 on deep potentials falling off faster than $1/r^2$ at large distances contains a general theory for the description of near-threshold bound and continuum states, which is well suited for application to realistic binary systems such as diatomic molecules or molecular ions. Section 4.2 connects the well established theory of Feshbach resonances with the empirical description that has become widely used in the cold-atoms community, and it formulates a threshold-insensitive parametrization of the Feshbach resonances which is relevant for the analysis of current experiments. The last section contains a short treatise on two-dimensional scattering, which reveals significant differences to the 3D case, in particular in the low-energy, near-threshold regime.

The first appendix describes scaling properties of classical and quantum systems governed by a conservative potential depending homogeneously on the coordinates. This is particularly useful for understanding if and where a given quantum mechanical system has a semiclassical or an anticlassical, extreme quantum limit. The second appendix contains a brief summary of the definitions and some important properties of special mathematical functions occurring in the solutions of various versions of the Schrödinger equation throughout the book.

The book is intended for advanced students and researchers. It is hoped that it will be useful for theorists and experimentalists alike. The level of abstraction is kept as low as at all possible, and deeper questions related to mathematical foundations of scattering theory, as discussed e.g. in *Methods of Modern Mathematical Physics, III. Scattering Theory* by Reed and Simon (Academic Press, New York, 1979), are passed by. The present book should be understandable for anyone with a basic knowledge of nonrelativistic quantum mechanics.

The conception of scattering theory presented in this book has grown over four decades of active involvement in the subject. For the comprehension of the recent developments, I have profited considerably from the input of talented young, unbiased students. In particular, with respect to the theory described in Chapter 4 of this book, original contributions of many students (and post-docs), and their critical views of previous work, have played a major role for achieving a mature formulation of rather general validity. In this context I would like to thank Johannes Trost, Petra Meerwald, Thomas Purr, Michael Moritz, Christopher Eltschka, Georg Jacoby, Carlo Meister, Alexander Jurisch, Eskender Mesfin, Florian Arnecke, Patrick Raab, Johannes Eiglsperger, Tim-Oliver Müller, Martin Fink, Alexander Kaiser, Frauke

Schwarz, Sebastian Schröter and Javier Madroñero. Discussions with Robin Côté of the University of Connecticut, with Manfred Kleber at the Physik Department in Garching and with Gerhard Rempe and Stephan Dürr of the Max Planck Institute for Quantum Optics proved very valuable. I am grateful to Wolfgang Domcke and Sebastian Schröter, and especially to Tim-Oliver Müller for meticulously checking the manuscript and drawing attention to several inconsistencies, and for making valuable suggestions which led to substantial improvements in the final version. Finally, I thank my wife Elfi for her encouragement and enduring patience during my engagement in this project.

Garching, Germany Harald Friedrich
February 2013

Contents

Chapter 1
Classical Scattering Theory

1.1 Relative Motion of Projectile and Target

Consider two particles, projectile and target, with masses m_1 and m_2 respectively, which interact via a time-independent potential V depending on the separation

$$\mathbf{r} = \mathbf{r}_1 - \mathbf{r}_2 \tag{1.1}$$

of their position vectors $\mathbf{r}_1$ and $\mathbf{r}_2$. In the absence of external forces, the centre of mass $\mathbf{R}_{\rm cm} = (m_1\mathbf{r}_1 + m_2\mathbf{r}_2)/(m_1 + m_2)$ moves uniformly, $\mathbf{R}_{\rm cm}(t) = \mathbf{R}_{\rm cm}(0) + \mathbf{V}_{\rm cm}t$. In the *centre-of-mass frame of reference*, that is the inertial system in which the centre of mass of the two particles is at rest, the position vectors of the two particles are

$$\mathbf{r}_1^{(\rm cm)} = \frac{m_2}{m_1 + m_2}\mathbf{r}, \qquad \mathbf{r}_2^{(\rm cm)} = -\frac{m_1}{m_1 + m_2}\mathbf{r}. \tag{1.2}$$

Scattering experiments in the laboratory usually involve a projectile initially moving freely towards a target at rest,

$$\mathbf{r}_1^{(\rm in,\,lab)}(t) = \mathbf{r}_1^{(\rm in,\,lab)}(0) + \mathbf{v}_1^{(\rm in,\,lab)}t, \qquad \mathbf{r}_2^{(\rm in,\,lab)}(t) = \mathbf{r}_2^{(\rm in,\,lab)}(0), \tag{1.3}$$

so the centre-of-mass velocity in the *laboratory frame of reference* is simply $\mathbf{V}_{\rm cm}^{(\rm lab)} = \dot{\mathbf{r}}_1^{(\rm in,\,lab)} m_1/(m_1 + m_2)$.

Throughout this book we shall focus on the *relative motion* of projectile and target, which contains the essential nontrivial physics of the scattering problem. The relevant coordinate is the relative distance (1.1). Transformation to the laboratory frame of reference is achieved via (1.2) and $\mathbf{r}_i^{(\rm lab)}(t) = \mathbf{r}_i^{(\rm cm)}(t) + \mathbf{R}_{\rm cm}^{(\rm lab)}(t)$, $i = 1, 2$. Details of such straightforward but cumbersome transformations are discussed, e.g., in paragraph 17 of [2].

Classically, the evolution of $\mathbf{r}(t)$ is described by Newton's equation of motion

$$\mu\ddot{\mathbf{r}} = -\nabla V(\mathbf{r}), \quad \mu = \frac{m_1 m_2}{m_1 + m_2}, \tag{1.4}$$

as for one particle with the *reduced mass* μ moving under the influence of the potential $V(\mathbf{r})$. In accordance with standard convention, we assume the asymptotic incoming velocity $\mathbf{v}_\infty = \lim_{t\to-\infty}\dot{\mathbf{r}}(t)$ to point in the direction of the positive z-axis,

H. Friedrich, *Scattering Theory*, DOI 10.1007/978-3-662-48526-2_1

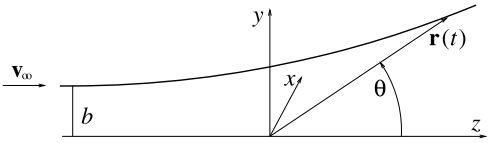

Fig. 1.1 Scattering of a particle with asymptotic incoming velocity $\mathbf{v}_\infty$

as illustrated in Fig. 1.1. We assume the potential $V(\mathbf{r})$ to vanish asymptotically, so the conserved total energy E of the system is just the incoming particle's initial kinetic energy, $E = \frac{1}{2}\mu v_\infty^2$, where $v_\infty = |\mathbf{v}_\infty|$. The perpendicular displacement of the incoming particle's asymptotic straight-line trajectory from the z-axis is the *impact parameter* b, so the incoming particle has an initial angular momentum $|\mathbf{L}| = \mu b v_\infty$ around the origin.

1.2 Deflection Function

From now on we assume that the potential $V(\mathbf{r})$ is radially symmetric; it depends only on the modulus r of the distance vector $\mathbf{r}$ and not on its orientation. The angular momentum $\mathbf{L} = \mu \mathbf{r} \times \dot{\mathbf{r}}$ is thus a conserved vector which always points in the same direction, and both $\mathbf{r}$ and $\dot{\mathbf{r}}$ must lie in the plane perpendicular to this direction. Any trajectory $\mathbf{r}(t)$ describing the scattering of the particle by the potential $V(r)$ is confined to a plane, the *scattering plane*. As already anticipated in Fig. 1.1, we choose it to be the y–z plane, and we assume that the positive x-axis points in the direction of $\mathbf{L}$, so $L = |\mathbf{L}| = L_x \geq 0$.

For motion in the y–z plane, the polar coordinates r, θ are defined via

$$x \equiv 0, \qquad y = r \sin\theta, \qquad z = r \cos\theta, \tag{1.5}$$

and the (conserved) angular momentum is

$$L = L_x = \mu(y\dot{z} - z\dot{y}) = -\mu r^2 \dot{\theta} = \mu b v_\infty. \tag{1.6}$$

Since the conserved energy is $E = \frac{1}{2}\mu v_\infty^2$, the impact parameter b is related to the angular momentum L and energy E via

$$L = b\sqrt{2\mu E}. \tag{1.7}$$

According to the geometry of Fig. 1.1, b and L are nonnegative, so

$$\dot{\theta} = -\frac{L}{\mu r^2} \leq 0, \tag{1.8}$$

which, for given L, uniquely defines $\dot{\theta}$ as function of r and shows that $\theta(t)$ is a monotonically decreasing function in time, starting from its initial value $\theta(t) \overset{t \to -\infty}{=} \pi$.

After the particle is scattered by the potential, it leaves to large r and its trajectory approaches a straight line deflected by the angle Θ from the forward direction. The deflection angle Θ depends on the energy E and the impact parameter b. For a given

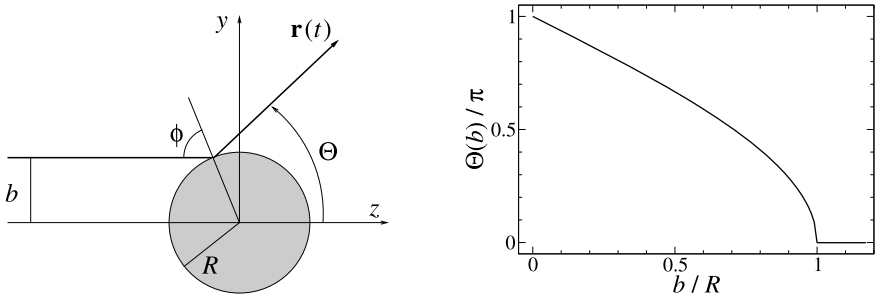

Fig. 1.2 Scattering by a hard sphere of radius R. Deflection function (1.9)

scattering experiment, the energy can be taken as fixed and known, so the observable features are determined by the function $\Theta(b)$, which is called the *deflection function*. We write the capital letter and emphasize that Θ retains the memory of possible clockwise revolutions around the scattering centre.

One of the simplest conceivable scattering problems is the scattering by a hard sphere of radius R as illustrated in the left-hand part of Fig. 1.2. The deflection angle is $\pi - 2\phi$, where $\sin\phi = b/R$,

$$\Theta(b) = \pi - 2\arcsin\left(\frac{b}{R}\right) = 2\arccos\left(\frac{b}{R}\right) \quad \text{for } 0 \le b \le R. \tag{1.9}$$

Obviously, trajectories with $b > R$ are not deflected, $\Theta(b) = 0$ for $b > R$. The deflection function (1.9) is shown in the right-hand part of Fig. 1.2.

More realistic scattering problems involve a smooth potential $V(r)$, for which the scattering trajectory cannot be constructed by such simple geometric means. In polar coordinates we have $E = \frac{1}{2}\mu(\dot{r}^2 + r^2\dot{\theta}^2) + V(r)$; with (1.8):

$$E = \frac{\mu}{2}\dot{r}^2 + \frac{L^2}{2\mu r^2} + V(r). \tag{1.10}$$

Equation (1.10) is a one-dimensional energy-conservation formula for the radial motion described by the coordinate r and the velocity $\dot{r}$. It shows that the evolution of $r(t)$ is as for one-dimensional motion of a particle with mass μ on the half-line $r \ge 0$ under the influence of an *effective potential*, V_{eff}. The effective potential consists of the potential energy $V(r)$ and the *centrifugal potential* $V_{\text{cent}}(r)$, which comes from the kinetic energy of angular motion and depends on the angular momentum L,

$$V_{\text{eff}}(r) = V(r) + V_{\text{cent}}(r), \quad V_{\text{cent}}(r) = \frac{L^2}{2\mu r^2}. \tag{1.11}$$

The effective potential helps us to understand the behaviour of a scattering trajectory for given energy E and impact parameter b (or angular momentum $L = b\sqrt{2\mu E}$) in very straightforward terms. The scattering process begins with $r \to \infty$ for $t \to -\infty$, and r decreases with time until it reaches the *classical turning point* r_{ctp}, which fulfills

$$E = V_{\text{eff}}(r_{\text{ctp}}) \tag{1.12}$$

and corresponds to the point of closest approach of target and projectile. For the hard-sphere case in Fig. 1.2, $r_{\rm ctp}$ is the sphere's radius R as long as $b \le R$. If $V_{\rm eff}(r) < E$ for all r, then the radial turning point is the origin, $r_{\rm ctp} = 0$. It is a useful convention to choose the time of closest approach to be $t = 0$: $r(t = 0) = r_{\rm ctp}$. For later (positive) times, r increases again until $r \to \infty$ for $t \to +\infty$.

The trajectory of the particle in the y–z-plane is most conveniently obtained via $\mathrm{d}\theta/\mathrm{d}r = \dot\theta/\dot r$ with $\dot\theta$ from (1.8) and $\dot r = \pm\sqrt{(2/\mu)[E - V_{\rm eff}(r)]}$ from (1.10),

$$\frac{\mathrm{d}\theta}{\mathrm{d}r} = \pm\frac{L}{r^2\sqrt{2\mu[E - V_{\rm eff}(r)]}}. \tag{1.13}$$

During the first half of the scattering process, $\dot r$ is negative (as is $\dot\theta$), so the plus sign on the right-hand side of (1.13) applies. During the second half, $\dot r$ is positive (in contrast to $\dot\theta$), so (1.13) applies with the minus sign. The polar angle of the point of closest approach, for which $r = r_{\rm ctp}$, is

$$\theta(r = r_{\rm ctp}) = \pi + \int_{\infty}^{r_{\rm ctp}} \frac{\mathrm{d}\theta}{\mathrm{d}r}\mathrm{d}r = \pi - \int_{r_{\rm ctp}}^{\infty} \frac{L \quad \mathrm{d}r}{r^2\sqrt{2\mu[E - V_{\rm eff}(r)]}}. \tag{1.14}$$

For an actual calculation, the scattering trajectory (r, θ) in the y–z plane can be obtained via

$$\theta(r) = \theta(r = r_{\rm ctp}) \pm \int_{r_{\rm ctp}}^{r} \frac{L \quad \mathrm{d}r'}{r'^2\sqrt{2\mu[E - V_{\rm eff}(r')]}}, \tag{1.15}$$

where the plus sign gives the points on the incoming half of the trajectory and the minus sign the points on the outgoing half. The deflection function follows from the expression (1.15) for the polar angle in the limit $r \to \infty$ on the outgoing branch of the trajectory,

$$\begin{aligned}\Theta(b) &= \theta(r_{\rm ctp}) - \int_{r_{\rm ctp}}^{\infty} \frac{L \quad \mathrm{d}r}{r^2\sqrt{2\mu[E - V_{\rm eff}(r)]}} = \pi - \int_{r_{\rm ctp}}^{\infty} \frac{2L \quad \mathrm{d}r}{r^2\sqrt{2\mu[E - V_{\rm eff}(r)]}} \\ &= \pi - \int_{r_{\rm ctp}}^{\infty} \frac{2b}{r^2}\left[1 - \frac{b^2}{r^2} - \frac{V(r)}{E}\right]^{-1/2} \mathrm{d}r. \end{aligned} \tag{1.16}$$

In the limit of large impact parameters, the effective potential (1.11) is dominated by the centrifugal term and the deflection angle tends to zero. For a potential falling off asymptotically as an inverse power of r,

$$V(r) \overset{r\to\infty}{\sim} \frac{C_\alpha}{r^\alpha}, \quad \alpha > 0, \tag{1.17}$$

the large-b behaviour of $\Theta(b)$ is easily calculated analytically. Changing the integration variable in (1.16) from r to $\xi = r/r_{\rm ctp}$ gives, for large b,

$$\Theta(b) = \pi - \int_1^{\infty} \frac{2\,\mathrm{d}\xi}{\sqrt{\xi^4 - \xi^2 + \varepsilon(\xi^4 - \xi^{4-\alpha})}}, \quad \text{where } \varepsilon = \left(\frac{r_{\rm ctp}}{b}\right)^2 - 1. \tag{1.18}$$

Expanding the integrand in terms of the small parameter $\varepsilon \overset{b\to\infty}{\sim} C_\alpha/(E\,b^\alpha)$ yields

$$\Theta(b) \overset{b\to\infty}{\sim} \frac{C_\alpha}{E\,b^\alpha}\frac{\pi\,\Gamma(\alpha)}{2^{\alpha-1}[\Gamma(\frac{\alpha}{2})]^2} = \frac{C_\alpha}{Eb^\alpha}\frac{\sqrt{\pi}\,\Gamma(\frac{\alpha+1}{2})}{\Gamma(\frac{\alpha}{2})}. \tag{1.19}$$

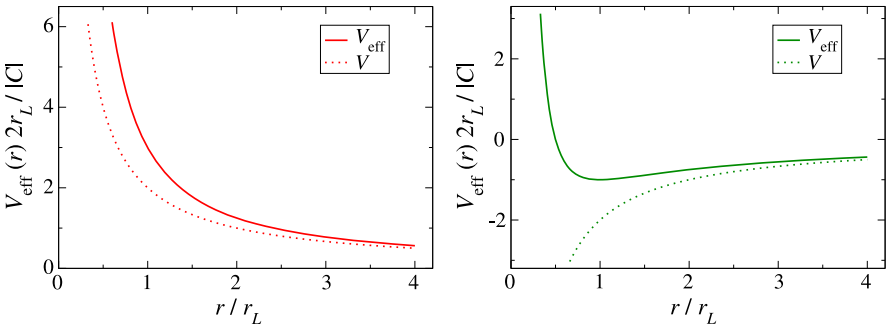

Fig. 1.3 Effective potential (1.21) for a repulsive ($C > 0$, *left-hand part*) and an attractive ($C < 0$, *right-hand part*) Kepler–Coulomb interaction. The *dotted lines* show the respective potential (1.20) without centrifugal contribution

1.2.1 Kepler–Coulomb Potential

The Kepler or Coulomb potential,

$$V(r) = \frac{C}{r}, \tag{1.20}$$

is important, because it describes gravitational and electrostatic interactions. For such a homogeneous potential of degree -1, the solutions of Newton's equation of motion (1.4) obey a simple scaling relation called Kepler's third law. If $\mathbf{r}(t)$ is a solution at energy E, then $s\mathbf{r}(s^{3/2}t)$ is a solution at energy E/s, see Appendix A.1. The geometric shape of a trajectory does not depend on the potential strength coefficient C, the impact parameter b and the energy E independently, but only on the ratio of C to the product Eb.

The weight of the centrifugal contribution in the effective potential (1.11) can be expressed via the length parameter

$$r_L = \frac{L^2}{\mu|C|}, \quad \text{so} \quad V_{\rm eff}(r) = \frac{|C|}{2r_L}\left[\pm 2\frac{r_L}{r} + \left(\frac{r_L}{r}\right)^2\right]. \tag{1.21}$$

In the repulsive case, $C > 0$, the plus sign in the square bracket applies; the effective potential is a monotonically decreasing function of r. In the attractive case, $C < 0$, $V_{\rm eff}(r)$ has a zero at $r_L/2$ and a minimum at r_L with $V_{\rm eff}(r_L) = -|C|/(2r_L)$. The effective potential (1.21) is shown for both the repulsive and the attractive case in Fig. 1.3.

The classical turning point is

$$r_{\rm ctp} = b\left(\sqrt{\gamma^2 + 1} \pm \gamma\right) \quad \text{with } \gamma = \frac{|C|}{2Eb}, \tag{1.22}$$

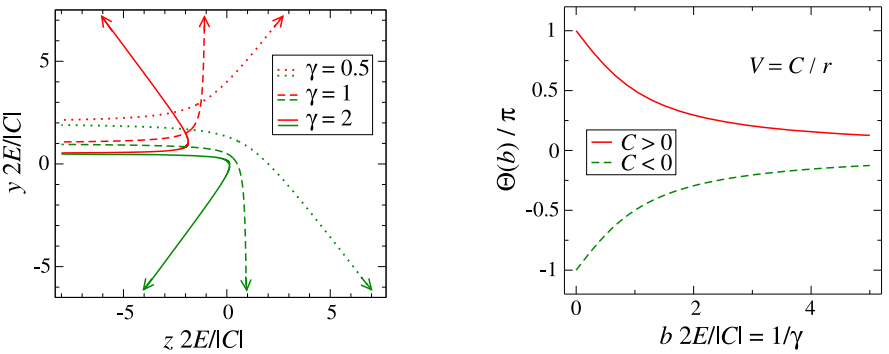

Fig. 1.4 Scattering trajectories (*left-hand part*) and deflection function *right-hand part* for the Kepler–Coulomb potential (1.20). The *red* (*green*) *lines* correspond to the repulsive (attractive) case $C > 0$ ($C < 0$). Lengths are in units of $|C|/(2E)$

where the plus (minus) sign applies for the repulsive (attractive) case $C > 0$ ($C < 0$) and the geometry of the trajectory is governed by the dimensionless parameter γ. With $\rho = r/b$, Eqs. (1.14) and (1.15) are as follows for the Kepler–Coulomb case:

$$\begin{aligned} \theta(\rho_{\mathrm{ctp}}) &= \pi - \int_{\rho_{\mathrm{ctp}}}^{\infty} \frac{\mathrm{d}\rho}{\rho\sqrt{\rho^2 \mp 2\gamma\rho - 1}}, \\ \theta(\rho) &= \theta(\rho_{\mathrm{ctp}}) \pm \int_{\rho_{\mathrm{ctp}}}^{\rho} \frac{\mathrm{d}\rho'}{\rho'\sqrt{\rho'^2 \mp 2\gamma\rho' - 1}}. \end{aligned} \tag{1.23}$$

The minus (plus) sign in the square root applies for the repulsive (attractive) case $C > 0$ ($C < 0$). Typical trajectories are shown in the left-hand part of Fig. 1.4. The axes are labelled with the b-independent dimensionless lengths $\rho\cos\theta/\gamma \equiv z2E/|C|$, $\rho\sin\theta/\gamma \equiv y2E/|C|$. The right-hand part of Fig. 1.4 shows the deflection function,

$$\Theta(b) = \pi - \int_{\rho_{\mathrm{ctp}}}^{\infty} \frac{2\,\mathrm{d}\rho}{\rho\sqrt{\rho^2 \mp 2\gamma\rho - 1}} = \pm 2\arccos\left(\frac{1}{\sqrt{\gamma^2+1}}\right). \tag{1.24}$$

1.2.2 Inverse-Power Potentials

As a more general ansatz, consider the inverse-power potential,

$$V(r) = \frac{C_\alpha}{r^\alpha}, \quad \alpha > 0. \tag{1.25}$$

This is a homogeneous potential of degree $-\alpha$, and, as a generalization of Kepler's third law, the solutions of Newton's equation of motion (1.4) obey the following scaling relation: If $\mathbf{r}(t)$ is a solution at energy E, then $s\mathbf{r}(s^{1+\alpha/2}t)$ is a solution at energy E/s^α, see Appendix A.1. The geometric shape of a trajectory does not

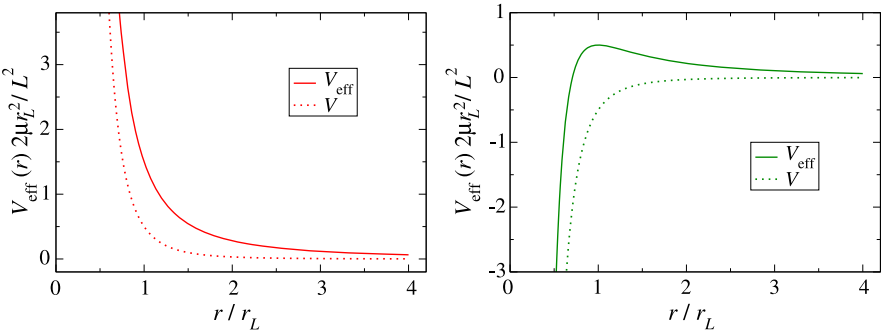

Fig. 1.5 Effective potential (1.26) for a repulsive ($C_\alpha > 0$, *left-hand part*) and an attractive ($C_\alpha < 0$, *right-hand part*) inverse-power potential with $\alpha = 4$. The *dotted lines* show the respective potential (1.25) without centrifugal contribution

depend on the potential strength coefficient C_α, the impact parameter b and the energy E independently, but only on the ratio of C_α to the product Eb^α. Although we are mainly interested in integer values of α on physical grounds, the discussion below is largely valid also for noninteger, real and positive α.

As a generalization of (1.21) we define

$$r_L = \left[\alpha\frac{\mu|C_\alpha|}{L^2}\right]^{1/(\alpha-2)}, \quad \text{so} \quad V_{\rm eff}(r) = \frac{L^2}{2\mu r_L^2}\left[\pm\frac{2}{\alpha}\left(\frac{r_L}{r}\right)^\alpha + \left(\frac{r_L}{r}\right)^2\right]. \quad (1.26)$$

For $C_\alpha > 0$, the plus sign in the square bracket applies; the effective potential is a monotonically decreasing function of r. For $C_\alpha = -|C_\alpha| < 0$, the minus sign applies, $V_{\rm eff}(r)$ has a zero at $r_L(2/\alpha)^{1/(\alpha-2)}$ and an extremum at r_L. For $\alpha < 2$ this extremum is a minimum, as in Sect. 1.2.1. For $\alpha > 2$, the extremum is a maximum. Such a "centrifugal barrier" is a characteristic property of all potentials with attractive tails falling off faster than $-1/r^2$. For the inverse-power tail (1.25) with $C_\alpha < 0$, the centrifugal barrier has its maximum at r_L and the barrier height is $V_{\rm eff}(r_L) = [1 - 2/\alpha]L^2/(2\mu r_L^2) > 0$. The effective potential (1.26) is shown for $\alpha = 4$, both for the repulsive and for the attractive case in Fig. 1.5.

Using (1.7), the equation defining turning points of the effective potential (1.26) can be written as

$$1 - \left(\frac{b}{r_{\rm ctp}}\right)^2 = \pm\frac{2}{\alpha}\gamma\left(\frac{b}{r_{\rm ctp}}\right)^\alpha \quad \text{with } \gamma = \frac{\alpha}{2}\frac{|C_\alpha|}{Eb^\alpha}. \quad (1.27)$$

In the repulsive case [plus sign in (1.27)], there is always one real solution for $r_{\rm ctp}$. In the attractive case, Eq. (1.27) always has one real solution for $r_{\rm ctp}$ if $\alpha < 2$.

For an attractive potential with $\alpha > 2$, Eq. (1.27) has no real solutions for large γ and two real solutions for small γ. For the value $\gamma_{\rm orb}$ separating these two regimes, the total energy E is exactly equal to the height $V_{\rm eff}(r_L)$ of the centrifugal barrier

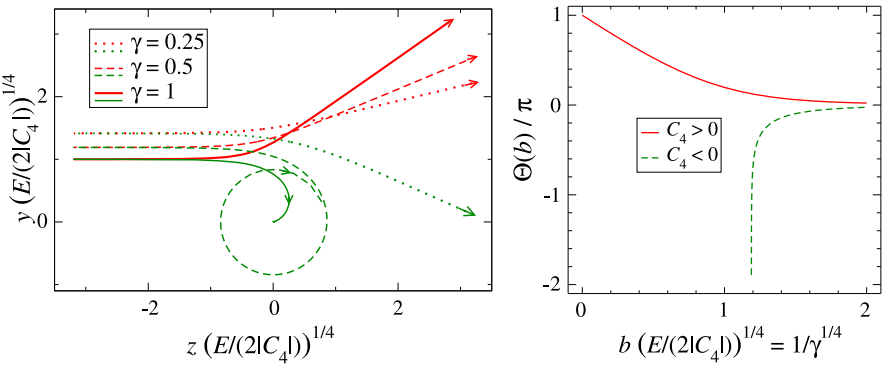

Fig. 1.6 Scattering trajectories (*left-hand part*) and deflection function (*right-hand part*) for the inverse-power potential (1.25) with $\alpha = 4$. The *red* (*green*) *lines* correspond to the repulsive (attractive) case $C_4 > 0$ ($C_4 < 0$). Lengths are in units of $(2|C_4|/E)^{1/4}$

and $r_{\rm ctp}$ is a double root of the equation; explicitly we have

$$\gamma_{\rm orb} = \left(1 - \frac{2}{\alpha}\right)^{(\alpha-2)/2} . \tag{1.28}$$

When $\gamma = \gamma_{\rm orb}$, the turning point is $r_{\rm ctp} = r_L = b\gamma_{\rm orb}^{1/(\alpha-2)}$ and Newton's equations (1.4) are solved by $\dot{r} = 0$, $\dot{\theta} = \text{const.}$ corresponding to uniform clockwise rotation on a circle of radius r_L. This motion is called *orbiting*. For fixed values of $|C_\alpha|$ and L, we have $\gamma \propto E^{(\alpha-2)/2}$, so $\gamma < \gamma_{\rm orb}$ corresponds to energies below the centrifugal barrier, where the radial motion is reflected at the outer turning point. For energies above the centrifugal barrier ($\gamma > \gamma_{\rm orb}$), there is no classical turning point and the incoming particle crashes into the origin $r = 0$ with ever increasing radial velocity. For the near-origin behaviour of the trajectory, Eq. (1.13) shows that

$$\frac{{\rm d}\theta}{{\rm d}r} \overset{r\to 0}{\sim} \frac{L}{\sqrt{2\mu|C_\alpha|}} r^{(\alpha-4)/2} \Rightarrow \int_{r_0}^{r} \frac{{\rm d}\theta}{{\rm d}r}{\rm d}r \overset{r\to 0}{\sim} c_1 - c_2 r^{(\alpha-2)/2}, \tag{1.29}$$

for a given r_0 with appropriate constants $c_{1,2}$. Since $(\alpha - 2)/2 > 0$, the polar angle converges to a finite limit during the crash to the origin.

Typical scattering trajectories are shown in the left-hand part of Fig. 1.6 for the inverse-power potential (1.25) with $\alpha = 4$. In this case $\gamma = 2|C_4|/(Eb^4)$. For $\gamma = \gamma_{\rm orb} = \frac{1}{2}$ and $C_4 < 0$, the incoming trajectory approaches the circular orbit for $t \to +\infty$. For smaller impact parameters, $\gamma > \gamma_{\rm orb}$, the incoming trajectory crashes into the origin and an outgoing trajectory cannot be determined unambiguously without further assumptions. The deflection function $\Theta(b)$ is shown in the right-hand part of Fig. 1.6. The abscissa is labelled with b in units of the length $(2|C_4|/E)^{1/4}$, i.e. with $1/\gamma^{1/4}$. For $C_4 > 0$, $\Theta(b)$ decreases monotonically from $\Theta(0) = \pi$ to zero; for $C_4 < 0$, $\Theta(b)$ increases monotonically from $-\infty$ in the orbiting case to zero. According to (1.19), $\Theta(b) \overset{b\to\infty}{\sim} \pm 3\pi\gamma/8$.

Scattering by attractive inverse-power potentials (1.25) depends crucially on whether the power α is larger or smaller than two, i.e. if there is a centrifugal barrier or not. The boundary separating these two regimes is provided by inverse-square potentials

$$V(r) = \frac{C_2}{r^2}, \qquad V_{\text{eff}}(r) = \frac{\tilde{L}^2}{2\mu r^2}, \quad \tilde{L}^2 = L^2 + 2\mu C_2. \tag{1.30}$$

As long as $\tilde{L}^2$ is greater than zero, the deflection function can be calculated in a very straightforward way. Since $\Theta(b)$ is identically zero for a free particle, the integral on the far right of the upper line of Eq. (1.16) must be equal to π for the free-particle case. This also holds for the effective potential (1.30), if we replace the true angular momentum L in the numerator of the integrand by $\tilde{L} = \sqrt{\tilde{L}^2}$, so

$$\Theta(b) = \pi\left(1 - \frac{L}{\tilde{L}}\right). \tag{1.31}$$

If $\tilde{L}^2 \leq 0$, the effective potential (1.30) has no turning point and the scattering trajectory crashes into the origin. For $\tilde{L}^2 < 0$, $\mathrm{d}\theta/\mathrm{d}r \overset{r\to 0}{\propto} 1/r$ according to (1.29), whereas $\mathrm{d}\theta/\mathrm{d}r \overset{r\to 0}{\propto} 1/r^2$ for $\tilde{L}^2 = 0$; in both cases the particle encircles the origin infinitely many times during the crash.

1.2.3 Lennard–Jones Potential

Realistic potentials have more structure than the inverse-power potentials discussed above. For example, the interaction of two neutral atoms with each other is characterized at large distances by an attractive tail proportional to $-1/r^6$, and it is strongly repulsive at very short distances comparable to the size of the atoms. A popular model for describing interatomic interactions is the Lennard–Jones potential,

$$V_{\text{LJ}}(r) = \frac{C_{12}}{r^{12}} - \frac{C_6}{r^6} = \mathscr{E}\left[\left(\frac{r_{\min}}{r}\right)^{12} - 2\left(\frac{r_{\min}}{r}\right)^{6}\right]. \tag{1.32}$$

It has a minimum at $r_{\min} = (2C_{12}/C_6)^{1/6}$, and $V_{\text{LJ}}(r_{\min}) = -\mathscr{E} = -{C_6}^2/(4C_{12})$.

We express the angular momentum in terms of a dimensionless quantity Λ,

$$\Lambda = \frac{L}{r_{\min}\sqrt{2\mu\mathscr{E}}}, \quad \text{so} \quad V_{\text{eff}} = \mathscr{E}\left[\left(\frac{r_{\min}}{r}\right)^{12} - 2\left(\frac{r_{\min}}{r}\right)^{6} + \Lambda^2\left(\frac{r_{\min}}{r}\right)^{2}\right]. \tag{1.33}$$

Λ^2 is the ratio of the centrifugal potential at $r_{\min}$ to the depth $\mathscr{E}$ of the potential (1.32). Figure 1.7 shows the effective potential (1.33) for $\Lambda^2 = 0, 1, 2$ and 3. Note that $V_{\text{eff}}(r)$ only has a local maximum if the angular momentum is less than a limiting value, $\Lambda < \Lambda_{\text{orb}}$. For $\Lambda = \Lambda_{\text{orb}}$, V_{eff} has a horizontal point of inflection at r_{orb}. From $V'_{\text{eff}}(r_{\text{orb}}) = 0$ and $V''_{\text{eff}}(r_{\text{orb}}) = 0$ we get

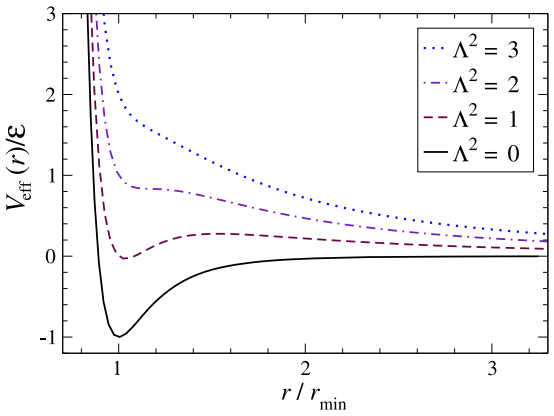

Fig. 1.7 Effective potential (1.33) for four values of Λ^2

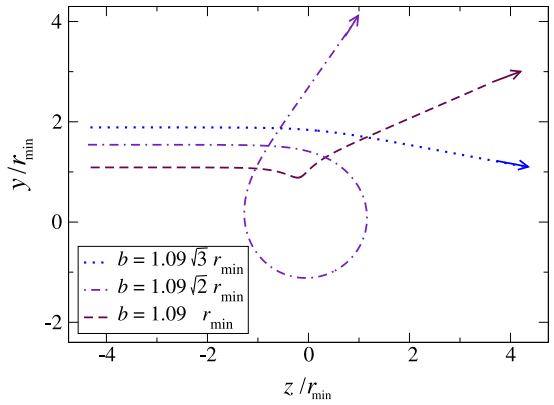

Fig. 1.8 Trajectories of a particle scattered by the Lennard–Jones potential (1.32) at energy $E = \mathscr{E}/(1.09)^2 \approx 0.84\mathscr{E}$. The three impact parameters correspond to $\Lambda^2 = 1$, $\Lambda^2 = 2$ and $\Lambda^2 = 3$, for which the effective potential is shown in Fig. 1.7

$$\begin{aligned} \frac{r_{\rm orb}}{r_{\rm min}} &= \left(\frac{5}{2}\right)^{1/6} \approx 1.165, \\ \Lambda^2_{\rm orb} &= \frac{18}{5}\left(\frac{2}{5}\right)^{2/3} \approx 1.954 \quad \text{and} \quad \frac{V_{\rm eff}(r_{\rm orb})}{\mathscr{E}} = \frac{4}{5}. \end{aligned} \tag{1.34}$$

If $E < \frac{4}{5}\mathscr{E}$, there will be an appropriate angular momentum $\Lambda < \Lambda_{\rm orb}$ for which the maximum of $V_{\rm eff}$, i.e. the top of the centrifugal barrier, coincides with E, so the conditions for orbiting are fulfilled. For $E = \frac{4}{5}\mathscr{E}$, orbiting occurs for $\Lambda = \Lambda_{\rm orb}$. If $E > \frac{4}{5}\mathscr{E}$, there is no orbiting.

Scattering trajectories are shown in Fig. 1.8 at energy $E/\mathscr{E} = 1/(1.09)^2 \approx 0.84$, which is just above the energy for which orbiting is possible. The impact parameters $b = r_{\rm min}\Lambda\sqrt{\mathscr{E}/E}$ correspond to $\Lambda^2 = 1, 2$ and 3 as featured in Fig. 1.7. In the closest collision ($\Lambda^2 = 1$), the particle passes above the centrifugal barrier associated with the attractive $-1/r^6$ potential tail, but instead of crashing into the origin it is reflected off the repulsive $1/r^{12}$ core at short distances. For the largest impact parameter ($\Lambda^2 = 3$), the radial motion is reflected by the centrifugal barrier, and the

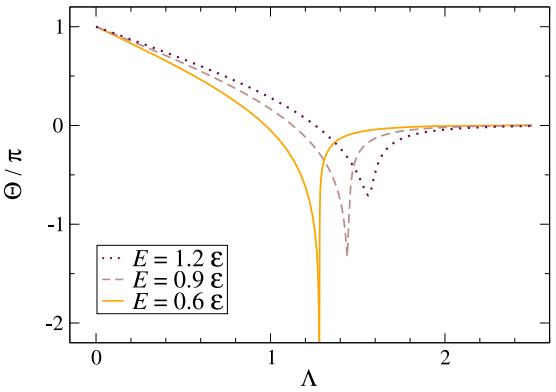

Fig. 1.9 Deflection function for scattering by the Lennard–Jones potential (1.32) for three energies. The abscissa is labelled by $\Lambda = \sqrt{E/\mathscr{E}}\, b/r_{\min}$

particle only weakly feels the attractive tail of the potential. The case in between, $\Lambda^2 = 2$, is close to the orbiting situation and the particle almost fulfills a complete revolution before leaving the interaction region.

Deflection functions for the Lennard–Jones potential (1.32) are shown in Fig. 1.9 for three energies. For $E/\mathscr{E} = 0.6$, orbiting occurs at $\Lambda \approx 1.281$. For $E/\mathscr{E} = 0.9$ and 1.2, orbiting is no longer possible, but pronounced minima of Θ with gradually decreasing depths remain.

1.3 Scattering Angle and Scattering Cross Sections

A typical scattering experiment involves a beam of incoming particles with uniform density n and asymptotic incoming velocity $\mathbf{v}_\infty = v_\infty \mathbf{e}_z$. The scattered particles are observed with a detector under an angle θ relative to the direction of incidence, see Fig. 1.10. The *scattering angle* θ varies between zero (forward scattering) and π (backward scattering).

The differential $\mathrm{d}\sigma$ is a quantitative measure for the flux of particles scattered into a differential solid angle $\mathrm{d}\Omega = \sin\theta\, \mathrm{d}\theta\, \mathrm{d}\phi$. It is defined as the number of particles passing a given (large) distance from the scattering centre in the direction of $\mathrm{d}\Omega$ per unit time, divided by the magnitude of the incoming current density, $|\mathbf{j}_{\mathrm{in}}| = n v_\infty$. If particles incident with impact parameter b are scattered into the angle θ, then, the particles scattered into the differential solid angle $\mathrm{d}\Omega$ are those with incoming trajectories passing through the differential area $\mathrm{d}b \times b\, \mathrm{d}\phi$ as shown in Fig. 1.10. The number of particles scattered into $\mathrm{d}\Omega$ per unit time is $n v_\infty \times b\, \mathrm{d}b\, \mathrm{d}\phi$, so

$$\mathrm{d}\sigma = b\, \mathrm{d}b\, \mathrm{d}\phi = b \left| \frac{\mathrm{d}b}{\mathrm{d}\theta} \right| \mathrm{d}\theta\, \mathrm{d}\phi = \frac{b}{\sin\theta} \left| \frac{\mathrm{d}b}{\mathrm{d}\theta} \right| \mathrm{d}\Omega . \tag{1.35}$$

The expressions in (1.35) contain the absolute value of $\mathrm{d}b/\mathrm{d}\theta$, because the observed yield is positive, regardless of whether $\mathrm{d}b/\mathrm{d}\theta$ is positive or negative.

The scattering angle $\theta \in [0, \pi]$ must not be confused with the deflection function $\Theta(b)$ discussed in Sect. 1.2. Among the particles observed under the scattering angle θ, there are those with incoming trajectories above the z-axis, as shown

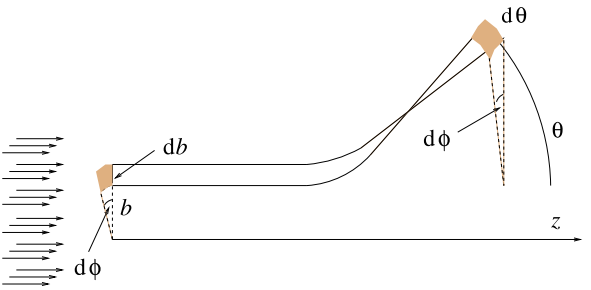

Fig. 1.10 Schematic illustration of a scattering experiment. Out of the uniform incoming beam, all trajectories with impact parameter between b and $b + \mathrm{d}b$ are observed with a scattering angle between θ and $\theta + \mathrm{d}\theta$

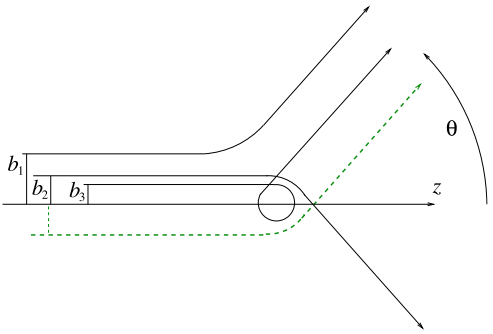

Fig. 1.11 Schematic illustration of different values of the deflection function corresponding to the same scattering angle θ: $\Theta(b_1) = \theta$, $\Theta(b_2) = -\theta$, $\Theta(b_3) = \theta - 2\pi$

in Fig. 1.10, for which $\Theta(b) = \theta$. However, there may also be particles with incoming trajectories below the z-axis, corresponding to a scattering plane rotated by π around the z-axis. An example is given by the dashed trajectory in Fig. 1.11 Such particles are detected under the scattering angle θ if $\Theta(b) = -\theta$. A scattering experiment in three dimensions usually does not discriminate between these two possibilities. Furthermore, one or more revolutions around the scattering centre are not detected, so observation under the scattering angle θ records all particles with impact parameter b for which $\pm(\Theta(b) + 2M\pi) = \theta$, i.e.,

$$\Theta(b) = \pm\theta - 2M\pi, \quad M = 0, 1, 2 \ldots . \tag{1.36}$$

The case $b = b_3$ in Fig. 1.11 is an example for $\Theta(b) = \theta - 2\pi$.

The *differential scattering cross section* as function of the scattering angle θ is obtained by summing the contributions (1.35) over all impact parameters fulfilling (1.36),

$$\frac{\mathrm{d}\sigma}{\mathrm{d}\Omega}(\theta) = \sum_i \frac{b_i}{\sin\theta}\left|\frac{\mathrm{d}b}{\mathrm{d}\theta}\right| = \sum_i \frac{b_i}{\sin\theta}\left[\left|\frac{\mathrm{d}\Theta}{\mathrm{d}b}\right|_{b_i}\right]^{-1}. \tag{1.37}$$

The area $\mathrm{d}\sigma$ corresponds to the area perpendicular to the incoming beam, through which all trajectories pass which are scattered into the solid angle $\mathrm{d}\Omega$. The expression on the far right of (1.37) is often preferred, because $\Theta(b)$ is an unambiguous function of the impact parameter b, defined on the interval $[0, \infty)$. In the preceeding expression, different terms in the sum correspond to different branches of the multivalued function $b(\theta)$.

The *integrated* or *total* scattering cross section σ is obtained by integrating the differential scattering cross section (1.37) over all angles of the unit sphere,

$$\sigma = \int \frac{\mathrm{d}\sigma}{\mathrm{d}\Omega}\mathrm{d}\Omega = 2\pi \int_0^\pi \frac{\mathrm{d}\sigma}{\mathrm{d}\Omega}(\theta)\sin\theta\,\mathrm{d}\theta. \tag{1.38}$$

The total scattering cross section corresponds to the area perpendicular to incidence through which all trajectories pass which are scattered at all.

For scattering by a hard sphere of radius R, the deflection function (1.9) is a bijective function of the impact parameter on the domain $b \in [0, R]$ where $\Theta = \theta$ and $b = R\cos(\theta/2)$, so

$$\frac{\mathrm{d}\sigma}{\mathrm{d}\Omega} = \frac{b}{\sin\theta}\left|\frac{\mathrm{d}b}{\mathrm{d}\theta}\right| = \frac{R^2}{4}. \tag{1.39}$$

Equation (1.39) shows that the hard sphere scatters isotropically. The total scattering cross section is, according to (1.38), simply 4π times the differential cross section (1.39), $\sigma = \pi R^2$, which is just the geometric cross section, i.e., the area of the obstacle as seen by the incident beam.

For a potential $V(r)$ which approaches zero smoothly as $r \to \infty$, the total scattering cross section is infinite, because even trajectories with very large impact parameters are scattered into small but nonvanishing scattering angles. For a potential falling off as $V(r) \sim C_\alpha/r^\alpha$ asymptotically, $\Theta(b) \propto 1/b^\alpha$ according to (1.19), and the differential scattering cross section (1.37) diverges in the forward direction as

$$\frac{\mathrm{d}\sigma}{\mathrm{d}\Omega}(\theta) \overset{\theta\to 0}{\sim} \frac{1}{\theta^{2+2/\alpha}}\frac{1}{\alpha}\left[\sqrt{\pi}\frac{|C_\alpha|}{E}\frac{\Gamma[(1+\alpha)/2]}{\Gamma(\alpha/2)}\right]^{2/\alpha}. \tag{1.40}$$

1.3.1 Kepler–Coulomb Potential

The Kepler–Coulomb potential $V(r) = C/r$ was introduced in Sect. 1.2.1, Eq. (1.20). The deflection function $\Theta(b)$ is given in (1.24) and shown in the right-hand part of Fig. 1.4. It is a bijective mapping of the interval $[0, \infty)$ onto a finite interval of deflection angles: $(0, \pi]$ in the repulsive case $C > 0$ and $[-\pi, 0)$ in the attractive case $C < 0$. The relation between scattering angle and deflection angle is $\theta = \Theta$ for $C > 0$ and $\theta = -\Theta$ for $C < 0$. Explicitly,

$$\begin{aligned} \Theta(b) &= \pm 2\arccos\left(\frac{1}{\sqrt{\gamma^2+1}}\right), \\ \gamma = \frac{|C|}{2Eb} &= \left|\tan\left(\frac{\theta}{2}\right)\right| \;\Rightarrow\; b = \left|\frac{C}{2E}\cot\left(\frac{\theta}{2}\right)\right|. \end{aligned} \tag{1.41}$$

The differential scattering cross section follows via (1.37),

$$\left|\frac{\mathrm{d}b}{\mathrm{d}\theta}\right| = \frac{|C|}{4E}\frac{1}{\sin^2(\theta/2)}, \quad \text{so} \quad \frac{\mathrm{d}\sigma}{\mathrm{d}\Omega} = \left(\frac{C}{4E}\right)^2 \frac{1}{\sin^4(\theta/2)} = \left(\frac{\mathrm{d}\sigma}{\mathrm{d}\Omega}\right)_{\text{Ruth}}, \tag{1.42}$$

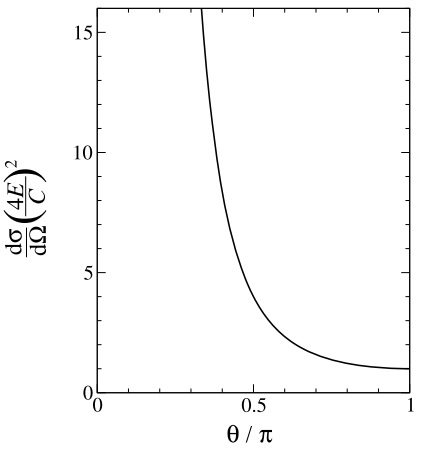

Fig. 1.12 Rutherford cross section (1.42) for scattering by the Kepler–Coulomb potential (1.20)

and it is shown in Fig. 1.12. This is the famous *Rutherford formula* for the differential cross section in Coulomb scattering. It does not discriminate between the repulsive case $C > 0$ and the attractive case $C < 0$.

1.3.2 Inverse-Power Potentials

Inverse-power potentials $V(r) = C_\alpha / r^\alpha$ were introduced in Sect. 1.2.2, Eq. (1.25). The deflection function is shown for the example $\alpha = 4$ in the right-hand part of Fig. 1.6. For the repulsive case, $C_\alpha > 0$, the deflection function $\Theta(b)$ is a bijective mapping of the interval $[0, \infty)$ onto $[0, \pi)$ and $\Theta = \theta$. The scattering cross section diverges in the forward direction according to (1.40) and is a monotonically decreasing function of the scattering angle. For an attractive inverse-power potential with $\alpha < 2$, there is no centrifugal barrier, and the scattering cross section is also a monotonically decreasing function of θ.

When $C_\alpha < 0$ and $\alpha > 2$, there is a centrifugal barrier and orbiting occurs when the parameter $\gamma = \alpha |C_\alpha| / (2Eb^\alpha)$ is equal to the value γ_{orb} given in Eq. (1.28), which, for given values of E and C_α, corresponds to the impact parameter

$$b_{\text{orb}} = \left(\frac{\alpha |C_\alpha|}{2E\gamma_{\text{orb}}} \right)^{1/\alpha} = \left(\frac{\alpha |C_\alpha|}{2E} \right)^{1/\alpha} \frac{\sqrt{\alpha}}{(\alpha - 2)^{(\alpha-2)/(2\alpha)}}. \tag{1.43}$$

As b increases from b_{orb} to infinity, $\Theta(b)$ grows from $-\infty$ to zero. For each scattering angle $\theta \in (0, \pi)$, there is an infinite sequence of impact parameters for which $\Theta + 2M\pi = \theta$ or $\Theta + 2M\pi = -\theta$. The derivative $|\mathrm{d}\Theta / \mathrm{d}b|$ is very large near orbiting, so the contribution of near-orbiting trajectories to the differential scattering cross section (1.37) is quite small. The small range of impact parameters near b_{orb} contributes rather uniformly to all scattering angles. The differential scattering cross section is shown in Fig. 1.13 for an inverse-power potential (1.25) with $\alpha = 4$.

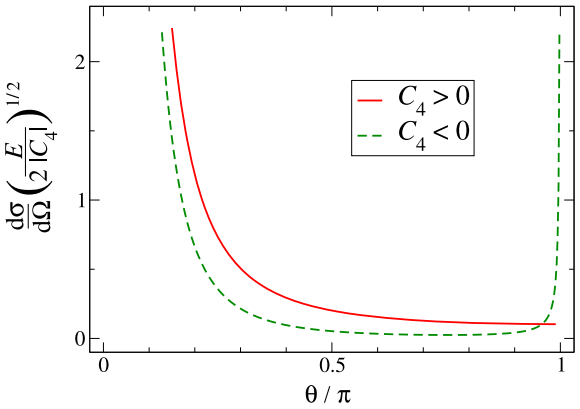

Fig. 1.13 Differential scattering cross section for an inverse-power potential (1.25) with $\alpha = 4$

Finite impact parameters for which $\Theta(b)$ is an odd multiple of π (corresponding to backward scattering) give a divergent contribution to the cross section due to the $\sin\theta$ in the denominator of the expression (1.37). Such divergent enhancement of the backward scattering cross section is referred to as *glory scattering*. The name stems from a similar effect in light scattering [1]. Note that the integration of the differential scattering cross section over a small finite range of angles near $\theta = \pi$ will lead to a finite result, because the diverging factor $1/\sin\theta$ in the cross section is compensated by the factor $\sin\theta$ in the differential $d\Omega$.

Glory scattering also occurs for finite impact parameters for which $\Theta(b)$ is an even multiple of π ("forward glory"). For potentials falling off smoothly to zero when $r \to \infty$, the effect of the forward glory is swamped by the generic forward divergence of the differential scattering cross section, see Eq. (1.40).

For an attractive inverse-power potential (1.25) with $\alpha > 2$, particles with impact parameters smaller than the orbiting value b_{orb} defined in (1.43) crash into the origin, where they may be absorbed by a variety of physical processes. The *absorption cross section* σ_{abs}, defined as the number of particles absorbed per unit time, divided by the incoming current density $n v_\infty$, is simply the area perpendicular to incidence through which the corresponding trajectories pass. Assuming that all particles incident with impact parameters $b < b_{\text{orb}}$ are absorbed yields

$$\sigma_{\text{abs}} = \pi b_{\text{orb}}^2 = \pi\alpha\left(\frac{|C_\alpha|}{2E}\right)^{2/\alpha}\left(\frac{1}{\alpha-2}\right)^{1-2/\alpha}. \tag{1.44}$$

For an inverse-square potential (1.30) with $C_2 < 0$, particles crash into the origin if $b \le \sqrt{|C_2|/E}$. If all these particles are absorbed,

$$\sigma_{\text{abs}} = \pi\frac{|C_2|}{E}, \tag{1.45}$$

which corresponds to the result (1.44) in the limit $\alpha \to 2$.

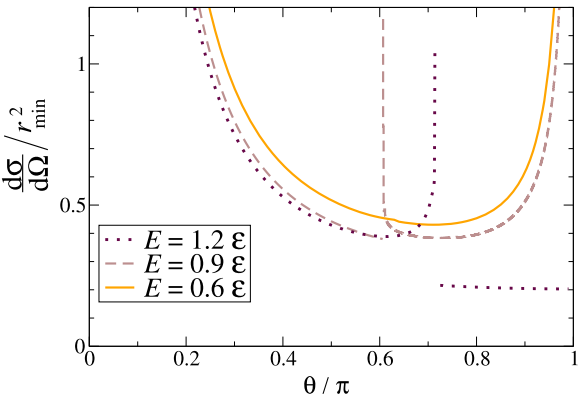

Fig. 1.14 Differential scattering cross section for the Lennard–Jones potential (1.32). For $E = 0.9\mathscr{E}$, there is a rainbow at $\theta_R \approx 0.61\pi$ and the dark side is towards smaller scattering angles. For $E = 1.2\mathscr{E}$, there is a rainbow at $\theta_R \approx 0.71\pi$ and the dark side is towards larger scattering angles

1.3.3 Lennard–Jones Potential

The Lennard–Jones potential (1.32) was discussed in Sect. 1.2.3, and deflection functions are shown in Fig. 1.9 for three energies. Differential scattering cross sections are shown in Fig. 1.14 for the same energies. At the lowest energy, $E = 0.6\mathscr{E}$, orbiting occurs and the behaviour of the cross section is qualitatively similar to that of the attractive $1/r^4$ potential shown in Fig. 1.13: there is divergence at backward angles corresponding to glory scattering, and the generic forward divergence. At $E = 0.9\mathscr{E}$, there is no orbiting, but the deflection function passes $-\pi$ for two finite values of the impact parameter, so glory scattering is still observable.

The deflection function at $E = 0.9\mathcal{E}$ has a minimum value $\Theta_{\min} \approx -1.39\pi$ for $\Lambda \approx 1.45$. At the corresponding scattering angle, $\theta_R = \Theta_{\min} + 2\pi \approx 0.61\pi$, the differential scattering cross section (1.37) diverges, because $\mathrm{d}\Theta/\mathrm{d}b$ vanishes. Such a divergence is called a *rainbow singularity*, because an analogous effect in light scattering is responsible for the rainbows in the sky [1]. The corresponding scattering angle θ_R is the *rainbow angle*. For $\theta > \theta_R \approx 0.61\pi$, there are five branches of $b(\theta)$ contributing to the scattering cross section (1.37), namely two with $\theta = \Theta + 2\pi$, two with $\theta = -\Theta$ and one with $\theta = \Theta$. The two branches with $\theta = \Theta + 2\pi$ coalesce at θ_R and no longer contribute for $\theta < \theta_R$, so only the three contributions with $\theta = \pm\Theta$ remain. For this rainbow, the regime $\theta < \theta_R$ is the *dark side* of the rainbow, while the regime $\theta > \theta_R$ is the *bright side* of the rainbow. The differential cross section (1.37) is noticeably smaller on the dark side of a rainbow than on the bright side.

At $E = 1.2\mathscr{E}$, the deflection function has a minimum $\Theta_{\min} \approx -0.71\pi$ at $\Lambda \approx 1.56$. The rainbow angle is now $\theta_R = -\Theta_{\min}$, and the dark side of the rainbow is $\theta > \theta_R$, while $\theta < \theta_R$ is the bright side. Note that $\Theta(b)$ never passes an odd multiple of π beyond $b = 0$, so there is no glory scattering at $E = 1.2\mathscr{E}$.

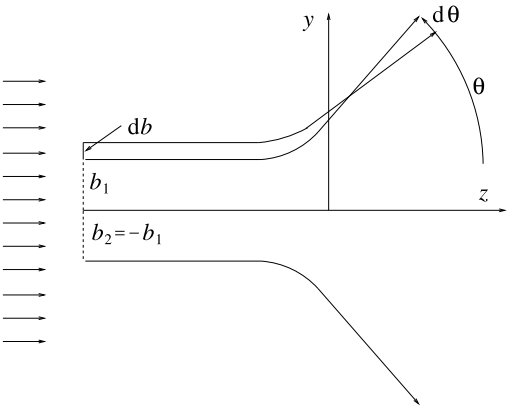

Fig. 1.15 Schematic illustration of a two-dimensional scattering experiment in the y–z plane. The impact parameter can be positive or negative (or zero), and the scattering angle θ varies between $-\pi$ and π

1.4 Classical Scattering in Two Spatial Dimensions

Two-dimensional scattering problems arise naturally when the motion of a particle is physically restricted to a plane. Furthermore, a three-dimensional scattering problem is effectively two-dimensional, if the physical system is translationally invariant in one direction, as is, e.g., the case for scattering of an atom by an infinitely long cylindrical wire.

As in three-dimensional scattering, we choose the z-axis to lie in the direction of incidence. The scattering potential is assumed to be radially symmetric, and the incoming particle with mass μ initially moves on a straight-line trajectory displaced by the impact parameter b from the z-axis. In three dimensions, this set-up is axially symmetric around the z-axis, and we chose the scattering plane to be the y–z plane with $b = L\sqrt{2\mu E} \geq 0$, see Fig. 1.1. In the 2D case, axial symmetry is replaced by reflection symmetry at the z-axis, and we could again choose the y–z plane such, that $b \geq 0$. We shall, however, adopt the more customary and convenient approach, where the y-z plane is assumed given by the physical system, so the impact parameter can be positive or negative (or zero), while the observable scattering angle θ varies between $-\pi$ and π—as sketched in Fig. 1.15.

For a given potential $V(r)$, the deflection function $\Theta(b)$ is the same as described in Sect. 1.2 for nonnegative b. Since the equations of motion are invariant under reflection at the z-axis, the deflection function for negative impact parameters follows via

$$\Theta(-b) = -\Theta(b), \tag{1.46}$$

i.e. the deflection function is an *antisymmetric* function of the impact parameter. When $\Theta(0) \neq 0$, i.e., $\lim_{b\to 0}\Theta(b) = m\pi$ with $m \neq 0$, then the deflection function shows a jump of $2m\pi$ at $b = 0$. As an example, Fig. 1.16 shows the deflection function for the Kepler–Coulomb potential $V(r) = C/r$, adapted to the two-dimensional case.

Particles scattered into a given scattering angle $\theta \in (0, \pi)$ are those with impact parameter b fulfilling (1.36). For each positive impact parameter b for which

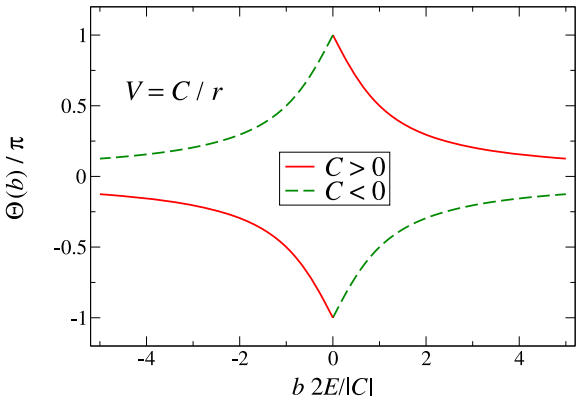

Fig. 1.16 Deflection function (1.24) for the Kepler–Coulomb potential, adapted to the two-dimensional case

$\Theta(b) = -\theta - 2M\pi$, the negative impact parameter $-b$ leads to the deflection angle $\Theta(-b) = \theta + 2M\pi$ because of (1.46). Trajectories of particles scattered into $-\theta$ are the reflections at the z-axis of those scattered into θ.

Adapting (1.36) to the two-dimensional case we formulate: A given scattering angle $\theta \in (-\pi, \pi)$ accommodates all particles with impact parameters $b \in (-\infty, \infty)$ for which

$$\Theta(b) = \theta - 2M\pi, \quad M = 0, \pm 1, \pm 2 \ldots . \tag{1.47}$$

Equation (1.8) in Sect. 1.2 can be generalized to accommodate negative angular momenta, for which $\theta(t)$ is a monotonically increasing function of time. One consequence is, that the integer M on the right-hand side of (1.47) can only be negative for negative impact parameters b, while it can only be positive for positive b, as already formulated in (1.36).

The differential $\mathrm{d}\lambda$ is a quantitative measure for the number of particles scattered into angles between θ and $\theta + \mathrm{d}\theta$ per unit time, normalized to the incoming current density $n\upsilon_\infty$. For each impact parameter fulfilling (1.47), these particles are those with incoming trajectories passing through the differential length $\mathrm{d}b$ as shown in Fig. 1.15. The number of particles scattered into $\mathrm{d}\theta$ per unit time is $n\upsilon_\infty \times \mathrm{d}b$, so

$$\mathrm{d}\lambda \equiv \mathrm{d}b = \left|\frac{\mathrm{d}b}{\mathrm{d}\theta}\right| \mathrm{d}\theta. \tag{1.48}$$

The *differential scattering cross section* as function of the scattering angle θ is obtained by summing the contributions (1.48) over all impact parameters fulfilling (1.47),

$$\frac{\mathrm{d}\lambda}{\mathrm{d}\theta} = \sum_i \left|\frac{\mathrm{d}b}{\mathrm{d}\theta}\right| = \sum_i \left[\left|\frac{\mathrm{d}\Theta}{\mathrm{d}b}\right|_{b_i}\right]^{-1}. \tag{1.49}$$

The length $\mathrm{d}\lambda$ corresponds to the length perpendicular to the incoming beam, through which all particles pass that are scattered into the angle $\mathrm{d}\theta$. From the symmetry with respect to reflection at the z-axis, it follows that the differential scattering cross section (1.49) is an even function of θ.

The *integrated* or *total* scattering cross section is obtained by integrating the differential cross section (1.49) over all scattering angles:

$$\lambda = \int_{-\pi}^{\pi} \frac{\mathrm{d}\lambda}{\mathrm{d}\theta} \mathrm{d}\theta. \tag{1.50}$$

It corresponds to the length perpendicular to the incoming beam, through which all particles pass that are scattered at all.

The formulae (1.49) and (1.50) for scattering cross sections in 2D differ from the corresponding formulae (1.37) and (1.38) in 3D in that they are missing the factor $b_i / \sin\theta$ coming from the definition of the solid angle. So, although the deflection function in 2D scattering is the same as in 3D—supplemented by Eq. (1.46) to accommodate negative impact parameters—the scattering cross sections for analogous systems in 2D and 3D do show differences.

Scattering by a hard sphere of radius R in 3D corresponds in 2D to the scattering by a hard disc of radius R, and Fig. 1.2 in Sect. 1.2 can be used as illustration in this case as well. The deflection function is given by (1.9) with (1.46), so $b = R\cos(\theta/2)$ and the differential cross section is, according to (1.49),

$$\frac{\mathrm{d}\lambda}{\mathrm{d}\theta} = \left|\frac{\mathrm{d}b}{\mathrm{d}\theta}\right| = \frac{R}{2}\left|\sin\left(\frac{\theta}{2}\right)\right|. \tag{1.51}$$

Note that scattering by a hard disc is, in contrast to scattering by a sphere, not isotropic. It is peaked at backward angles, $\theta \to \pm\pi$, and it vanishes towards forward angles $\theta \to 0$. The depletion at forward angles is easily understood considering that particles scattered into small angles hit the disc near the edge of its projection onto the line perpendicular to incidence, i.e. for b near $\pm R$. In 3D, a whole circle of impact parameters with b near R and azimuthal angles from zero to 2π contributes to scattering into small angles. The integrated cross section for scattering by the hard disc is

$$\lambda = \frac{R}{2}\int_{-\pi}^{\pi} \left|\sin\left(\frac{\theta}{2}\right)\right| \mathrm{d}\theta = 2R, \tag{1.52}$$

which is the geometric cross section, i.e., the length occupied by the disc in the path of the incident particles.

As in 3D scattering, the integrated cross section is infinite for a potential falling off smoothly as $r \to \infty$. For $V(r) \overset{r\to\infty}{\sim} C_\alpha / r^\alpha$, the deflection function behaves according to (1.19) and the differential scattering cross section (1.49) diverges in the forward direction as

$$\frac{\mathrm{d}\lambda}{\mathrm{d}\theta} \overset{\theta\to 0}{\sim} \frac{1}{|\theta|^{1+1/\alpha}} \frac{1}{\alpha}\left[\sqrt{\pi}\frac{|C_\alpha|}{E}\frac{\Gamma[(1+\alpha)/2]}{\Gamma(\alpha/2)}\right]^{1/\alpha}. \tag{1.53}$$

Comparing the forward divergence in 2D (1.53) and 3D (1.40) gives the appealingly simple result,

$$\left[\frac{\mathrm{d}\lambda}{\mathrm{d}\theta}(\theta)\right]_{\mathrm{2D}} \overset{\theta\to 0}{\sim} \sqrt{\frac{1}{\alpha}\left[\frac{\mathrm{d}\sigma}{\mathrm{d}\Omega}(|\theta|)\right]_{\mathrm{3D}}}. \tag{1.54}$$

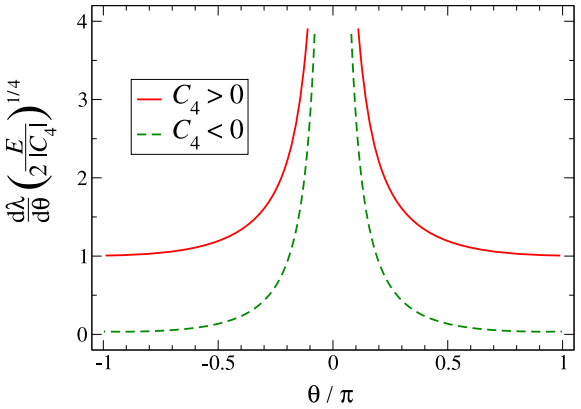

Fig. 1.17 Differential scattering cross section in two dimensions for an inverse-power potential (1.25) with $\alpha = 4$

For the Kepler–Coulomb potential $V(r) = C/r$, the deflection function is given analytically in (1.24) and displayed for the 2D situation in Fig. 1.16. The differential scattering cross section in 2D follows immediately via (1.49),

$$\frac{d\lambda}{d\theta} = \frac{|C|}{4E} \frac{1}{\sin^2(\theta/2)}. \tag{1.55}$$

In this case, the relation (1.54), with $\alpha = 1$, is not only valid asymptotically for $\theta \to 0$; it is an equality for all scattering angles.

The cross sections for the other examples discussed in Sect. 1.3 can also be derived via (1.49) using the deflection functions given in Sect. 1.2. Apart from the slower divergence at forward angles, a main difference is the absence of the glory singularity, which is due to the factor $1/\sin\theta$ in the 3D case. A main manifestation of orbiting and near-orbiting situations in 3D scattering, namely glory scattering at backward angles, is thus missing in the 2D cross sections. Figure 1.17 shows the differential scattering cross section (1.49) for an inverse-power potential $V(r) = C_4/r^4$. The ordinate is labelled with the cross section in units of the length $(2|C_4|/E)^{1/4}$.

For scattering by an attractive inverse-power potential $V(r) = C_\alpha/r^\alpha$, with $\alpha > 2$, orbiting occurs for impact parameters $|b| = b_{\rm orb}$, with $b_{\rm orb}$ given by (1.43). Assuming that all particles with impact parameters $|b| < b_{\rm orb}$ are absorbed, the absorbtion cross section is

$$\lambda_{\rm abs} = 2b_{\rm orb}. \tag{1.56}$$

The differential cross section for scattering by the Lennard–Jones potential (1.32) in two dimensions follows via (1.49)—and (1.46)—from the deflection functions discussed in Sect. 1.3.3, see Fig. 1.9. They are shown in Fig. 1.18 for the same energies as in Fig. 1.9 and Sect. 1.3.3. The rainbow singularities for $E = 0.9\mathscr{E}$ (at $\theta_{\rm R} \approx 0.61\pi$) and for $E = 1.2\mathscr{E}$ (at $\theta_{\rm R} \approx 0.71\pi$) are manifest, as in the 3D case.

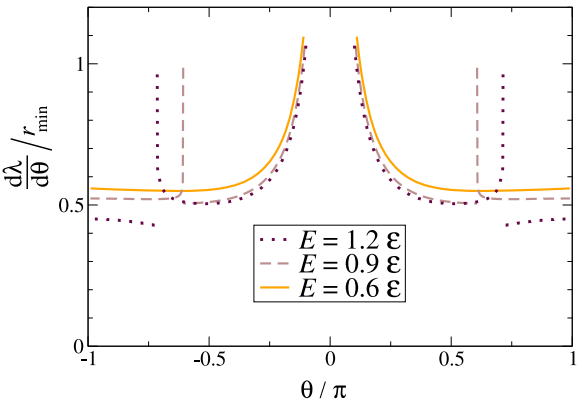

Fig. 1.18 Differential scattering cross section in two dimensions for the Lennard–Jones potential (1.32). For $E = 0.9\mathscr{E}$, there are rainbows at $|\theta| = \theta_R \approx 0.61\pi$ and the dark sides are towards smaller values of $|\theta|$. For $E = 1.2\mathscr{E}$, there are rainbows at $|\theta| = \theta_R \approx 0.71\pi$ and the dark sides are towards larger values of $|\theta|$

References

1. Adam, J.A.: The mathematical physics of rainbows and glories. Phys. Rep. **356**, 229–365 (2002)
2. Landau, L.D., Lifshitz, E.M.: Course of Theoretical Physics. Mechanics, vol. 1. 3rd edn. Butterworth-Heinemann, Stoneham (1976)

Chapter 2
Elastic Scattering by a Conservative Potential

2.1 Scattering Amplitude and Scattering Cross Section

In quantum mechanics the relative motion of a projectile and a target is described by a complex-valued wave function ψ which depends on the relative distance $\mathbf{r}$ of the projectile from the target. The wave function is assumed to obey the time-independent Schrödinger equation for a particle with (reduced) mass μ in the potential $V(\mathbf{r})$,

$$\left[-\frac{\hbar^2}{2\mu}\Delta + V(\mathbf{r})\right]\psi(\mathbf{r}) = E\psi(\mathbf{r}). \tag{2.1}$$

In order to describe elastic scattering at energy $E = \hbar^2 k^2/(2\mu)$, we look for solutions of (2.1), which at large distances obey boundary conditions corresponding to an incoming plane wave and an outgoing, scattered spherical wave, as sketched in Fig. 2.1,

$$\psi(\mathbf{r}) \overset{r\to\infty}{\sim} \mathrm{e}^{\mathrm{i}kz} + f(\theta,\phi)\frac{\mathrm{e}^{\mathrm{i}kr}}{r}. \tag{2.2}$$

Although a real scattering event is a time-dependent process, the description via stationary solutions of the time-independent Schrödinger equation is adequate in most experimental situations [30]. The explicit form of the two terms on the right-hand side of (2.2) implies that the motion of the particle is asymptotically ($r \to \infty$) free, which places some constraints on the large-distance behaviour of the potential $V(\mathbf{r})$. Unless stated otherwise, we assume that the potential falls off faster than $1/r^2$ at large distances, $r^2 V(\mathbf{r}) \overset{r\to\infty}{\longrightarrow} 0$.

The particle flux associated with the quantum mechanical wave function is described via the *current density* $\mathbf{j}(\mathbf{r})$. Classically, $\mathbf{j}(\mathbf{r})$ would be the product of particle density and velocity. In the corresponding quantum mechanical expression, the velocity is replaced by $\hat{\mathbf{p}}/\mu$, where $\hat{\mathbf{p}} = (\hbar/\mathrm{i})\nabla$ is the momentum operator conjugate

H. Friedrich, *Scattering Theory*, DOI 10.1007/978-3-662-48526-2_2

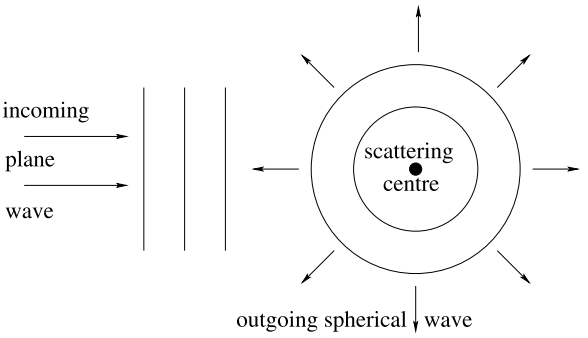

Fig. 2.1 Schematic illustration of the incoming plane wave and the outgoing spherical wave as described by a solution of (2.1) obeying the boundary conditions (2.2)

to $\mathbf{r}$,

$$\mathbf{j}(\mathbf{r}) = \Re\left[\psi^*(\mathbf{r})\frac{\hat{\mathbf{p}}}{\mu}\psi(\mathbf{r})\right] = \frac{\hbar}{2\mathrm{i}\mu}\psi^*(\mathbf{r})\nabla\psi(\mathbf{r}) + \mathrm{cc}; \tag{2.3}$$

"cc" stands for the complex conjugate of the preceding term.

From the first term on the right-hand side of (2.2) we find that the current density associated with the incoming plane wave is $\mathbf{j}_{\mathrm{in}} = \hat{\mathbf{e}}_z \hbar k/\mu$, corresponding to a wave of unit spatial density moving with velocity $v = \hbar k/\mu$ in the direction of $\hat{\mathbf{e}}_z$, the unit vector in z-direction. The second term on the right-hand side of (2.2) describes an outgoing spherical wave, modulated by the *scattering amplitude* $f(\theta, \phi)$, which has the physical dimensions of a length. Inserted in (2.3) this term generates an outgoing current density which is given to leading order by

$$\mathbf{j}_{\mathrm{out}}(\mathbf{r}) = \frac{\hbar k}{\mu}\left|f(\theta,\phi)\right|^2 \frac{\hat{\mathbf{e}}_{\mathbf{r}}}{r^2} + O\left(\frac{1}{r^3}\right), \tag{2.4}$$

where $\hat{\mathbf{e}}_{\mathbf{r}} = \mathbf{r}/r$ is the radial unit vector. Asymptotically, the flux of particle density scattered into the solid angle $\mathrm{d}\Omega = \sin\theta \mathrm{d}\theta\mathrm{d}\phi$ is $\lim_{r\to\infty}\mathbf{j}_{\mathrm{out}}(\mathbf{r})\cdot\mathbf{ds}$ with $\mathbf{ds} = \hat{\mathbf{e}}_{\mathbf{r}} r^2 \mathrm{d}\Omega$, i.e., $(\hbar k/\mu)|f(\theta,\phi)|^2\mathrm{d}\Omega$. The differential scattering cross section is given by this flux, normalized to the incoming current density $|\mathbf{j}_{\mathrm{in}}| = \hbar k/\mu$,

$$\mathrm{d}\sigma = \left|f(\theta,\phi)\right|^2 \mathrm{d}\Omega, \qquad \frac{\mathrm{d}\sigma}{\mathrm{d}\Omega} = \left|f(\theta,\phi)\right|^2. \tag{2.5}$$

Integrating over all directions θ, ϕ yields the *integrated* or *total* elastic scattering cross section,

$$\sigma = \int \frac{\mathrm{d}\sigma}{\mathrm{d}\Omega}\mathrm{d}\Omega = \int_0^{2\pi}\mathrm{d}\phi \int_0^{\pi} \sin\theta \mathrm{d}\theta \left|f(\theta,\phi)\right|^2. \tag{2.6}$$

As in the classical case, see Eqs. (1.37), (1.38) in Sect. 1.3, σ has the physical dimensions of an area; $\mathrm{d}\sigma$ can be interpreted as the area in the plane perpendicular to the direction of incidence, through which the incoming flux passes which is scattered into the outgoing direction $\mathrm{d}\Omega$. Correspondingly, σ describes the area through which all the flux passes which is scattered at all.

Each solution of the stationary Schrödinger equation (2.1) fulfills the *continuity equation* in the form,

$$\nabla \cdot \mathbf{j} = -\frac{\partial \rho}{\partial t} = 0, \quad \text{or, equivalently,} \quad \oint \mathbf{j} \cdot \mathrm{d}\mathbf{s} = 0. \tag{2.7}$$

This states that the net flux through any closed surface vanishes, which is an expression of particle conservation. For the surface of a large sphere with radius $r \to \infty$, the integrated contribution from the incoming plane wave, $I_{\text{in}} = \oint \mathbf{j}_{\text{in}} \cdot \mathrm{d}\mathbf{s}$, vanishes because of symmetry. The contribution I_{out} from the outgoing current density is positive unless the scattering amplitude $f(\theta, \phi)$ vanishes identically,

$$I_{\text{out}} = \lim_{r\to\infty} \oint \mathbf{j}_{\text{out}}(\mathbf{r}) \cdot \mathrm{d}\mathbf{s} = \frac{\hbar k}{\mu} \int \left| f(\Omega) \right|^2 \mathrm{d}\Omega = \frac{\hbar k}{\mu}\sigma. \tag{2.8}$$

The fact that $I_{\text{in}} + I_{\text{out}}$ does not vanish does not contradict Eq. (2.7), because the total current density $\mathbf{j}$ is not merely the sum of $\mathbf{j}_{\text{in}}$ and $\mathbf{j}_{\text{out}}$, but contains a contribution from the interference of plane and spherical waves,

$$\mathbf{j}(\mathbf{r}) \overset{r\to\infty}{\sim} \mathbf{j}_{\text{in}} + \mathbf{j}_{\text{out}}(r) + \mathbf{j}_{\text{int}}(r). \tag{2.9}$$

The interference term is, including terms up to $O(1/r^2)$,

$$\mathbf{j}_{\text{int}}(r) \overset{r\to\infty}{\sim} \frac{\hbar}{2\mu} f(\theta,\phi) \left[k \frac{\mathrm{e}^{\mathrm{i}k(r-z)}}{r} (\hat{\mathbf{e}}_{\mathbf{r}} + \hat{\mathbf{e}}_z) + \mathrm{i} \frac{\mathrm{e}^{\mathrm{i}k(r-z)}}{r^2} \hat{\mathbf{e}}_{\mathbf{r}} \right] + \text{cc} + \cdots, \tag{2.10}$$

where $\cdots$ stands for vector contributions orthogonal to $\hat{\mathbf{e}}_{\mathbf{r}}$. The contribution of this interference term to the flux through the surface element $\mathrm{d}\mathbf{s} = \hat{\mathbf{e}}_{\mathbf{r}} r^2 \mathrm{d}\Omega$ of a sphere with large radius r is,

$$\mathbf{j}_{\text{int}}(r) \cdot \mathrm{d}\mathbf{s} = \frac{\hbar}{2\mu} f(\theta,\phi) \mathrm{e}^{\mathrm{i}kr(1-\cos\theta)} \big[kr(1+\cos\theta) + \mathrm{i} \big] \mathrm{d}\Omega + \text{cc}. \tag{2.11}$$

The contribution $I_{\text{int}} = \lim_{r\to\infty} \oint \mathbf{j}_{\text{int}}(\mathbf{r}) \cdot \mathrm{d}\mathbf{s}$ to the total flux through the surface of the sphere with large radius r is obtained by integrating the expression (2.11) over $\mathrm{d}\Omega$ and taking the limit $r \to \infty$. The contribution due to the "i" in the square bracket vanishes, because $\lim_{\gamma\to\infty} \int_{-1}^{1} f(x) \mathrm{e}^{\mathrm{i}\gamma(1-x)} \mathrm{d}x = 0$, with $kr \equiv \gamma$, $x = \cos\theta$. A non-vanishing result is obtained from the preceding term proportional to kr via the identity

$$\lim_{\gamma\to\infty} \gamma \int_{-1}^{+1} (1+x) f(x) \mathrm{e}^{\mathrm{i}\gamma(1-x)} \mathrm{d}x = 2\mathrm{i} f(1), \quad \text{namely,} \tag{2.12}$$

$$\begin{aligned} I_{\text{int}} &= \lim_{r\to\infty} \int_0^{2\pi} \mathrm{d}\phi \int_{-1}^{+1} \mathrm{d}\cos\theta \, \mathbf{j}_{\text{int}}(r) \cdot \mathrm{d}\mathbf{s} \\ &= \frac{\hbar}{\mu} 2\pi \mathrm{i} f(\theta = 0) + \text{cc} = -\frac{\hbar}{\mu} 4\pi \Im\big[f(\theta = 0) \big]. \end{aligned} \tag{2.13}$$

Particle conservation requires that I_{int} exactly cancels the contribution I_{out} as given in (2.8), so

$$\sigma = \frac{4\pi}{k}\Im\big[f(\theta = 0)\big]. \tag{2.14}$$

Equation (2.14) is known as the *optical theorem*. It shows that destructive interference between the plane wave and the scattered wave in the forward direction $\theta = 0$ compensates the loss of flux through the scattering process. Note that $f(\theta, \phi)$ becomes independent of ϕ for $\theta = 0$.

2.2 Lippmann–Schwinger Equation and Born Approximation

The Schrödinger equation (2.1) can be rewritten as

$$\left(E + \frac{\hbar^2}{2\mu}\Delta\right)\psi(\mathbf{r}) = V(\mathbf{r})\psi(\mathbf{r}) \tag{2.15}$$

and transformed into an integral equation with the help of the *free-particle Green's function* $\mathcal{G}(\mathbf{r}, \mathbf{r}')$, which fulfills

$$\left(E + \frac{\hbar^2}{2\mu}\Delta_{\mathbf{r}}\right)\mathcal{G}\big(\mathbf{r}, \mathbf{r}'\big) = \delta\big(\mathbf{r} - \mathbf{r}'\big) \tag{2.16}$$

and is explicitly given by

$$\mathcal{G}(\mathbf{r}, \mathbf{r}') = -\frac{\mu}{2\pi\hbar^2}\frac{\mathrm{e}^{\mathrm{i}k|\mathbf{r}-\mathbf{r}'|}}{|\mathbf{r} - \mathbf{r}'|}. \tag{2.17}$$

A wave function $\psi(\mathbf{r})$ obeying the integral equation

$$\psi(\mathbf{r}) = \mathrm{e}^{\mathrm{i}kz} + \int \mathcal{G}(\mathbf{r}, \mathbf{r}')V(\mathbf{r}')\psi(\mathbf{r}')\mathrm{d}\mathbf{r}' \tag{2.18}$$

necessarily obeys the Schrödinger equation (2.15). This would also hold, if the first term $\mathrm{e}^{\mathrm{i}kz}$ were replaced by $\mathrm{e}^{-\mathrm{i}kz}$ or any other solution of the "homogeneous" version, $[E + (\hbar^2/(2\mu))\Delta]\psi(\mathbf{r}) = 0$, of Eq. (2.15).[1]

Equation (2.18) is called the *Lippmann–Schwinger equation*. It is essentially equivalent to the Schrödinger equation (2.1), but has the advantage, that the boundary conditions (2.2) are automatically fulfilled. To see this we make use of the explicit form of the Green's function (2.17) for $|\mathbf{r}| \gg |\mathbf{r}'|$:

$$\mathcal{G}\big(\mathbf{r}, \mathbf{r}'\big) = -\frac{\mu}{2\pi\hbar^2}\frac{\mathrm{e}^{\mathrm{i}kr}}{r}\left[\mathrm{e}^{-\mathrm{i}\mathbf{k}_{\mathbf{r}}\cdot\mathbf{r}'} + O\left(\frac{r'}{r}\right)\right], \tag{2.19}$$

[1] Equation (2.15) is homogeneous, whether or not the right-hand side is replaced by zero. The present terminology is adapted from applications to genuinely inhomogeneous differential equations, where the right-hand side is a given function independent of the solution being sought.

where $\mathbf{k_r} = k\hat{\mathbf{e}}_\mathbf{r}$ is the wave vector which has the same length as the wave vector $k\hat{\mathbf{e}}_z$ of the incoming plane wave but points in the direction of the radial vector $\hat{\mathbf{e}}_\mathbf{r}$ (without prime). Inserting (2.19) into (2.18) gives the asymptotic form (2.2) with

$$f(\theta,\phi) = -\frac{\mu}{2\pi\hbar^2}\int \mathrm{e}^{-\mathrm{i}\mathbf{k_r}\cdot\mathbf{r}'}\,V(\mathbf{r}')\psi(\mathbf{r}')\mathrm{d}\mathbf{r}'. \tag{2.20}$$

Equation (2.20) is an exact expression for the scattering amplitude f, but its evaluation requires the knowledge of the exact solution ψ of the Schrödinger (or Lippmann–Schwinger) equation. If, in addition to fulfilling $r^2V(\mathbf{r}) \overset{r\to\infty}{\longrightarrow} 0$, the potential is less singular than $1/r^2$ at the origin, $r^2V(\mathbf{r}) \overset{r\to 0}{\longrightarrow} 0$ (and a continuous function of $\mathbf{r}$), then the integral on the right-hand side of (2.20) converges for all values of $\mathbf{k_r}$.

If the influence of the potential V can be regarded to be small, the Lippmann–Schwinger equation (2.20) can be used to construct a perturbation series. Inserting the explicit form (2.18) for $\psi(\mathbf{r}')$ into (2.20) gives

$$\begin{aligned} f(\theta,\phi) = -\frac{\mu}{2\pi\hbar^2}\Bigg[&\int \mathrm{d}\mathbf{r}'\mathrm{e}^{-\mathrm{i}\mathbf{k_r}\cdot\mathbf{r}'}V(\mathbf{r}')\mathrm{e}^{\mathrm{i}kz'} \\ &+ \int \mathrm{d}\mathbf{r}'\mathrm{e}^{-\mathrm{i}\mathbf{k_r}\cdot\mathbf{r}'}V(\mathbf{r}')\int \mathrm{d}\mathbf{r}''\mathscr{G}(\mathbf{r}',\mathbf{r}'')V(\mathbf{r}'')\psi(\mathbf{r}'')\Bigg]. \end{aligned} \tag{2.21}$$

Repeatedly inserting the explicit form (2.18) for the exact wave function ψ generates a series of approximations ordered by the number of times the potential V appears in the (multiple) integral. This series is called the *Born series*. Keeping only the first term on the upper line of Eq. (2.21) defines the *Born approximation* in first order,

$$f^{\mathrm{Born}}(\theta,\phi) = -\frac{\mu}{2\pi\hbar^2}\int \mathrm{d}\mathbf{r}'\mathrm{e}^{-\mathrm{i}\mathbf{k_r}\cdot\mathbf{r}'}V(\mathbf{r}')\mathrm{e}^{\mathrm{i}kz'} = -\frac{\mu}{2\pi\hbar^2}\int \mathrm{d}\mathbf{r}'\mathrm{e}^{-\mathrm{i}\mathbf{q}\cdot\mathbf{r}'}V(\mathbf{r}'), \tag{2.22}$$

where $\hbar\mathbf{q}$ is the momentum transferred from the incoming wave travelling in the direction of $\hat{\mathbf{e}}_z$ to the outgoing wave travelling in the direction of $\hat{\mathbf{e}}_\mathbf{r}$,

$$\mathbf{q} = k(\hat{\mathbf{e}}_\mathbf{r} - \hat{\mathbf{e}}_z). \tag{2.23}$$

The scattering amplitude in Born approximation is essentially the Fourier transform of the potential; its dependence on the scattering angle(s) enters through the wave vector of momentum transfer (2.23). The polar angle θ is related to the wave number $q = |\mathbf{q}|$ via

$$q = 2k\sin(\theta/2), \tag{2.24}$$

see Fig. 2.2. If the potential V is real and radially symmetric, $V = V(r)$, then f^{Born} is a real function depending only on the wave number q. The scattering amplitude in Born approximation thus necessarily violates the optical theorem (2.14).

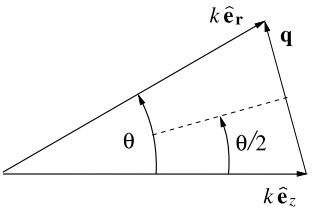

Fig. 2.2 Illustration of the relation (2.24) connecting the polar angle θ with the wave vector $\mathbf{q}$ of momentum transfer

Inserting $e^{ikz''}$ for $\psi(\mathbf{r}'')$ in the integral in the lower line of Eq. (2.21) defines the *second-order Born approximation*. Including the contribution $\int \mathscr{G}(\mathbf{r}'', \mathbf{r}''')V(\mathbf{r}''')d\mathbf{r}'''$ paves the way to higher-order terms.

2.3 Radially Symmetric Potentials

2.3.1 Angular Momentum

When the potential is radially symmetric, $V(\mathbf{r}) = V(r)$, the orbital angular momentum $\hat{\mathbf{L}} = \mathbf{r} \times \hat{\mathbf{p}}$ is a conserved quantity. The three components of $\hat{\mathbf{L}}$ commute with $\hat{\mathbf{L}}^2$ but not with each other, $[\hat{L}_x, \hat{L}_y] = i\hbar\hat{L}_z$. The space of angular functions can be spanned by simultaneous eigenstates of $\hat{\mathbf{L}}^2$ and one component of $\hat{\mathbf{L}}$, which is usually chosen to be $\hat{L}_z$. In coordinate representation, these states are the *spherical harmonics* $Y_{l,m}(\theta, \phi)$, which are labelled by the angular momentum quantum number l and the azimuthal quantum number m,

$$\begin{aligned} &\hat{\mathbf{L}}^2 Y_{l,m}(\theta,\phi) = l(l+1)\hbar^2 Y_{l,m}(\theta,\phi), \quad l = 0, 1, 2, \ldots; \\ &\hat{L}_z Y_{l,m}(\theta,\phi) = m\hbar Y_{l,m}(\theta,\phi), \quad m = -l, -l+1, \ldots, l-1, l. \end{aligned} \tag{2.25}$$

The general structure[2] of the spherical harmonics is,

$$Y_{l,m}(\theta,\phi) = e^{im\phi} \sin^{|m|}(\theta) \mathrm{Pol}_{l-|m|}(\cos\theta), \tag{2.26}$$

where $\mathrm{Pol}_\lambda(x)$ stands for a polynomial of degree λ in x. They are orthonormal,

$$\begin{aligned} \int Y_{l,m}(\Omega)^* Y_{l',m'}(\Omega) d\Omega &= \int_0^{2\pi} d\phi \int_{-1}^{+1} d\cos\theta \, Y_{l,m}(\theta,\phi)^* Y_{l',m'}(\theta,\phi) \\ &= \delta_{l,l'}\delta_{m,m'}, \end{aligned} \tag{2.27}$$

and obey the following relations:

$$Y_{l,m}(\theta - \pi, \phi + \pi) = Y_{l,-m}(\theta,\phi) = (-1)^l Y_{l,m}(\theta,\phi). \tag{2.28}$$

[2] For precise definitions of the $Y_{l,m}$ and other special functions see Appendix B.

For vanishing azimuthal quantum number, $m = 0$, the spherical harmonics do not depend on ϕ and are proportional to *Legendre polynomials* [1] of $\cos\theta$,

$$Y_{l,m=0}(\theta) = \sqrt{\frac{2l+1}{4\pi}} P_l(\cos\theta). \tag{2.29}$$

The Legendre polynomials fulfill the orthogonality relation

$$\int_{-1}^{1} P_l(x) P_{l'}(x) \mathrm{d}x = \frac{2}{2l+1} \delta_{l,l'}, \tag{2.30}$$

and for two vectors $\mathbf{a}$, $\mathbf{b}$, with $|\mathbf{a}| \leq |\mathbf{b}|$ we have

$$\frac{1}{|\mathbf{a}-\mathbf{b}|} = \sum_{l=0}^{\infty} \frac{|\mathbf{a}|^l}{|\mathbf{b}|^{l+1}} P_l(\cos\theta), \tag{2.31}$$

where θ is the angle between $\mathbf{a}$ and $\mathbf{b}$. For $|\mathbf{a}| = |\mathbf{b}|$ Eq. (2.31) yields

$$\sum_{l=0}^{\infty} P_l(\cos\theta) = \frac{1}{2\sin(\theta/2)}. \tag{2.32}$$

2.3.2 Partial-Waves Expansion

For a radially symmetric potential, the Schrödinger equation (2.1) is rotationally invariant, but the boundary conditions (2.2) for the scattering wave function $\psi(\mathbf{r})$ are not. So ψ is not an eigenfunction of angular momentum, but it can be expanded in eigenfunctions of angular momentum. Since rotational symmetry around the z-axis is conserved both by the Schrödinger equation (2.1) and the boundary conditions (2.2), the azimuthal quantum number m is conserved. Since the incoming plane wave has $m = 0$, the same can be assumed for the full wave function $\psi(\mathbf{r})$, which thus no longer depends on the azimuthal angle ϕ,

$$\psi(\mathbf{r}) = \psi(r,\theta) = \sum_{l=0}^{\infty} \frac{u_l(r)}{r} P_l(\cos\theta). \tag{2.33}$$

Equation (2.33) represents an expansion of the full scattering wave $\psi(\mathbf{r})$ in *partial waves*, each such partial wave being labelled by its orbital angular momentum quantum number l. The contribution of each partial wave is determined by its *radial wave function* $u_l(r)$. From the spherical representation of the Laplacian we have

$$-\frac{\hbar^2}{2\mu}\Delta = -\frac{\hbar^2}{2\mu}\left(\frac{\partial^2}{\partial r^2} + \frac{2}{r}\frac{\partial}{\partial r}\right) + \frac{\hat{\mathbf{L}}^2}{2\mu r^2}, \tag{2.34}$$

and inserting the expansion (2.33) into the Schrödinger equation (2.1) leads to the equations

$$\left[-\frac{\hbar^2}{2\mu}\frac{\mathrm{d}^2}{\mathrm{d}r^2}+\frac{l(l+1)\hbar^2}{2\mu r^2}+V(r)\right]u_l(r)=Eu_l(r) \tag{2.35}$$

for the radial wave functions $u_l(r)$. The $1/r$ on the right-hand side of (2.33) ensures that the *radial Schrödinger equation* (2.35) contains only the second and not the first derivative of u_l, so it has the form of a Schrödinger equation for a particle moving in one dimension under the influence of the effective potential

$$V_{\mathrm{eff}}(r)=V(r)+V_{\mathrm{cent}}(r),\quad V_{\mathrm{cent}}(r)=\frac{l(l+1)\hbar^2}{2\mu r^2}, \tag{2.36}$$

subject to the condition that the coordinate r is nonnegative, $r\geq 0$. In the space of all possible radial wave functions in the lth partial wave, the unitary scalar product of two radial wave functions, u_l and $\tilde{u}_l$ is defined as

$$\langle u_l|\tilde{u}_l\rangle=\int_0^\infty u_l(r)^*\tilde{u}_l(r)\mathrm{d}r. \tag{2.37}$$

The effective potential (2.36) is essentially the same as in the classical description, see Eq. (1.11) in Sect. 1.2, except that the square of the angular momentum in the centrifugal potential is expressed via its quantum mechanical eigenvalue $l(l+1)\hbar^2$.

2.3.3 Scattering Phase Shifts

In the absence of the potential $V(r)$, the radial Schrödinger equation (2.35) represents the angular momentum components of the free-particle wave equation, and its solutions can be written as functions of the dimensionless product kr. Two linearly independent solutions of the radial free-particle equation are,

$$u_l^{(\mathrm{s})}(kr)=krj_l(kr),\qquad u_l^{(\mathrm{c})}(kr)=-kry_l(kr), \tag{2.38}$$

where j_l and y_l stand for the *spherical Bessel functions* of the first and second kind, respectively (see Appendix B.4 and Ref. [1]). Their asymptotic behaviour is given by

$$\begin{aligned} u_l^{(\mathrm{s})}(kr) &\overset{kr\to\infty}{=} \sin\left(kr-l\frac{\pi}{2}\right)+O\left(\frac{1}{kr}\right),\\ u_l^{(\mathrm{c})}(kr) &\overset{kr\to\infty}{=} \cos\left(kr-l\frac{\pi}{2}\right)+O\left(\frac{1}{kr}\right). \end{aligned} \tag{2.39}$$

For small values of kr, the radial free-particle wave functions (2.38) behave as,

$$\begin{aligned} u_l^{(\mathrm{s})}(kr) &\overset{kr\to 0}{\sim} \frac{\sqrt{\pi}(kr)^{l+1}}{2^{l+1}\Gamma(l+\frac{3}{2})}\left[1-\frac{(kr)^2}{4l+6}\right], \\ u_l^{(\mathrm{c})}(kr) &\overset{kr\to 0}{\sim} \frac{2^l\Gamma(l+\frac{1}{2})}{\sqrt{\pi}(kr)^l}\left[1+\frac{(kr)^2}{4l-2}\right]. \end{aligned} \tag{2.40}$$

The wave function $u_l^{(\mathrm{s})}$ is the physical, *regular* solution; $u_l^{(\mathrm{c})}$ is an unphysical, *irregular* solution. For $l>0$, the irregular solution $u_l^{(\mathrm{c})}$ is not square integrable due to the divergence at $r\to 0$; for $l=0$ its contribution proportional to $1/r$ in the full wave function (2.33) would lead to a delta-function contribution in $\Delta\psi$, which cannot be compensated by any other term in the Schrödinger equation (2.1).

For a potential $V(r)$ less singular than $1/r^2$ at the origin, the effective potential (2.36) is dominated near $r=0$ by the centrifugal term, so we can expect two linearly independent solutions of (2.35), u_l^{reg} and $u_l^{\mathrm{irr}}(r)$, whose small-distance behaviour is

$$u_l^{\mathrm{reg}}(r) \overset{r\to 0}{\propto} r^{l+1}, \qquad u_l^{\mathrm{irr}}(r) \overset{r\to 0}{\propto} r^{-l}. \tag{2.41}$$

Here u_l^{reg} denotes the physical, regular solution; u_l^{irr} is an unphysical, irregular solution. In the following, we shall mostly be dealing with regular solutions of the radial Schrödinger equation, which vanish for $r\to 0$, and we shall dispense with the superscript "reg" unless it is explicitly needed.

At large distances, the effective potential (2.36) is again dominated by the centrifugal term, because we have assumed that $V(r)$ falls off faster than $1/r^2$. The regular solution of the radial Schrödinger equation (2.35) can, at large distances, be taken to be a superposition of the two radial free-particle wave functions (2.38) obeying (2.39),

$$u_l(r) \overset{r\to\infty}{\propto} Au_l^{(\mathrm{s})}(kr) + Bu_l^{(\mathrm{c})}(kr) \overset{r\to\infty}{\propto} \sin\left(kr - l\frac{\pi}{2} + \delta_l\right), \tag{2.42}$$

with $\tan\delta_l = B/A$. Since the potential is real, we can assume that u_l is, except for a constant complex factor, a real function of r, so that the ratio B/A and the phase δ_l are real. The phases δ_l, $l=0,1,2,\ldots$, contain the information about the effect of the potential on the asymptotic behaviour of the wave function (2.33). They are called *scattering phase shifts*, because they determine the scattering amplitude, as shown in the following.

The partial-waves expansion of the incoming plane wave is

$$\mathrm{e}^{\mathrm{i}kz} = \sum_{l=0}^{\infty}(2l+1)\mathrm{i}^l j_l(kr)P_l(\cos\theta), \tag{2.43}$$

where the j_l are the spherical Bessel functions of the first kind, already introduced in Eq. (2.38). At large distances, the full wave function consists of the plane wave

(2.43) and an outgoing spherical wave according to (2.2). The scattering amplitude f depends only on the polar angle θ, because the whole wave function does not depend on the azimuthal angle ϕ. We expand f into partial-wave contributions,

$$f(\theta) = \sum_{l=0}^{\infty} f_l P_l(\cos\theta), \tag{2.44}$$

with constant coefficients f_l, the *partial-wave scattering amplitudes*. Expressing the sum of plane and spherical wave in the form (2.33) gives an explicit expression for the asymptotic behaviour of the radial wave functions,

$$\begin{aligned} u_l(r) &\overset{r\to\infty}{\sim} \mathrm{i}^l\left[\frac{2l+1}{k}\sin\left(kr - l\frac{\pi}{2}\right) + f_l \mathrm{e}^{\mathrm{i}(kr - l\pi/2)}\right] \\ &= \mathrm{i}^l\left[\left(\frac{2l+1}{k} + \mathrm{i}f_l\right)\sin\left(kr - l\frac{\pi}{2}\right) + f_l\cos\left(kr - l\frac{\pi}{2}\right)\right]. \end{aligned} \tag{2.45}$$

Comparing Eqs. (2.45) and (2.42) shows that the coefficients of the sine and cosine terms in the square bracket in the lower line of (2.45) can be interpreted as the coefficients A and B in (2.42), for which $\tan\delta_l = B/A$. With the coefficients in (2.45),

$$\cot\delta_l = \frac{A}{B} \equiv \frac{2l+1}{kf_l} + \mathrm{i} \quad \Rightarrow \quad \cot\delta_l - \mathrm{i} = \frac{\mathrm{e}^{-\mathrm{i}\delta_l}}{\sin\delta_l} = \frac{2l+1}{kf_l}, \tag{2.46}$$

which leads to

$$f_l = \frac{2l+1}{k}\mathrm{e}^{\mathrm{i}\delta_l}\sin\delta_l = \frac{2l+1}{2\mathrm{i}k}\left(\mathrm{e}^{2\mathrm{i}\delta_l} - 1\right). \tag{2.47}$$

With (2.45) the asymptotic form of the radial wave functions is,

$$u_l(r) \overset{r\to\infty}{\sim} \frac{2l+1}{k}\mathrm{i}^l\mathrm{e}^{\mathrm{i}\delta_l}\sin\left(kr - l\frac{\pi}{2} + \delta_l\right), \tag{2.48}$$

and the asymptotic form of the full wave function (2.33) is

$$\psi(\mathbf{r}) \overset{r\to\infty}{\sim} \sum_{l=0}^{\infty}\frac{2l+1}{kr}\mathrm{i}^l\mathrm{e}^{\mathrm{i}\delta_l}\sin\left(kr - l\frac{\pi}{2} + \delta_l\right)P_l(\cos\theta). \tag{2.49}$$

The explicit expression, (2.44) with (2.47), for the scattering amplitude allows us to express the differential scattering cross section in terms of the scattering phase shifts δ_l,

$$\frac{\mathrm{d}\sigma}{\mathrm{d}\Omega} = \left|f(\theta)\right|^2 = \frac{1}{k^2}\sum_{l,l'}\mathrm{e}^{\mathrm{i}(\delta_l - \delta_{l'})}(2l+1)\sin\delta_l\left(2l'+1\right)\sin\delta_{l'}P_l(\cos\theta)P_{l'}(\cos\theta). \tag{2.50}$$

For the integrated scattering cross section we can exploit the orthogonality (2.30) of the Legendre polynomials,

$$\sigma = \sum_{l=0}^{\infty} \frac{4\pi}{2l+1} |f_l|^2 = \frac{4\pi}{k^2} \sum_{l=0}^{\infty} (2l+1) \sin^2 \delta_l = \frac{\pi}{k^2} \sum_{l=0}^{\infty} (2l+1) \left| e^{2i\delta_l} - 1 \right|^2. \quad (2.51)$$

The integrated scattering cross section is the incoherent sum of the contributions $\sigma_{[l]}$,

$$\sigma = \sum_{l=0}^{\infty} \sigma_{[l]}, \quad \sigma_{[l]} = \frac{4\pi}{k^2} (2l+1) \sin^2 \delta_l. \quad (2.52)$$

The maximum contribution of a given partial wave l to the integrated cross section is realized when δ_l is an odd multiple of $\frac{\pi}{2}$, so $\sin^2 \delta_l = 1$,

$$(\sigma_{[l]})_{\max} = \frac{4\pi}{k^2} (2l+1). \quad (2.53)$$

2.3.4 Normalization of Radial Wave Functions

A radial wave function $u_b(r)$ describing a negative-energy bound state in a given partial wave l is square-integrable and can be normalized to unity,

$$\langle u_b | u_b \rangle = \int_0^{\infty} u_b(r)^* u_b(r) dr = 1. \quad (2.54)$$

The regular solutions $u_l^{(k)}(r)$ of the radial Schrödinger equation at positive energies, $E = \hbar^2 k^2/(2\mu)$ $[k > 0]$, are orthogonal,

$$\left\langle u_l^{(k)} \middle| u_l^{(k')} \right\rangle = \int_0^{\infty} u_l^{(k)}(r)^* u_l^{(k')}(r) dr = 0 \quad \text{for } k \neq k', \quad (2.55)$$

but the integral diverges for $k = k'$, because the integrand is asymptotically proportional to $\sin^2(kr - \frac{\pi}{2} l + \delta_l)$. We can write

$$\left\langle u_l^{(k)} \middle| u_l^{(k')} \right\rangle \propto \delta(k - k'), \quad (2.56)$$

but this relation is not so useful as long as the proportionality constant is not known.

For pure sine waves of unit amplitude, $u_s^{(k)} = \sin(kr)$ $[k > 0]$, it is easy to see that

$$\left\langle u_s^{(k)} \middle| u_s^{(k')} \right\rangle = \int_0^{\infty} \sin(kr) \sin(k'r) dr = \frac{\pi}{2} \delta(k - k'). \quad (2.57)$$

The right-hand side of Eq. (2.57) remains unchanged, if we replace the wave functions $u_s^{(k)}$ by regular solutions of the radial Schrödinger equation which behave

asymptotically as $\sin(kr - \frac{\pi}{2}l + \delta_l)$. For $k \neq k'$ this follows according to (2.55). For $k = k'$ we can divide the integral from $r = 0$ to $r = \infty$ into a finite integral from $r = 0$ to some arbitrarily large but finite radius r_{large}, and an integral from r_{large} to $r = \infty$, which is the infinite part that determines the prefactor of the delta function. In the latter integral, the radial wave function is well described by the sine with unit amplitude, and the shift of argument, $-\frac{\pi}{2}l + \delta_l$, does not affect the result. We can thus define regular radial wave functions that are *normalized in wave number* as follows:

$$u_l^{(k)}(r) \overset{r\to\infty}{\sim} \sqrt{\frac{2}{\pi}} \sin\left(kr - l\frac{\pi}{2} + \delta_l\right) \quad \Longrightarrow \quad \left\langle u_l^{(k)} \middle| u_l^{(k')} \right\rangle = \delta\big(k - k'\big). \tag{2.58}$$

The identity

$$\delta\big(k - k'\big) = \frac{\mathrm{d}E}{\mathrm{d}k}\delta\big(E - E'\big) = \frac{\hbar^2 k}{\mu}\delta\big(E - E'\big) \tag{2.59}$$

leads to the appropriate definition of the regular radial wave functions $\bar{\mathrm{u}}_l^{(E)}$, which are *normalized in energy*,

$$\bar{\mathrm{u}}_l^{(E)}(r) \overset{r\to\infty}{\sim} \sqrt{\frac{2\mu}{\pi\hbar^2 k}} \sin\left(kr - l\frac{\pi}{2} + \delta_l\right) \quad \Longrightarrow \quad \left\langle \bar{\mathrm{u}}_l^{(E)} \middle| \bar{\mathrm{u}}_l^{(E')} \right\rangle = \delta\big(E - E'\big). \tag{2.60}$$

2.3.5 Radial Lippmann–Schwinger Equation

The radial Schrödinger equation (2.35) can be rewritten as

$$\left[E + \frac{\hbar^2}{2\mu}\frac{\mathrm{d}^2}{\mathrm{d}r^2} - \frac{l(l+1)\hbar^2}{2\mu r^2}\right] u_l(r) = V(r)u_l(r) \tag{2.61}$$

and transformed into an integral equation with the help of the *radial free-particle Green's function* $\mathscr{G}_l(r, r')$, which fulfills

$$\left[E + \frac{\hbar^2}{2\mu}\frac{\mathrm{d}^2}{\mathrm{d}r^2} - \frac{l(l+1)\hbar^2}{2\mu r^2}\right] \mathscr{G}_l\big(r, r'\big) = \delta\big(r - r'\big) \tag{2.62}$$

and is explicitly given by

$$\mathscr{G}_l\big(r, r'\big) = -\frac{2\mu}{\hbar^2 k} u_l^{(\mathrm{s})}(kr_<) u_l^{(\mathrm{c})}(kr_>); \tag{2.63}$$

here $u_l^{(\mathrm{s})}$ and $u_l^{(\mathrm{c})}$ stand for the regular and irregular free-particle radial waves as defined in (2.38), and $r_<$ stands for the smaller while $r_>$ stands for the larger of the

two radial coordinates r and r'. A wave function obeying the integral equation

$$u_l(r) = u_l^{(\mathrm{s})}(kr) + \int_0^\infty \mathscr{G}_l(r, r')\, V(r')\, u_l(r') \tag{2.64}$$

necessarily obeys the radial Schrödinger equation (2.61). This would also hold if the first term $u_l^{(\mathrm{s})}(kr)$ were replaced by any other solution of the "homogeneous" version $[E + \cdots]u_l(r) = 0$ of Eq. (2.61).[3]

Equation (2.64) is the *radial Lippmann–Schwinger equation* in the lth partial wave. Asymptotically, $r \to \infty$, we can assume $r = r_>$ and $r' = r_<$ in the radial Green's function, so the factor $u_l^{(\mathrm{c})}(kr_>) = u_l^{(\mathrm{c})}(kr)$ can be drawn out of the integral over r',

$$u_l(r) \overset{r\to\infty}{\sim} u_l^{(\mathrm{s})}(kr) - \left[\frac{2\mu}{\hbar^2 k}\int_0^\infty u_l^{(\mathrm{s})}(kr')\, V(r')\, u_l(r')\,\mathrm{d}r'\right] u_l^{(\mathrm{c})}(kr). \tag{2.65}$$

Comparing with Eq. (2.42) shows that the coefficient of $u_l^{(\mathrm{c})}(kr)$ in (2.65) is the tangent of the scattering phase shift,

$$\tan\delta_l = -\frac{2\mu}{\hbar^2 k}\int_0^\infty u_l^{(\mathrm{s})}(kr)\, V(r)\, u_l(r)\,\mathrm{d}r. \tag{2.66}$$

The expression on the right-hand side of (2.66) cannot be evaluated explicitly, because it still contains the (usually unknown) exact solution u_l of the radial Schrödinger equation. It does, however, offer a possibility for approximation in the spirit of the Born approximation. Replacing $u_l(r)$ in the integrand in (2.66) by the regular free-particle radial wave $u_l^{(\mathrm{s})}(kr)$ gives an explicit but approximate expression for $\tan\delta_l$, in the spirit of the first-order Born approximation:

$$\tan\delta_l^{\mathrm{Born}} = -\frac{2\mu}{\hbar^2 k}\int_0^\infty \left[u_l^{(\mathrm{s})}(kr)\right]^2 V(r)\,\mathrm{d}r. \tag{2.67}$$

Note that the right-hand side of (2.67) is a smooth function of k that always remains finite. Hence δ_l^{Born} as function of k can never cross an odd multiple of $\frac{\pi}{2}$. Equation (2.67) can only be a useful approximation when the phase shifts are restricted to a small interval around zero (or an integer multiple of π); for potentials which are bounded and short ranged, this happens both in the limit of high energies and in the limit of large angular momentum quantum numbers l, see Sect. 2.6.4.

[3] See footnote in Sect. 2.2.

2.3.6 S-Matrix

The asymptotic behaviour of the radial wave function (2.48) can be written as

$$u_l(r) \overset{r\to 0}{\sim} \frac{2l+1}{2k} \mathrm{i}^{l+1} \left[\mathrm{e}^{-\mathrm{i}(kr - l\pi/2)} - \mathrm{e}^{2\mathrm{i}\delta_l} \mathrm{e}^{+\mathrm{i}(kr - l\pi/2)} \right]$$
$$= \frac{2l+1}{2k} \mathrm{i}^{2l+1} \left[\mathrm{e}^{-\mathrm{i}kr} - (-1)^l \mathrm{e}^{2\mathrm{i}\delta_l} \mathrm{e}^{+\mathrm{i}kr} \right]. \tag{2.68}$$

In both lines of (2.68), the square bracket contains an incoming radial wave proportional to $\mathrm{e}^{-\mathrm{i}kr\cdots}$ and an outgoing radial wave proportional to $\mathrm{e}^{+\mathrm{i}kr\cdots}$. The factor $\mathrm{e}^{2\mathrm{i}\delta_l}$ in the outgoing wave is the contribution of the lth partial wave to the *scattering matrix* or S-matrix,

$$S_l = \mathrm{e}^{2\mathrm{i}\delta_l}. \tag{2.69}$$

For the radial potential $V(r)$, the S-matrix is diagonal, because there is no coupling between the radial Schrödinger equations (2.35) of different l.

The S-matrix is *unitary*, which, for the partial-wave contribution (2.69) means $|S_l| = 1$. This is an expression of particle conservation and is fulfilled as long as the scattering phase shifts δ_l are real. Equation (2.53) is based on the assumption, that the phase shifts are real, i.e., that the S-matrix is unitary. Its right-hand side $(4\pi/k^2)(2l+1)$ is hence called the *unitarity limit* of the contribution of the respective partial wave to the integrated scattering cross section.

For real δ_l, the scattering amplitude (2.44) with the partial-wave amplitudes (2.47) can be decomposed into real and imaginary parts as follows:

$$f(\theta) = \sum_{l=0}^{\infty} \frac{2l+1}{k} \left[\cos\delta_l \sin\delta_l + \mathrm{i}\sin^2\delta_l \right] P_l(\cos\theta). \tag{2.70}$$

For the forward direction, $\theta = 0$, we insert $P_l(1) = 1$ and recall Eq. (2.51),

$$\Im\left[f(\theta=0)\right] = \sum_{l=0}^{\infty} \frac{2l+1}{k} \sin^2\delta_l = \frac{k}{4\pi}\sigma, \tag{2.71}$$

thus recovering the optical theorem (2.14). The unitarity of the S-matrix is an expression of particle conservation. Note that the radial Born approximation (2.67) yields real phase shifts and a unitary S-matrix, so it is compatible with particle conservation. This is in contrast to the Born approximation (2.22) for the scattering amplitude. For a radially symmetric potential V, the Born scattering amplitude (2.22) is a real function of the modulus of the momentum transfer vector (2.23) and necessarily violates the optical theorem.

2.3.7 Determination of the Scattering Phase Shifts

The boundary condition $u_l(r) \overset{r\to 0}{\propto} r^{l+1}$ uniquely determines the radial wave function except for a constant factor. The scattering phase shifts δ_l can be calculated by integrating the radial Schrödinger equation (2.35) with this boundary condition from small r to a finite radius r_m, where the potential $V(r)$ has already fallen off sufficiently to be negligible. Matching the logarithmic derivative u_l'/u_l to the logarithmic derivative of a superposition (2.42) of the free-particle wave functions at $r = r_\mathrm{m}$ yields $\tan\delta_l$.

Due to the influence of the potential at short distances, the nodes (beyond $r = 0$) and antinodes of the radial wave function $u_l(r)$ are shifted relative to those of the regular free-particle wave function $u_l^{(\mathrm{s})}$. This leads to asymptotic *spatial shifts* d_l, which are related to the phase shifts δ_l by $d_l = \delta_l/k$, as can be seen by writing u_l as

$$u_l(r) \overset{r\to\infty}{\propto} \sin\left[k\left(r + \frac{\delta_l}{k}\right) - l\frac{\pi}{2}\right]. \tag{2.72}$$

For a repulsive potential V, the radial wave function is suppressed at small distances and its nodes (beyond $r = 0$) and antinodes are pushed to larger values of r by the potential; the spatial shifts, and hence also the phase shifts, are negative. The simplest example is scattering by a hard sphere of radius R. For $r > R$, the potential vanishes, and the radial wave function can be written as $Au_l^{(\mathrm{s})}(kr) + Bu_l^{(\mathrm{c})}(kr)$, see Eq. (2.42). The wave function must vanish for $r \le R$, so the inner boundary condition is pushed out from $r = 0$ to $r = R$. The condition $Au_l^{(\mathrm{s})}(kR) + Bu_l^{(\mathrm{c})}(kR) = 0$ yields

$$\frac{B}{A} = -\frac{u_l^{(\mathrm{s})}(kR)}{u_l^{(\mathrm{c})}(kR)} = \frac{j_l(kR)}{y_l(kR)}, \qquad \delta_l = \arctan\left(\frac{j_l(kR)}{y_l(kR)}\right). \tag{2.73}$$

From (2.40) and (2.39), the low- and high-energy behaviour of the hard-sphere phase shifts is

$$\begin{aligned} \delta_l &\overset{kR\to 0}{\sim} -\frac{\pi}{\Gamma(l+\frac{3}{2})\Gamma(l+\frac{1}{2})}\left(\frac{kR}{2}\right)^{2l+1}\left[1 - \left(\frac{kR}{2}\right)^2\left(\frac{1}{l-\frac{1}{2}} + \frac{1}{l+\frac{3}{2}}\right)\right], \\ \delta_l &\overset{kR\to\infty}{\sim} -kR + l\frac{\pi}{2} \end{aligned} \tag{2.74}$$

for $l > 0$, while $\delta_{l=0} = -kR$ for all k. Note that the high-energy behaviour in the lower line of (2.74) implies that the radial wave function (2.72) has the same asymptotic behaviour in all partial waves in the high-energy limit,

$$u_l(r) \overset{r\to\infty, kR\to\infty}{\propto} \sin(kr - kR). \tag{2.75}$$

This is because, for any angular momentum l, the radial classical turning point always reaches the radius R of the hard sphere at a sufficiently high energy, and the

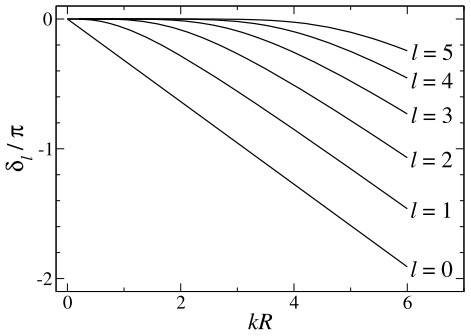

Fig. 2.3 Scattering phase shifts (2.73) for scattering by a hard sphere of radius R

influence of the centrifugal potential diminishes continuously as the energy rises further above this value. The phase shifts (2.73) for scattering by a hard sphere are shown in Fig. 2.3 for partial waves from $l = 0$ to $l = 5$.

For an attractive potential, the oscillations are of smaller wavelength in the interaction region and a given node (beyond $r = 0$) or antinode is pulled in to shorter distances by the potential; the spatial shift and the phase shift are positive. The behaviour of the phase shift depends on whether the effective potential features an attractive well that is deep enough to support one or more bound states, and the near-threshold behaviour of the phase shift depends sensitively on whether or not there is a bound state close to threshold.

2.3.8 *Near-Threshold Behaviour of the Scattering Phase Shifts*

The leading near-threshold behaviour of the phase shifts can be derived from the small-argument behaviour of the free-particle solutions. At distances r beyond the range of the potential, the radial wave function $u_l(r)$ is a superposition of the free-particle wave functions (2.38); towards threshold, $k \to 0$, the product kr tends to zero so we can make use of the small-argument expressions (2.40),

$$\begin{aligned} u_l(r) &\overset{kr\to 0}{\propto} u_l^{(\mathrm{s})}(kr) + \tan\delta_l u_l^{(\mathrm{c})}(kr) \\ &\sim \frac{\sqrt{\pi}k^{l+1}}{2^{l+1}\Gamma(l+\frac{3}{2})}\left[r^{l+1} + \tan\delta_l \frac{2^{2l+1}\Gamma(l+\frac{1}{2})\Gamma(l+\frac{3}{2})}{\pi k^{2l+1} r^l}\right]. \end{aligned} \tag{2.76}$$

Directly at threshold, the radial Schrödinger equation (2.35) has a regular solution $u_l^{(0)}(r)$ which is defined up to a constant by the boundary condition $u_l^{(0)}(0) = 0$ and is function of r only. The wave function (2.76) must become proportional to this

k-independent solution for $k \to 0$, so in the second term in the square bracket in the lower line of Eq. (2.76), the k-dependence of $\tan\delta_l$ must compensate the factor k^{2l+1} in the denominator, $\tan\delta \overset{k\to 0}{\propto} k^{2l+1}$. More explicitly,

$$\tan\delta_l \overset{k\to 0}{\sim} -\frac{\pi}{\Gamma(l+\frac{1}{2})\Gamma(l+\frac{3}{2})}\left(\frac{a_l k}{2}\right)^{2l+1}. \tag{2.77}$$

The characteristic length a_l appearing on the right-hand side of (2.77) is the *scattering length* in the lth partial wave.

The proportionality to k^{2l+1} in (2.77) expresses growing suppression with increasing l due to the influence of the centrifugal barrier separating the asymptotic region of free-particle motion from the interaction region at small distances. It is typical for the l-dependence of quantum mechanical quantities involving a centrifugal barrier and is generally referred to as *Wigner's threshold law*.

Equation (2.77) implies that the leading behaviour of the partial-wave scattering amplitude (2.47) is

$$f_l \overset{k\to 0}{\propto} k^{2l}, \tag{2.78}$$

which means that small l-values dominate the scattering amplitude (2.44) and the scattering cross sections (2.50), (2.51) at low energies. For s-waves, Eq. (2.77) reads

$$\tan\delta_0 \overset{k\to 0}{\sim} -ak, \tag{2.79}$$

where we have dropped the subscript on the a, as is customary. The s-wave scattering length a in (2.79) is generally referred to as *the* scattering length, a concept introduced by Fermi and Marshall in 1947 [15]. From (2.78) it follows that only the s-wave retains a nonvanishing contribution to the scattering amplitude (2.44) in the limit $k \to 0$,

$$\lim_{k\to 0} f(\theta) = f_0 P_0 \sim -a \quad \Longrightarrow \quad \lim_{k\to 0}\frac{\mathrm{d}\sigma}{\mathrm{d}\Omega} = a^2 \quad \text{and} \quad \lim_{k\to 0}\sigma = 4\pi a^2. \tag{2.80}$$

For hard-sphere scattering, the scattering length is the radius of the sphere, and the threshold limit of the quantum mechanical integrated scattering cross section is $4\pi R^2$, which is four times the classical cross section, see Eq. (1.39) in Sect. 1.3.

The definition (2.79) of the scattering length for s-waves is universally accepted. For $l > 0$, the definitions of the scattering length vary. Some authors, e.g. [44], even call the whole coefficient of k^{2l+1} in (2.77) scattering length, although this coefficient has the physical dimension of a length to the power $2l+1$. The definition (2.77) ensures that a_l is a length and that for scattering by a hard sphere of radius R we have $a_l = R$ for all l, as can be seen by comparing with (2.74).

With (2.77), the threshold solution of the radial Schrödinger equation (2.35) behaves asymptotically as,

$$u_l^{(0)}(r) \overset{r\to\infty}{\propto} r^{l+1} - \frac{a_l^{2l+1}}{r^l}, \tag{2.81}$$

so the scattering length appears as the zero of the asymptotic behaviour of the threshold solution of the radial Schrödinger equation. The leading term in (2.81) is proportional to r^{l+1} and comes naturally by integrating outwards under the centrifugal potential. The proportionality of the next-to-leading term to r^{-l} is not so universal and is subject to conditions on the asymptotic fall-off of the potential $V(r)$. For a potential falling off asymptotically as an inverse power of r, $V(r) \overset{r\to\infty}{\propto} 1/r^{\alpha}$, $\alpha > 2$, the next-to-leading term is proportional to r^{-l} *only* if

$$\alpha > 2l + 3, \tag{2.82}$$

as is shown later in Sect. 2.6. The definition (2.77) of the partial-wave scattering length and the behaviour (2.81) of the threshold wave function apply only for potentials which fall off faster than $1/r^{2l+3}$ at large distances. The s-wave scattering length is well defined for potentials falling off faster than $1/r^3$, the p-wave ($l = 1$) scattering length for potentials falling off faster than $1/r^5$.

When the scattering length vanishes, the threshold solution (2.81) is asymptotically proportional to r^{l+1}, just as the regular solution of the radial Schrödinger equation for the centrifugal potential alone. An infinite scattering length, $|a_l| \to \infty$, implies that the threshold solution of the radial Schrödinger equation (2.35) decays as $1/r^l$ for large distances. For $l > 0$ this means that there is a normalizable wave function solving the radial Schrödinger equation at $E = 0$, i.e., a bound state exactly at threshold.

For s-waves, Eq. (2.81) reads

$$u_{l=0}^{(0)} \overset{r\to\infty}{\propto} r - a \propto 1 - \frac{r}{a}. \tag{2.83}$$

An infinite s-wave scattering length means that the threshold solution becomes constant at large distances. One speaks of a bound state at threshold in this case as well, even though the wave function is not normalizable.

The scattering length depends very sensitively on whether there is a bound state very close to threshold, or whether the potential just fails to bind a further bound state. This is easily demonstrated via the simple but instructive example of an attractive sharp-step potential,

$$V(r) = \begin{cases} -V_S & \text{for } r \le L, \\ 0 & \text{for } r > L, \end{cases} \qquad V_S = \frac{\hbar^2 K_S^2}{2\mu}. \tag{2.84}$$

When $K_S L = \frac{\pi}{2}$, which corresponds to a depth V_S equal to the energy $E_0 = (\frac{\pi}{2}\hbar)^2/(2\mu L^2)$, the potential (2.84) has a threshold solution which becomes constant for $r > L$. For a slightly deeper step, $V_S = 1.4E_0$, the potential supports a weakly bound state at the energy $E_b \approx -0.189E_0$, indicated by the horizontal dotted brown line in the left half of Fig. 2.4; the associated bound-state wave function is shown as dashed brown line. As is customary in such illustrations, the zero-axis for a wave function is chosen to lie at the energy for which it solves the Schrödinger equation. The threshold solution at $E = 0$ (solid blue line) is not very different

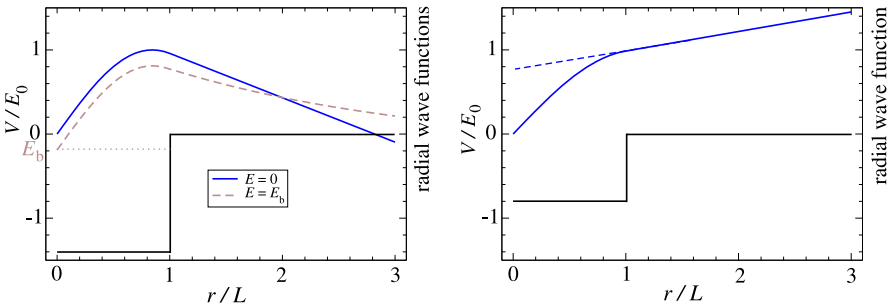

Fig. 2.4 Sharp-step potential (2.84). The energy is given in units of $E_0 = (\frac{\pi}{2}\hbar)^2/(2\mu L^2)$. For $V_S = E_0$, the s-wave radial Schrödinger equation has a zero-energy solution which becomes constant for $r \geq L$. The left half of the figure shows the case $V_S = 1.4E_0$, for which the potential supports a bound state at the energy $E_b \approx -0.189E_0$, indicated by the *horizontal dotted brown line*. The bound-state wave function is shown as *dashed brown line*, and its zero-axis lies at its energy E_b. The threshold solution is shown as *solid blue line* with zero-axis at $E = 0$; for $r > L$ it is a linear function which cuts the axis at a distance defining the scattering length a. The right half of the figure shows the case $V_S = 0.8E_0$, for which there is no bound state; the threshold solution (*solid blue line*) is a straight line for $r > L$, and the extrapolation of this line to smaller r-values leads to an intersection with the r-axis at a large negative value, corresponding to a large negative scattering length a

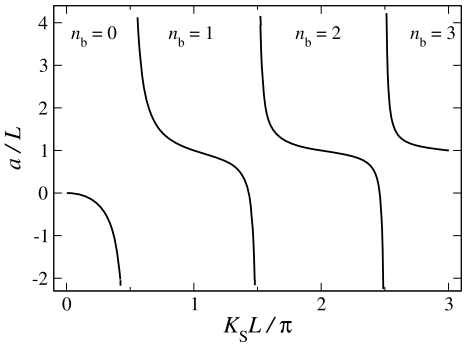

Fig. 2.5 Scattering length for the sharp-step potential as function of the threshold wave number K_S, as given by Eq. (2.85). Each pole indicates the existence of a bound state at threshold; n_b is the number of bound states supported by the potential for values of K_S between successive poles

from the bound-state wave function for $r \leq L$. For $r > L$ the potential vanishes, so the threshold solution assumes its asymptotic behaviour (2.83) corresponding to a linear fall-off; it cuts the r-axis at a value defining the scattering length a ($\approx 2.8L$ in the present case). The right half of Fig. 2.4 shows a shallower step, $V_S = 0.8E_0$, for which the potential just fails to support a bound state. The threshold solution (solid blue line) now *grows* linearly for $r > L$. Extrapolation of this linear behaviour to smaller r-values eventually leads to a crossing of the r-axis at a large negative value, corresponding to a large negative scattering length. The dependence of the scattering length on the potential depth V_S, or on the related threshold wave number $K_S = \sqrt{2\mu V_S}/\hbar$, can be easily deduced from the threshold solution $u^{(0)}_{l=0}(r) \overset{r \leq L}{\propto} \sin(K_S r)$. Its logarithmic derivative at $r = L$ is $K_S \cot(K_S L)$ which

must be equal to $1/(L-a)$ according to (2.83), so [24]

$$a = L - \frac{\tan(K_S L)}{K_S}. \tag{2.85}$$

Figure 2.5 shows the behaviour of the scattering length as function of the threshold wave number K_S. It is typical for the behaviour of the scattering length of a potential as function of a parameter which can tune the number and positions of bound states in the potential. The scattering length has a pole whenever there is a bound state at threshold. Before the first pole ($K_S L < 0.5\pi$ in Fig. 2.5), the potential has no bound states. The number of bound states increases by one every time K_S increases through a pole.

A quantitative relation between the diverging scattering length and the vanishing eigenenergy of a near-threshold bound state can be derived quite generally as follows: Assume that there is a bound s-state at an energy $E_b = -\hbar^2\kappa_b^2/(2\mu)$ very close to threshold. Beyond the range of the potential, the radial wave function $u_{l=0}^{(\kappa_b)}$ at this energy is proportional to $e^{-\kappa_b r}$ and behaves as

$$u_{l=0}^{(\kappa_b)}(r) \propto 1 - r\left[\kappa_b + O\left(\kappa_b^2\right)\right] \quad (\kappa_b < 0). \tag{2.86}$$

The terms below order κ_b^2 in (2.86) are compatible with (2.83) if we assume

$$\frac{1}{a} \overset{\kappa_b \to 0}{\sim} \kappa_b + O\left(\kappa_b^2\right). \tag{2.87}$$

This is plausible, since the radial Schrödinger equation at energy E_b differs from the radial Schrödinger equation at threshold by a term of order κ_b^2. Equation (2.87) implies the following relation between the scattering length a and the inverse penetration depth κ_b of a bound state very near threshold,

$$a \overset{\kappa_b \to 0}{\sim} \frac{1}{\kappa_b} + O\left(\kappa_b^0\right). \tag{2.88}$$

Conversely, a large positive scattering length a implies a near-threshold bound state, whose energy is given by,

$$E_b = -\frac{\hbar^2\kappa_b^2}{2\mu} \overset{a \to \infty}{\sim} -\frac{\hbar^2}{2\mu a^2} + O\left(\frac{1}{a^3}\right). \tag{2.89}$$

When the potential just fails to bind a further bound state, there may be a solution $u_{l=0}^{v}$ of the s-wave radial Schrödinger equation which is asymptotically proportional to $e^{+\kappa_v r}$ with a very small positive κ_v. By the same arguments as above, such a solution of (2.35) gives rise to a large negative scattering length, $a \overset{\kappa_v \to 0}{\sim} -1/\kappa_v + O(\kappa_v^0)$. In such a situation one speaks of a *virtual state* at the energy $E_v = -\hbar^2\kappa_v^2/(2\mu)$ [33, 44].

The unambiguous identification of a virtual state poses a problem. The discrete energy of a genuine bound state is easily found via the condition that the wave

function must decay to zero as $e^{-\kappa r}$ at large distances. When solving the radial Schrödinger equation, e.g. by integrating it from smaller to larger r-values, any contribution from the exponentially growing solution soon becomes dominant and indicates that the energy under consideration is not a bound-state eigenvalue. On the other hand, the solution proportional to $e^{+\kappa r}$ cannot be unambiguously defined, unless the potential vanishes exactly after some finite, preferably short, distance. Any contribution of the solution proportional to $e^{-\kappa r}$ is soon dominated by the exponentially growing term, so it is very difficult in practice to decide, whether the contribution of the decaying solution vanishes exactly or not. This problem is aggravated as κ increases, so the concept of virtual states is most useful very close to threshold.

For a potential which falls off sufficiently rapidly at large distances, the next-to-leading behaviour of the scattering phase shifts near threshold, following the leading term (2.77), can be derived from solutions of the radial Schrödinger equation at threshold [3]. This is shown below for s-waves, $l = 0$. We shall drop the subscript $l = 0$, but remember that we are dealing with s-waves.

Let $u^{(0)}$ and $u^{(k)}$ be regular radial wave functions that solve the radial Schrödinger equation at threshold and for wave number $k > 0$,

$$\frac{\mathrm{d}^2 u^{(0)}}{\mathrm{d}r^2} = \frac{2\mu}{\hbar^2} V(r) u^{(0)}(r), \qquad \frac{\mathrm{d}^2 u^{(k)}}{\mathrm{d}r^2} = \left(\frac{2\mu}{\hbar^2} V(r) - k^2 \right) u^{(k)}(r). \tag{2.90}$$

There are two alternative representations for the integral

$$I_u(r_0) = \int_0^{r_0} \left[u^{(0)}(r) \frac{\mathrm{d}^2 u^{(k)}}{\mathrm{d}r^2} - u^{(k)}(r) \frac{\mathrm{d}^2 u^{(0)}}{\mathrm{d}r^2} \right] \mathrm{d}r. \tag{2.91}$$

One involves multiplying the first of the two equations (2.90) by $u^{(k)}$, the second by $u^{(0)}$, and integrating the difference; this leads to

$$I_u(r_0) = -k^2 \int_0^{r_0} u^{(0)}(r) u^{(k)}(r) \mathrm{d}r. \tag{2.92}$$

An alternative representation of the integral (2.91) is obtained by partial integration,

$$I_u(r_0) = \left[u^{(0)}(r) \frac{\mathrm{d}u^{(k)}}{\mathrm{d}r} - u^{(k)}(r) \frac{\mathrm{d}u^{(0)}}{\mathrm{d}r} \right]_0^{r_0} = u^{(0)}(r_0) \left. \frac{\mathrm{d}u^{(k)}}{\mathrm{d}r} \right|_{r_0} - u^{(k)}(r_0) \left. \frac{\mathrm{d}u^{(0)}}{\mathrm{d}r} \right|_{r_0}. \tag{2.93}$$

Contributions from the lower limit of integration, $r = 0$, vanish, because the regular solutions $u(r)$ vanish for $r \to 0$.

We now repeat the procedure for two (not necessarily regular) radial wave functions, $w^{(0)}$ and $w^{(k)}$, which solve the *free-particle* radial Schrödinger equation at threshold and for wave number $k > 0$,

$$\frac{\mathrm{d}^2 w^{(0)}}{\mathrm{d}r^2} = 0, \qquad \frac{\mathrm{d}^2 w^{(k)}}{\mathrm{d}r^2} = -k^2 w^{(k)}(r). \tag{2.94}$$

The integral

$$I_w(r_0) = \int_0^{r_0} \left[w^{(0)}(r) \frac{\mathrm{d}^2 w^{(k)}}{\mathrm{d}r^2} - w^{(k)}(r) \frac{\mathrm{d}^2 w^{(0)}}{\mathrm{d}r^2} \right] \mathrm{d}r \tag{2.95}$$

can, in analogy to (2.92) and (2.93), be written as

$$I_w(r_0) = -k^2 \int_0^{r_0} w^{(0)}(r) w^{(k)}(r) \mathrm{d}r, \quad \text{or as} \tag{2.96}$$

$$I_w(r_0) = w^{(0)}(r_0) \frac{\mathrm{d}w^{(k)}}{\mathrm{d}r}\bigg|_{r_0} - w^{(k)}(r_0) \frac{\mathrm{d}w^{(0)}}{\mathrm{d}r}\bigg|_{r_0} - w^{(0)}(0) \frac{\mathrm{d}w^{(k)}}{\mathrm{d}r}\bigg|_0 + w^{(k)}(0) \frac{\mathrm{d}w^{(0)}}{\mathrm{d}r}\bigg|_0 . \tag{2.97}$$

Equation (2.97) includes the contributions from the lower integration limit, $r = 0$, because the free-particle solutions $w(r)$ are *not* assumed to vanish at $r = 0$. Instead, they shall be assumed to be asymptotically equal to the regular solutions $u(r)$, which behave as (2.83) and (2.42). Explicitly and with appropriate normalization:

$$\begin{aligned} w^{(0)}(r) &= 1 - \frac{r}{a}, & w^{(k)}(r) &= -\frac{1}{ka} \sin(kr + \delta); \\ u^{(0)}(r) &\overset{r\to\infty}{\sim} 1 - \frac{r}{a}, & u^{(k)}(r) &\overset{r\to\infty}{\sim} -\frac{1}{ka} \sin(kr + \delta). \end{aligned} \tag{2.98}$$

According to (2.92) and (2.96), the difference of the integrals (2.91) and (2.95) is,

$$I_u(r_0) - I_w(r_0) = k^2 \int_0^{r_0} \left[w^{(0)}(r) w^{(k)}(r) - u^{(0)}(r) u^{(k)}(r) \right] \mathrm{d}r. \tag{2.99}$$

The integral converges in the limit $r_0 \to \infty$, provided that the regular solutions $u(r)$ approach their asymptotic forms $w(r)$ sufficiently fast,

$$I_u(r_0) - I_w(r_0) \overset{r_0\to\infty}{\sim} k^2 I(k), \quad I(k) = \int_0^{\infty} \left[w^{(0)}(r) w^{(k)}(r) - u^{(0)}(r) u^{(k)}(r) \right] \mathrm{d}r. \tag{2.100}$$

Note that $I(k)$ has the physical dimension of a length. When expressing the difference $I_u(r_0) - I_w(r_0)$ via Eqs. (2.93) and (2.97), the contributions from the upper integration limit r_0 vanish, so

$$I_u(r_0) - I_w(r_0) \overset{r_0\to\infty}{\sim} w^{(0)}(0) \frac{\mathrm{d}w^{(k)}}{\mathrm{d}r}\bigg|_0 - w^{(k)}(0) \frac{\mathrm{d}w^{(0)}}{\mathrm{d}r}\bigg|_0 = -\frac{\cos\delta}{a} - \frac{\sin\delta}{ka^2}. \tag{2.101}$$

Equating the right-hand side of (2.101) with $k^2 I(k)$ yields

$$ka \cot\delta = -\left[1 + k^2 a I(k) / \cos\delta \right]^{-1}. \tag{2.102}$$

In the limit of small wave numbers, $\cos\delta$ tends to unity and $I(k)$ assumes a certain value which is usually expressed in terms of the *effective range*, $r_{\text{eff}} = 2\lim_{k\to 0} I(k)$, so the leading near-threshold behaviour of Eq. (2.102) is,

$$k\cot\delta \overset{k\to 0}{\sim} -\frac{1}{a} + \frac{1}{2}r_{\text{eff}}k^2 + O\big(k^4\big), \qquad r_{\text{eff}} = 2\int_0^\infty \Big(\big[w^{(0)}(r)\big]^2 - \big[u^{(0)}(r)\big]^2\Big)\mathrm{d}r. \tag{2.103}$$

Translating this into an expansion for the scattering phase shift itself gives,

$$\delta \overset{k\to 0}{\sim} -ka + \frac{k^3}{3}\left[a^3 - \frac{3}{2}r_{\text{eff}}\,a^2\right] + O\big(k^5\big) \pmod{\pi}. \tag{2.104}$$

Equation (2.103) features the two leading terms of the *effective-range expansion*. For potentials which fall off faster than any inverse power of r at large distances, $k\cot\delta$ is known to be an analytical function of energy, i.e. of k^2. The same applies for nonvanishing angular momenta to the function $k^{2l+1}\cot\delta_l$ [12]. Note, however, that most realistic potentials do not fall off so quickly, but rather as an inverse power of r, $V(r) \overset{r\to\infty}{\propto} 1/r^\alpha$, see Sect. 2.6. In such cases, $k\cot\delta$ is not an analytical function of k^2, and the second term in (2.103) can only be defined in general when $\alpha > 5$.

The scattering length a has an immediate physical significance, because it determines the near-threshold limits of the differential and the integrated scattering cross sections according to Eq. (2.80). Only when the potential is repulsive or so weakly attractive that it is not near to supporting a bound state, can the scattering length and the effective range r_{eff} be related to a distance up to which the potential has nonnegligible values. For scattering by a hard sphere of radius R, we have $a = R$ and $r_{\text{eff}} = \frac{2}{3}R$, so the k^3-term in (2.104) vanishes, as do all higher terms.

As soon as the potential is attractive enough to support one or more bound states, the proximity of a bound (or virtual) state to threshold dominantly influences the scattering length as illustrated for the attractive sharp-step potential in Fig. 2.5. The behaviour of the effective range is strongly correlated to the behaviour of the scattering length. When $a = 0$, for example, which happens for the sharp-step potential (2.84), (2.85) whenever $K_S L$ is an integer multiple of π, there is no bound or virtual state near threshold, the effective range diverges, but the product $a^2 r_{\text{eff}}$ in (2.104) remains finite.

2.3.9 Levinson's Theorem

If the effective potential (2.36) features a sufficiently deep attractive well, then the radial wave function shows oscillations in the region of this well. As the energy approaches the threshold from above, these inner oscillations can persist all the way down to $E = 0$. Matching the radial wave function u_l to a superposition of free-particle waves at a matching radius r_{m} beyond the range of the potential only determines the phase shift δ_l to within an integer multiple of π. By comparing $u_l(r)$ to

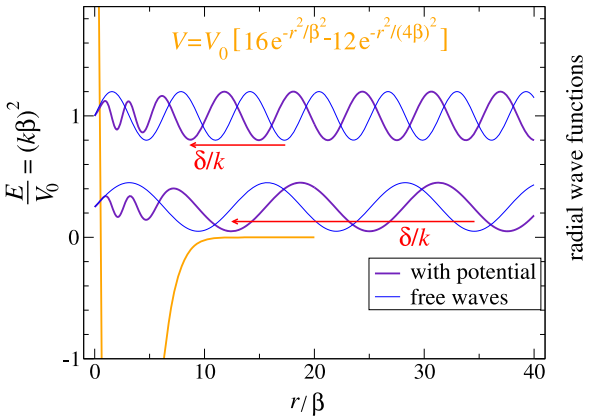

Fig. 2.6 Solutions of the radial Schrödinger equation (2.35) for $l = 0$. The *thick violet lines* show the wave functions in the potential (2.105) (*orange line*) for $E = V_0$ and $E = 0.25V_0$; the *thin blue lines* are the free waves $\propto \sin(kr)$. The zero-axes for the wave functions lie at the respective energies. The *red arrows* show the spatial shift from the third minimum of the free wave to the third minimum of the wave function in the potential

the regular free-particle wave $u_l^{(s)}(kr)$ in the whole range of r-values from $r = 0$ to $r = r_m$ we can also keep track of an additional integer multiple of π corresponding to spatial shifts by as many half-waves.

This is illustrated in Fig. 2.6 which shows radial wave functions for s-waves in the model potential

$$V(r) = V_0\big[16\mathrm{e}^{-r^2/\beta^2} - 12\mathrm{e}^{-r^2/(4\beta)^2}\big], \quad V_0 = \frac{\hbar^2}{2\mu\beta^2}. \tag{2.105}$$

This potential consists of a repulsive Gaussian of height $16V_0$ and range β and an attractive Gaussian tail of depth $12V_0$ and range 4β. It is qualitatively similar to the Lennard–Jones potential (1.32) studied in Sect. 1.2.3, but there are two important differences: it falls off faster than any inverse power of r at large distances, and it remains bounded at small distances. The radial wave functions $u_{l=0}(r)$ (with conveniently chosen amplitudes) are shown in Fig. 2.6 as thick violet lines for the two energies $E = 0.25V_0$ and $E = V_0$, together with the respective free-particle wave functions $\propto \sin(kr)$ (thin blue lines). [The zero-axis for a wave function is again chosen to lie at the energy for which it solves the Schrödinger equation.] The red arrows show the spatial shift from the third minimum of the free-particle wave function to the third minimum of the radial wave function obtained with the potential. This spatial shift contains a contribution $\tilde{d}$ not larger than the range of the potential, plus an integer number n_{hw} of half waves, $d = \tilde{d} + n_{hw}\lambda/2$. The wavelength $\lambda = 2\pi/k$ (beyond the range of the potential) diverges towards threshold, so the spatial shift $d = \tilde{d} + n_{hw}\pi/k$ is dominated by the term containing n_{hw}. For the phase

shift, this implies

$$\lim_{k\to 0} \delta_l(k) = n_{\mathrm{hw}}\pi, \tag{2.106}$$

where n_{hw} is the number of additional nodes in the radial wave function, compared to the free-particle wave. Equation (2.106) is also valid for angular momenta $l > 0$. The number n_{hw} of additional nodes is well defined towards threshold, because those nodes of u_l (beyond $r = 0$) which are not additional nodes due to attractive behaviour of the potential V at short distances wander to infinity in the limit $k \to 0$, as do the nodes (beyond $r = 0$) of the free-particle wave $u_l^{(\mathrm{s})}$.

Since the potential $V(r)$ falls off faster than $1/r^2$ at large distances and is less singular than $1/r^2$ at small distances, it supports at most a finite number of bound states [16]. The number n_{b} of bound states supported by the effective potential V_{eff} in the lth partial wave is equal to the number n_{hw} of additional nodes in the radial wave function near threshold. To see this, recall that the ground-state wave function in a potential well has no nodes, and that the number of nodes increases by one for each successive excited state. A wave function solving the radial Schrödinger equation at a positive energy very near threshold has one more node in the interaction region than the highest bound state; this is a necessary condition for its orthogonality to all the bound eigenfunctions in the potential well.

If $V(r)$ is bounded, its influence becomes negligible at high energies,

$$\lim_{k\to\infty} \delta_l(k) = 0. \tag{2.107}$$

In the high-energy limit, the nodes of u_l and of the free-particle wave $u_l^{(\mathrm{s})}$ coalesce and u_l has no additional nodes. This holds also for potentials which are not necessarily bounded, but less singular than $1/r^2$ for $r \to 0$. If we consider δ_l as a continuous function of wave number (or energy), then combining Eqs. (2.107) and (2.106), with $n_{\mathrm{hw}} = n_{\mathrm{b}}$, yields

$$\lim_{k\to 0} \delta_l(k) - \lim_{k\to\infty} \delta_l(k) = n_{\mathrm{b}}\pi, \tag{2.108}$$

where n_{b} is the number of bound states in the lth partial wave. Equation (2.108) was first derived by Levinson in 1949 [28] and is known as *Levinson's theorem*.

There is one exception to the rule (2.106), and hence also to (2.108), namely when there is an s-wave bound state exactly at threshold, with $|a| = \infty$ according to (2.83). The threshold wave function is asymptotically proportional to $\cos(kr)$ in the limit $k \to 0$, which corresponds to a phase shift of $\pi/2$ relative to the free-particle wave $\sin(kr)$, so $\delta_{l=0}(k)$ converges to an odd multiple of $\pi/2$ for $k \to 0$.

The model potential (2.105) falls off faster than any inverse power of r at large distances, so the leading near-threshold behaviour of the phase shifts is given by (2.77) for all l. Furthermore, the potential is bounded so the phase shifts obey Levinson's theorem (2.108). Figure 2.7 shows the corresponding phase shifts as functions of the scaled wave number $k\beta$ for angular momentum quantum numbers up to $l = 15$.

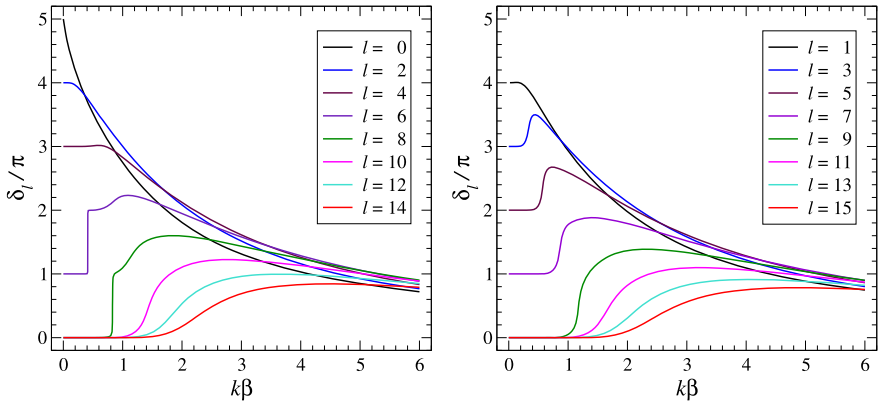

Fig. 2.7 Phase shifts for scattering by the model potential (2.105) as functions of the scaled wave number $k\beta$ for angular momentum quantum numbers up to $l = 15$. Even and odd l are shown in separate panels to avoid overcrowding in the figure

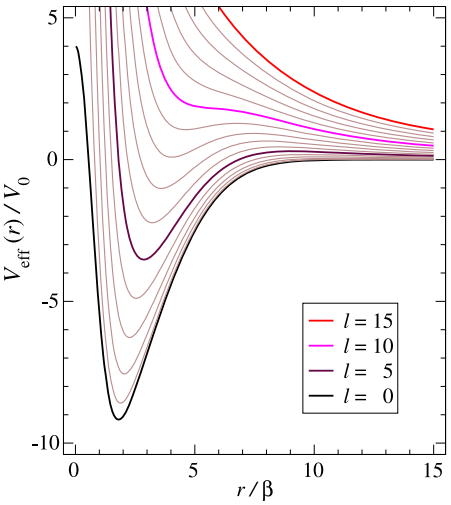

Fig. 2.8 Effective potentials (2.36) for the model potential (2.105) and angular momenta up to $l = 15$

Some features in Fig. 2.7 can be understood by looking at the effective potentials (2.36), which are shown in Fig. 2.8. The number n_b of bound states, corresponding to the threshold value $n_\mathrm{b}\pi$ of δ_l, decreases from five for $l = 0$ to zero for $l = 8$, where the minimum of the effective potential already lies above the threshold $E = 0$. There are no bound states above threshold, but *almost bound states* can form at certain energies below the maximum of the potential barrier formed by the centrifugal potential V_cent and the attractive potential V. Such almost bound states above the threshold of a potential are called *potential resonances* or *shape resonances*, and they lead to more or less sudden jumps of the phase shift by π, as seen for many of the partial waves in Fig. 2.7. Potential or shape resonances are the subject of the following Sect. 2.3.10.

2.3.10 Potential Resonances (Shape Resonances)

A resonance is a state of a system which is almost bound and decays with certain lifetime. *Potential resonances*, also called *shape resonances*, appear in a potential landscape as states, whose energy is high enough to decay into a continuum, but whose rapid decay is inhibited by the shape of the potential, e.g., by a barrier whose maximum lies above the energy of the resonant state. In contrast, *Feshbach resonances*, which are discussed in Sect. 3.5, are bound states in a given degree of freedom (or set of degrees of freedom) which can decay via coupling into one or more independent degrees of freedom supporting appropriate continuum states. Since resonant states are associated with a lifetime, it is helpful to discuss the time evolution of the scattering event.

2.3.10.1 Time Evolution of a Scattering Event

Consider a single partial wave whose stationary solutions of the time-independent radial Schrödinger equation (2.35) behave asymptotically as,

$$u_l(r) \overset{r\to\infty}{\sim} \mathrm{e}^{-\mathrm{i}(kr-l\pi/2)} - \mathrm{e}^{2\mathrm{i}\delta_l}\mathrm{e}^{+\mathrm{i}(kr-l\pi/2)}, \tag{2.109}$$

as in (2.68), except for normalization. The time-independent equation (2.35) becomes the time-dependent radial Schrödinger equation if the right-hand side Eu_l is replaced by $\mathrm{i}\hbar\partial u_l/\partial t$, and the radial wave functions $u_l(r)$ become solutions of this time-dependent equation through multiplication by $\mathrm{e}^{-\mathrm{i}\omega t}$,

$$u^{(k)}(r,t) = u(r)\mathrm{e}^{-\mathrm{i}\omega t}, \qquad \omega(k) = \frac{\hbar k^2}{2\mu}. \tag{2.110}$$

Since this subsection deals exclusively with a single partial wave l, the subscript l is dropped in Eq. (2.110), but a superscript (k) is included to record the wave number k, resp. energy $E = \hbar^2k^2/(2\mu)$, for which the wave function is an eigenstate of the radial Hamiltonian. The dependence of the circular frequency ω on the wave number k is the usual *dispersion relation* for matter waves.

The general solution of the time-dependent radial Schrödinger equation is a superposition of the wave functions (2.110) with an amplitude function $\phi(k)$,

$$u(r,t) = \int_0^\infty u^{(k)}(r,t)\phi(k)\mathrm{d}k. \tag{2.111}$$

We can construct almost monochromatic wave packets by assuming that the amplitude function $\phi(k)$ is strongly peaked around a mean wave number $\bar{k} > 0$ and vanishes rapidly away from $\bar{k}$. Then the lower integration limit in (2.111) can be changed to $-\infty$ and, in the small range of k-values filtered out by $\phi(k)$, we can

approximate $\omega(k)$ by its first-order Taylor expansion,

$$\omega(k) \approx \bar{\omega} + \bar{v}(k - \bar{k}), \quad \bar{\omega} = \omega(\bar{k}),\ \bar{v} = \left.\frac{\mathrm{d}\omega}{\mathrm{d}k}\right|_{\bar{k}} = \frac{\hbar\bar{k}}{\mu}. \tag{2.112}$$

At large distances r, the contribution u^{in} of the first term on the right-hand side of (2.109) to the superposition (2.111) is thus

$$\begin{aligned} u^{\mathrm{in}}(r,t) &= \int_{-\infty}^{\infty} \mathrm{e}^{-\mathrm{i}(kr+\omega t-l\pi/2)}\phi(k)\mathrm{d}k \\ &\approx \mathrm{e}^{-\mathrm{i}\bar{k}r-\mathrm{i}\bar{\omega}t}\,\mathrm{i}^l \int_{-\infty}^{\infty} \mathrm{e}^{-\mathrm{i}(k-\bar{k})(r+\bar{v}t)}\tilde{\phi}(k-\bar{k})\mathrm{d}(k-\bar{k}), \end{aligned} \tag{2.113}$$

where we have changed the integration variable from k to $k - \bar{k}$ and replaced $\phi(k)$ by the function $\tilde{\phi}(k - \bar{k})$, which is peaked around argument zero. The integral in (2.113) is essentially the Fourier transform of $\tilde{\phi}$ and is a function of the conjugate variable $r + \bar{v}t$,

$$u^{\mathrm{in}}(r,t) = \mathrm{e}^{-\mathrm{i}\bar{k}r-\mathrm{i}\bar{\omega}t}\Psi(r+\bar{v}t). \tag{2.114}$$

Since $\tilde{\phi}$ is narrowly peaked in wave number, Ψ represents a wave packet broadly spread in coordinate space; a possible choice is

$$\tilde{\phi}(q) \propto \mathrm{e}^{-B^2q^2/2} \quad \Longrightarrow \quad \Psi(x) \propto \mathrm{e}^{-x^2/(2B^2)}. \tag{2.115}$$

For large negative times t, the wave function (2.114) represents an almost monochromatic radial wave packet, which is broadly localized around $r = -\bar{v}t$ and travels towards the origin with group velocity $-\bar{v} = -\hbar\bar{k}/\mu$.

The contribution u^{out} of the second term on the right-hand side of (2.109) to the superposition (2.111) contains the S-matrix as factor in the integrand. In the small range of k-values filtered out by the amplitude function $\phi(k)$, the scattering phase shift $\delta_l(k)$ is well approximated by its first-order Taylor expansion,

$$\delta_l(k) \approx \delta_l(\bar{k}) + (k - \bar{k})\left.\frac{\mathrm{d}\delta_l}{\mathrm{d}k}\right|_{\bar{k}}. \tag{2.116}$$

At large distances r, the contribution u^{out} of the second term on the right-hand side of (2.109) to the superposition (2.111) is thus

$$\begin{aligned} u^{\mathrm{out}}(r,t) &= -\int_{-\infty}^{\infty} \mathrm{e}^{+\mathrm{i}(kr-\omega t-l\pi/2)}\mathrm{e}^{2\mathrm{i}\delta_l}\phi(k)\mathrm{d}k \\ &\approx -\mathrm{e}^{+\mathrm{i}\bar{k}r-\mathrm{i}\bar{\omega}t}\mathrm{e}^{2\mathrm{i}\delta_l(\bar{k})}(-\mathrm{i})^l \int_{-\infty}^{\infty} \mathrm{e}^{-\mathrm{i}(k-\bar{k})[-(r-\bar{v}t+\Delta r)]}\tilde{\phi}(k-\bar{k})\mathrm{d}(k-\bar{k}) \end{aligned} \tag{2.117}$$

with

$$\Delta r = 2\frac{\mathrm{d}\delta_l}{\mathrm{d}k}\bigg|_{\bar{k}}. \tag{2.118}$$

The integral in (2.117) is essentially the same Fourier transform of $\tilde{\phi}$ as in (2.113), but the conjugate variable is $-(r - \bar{v}t + \Delta r)$ instead of $r + \bar{v}t$, so

$$u^{\mathrm{out}}(r,t) = \mathrm{e}^{+\mathrm{i}\bar{k}r - \mathrm{i}\bar{\omega}t}\mathrm{e}^{2\mathrm{i}\delta_l(\bar{k})}(-1)^l \Psi\big[-(r - \bar{v}t + \Delta r)\big]. \tag{2.119}$$

For large positive times t, the wave function (2.119) represents an almost monochromatic radial wave packet, which is broadly localized around $r = \bar{v}t - \Delta r$ and travels away from the origin with group velocity $\bar{v} = \hbar\bar{k}/\mu$. Relative to a free particle which travels inward with velocity $-\bar{v}$, reaches the origin at $t = 0$ and then travels outward with velocity $\bar{v}$, the wave packet (2.119) lags behind by the *space shift* Δr, which is related to the k-derivative of the phase shift via (2.118). This space shift is related to a *time delay* Δt,

$$\Delta t = \frac{\Delta r}{\bar{v}} = 2\frac{\mu}{\hbar\bar{k}}\frac{\mathrm{d}\delta_l}{\mathrm{d}k}\bigg|_{\bar{k}} = 2\hbar\frac{\mathrm{d}\delta_l}{\mathrm{d}E}\bigg|_{\bar{E}}, \tag{2.120}$$

where $\bar{E} = \hbar^2\bar{k}^2/(2\mu)$ is the energy corresponding to the mean wave number $\bar{k}$ of the wave packet. The expression (2.120) relates the energy derivative of the scattering phase shift to the time delay of a radial wave packet, relative to the time evolution for a free particle reflected at $r = 0$. It was first derived by Eisenbud and Wigner [51] and is referred to as the *Wigner time delay*.

The Wigner time delay is a valid concept for almost monochromatic wave packets, which are necessarily broad in coordinate space. This is no restriction for a scattering scenario, where incoming and outgoing waves can move freely over large distances.

When the scattering phase shift δ_l decreases with increasing energy or wave number, the space shift (2.118) and the time delay (2.120) are negative; the scattered wave packet returns earlier than expected for a free particle. For scattering by a hard sphere, see (2.73), (2.74) and Fig. 2.3, we have $\Delta r = -2R$ for $l = 0$ and $\Delta r \overset{kR\to\infty}{\sim} -2R$ for $l > 0$. A space shift of $-2R$ simply means that the wave packet returns at the same time as a free particle reflected at $r = R$ rather than at $r = 0$, and the corresponding time *gain* is $2R/\bar{v}$. For a potential whose influence is negligible beyond a certain range R_V, the space shift can never be less than $-2R_V$, because the wave packet cannot return faster than a free particle reflected at $r = R_V$. This puts lower bounds on k-derivatives and energy derivatives of the scattering phase shifts, as already discussed in [51],

$$\frac{\mathrm{d}\delta_l}{\mathrm{d}k} \geq -R_V, \qquad \frac{\mathrm{d}\delta_l}{\mathrm{d}E} \geq -\frac{R_V}{\hbar\upsilon} = -\frac{\mu R_V}{\hbar^2 k}. \tag{2.121}$$

For a potential $V(r)$ falling off sufficiently fast at large distances, the range of its "influence" can usually be estimated as the range over which $V(r)$ has nonnegligible

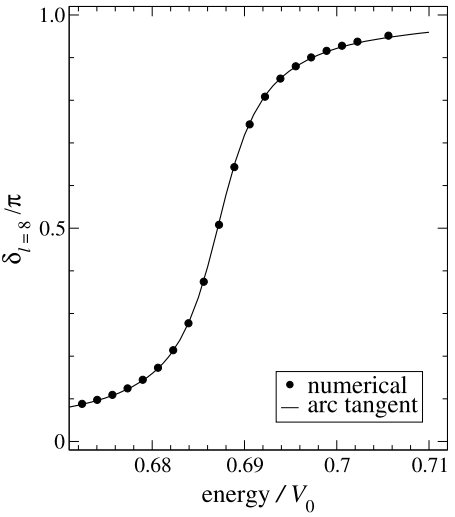

Fig. 2.9 Phase shifts near the $l = 8$ shape resonance in the model potential (2.105). The *dots* were obtained by numerically solving the radial Schrödinger equation and the *solid line* is the analytical function (2.122) with the parameters given in (2.123)

values. The s-wave scattering length a can, however, assume arbitrarily large values if there is an s-wave bound state sufficiently close to threshold, see (2.88). In this case, $\delta_{l=0}(k) \sim -ak$ near threshold, and $-a$ is the lower bound on $\mathrm{d}\delta_{l=0}/\mathrm{d}k$.

There is no upper bound on the energy derivative of the phase shift, i.e., on the delay experienced in a given partial wave during the scattering process. This is already indicated in the sharp jump by π of $\delta_{l=6}$ at $k\beta \approx 0.41$ and of $\delta_{l=8}$ at $k\beta \approx 0.83$ in Fig. 2.7. These jumps are typical signatures of resonances which decay with a finite lifetime.

2.3.10.2 Resonant Behaviour of Phase Shifts

As a typical example for a potential resonance, let's focus on the partial wave $l = 8$ in the model potential (2.105). The jump by π around $k\beta = 0.829$ is well described by the analytical expression

$$\delta_l(E) = \delta_{\mathrm{bg}} - \arctan\left(\frac{\Gamma/2}{E - E_{\mathrm{R}}}\right), \tag{2.122}$$

where E_{R} is the *resonance position*, Γ is the *resonance width*, and δ_{bg} is a smoothly energy-dependent *background phase shift*. The branch of the arcus-tangent function in (2.122) is chosen such that $-\arctan(1/x)$ rises smoothly from zero to π as x varies from $-\infty$ to ∞. Figure 2.9 shows the phase shifts calculated by numerically solving the radial Schrödinger equation (filled dots) together with the function (2.122) (solid line). The parameters for the fit in Fig. 2.9 are

$$\delta_{\mathrm{bg}} = 0.01, \qquad E_{\mathrm{R}} = 0.6872 V_0, \qquad \Gamma = 0.0073 V_0. \tag{2.123}$$

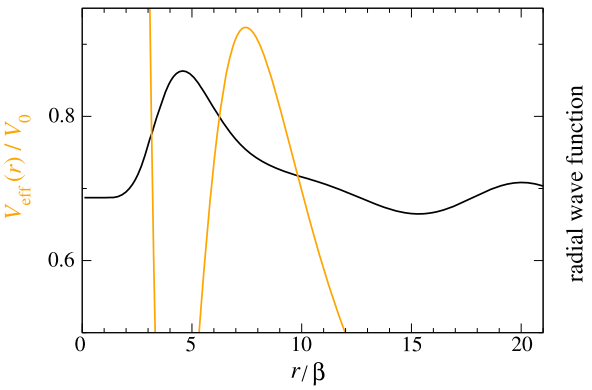

Fig. 2.10 Solution of the radial Schrödinger equation (2.35) with the model potential (2.105) in the partial wave $l = 8$ at energy $E = E_{\rm R} = 0.6872V_0$. The *orange line* shows the effective potential (2.36)

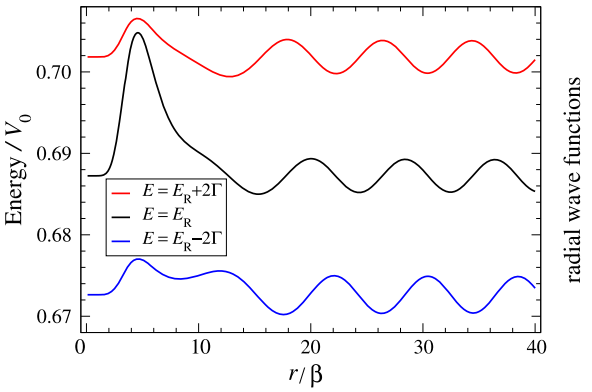

Fig. 2.11 Radial wave function at the resonance energy $E_{\rm R}$ as in Fig. 2.10, and at 2Γ below and above $E_{\rm R}$

The nature of the resonance as an almost bound state trapped by the centrifugal barrier is illustrated in Fig. 2.10, which shows the solution of the radial Schrödinger equation at the resonance energy $E_{\rm R}$. The wave function has significant amplitude in the classically allowed region on the near side of the barrier and connects through the classically forbidden region under the barrier to the asymptotic regime. The enhancement of the amplitude in the potential well at small distances is restricted to energies close to $E_{\rm R}$. This is illustrated in Fig. 2.11, which also shows the radial wave functions at energies 2Γ below and above $E_{\rm R}$. Figure 2.11 also shows that the wave function at energy 2Γ above $E_{\rm R}$ has one more node at small distances, and beyond the barrier it is shifted by a half wave relative to the wave function at energy 2Γ below $E_{\rm R}$.

The picture of a resonance as an almost bound state decaying in time can be served by looking for a solution of the radial Schrödinger equation (2.35) whose asymptotic form (2.68),

$$u_l(r) \overset{r\to\infty}{\propto} \mathrm{e}^{-\mathrm{i}\delta_l}\mathrm{e}^{-\mathrm{i}(kr-l\pi/2)} - \mathrm{e}^{+\mathrm{i}\delta_l}\mathrm{e}^{+\mathrm{i}(kr-l\pi/2)}, \tag{2.124}$$

contains only the outgoing term proportional to $\mathrm{e}^{+\mathrm{i}(kr-l\pi/2)}$, which implies that the ratio $\mathrm{e}^{-\mathrm{i}\delta_l}/\mathrm{e}^{+\mathrm{i}\delta_l}$ vanishes. This cannot be achieved as long as the scattering phase

shifts δ_l are real and the S-matrix is unitary, but, as realized by Gamow [19] and Siegert [42], both conditions can be relaxed by allowing complex energies E.

Assume that there is an energy $\mathscr{E} = E_{\mathrm{re}} + \mathrm{i}E_{\mathrm{im}}$ in the complex plane, for which there exists a solution of the radial Schrödinger equation with the asymptotic behaviour (2.124) but with $\mathrm{e}^{-\mathrm{i}\delta_l(\mathscr{E})} = 0$. Constructing the corresponding time-dependent wave function via multiplication with $\mathrm{e}^{-\mathrm{i}\mathscr{E}t/\hbar}$ leads to a time dependence of the probability distribution, $|u_l|^2 \propto \mathrm{e}^{2E_{\mathrm{im}}t/\hbar}$, and a negative imaginary part E_{im} describes a state decaying in time. The *lifetime* of the decaying resonant state is $-\hbar/(2E_{\mathrm{im}})$.

Assume that the function $\mathrm{e}^{-\mathrm{i}\delta_l(E)}$ is an analytical function of E, at least in a close neighbourhood of $\mathscr{E}$, so it can be approximated by a Taylor expansion to first order,

$$\mathrm{e}^{-\mathrm{i}\delta_l(E)} \approx C(E - \mathscr{E}). \tag{2.125}$$

If the imaginary part E_{im} of $\mathscr{E}$ is small, so that the domain where (2.125) is accurate overlaps with the real axis, then for *real* energies E in this domain we can also write,

$$\mathrm{e}^{+\mathrm{i}\delta_l(E)} = \left[\mathrm{e}^{-\mathrm{i}\delta_l(E)}\right]^* \approx C^*\left(E - \mathscr{E}^*\right). \tag{2.126}$$

For the S-matrix $S_l = \mathrm{e}^{+\mathrm{i}\delta_l(E)}/\mathrm{e}^{-\mathrm{i}\delta_l(E)}$ this gives,

$$S_l = \left(\frac{C^*}{C}\right)\frac{E - E_{\mathrm{re}} + \mathrm{i}E_{\mathrm{im}}}{E - E_{\mathrm{re}} - \mathrm{i}E_{\mathrm{im}}}, \tag{2.127}$$

and for the argument $2\delta_l$ of the S-matrix this implies

$$2\delta_l = -2\arg(C) + 2\arctan\left(\frac{E_{\mathrm{im}}}{E - E_{\mathrm{re}}}\right). \tag{2.128}$$

This is exactly the form (2.122) with the resonance position at $E_{\mathrm{R}} = E_{\mathrm{re}}$, the resonance width $\Gamma = -2E_{\mathrm{im}}$ and the background phase shift $\delta_{\mathrm{bg}} = -\arg(C)$. The lifetime τ_{R} of the resonance is related to its width via

$$\tau_{\mathrm{R}} = \frac{\hbar}{\Gamma}. \tag{2.129}$$

From (2.125) it follows that the S-matrix has a pole at energy $E = E_{\mathrm{R}} - \mathrm{i}\Gamma/2$. The real part of this pole is the resonance position and minus twice the imaginary part is the resonance width. If the pole is sufficiently close to the real axis, i.e., if the resonance width is sufficiently small, the pole leads to a jump by π in the scattering phase shift, as described by the arcus-tangent formula (2.122). The width is then the energy interval over which the arcus-tangent contribution to the phase shift increases from $\frac{1}{4}\pi$ to $\frac{3}{4}\pi$. If the background phase shift is negligibly small, then the contribution of the lth partial wave to the integrated cross section (2.52) is, near resonance,

$$\sigma_{[l]} = \frac{4\pi}{k^2}(2l+1)\sin^2\delta_l = \frac{4\pi}{k^2}\frac{2l+1}{1+\cot^2\delta_l} = \frac{4\pi}{k^2}\frac{(2l+1)(\Gamma/2)^2}{(E - E_{\mathrm{R}})^2 + (\Gamma/2)^2}. \tag{2.130}$$

The formula (2.130) is known as the *Breit–Wigner formula* for resonance scattering [50].

For the pure arcus-tangent form (2.122) of the resonant phase shift, we have

$$\frac{\mathrm{d}\delta_l}{\mathrm{d}E} = \frac{\Gamma/2}{(E - E_\mathrm{R})^2 + (\Gamma/2)^2}, \tag{2.131}$$

so the resonance width is related to the energy derivative of the phase shift at resonance by

$$\Gamma = 2\left[\frac{\mathrm{d}\delta_l}{\mathrm{d}E}\bigg|_{E=E_\mathrm{R}}\right]^{-1}. \tag{2.132}$$

From the formula (2.120), the Wigner time delay at an energy near resonance is

$$\Delta t = 2\hbar\frac{\mathrm{d}\delta_l}{\mathrm{d}E} = \frac{\hbar\Gamma}{(E - E_\mathrm{R})^2 + (\Gamma/2)^2}. \tag{2.133}$$

Remember that Eq. (2.120) was derived for almost monochromatic wave packets with a very small uncertainty in momentum or energy. For such an almost monochromatic wave packet with incident energy corresponding to the resonant energy E_R, the Wigner time delay is $4\hbar/\Gamma$, i.e. four times the lifetime τ_R, which is twice as large as one might expect for a particle that enters and leaves the resonant state on the time scale τ_R. The Wigner time delay decreases as the energy is detuned from centre of the resonance at E_R.

For less sudden jumps of the phase shift, which may not be so well described by the pure arcus-tangent form (2.122), it may nevertheless make sense to speak of a resonance. A reasonable definition for the position E_R of the resonance is the energy for which the derivative $\mathrm{d}\delta_l/\mathrm{d}E$ is maximal, i.e., the energy of maximal Wigner time delay. Equation (2.132) can then serve as a definition of the resonant width, even if the energy dependence of δ_l is not very close to the arcus-tangent form (2.122). Different definitions of a resonance, e.g. as a maximum of the energy derivative of the scattering phase shift or as a pole of the S-matrix in the complex energy plane, tend to agree when the resonance is narrow. The definition of a resonance becomes increasingly ambiguous with increasing width.

2.3.11 Scattering Cross Sections

The observable cross sections depend on the scattering phase shifts according to Eqs. (2.50) and (2.51). Figure 2.12 shows the differential cross section (2.50) for scattering by the model potential (2.105) as a function of energy for the scattering angle $\theta = 30°$. In the limit $k \to 0$ it approaches the square of the scattering length a, which is given by $a \approx 18.78\beta$ in this case, so the limiting value is near $353\beta^2$. Sharp features are observed near $E = 0.17V_0$ ($k\beta \approx 0.4115$), where there is a sharp

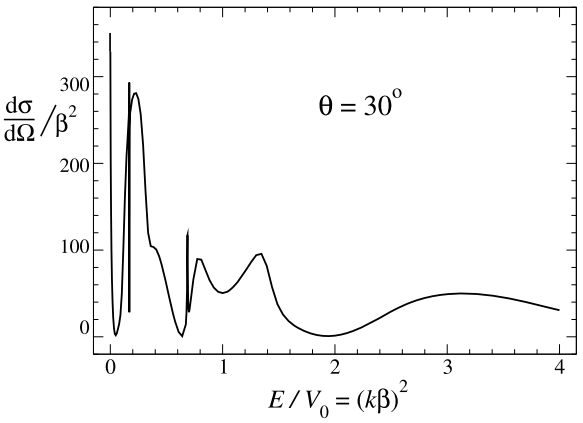

Fig. 2.12 Differential scattering cross section for the model potential (2.105) as function of energy for $\theta = 30°$

resonance in the $l = 6$ partial wave, and at near $E = 0.6872V_0$ corresponding to the $l = 8$ resonance discussed in connection with Figs. 2.9–2.11.

Angular distributions are shown in Fig. 2.13 for several values of the energy resp. scaled momentum $k\beta$. For $k\beta = 0.05$, the cross section has dropped from its threshold value but is still largely isotropic. At $k\beta = 0.275$ the s-wave phase shift is close to an integral multiple of π; the cross section is strongly suppressed and is no longer near isotropic. Near a resonance in a given partial wave, the respective phase shift rises through π and becomes an odd multiple of $\frac{\pi}{2}$ at some point in this process. The contribution of the partial wave to the integrated cross section reaches its unitarity limit (2.53) in this case, and the angular distribution of the differential cross section can be expected to show the imprint of the corresponding term

$$\left(\frac{\mathrm{d}\sigma}{\mathrm{d}\Omega}\right)_l = \frac{(2l+1)^2}{k^2} P_l(\cos\theta)^2. \tag{2.134}$$

The middle panels of Fig. 2.13 show the differential scattering cross sections at $k\beta = 0.4115$, where $\delta_{l=6}$ is close to $\frac{3}{2}\pi$, and at $k\beta = 0.829$, where $\delta_{l=8}$ is close to $\frac{1}{2}\pi$. The dashed lines show the term (2.134) for these cases. Towards higher momenta, the angular distributions show an increasing localization towards forward directions, see bottom right panel showing the results for $k\beta = 2$.

The Born approximation to the scattering cross section is easily evaluated for the model potential (2.105). The scattering amplitude (2.22) in this case is

$$f^{\mathrm{Born}}(\theta) = 4\pi\beta\left(48\mathrm{e}^{-4\beta^2q^2} - \mathrm{e}^{-\beta^2q^2/4}\right), \quad q = 2k\sin\left(\frac{\theta}{2}\right). \tag{2.135}$$

The resulting differential cross section $|f^{\mathrm{Born}}(\theta)|^2$ reproduces the tendency to forward peaking, as shown for $k\beta = 2$ by the dashed line in the bottom right panel of Fig. 2.13, but quantitatively, it is still catastrophically wrong at this value of $k\beta$.

Whereas the classical integrated scattering section diverges for all potentials which vanish smoothly for $R \to \infty$ (see discussion around Eq. (1.40) in Sect. 1.3),

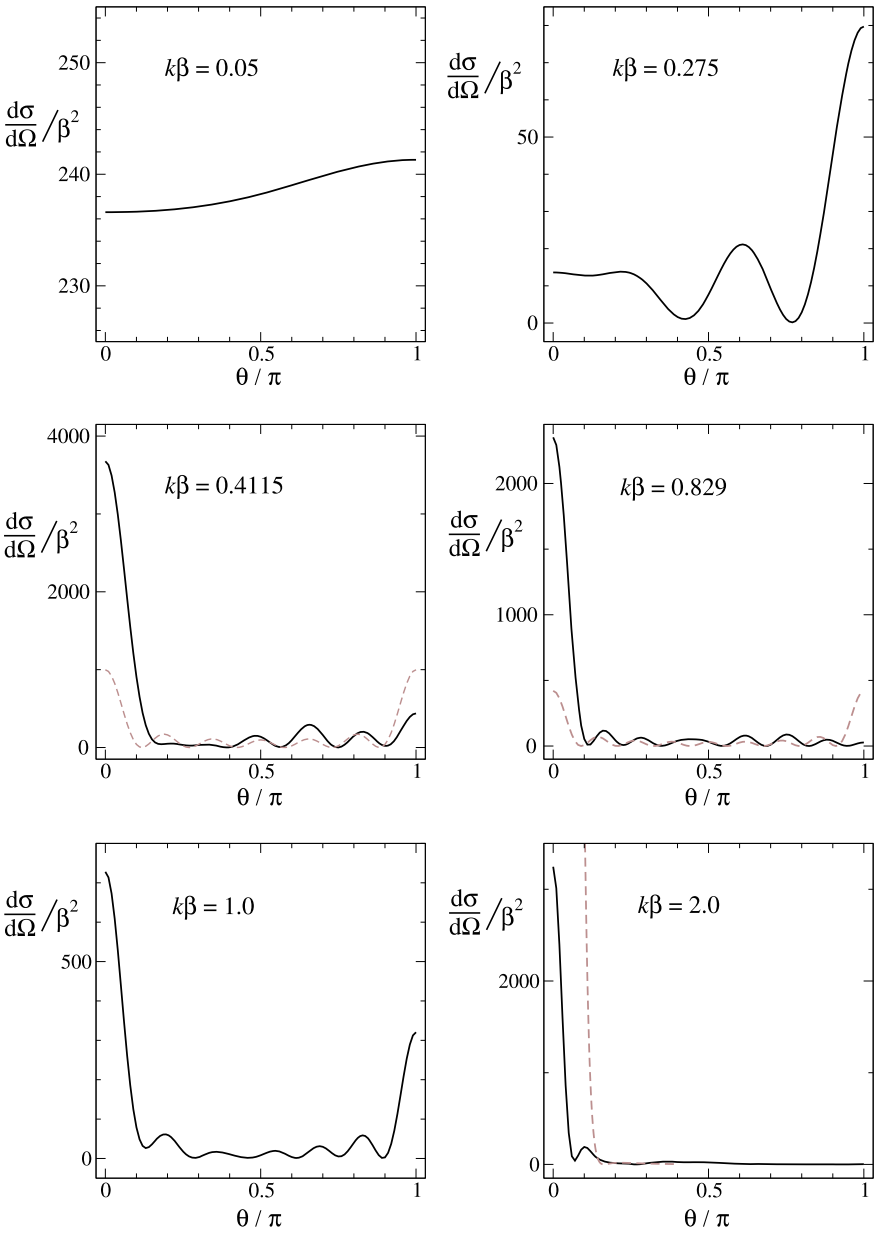

Fig. 2.13 Angular distributions for the differential cross sections for scattering by the model potential (2.105). The *dashed lines* at $k\beta = 0.4115$ and $k\beta = 0.829$ show the function $(2l+1)^2 P_l(\cos\theta)^2/k^2$ for $l = 6$ and $l = 8$, respectively. The *dashed line* at $k\beta = 2.0$ shows the result of the Born approximation (2.135)

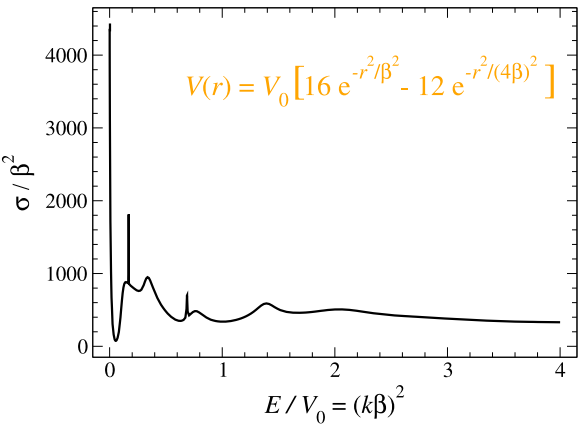

Fig. 2.14 Integrated cross section for scattering by the model potential (2.105)

the quantum mechanical integrated cross section remains finite for potentials falling off faster than $1/r^2$. The integrated cross section σ for scattering by the model potential (2.105) is shown in Fig. 2.14 as function of energy. The threshold value is $\sigma \overset{E\to 0}{\sim} 4\pi a^2 \approx 4440\beta^2$. The integrated cross section goes through a deep minimum below $(k\beta)^2 = 0.1$. This is because the s-wave phase shift goes through an integer multiple of π at $(k\beta)^2 \approx 0.075$, while the contributions from all other partial waves are still small. Such an effect was first observed in the 1920's in scattering of slow electrons by atoms and molecules [36, 45, 46] and is now referred to as the *Ramsauer–Townsend Minimum*. Near $(k\beta)^2 = 0.17$ and $(k\beta)^2 = 0.69$, the integrated cross section shows the typical Breit–Wigner behaviour (2.130) due to the narrow and isolated resonances in the $l = 6$ and $l = 8$ partial waves. The peak height above the smooth background is $(2l+1)4\pi/k^2$ corresponding to $965\beta^2$ and $311\beta^2$, respectively.

2.4 The WKB Approximation

Shortly after Schrödinger published his wave equation for quantum mechanics in 1926, Schrödinger [38] Wentzel [49], Kramers [26] and Brillouin [9] formulated an approximate method of solution which is now known as the "WKB" method. The method had been formulated in 1923 for such second-order differential equations by Jeffreys—and published in 1925 [23], but he had not, of course, been able to refer to Schrödinger's work which came later. The WKB approximation is a semiclassical approximation, which can be expected to work well when physical actions are large compared to Planck's constant $\hbar$. For a comprehensive review see Ref. [2].

2.4.1 Definition and Accuracy of WKB Wave Functions

For a free particle of mass μ moving in one spatial dimension with constant momentum $p = \hbar k$, the quantum mechanical wave function is proportional to e^{ikr}. In

the presence of a potential $V(r)$, the *local classical momentum* $p(r)$ is a function of r,

$$p(r) = \pm\sqrt{2\mu\big[E - V(r)\big]} = \pm\hbar\sqrt{k^2 - 2\mu V(r)/\hbar^2}; \tag{2.136}$$

it is real in the *classically allowed region* $E \geq V(r)$ and purely imaginary in the *classically forbidden region* $E < V(r)$. In the WKB approximation, the exponential form of the wave function is retained in the presence of the potential, but the product kr in the exponent is replaced by the integral $\int^r p(r')\mathrm{d}r'/\hbar$, in order to account for the spatial variation of p. The integral $\int^r p(r')\mathrm{d}r'$ has the physical dimension of an action and is referred to as an *action integral*. In order to satisfy the continuity equation $\mathrm{d}j_r/\mathrm{d}r = 0$ for the radial current density $j_r = u^* u'\hbar/(2\mathrm{i}\mu) + \mathrm{cc}$, the exponential term is complemented with the prefactor $1/\sqrt{p(r)}$. The resulting expression for the WKB wave function is

$$u^{\mathrm{WKB}}(r) \propto \frac{1}{\sqrt{p(r)}} \mathrm{e}^{\pm\frac{\mathrm{i}}{\hbar}\int^r p(r')\mathrm{d}r'}. \tag{2.137}$$

The lower limit of the action integral in the exponent in (2.137) can be chosen according to convenience. Changing the lower limit amounts to multiplying the right-hand side of (2.137) by an overall phase.

The WKB wave function (2.137) obeys the following differential equation,

$$\frac{\mathrm{d}^2 u^{\mathrm{WKB}}}{\mathrm{d}r^2} + \frac{p(r)^2}{\hbar^2} u^{\mathrm{WKB}}(r) + \left(\frac{p''}{2p(r)} - \frac{3}{4}\frac{(p')^2}{p(r)^2}\right) u^{\mathrm{WKB}}(r) = 0, \tag{2.138}$$

whereas the Schrödinger equation for the quantum mechanical wave function $u(r)$ reads $u'' + (p^2/\hbar^2)u(r) = 0$. The WKB approximation can be expected to be good when the third term on the left-hand side of Eq. (2.138) is small compared to the second term, i.e., the absolute value of the function

$$Q(r) = \hbar^2\left(\frac{3}{4}\frac{(p')^2}{p^4} - \frac{p''}{2p^3}\right) = \frac{1}{16\pi^2}\left[2\lambda\frac{\mathrm{d}^2\lambda}{\mathrm{d}r^2} - \left(\frac{\mathrm{d}\lambda}{\mathrm{d}r}\right)^2\right] \tag{2.139}$$

should be small. The function $\lambda(r)$ in (2.139) is the *local de Broglie wave length*,

$$\lambda(r) = \frac{2\pi\hbar}{p(r)}. \tag{2.140}$$

The validity condition for the WKB approximation is

$$\big|Q(r)\big| \ll 1. \tag{2.141}$$

It is a *local* property of the Schrödinger equation. The validity condition is often given as $|\lambda'| \ll 1$, which is mostly but not always compatible with the condition (2.141). One notable exception is the case of a potential proportional to $1/r^4$ at energy $E = 0$. In this case, $\lambda(r) \propto r^2$, so the two terms in (2.139) cancel and the

WKB wave function is an exact solution of the Schrödinger equation for all r; on the other hand, $|\lambda'|$ grows to infinity for large r.

When the function $Q(r)$ defined in (2.139) is significantly nonvanishing, the WKB approximation is not reliable, which has led to the name *badlands function* for $Q(r)$—or for the simpler expression $|\lambda'|$ [13]. A more positive attitude is expressed by calling $Q(r)$ the *quantality function*, because the regions where it is nonnegligible are those where quantum mechanical effects are important.

2.4.2 Connection Across a Classical Turning Point

At a classical turning point r_{ctp}, the local classical momentum vanishes, the WKB wave function has a singularity, and the quantality function diverges. On the classically forbidden side of r_{ctp}, the local classical momentum is purely imaginary, and the WKB wave function is a superposition of two linearly independent WKB wave functions, u_-^{WKB} which decays exponentially, and u_+^{WKB} which grows exponentially with increasing separation from r_{ctp},

$$u_{\mathrm{forb}}^{\mathrm{WKB}}(r) = A_- u_-^{\mathrm{WKB}}(r) + A_+ u_+^{\mathrm{WKB}}(r), \qquad u_\pm^{\mathrm{WKB}}(r) = \frac{1}{\sqrt{|p(r)|}} \mathrm{e}^{\pm\frac{1}{\hbar}\left|\int_{r_{\mathrm{ctp}}}^{r} p(r')\mathrm{d}r'\right|}; \tag{2.142}$$

the lower integration limit in the action integral has been chosen, as is customary, to be the classical turning point r_{ctp}. If r_{ctp} is the only classical turning point, then the exponentially growing contribution should vanish in a physically reasonable wave function, which is thus proportional to u_-^{WKB}. The real function $u_-^{\mathrm{WKB}}(r)$ on the classically allowed side of r_{ctp} must be related to a real-valued superposition $u_{\mathrm{all}}^{\mathrm{WKB}}$ of the two linearly independent wave functions (2.137) on the classically allowed side of r_{ctp}; this superposition can be expressed in terms of an amplitude A and a phase ϕ as

$$u_{\mathrm{all}}^{\mathrm{WKB}}(r) = \frac{A}{\sqrt{p(r)}} \cos\left(\frac{1}{\hbar}\left|\int_{r_{\mathrm{ctp}}}^{r} p\big(r'\big)\mathrm{d}r'\right| - \frac{\phi}{2}\right). \tag{2.143}$$

Writing the cosine on the right-hand side of (2.143) as a sum of an incoming and a reflected wave,

$$\cos\left(\frac{1}{\hbar}\left|\int_{r_{\mathrm{ctp}}}^{r} p\big(r'\big)\mathrm{d}r'\right| - \frac{\phi}{2}\right) \propto \mathrm{e}^{-\frac{\mathrm{i}}{\hbar}\left|\int_{r_{\mathrm{ctp}}}^{r} p(r')\mathrm{d}r'\right|} + \mathrm{e}^{-\mathrm{i}\phi}\mathrm{e}^{+\frac{\mathrm{i}}{\hbar}\left|\int_{r_{\mathrm{ctp}}}^{r} p(r')\mathrm{d}r'\right|}, \tag{2.144}$$

reveals that ϕ is the phase loss of the WKB wave due to reflection at the classical turning point r_{ctp}, the *reflection phase* at r_{ctp} [17]. The connection across the classical turning point is expressed in the *connection formula*,

$$\frac{1}{\sqrt{|p(r)|}} \mathrm{e}^{-\frac{1}{\hbar}\left|\int_{r_{\mathrm{ctp}}}^{r} p(r')\mathrm{d}r'\right|} \longrightarrow \frac{A}{\sqrt{p(r)}} \cos\left(\frac{1}{\hbar}\left|\int_{r_{\mathrm{ctp}}}^{r} p\big(r'\big)\mathrm{d}r'\right| - \frac{\phi}{2}\right). \tag{2.145}$$

Due to the divergence of the WKB wave function at r_{ctp}, it is not immediately clear how to choose the amplitude A and the reflection phase ϕ in (2.145). This is the so-called "connection problem" of the WKB approximation at a classical turning point. A prescription for connection can be obtained by assuming a linear behaviour of the potential in a sufficiently large region around the classical turning point,

$$V(r) = (r - r_{\mathrm{ctp}})V'(r_{\mathrm{ctp}}). \tag{2.146}$$

The Schrödinger equation with the linear potential (2.146) can be solved analytically. If, for example, $\mathrm{d}V/\mathrm{d}r$ is negative at r_{ctp}, then the classically allowed region is $r > r_{\mathrm{ctp}}$ and the physically reasonable solution of the Schrödinger equation with the potential (2.146) is, except for an arbitrary overall normalization constant, an Airy function (see Appendix B.4),

$$u(r) = \mathrm{Ai}\big(\xi^{1/3}(r_{\mathrm{ctp}} - r)\big), \quad \xi = -\frac{2\mu}{\hbar^2}V'(r_{\mathrm{ctp}}) > 0. \tag{2.147}$$

Inserting the asymptotic behaviour of the Airy function for large positive or negative values of the dimensionless argument $\xi^{1/3}(r - r_{\mathrm{ctp}})$ in (2.147) gives,

$$u(r) \sim \frac{1}{2\sqrt{\pi}}\big[\xi^{1/3}(r - r_{\mathrm{ctp}})\big]^{-1/4}\mathrm{e}^{-\zeta} \tag{2.148}$$

on the classically forbidden side $r < r_{\mathrm{ctp}}$, and

$$u(r) \sim \frac{1}{\sqrt{\pi}}\big[\xi^{1/3}(r - r_{\mathrm{ctp}})\big]^{-1/4}\cos\left(\zeta - \frac{\pi}{4}\right) \tag{2.149}$$

on the allowed side $r > r_{\mathrm{ctp}}$. The local classical momentum is $p(r) = \hbar\sqrt{\xi(r - r_{\mathrm{ctp}})}$, and the dimensionless variable ζ in (2.148), (2.149) is

$$\zeta = \frac{2}{3}\sqrt{\xi}|r - r_{\mathrm{ctp}}|^{3/2} = \frac{1}{\hbar}\left|\int_{r_{\mathrm{ctp}}}^{r} p\big(r'\big)\mathrm{d}r'\right|. \tag{2.150}$$

Comparing (2.148) with the left-hand side of the connection formula (2.145) and (2.149) with the right-hand side shows that, for the linear potential (2.146), the appropriate values of the amplitude A and the reflection phase ϕ in the connection formula (2.145) are

$$A = 2, \qquad \phi = \frac{\pi}{2}. \tag{2.151}$$

The potential (2.146) is shown in Fig. 2.15 together with the exact wave function (2.147) and its WKB approximations on the classically forbidden and allowed sides of the classical turning point.

It is important to understand, that the WKB approximation can be highly accurate away from a classical turning point, even in cases when a linear approximation is not justified near the classical turning point. A simple example is the radial Schrödinger equation (2.35) for s-waves in the absence of a potential. The quantality function

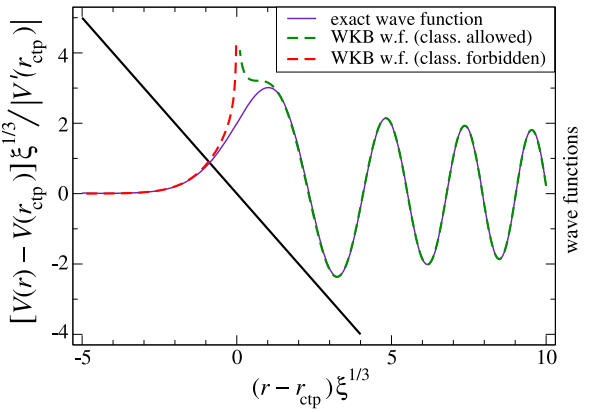

Fig. 2.15 The *solid black line* shows the linear potential (2.146) around its classical turning point $r_{\rm ctp}$. The decaying WKB wave function on the classically forbidden side of $r_{\rm ctp}$ (*dashed red line*) is connected via (2.145) with (2.151) to the oscillating WKB wave function on the classically allowed side of $r_{\rm ctp}$ (*dashed green line*). The quantities plotted are scaled with the inverse length $\xi^{1/3}$, see Eq. (2.147), and are dimensionless

vanishes for $r > 0$, so the WKB approximation is exact for all $r > 0$. The WKB wave function $u_{l=0}(r) \propto \cos(kr - \frac{1}{2}\phi)$ is, however, only equal to the regular free particle solution $\propto \sin(kr)$ if we choose the reflection phase at the classical turning point $r_{\rm ctp} = 0$ to be $\phi = \pi$.

For a potential that vanishes asymptotically as an inverse power of the distance, $V(r) \overset{r\to\infty}{\propto} 1/r^\alpha$ with $\alpha > 0$, the asymptotic behaviour of the local de Broglie wave length (2.140) at a positive energy $E = \hbar^2 k^2/(2\mu)$ is,

$$\lambda(r) = \frac{2\pi}{k} + O\left(\frac{1}{r^\alpha}\right), \tag{2.152}$$

so the quantality function (2.139) vanishes asymptotically, and the WKB approximation becomes exact for $r \to \infty$. The amplitude of a wave function is generally subject to a convenient choice of normalization, but a WKB wave function such as (2.143) can only be a good approximation of an exact wave function $u(r)$ asymptotically, if the reflection phase ϕ is chosen correctly. It can be shown [47], that the error of the appropriately normalized WKB wave function with correctly chosen reflection phase decays as $1/r^{\alpha+1}$ asymptotically.

An instructive example is the inverse-square potential

$$V_2(r) = \frac{C_2}{r^2} = \frac{\hbar^2}{2\mu}\frac{\gamma}{r^2}, \tag{2.153}$$

where γ is a dimensionless constant, which is equal to $l(l+1)$ if we interpret V_2 as the centrifugal potential in the partial wave l. The Schrödinger equation, expressed

in terms of the scaled coordinate $\rho = kr$, reads

$$-\frac{\mathrm{d}^2 u}{\mathrm{d}\rho^2} + \frac{\gamma}{\rho^2} u(\rho) = u(\rho). \tag{2.154}$$

It has as regular solution

$$u^{\mathrm{reg}}(\rho) = \sqrt{\frac{\pi}{2}} \sqrt{\rho} J_\nu(\rho) \quad \text{with } \nu = \sqrt{\gamma + \frac{1}{4}}, \tag{2.155}$$

where J_ν is an ordinary Bessel function, see Appendix B.4. If $\gamma = l(l+1)$, then the order of the Bessel function is $\nu = l + \frac{1}{2}$, and u^{reg} is the regular free-particle radial wave function $u_l^{(\mathrm{s})}$ introduced in Sect. 2.3.3, Eq. (2.38). The limiting behaviour of the wave function (2.155) for small and for large argument is,

$$\begin{aligned} u^{\mathrm{reg}}(\rho) &\overset{\rho \to 0}{\sim} \frac{\sqrt{\pi}}{\Gamma(\nu+1)} \left(\frac{\rho}{2}\right)^{\nu+1/2}, \\ u^{\mathrm{reg}}(\rho) &\overset{\rho \to \infty}{\sim} \left(1 - \frac{\gamma(\gamma-2)}{8\rho^2}\right) \cos\left[\rho - \nu\frac{\pi}{2} - \frac{\pi}{4}\right] \\ &\quad - \frac{\gamma}{2\rho} \sin\left[\rho - \nu\frac{\pi}{2} - \frac{\pi}{4}\right] + O\left(\frac{1}{\rho^3}\right). \end{aligned} \tag{2.156}$$

For $\gamma \geq 0$, the classical turning point is given by $\rho_{\mathrm{ctp}} = kr_{\mathrm{ctp}} = \sqrt{\gamma}$ and the appropriately scaled local classical momentum is $p(\rho) = \sqrt{1 - \gamma/\rho^2}$. The asymptotic behaviour of the WKB wave functions $u_{\mathrm{forb}}^{\mathrm{WKB}}$ on the classically forbidden and $u_{\mathrm{all}}^{\mathrm{WKB}}$ on the classically allowed side of ρ_{ctp} is,

$$\begin{aligned} u_{\mathrm{forb}}^{\mathrm{WKB}}(\rho) &\overset{\rho \to 0}{\propto} \rho^{\sqrt{\gamma}+1/2}, \\ u_{\mathrm{all}}^{\mathrm{WKB}}(\rho) &\overset{\rho \to \infty}{\propto} \left(1 - \frac{\gamma(\gamma-2)}{8\rho^2}\right) \cos\left[\rho - \sqrt{\gamma}\frac{\pi}{2} - \frac{\phi}{2}\right] \\ &\quad - \frac{\gamma}{2\rho} \sin\left[\rho - \sqrt{\gamma}\frac{\pi}{2} - \frac{\phi}{2}\right] + O\left(\frac{1}{\rho^3}\right), \end{aligned} \tag{2.157}$$

where ϕ is the reflection phase as in Eq. (2.143).

Compared to the exact wave function (2.156), the WKB wave function (2.157) has the wrong power-behaviour near the origin and, if the reflection phase ϕ is taken to be $\frac{\pi}{2}$, the wrong asymptotic phase. Both deficits can be remedied, if the WKB wave function is calculated not with the true strength parameter γ in the potential (2.153), but with the modified strength parameter γ' defined by

$$\gamma' = \gamma + \frac{1}{4}. \tag{2.158}$$

If V_2 is the centrifugal potential, then (2.158) amounts to replacing $\gamma = l(l+1)$ by $(l+\frac{1}{2})^2$. The modification (2.158) for the evaluation of WKB wave functions is called the *Langer modification* [27].

On the classically allowed side of the turning point, choosing the conventional value $\frac{\pi}{2}$ for the reflection phase ϕ in the WKB wave (2.157) and applying the Langer modification (2.158) guarantees the correct phase in the leading asymptotic term, which oscillates with constant amplitude, but the next two terms with amplitudes proportional to $1/(kr)$ and $1/(kr)^2$, respectively, acquire wrong prefactors. The error in the WKB wave constructed via the Langer modification is asymptotically proportional to $1/(kr)$.

An alternative to the Langer modification is to retain the correct coefficient γ in the potential (2.153), and to determine the reflection phase ϕ such that the WKB wave function has the correct phase asymptotically. Comparing (2.156) and (2.157) shows that the appropriate choice for the reflection phase in this case is

$$\phi = \frac{\pi}{2} + \left(\sqrt{\gamma + \frac{1}{4}} - \sqrt{\gamma}\right)\pi. \tag{2.159}$$

With the reflection phase given by (2.159), all terms up to and including $1/(kr)^2$ in the WKB wave function (2.157) agree in amplitude and phase with the corresponding terms in the exact wave function (2.156); the error in the WKB wave function decays asymptotically as $1/(kr)^3$, which agrees with the observation made after Eq. (2.152) above and is two orders better than with the Langer modification. For s-waves ($l = 0$), the prescription (2.159) gives $\phi = \pi$, in agreement with the discussion in the paragraph after Eq. (2.151).

Now consider a general repulsive inverse-power potential,

$$V_\alpha^{\text{rep}}(r) = \frac{C_\alpha}{r^\alpha} = \frac{\hbar^2}{2\mu}\frac{(\beta_\alpha)^{\alpha-2}}{r^\alpha}, \quad \alpha \neq 2. \tag{2.160}$$

In the second expression on the right-hand side of (2.160), the strength parameter C_α is expressed via a quantum mechanical length $\beta_\alpha = (2\mu C_\alpha/\hbar^2)^{1/(\alpha-2)}$, which does not exist in classical mechanics. In terms of the scaled coordinate $\rho = kr$, the Schrödinger equation with the potential (2.160) reads,

$$-\frac{\mathrm{d}^2 u}{\mathrm{d}\rho^2} + \left(\frac{\rho_{\text{ctp}}}{\rho}\right)^\alpha u(\rho) = u(\rho). \tag{2.161}$$

The quantum mechanical properties of the potential (2.160) depend not on energy E (or wave number k) and strength parameter C_α (or characteristic quantum length β_α) independently, but only on the dimensionless product $k\beta_\alpha$, which enters Eq. (2.161) via the *reduced* or *scaled classical turning point* ρ_{ctp},

$$\rho_{\text{ctp}} = kr_{\text{ctp}} = (k\beta_\alpha)^{1-2/\alpha}, \quad k\beta_\alpha = \rho_{\text{ctp}}^{\alpha/(\alpha-2)}. \tag{2.162}$$

Table 2.1 Conditions for the semiclassical and the anticlassical, extreme quantum limit of the Schrödinger equation with a repulsive inverse-power potential C_α/r^α, cf. (2.153), (2.160)

	Semiclassical limit			Anticlassical, extreme quantum limit		
$\alpha > 2$	$E \to \infty$	$C_\alpha \to \infty$	$\beta_\alpha \to \infty$	$E \to 0$	$C_\alpha \to 0$	$\beta_\alpha \to 0$
$\alpha = 2$		$C_2 \to \infty$	$\gamma \to \infty$		$C_2 \to 0$	$\gamma \to 0$
$0 < \alpha < 2$	$E \to 0$	$C_\alpha \to \infty$	$\beta_\alpha \to 0$	$E \to \infty$	$C_\alpha \to 0$	$\beta_\alpha \to \infty$

The scaled classical turning point can be seen as a typical classical action, namely $p_\infty r_{\mathrm{ctp}} = \hbar k r_{\mathrm{ctp}}$ in units of Planck's constant $\hbar$. The limit $\rho_{\mathrm{ctp}} \to \infty$ thus corresponds to the *semiclassical limit* of large actions, while $\rho_{\mathrm{ctp}} \to 0$ represents the *anticlassical, extreme quantum limit* of small actions for the Schrödinger equation (2.161).

For $\alpha > 2$, the power $1 - 2/\alpha$ in (2.162) is positive, and the semiclassical limit corresponds to the limit of high energies (or wave numbers). For $0 < \alpha < 2$, however, the power $1 - 2/\alpha$ is negative, and the semiclassical limit is towards threshold, $k \to 0$, whereas the high-energy limit $k \to \infty$ defines the anticlassical, extreme quantum limit. Coulomb potentials, for which $\alpha = 1$, are unusual in that the semiclassical limit is towards threshold $E = 0$, while the anticlassical, extreme quantum limit, is at high energies. For the inverse-square potential (2.153), the scaled classical turning point $kr_{\mathrm{ctp}} = \sqrt{\gamma}$ does not depend on energy. A semiclassical limit is reached neither for $k \to \infty$ nor for $k \to 0$, but for $\gamma \to \infty$ corresponding to a large strength coefficient of the potential term in the Schrödinger equation. A large strength coefficient C_α of the potential also defines the semiclassical limit for inverse-power potentials (2.160) with $\alpha \neq 2$. This is obviously so for $\alpha > 2$, where large values of $(k\beta_\alpha)^{1-2/\alpha}$ are reached for large k and/or large β_α, and it also holds for $0 < \alpha < 2$, where $C_\alpha \propto 1/(\beta_\alpha)^{2-\alpha}$ and the semiclassical limit is reached for $(k\beta_\alpha)^{(2-\alpha)/\alpha} \to 0$. A summary of the conditions for the semiclassical and the anticlassical, extreme quantum limit of the Schrödinger equation with a repulsive inverse-power potential C_α/r^α is given in Table 2.1. Analogous results are derived in Appendix A.2 for homogeneous potentials in general.

For the inverse-power potential $V_\alpha = C_\alpha/r^\alpha$, the local de Broglie wavelength becomes proportional to $r^{\alpha/2}$ for $r \to 0$, so both contributions to the quantality function (2.139) are proportional to $r^{\alpha-2}$ in this limit. For $\alpha > 2$, the WKB approximation becomes increasingly accurate with decreasing r and it becomes exact in the limit $r \to 0$. The small-r behaviour of the regular solution of the Schrödinger equation with the inverse-power potential (2.161) is thus, for $\alpha > 2$, correctly given by the WKB expression,

$$u(r) \overset{r\to 0}{\propto} r^{\alpha/4} \exp\left[-\frac{2}{\alpha-2}\left(\frac{\beta_\alpha}{r}\right)^{(\alpha-2)/2}\right], \quad \alpha > 2, \tag{2.163}$$

see also Eq. (2.183) below.

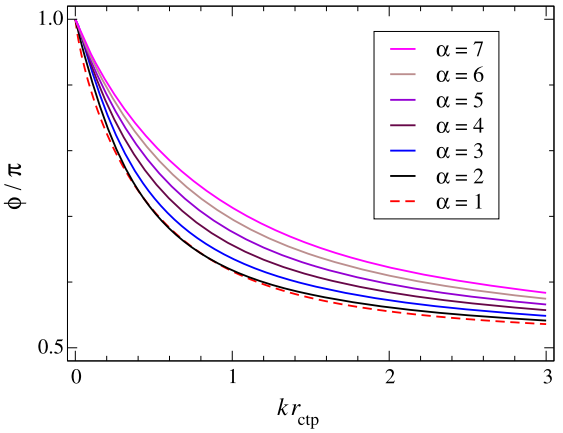

Fig. 2.16 Reflection phase ϕ for repulsive inverse-power potentials (2.160) as function of the scaled classical turning point $\rho_{\rm ctp} = kr_{\rm ctp}$. The reflection phase is defined by the requirement that the WKB wave function (2.143) be asymptotically in phase with the regular solution of the Schrödinger equation (2.161). For the inverse-square potential (2.153), the scaled classical turning point is $\sqrt{\gamma}$ and is independent of energy; ϕ is given analytically by Eq. (2.159) in this case. For $\alpha > 2$, the semiclassical limit $\rho_{\rm ctp} \to \infty$ corresponds to the high-energy limit $k \to \infty$ according to (2.162), and the anticlassical, extreme quantum limit $\rho_{\rm ctp} \to 0$ is towards threshold, $k \to 0$. For $\alpha = 1$, the reverse is true. The reflection phase (*red dashed line*) is given analytically by Eq. (2.167) in this case. (Adapted from [47])

For $\alpha > 1$, the action integral appearing in the WKB wave function (2.143) on the classically allowed side of the turning point is, expressed in the scaled coordinate $\rho = kr$,

$$\int_{\rho_{\rm ctp}}^{\rho} \sqrt{1 - \left(\frac{\rho_{\rm ctp}}{\rho'}\right)^{\alpha}}\, {\rm d}\rho' \overset{\rho\to\infty}{\sim} \rho - \rho_{\rm ctp} \frac{\sqrt{\pi}}{2} \frac{\Gamma(1-\frac{1}{\alpha})}{\Gamma(\frac{3}{2}-\frac{1}{\alpha})} + O\left(\left[\frac{\rho_{\rm ctp}}{\rho}\right]^{\alpha-1}\right). \quad (2.164)$$

The appropriate reflection phase ϕ, with which the asymptotic phase of the WKB wave function agrees with the phase of the regular solution of the Schrödinger equation, is obtained by comparing the WKB wave function (2.143) with the exact solution $u^{\rm reg}$. The results based on a numerical solution of the Schrödinger equation are shown as function of $\rho_{\rm ctp} = kr_{\rm ctp} = (k\beta_\alpha)^{1-2/\alpha}$ in Fig. 2.16 for $\alpha = 3$ to $\alpha = 7$, together with the reflection phase (2.159) for the inverse-square potential (2.153) as function of $kr_{\rm ctp} = \sqrt{\gamma}$.

For $\alpha = 1$, $\rho_{\rm ctp} = 1/(k\beta_1)$ and Eq. (2.164) is replaced by

$$\int_{\rho_{\rm ctp}}^{\rho} \sqrt{1 - \frac{\rho_{\rm ctp}}{\rho'}}\, {\rm d}\rho' \overset{\rho\to\infty}{\sim} \rho - \frac{\rho_{\rm ctp}}{2}\big[1 + \ln(4\rho) - \ln(\rho_{\rm ctp})\big]. \quad (2.165)$$

The regular solution of (2.161) is a Coulomb function [see Sect. 2.5.1 and, in particular, Eq. (2.200) below] whose asymptotic behaviour is,

$$u^{\mathrm{reg}}(\rho) \overset{\rho\to\infty}{\sim} \cos\left(\rho - \frac{\rho_{\mathrm{ctp}}}{2}\ln(2\rho) - \frac{\pi}{2} + \sigma_0\right), \quad \sigma_0 = \arg\left[\Gamma\left(1 + \mathrm{i}\frac{\rho_{\mathrm{ctp}}}{2}\right)\right]. \tag{2.166}$$

The reflection phase for $\alpha = 1$ is thus

$$\phi = \pi - \rho_{\mathrm{ctp}}\left[1 - \ln(\rho_{\mathrm{ctp}}/2)\right] - 2\sigma_0. \tag{2.167}$$

The reflection phase (2.167) as function of $\rho_{\mathrm{ctp}} = kr_{\mathrm{ctp}}$ is included as dashed red line in Fig. 2.16.

Figure 2.16 shows that the reflection phases only reach the value $\frac{\pi}{2}$, as expected from the linear approximation of the potential, in the semiclassical limit $\rho_{\mathrm{ctp}} \to \infty$. For decreasing values of ρ_{ctp}, the reflection phases increase monotonically and reach the value π in the anticlassical limit $\rho_{\mathrm{ctp}} \to 0$. The leading behaviour of ϕ near the semiclassical limit is [47],

$$\phi \overset{\rho_{\mathrm{ctp}}\to\infty}{\sim} \frac{\pi}{2} + \frac{\sqrt{\pi}}{\rho_{\mathrm{ctp}}}\frac{(\alpha+1)\Gamma(\frac{1}{\alpha})}{12\alpha\Gamma(\frac{1}{2}+\frac{1}{\alpha})} + O\left(\frac{1}{(\rho_{\mathrm{ctp}})^3}\right). \tag{2.168}$$

This equation holds for all powers $\alpha > 0$. Remember, however, that for $\alpha < 2$ the semiclassical limit $\rho_{\mathrm{ctp}} \to \infty$ corresponds to $k \to 0$.

In the anticlassical, extreme quantum limit, we have [18]

$$\phi \overset{\rho_{\mathrm{ctp}}\to 0}{\sim} \pi - \sqrt{\pi}\frac{\Gamma(1-\frac{1}{\alpha})}{\Gamma(\frac{3}{2}-\frac{1}{\alpha})}\rho_{\mathrm{ctp}} + 2\nu^{2\nu}\frac{\Gamma(1-\nu)}{\Gamma(1+\nu)}k\beta_\alpha \quad \text{for } \nu = \frac{1}{\alpha-2} < 1. \tag{2.169}$$

The restriction $\nu < 1$ implies $\alpha > 3$; the threshold $k \to 0$ corresponds to the anticlassical limit in these cases.

2.4.3 WKB Phase Shifts

At a given energy $E = \hbar^2k^2/(2\mu)$, the radial Schrödinger equation (2.35) with the effective potential $V_{\mathrm{eff}}(r) = V(r) + l(l+1)\hbar^2/(2\mu r^2)$ features an outermost classical turning point r_{ctp}, which may be at the origin in case $E > V_{\mathrm{eff}}(r)$ for all $r > 0$. The WKB wave function in the classically allowed region beyond r_{ctp} in the partial wave l has the form (2.143),

$$u_l^{\mathrm{WKB}}(r) \propto \frac{1}{\sqrt{p_l(r)}}\cos\left(\frac{1}{\hbar}\int_{r_{\mathrm{ctp}}}^{r} p_l(r')\mathrm{d}r' - \frac{\phi}{2}\right). \tag{2.170}$$

The local classical momentum $p_l(r)$ carries the subscript l to remind us that its definition explicitly includes the centrifugal potential,

$$p_l(r) = \sqrt{2\mu\left[E - V(r) - \frac{l(l+1)\hbar^2}{2\mu r^2}\right]}. \tag{2.171}$$

We assume that the potential $V(r)$ falls off faster than $1/r^2$ at large distances, so the asymptotic behaviour of the regular solution of the radial Schrödinger equation (2.35) is

$$u_l(r) \overset{r\to\infty}{\propto} \sin\left(kr - l\frac{\pi}{2} + \delta_l\right). \tag{2.172}$$

Comparing this with the asymptotic behaviour of the WKB wave function (2.170) establishes a relation between the reflection phase ϕ at the outermost classical turning point and the scattering phase shift δ_l,

$$\begin{aligned}\delta_l &= l\frac{\pi}{2} + \frac{\pi}{2} - \frac{\phi}{2} + \lim_{r\to\infty}\frac{1}{\hbar}\left(\int_{r_{\mathrm{ctp}}}^{r} p_l(r')\mathrm{d}r' - kr\right)\\ &= (l+1)\frac{\pi}{2} - \frac{\phi}{2} + \frac{1}{\hbar}\int_{r_{\mathrm{ctp}}}^{\infty}\big[p_l(r) - \hbar k\big]\mathrm{d}r - kr_{\mathrm{ctp}}.\end{aligned} \tag{2.173}$$

By definition, the correct reflection phase ϕ yields the correct scattering phase shift δ_l via (2.173). A semiclassical approximation δ_l^{WKB} to the scattering phase shift is obtained by inserting $\frac{\pi}{2}$ for ϕ according to (2.145) and invoking the Langer modification (2.158), i.e. replacing $\sqrt{l(l+1)}$ by $l + \frac{1}{2} \equiv l'$ for the evaluation of the action integral in (2.173),

$$\delta_l^{\mathrm{WKB}} = l'\frac{\pi}{2} + \frac{1}{\hbar}\int_{r_{\mathrm{ctp}}}^{\infty}\left(\sqrt{2\mu\big[E - V(r)\big] - \big(l'\big)^2\hbar^2/r^2} - \hbar k\right)\mathrm{d}r - kr_{\mathrm{ctp}}. \tag{2.174}$$

Equation (2.174) represents the conventional WKB approximation for the scattering phase shift in the partial wave l. For potentials $V(r)$ falling off faster than $1/r^2$ at large distances, it can be expected to become increasingly accurate for large l, because the centrifugal potential becomes increasingly dominant.

Since the right-hand side of (2.174) contains an explicit functional dependence on the angular momentum quantum number l, or rather on $l' = l + \frac{1}{2}$, we can pretend that the angular momentum quantum number is a continuous variable and evaluate the derivative of the phase shift with respect to this variable,

$$\frac{\mathrm{d}\delta_l^{\mathrm{WKB}}}{\mathrm{d}l} = \frac{\pi}{2} - \int_{r_{\mathrm{ctp}}}^{\infty}\frac{1}{r^2}\frac{l'\hbar}{\sqrt{2\mu[E - V(r)] - (l')^2\hbar^2/r^2}}\mathrm{d}r. \tag{2.175}$$

Due to the variation of r_{ctp} with l, the derivative of the integral in (2.174) contains a term corresponding to minus the integrand at r_{ctp} times $\mathrm{d}r_{\mathrm{ctp}}/\mathrm{d}l$. Since the square

root vanishes at $r_{\rm ctp}$ by definition of the classical turning point, this term reduces to $k\mathrm{d}r_{\rm ctp}/\mathrm{d}l$, which cancels with the l-derivative of the last term $-kr_{\rm ctp}$ on the right-hand side of (2.174).

From a (semi-)classical point of view, it is natural to identify the quantity $l'\hbar$ with the classical orbital angular momentum L, whereby the right-hand side of (2.175) turns out to be half the classical deflection function as defined in Eq. (1.16) in Sect. 1.2:

$$\Theta(L) = 2\frac{\mathrm{d}\delta_l^{\rm WKB}}{\mathrm{d}l}, \quad L = \left(l + \frac{1}{2}\right)\hbar. \tag{2.176}$$

This relation connects the quantum mechanical phase shifts to the classical trajectories labelled by an impact parameter b corresponding to angular momentum $L = b\sqrt{2\mu E}$. For potentials falling off faster than $1/r^2$ at large distances, the approximations involved, i.e. the WKB approximation with Langer modification and the assumption of a continuous angular momentum quantum number, can be expected to be increasingly reliable for large angular momenta corresponding to large impact parameters, i.e. for *peripheral scattering*.

At the other limit, i.e. for s-waves ($l = 0$), the conventional WKB approximation can not be expected to work well. The relation (2.173) connecting the phase shift with the reflection phase at the outer classical turning point is, however, always valid. For the repulsive inverse-power potentials (2.160), we observe that

$$\frac{1}{\hbar}\int_{r_{\rm ctp}}^{r} p_{l=0}(r')\mathrm{d}r' \overset{r\to\infty}{\sim} kr - kr_{\rm ctp}\frac{\sqrt{\pi}}{2}\frac{\Gamma(1-\frac{1}{\alpha})}{\Gamma(\frac{3}{2}-\frac{1}{\alpha})} + O\left(\left[\frac{r_{\rm ctp}}{r}\right]^{\alpha-1}\right) \tag{2.177}$$

according to (2.164). The s-wave phase shift for scattering by the repulsive inverse-power potential (2.160) is thus related to the reflection phase ϕ by

$$\delta_{l=0} = -\rho_{\rm ctp}\frac{\sqrt{\pi}}{2}\frac{\Gamma(1-\frac{1}{\alpha})}{\Gamma(\frac{3}{2}-\frac{1}{\alpha})} - \frac{\phi}{2} + \frac{\pi}{2}. \tag{2.178}$$

Inserting the high-$\rho_{\rm ctp}$ expansion (2.168) for the reflection phase gives the appropriate limiting behaviour of the phase shift,

$$\delta_{l=0} \overset{\rho_{\rm ctp}\to\infty}{\sim} -\rho_{\rm ctp}\frac{\sqrt{\pi}}{2}\frac{\Gamma(1-\frac{1}{\alpha})}{\Gamma(\frac{3}{2}-\frac{1}{\alpha})} + \frac{\pi}{4} + O\left(\frac{1}{\rho_{\rm ctp}}\right). \tag{2.179}$$

For $\alpha > 2$, Eq. (2.179) describes the high-energy limit of the phase shift.

When inserting the near-threshold expansion (2.169) for the reflection phase in (2.173), the first two terms from $-\phi/2$ cancel the constant term $\frac{\pi}{2}$ and the contribution from the action integral leaving

$$\delta_{l=0} \overset{k\to 0}{\sim} -\nu^{2\nu}\frac{\Gamma(1-\nu)}{\Gamma(1+\nu)}k\beta_\alpha, \quad \nu = \frac{1}{\alpha-2} < 1. \tag{2.180}$$

Table 2.2 Scattering lengths (2.181) for repulsive inverse-power potentials (2.160) in units of β_α

α	4	5	6	7	8	$\alpha \to \infty$
a/β_α	1	0.729011	0.675978	0.666083	0.669594	1

We thus have an explicit expression for the scattering length for repulsive inverse-power potentials (2.160) with $\alpha > 3$,

$$a = \nu^{2\nu} \frac{\Gamma(1-\nu)}{\Gamma(1+\nu)} \beta_\alpha. \tag{2.181}$$

Note that the leading near-threshold energy dependence of the reflection phase, contained in the term proportional to $\rho_{\text{ctp}} = (k\beta_\alpha)^{1-2/\alpha}$, is of lower order than k, but since this term cancels with the leading energy-dependent contribution from the WKB action integral, the leading contribution to $\delta_{l=0}$ is actually proportional to k, in accordance with Wigner's threshold law.

Equations (2.180) and (2.181) can also be derived directly from the zero-energy solution of the radial Schrödinger equation (2.35). For the repulsive inverse-power potential (2.160), the regular s-wave solution is

$$u^{(0)}_{l=0}(r) \propto \sqrt{\frac{r}{\beta_\alpha}} K_\nu\left(2\nu\left(\frac{\beta_\alpha}{r}\right)^{1/(2\nu)}\right), \tag{2.182}$$

where K_ν is a modified Bessel function [1], see Appendix B.4. The large-argument behaviour K_ν gives the small-r behaviour of $u^{(0)}_{l=0}(r)$,

$$u^{(0)}_{l=0}(r) \overset{r\to 0}{\propto} \left(\frac{r}{\beta_\alpha}\right)^{\alpha/4} \mathrm{e}^{-2\nu(\beta_\alpha/r)^{1/(2\nu)}}. \tag{2.183}$$

For any $\alpha > 2 \Leftrightarrow \nu > 0$, this agrees with the WKB result (2.163). The asymptotic ($r \to \infty$) behaviour of $u^{(0)}_{l=0}(r)$ follows from the small-argument behaviour of K_ν,

$$u^{(0)}_{l=0}(r) \overset{r\to\infty}{\propto} \frac{\nu^{-\nu}}{\Gamma(1-\nu)} \frac{r}{\beta_\alpha} - \frac{\nu^{\nu}}{\Gamma(1+\nu)} + O\left(\left(\frac{\beta_\alpha}{r}\right)^{\alpha-3}\right). \tag{2.184}$$

For $\nu < 1 \Leftrightarrow \alpha > 3$, this agrees with (2.83) when the scattering length is given by (2.181). For repulsive inverse-power potentials (2.160) with $\alpha > 3$, the scattering length (2.181) scales with the characteristic quantum length β_α; the prefactor depends on the power α and is in general close to unity. Numerical values of the scattering length in units of β_α are given for $\alpha = 4, \ldots, 8$ in Table 2.2.

2.5 Coulombic Potentials

The previous sections of this chapter were mainly concerned with potentials $V(r)$ which vanish faster than $1/r^2$ at large distances, i.e. faster than the centrifugal po-

tential in the radial Schrödinger equation. The scattering problem is qualitatively different for potentials which fall off slower than $1/r^2$. This includes the important class of the Coulombic potentials, which are asymptotically proportional to $1/r$ and describe the interaction between two electrically charged particles. The present section starts with the description of scattering by a pure Coulomb potential, which is proportional to $1/r$ in the whole range of distances from $r \to 0$ to $r \to \infty$. The subsequent subsections treat modified Coulomb potentials, which are proportional to $1/r$ at large distances but deviate from the pure Coulomb shape at small distances.

2.5.1 Pure Coulomb Potential

The strength parameter C of a pure Coulomb potential,

$$V(r) = \frac{C}{r}, \tag{2.185}$$

has the physical dimension energy$\times$length and is generally given by $C = \pm Z_1 Z_2 e^2$, where $Z_1 e$ and $Z_2 e$ are the charges of projectile and target, respectively. Rewriting the Schrödinger equation (2.1) in terms of the scaled coordinate $\boldsymbol{\rho} = k\mathbf{r}$,

$$\left[-\Delta_{\boldsymbol{\rho}} + \frac{2\eta}{\rho}\right]\psi = \psi, \tag{2.186}$$

shows that the influence of the Coulomb potential is quantitatively expressed via the dimensionless *Sommerfeld parameter*,

$$\eta = \frac{\mu C}{\hbar^2 k}, \tag{2.187}$$

which corresponds to the ratio of C to $2E/k = \hbar\upsilon$. The Sommerfeld parameter (2.187) is positive for repulsive and negative for attractive Coulomb potentials. It is related to a quantum mechanical length scale a_C, which does not exist in classical mechanics,

$$a_C = \frac{1}{|\eta| k} = \frac{\hbar^2}{\mu |C|}, \quad |\eta| = \frac{1}{a_C k}. \tag{2.188}$$

For an attractive Coulomb potential, $C < 0$, a_C is the *Bohr radius*, which describes the spatial extension of the ground-state wave function in the potential (2.185). For a repulsive Coulomb potential, $C \equiv C_1 > 0$, $a_C = 2\beta_1$, where β_1 is the characteristic quantum length introduced in Eq. (2.160), and η is related to the scaled classical turning point of the s-wave radial Schrödinger equation [cf. Eq. (2.161)] via

$$2\eta = \rho_{\mathrm{ctp}} = k r_{\mathrm{ctp}} = (k\beta_1)^{-1}. \tag{2.189}$$

The stationary Schrödinger equation (2.186) has an analytical solution[4] ψ_{C}, whose asymptotic behaviour comes close to the expression (2.2) on which the description of scattering has so far been based, namely

$$\psi_{\mathrm{C}}(\mathbf{r}) = \mathrm{e}^{-\frac{\pi}{2}\eta}\Gamma(1+\mathrm{i}\eta)\mathrm{e}^{\mathrm{i}kz}F\big(-\mathrm{i}\eta, 1; \mathrm{i}k[r-z]\big). \tag{2.190}$$

Here F is the confluent hypergeometric function, which is defined and discussed in Appendix B.5. For large values of $k(r-z)$, the wave function (2.190) behaves as

$$\begin{aligned}\psi_{\mathrm{C}}(\mathbf{r}) = {} & \mathrm{e}^{\mathrm{i}[kz+\eta\ln(k[r-z])]}\left[1+\frac{\eta^2}{\mathrm{i}k[r-z]}+\cdots\right] \\ & + f_{\mathrm{C}}(\theta)\frac{\mathrm{e}^{\mathrm{i}(kr-\eta\ln 2kr)}}{r}\left[1+\frac{(1+\mathrm{i}\eta)^2}{\mathrm{i}k[r-z]}+\cdots\right];\end{aligned} \tag{2.191}$$

the function $f_{\mathrm{C}}(\theta)$ is the *Coulomb scattering amplitude*,

$$f_{\mathrm{C}}(\theta) = \frac{-\eta}{2k\sin^2(\theta/2)}\mathrm{e}^{-\mathrm{i}(\eta\ln[\sin^2(\theta/2)]-2\sigma_0)}, \quad \sigma_0 = \arg\big[\Gamma(1+\mathrm{i}\eta)\big]. \tag{2.192}$$

For $r\to\infty$, the term on the upper line of Eq. (2.191) resembles a plane wave except in forward direction where $r-z=0$. The additional term following $\mathrm{i}kz$ in the exponent is logarithmic in $\rho = kr$, i.e. of order ρ^0, and its derivative with respect to r or ρ introduces a factor of order ρ^{-1}, which can be neglected asymptotically. Similar arguments apply for the outgoing spherical wave in the lower line of Eq. (2.191). The asymptotic expressions for the current densities, which are used to define scattering cross sections as in Sect. 2.1, are thus obtained via the leading terms, $\mathrm{i}kz$ and $\mathrm{i}kr$, in the respective exponents, yielding

$$\begin{aligned}\mathbf{j}_{\mathrm{in}}(\mathbf{r}) &\overset{kr\to\infty}{\sim} \frac{\hbar k}{\mu}\mathbf{e}_z + O\left(\frac{1}{r}\right), \\ \mathbf{j}_{\mathrm{out}}(\mathbf{r}) &\overset{kr\to\infty}{\sim} \frac{\hbar k}{\mu}\big|f_{\mathrm{C}}(\theta)\big|^2\frac{\mathbf{e}_{\mathbf{r}}}{r^2} + O\left(\frac{1}{r^3}\right).\end{aligned} \tag{2.193}$$

Just as in Eq. (2.5) in Sect. 2.1, the differential scattering cross section is given by the absolute square of the scattering amplitude which, in this case, is the Coulomb scattering amplitude (2.192),

$$\frac{\mathrm{d}\sigma}{\mathrm{d}\Omega} = \big|f_{\mathrm{C}}(\theta)\big|^2 = \frac{\eta^2}{4k^2}\frac{1}{\sin^4(\theta/2)} = \left(\frac{C}{4E}\right)^2\frac{1}{\sin^4(\theta/2)} = \left(\frac{\mathrm{d}\sigma}{\mathrm{d}\Omega}\right)_{\mathrm{Ruth}}. \tag{2.194}$$

The Schrödinger equation (2.186) depends explicitly on the Sommerfeld parameter η, and so it is not surprising that the Coulomb scattering amplitude (2.192) depends on η. The modulus of f_{C} does not depend on k and η independently, but

[4] For a detailed but compact derivation of Eqs. (2.190)–(2.192), see Sect. 14.6.1 of [33].

only on the ratio $\eta/2k$, which is equal to $C/(4E)$. The quantum mechanical result (2.194) is actually identical to the classical differential cross section (1.42) for scattering by a Coulomb potential. This is an unusual coincidence and peculiar to the scattering problem in three dimensions. For a potential of the form (2.185) in two spatial dimensions, the quantum mechanical cross section is not identical to the classical result (1.55), as discussed later in Sect. 4.3.6 in Chap. 4.

A further remarkable coincidence related to Coulomb scattering in three spatial dimensions is provided by the Born approximation. Although the condition $E \gg V(r)$ cannot be fulfilled for the Coulomb potential, a naïve implementation of Eq. (2.22) with the Coulomb potential (2.185) yields

$$f_{\mathrm{C}}^{\mathrm{Born}}(\theta) = -\frac{\mu}{2\pi\hbar^2}\int \mathrm{e}^{-\mathrm{i}\mathbf{q}\cdot\mathbf{r}}\frac{C}{r}\mathrm{d}\mathbf{r} = -\frac{2\mu C}{\hbar^2 q^2} = -\frac{C}{4E}\frac{1}{\sin^2(\theta/2)}, \tag{2.195}$$

so the differential scattering cross section in Born approximation is,

$$\left(\frac{\mathrm{d}\sigma_{\mathrm{C}}}{\mathrm{d}\Omega}\right)^{\mathrm{Born}} = \left|f_{\mathrm{C}}^{\mathrm{Born}}(\theta)\right|^2 = \left(\frac{\mathrm{d}\sigma}{\mathrm{d}\Omega}\right)_{\mathrm{Ruth}}. \tag{2.196}$$

It is a coincidence of Coulomb scattering in three spatial dimensions, that the classical expression (1.42), the quantum mechanical expression (2.194) and the Born approximation (2.196) all yield the same result, namely the Rutherford cross section. Note, however, that the Coulomb scattering amplitude (2.195) in Born approximation is real and contains none of the phase information of the true quantum mechanical amplitude (2.192).

For the Coulomb potential (2.185), the effective potential in the partial wave l is,

$$V_{\mathrm{eff}}(r) = \frac{C}{r} + \frac{\hbar^2}{2\mu}\frac{l(l+1)}{r^2}, \tag{2.197}$$

and the radial Schrödinger equation (2.35) can be written in terms of the scaled coordinate $\rho = kr$ as

$$\left[-\frac{\mathrm{d}^2}{\mathrm{d}\rho^2} + \frac{l(l+1)}{\rho^2} + \frac{2\eta}{\rho}\right]u_l(\rho) = u_l(\rho). \tag{2.198}$$

Its (appropriately normalized) regular solution is the *regular Coulomb function* [52]

$$F_l(\eta,\rho) = 2^l \mathrm{e}^{-\frac{\pi}{2}\eta}\frac{|\Gamma(l+1+\mathrm{i}\eta)|}{(2l+1)!}\mathrm{e}^{-\mathrm{i}\rho}\rho^{l+1}F(l+1-\mathrm{i}\eta, 2l+2; 2\mathrm{i}\rho), \tag{2.199}$$

where F again stands for the confluent hypergeometric function, see Appendix B.5. For a given value of the Sommerfeld parameter η, the large-ρ behaviour of F_l is,

$$F_l(\eta,\rho) \overset{\rho\to\infty}{\sim} \sin\left(\rho - \eta\ln(2\rho) - l\frac{\pi}{2} + \sigma_l\right). \tag{2.200}$$

In addition to the terms $\rho - l\frac{\pi}{2}$ familiar from the free particle's radial wave functions introduced in Sect. 2.3.3, the argument of the sine in (2.200) contains the characteristic logarithmic term $-\eta \ln(2\rho)$ and the *Coulomb phase* σ_l,

$$\sigma_l = \arg\bigl[\Gamma(l+1+\mathrm{i}\eta)\bigr]. \tag{2.201}$$

For vanishing Sommerfeld parameter η, the regular Coulomb function (2.199) becomes the regular radial free-particle wave function $u_l^{(\mathrm{s})}(kr)$ defined in Eq. (2.38).

The *irregular* Coulomb function whose asymptotic phase differs by $\pi/2$ from that of (2.200) is called $G_l(\eta, \rho)$ [52]; it is defined as the solution of Eq. (2.198) which, for given η, behaves asymptotically (large ρ) as

$$G_l(\eta, \rho) \overset{\rho\to\infty}{\sim} \cos\left(\rho - \eta\ln(2\rho) - l\frac{\pi}{2} + \sigma_l\right). \tag{2.202}$$

An explicit expression is given in Refs. [5, 43] in terms of Whittaker functions, which can be rewritten [1] in terms of the confluent hypergeometric function $U(a, b; z)$ (see Appendix B.5),

$$\begin{aligned} G_l(\eta, \rho) &= \mathrm{i}F_l(\eta, \rho) \\ &\quad + \mathrm{e}^{\frac{\pi}{2}\eta}\frac{|\Gamma(l+1+\mathrm{i}\eta)|}{\Gamma(l+1+\mathrm{i}\eta)}\mathrm{e}^{-\mathrm{i}(\rho - l\frac{\pi}{2})}(2\mathrm{i}\rho)^{l+1}U(l+1-\mathrm{i}\eta, 2l+2; 2\mathrm{i}\rho). \end{aligned} \tag{2.203}$$

For vanishing η, the irregular Coulomb function G_l becomes the irregular radial free-particle wave function $u_l^{(\mathrm{c})}(kr)$ defined in (2.38).

The small-ρ behaviour of the regular Coulomb function is, for fixed η [1],

$$F_l(\eta, \rho) \overset{\rho\to 0}{\sim} 2^l \mathrm{e}^{-\frac{\pi}{2}\eta}\frac{|\Gamma(l+1+\mathrm{i}\eta)|}{(2l+1)!}\rho^{l+1}. \tag{2.204}$$

Exploiting the ρ-independence of the Wronskian [1],

$$\frac{\partial F_l}{\partial\rho}G_l(\eta, \rho) - \frac{\partial G_l}{\partial\rho}F_l(\eta, \rho) = 1, \tag{2.205}$$

we can derive the small-ρ behaviour of the irregular Coulomb function for fixed η,

$$G_l(\eta, \rho) \overset{\rho\to 0}{\sim} \frac{\mathrm{e}^{\frac{\pi}{2}\eta}(2l)!}{2^l|\Gamma(l+1+\mathrm{i}\eta)|}\rho^{-l}. \tag{2.206}$$

The partial-waves expansion of the Coulomb scattering amplitude is rarely used explicitly, because of its poor convergence properties [20], but it is helpful to record the partial-waves decomposition of the full wave function (2.190) [8],

$$\psi_{\mathrm{C}}(\mathbf{r}) = \sum_{l=0}^{\infty}(2l+1)\mathrm{i}^l\mathrm{e}^{\mathrm{i}\sigma_l}\frac{F_l(\eta, kr)}{kr}P_l(\cos\theta). \tag{2.207}$$

This is the Coulomb-wave analogy to the partial-wave decomposition (2.43) of the free particle's plane wave. The free particle's regular radial wave function $u_l^{(\mathrm{s})}(kr) = kr j_l(kr)$ is replaced by the regular Coulomb function $F_l(\eta, kr)$, and there is an additional phase factor $\mathrm{e}^{\mathrm{i}\sigma_l}$.

2.5.2 Modified Coulomb Potential; General Considerations

A pure Coulomb potential (2.185) describes the electrostatic interaction of two charged point particles. The more realistic case involves deviations from the pure Coulomb shape at short distances, due to the effects of finite size and/or internal structure of target and/or projectile. These deviations can be accounted for by an additional short-range potential V_{sr}, which we assume to be radially symmetric.

$$V(r) = \frac{C}{r} + V_{\mathrm{sr}}(r). \tag{2.208}$$

In a typical scattering scenario, projectile and target are well separated initially, so the incoming wave can be expected to have the same form as for the pure Coulomb potential in the upper line of Eq. (2.191). The outgoing spherical wave has an additional contribution, which has the same structure as the lower line of (2.191), but is due to the additional short-range potential V_{sr}. The scattering process is thus described by solutions of the Schrödinger equation (2.1) which have the following asymptotic behaviour:

$$\begin{aligned}\psi(\mathbf{r}) &\overset{r\to\infty}{\sim} \psi_{\mathrm{C}}(\mathbf{r}) + \tilde{f}(\theta)\frac{\mathrm{e}^{\mathrm{i}(kr-\eta\ln 2kr)}}{r} \\ &\overset{r\to\infty}{\sim} \mathrm{e}^{\mathrm{i}[kz+\eta\ln(k[r-z])]} + \left[f_{\mathrm{C}}(\theta) + \tilde{f}(\theta)\right]\frac{\mathrm{e}^{\mathrm{i}(kr-\eta\ln 2kr)}}{r}.\end{aligned} \tag{2.209}$$

Here $\tilde{f}$ is an additional scattering amplitude due to the additional short-range potential V_{sr}. Since the total scattering amplitude is the sum of the Coulomb scattering amplitude (2.192) and the additional scattering amplitude $\tilde{f}$, the differential scattering cross section is

$$\frac{\mathrm{d}\sigma}{\mathrm{d}\Omega} = \left|f_{\mathrm{C}}(\theta) + \tilde{f}(\theta)\right|^2 = \left(\frac{\mathrm{d}\sigma}{\mathrm{d}\Omega}\right)_{\mathrm{Ruth}} + \left|\tilde{f}(\theta)\right|^2 + f_{\mathrm{C}}^*(\theta)\tilde{f}(\theta) + f_{\mathrm{C}}(\theta)\tilde{f}^*(\theta). \tag{2.210}$$

Apart from the Rutherford scattering cross section and the modulus squared of the additional scattering amplitude $\tilde{f}$, the differential cross section (2.210) also contains interference terms. Note that $\tilde{f}$ is *not* the scattering amplitude for scattering by the short-range potential alone.

The partial-waves expansion of the full wave function $\psi(\mathbf{r})$ is as expressed by Eq. (2.33). The effective potential in the partial wave l is,

$$V_{\mathrm{eff}}(r) = \frac{C}{r} + V_{\mathrm{sr}}(r) + \frac{\hbar^2}{2\mu}\frac{l(l+1)}{r^2}, \tag{2.211}$$

and the radial wave functions $u_l(r)$ are regular solutions of the radial Schrödinger equation,

$$\left[\frac{\hbar^2}{2\mu}\left(-\frac{\mathrm{d}^2 u_l}{\mathrm{d}r^2}+\frac{l(l+1)}{r^2}+\frac{2\eta k}{r}\right)+V_{\mathrm{sr}}(r)\right]u_l(r)=Eu_l(r)=\frac{\hbar^2k^2}{2\mu}u_l(r). \quad (2.212)$$

Beyond the range of V_{sr}, the radial Schrödinger equation (2.212) is as for a pure Coulomb potential, so the regular radial wave function becomes a superposition of the regular and irregular Coulomb wave functions introduced in Sect. 2.5.1,

$$u_l(r)\overset{r\to\infty}{\sim} AF_l(\eta,kr)+BG_l(\eta,kr)\overset{kr\to\infty}{\propto}\sin\left(kr-\eta\ln(2kr)-l\frac{\pi}{2}+\sigma_l+\tilde{\delta}_l\right), \quad (2.213)$$

with $\tan\tilde{\delta}_l = B/A$. The additional asymptotic phase shifts $\tilde{\delta}_l$ now account for the influence of the short-range potential V_{sr} on the asymptotic behaviour of the radial wave functions. Note that the phases $\tilde{\delta}_l$ are *not* the scattering phase shifts for the short-range potential V_{sr} alone, i.e. in the absence of the Coulomb potential.

A partial-waves expansion may not be practicable for the Coulomb scattering amplitude f_{C}, which is known analytically anyhow, but it does make sense for the additional amplitude $\tilde{f}$, which is due to the additional short-range potential and can be expected to have better convergence properties,

$$\tilde{f}(\theta)=\sum_{l=0}^{\infty}\tilde{f}_l P_l(\cos\theta). \quad (2.214)$$

The representation (2.207) of the Coulomb wave function ψ_{C} can be used to express the asymptotic form of the full wave function, as given in the upper line of (2.209), in the form (2.33). This gives an explicit expression for the asymptotic behaviour of the radial wave functions,

$$\begin{aligned}
u_l(r) &\overset{r\to\infty}{\sim} \mathrm{i}^l\frac{2l+1}{k}\mathrm{e}^{\mathrm{i}\sigma_l}\sin\left(kr-\eta\ln(2kr)-l\frac{\pi}{2}+\sigma_l\right)+\tilde{f}_l\mathrm{e}^{\mathrm{i}(kr-\eta\ln(2kr))}\\
&= \mathrm{i}^l\left[\frac{2l+1}{k}\mathrm{e}^{\mathrm{i}\sigma_l}\sin\left(kr-\eta\ln(2kr)-l\frac{\pi}{2}+\sigma_l\right)\right.\\
&\quad \left.+\tilde{f}_l\mathrm{e}^{-\mathrm{i}\sigma_l}\mathrm{e}^{\mathrm{i}(kr-\eta\ln(2kr)-l\frac{\pi}{2}+\sigma_l)}\right]\\
&= \mathrm{i}^l\left[\left(\frac{2l+1}{k}\mathrm{e}^{\mathrm{i}\sigma_l}+\mathrm{i}\tilde{f}_l\mathrm{e}^{-\mathrm{i}\sigma_l}\right)\sin\left(kr-\eta\ln(2kr)-l\frac{\pi}{2}+\sigma_l\right)\right.\\
&\quad \left.+\tilde{f}_l\mathrm{e}^{-\mathrm{i}\sigma_l}\cos\left(kr-\eta\ln(2kr)-l\frac{\pi}{2}+\sigma_l\right)\right]. \quad (2.215)
\end{aligned}$$

Comparing Eqs. (2.215) and (2.213) shows that

$$\cot\tilde{\delta}_l=\frac{A}{B}=\frac{2l+1}{k\tilde{f}_l}\mathrm{e}^{2\mathrm{i}\sigma_l}+\mathrm{i}\quad\Rightarrow\quad\cot\tilde{\delta}_l-\mathrm{i}=\frac{\mathrm{e}^{-\mathrm{i}\tilde{\delta}_l}}{\sin\tilde{\delta}_l}=\frac{2l+1}{k\tilde{f}_l}\mathrm{e}^{2\mathrm{i}\sigma_l}, \quad (2.216)$$

similar to the result (2.46) derived for potentials falling off faster than $1/r^2$. For the partial-wave amplitudes $\tilde{f}_l$ due to the short-range potential V_{sr} in the presence of a Coulomb potential we obtain

$$\tilde{f}_l = \frac{2l+1}{k} \mathrm{e}^{2\mathrm{i}\sigma_l} \mathrm{e}^{\mathrm{i}\tilde{\delta}_l} \sin\tilde{\delta}_l = \frac{2l+1}{2\mathrm{i}k} \mathrm{e}^{2\mathrm{i}\sigma_l} \left(\mathrm{e}^{2\mathrm{i}\tilde{\delta}_l} - 1\right), \tag{2.217}$$

where $\tilde{\delta}_l$ now stands for the additional asymptotic phase shift due to the short-range modification of the Coulomb potential.

So the partial-waves method can be used to obtain differential scattering cross sections for a Coulomb potential modified at small distances. The additional phase shifts $\tilde{\delta}_l$, relative to the pure Coulomb case, are obtained by integrating the radial Schrödinger equation (2.212) and matching the regular solution $u_l(r)$ to a superposition (2.213) of regular and irregular Coulomb functions at some distance beyond the range of the short-range potential V_{sr}. The additional scattering amplitude (2.214), with partial-wave amplitudes $\tilde{f}_l$ given by (2.217) is then inserted into the expression (2.210). Note that the integrated elastic scattering cross section σ diverges in the presence of a Coulomb potential because of the $1/\sin^4(\theta/2)$ behaviour of the differential cross section towards forward directions.

For the effective potential (2.211), a Lippmann–Schwinger equation focussing on the effect of the additional short-range potential V_{sr} can be derived by rewriting the radial Schrödinger equation (2.212) as

$$\left[E + \frac{\hbar^2}{2\mu}\left(\frac{\mathrm{d}^2}{\mathrm{d}r^2} - \frac{l(l+1)}{r^2} - \frac{2\eta k}{r}\right)\right] u_l(r) = V_{\mathrm{sr}}(r) u_l(r). \tag{2.218}$$

Adapting the treatment discussed for potentials falling off faster than $1/r^2$ in Sect. 2.3.5 to the present case, we can transform Eq. (2.218) into an integral equation with the help of the *radial Coulomb Green's function*, $\mathscr{G}_l^{\mathrm{C}}(r, r')$, which fulfills

$$\left[E + \frac{\hbar^2}{2\mu}\left(\frac{\mathrm{d}^2}{\mathrm{d}r^2} - \frac{l(l+1)}{r^2} - \frac{2\eta k}{r}\right)\right] \mathscr{G}_l^{\mathrm{C}}\left(r, r'\right) = \delta\left(r - r'\right) \tag{2.219}$$

and is explicitly given by

$$\mathscr{G}_l^{\mathrm{C}}\left(r, r'\right) = -\frac{2\mu}{\hbar^2 k} F_l(\eta, kr_<) G_l(\eta, kr_>), \tag{2.220}$$

where F_l and G_l are the regular and irregular Coulomb functions introduced in Sect. 2.5.1. Again, $r_<$ is the smaller and $r_>$ the larger of the two radial coordinates r and r'. A wave function obeying the integral equation

$$u_l(r) = F_l(\eta, kr) + \int_0^\infty \mathscr{G}_l^{\mathrm{C}}\left(r, r'\right) V_{\mathrm{sr}}\left(r'\right) u_l\left(r'\right) \mathrm{d}r' \tag{2.221}$$

necessarily obeys the radial Schrödinger equation (2.218). Equation (2.221) is the radial Lippmann–Schwinger equation, adapted for the case of a modified Coulomb

potential. Asymptotically, $r \to \infty$, we can assume $r = r_>$ and $r' = r_<$, so

$$u_l(r) \overset{r\to\infty}{\sim} F_l(\eta, kr) - \left[\frac{2\mu}{\hbar^2 k}\int_0^\infty F_l\big(\eta, kr'\big)V_{\rm sr}\big(r'\big)u_l\big(r'\big)\right]G_l\big(\eta, kr'\big)\mathrm{d}r', \quad (2.222)$$

and the coefficient of $G_l(\eta, kr')$ is the tangent of the additional phase shift $\tilde{\delta}_l$ due to the short-range potential $V_{\rm sr}$,

$$\tan\tilde{\delta}_l = -\frac{2\mu}{\hbar^2 k}\int_0^\infty F_l\big(\eta, kr'\big)V_{\rm sr}\big(r'\big)u_l\big(r'\big)\mathrm{d}r'. \quad (2.223)$$

An explicit approximate expression for $\tan\tilde{\delta}_l$ in the spirit of the Born approximation is obtained by replacing the exact wave function u_l in the integrand by the regular Coulomb function F_l,

$$\tan\tilde{\delta}_l^{\rm DWBA} = -\frac{2\mu}{\hbar^2 k}\int_0^\infty \big[F_l\big(\eta, kr'\big)\big]^2 V_{\rm sr}\big(r'\big)\mathrm{d}r'. \quad (2.224)$$

Since this is a Born-type approximation for the phase shifts relative to the regular Coulomb wave rather than relative to the free-particle wave as in (2.67), the approximation (2.224) is referred to as the *distorted-wave* Born approximation (DWBA)—for the additional phase shift due to the short-range potential $V_{\rm sr}$.

Since the Coulomb potential falls off slower than the centrifugal potential at large distances, it dominates the asymptotic behaviour of the effective potential in every partial wave. The behaviour of the additional phase shifts $\tilde{\delta}_l$ as functions of energy depends crucially on whether the underlying Coulomb potential is repulsive or attractive. These very different situations are treated separately in the next two subsections.

2.5.3 *Modified Repulsive Coulomb Potential*

First consider the case that the underlying Coulomb potential C/r is repulsive,

$$C > 0, \quad \eta = |\eta| = \frac{1}{a_C k} > 0. \quad (2.225)$$

At near-threshold energies, the radial wave function is suppressed under the Coulomb barrier. The near-threshold behaviour of the additional phase shifts $\tilde{\delta}_l$ due to the short-range potential can be derived from the small-ρ behaviour of the Coulomb functions. The small-ρ limits (2.204) and (2.206) apply for a fixed value of the Sommerfeld parameter, which is related to the wavenumber k via (2.225). Towards threshold $k \to 0$, we exploit the relation (B.18) in Appendix B.3

$$\big|\Gamma(l+1+\mathrm{i}\eta)\big| \overset{|\eta|\to\infty}{\sim} \sqrt{2\pi}\,\mathrm{e}^{-\frac{\pi}{2}|\eta|}|\eta|^{l+1/2} \quad (2.226)$$

to obtain the limiting near-threshold behaviour of the Coulomb functions for given value of the distance $r = a_C \rho\eta$,

$$\begin{aligned} F_l(\eta, kr) &\overset{k\to 0}{\sim} \sqrt{\pi}\,\mathrm{e}^{-\pi\eta}\sqrt{kr}\,I_{2l+1}\left(\sqrt{\frac{8r}{a_C}}\right), \\ G_l(\eta, kr) &\overset{k\to 0}{\sim} \frac{2}{\sqrt{\pi}}\mathrm{e}^{\pi\eta}\sqrt{kr}\,K_{2l+1}\left(\sqrt{\frac{8r}{a_C}}\right). \end{aligned} \tag{2.227}$$

Here I_{2l+1} and K_{2l+1} are the modified Bessel functions as described in Appendix B.4. Their small- and large-argument behaviour is,

$$\begin{aligned} &I_{2l+1}\left(\sqrt{\frac{8r}{a_C}}\right) \overset{r\to 0}{\sim} \frac{(2r/a_C)^{l+1/2}}{(2l+1)!}, \qquad I_{2l+1}\left(\sqrt{\frac{8r}{a_C}}\right) \overset{r\to\infty}{\sim} \left(\frac{8r}{a_C}\right)^{-1/4} \frac{\mathrm{e}^{\sqrt{8r/a_C}}}{\sqrt{2\pi}}, \\ &K_{2l+1}\left(\sqrt{\frac{8r}{a_C}}\right) \overset{r\to 0}{\sim} \frac{(2l)!/2}{(2r/a_C)^{l+1/2}}, \qquad K_{2l+1}\left(\sqrt{\frac{8r}{a_C}}\right) \overset{r\to\infty}{\sim} \left(\frac{8r}{a_C}\right)^{-1/4} \frac{\mathrm{e}^{-\sqrt{8r/a_C}}}{\sqrt{2/\pi}}. \end{aligned} \tag{2.228}$$

Beyond the range of V_{sr}, the regular solution of the radial Schrödinger equation (2.212) has the following limiting behaviour towards threshold,

$$\begin{aligned} u_l(r) &\propto F_l(\eta, kr) + \tan\tilde{\delta}_l G_l(\eta, kr) \overset{k\to 0}{\sim} \sqrt{\pi}\,\mathrm{e}^{-\pi\eta}\sqrt{k} \\ &\times \left[\sqrt{r}\,I_{2l+1}\left(\sqrt{\frac{8r}{a_C}}\right) + \tan\tilde{\delta}_l \frac{2}{\pi}\mathrm{e}^{2\pi\eta}\sqrt{r}\,K_{2l+1}\left(\sqrt{\frac{8r}{a_C}}\right)\right]. \end{aligned} \tag{2.229}$$

Similar to the discussion involving Eq. (2.76) in Sect. 2.3.8, the k-dependence of $\tan\tilde{\delta}$ must cancel the k-dependence of $\mathrm{e}^{2\pi\eta}$ in the limit $k \to 0$, because the whole square bracket converges to a k-independent function of r in this limit, so

$$\tan\tilde{\delta}_l \overset{k\to 0}{\propto} \mathrm{e}^{-2\pi\eta} \tag{2.230}$$

for all partial waves l. The phase shifts $\tilde{\delta}_l$ are strongly suppressed towards threshold, because the repulsive Coulomb barrier smothers the influence of the short-range potential V_{sr}. For a short-range potential without a Coulomb field, the effective-range expansion (2.103) was formulated for $k\cot\delta_{l=0}$ in the case of s-waves, and it is an expansion for $k^{2l+1}\cot\delta_l$ when $l > 0$. In the presence of a repulsive Coulomb field, an effective-range expansion can be formulated as a series expansion for the quantity $\cot\tilde{\delta}_l/(\mathrm{e}^{2\pi\eta} - 1)$ [22, 25, 48].

If the effective potential (2.211), including the centrifugal term and the repulsive Coulomb behaviour at large distances, features a sufficiently deep attractive well at small distances, then it may support a finite number of bound states. The discussion of Sect. 2.3.9 can be adapted for the present situation. Compared to the pure

Coulomb wave $F_l(\eta, kr)$, the regular solution $u_l(r)$ of the radial Schrödinger equation features additional nodes at short distances. Additional short-distance nodes persist for $k \to 0$, while the nodes related to the asymptotic oscillations of the wave function wander to infinity in this limit, as do the nodes (beyond $r = 0$) of the pure Coulomb wave $F_l(\eta, kr)$. The number of (additional) short-distance nodes at threshold corresponds to the number n_b of bound states supported by the effective potential in the partial wave l, and it corresponds to a threshold value of $n_\mathrm{b}\pi$ for the additional phase shift due to the short-range deviations of the potential $V(r)$ from the pure Coulomb shape. As long as $V(r)$ is less singular than $1/r^2$ at short distances, its influence becomes negligible at high energies, so the nodes of $u_l(r)$ and of $F_l(\eta, kr)$ coalesce and $\tilde{\delta}_l \overset{k\to\infty}{\longrightarrow} 0$. Levinson's theorem (2.108), formulated in Sect. 2.3.9 for the scattering phase shifts due to a potential falling off faster than $1/r^2$ at large distances, also applies in the case of a modified repulsive Coulomb potential for the additional phase shifts $\tilde{\delta}_l$ due to the short-range deviations of the potential from the pure Coulomb shape,

$$\lim_{k\to 0} \tilde{\delta}_l(k) - \lim_{k\to\infty} \tilde{\delta}_l(k) = n_\mathrm{b}\pi. \tag{2.231}$$

As an example consider the modified Coulomb potential consisting of the model potential (2.105) in conjunction with a smoothed expression

$$V_C^{\mathrm{smooth}}(r) = \frac{C}{r}\mathrm{erf}\left(\frac{r}{\beta}\right) = \frac{\hbar^2}{\mu a_C}\frac{\mathrm{erf}(r/\beta)}{r} \tag{2.232}$$

for the Coulomb potential,

$$V(r) = V_0\left[16\mathrm{e}^{-r^2/\beta^2} - 12\mathrm{e}^{-r^2/(4\beta)^2}\right] + \frac{\hbar^2}{\mu a_C}\frac{\mathrm{erf}(r/\beta)}{r}, \quad V_0 = \frac{\hbar^2}{2\mu\beta^2}. \tag{2.233}$$

The *error function* $\mathrm{erf}(x)$ is a smooth function which vanishes proportional to x for $x \to 0$ and tends rapidly to unity for large x, see Appendix B.2. For the modified Coulomb potential (2.233) the short-range potential V_sr describing the deviation from the pure Coulomb shape is explicitly,

$$V_\mathrm{sr}(r) = V_0[\cdots] + \frac{\hbar^2}{\mu a_C}\frac{\mathrm{erf}(r/\beta) - 1}{r}. \tag{2.234}$$

For the model calculations below, the strength C of the Coulomb potential is chosen such that the length $a_C = \hbar^2/(\mu C)$ is equal to the length scale β in V_sr.

The left-hand part of Fig. 2.17 shows the additional phase shifts $\tilde{\delta}_l$ for partial waves up to $l = 7$ and scaled wave numbers up to $k\beta = 6$. Their behaviour is qualitatively similar to that of the scattering phase shifts for the short-range potential (2.105) as can be seen by comparing with Fig. 2.7 in Sect. 2.3.7. It can be under-

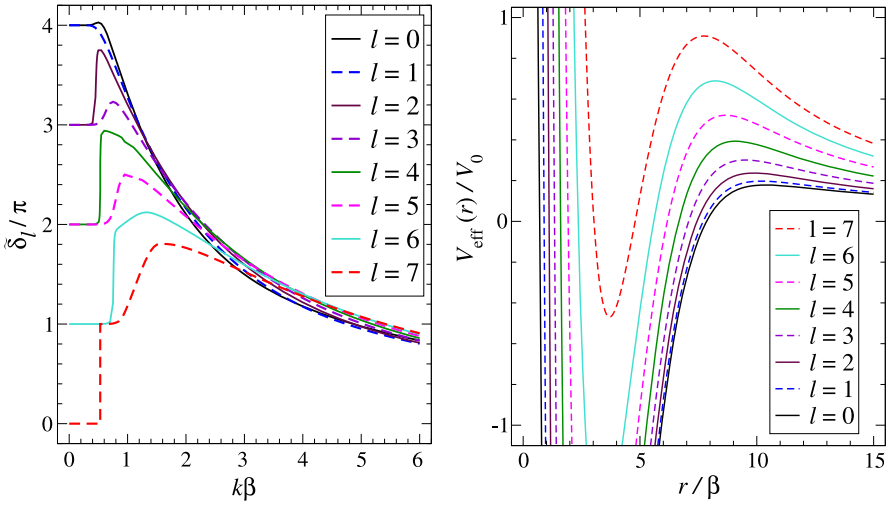

Fig. 2.17 The *left-hand part* shows the additional phase shifts $\tilde{\delta}_l$ in the modified repulsive Coulomb potential (2.233) for partial waves up to $l = 7$ and scaled wave numbers up to $k\beta = 6$. The *right-hand part* shows the effective potentials (2.211) in the respective partial waves

stood by looking at the effective potentials in the respective partial waves, which are shown in the right-hand part of Fig. 2.17. All $\tilde{\delta}_l$ tend rapidly to $n_{\rm b}\pi$ at threshold, according to (2.230) and (2.231). The repulsive barrier is a combination of the centrifugal potential and the repulsive Coulomb term and is higher and broader than the centrifugal barrier without the underlying Coulomb potential. At the same time, the depth of the attractive well at short distances is reduced by the repulsive Coulomb term, and the effective potential supports one less bound state in half of the cases.

2.5.4 *Modified Attractive Coulomb Potential, Quantum-Defect Theory*

When the underlying Coulomb potential is attractive,

$$C < 0, \quad \eta = -|\eta| = -\frac{1}{a_C k} < 0, \tag{2.235}$$

the situation is very different from the repulsive case. The effective potential is asymptotically dominated by the attractive Coulomb potential in all partial waves. Equation (2.226) holds also in the attractive case, and exploiting Eqs. (2.204) and

(2.206) yields

$$\begin{aligned} F_l(\eta, kr) &\overset{k\to 0}{\sim} \sqrt{\pi kr}\, J_{2l+1}\left(\sqrt{\frac{8r}{a_C}}\right), \\ G_l(\eta, kr) &\overset{k\to 0}{\sim} -\sqrt{\pi kr}\, Y_{2l+1}\left(\sqrt{\frac{8r}{a_C}}\right), \end{aligned} \tag{2.236}$$

where J_{2l+1} and Y_{2l+1} are the ordinary Bessel functions, see Appendix B.4. Towards threshold, the amplitudes of F_l an G_l vanish proportional to $\sqrt{k}$, so the limit $k \to 0$ is more conveniently studied with the renormalized Coulomb functions,

$$\bar{\mathrm{F}}_l(\eta, kr) = \sqrt{\frac{2\mu}{\pi\hbar^2 k}}\, F_l(\eta, kr), \quad \bar{\mathrm{G}}_l(\eta, kr) = \sqrt{\frac{2\mu}{\pi\hbar^2 k}}\, G_l(\eta, kr). \tag{2.237}$$

This renormalization corresponds to normalization in energy, as described in Sect. 2.3.4. The renormalized functions converge to well defined limits at threshold. With the abbreviation $z = \sqrt{8r/a_C}$,

$$\begin{aligned} \bar{\mathrm{F}}_l(\eta, kr) &\overset{k\to 0}{\sim} \sqrt{\frac{2\mu r}{\hbar^2}}\, J_{2l+1}(z) \overset{r\to\infty}{\sim} \sqrt{\frac{2\mu}{\pi\hbar^2}} \left(\frac{a_C r}{2}\right)^{\frac{1}{4}} \sin\left(z - \left(l + \frac{1}{4}\right)\pi\right), \\ \bar{\mathrm{G}}_l(\eta, kr) &\overset{k\to 0}{\sim} -\sqrt{\frac{2\mu r}{\hbar^2}}\, Y_{2l+1}(z) \overset{r\to\infty}{\sim} \sqrt{\frac{2\mu}{\pi\hbar^2}} \left(\frac{a_C r}{2}\right)^{\frac{1}{4}} \cos\left(z - \left(l + \frac{1}{4}\right)\pi\right). \end{aligned} \tag{2.238}$$

Beyond the range of the short-range modification of the attractive Coulomb potential, the energy-normalized regular solution of the radial Schrödinger equation (2.212) is

$$\begin{aligned} \bar{\mathrm{u}}_l(r) &= \cos\tilde{\delta}_l \bar{\mathrm{F}}_l(\eta, kr) + \sin\tilde{\delta}_l \bar{\mathrm{G}}_l(\eta, kr) \\ &\overset{k\to 0}{\sim} \sqrt{\frac{2\mu r}{\hbar^2}} \cos\tilde{\delta}_l \left[J_{2l+1}\left(\sqrt{\frac{8r}{a_C}}\right) - \tan\tilde{\delta}_l\, Y_{2l+1}\left(\sqrt{\frac{8r}{a_C}}\right)\right]. \end{aligned} \tag{2.239}$$

In the limit $k \to 0$, the big square bracket in the lower line of Eq. (2.239) is independent of k, as long as $\tan\tilde{\delta}_l$ tends to a well defined value in this limit; this value need not be zero. The additional phase shift due to the short-range modification of an attractive Coulomb potential tends to a constant, $\tilde{\delta}_l(0)$, at threshold, and, in contrast to the scattering phase shifts for potentials falling off faster than $1/r^2$, this constant need not be an integer multiple of π. From (2.238) and (2.239) the asymptotic behaviour of the energy-normalized regular radial wave function at threshold is

$$\bar{\mathrm{u}}_l(r) \overset{r\to\infty, E=0}{\sim} \sqrt{\frac{2\mu}{\pi\hbar^2}} \left(\frac{a_C r}{2}\right)^{\frac{1}{4}} \sin\left(\sqrt{\frac{8r}{a_C}} - \left(l + \frac{1}{4}\right)\pi + \tilde{\delta}_l(0)\right). \tag{2.240}$$

In contrast to the situation for potentials falling off faster than $1/r^2$, or for modified repulsive Coulomb potentials, see Eq. (2.229), the nodes of radial wave function (2.239) beyond the range of $V_{\rm sr}$ do not wander to infinity in the limit $k \to 0$. The threshold wave function $u_l^{(0)}$ with the asymptotic form (2.240) has an infinite sequence of well defined nodes. This is a manifestation of the fact, that the potential supports an infinite number of bound states. Levinson's theorem (2.231), which for a modified repulsive Coulomb potential relates the threshold value of $\tilde{\delta}_l$ to the number of bound states, can not be carried over directly to the case of a modified attractive Coulomb potential. A generalized version of the theorem involving the number of additional bound states due to the short-range deviations from the pure attractive Coulomb potential has been formulated by Rosenberg [37]; see also the discussion of Figs. 2.19 and 2.20 below.

As an example we again consider the model potential (2.105) in conjunction with the smoothed Coulomb potential (2.232), which is, however, now taken to be attractive,

$$V(r) = V_0\big[16\mathrm{e}^{-r^2/\beta^2} - 12\mathrm{e}^{-r^2/(4\beta)^2}\big] - \frac{\hbar^2}{\mu a_C}\frac{\mathrm{erf}(r/\beta)}{r}, \quad V_0 = \frac{\hbar^2}{2\mu\beta^2}. \tag{2.241}$$

The potential $V_{\rm sr}$ describing the short-range deviation of $V(r)$ from the pure Coulomb shape now is

$$V_{\rm sr}(r) = V_0[\cdots] - \frac{\hbar^2}{\mu a_C}\frac{\mathrm{erf}(r/\beta) - 1}{r}. \tag{2.242}$$

Again we assume that the characteristic length a_C of the Coulomb potential, which now corresponds to the Bohr radius, is equal to the length β. The behaviour of the additional phase shifts $\tilde{\delta}_l$ is shown in the left-hand part of Fig. 2.18, while the effective potentials are shown in the right-hand part. As already observed in Sect. 1.2.1, the centrifugal potential in combination with an attractive Coulomb potential does *not* form a centrifugal barrier, see Fig. 1.3. For partial waves up to and including $l = 3$, there is no barrier separating the inner well of the potential from the outer attractive Coulombic tail. The threshold values of the additional phase shifts $\tilde{\delta}_l$ are clearly not integer multiples of π, and this holds also for $l = 4$ and $l = 5$. For some higher angular momentum quantum numbers, a potential barrier can form between the inner well and the distant long-range attractive tail, where the short-range potential is negligible and the Coulomb potential dominates over the centrifugal term.

At negative energies $E = -\hbar^2\kappa^2/(2\mu)$, $\kappa = \sqrt{-2\mu E/\hbar^2}$, the radial Schrödinger equation (2.212) is replaced by

$$\left[\frac{\hbar^2}{2\mu}\left(-\frac{\mathrm{d}^2}{\mathrm{d}r^2} + \frac{l(l+1)}{r^2} + \frac{2\eta\kappa}{r}\right) + V_{\rm sr}(r)\right]u_l(r) = -\frac{\hbar^2\kappa^2}{2\mu}u_l(r), \tag{2.243}$$

where the definition (2.187) of the Sommerfeld parameter has been adapted to subthreshold energies,

$$\eta = \frac{\mu C}{\hbar^2\kappa} = -\frac{1}{a_C\kappa} < 0. \tag{2.244}$$

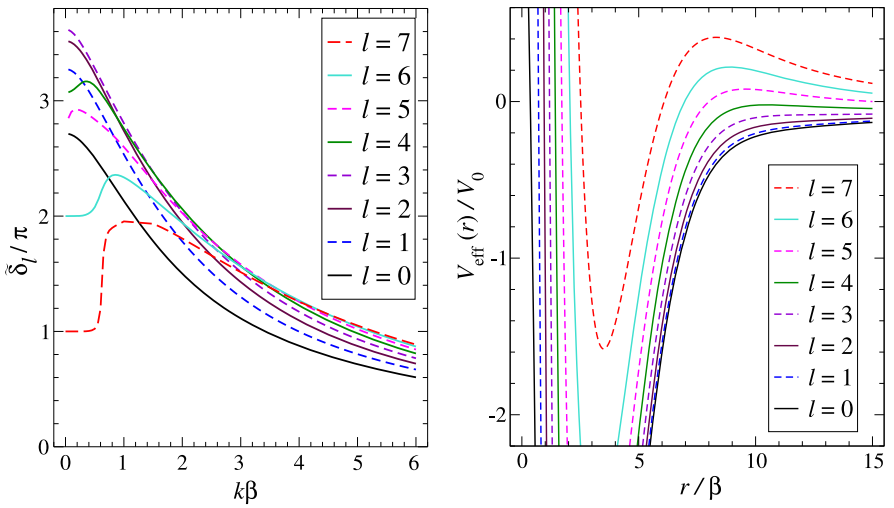

Fig. 2.18 The *left-hand part* shows the additional phase shifts $\tilde{\delta}_l$ in the modified attractive Coulomb potential (2.241) with $a_C = \beta$ for partial waves up to $l = 7$ and scaled wave numbers up to $k\beta = 6$. The *right-hand part* shows the effective potential (2.211) in the respective partial waves. At very large distances, the short-range potential is negligible and the Coulomb potential dominates over the centrifugal term, so the effective potential approaches zero from below in all partial waves

Beyond the range of the short-range potential $V_{\rm sr}$, the decaying, bound-state solutions of (2.243) are proportional to Whittaker functions (see Appendix B.5),

$$u_l^{(\kappa)}(r) \propto W_{|\eta|,l+\frac{1}{2}}(2\kappa r) \overset{\kappa r \to \infty}{\sim} (2\kappa r)^{|\eta|} \mathrm{e}^{-\kappa r}. \tag{2.245}$$

Bound states exist at discrete energies $E_n = -\hbar^2 \kappa_n^2/(2\mu)$, for which the regular solution $u_l^{(\kappa_n)}(r)$, which vanishes for $r \to 0$, matches to the decaying form (2.245) asymptotically. In the absence of a short-range potential, i.e. for a pure attractive Coulomb potential, the solution of (2.243) has the form (2.245) for all r, and the boundary condition $u_l^{(\kappa)}(0) = 0$ is fulfilled for integer values of $|\eta|$ larger than l,

$$|\eta| = n \Rightarrow \kappa_n = \frac{1}{n a_C}, \qquad E_n = -\frac{\mathscr{R}}{n^2}, \quad n = l+1, l+2, l+3, \ldots. \tag{2.246}$$

The radial eigenfunction in the partial wave l is

$$u_{n,l}^{(C)}(r) = \frac{(-1)^{n-l-1}}{n\sqrt{a_C (n+l)!(n-l-1)!}} W_{n,l+\frac{1}{2}}\left(\frac{2r}{n a_C}\right). \tag{2.247}$$

For a given *principal quantum number* n, the number of radial nodes (beyond zero) is

$$n_{\rm r} = n - l - 1 \tag{2.248}$$

and serves as the *radial quantum number*, which labels the bound states in a given partial wave, starting with $n_r = 0$ for the ground state. The bound-state energy eigenvalues (2.246) are well known from the quantization in hydrogen-like atoms; the energy $\mathscr{R}$ is the *Rydberg energy*,

$$\mathscr{R} = \frac{\hbar^2}{2\mu a_C^2} = \frac{\mu C^2}{2\hbar^2}. \tag{2.249}$$

The bound-state eigenfunctions (2.247) in the pure attractive Coulomb potential are normalized to unity, $\int_0^\infty [u_{n,l}^{(C)}(r)]^2 \mathrm{d}r = 1$. At any given distance r, their amplitude decreases to zero as $n \to \infty$, while their spatial extension grows with the increasing number of oscillations. Renormalized bound-state wave functions defined by

$$\bar{\mathrm{u}}_{n,l}^{(C)}(r) = \sqrt{\frac{n^3}{2\mathscr{R}}} u_{n,l}^{(C)}(r) \tag{2.250}$$

have the property, that they converge to a well-defined wave function for $n \to \infty$. This is the same limit that is reached by the energy-normalized continuum wave functions $\bar{\mathrm{F}}_l$, as defined in (2.237), when approaching the threshold from above [16],

$$\lim_{n\to\infty} \bar{\mathrm{u}}_{n,l}^{(C)}(r) = \sqrt{\frac{2\mu r}{\hbar^2}} J_{2l+1}\left(\sqrt{\frac{8r}{a_C}}\right) = \lim_{E\to 0} \bar{\mathrm{F}}_l(\eta, kr), \tag{2.251}$$

compare Eq. (2.238) above.

When the potential deviates from the pure Coulomb shape at small distances, the regular solution of the radial Schrödinger equation (2.243) has the form (2.245) beyond the range of the short-range deviations, but it is different for small r. For a given angular momentum quantum number l, bound states now exist for values $\tilde{n}$ of $|\eta|$ which are not necessarily integer,

$$|\eta| = \tilde{n} = n - \mu_n \Rightarrow \kappa_n = \frac{1}{\tilde{n} a_C} = \frac{1/a_C}{n - \mu_n}, \quad E_n = -\frac{\mathscr{R}}{(n-\mu_n)^2}. \tag{2.252}$$

The quantization formula on the far right of Eq. (2.252) is called *Rydberg formula*, and the infinite sequence of energy eigenvalues is called a *Rydberg series*. The dependence of E_n on quantum number n is not identical, but similar to that in Eq. (2.246) for a pure attractive Coulomb potential. The infinitely many weakly bound *Rydberg states* form a "quasicontinuum" below threshold—as opposed to the true continuum above threshold. The *effective quantum number*,[5]

$$\tilde{n} = n - \mu_n, \tag{2.253}$$

[5] Alternative notations for the effective quantum number are ν_n [41] and n^* [16].

differs from the respective integer quantum number n by the *quantum defect* μ_n. The concept of quantum defects originated in the early days of quantum mechanics, even before Schrödinger formulated his wave equation in 1926. Quantum defects were used to explain the bound-state energy spectra of alkali atoms, see e.g. [6]. At large distances, the valence electron in an alkali atom experiences an ordinary Coulomb potential, as in a hydrogen atom, because the Z-fold positive charge of the atomic nucleus is largely screened by the $Z-1$ electrons in the filled shells. The potential is more attractive at small distances due to a decrease of this screening effect, which leads a decrease in the energy eigenvalues, relative to the hydrogen-atom case, and this decrease can be described by positive quantum defects in the Rydberg formula (2.252). It is, of course, always possible to write an infinite series of energies as in (2.252), but the physical relevance of the Rydberg formula is founded on the recognition that the quantum defects μ_n depend weakly on n and converge to a well defined limit for $n \to \infty$, as shown below.

If the radial bound-state wave functions $u_{n,l}(r)$ in the modified attractive Coulomb potential are normalized to unity, then the corresponding energy-normalized bound states wave functions $\bar{\mathrm{u}}_{n,l}(r)$ are defined in analogy to (2.250) as

$$\bar{\mathrm{u}}_{n,l}(r) = \sqrt{\frac{\tilde{n}^3}{2\mathscr{R}}}\, u_{n,l}(r), \tag{2.254}$$

i.e., the principal quantum number n in the square root is replaced by the effective quantum number $\tilde{n} = n - \mu_n$. As $n \to \infty$, the renormalized bound-state wave functions (2.254) converge from below to the threshold solution of the radial Schrödinger equation (2.243), which is the same limit as is reached by the energy-normalized continuum wave functions when approaching the threshold from above. Its asymptotic behaviour is given by (2.240), so

$$\lim_{n\to\infty} \bar{\mathrm{u}}_{n,l}(r) \overset{r\to\infty}{\sim} \sqrt{\frac{2\mu}{\pi\hbar^2}} \left(\frac{a_C r}{2}\right)^{\frac{1}{4}} \sin\left(\sqrt{\frac{8r}{a_C}} - \left(l+\frac{1}{4}\right)\pi + \tilde{\delta}_l(0)\right). \tag{2.255}$$

Beyond the range of the short-range modifications of the Coulomb potential, the bound-state wave functions $\bar{\mathrm{u}}_{n,l}(r)$ are proportional to the Whittaker functions $W_{\tilde{n},l+\frac{1}{2}}(2r/(\tilde{n}a_C))$. As $\tilde{n} = n - \mu_n$ grows to infinity, the limit of these Whittaker functions is (see formula 9.229 of [21]),

$$W_{\tilde{n},l+\frac{1}{2}}(2\kappa r) \overset{\tilde{n}\to\infty}{\propto} (a_C r)^{1/4} \sin\left(\sqrt{\frac{8r}{a_C}} - (n-\mu_n)\pi - \frac{\pi}{4}\right). \tag{2.256}$$

Compatibility with Eqs. (2.240) and (2.255) requires

$$\pi \lim_{n\to\infty} \mu_n = \tilde{\delta}_l(0) = \lim_{E\to 0} \tilde{\delta}_l(E) \pmod{\pi}. \tag{2.257}$$

Equation (2.257) was first formulated by Seaton [40, 41] and deserves to be called *Seaton's theorem*. Its physical interpretation is straightforward. At threshold,

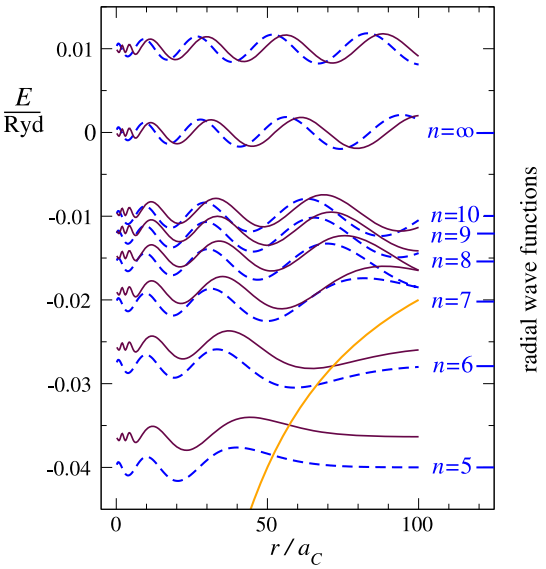

Fig. 2.19 Radial wave functions for the modified attractive Coulomb potential (2.241) in the partial wave $l = 0$ (*solid maroon lines*). The bound states are shifted in energy relative to the pure Coulomb bound states at $E_n = -\mathscr{R}/n^2$, the radial wave functions of which are shown as *dashed blue lines*. The phase shifts due to the short-range modification of the pure Coulomb potential persist to the threshold, $E = 0$ corresponding to $n = \infty$, and continue smoothly to the continuum states at positive energy. The *orange line* shows the Coulombic tail of the potential

the short-range potential $V_{\rm sr}$ leads to an asymptotic shift $\tilde{\delta}_l(0)$ in the phase of the threshold solution (2.240) of the radial Schrödinger equation in the partial wave l relative to the pure Coulomb wave. This phase shift represents the threshold limit of the additional phase shift $\tilde{\delta}_l(E)$ in the scattering states above threshold. Below threshold, the short-range potential $V_{\rm sr}$ induces energy shifts of the bound states relative to the bound-state energies in the pure Coulomb case, and these shifts are, in each partial wave l, quantified by the series of quantum defects μ_n. The quantum defect is also associated with a phase shift in the outer part of the radial wave function. A quantum defect of unity gives the energy level at E_n a new label, namely E_{n+1}, without changing its value; it amounts to a shift of one half-wave in the outer part of the radial wave function, i.e. to a phase shift of π. Fractional quantum defects correspond to shifts by fractions of half waves. Approaching threshold from below, the phase shifts $\pi\mu_n$ in the outer parts of the bound-state wave functions converge to the same limit as the phase shifts in the continuum states approaching threshold from above.

As an example we again consider the modified Coulomb potential (2.241). We had chosen $a_C = \beta$, so the Rydberg energy is equal to the coefficient V_0. The radial wave functions in the partial wave $l = 0$ are shown in Fig. 2.19 for several bound states, at threshold, and in the continuum. The bound state wave functions are normalized according to (2.254), so that they merge smoothly into the energy-normalized continuum wave functions above threshold. Due to the short-range modification of the attractive Coulomb potential, the bound states are shifted in energy, and their wave functions are shifted in phase, relative to the pure Coulomb case (dashed blue lines). These phase shifts persist to the threshold, $E = 0$ corresponding to $n = \infty$, and they connect smoothly to the additional phase shifts $\tilde{\delta}_{l=0}$ of the continuum states.

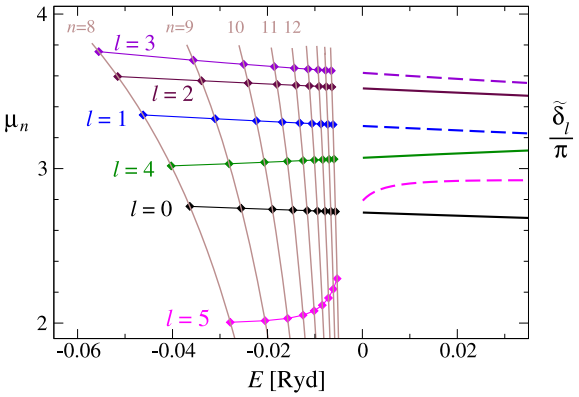

Fig. 2.20 The *left-hand part* ($E < 0$) shows bound states of the modified attractive Coulomb potential (2.241) as diamonds in the E_n–μ_n plane. In each partial wave l, they appear as the intersections of a smooth quantum-defect function $\mu^{\rm QD}(E)$ with the family of curves (2.258), which are shown as *thin brown lines*. Each quantum-defect function can be continued smoothly to energies above threshold where it represents $1/\pi$ times the additional phase shift $\tilde{\delta}_l$. For $l = 5$, a shape resonance appears near threshold; the resonant feature appears as a rise in the phase shift $\tilde{\delta}_l$ above and a rise in the quantum defects below threshold

The Rydberg formula (2.252) can be rewritten as

$$\mu_n = n - |\eta| = n - \sqrt{-\frac{\mathscr{R}}{E}}. \tag{2.258}$$

The weak dependence of μ_n on n and hence, in particular, on E, implies that the quantum defects can be interpolated to a smooth *quantum-defect function* $\mu^{\rm QD}(E)$, $\mu_n = \mu^{\rm QD}(E_n)$. The bound states are given as the intersections of $\mu^{\rm QD}(E)$ with the family of curves $n - |\eta|$. This is illustrated in the left-hand part ($E < 0$) of Fig. 2.20, where the bound states are plotted for each partial wave from $l = 0$ to $l = 5$ as diamonds in the E_n–μ_n plane.

The quantum defects are, strictly speaking, only defined modulo unity, and the additional phase shifts $\tilde{\delta}_l$ modulo π. Since the bound-state energies fix the effective quantum numbers $n - \mu_n$ according to (2.252), the integer part of μ_n depends on where we start counting for the bound-state quantum numbers. We assign the radial quantum number $n_{\rm r} = 0$ corresponding to the principal quantum number $n = l + 1$ to the lowest bound state in a given partial wave and count upwards from there. If μ_n is an integer, then the corresponding energy eigenvalue $-\mathscr{R}/(n - \mu_n)^2$ is the same as that of the pure-Coulomb state with principal quantum number $n - \mu_n$, but the radial wave function in the modified Coulomb potential has μ_n nodes more than the pure Coulomb wave at the same energy. When μ_n lies between two integers, n_μ and $n_\mu + 1$, then the radial wave function has n_μ nodes more than the wave function of the next-highest pure Coulomb state with principal quantum number $n - n_\mu$, and $n_\mu + 1$ nodes more than the wave function of the next-lowest with principal quantum number $n - n_\mu - 1$. The quantum defects in Fig. 2.20 all turn out to lie between

two and four. This reflects the fact that the radial wave functions in the modified attractive Coulomb potential have three or four nodes more than the wave functions of the next-lowest state in the pure Coulomb potential. The quantum defects of the $l = 0$ bound states lie near 2.7, and their wave functions, which are shown as maroon lines in Fig. 2.19, each have three nodes more than the pure Coulomb waves (dashed blue lines) at slightly lower energy.

For each partial wave l, the smooth curve $\mu^{\mathrm{QD}}(E)$ can be continued to energies above threshold where it represents $1/\pi$ times the additional phase shift $\tilde{\delta}_l$ in the respective partial wave. These phase shifts were already shown in the left-hand part of Fig. 2.18; in the right-hand part ($E > 0$) of Fig. 2.20 they are shown as functions of energy in a small range near threshold. In the $l = 5$ partial wave, there is a shape resonance close to threshold. The associated rise of $\tilde{\delta}_l$ extends to a hundredth of the Rydberg energy above threshold, starting a few hundredths of the Rydberg energy below threshold, where it is manifest as a rise in the quantum defects. In a modified attractive Coulomb potential, such resonant features of finite width can straddle the threshold, as is discussed in more detail in Sect. 3.7 in Chap. 3. An analogous behaviour does not occur for a modified repulsive Coulomb potential, or for the scattering phase shifts of a potential falling off faster than $1/r^2$, because the phase shift involved necessarily approaches an integer multiple of π at threshold.

For an attractive Coulomb potential modified by deviations from the pure Coulomb shape at small distances, the effects of these deviations on the near-threshold states in a given partial wave, both above and below threshold, are accounted for by the quantum-defect function $\mu^{\mathrm{QD}}(E)$. It is a smooth function of energy everywhere, including the near-threshold regime $E \approx 0$. At above-threshold energies, $\mu^{\mathrm{QD}}(E)$ is related to the additional phase shift $\tilde{\delta}_l$,

$$\pi\,\mu^{\mathrm{QD}}(E) = \tilde{\delta}_l(E) \pmod{\pi}. \tag{2.259}$$

At below-threshold energies, the large-distance oscillations of the bound-state wave functions are shifted by the phase $\pi\,\mu^{\mathrm{QD}}$ with respect to bound states of similar energy in the pure Coulomb potential, but these phase shifts are related to the binding energies via the effective quantum number: $\pi\,\mu^{\mathrm{QD}} = -\pi\tilde{n} \pmod{\pi}$, compare Eq. (2.256). The energies E_n of the bound states are thus determined as the intersections of $\mu^{\mathrm{QD}}(E)$ with the curves $n - \sqrt{-\mathscr{R}/E}$, see Eq. (2.258).

The effect of the short-range deviations from the pure Coulomb potential can be collected into one single formula,

$$\mu^{\mathrm{QD}}(E) + \nu(E) = 0 \pmod{1}, \tag{2.260}$$

by introducing a function $\nu(E)$ which has different interpretations below and above threshold. Below threshold it stands for the effective quantum number, treated as a continuous variable, the *continuous effective quantum number*,

$$\nu(E) \equiv \tilde{n} \equiv |\eta| = \sqrt{-\mathscr{R}/E} \quad \text{for } E < 0; \tag{2.261}$$

above threshold it stands for the additional scattering phase shift divided by $-\pi$,

$$\nu(E) = -\frac{1}{\pi}\tilde{\delta}_l(E) \quad \text{for } E > 0. \tag{2.262}$$

Equations (2.260), (2.261) and (2.262) make up the content of (single-channel) *quantum-defect theory* (QDT). It describes the smooth transition from the true continuum above threshold to the quasi-continuum of Rydberg states below threshold, as expressed in Seaton's theorem (2.257). Knowledge of the threshold limit $\tilde{\delta}_l(0)$ of the additional phase shift with a given accuracy determines the eigenenergies of an infinite number of bound states with ever improving accuracy for $n \to \infty$.

2.6 Potentials Falling off as $1/r^\alpha$, $\alpha > 2$

Potentials with Coulombic tails falling off as $1/r$ at large distances are rightly called "long ranged". They require special treatment in scattering theory, as given in the previous section. The term "short ranged" is generally used for potentials falling off faster than any inverse power of the distance, such as the model potential (2.105) discussed in Sect. 2.3. Their asymptotic fall-off is typically characterized by a well defined range parameter, both classically and in quantum mechanics. Potentials falling off asymptotically as an inverse power of r, $V(r) \overset{r\to\infty}{\propto} 1/r^\alpha$, are usually also called "long ranged" even when $\alpha > 2$ [29, 34], although their properties are in many aspects closer to those of short-range potentials than to the genuinely long-range Coulombic potentials. Most of the theory presented in Sects. 2.1 to 2.3, in particular the partial-waves expansion with scattering phase shifts that tend to an integral multiple of π at threshold, applies for all potentials that fall off faster than the centrifugal potential, i.e. faster than $1/r^2$, at large distances. There are, however, some aspects in which the properties of potentials with inverse-power tails differ from those of genuinely short-range potentials; these aspects are illuminated in this section.

2.6.1 Near-Threshold Behaviour of Scattering Phase Shifts

The near-threshold behaviour of scattering phase shifts was discussed in Sect. 2.3.8 in connection with the asymptotic behaviour of the threshold solution ($E = 0$) of the radial Schrödinger equation (2.35). This was given in Eq. (2.81), which is repeated here for convenience:

$$u_l^{(0)}(r) \overset{r\to\infty}{\propto} r^{l+1} - \frac{a_l^{2l+1}}{r^l}; \tag{2.263}$$

a_l is the scattering length in the partial wave l, as defined in Sect. 2.3.8. For all potentials $V(r)$ falling off faster than $1/r^2$ at large distances, the leading term proportional to r^{l+1} is a natural consequence of the repulsive centrifugal potential, which

is always dominant at sufficiently large distances. The fact that the next-to-leading term is $2l + 1$ powers of r lower than the leading term is nontrivial and requires a sufficiently rapid fall-off of $V(r)$ for large r. Equation (2.263) is obviously valid for all partial waves l if $V(r)$ vanishes exactly beyond some finite distance, and it also holds if $V(r)$ falls off faster than any inverse power of r. For a potential tail falling off as $1/r^\alpha$, $\alpha > 2$, its validity is limited to the partial waves $l < (\alpha - 3)/2$, as shown in the following.

Consider a potential behaving asymptotically as

$$V(r) \overset{r\to\infty}{\sim} V_\alpha(r) = \frac{C_\alpha}{r^\alpha} = \pm\frac{\hbar^2}{2\mu}\frac{(\beta_\alpha)^{\alpha-2}}{r^\alpha}, \quad \alpha > 2. \tag{2.264}$$

Such behaviour is ubiquitous in nature. It applies, e.g., with $\alpha = 6$ for the van der Waals potential between two uncharged polarizable particles such as atoms or molecules, with $\alpha = 4$ for the interaction of a charged particle with a polarizable neutral, and with $\alpha = 3$ for the resonant dipole-dipole interaction of two identical atoms in different internal states. In quantum mechanics, the inverse-power term possesses a characteristic length β_α which does not exist in classical mechanics. It is related to the strength coefficient C_α via

$$\beta_\alpha = \left(\frac{2\mu|C_\alpha|}{\hbar^2}\right)^{1/(\alpha-2)}. \tag{2.265}$$

The length β_α has been called "van der Waals length" for attractive inverse-power tails with $\alpha = 6$ [32]. Since the theory does not depend on whether or not the potential tail is associated with a van der Waals interaction, it seems appropriate to choose a more general name, such as the *characteristic quantum length* associated with the inverse-power term C_α/r^α, as already done in connection with repulsive inverse-power potentials in Sect. 2.4.

At large distances r, the radial Schrödinger equation at threshold ($E = 0$) for a potential fulfilling (2.264) reads

$$\left(-\frac{\mathrm{d}^2}{\mathrm{d}r^2} + \frac{l(l+1)}{r^2} \pm \frac{\beta^{\alpha-2}}{r^\alpha}\right)u_l^{(0)}(r) = 0; \tag{2.266}$$

we dispense with the subscript on the characteristic quantum length β, as long as only one power α is in the focus of attention. The solutions of Eq. (2.266) are known analytically,

$$u_l^{(0)}(r) = \sqrt{\frac{r}{\beta}}\big[A\mathscr{C}_\nu(\zeta) + B\mathscr{D}_\nu(\zeta)\big], \tag{2.267}$$

where $\mathscr{C}_\nu$ and $\mathscr{D}_\nu$ stand for Bessel functions whose order ν and argument ζ are

$$\nu = \frac{2l+1}{\alpha-2}, \qquad \zeta = \frac{2}{\alpha-2}\left(\frac{\beta}{r}\right)^{(\alpha-2)/2}. \tag{2.268}$$

In the attractive case, for which the "±" in front of the inverse-power term in (2.266) is a "−", $\mathscr{C}_\nu$ and $\mathscr{D}_\nu$ are the ordinary Bessel functions J_ν and Y_ν. In the repulsive case, for which the "±" in front of the inverse-power term in (2.266) is a "+", $\mathscr{C}_\nu$ and $\mathscr{D}_\nu$ are the modified Bessel functions I_ν and K_ν, see Appendix B.4.

Large distances r correspond to small arguments ζ of the Bessel functions in (2.267). For the repulsive case, the small-argument expansions of the modified Bessel functions are [1]

$$I_\nu(\zeta) \overset{\zeta\to 0}{\sim} \frac{(\zeta/2)^\nu}{\Gamma(1+\nu)}\big[1+O\big(\zeta^2\big)\big], \qquad K_\nu(\zeta) \overset{\zeta\to 0}{\sim} \frac{\Gamma(\nu)}{2(\zeta/2)^\nu}\big[1+O\big(\zeta^2\big)\big]. \tag{2.269}$$

Since

$$\left(\frac{\zeta}{2}\right)^\nu = \left(\frac{1}{\alpha-2}\right)^{(2l+1)/(\alpha-2)}\left(\frac{\beta}{r}\right)^{l+1/2} \quad \text{and} \quad \zeta^2 \propto \left(\frac{\beta}{r}\right)^{\alpha-2}, \tag{2.270}$$

the asymptotic behaviour of the wave function (2.267) is,

$$u_l^{(0)}(r) \overset{r\to\infty}{\propto} A'\left(\frac{\beta}{r}\right)^l + B'\left(\frac{r}{\beta}\right)^{l+1}\left[1+O\left(\left(\frac{\beta}{r}\right)^{\alpha-2}\right)\right], \tag{2.271}$$

where the first term originates from the I_ν-contribution and the second term from the K_ν-contribution in (2.267). If $2l+1<\alpha-2$, then the $O((\beta/r)^{\alpha-2})$ in the square bracket leads to a contribution of higher order than l in $1/r$, the asymptotic expression (2.263) is valid and defines the scattering length in the partial wave l. On the other hand, if $2l+1>\alpha-2$, then the $O((\beta/r)^{\alpha-2})$ in the square bracket leads to a contribution of lower order than l in $1/r$. In this case, (2.263) is not valid, and a scattering length in the partial wave l cannot be defined. Similar arguments apply for the attractive case, where the modified Bessel functions I_ν and K_ν are replaced by the ordinary Bessel functions J_ν and Y_ν.

For $2l+1>\alpha-2$ corresponding to $2l+3>\alpha$, the leading near-threshold behaviour of $\tan\delta_l$ can be obtained using the expression (2.66) derived with the help of the radial Lippmann–Schwinger equation. Changing the integration variable in (2.66) from r to $\rho=kr$ yields,

$$\tan\delta_l = -\frac{2\mu}{\hbar^2k^2}\int_0^\infty u_l^{(\mathrm{s})}(\rho)V\left(\frac{\rho}{k}\right)u_l(\rho)\mathrm{d}\rho. \tag{2.272}$$

Towards threshold, $k\to 0$, the regular solution of the Schrödinger equation $u_l(\rho)$ is, beyond the range of V, dominated by the centrifugal potential. The potential V is a function of the distance r and is given by the inverse-power term V_α at large distances. Its range is characterized by the quantum mechanical length β, and it shrinks to ever smaller values of ρ for $k\to 0$. Beyond this range, the regular radial wave function has the form $u_l^{(\mathrm{s})}(\rho)+\tan\delta_l u_l^{(\mathrm{c})}(\rho)$ and can be replaced by $u_l^{(\mathrm{s})}$, because $\tan\delta_l$ tends to zero for $k\to 0$. Furthermore, in the limit $k\to 0$, the integral in (2.272) is dominated by contributions from large arguments $r=\rho/k$ of the po-

tential V, which can thus be replaced by its asymptotic form V_α defined in (2.264). Inserting V_α in (2.272) and replacing u_l by $u_l^{(\mathrm{s})}$ gives

$$\tan\delta_l \overset{k\to 0}{\sim} \mp(k\beta)^{\alpha-2}\int_0^\infty \frac{u_l^{(\mathrm{s})}(\rho)^2}{\rho^\alpha}\mathrm{d}\rho. \tag{2.273}$$

The integrand in (2.273) falls off as $1/\rho^\alpha$ at large scaled distances, because $u_l^{(\mathrm{s})}$ approaches $\sin(\rho - l\frac{\pi}{2})$ for large ρ. For small ρ, $u_l^{(\mathrm{s})}(\rho)$ is proportional to ρ^{l+1}, so the integrand is proportional to $\rho^{2l+2-\alpha}$. The integral converges when $2l+2-\alpha > -1$, i.e. when $\alpha < 2l+3$.

The integral on the right-hand side of (2.273) can be evaluated analytically for the inverse-power potential V_α of (2.264) with $\alpha < 2l+3$,

$$\tan\delta_l \overset{k\to 0}{\sim} \mp\frac{\pi}{4}\frac{\Gamma(\alpha-1)\Gamma(l+\frac{3}{2}-\frac{\alpha}{2})}{[\Gamma(\frac{\alpha}{2})]^2\Gamma(l+\frac{1}{2}+\frac{\alpha}{2})}\left(\frac{k\beta}{2}\right)^{\alpha-2}, \quad \alpha < 2l+3. \tag{2.274}$$

Note that the right-hand side of (2.274) is determined exclusively by the asymptotic inverse-power behaviour of the potential and does not depend on deviations from this form at smaller distances.

For $\alpha > 2l+3$, the asymptotic form of the threshold solution is given by (2.263). The leading near-threshold behaviour of the scattering phase shift is as given in Eq. (2.77) in Sect. 2.3.8, with a scattering length a_l depending on the whole potential, not only its asymptotic behaviour.

2.6.2 The Special Case $2l+3=\alpha$

If the power α characterizing the asymptotic fall-off of the potential is odd, then $(\alpha-3)/2$ is an integer, and the angular momentum quantum number $l = (\alpha-3)/2$ lies in between the two cases expressed in Eq. (2.77) in Sect. 2.3.8 and Eq. (2.274) above. For this value of l, the Bessel functions in the zero-energy solutions (2.267) of the radial Schrödinger equation (2.266) have the following order and argument:

$$\nu = 1, \quad \zeta = \frac{1}{l+\frac{1}{2}}\left(\frac{\beta}{r}\right)^{l+1/2}. \tag{2.275}$$

If the inverse-power term in (2.266) is attractive, i.e. the "$\pm$" is a "$-$", then the two linearly independent threshold solutions $u_l^{(0)}$ and $w_l^{(0)}$ at large distances are,

$$\begin{aligned} u_l^{(0)}(r) &\overset{r\to\infty}{\sim} \sqrt{\frac{r}{\beta}}J_1(\zeta) \overset{r/\beta\to\infty}{\sim} \frac{1}{2l+1}\left(\frac{\beta}{r}\right)^l + O\left(\left(\frac{\beta}{r}\right)^{3l+1}\right), \\ w_l^{(0)}(r) &\overset{r\to\infty}{\sim} \sqrt{\frac{r}{\beta}}Y_1(\zeta) \overset{r/\beta\to\infty}{\sim} -\frac{2l+1}{\pi}\left(\frac{r}{\beta}\right)^{l+1} + \frac{1}{\pi}\left(\frac{\beta}{r}\right)^l \ln\left(\frac{\beta}{r}\right) + \cdots, \end{aligned} \tag{2.276}$$

where $\cdots$ stands for residual terms that start with a contribution proportional to $(\beta/r)^l$ *without* the logarithmic factor. For $r/\beta \to \infty$, the second term in the expansion of $w_l^{(0)}(r)$, containing the logarithmic factor, is stronger than these residual terms and also stronger than the contribution from $u_l^{(0)}(r)$. Retaining only the two strongest terms from $w_l^{(0)}(r)$ leads to the following relation for the large-distance behaviour of the regular solution of the radial Schrödinger equation (2.35) in the near-threshold limit:

$$\lim_{kr\to 0, r\to\infty} \left[u_l^{(\mathrm{s})}(kr) + \tan\delta_l u_l^{(\mathrm{c})}(kr)\right] \propto \lim_{r/\beta\to\infty} \left[(2l+1)\left(\frac{r}{\beta}\right)^{l+1} - \left(\frac{\beta}{r}\right)^{l} \ln\left(\frac{\beta}{r}\right)\right]. \tag{2.277}$$

Note that as already observed for the case $2l+3 > \alpha$ in Eq. (2.274), the right-hand side of (2.277) is completely determined by the asymptotic inverse-power form of the potential and independent of deviations from this form at smaller distances. For $u_l^{(\mathrm{s})}(kr)$ and $u_l^{(\mathrm{c})}(kr)$ on the left-hand side of (2.277), we insert the leading small-argument behaviour from (2.40). For easier comparison of both sides of the equation, we replace the product kr on the left-hand side by $(k\beta)(r/\beta)$, while on the right-hand side we replace the ratio β/r in the logarithm by $(k\beta)/(kr)$. Matching the left- and right-hand sides of (2.277) thus leads to the requirement

$$\left(\frac{r}{\beta}\right)^{l+1} + \tan\delta_l \frac{2^{2l+1}\Gamma(l+\frac{1}{2})\Gamma(l+\frac{3}{2})}{\pi(k\beta)^{2l+1}} \left(\frac{\beta}{r}\right)^{l} \propto (2l+1)\left(\frac{r}{\beta}\right)^{l+1} - \left(\frac{\beta}{r}\right)^{l} \left[\ln(k\beta) - \ln(kr)\right] \tag{2.278}$$

for $kr \to 0$ and $r/\beta \to \infty$. For $kr \to 0$, the absolute value of $\ln(kr)$ is small compared to the absolute value of $\ln(k\beta)$ when $r \gg \beta$. If we ignore the term $\ln(kr)$ on the right-hand side, then Eq. (2.278) is fulfilled when

$$\tan\delta_l \overset{k\to 0}{\sim} -\frac{\pi}{\Gamma(l+\frac{1}{2})\Gamma(l+\frac{3}{2})} \left(\frac{k\beta}{2}\right)^{2l+1} \frac{\ln(k\beta)}{(2l+1)}. \tag{2.279}$$

If the inverse-power term in (2.266) is repulsive, i.e. the "$\pm$" is a "$+$", then the two linearly independent threshold solutions $u_l^{(0)}$ and $w_l^{(0)}$ at large distances are as in (2.276), but the ordinary Bessel functions $J_1(\zeta)$ and $Y_1(\zeta)$ are replaced by the modified Bessel functions $I_1(\zeta)$ and $K_1(\zeta)$. In the expression for $w_l^{(0)}$ in (2.276), this leads to an irrelevant factor $\frac{2}{\pi}$ and to a "$+$" instead of a "$-$" in front of the first term on the right-hand side. In this case, the "$-$" on the right-hand side of (2.279) is replaced by a "$+$".

The relation $2l+1 = \alpha - 2$ can be used to replace the angular momentum quantum number l by the power α in Eq. (2.279)—and in the corresponding equation for

the repulsive case,

$$\tan\delta_l \overset{k\to 0}{\sim} \pm\frac{\pi/2}{[\Gamma(\frac{\alpha}{2})]^2}\left(\frac{k\beta}{2}\right)^{\alpha-2}\ln(k\beta); \tag{2.280}$$

the "$\pm$" is a "$+$" in the repulsive and a "$-$" in the attractive case. The right-hand sides of (2.279) and (2.280) depend only on the asymptotic inverse-power part of the potential. They are only marginally the leading term; the next contribution is of order $k^{2l+1} = k^{\alpha-2}$ *without* the logarithmic factor and contains effects due to deviations of the potential from the inverse-power form at smaller distances.

2.6.3 Modified Effective-Range Expansions

For potentials falling off faster than any power of the distance asymptotically, the quantity $k^{2l+1}\cot\delta_l$ can generally be expanded in powers of k^2. The first two terms of this "effective-range" expansion are given for s-waves in Sect. 2.3.8, see Eqs. (2.103), (2.104). The results of the previous two subsections indicate that the applicability of the effective-range expansion is limited for potentials falling off as $1/r^\alpha$ ($\alpha > 2$). For s-waves ($l = 0$) a scattering length a can only be defined if $\alpha > 3$. The next term in the expansion (2.104) contains the effective range

$$r_{\text{eff}} = 2\int_0^\infty \left(\left[w^{(0)}(r)\right]^2 - \left[u^{(0)}(r)\right]^2\right)\mathrm{d}r. \tag{2.281}$$

In this expression $u^{(0)}$ stands for the regular solution of the radial Schrödinger equation, for $l = 0$, whose asymptotic behaviour is $u^{(0)}(r) \overset{r\to\infty}{\sim} 1 - r/a$ while $w^{(0)}$ is the, not necessarily regular, solution of the free particle's equation which carries this asymptotic form down all the way to $r = 0 : w^{(0)}(r) = 1 - r/a$, compare Eq. (2.98) in Sect. 2.3.8. The convergence of the integral in (2.281) depends on how rapidly $u^{(0)}(r)$ approaches its asymptotic form, and this, in turn, depends on the asymptotic fall-off of $V(r)$.

For a potential falling off as an inverse power according to (2.264), the threshold solutions of the radial Schrödinger equation are, at large distances, of the form $\sqrt{r/\beta}\mathscr{C}_\nu(\zeta)$; here $\mathscr{C}_\nu(\zeta)$ stands for a Bessel function whose order ν and argument ζ are given by (2.270); for $l = 0$:

$$\nu = \frac{1}{\alpha - 2}, \quad \zeta = 2\nu\left(\frac{\beta}{r}\right)^{1/(2\nu)}. \tag{2.282}$$

As already observed for arbitrary l in Sect. 2.6.1, the Bessel functions J_ν (for an attractive $1/r^\alpha$ potential) and I_ν (in the repulsive case) lead to a near-threshold wave function proportional to $(\beta/r)^l$ asymptotically, i.e. to a constant for $l = 0$, while

$$\sqrt{\frac{r}{\beta}}\begin{pmatrix} Y_\nu(\zeta) \\ K_\nu(\zeta)\end{pmatrix} \overset{r/\beta\to\infty}{\propto} \frac{r}{\beta}\left[1 + O\left(\left(\frac{\beta}{r}\right)^{\alpha-2}\right)\right], \tag{2.283}$$

see Eq. (2.271). The asymptotic behaviour of $u^{(0)}$ is thus

$$u^{(0)}(r) \overset{r\to\infty}{\sim} 1 - \frac{r}{a} + O\left(\left(\frac{\beta}{r}\right)^{\alpha-3}\right)$$

$$\Rightarrow \quad \left[u^{(0)}(r)\right]^2 \overset{r\to\infty}{\sim} \left(1 - \frac{r}{a}\right)^2 + O\left(r^{4-\alpha}\right). \tag{2.284}$$

Consequently, the integrand in (2.281) falls off as $r^{4-\alpha}$ asymptotically, and this must be faster than $1/r$ for the integral to converge. A finite expression for the effective range (2.281) requires $\alpha > 5$, i.e., the potential must fall off faster than $1/r^5$ asymptotically.

There is one exception to this condition. If the scattering length a is infinite, i.e., if there is a bound state exactly at threshold, then the wave function (2.267) contains only the J_ν or I_ν contribution, so $u^{(0)}(r) \overset{r\to\infty}{\sim} 1 + O(r^{2-\alpha})$ and the integrand in (2.281) falls off as $r^{2-\alpha}$ asymptotically. In this case, $\alpha > 3$ is sufficient for the integral to converge. When there is an s-wave bound state exactly at threshold, the leading near-threshold behaviour of the s-wave scattering phase shift is, according to (2.103),

$$\cot\delta_{l=0} \overset{k\to 0}{\sim} \frac{r_{\text{eff}}k}{2}, \tag{2.285}$$

and this holds for all potentials falling off faster than $1/r^3$ asymptotically.

When the potential falls off as $1/r^\alpha$ asymptotically, with $\alpha > 3$, then the effective-range expansion for the s-wave scattering phase shift starts as in (2.103), but the expansion in powers of k^2 does not continue indefinitely. As shown above, the k^2-term (generally) requires $\alpha > 5$, and analogous considerations [29] show that the expansion (2.103) is only valid up to terms k^{2n} with $2n < \alpha - 3$. Higher terms include odd powers of k and can also contain non-analytic, logarithmic factors.

These observations further limit the practical use of the effective-range expansion (2.103). When both target and projectile are spherical, the highest power α of practical significance is $\alpha = 7$, which occurs in the interaction between two neutral polarizable atoms (or molecules) when the electrostatic van der Waals interaction ($\propto 1/r^6$ at large distances) is corrected for asymptotically relevant retardation effects [11]. In this case the leading, constant term in the expansion for $k^{2l+1}\cot\delta_l$, which defines the scattering length, exists only for $l = 0$ and $l = 1$. The expansion holds up to the second term proportional to k^2 only for $l = 0$, and the expansion is not valid up to the k^4-term, even for $l = 0$. The naïve expansion (2.103) has to be modified substantially for potentials falling off as an inverse power at large distances.

Such a *modified effective-range expansion* was formulated by O'Malley, Spruch and Rosenberg [34] in 1961 for the important case of a potential with an attractive tail proportional to $1/r^4$, as occurs in the interaction of a charged particle with a polarizable neutral partner. Up to and including terms of order k^2, the modified

effective-range expansion for s-waves reads

$$k\cot\delta_{l=0} \overset{k\to 0}{\sim} -\frac{1}{a} + \frac{\pi}{3a^2}\beta^2 k + \frac{4\beta^2}{3a}k^2\ln\left(\frac{k\beta}{4}\right) + \left[\frac{\tilde{r}_{\text{eff}}}{2} + \frac{\pi}{3}\beta + \left(\frac{20}{9} - \frac{8}{3}\psi\left(\frac{3}{2}\right)\right)\frac{\beta^2}{a} - \frac{\pi\beta^3}{3a^2} - \frac{\pi^2}{9a^3}\right]k^2, \tag{2.286}$$

where ψ is the digamma function, $\psi(z) = \Gamma'(z)/\Gamma(z)$, $\psi(\frac{3}{2}) = 0.0364899740\ldots$ (see Appendix B.3). The *modified effective range* $\tilde{r}_{\text{eff}}$ is defined as in Eq. (2.281), except that $w^{(0)}(r)$ now is the, not necessarily regular, radial wave function that solves the s-wave radial Schrödinger equation containing the attractive inverse-power potential $V_{\alpha=4}$, as defined in (2.264), with "$-$" on the far-right, and behaves asymptotically as $w^{(0)}(r) \overset{r\to\infty}{\sim} 1 - r/a$. Beyond the s-wave, i.e. for $l \geq 1$, the condition $2l + 3 > \alpha$ is always fulfilled for $\alpha = 4$, so the leading near-threshold behaviour of the scattering phase shifts is given by,

$$\tan\delta_l \overset{k\to 0}{\sim} \frac{\pi(k\beta)^2}{(2l+3)(2l+1)(2l-1)}, \quad l \geq 1, \tag{2.287}$$

in accordance with (2.274).

For a potential asymptotically proportional to $1/r^3$, the condition treated in Sect. 2.6.2 is fulfilled for s-waves and Eq. (2.280) becomes

$$\tan\delta_{l=0} \overset{k\to 0}{\sim} \pm k\beta\ln(k\beta) + O(k). \tag{2.288}$$

Towards threshold, the s-wave partial-wave scattering amplitude diverges logarithmically (see Eq. (2.47) in Sect. 2.3.3),

$$f_{l=0} \overset{k\to 0}{\sim} \pm\beta\ln(k\beta), \tag{2.289}$$

so the differential scattering cross section also diverges logarithmically towards threshold. Later on, in Sect. 4.1.5, an extension of Eq. (2.288) is presented, in which the right-hand side contains *all* terms of order k, and also those of order k^2, so that the next term is of order k^3, see Eq. (4.129) in Sect. 4.1.3.

All nonvanishing angular momentum quantum numbers $l > 0$ fulfill the condition $2l + 3 > \alpha$, so $\tan\delta_l \overset{k\to 0}{\propto} k$ according to (2.274). It follows that all partial-wave scattering amplitudes f_l with $l > 0$ tend to a finite limit and all partial waves $l > 0$ give a finite contribution to the scattering cross section at threshold. The magnitude of these contributions decreases with increasing l according to (2.274),

$$\tan\delta_l \overset{k\to 0}{\sim} \mp\frac{1}{2l(l+1)}k\beta, \qquad f_l \overset{k\to 0}{\sim} \mp\frac{2l+1}{2l(l+1)}\beta \quad \text{for } \alpha = 3, l > 0. \tag{2.290}$$

2.6.4 Peripheral Scattering

The right-hand side of Eq. (2.274) is the result of the radial Born approximation for the phase shift, when the potential is taken to be the inverse-power potential V_α defined in (2.264), compare Eq. (2.67) in Sect. 2.3.5:

$$\tan\delta_l^{\text{Born}} = \mp\frac{\pi}{4}\left(\frac{k\beta}{2}\right)^{\alpha-2}\frac{\Gamma(\alpha-1)\Gamma(l+\frac{3}{2}-\frac{\alpha}{2})}{[\Gamma(\frac{\alpha}{2})]^2\Gamma(l+\frac{1}{2}+\frac{\alpha}{2})}, \quad l > \frac{\alpha-3}{2}. \tag{2.291}$$

This result was given by Dalgarno et al. in Ref. [14]. For increasing angular momentum quantum number l, the centrifugal potential becomes increasingly dominant and the accuracy of the radial Born approximation (2.291) improves, $\tan\delta_l^{\text{Born}} \overset{l\to\infty}{\sim} \tan\delta_l$. The availability of the analytical formula (2.291) for large l is very helpful for the actual calculation of scattering cross sections, because it means that the radial Schrödinger equation need only be solved explicitly for a finite, preferably small number of partial waves.

A simplification of Eq. (2.291), valid for large l, can be derived via *Stirling's formula* (B.17) [see Appendix B.3],

$$\Gamma(z) \overset{z\to\infty}{\sim} \sqrt{2\pi}\,\mathrm{e}^{-z}z^{z-1/2}\left[1+O\left(\frac{1}{z}\right)\right]. \tag{2.292}$$

Applying (2.292) to the two gamma functions with l-dependent arguments in (2.291) gives

$$\tan\delta_l \approx \delta_l \overset{l\to\infty}{\sim} \mp\frac{\pi}{4}\left(\frac{k\beta}{2}\right)^{\alpha-2}\frac{\Gamma(\alpha-1)}{[\Gamma(\frac{\alpha}{2})]^2}\left(l+\frac{3-\alpha}{2}\right)^{1-\alpha}. \tag{2.293}$$

Treating l as a continuous variable and taking the derivative of the expression for $\tan\delta_l \approx \delta_l \pmod\pi$ with respect to l yields

$$\frac{\mathrm{d}\delta_l}{\mathrm{d}l} \overset{l\to\infty}{\sim} \pm\frac{\pi}{2^\alpha}(k\beta)^{\alpha-2}\frac{\Gamma(\alpha)/[\Gamma(\frac{\alpha}{2})]^2}{(l+\frac{3-\alpha}{2})^\alpha} = \frac{\pi}{2^\alpha}\frac{C_\alpha}{E}\frac{\Gamma(\alpha)}{[\Gamma(\frac{\alpha}{2})]^2}\left(\frac{k}{l+\frac{3-\alpha}{2}}\right)^\alpha, \tag{2.294}$$

where the relations $k^2 = 2\mu E/\hbar^2$ and $\pm\beta^{\alpha-2} = 2\mu C_\alpha/\hbar^2$ were used to generate the expression on the far right.

The phase-shift derivative (2.294) can be related to the classical deflection function $\Theta(b)$ familiar from Chap. 1. The classical impact parameter b is related to the angular momentum L via $L = p_\infty b$, so

$$L = \hbar k b \equiv \hbar l \quad \Rightarrow \quad \frac{l+\frac{3-\alpha}{2}}{k} \overset{l\to\infty}{\approx} \frac{l}{k} = b. \tag{2.295}$$

Recalling the formula (1.19) in Sect. 1.2 describing the large-b behaviour of the classical deflection function $\Theta(b)$ shows,

$$\Theta(b) \overset{b\to\infty}{\sim} \frac{C_\alpha}{Eb^\alpha} \frac{\pi\Gamma(\alpha)}{2^{\alpha-1}[\Gamma(\frac{\alpha}{2})]^2} \overset{l\to\infty}{\sim} 2\frac{\mathrm{d}\delta_l}{\mathrm{d}l}. \tag{2.296}$$

The relation $\Theta(b) \overset{b\to\infty}{\sim} 2\mathrm{d}\delta_l/\mathrm{d}l$ was also derived without reference to a particular shape of the potential in the semiclassical WKB framework in Sect. 2.4.3, see Eq. (2.176). For large angular momentum quantum numbers l, corresponding classically to large impact parameters b, the quantum mechanical phase shifts are transparently connected via this relation to the classical deflection function. Note however, that the contribution of impact parameters near b to the classical total scattering cross section is $2\pi b\mathrm{d}b$, and summation over all contributions, i.e. integrating over all b leads to an infinite result. In quantum mechanics, the contribution of the partial wave $l \equiv kb$ is, according to (2.52),

$$\sigma_{[l]} = \frac{4\pi}{k^2}(2l+1)\sin^2\delta_l \approx 2\pi b\mathrm{d}b\big[2\sin^2\delta_l\big]. \tag{2.297}$$

In order to obtain the expression on the far right of (2.297), one factor $1/k$ is interpreted as $\mathrm{d}l/k$, with $\mathrm{d}l = 1$ as the small increment in l, and $\mathrm{d}l/k$ is equated with $\mathrm{d}b$. The statistical average of $2\sin^2\delta_l$ is unity, and inserting this value in the square bracket in (2.297) recovers the classical expectation. The decrease of $\sin^2\delta_l$ with increasing l quenches the contributions of the high angular momenta to the quantum mechanical total scattering cross section. For a given energy (fixed k), we have $\delta_l \overset{l\to\infty}{\propto} 1/l^{\alpha-1}$ according to (2.293), so $(2l+1)\sin^2\delta_l \overset{l\to\infty}{\propto} 1/l^{2\alpha-3}$ and summation over all l to infinity converges to a finite value if $2\alpha - 3 > 1$, i.e. if $\alpha > 2$. For a potential falling off faster than $1/r^2$ at large distances, the quantum mechanical total scattering cross section at a given energy E is finite.

2.6.5 The Lennard–Jones Potential

A model potential that is widely used to describe inter-atomic interactions is the Lennard–Jones potential, which was already discussed in Sects. 1.2.3 and 1.3.3,

$$V_{\mathrm{LJ}}(r) = \mathscr{E}\left[\left(\frac{r_{\min}}{r}\right)^{12} - 2\left(\frac{r_{\min}}{r}\right)^{6}\right]. \tag{2.298}$$

The quantum mechanical properties of the potential (2.298) are characterized by the ratio of the energy $\mathscr{E}$ to the energy scale $\hbar^2/(2\mu r_{\min}^2)$ provided by the length $r_{\min}$,

$$B_{\mathrm{LJ}} = \frac{\mathscr{E}}{\hbar^2/(2\mu r_{\min}^2)}. \tag{2.299}$$

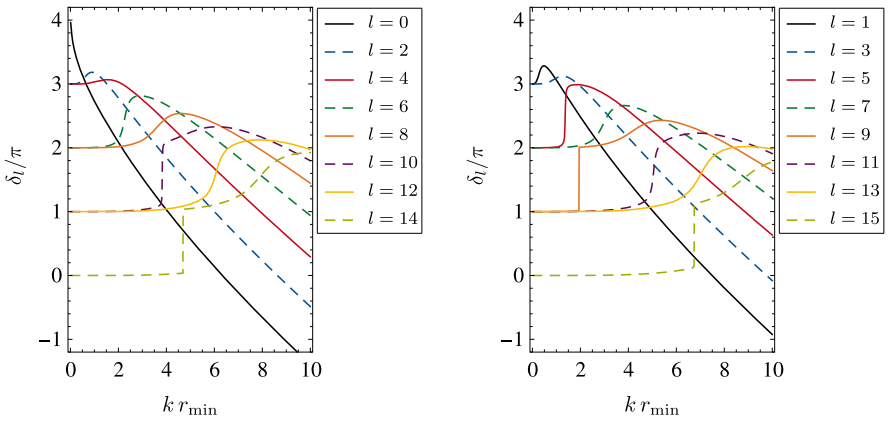

Fig. 2.21 Phase shifts for scattering by the Lennard–Jones potential (2.298) with $B_{\mathrm{LJ}} = 240$. Even and odd partial waves are shown in separate panels to avoid overcrowding in the figure

In terms of the scaled Lennard–Jones coordinate $s = r/r_{\min}$, the radial Schrödinger equation (2.35) with the potential (2.298) reads

$$-\frac{\mathrm{d}^2 u_l}{\mathrm{d}s^2} + \left[\frac{l(l+1)}{s^2} + B_{\mathrm{LJ}}\left(\frac{1}{s^{12}} - \frac{2}{s^6}\right)\right] u_l(s) = (k r_{\min})^2 u_l(s). \tag{2.300}$$

For the special value $B_{\mathrm{LJ}} = 240$, the potential (2.298) supports four bound states in the partial wave $l = 0$, three in the partial waves $l = 1$ to $l = 4$, two in the partial waves $l = 5$ to $l = 8$ and one in the partial waves $l = 9$ to $l = 13$. The scattering phase shifts are shown as functions of the scaled momentum $k r_{\min}$ for partial waves up to $l = 15$ in Fig. 2.21. The near-threshold behaviour of the phase shifts is quite similar to that shown in Fig. 2.7 for the short-range model potential (2.105). All phase shifts tend to an integer multiple of π at threshold. The observation that the number of short-distance nodes of the radial wave function at near-threshold energies corresponds to the number n_{b} of bound states supported by the effective potential applies in the present case, so it makes sense to start $\delta_l(k)$ with the value $n_{\mathrm{b}}\pi$ at threshold. However, the other condition for the validity of Levinson's theorem (2.108), namely that the phase shifts tend to zero in the high-energy limit, is not fulfilled for the Lennard–Jones potential (2.298). This is because the small-distance behaviour of the potential is dominated by the repulsive $1/r^{12}$ term, which is *more singular* than $1/r^2$, i.e. than the centrifugal potential. Hence the small-distance nodes of the radial wave function do not coalesce with the nodes of the free particle's radial wave function at high energies. The high-energy behaviour of the s-wave phase shift follows from (2.179) for the special case $\alpha = 12$, and for $l > 0$ we add a contribution $l\frac{\pi}{2}$, so

$$\delta_l \overset{k\to\infty}{\sim} -(k\beta_{12})^{5/6}\frac{\sqrt{\pi}}{2}\frac{\Gamma(\frac{11}{12})}{\Gamma(\frac{17}{12})} + \left(l + \frac{1}{2}\right)\frac{\pi}{2}, \quad \beta_{12} = r_{\min}(B_{\mathrm{LJ}})^{1/10}. \tag{2.301}$$

The high-energy decrease of the scattering phase shifts is already visible in the range covered in Fig. 2.21, and it is qualitatively similar to the decrease of the phase shifts in hard-sphere scattering, as described by the lower equation (2.74) and shown in Fig. 2.3. The additive term $l\frac{\pi}{2}$ accounting for the l-dependence of the high-energy limit can be derived mathematically [7], but it can also be understood by the reasoning already applied in the case of hard-sphere scattering in Sect. 2.3.7. Since the potential is more singular than $1/r^2$ at small distances, it dominates over the centrifugal potential in the high-energy limit, and the asymptotic behaviour of the radial wave functions $u_l(r)$ becomes independent of l in this limit, compare with Eq. (2.75) for the hard-sphere case. Since this behaviour is $u_l(r) \overset{r\to\infty}{\propto} \sin(kr - l\frac{\pi}{2} + \delta_l)$, the term $+l\frac{\pi}{2}$ in the expression for the phase shift serves to eliminate the l-dependence of $u_l(r)$ in the high-energy limit.

2.7 Potentials with Inverse-Square Tails

This section is devoted to potentials which fall off as $1/r^2$ at large distances. They represent the watershed between potentials which are asymptotically stronger and those which are asymptotically weaker than the centrifugal potential in the radial Schrödinger equation.

2.7.1 Pure Inverse-Square Potential

Consider the pure inverse-square potential,

$$V_2(r) = \frac{C_2}{r^2} = \frac{\hbar^2}{2\mu}\frac{\gamma}{r^2}. \tag{2.302}$$

The radial Schrödinger equation with the potential V_2 in the partial wave l reads,

$$-\frac{\mathrm{d}^2 u_l}{\mathrm{d}r^2} + \left[\frac{l(l+1)+\gamma}{r^2}\right] u_l(r) = k^2 u_l(r). \tag{2.303}$$

As for the free-particle case, Eq. (2.303) has no characteristic scale of length or energy. Its solutions are not functions of wave number k and distance r independently, they are functions of the scaled coordinate kr (for $k > 0$). An easy way to obtain the solutions of (2.303) is to rewrite the coefficient of $1/r^2$ in the effective potential,

$$l(l+1)+\gamma = l_\gamma(l_\gamma+1) \quad \Rightarrow \quad l_\gamma = \sqrt{\left(l+\frac{1}{2}\right)^2 + \gamma} - \frac{1}{2}. \tag{2.304}$$

Two linearly independent solutions of (2.303) are then,

$$u_{l_\gamma}^{(\mathrm{s})}(kr) = \sqrt{\frac{\pi}{2}kr}\, J_{l_\gamma+\frac{1}{2}}(kr), \qquad u_{l_\gamma}^{(\mathrm{c})}(kr) = -\sqrt{\frac{\pi}{2}kr}\, Y_{l_\gamma+\frac{1}{2}}(kr). \tag{2.305}$$

If l_γ happens to be a nonnegative integer, then the wave functions (2.305) are just the free-particle's radial waves corresponding to angular momentum quantum number l_γ instead of l, as defined in Eq. (2.38) in Sect. 2.3.3. In the more general case, it seems appropriate to base the definitions on the ordinary Bessel functions J and Y rather than on the spherical Bessel functions j and y, see Appendix B.4. The properties of the solutions of (2.303) depend significantly on the sign of the argument of the square root on the far right of (2.304).

2.7.1.1 The "Under-Critical" Case

The "under-critical" case is defined by the condition

$$\left(l+\frac{1}{2}\right)^2+\gamma>0, \tag{2.306}$$

which implies that $l_\gamma+\frac{1}{2}$ is real and positive. In this case, the small-argument and large-argument behaviour of the radial wave functions (2.305) is analogous to that given in the corresponding formulae (2.39), (2.40) for the free-particle case,

$$u_{l_\gamma}^{(\mathrm{s})}(kr) \overset{kr\to\infty}{\sim} \sin\left(kr-l_\gamma\frac{\pi}{2}\right), \qquad u_{l_\gamma}^{(\mathrm{c})}(kr) \overset{kr\to\infty}{\sim} \cos\left(kr-l_\gamma\frac{\pi}{2}\right). \tag{2.307}$$

$$u_{l_\gamma}^{(\mathrm{s})}(kr) \overset{kr\to 0}{\sim} \frac{\sqrt{\pi}(kr)^{l_\gamma+1}}{2^{l_\gamma+1}\Gamma(l_\gamma+\frac{3}{2})}, \qquad u_{l_\gamma}^{(\mathrm{c})}(kr) \overset{kr\to 0}{\sim} \frac{2^{l_\gamma}\Gamma(l_\gamma+\frac{1}{2})}{\sqrt{\pi}(kr)^{l_\gamma}}. \tag{2.308}$$

The wave function $u_{l_\gamma}^{(\mathrm{s})}(kr)$ vanishes for $kr\to 0$ and plays the role of the regular solution of (2.303). Its asymptotic phase shift, relative to the free-particle's regular radial wave $u_l^{(\mathrm{s})}$, is given by

$$\delta_l=(l-l_\gamma)\frac{\pi}{2}=\left[l+\frac{1}{2}-\sqrt{\left(l+\frac{1}{2}\right)^2+\gamma}\right]\frac{\pi}{2}. \tag{2.309}$$

In a given partial wave l, the phase shift (2.309) does not depend on energy. For a given value of γ, Eq. (2.306) is always fulfilled for sufficiently large l, and the scattering phase shift tends to zero as

$$\delta_l \overset{l\to\infty}{\sim} -\frac{\gamma\pi}{4l+2}; \tag{2.310}$$

this corresponds to (2.293) with $\alpha=2$. The partial-wave scattering amplitude (2.47) behaves as,

$$f_l \overset{\delta_l\to 0}{\sim} \frac{2l+1}{k}\delta_l \overset{l\to\infty}{\sim} -\frac{\gamma}{k}\frac{\pi}{2}. \tag{2.311}$$

With Eq. (2.32) from Sect. 2.3.1 we can derive an explicit expression for the forwardly diverging part of the scattering amplitude and cross section,

$$f(\theta) \overset{\theta\to 0}{\sim} -\frac{\gamma\pi}{4k\sin(\theta/2)} \quad \Rightarrow \quad \frac{\mathrm{d}\sigma}{\mathrm{d}\Omega} \overset{\theta\to 0}{\sim} \frac{(\gamma\pi)^2}{16k^2\sin^2(\theta/2)} \overset{\theta\to 0}{\sim} \frac{(\gamma\pi)^2}{4k^2\theta^2}. \tag{2.312}$$

The proportionality of $\mathrm{d}\sigma/\mathrm{d}\Omega$ to $1/\theta^2$ in the forward direction is less singular by one power of θ than the corresponding classical result, see Eq. (1.40) in Sect. 1.3. Nevertheless, the integral of $\mathrm{d}\sigma/\mathrm{d}\Omega$ over the polar angle θ (with the differential $\mathrm{d}\cos\theta = \sin\theta\mathrm{d}\theta$) still diverges.

2.7.1.2 The "Over-Critically Attractive" Case

The "over-critically attractive" case is defined by the condition

$$\left(l+\frac{1}{2}\right)^2 + \gamma < 0. \tag{2.313}$$

This can happen for an attractive inverse-square potential (2.302) with $\gamma < -\frac{1}{4}$ for a finite number of the lower l-values. If we equate $(l+\frac{1}{2})^2\hbar^2$ with the square of the angular momentum L in the spirit of the Langer modification (2.158), then the condition (2.313) corresponds to the classical condition $L^2 + 2\mu C_2 < 0$, which was discussed at the end of Sect. 1.2.2 and for which incoming trajectories crash into the origin while encircling it an infinite number of times.

In the over-critically attractive case (2.313), the order of the Bessel functions in (2.305) becomes imaginary,

$$l_\gamma + \frac{1}{2} = \sqrt{\left(l+\frac{1}{2}\right)^2 + \gamma} = \pm\mathrm{i}\tau, \quad \tau = \sqrt{|\gamma| - \left(l+\frac{1}{2}\right)^2} > 0. \tag{2.314}$$

The two linearly independent solutions of (2.303), defined in analogy to (2.305),

$$u^{(\mathrm{s})}_{l_\gamma}(kr) = \sqrt{\frac{\pi}{2}kr}\,J_{\mathrm{i}\tau}(kr), \qquad u^{(\mathrm{c})}_{l_\gamma}(kr) = -\sqrt{\frac{\pi}{2}kr}\,Y_{\mathrm{i}\tau}(kr), \tag{2.315}$$

are now complex. Real-valued linearly independent superpositions can be constructed, e.g. as follows:

$$\begin{aligned} u^{(\mathrm{s})}_{\tau}(kr) &= \cosh\left(\frac{\pi\tau}{2}\right)u^{(\mathrm{s})}_{l_\gamma}(kr) + \mathrm{i}\sinh\left(\frac{\pi\tau}{2}\right)u^{(\mathrm{c})}_{l_\gamma}(kr) \overset{kr\to\infty}{\sim} \sin\left(kr+\frac{\pi}{4}\right), \\ u^{(\mathrm{c})}_{\tau}(kr) &= \cosh\left(\frac{\pi\tau}{2}\right)u^{(\mathrm{c})}_{l_\gamma}(kr) - \mathrm{i}\sinh\left(\frac{\pi\tau}{2}\right)u^{(\mathrm{s})}_{l_\gamma}(kr) \overset{kr\to\infty}{\sim} \cos\left(kr+\frac{\pi}{4}\right). \end{aligned} \tag{2.316}$$

The small-argument behaviour of the real-valued solutions (2.316) is,

$$\begin{aligned} u_\tau^{(\mathrm{s})}(kr) &\overset{kr\to 0}{\sim} \frac{\sqrt{\pi kr/2}}{2\cosh(\pi\tau/2)}\left[\frac{(kr/2)^{\mathrm{i}\tau}}{\Gamma(1+\mathrm{i}\tau)}+\frac{(kr/2)^{-\mathrm{i}\tau}}{\Gamma(1-\mathrm{i}\tau)}\right], \\ u_\tau^{(\mathrm{c})}(kr) &\overset{kr\to 0}{\sim} \frac{\mathrm{i}\sqrt{\pi kr/2}}{2\sinh(\pi\tau/2)}\left[\frac{(kr/2)^{\mathrm{i}\tau}}{\Gamma(1+\mathrm{i}\tau)}-\frac{(kr/2)^{-\mathrm{i}\tau}}{\Gamma(1-\mathrm{i}\tau)}\right]. \end{aligned} \tag{2.317}$$

According to (2.317), the two linearly independent functions $u_\tau^{(\mathrm{s})}$ and $u_\tau^{(\mathrm{c})}$ both fulfill the boundary condition $u_l(r) \overset{r\to 0}{\longrightarrow} 0$. In the over-critically attractive case, this condition is not sufficient to unambiguously define a regular solution of the radial Schrödinger equation (2.303).

Directly at threshold, $k = 0$, the radial wave functions cannot be expressed as functions of kr. Two linearly independent solutions of (2.303) at threshold are,

$$u_{l_\gamma}^{(+)}(r) = \left(\frac{r}{\beta}\right)^{\frac{1}{2}+\mathrm{i}\tau} = \sqrt{\frac{r}{\beta}}\mathrm{e}^{\mathrm{i}\tau\ln(r/\beta)}, \qquad u_{l_\gamma}^{(-)}(r) = \left(\frac{r}{\beta}\right)^{\frac{1}{2}-\mathrm{i}\tau} = \sqrt{\frac{r}{\beta}}\mathrm{e}^{-\mathrm{i}\tau\ln(r/\beta)}. \tag{2.318}$$

The length β is introduced so that the argument of the logarithm is dimensionless. Its choice is completely arbitrary, reflecting the fact that the radial Schrödinger equation (2.303) has no length scale. A real-valued threshold solution of (2.303) can be constructed as a linear combination of the two solutions (2.318),

$$u_{l_\gamma}^{(0)}(r) \propto \sqrt{r}\sin\left[\tau\ln\left(\frac{r}{\beta}\right)\right]. \tag{2.319}$$

Since the length β is arbitrary, so is the phase of the sine in (2.319). Changing β to β' is equivalent to adding a phase $\tau\ln(\beta/\beta')$. The wave function (2.319) has a node whenever the argument of the sine is an integer multiple of π. For a given choice of β this gives an infinite series of nodes r_n,

$$r_n = \beta\mathrm{e}^{n\pi/\tau}, \quad n = 0, \pm1, \pm2, \pm3, \ldots. \tag{2.320}$$

Infinitely many nodes accumulate at $r = 0$ for $n \to -\infty$ and infinitely many nodes extend to $r \to \infty$ for $n \to +\infty$. The ratio of two successive nodes is

$$\frac{r_{n+1}}{r_n} = \mathrm{e}^{\pi/\tau}. \tag{2.321}$$

Choosing a value for β or fixing the position of one node determines the positions of all other nodes via (2.320) or (2.321).

When (2.313) is fulfilled, then the radial Schrödinger equation (2.303) also has physically meaningful solutions for negative energies $E = -\hbar^2\kappa^2/(2\mu)$, in particular the solution

$$u_\tau^{(\kappa)}(\kappa r) = \sqrt{\frac{2}{\pi}\kappa r}\,K_{\mathrm{i}\tau}(\kappa r), \tag{2.322}$$

where K stands for the modified Bessel function, see Appendix B.4. The asymptotic large-argument behaviour of the wave function (2.322),

$$u_\tau^{(\kappa)}(\kappa r) \overset{\kappa r \to \infty}{\sim} \mathrm{e}^{-\kappa r}, \tag{2.323}$$

fulfills the boundary condition for bound states. At the same time,

$$u_\tau^{(\kappa)}(\kappa r) \overset{\kappa r \to 0}{\sim} -\frac{\sqrt{2\pi\kappa r}}{\sinh(\pi\tau)|\Gamma(1+\mathrm{i}\tau)|} \sin\left(\tau \ln\left(\frac{\kappa r}{2}\right) - \sigma_\tau\right), \tag{2.324}$$

where σ_τ is a phase defined by

$$\sigma_\tau = \arg\bigl[\Gamma(1+\mathrm{i}\tau)\bigr]. \tag{2.325}$$

The radial wave functions $u_\tau^{(\kappa)}(\kappa r)$ as given in (2.322) represent normalizable solutions of the radial Schrödinger equation (2.303) at all negative energies. This is a manifestation of the fact that there is no energy scale for the inverse-square potential (see also Appendix A).

Morse and Feshbach pointed out that the dilemma of a seemingly continuous bound-state spectrum can be overcome by requiring bound states with different energies to be orthogonal, see Sect. 12.3, p. 1666, of Ref. [31]. This leads to the condition

$$\sin\left[\tau \ln\left(\frac{\kappa_1}{\kappa_2}\right)\right] = 0 \tag{2.326}$$

for each pair $u_\tau^{(\kappa_1)}$, $u_\tau^{(\kappa_2)}$ of radial wave functions (2.322). Taking one arbitrary energy $E_0 = -\hbar^2\kappa_0^2/(2\mu)$ as reference bound-state energy, the whole series of bound-state energies $E_n = -\hbar^2\kappa_n^2/(2\mu)$ can be defined by,

$$\begin{aligned} &\tau \ln\left(\frac{\kappa_0}{\kappa_n}\right) = n\pi \quad \Leftrightarrow \quad n = -\frac{\tau}{2\pi} \ln\left(\frac{E_n}{E_0}\right) \quad \Leftrightarrow \quad E_n = E_0 \mathrm{e}^{-2\pi n/\tau}, \\ &n = 0, \pm 1, \pm 2, \ldots. \end{aligned} \tag{2.327}$$

For $n \to +\infty$, the energies E_n converge from below to the continuum threshold $E = 0$. The exponentially converging series is characterized by a constant ratio of successive bound-state energies,

$$\frac{E_{n+1}}{E_n} = \mathrm{e}^{-2\pi/\tau}, \qquad \frac{E_n}{E_{n+1}} = \mathrm{e}^{+2\pi/\tau}. \tag{2.328}$$

Series of levels obeying (2.328) for $n \to \infty$ are called *dipole series*, because overcritically attractive $1/r^2$ potentials typically occur in the interaction of a charged particle and an overall neutral dipole.

For $n \to -\infty$, the energies E_n in (2.327) tend exponentially to $-\infty$; there is no lower bound on the bound state energies. This is an unphysical feature, as is the arbitrariness in the choice of reference energy E_0 in such a pure dipole series. Both deficits are overcome when the singular inverse-square behaviour of the potential at small distances is replaced by a more realistic, less singular r-dependence.

2.7.1.3 The "Critically Attractive" Case

In between the under-critical case (2.306) and the over-critically attractive case (2.313) lies the "critically attractive case", which is defined by the condition

$$\left(l+\frac{1}{2}\right)^2+\gamma=0 \quad \Rightarrow \quad l_\gamma+\frac{1}{2}=0. \tag{2.329}$$

In this case, the order of the Bessel functions in the definition (2.305) of the radial wave functions $u^{(\mathrm{s})}_{l_\gamma}$ and $u^{(\mathrm{c})}_{l_\gamma}$ vanishes exactly,

$$u^{(\mathrm{s})}_{l_\gamma}(kr)=\sqrt{\frac{\pi}{2}kr}\,J_0(kr), \qquad u^{(\mathrm{c})}_{l_\gamma}(kr)=-\sqrt{\frac{\pi}{2}kr}\,Y_0(kr). \tag{2.330}$$

The large-argument behaviour of the two radial wave functions (2.330) is

$$u^{(\mathrm{s})}_{l_\gamma}(kr) \overset{kr\to\infty}{\sim} \sin\left(kr+\frac{\pi}{4}\right), \qquad u^{(\mathrm{c})}_{l_\gamma}(kr) \overset{kr\to\infty}{\sim} \cos\left(kr+\frac{\pi}{4}\right), \tag{2.331}$$

and the small-argument behaviour follows from the small-argument behaviour of the ordinary Bessel functions J_0 and Y_0,

$$u^{(\mathrm{s})}_{l_\gamma}(kr) \overset{kr\to 0}{\sim} \sqrt{\frac{\pi}{2}kr}, \qquad u^{(\mathrm{c})}_{l_\gamma}(kr) \overset{kr\to 0}{\sim} -\sqrt{\frac{2}{\pi}kr}\left[\ln\left(\frac{kr}{2}\right)+\gamma_{\mathrm{E}}+O\big((kr)^2\big)\right]; \tag{2.332}$$

here $\gamma_{\mathrm{E}}=0.5772\ldots$ is Euler's constant, see Appendix B.3.

The critically attractive case (2.329) corresponds to an effective angular momentum quantum number $l_\gamma=-\frac{1}{2}$ and an inverse-square potential $-\hbar^2/(8\mu r^2)$. This attractive inverse-square potential occurs as the s-wave centrifugal potential in the radial Schrödinger equation for scattering in two rather than three spatial dimensions, and it is discussed in more detail in Sect. 4.3 in Chap. 4.

2.7.2 Modified Inverse-Square Potential

Consider a potential $V(r)$ which behaves as the inverse-square potential (2.302) at large distances,

$$V(r) \overset{r\to\infty}{\sim} V_2(r)=\frac{\hbar^2}{2\mu}\frac{\gamma}{r^2}, \tag{2.333}$$

but is less singular than $1/r^2$ at small distances. At distances large enough for the deviations of $V(r)$ from the pure inverse-square form (2.302) to be negligible, the real-valued regular solution $u_l(r)$ of the radial Schrödinger equation (2.35) becomes a superposition of the two real-valued solutions of (2.303), as defined in the previous subsection.

2.7.2.1 The Under-Critical Case

Consider first the case that the inverse-square tail (2.333) is under-critical, i.e. that it fulfills (2.306) and l_γ is a real number larger than $-\frac{1}{2}$. In this case, the two real-valued solutions of (2.303) are the functions $u_{l\gamma}^{(\mathrm{s})}(kr)$ and $u_{l\gamma}^{(\mathrm{c})}(kr)$ as defined in Eq. (2.305), and the asymptotic behaviour of $u_l(r)$ can be expressed with the help of an additional phase shift $\tilde{\delta}_l$,

$$u_l(r) \overset{r\to\infty}{\propto} u_{l\gamma}^{(\mathrm{s})}(r) + \tan\tilde{\delta}_l u_{l\gamma}^{(\mathrm{c})}(r) \overset{kr\to\infty}{\propto} \sin\left(kr - l_\gamma\frac{\pi}{2} + \tilde{\delta}_l\right) = \sin\left(kr - l\frac{\pi}{2} + \delta_l\right). \tag{2.334}$$

The asymptotic phase shift δ_l of the radial wave function (2.334) relative to the free-particle wave consists of the energy-independent phase shift $(l - l_\gamma)\frac{\pi}{2}$ due to the inverse-square tail and the additional phase shift $\tilde{\delta}_l$ due to the deviations of the full potential from the pure inverse-square form (2.302),

$$\delta_l(k) = (l - l_\gamma)\frac{\pi}{2} + \tilde{\delta}_l(k). \tag{2.335}$$

For the near-threshold behaviour of $\tilde{\delta}_l$, we adapt the discussion of Sect. 2.3.8 to the present situation. In analogy to Eq. (2.76), we can write the asymptotic behaviour (2.334) as

$$\begin{aligned} u_l(r) &\overset{kr\to 0}{\propto} u_{l_\gamma}^{(\mathrm{s})}(kr) + \tan\tilde{\delta}_l u_{l_\gamma}^{(\mathrm{c})}(kr) \\ &\sim \frac{\sqrt{\pi}k^{l_\gamma+1}}{2^{l_\gamma+1}\Gamma(l_\gamma+\frac{3}{2})}\left[r^{l_\gamma+1} + \tan\tilde{\delta}_l \frac{2^{2l_\gamma+1}\Gamma(l_\gamma+\frac{1}{2})\Gamma(l_\gamma+\frac{3}{2})}{\pi k^{2l_\gamma+1} r^{l_\gamma}}\right]. \end{aligned} \tag{2.336}$$

As in Sect. 2.3.8, we argue that the square bracket must become independent of k in the limit $k \to 0$ so that, in analogy to (2.77),

$$\tan\tilde{\delta}_l \overset{k\to 0}{\sim} \mp\frac{\pi}{\Gamma(l_\gamma+\frac{1}{2})\Gamma(l_\gamma+\frac{3}{2})}\left(\frac{\tilde{a}_l k}{2}\right)^{2l_\gamma+1}. \tag{2.337}$$

The quantity $\tilde{a}_l$ has the dimension of a length and is assumed to be nonnegative. This is necessary, because the power $2l_\gamma + 1$, to which $\tilde{a}_l k/2$ is raised in (2.337), is generally not an odd integer as in (2.77), but can be any positive real number. The length $\tilde{a}_l$ can be interpreted as a scattering length (in the partial wave l) describing the near-threshold behaviour of the tangent of the additional phase shift $\tilde{\delta}_l$. Note that the full phase shift in the partial wave l consists of $\tilde{\delta}_l$ on top of the energy-independent background term according to (2.335).

The derivation of Eq. (2.337) implies that the large-distance behaviour of the regular threshold solution of the radial Schrödinger equation is, in analogy to (2.81),

$$u_l^{(0)}(r) \overset{r\to\infty}{\propto} r^{l_\gamma+1} \mp \frac{\tilde{a}_l^{2l_\gamma+1}}{r^{l_\gamma}}. \tag{2.338}$$

When the deviation of the full potential $V(r)$ from the inverse-square form (2.302) falls of as $1/r^\alpha$, $\alpha > 2$, at large distances, then the derivation of Eqs. (2.337) and (2.338) requires $\alpha - 2 > 2l_\gamma + 1$, i.e. $\alpha > 2l_\gamma + 3$, for the reasons discussed in Sect. 2.6.1. Otherwise, $\tan\tilde{\delta}_l$ is of order $k^{\alpha-2}$ near threshold.

If the short-range deviation of the full potential $V(r)$ from the pure inverse-square form (2.302) is so attractive that the effective potential in the partial wave l supports one or more bound states, then the discussions in Sect. 2.3.9 and Sect. 2.5.3 on the additional nodes of the threshold solution of the radial Schrödinger equation at small distances can be adapted to the present situation, and Levinson's theorem can be formulated as,

$$\lim_{k\to 0}\tilde{\delta}_l(k) - \lim_{k\to\infty}\tilde{\delta}_l(k) = \lim_{k\to 0}\delta_l(k) - \lim_{k\to\infty}\delta_l(k) = n_\mathrm{b}\pi, \tag{2.339}$$

where n_b is the number of bound states in the partial wave l. Equation (2.339) can be formulated for the full phase shifts δ_l, in relation to the free-particle solutions of the radial Schrödinger equation, because these differ from the additional phase shifts $\tilde{\delta}_l$ only via an energy-independent term according to (2.335).

2.7.2.2 The Over-Critically Attractive Case

Now consider the case that the inverse-square tail (2.302) is over-critically attractive, i.e. that it fulfills (2.313) and $l_\gamma + \frac{1}{2} = \mathrm{i}\tau$, $\tau = \sqrt{|\gamma| - (l+\frac{1}{2})^2} > 0$. At sufficiently large distances, where the deviations of the full potential $V(r)$ from the pure inverse-square form (2.302) are negligible, the real-valued regular solution $u_l(r)$ of the radial Schrödinger equation (2.35) is a superposition of the two linearly independent solutions (2.316),

$$u_l(r) \overset{r\to\infty}{\propto} u_\tau^{(\mathrm{s})}(kr) + \tan\tilde{\delta}_l u_\tau^{(\mathrm{c})}(kr) \overset{kr\to\infty}{\propto} \sin\left(kr + \frac{\pi}{4} + \tilde{\delta}_l\right). \tag{2.340}$$

Comparing to the asymptotic phase of the free particle's regular wave function (2.39) shows that $\tilde{\delta}_l$ is, in this case, related to the actual scattering phase shift δ_l by

$$\delta_l(k) = \left(l + \frac{1}{2}\right)\frac{\pi}{2} + \tilde{\delta}_l(k). \tag{2.341}$$

Inserting the small-argument ($kr \to 0$) expansions (2.317) into the asymptotic form (2.340) gives

$$u_\tau^{(\mathrm{s})}(kr) + \tan\tilde{\delta}_l u_\tau^{(\mathrm{c})}(kr)$$
$$\overset{kr\to 0}{\sim} \frac{\sqrt{\pi kr/2}}{|\Gamma(1+\mathrm{i}\tau)|}\left[\frac{\cos[\tau\ln(kr/2)-\sigma_\tau]}{\cosh(\pi\tau/2)} - \tan\tilde{\delta}_l \frac{\sin[\tau\ln(kr/2)-\sigma_\tau]}{\sinh(\pi\tau/2)}\right]$$
$$\propto \sqrt{r}\cos\left[\tau\ln\left(\frac{kr}{2}\right) - \sigma_\tau + \Delta\right], \tag{2.342}$$

where $\sigma_\tau = \arg[\Gamma(1+\mathrm{i}\tau)]$ is the phase defined in (2.325), and Δ is an angle for which $\tan\Delta = \tan\tilde{\delta}_l/\tanh(\pi\tau/2)$. In order that the wave function (2.342) become independent of k (except for an overall factor) in the limit $kr \to 0$, the phase Δ must compensate the leading k-dependence in the argument of the cosine, $\Delta \overset{k\to 0}{\sim} -\tau\ln(k\beta/2)$, where β is an arbitrary length, which is introduced to make the argument of the logarithm dimensionless. The angle Δ grows logarithmically to infinity for $k \to 0$, and the phase shift $\tilde{\delta}_l$ behaves in much the same way. To see this, we write $\tilde{\delta}_l = \Delta + \varepsilon$ and deduce

$$\tan(\Delta+\varepsilon) = \tanh\left(\frac{\pi\tau}{2}\right)\tan\Delta$$
$$\Rightarrow \quad \tan\varepsilon = \left[\tanh\left(\frac{\pi\tau}{2}\right) - 1\right]\frac{\tan\Delta}{1+\tanh(\pi\tau/2)\tan^2\Delta}. \tag{2.343}$$

Since τ is real and positive, $\tanh(\pi\tau/2)$ is a real number between zero and unity. The square bracket on the far right of (2.343) is thus a finite negative number, and the quotient with the numerator $\tan\Delta$ varies between zero, when Δ is an even or odd multiple of $\frac{\pi}{2}$, and its maximum value $1/(2\sqrt{\tanh(\pi\tau/2)})$. As Δ grows logarithmically to infinity, the difference ε between $\tilde{\delta}_l$ and Δ remains limited to values between zero and some finite angle between $-\frac{\pi}{2}$ and zero. We can conclude that

$$\tilde{\delta}_l \overset{k\to 0}{\approx} -\tau\ln\left(\frac{k\beta}{2}\right). \tag{2.344}$$

Approaching threshold from above, $k \to 0$, the regular radial wave function converges to a well-defined threshold solution which behaves as (2.319) beyond the range of the short-range deviations of $V(r)$ from the pure inverse-square form (2.302). The length β is now no longer arbitrary, but determined (to within a factor $\mathrm{e}^{n\pi/\tau}$ with integer n) by the short-range part of the potential. Approaching threshold from below, $\kappa \to 0$, the nodes of the bound state wave functions (2.324) must converge to the nodes of the threshold solution, which are given by (2.320) at large distances. This is achieved for values κ_n with

$$\tau\ln\left(\frac{\kappa_n\beta}{2}\right) - \sigma_\tau + n\pi = 0 \quad \Leftrightarrow \quad \kappa_n = \frac{2}{\beta}\mathrm{e}^{(\sigma_\tau - n\pi)/\tau}. \tag{2.345}$$

The near-threshold behaviour of the bound-state energies is thus,

$$E_n \overset{n\to\infty}{\sim} -\frac{2\hbar^2}{\mu\beta^2}\mathrm{e}^{2(\sigma_\tau - n\pi)/\tau}. \tag{2.346}$$

2.7.2.3 The Critically Attractive Case

When the condition (2.329) is fulfilled, the regular solution of the radial Schrödinger equation (2.35) is asymptotically a superposition of the two wave functions (2.330), determined by a phase $\tilde{\delta}$,

$$u_l(r) \overset{r\to\infty}{\propto} \sqrt{kr}\big[J_0(kr) - \tan\tilde{\delta}_l Y_0(kr)\big] \overset{kr\to\infty}{\propto} \sin\left(kr + \frac{\pi}{4} + \tilde{\delta}_l\right) = \sin\left(kr - l\frac{\pi}{2} + \delta_l\right). \tag{2.347}$$

As in the over-critically attractive case, the phase $\tilde{\delta}_l$ is related to the actual scattering phase shift δ_l by Eq. (2.341). This agrees with the formula (2.335) when $l_\gamma = -\frac{1}{2}$.

In order to obtain the near-threshold behaviour of the phase $\tilde{\delta}_l$, we insert the small-argument expressions for the Bessel functions in (2.347), see also Eq. (2.332) in Sect. 2.7.1,

$$\sqrt{kr}\big[J_0(kr) - \tan\tilde{\delta}_l Y_0(kr)\big] \overset{kr\to 0}{\sim} \sqrt{kr}\left[1 - \frac{2}{\pi}\tan\tilde{\delta}_l\left(\ln\left(\frac{kr}{2}\right) + \gamma_\mathrm{E}\right)\right]. \tag{2.348}$$

We rewrite the big square bracket on the right-hand side of (2.348) as

$$\left[\cdots\right] = \tan\tilde{\delta}_l\left[\cot\tilde{\delta}_l - \ln\left(\left[\frac{kr}{2}\mathrm{e}^{\gamma_\mathrm{E}}\right]^{2/\pi}\right)\right] \tag{2.349}$$

and observe that the big-square bracket on the right-hand side of (2.349) tends to a k-independent limit for $k \to 0$ if $\cot\tilde{\delta}_l$ behaves as

$$\cot\tilde{\delta}_l \overset{k\to 0}{\sim} \ln\left(\left[\frac{k\tilde{a}_l}{2}\mathrm{e}^{\gamma_\mathrm{E}}\right]^{2/\pi}\right) = \frac{2}{\pi}\left(\ln\left(\frac{k\tilde{a}_l}{2}\right) + \gamma_\mathrm{E}\right). \tag{2.350}$$

Equation (2.350) defines the scattering length $\tilde{a}_l$ in the partial wave l for the critically attractive case. In the limit $k \to 0$, the wave function (2.348) converges to a k-independent limit $u_l^{(0)}$,

$$u_l(r) \overset{k\to 0}{\propto} u_l^{(0)}(r) \overset{r\to\infty}{\propto} -\sqrt{r}\ln\left(\frac{r}{\tilde{a}_l}\right). \tag{2.351}$$

The wave function on the far right of (2.351) has exactly one node (beyond $r = 0$), and this node lies at $r = \tilde{a}_l$.

2.7.3 *Example: Inverse-Square Potential with Hard Sphere*

As an example, consider the case of a hard sphere of radius R in conjunction with an inverse-square potential (2.302) for $r > R$. This potential is not less singular

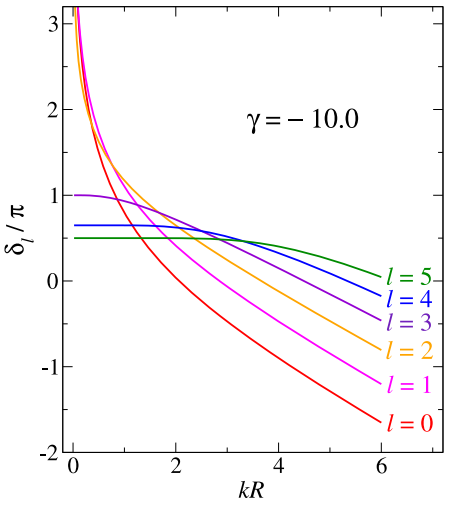

Fig. 2.22 Phase shifts for scattering by a hard sphere of radius R in the presence of an inverse-square potential (2.302) with $\gamma = -10.0$. For $l \geq 3$, the effective potential is under-critical; the scattering phase shifts are given by (2.335) and converge to the finite limit $(l - l_\gamma)\frac{\pi}{2}$ at threshold. The effective potential is over-critically attractive for $l = 0$, 1 and 2; in these cases the scattering phase shifts are given by (2.341) and grow logarithmically to infinity at threshold according to (2.344)

than $1/r^2$ at small distances, and the phase shifts $\tilde{\delta}_l$ don't vanish in the high-energy limit. The example is, however, useful for illustrating the low-energy behaviour of the phase shifts. Beyond the radius R, the radial wave function is a superposition of the solutions (2.305) in the under-critical case (2.306), and of the solutions (2.316) in the over-critically attractive case (2.313). In the under-critical case, the scattering phase shift δ_l is given by

$$\delta_l = (l - l_\gamma)\frac{\pi}{2} + \tilde{\delta}_l, \qquad \tan\tilde{\delta}_l = -\frac{u^{(\mathrm{s})}_{l_\gamma}(kR)}{u^{(\mathrm{c})}l_\gamma(kR)} = \frac{J_{l_\gamma+\frac{1}{2}}(kR)}{Y_{l_\gamma+\frac{1}{2}}(kR)}. \tag{2.352}$$

In the over-critically attractive case, the scattering phase shift δ_l is given by

$$\delta_l = \left(l + \frac{1}{2}\right)\frac{\pi}{2} + \tilde{\delta}_l, \qquad \tan\tilde{\delta}_l = -\frac{u^{(\mathrm{s})}_\tau(kR)}{u^{(\mathrm{c})}_\tau(kR)} = \mathrm{i}\tanh\left(\frac{\pi\tau}{2}\right)\frac{J_{\mathrm{i}\tau}(kR) + J_{-\mathrm{i}\tau}(kR)}{J_{\mathrm{i}\tau}(kR) - J_{-\mathrm{i}\tau}(kR)}. \tag{2.353}$$

We choose $\gamma = -10.0$. For this strength of $V_2(r)$, the effective potential is under-critical in all partial waves $l \geq 3$, while it is over-critically attractive for $l = 0$, $l = 1$ and $l = 2$. In Table 2.3 we list the values for the characteristic parameters of the over-critically attractive potential in these partial waves.

The scattering phase shifts for the hard-sphere example are shown as function of kR for partial waves up to $l = 5$ in Fig. 2.22. For $l \geq 3$, the phase shifts converge to the finite value $(l - l_\gamma)\frac{\pi}{2}$ at threshold, in accordance with Eqs. (2.335) and (2.337). In the over-critically attractive partial waves $l \leq 2$, the phase shifts diverge at threshold in accordance with (2.344).

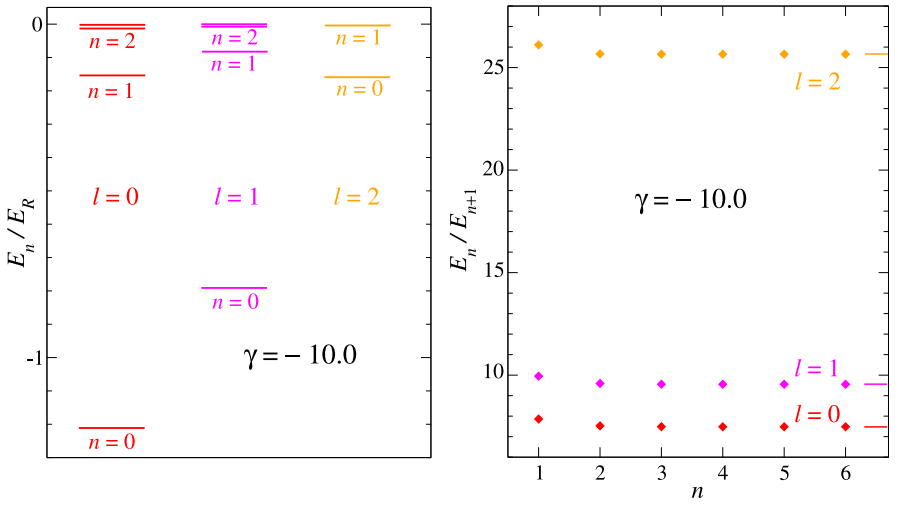

Fig. 2.23 For an attractive inverse-square potential (2.302) with $\gamma = -10.0$, cut off by a hard-sphere at radius R, the *left-hand part* shows the bound-state energies, in units of the energy E_R defined in Eq. (2.354), for the over-critically attractive partial waves $l = 0, 1,$ and 2. The *right-hand part* shows the ratios of successive energy eigenvalues in the respective partial wave. The *horizontal lines* at the right-hand edge of the figure correspond to the ratios (2.328) expected for the strength parameter $\gamma = -10$, as given in the last three columns of Table 2.3

Table 2.3 For $\gamma = -10.0$, the table shows the values of the parameter τ defined by (2.314), the phase σ_τ defined by (2.325) and the ratio $e^{2\pi/\tau}$ in (2.328) for the over-critically attractive partial waves $l = 0$, $l = 1$ and $l = 2$

$\tau(0)$	$\tau(1)$	$\tau(2)$	$\sigma_\tau(0)$	$\sigma_\tau(1)$	$\sigma_\tau(2)$	$e^{2\pi/\tau}(0)$	$e^{2\pi/\tau}(1)$	$e^{2\pi/\tau}(2)$
3.1225	2.7839	1.9365	1.1915	0.8217	0.08524	7.4800	9.5543	25.652

All regular wave functions have a node at $r = R$, so we can choose the length in Eqs. (2.319) and (2.320) as $\beta = R$. The natural energy scale is now

$$E_R = \frac{\hbar^2}{2\mu R^2} = \frac{\hbar^2}{2\mu\beta^2}. \tag{2.354}$$

The inner boundary condition for the bound-state wave functions (2.322) is that they have a node at $r = R$, so the values κ_n defining the bound-state eigenenergies $E_n = -\hbar^2\kappa_n^2/(2\mu)$ are given by the zeros of the modified Bessel function, $K_{i\tau}(\kappa_n R) = 0$. The left-hand part of Fig. 2.23 shows the spectrum of bound-state energies in the over-critically attractive partial waves. The spectrum in each partial wave is very sparse, because the energies converge very rapidly, exponentially, to the threshold. The right-hand part of the figure shows the ratios E_n/E_{n+1} in the respective partial wave. The ratio very rapidly approaches the expectation (2.328) characteristic of a dipole series. The limiting values $e^{2\pi/\tau}$ of this ratio are listed in

the last three columns of Table 2.3 and shown as horizontal lines at the right-hand edge of Fig. 2.23.

2.8 Nonvanishing Angular Momentum of Projectile and/or Target

The theory presented so far has been based on the interaction potential between target and projectile without any consideration of effects due to their internal structure. A first extension of this simple picture is to account for the fact that the projectile and/or target, in its respective rest frame, need not have vanishing angular momentum. Such a nonvanishing *internal angular momentum* is called "spin" in the case of atomic nuclei. For atoms and molecules, the label "spin" is usually used only for that part of the angular momentum which originates from the spin degrees of freedom of the electrons involved—in contrast to the orbital part of their angular momentum. This distinction is not important in the following, so the term "spin" is used for the total internal angular momentum of the projectile and of the target, and the term "orbital angular momentum" refers to the angular momentum of relative motion.

2.8.1 General Formalism for Treating Spins

The internal angular momentum of the projectile (target) is described by the operator $\hat{\mathbf{I}}_\mathrm{p}$ ($\hat{\mathbf{I}}_\mathrm{t}$) and the associated angular momentum eigenstates $|I_\mathrm{p} M_\mathrm{p}\rangle$ ($|I_\mathrm{t} M_\mathrm{t}\rangle$) are eigenstates of its square and of the component along a certain direction, which is conveniently taken to be the z-direction,

$$\begin{aligned} \hat{\mathbf{I}}_\mathrm{p}^2 |I_\mathrm{p} M_\mathrm{p}\rangle &= I_\mathrm{p}(I_\mathrm{p}+1)\hbar^2 |I_\mathrm{p} M_\mathrm{p}\rangle, \qquad & \hat{I}_{\mathrm{p},z} |I_\mathrm{p} M_\mathrm{p}\rangle &= M_\mathrm{p}\hbar |I_\mathrm{p} M_\mathrm{p}\rangle, \\ \hat{\mathbf{I}}_\mathrm{t}^2 |I_\mathrm{t} M_\mathrm{t}\rangle &= I_\mathrm{t}(I_\mathrm{t}+1)\hbar^2 |I_\mathrm{t} M_\mathrm{t}\rangle, \qquad & \hat{I}_{\mathrm{t},z} |I_\mathrm{t} M_\mathrm{t}\rangle &= M_\mathrm{t}\hbar |I_\mathrm{t} M_\mathrm{t}\rangle. \end{aligned} \tag{2.355}$$

We assume that the magnitudes of the projectile spin and the target spin, as quantified by the quantum numbers I_p and I_t, are fixed throughout the scattering process, but their orientations, as expressed via the component quantum numbers M_p and M_t, can change. The available spin states of the projectile (of the target) form a $(2I_\mathrm{p}+1)$-dimensional (a $(2I_\mathrm{t}+1)$-dimensional) space, a *spin multiplet* spanned by the eigenstates of the z-component of the respective spin,

$$M_\mathrm{p} = -I_\mathrm{p}, -I_\mathrm{p}+1, \ldots, M_\mathrm{p}, \qquad M_\mathrm{t} = -I_\mathrm{t}, -I_\mathrm{t}+1, \ldots, M_\mathrm{t}. \tag{2.356}$$

The *uncoupled* combined spin states,

$$\Upsilon_{M_\mathrm{p}, M_\mathrm{t}} \equiv |I_\mathrm{p}, M_\mathrm{p}\rangle |I_\mathrm{t}, M_\mathrm{t}\rangle, \tag{2.357}$$

form a basis of the $(2I_\mathrm{p}+1)(2I_\mathrm{t}+1)$-dimensional space of all possible components of the projectile and target spins. The total wave function of the projectile-target system consists, after separation of the centre-of-mass motion, of a spatial part depending on the relative distance coordinate $\mathbf{r}$ and a spin part depending on the spin-component quantum numbers M_p and M_t. It can be expanded in the spin states as

$$\psi(\mathbf{r}, M_\mathrm{p}, M_\mathrm{t}) = \sum_{i_\mathrm{s}=1}^{(2I_\mathrm{p}+1)(2I_\mathrm{t}+1)} \psi_{i_\mathrm{s}}(\mathbf{r})\Upsilon_{i_\mathrm{s}}(M_\mathrm{p}, M_\mathrm{t}). \tag{2.358}$$

The index i_s covers all $(2I_\mathrm{p}+1)(2I_\mathrm{t}+1)$ spin states Υ_{i_s}. These may be the states of the uncoupled basis (2.357), but any other basis of spin space can also serve the purpose. The individual spin states Υ_{i_s} define a "spin channel", and the component wave functions $\psi_{i_\mathrm{s}}(\mathbf{r})$ are the *spin-channel wave functions* in the respective spin channels.

The Hamiltonian describing the relative motion of projectile and target may also act on the spin degrees of freedom. The Schrödinger equation is

$$\left[-\frac{\hbar^2}{2\mu}\Delta + \hat{V}\right]\psi(\mathbf{r}, M_\mathrm{p}, M_\mathrm{t}) = E\psi(\mathbf{r}, M_\mathrm{p}, M_\mathrm{t}), \tag{2.359}$$

and the potential energy operator $\hat{V}$ now acts also in spin space. In order to describe the scattering process we look for solutions of (2.359) obeying the following boundary conditions,

$$\psi \overset{r\to\infty}{\sim} \mathrm{e}^{\mathrm{i}kz}\Upsilon_{i_\mathrm{s}} + \sum_{j_\mathrm{s}=1}^{(2I_\mathrm{p}+1)(2I_\mathrm{t}+1)} f_{i_\mathrm{s},j_\mathrm{s}}(\theta,\phi)\frac{\mathrm{e}^{\mathrm{i}kr}}{r}\Upsilon_{j_\mathrm{s}}. \tag{2.360}$$

An elastic scattering process doesn't only change the direction of relative motion of target and projectile, it can also change the spin part of the wave function. The wave function (2.360) describes a scattering process, in which the state of the projectile and target spins is initially given by Υ_{i_s}. The outgoing spherical wave is a superposition of components corresponding to the various possible spin states, which are labelled by Υ_{j_s}. The scattering amplitude $f_{i_\mathrm{s},j_\mathrm{s}}$ describes the scattering process accompanied by a change of spin state from Υ_{i_s} to Υ_{j_s}, and the associated differential scattering cross section is,

$$\left(\frac{\mathrm{d}\sigma}{\mathrm{d}\Omega}\right)_{i_\mathrm{s}\to j_\mathrm{s}} = \left|f_{i_\mathrm{s},j_\mathrm{s}}(\theta,\phi)\right|^2. \tag{2.361}$$

The spin-dependent scattering amplitudes $f_{i_\mathrm{s},j_\mathrm{s}}$ generally depend not only on the polar angle θ, but also on the azimuthal angle ϕ.

In many scattering experiments, the spin states are not controlled or measured. When the initial state of the spin components is unknown, the quantum mechanical description of the scattering process is best based on a statistical average over all

possible initial spin states. When the final state of the spin components is not registered, the observed yield is the sum over the contributions from all possible spin states. The differential scattering cross section observed in an experiment which does not register the spin states is obtained by averaging over all initial spin states and summing over all final spin states,

$$\frac{\mathrm{d}\sigma}{\mathrm{d}\Omega} = \frac{1}{(2I_\mathrm{p}+1)(2I_\mathrm{t}+1)} \sum_{i_\mathrm{s},j_\mathrm{s}} \left| f_{i_\mathrm{s},j_\mathrm{s}}(\theta,\phi) \right|^2. \tag{2.362}$$

If the interaction between projectile and target is independent of their spins, then the spin-changing amplitudes, $j_\mathrm{s} \neq i_\mathrm{s}$, vanish, while the spin-state conserving amplitudes are all equal to one and the same amplitude f. In this case the sum over the $(2I_\mathrm{p}+1)(2I_\mathrm{t}+1)$ identical contributions in (2.362) simply cancels the prefactor,

$$f_{i_\mathrm{s},j_\mathrm{s}} = \delta_{i_\mathrm{s},j_\mathrm{s}} f(\theta,\phi) \quad \Longrightarrow \quad \frac{\mathrm{d}\sigma}{\mathrm{d}\Omega} = \left| f(\theta,\phi) \right|^2. \tag{2.363}$$

In the presence of nonvanishing spins, the reduction of the partial differential equation (2.359) to ordinary differential equations for radial wave functions is more complicated than in the spinless case discussed in Sect. 2.3. The partial-waves expansion for each spin-channel wave function associated with the spin state χ_{i_s} in (2.358) is

$$\psi_{i_\mathrm{s}}(\mathbf{r}) = \sum_{l=0}^{\infty} \sum_{m=-l}^{l} \frac{u_{i_\mathrm{s},l,m}(r)}{r} Y_{l,m}(\theta,\phi). \tag{2.364}$$

In contrast to the partial-waves expansion (2.33) in Sect. 2.3.2, we can no longer assume that the z-component of the orbital angular momentum vanishes. Since the expansion (2.364) involves the spherical harmonics $Y_{l,m}$ rather than the Legendre polynomials P_l used in (2.33), the definition of the radial wave function $u_{l,m=0}$ in (2.364) differs from the definition of u_l in (2.33) by a factor $\sqrt{4\pi/(2l+1)}$, compare Eq. (2.29). Inserting the expansion (2.358) with the partial-waves decompositions (2.364) into the Schrödinger equation (2.359) leads to the following set of coupled equations for the *radial spin-channel wave functions* $u_{i_\mathrm{s},l,m}$:

$$\left[-\frac{\hbar^2}{2\mu} \frac{\mathrm{d}^2}{\mathrm{d}r^2} + \frac{l(l+1)\hbar^2}{2\mu r^2} \right] u_{i_\mathrm{s},l,m}(r) + \sum_{j_\mathrm{s},l',m'} V\big(i_\mathrm{s},l,m;j_\mathrm{s},l',m'\big) u_{j_\mathrm{s},l',m'}(r) = E u_{i_\mathrm{s},l,m}(r). \tag{2.365}$$

The potential energy operator $\hat{V}$ now appears as a matrix of radial potentials defined by

$$V\big(i_\mathrm{s},l,m;j_\mathrm{s},l',m'\big) = \big\langle \chi_{i_\mathrm{s}}(M_\mathrm{p},M_\mathrm{t}) Y_{l,m}(\theta,\phi) \big| \hat{V} \big| \chi_{j_\mathrm{s}}(M_\mathrm{p},M_\mathrm{t}) Y_{l',m'}(\theta,\phi) \big\rangle. \tag{2.366}$$

The matrix element on the right-hand side of (2.366) involves integration over the angles θ and ϕ and summation over the spin-component quantum numbers M_p and M_t; it remains a (not necessarily local) radial potential for functions of the radial coordinate r. The set of Eq. (2.365) represents the *radial coupled-channel equations* for the case that the channels are defined by the spin states of projectile and target together with the orbital angular momentum states of relative motion.

Which combinations of channel label j_s and angular momentum quantum number l', m' are to be included in the sum in (2.365) for given i_s, l and m depends on the projectile and target spins. Instead of the uncoupled basis (2.357), the spin states can also be expressed in terms of eigenstates $|I, M_I\rangle$ of the total internal angular momentum $\hat{\mathbf{I}} = \hat{\mathbf{I}}_\mathrm{p} + \hat{\mathbf{I}}_\mathrm{t}$,

$$\hat{\mathbf{I}}^2 |I, M_I\rangle = I(I+1)\hbar^2 |I, M_I\rangle, \qquad \hat{I}_z |I, M_I\rangle = M_I \hbar |I, M_I\rangle. \tag{2.367}$$

The coupled spin states (2.367) can be expanded in the uncoupled basis (2.357),

$$|I, M_I\rangle = \sum_{M_\mathrm{p}, M_\mathrm{t}} \langle I_\mathrm{p}, M_\mathrm{p}; I_\mathrm{t}, M_\mathrm{t} | I, M_I\rangle |I_\mathrm{p}, M_\mathrm{p}\rangle |I_\mathrm{t}, M_\mathrm{t}\rangle. \tag{2.368}$$

The quantum number I for the total spin, meaning the total internal angular momentum of projectile and target, can assume any of the values

$$I = |I_\mathrm{p} - I_\mathrm{t}|, |I_\mathrm{p} - I_\mathrm{t}| + 1, \ldots, I_\mathrm{p} + I_\mathrm{t}; \tag{2.369}$$

for each value I of the total spin, the quantum number M_I for its z-component can assume any of the $2I + 1$ values

$$M_I = -I, -I + 1, \ldots, +I. \tag{2.370}$$

The expansion coefficients $\langle I_\mathrm{p}, M_\mathrm{p}; I_\mathrm{t}, M_\mathrm{t} | I, M_I\rangle$ in (2.368) are the *Clebsch–Gordan coefficients* [39]; they are nonvanishing only when the total spin I is in the range given by (2.369) and the component quantum numbers obey $M_I = M_\mathrm{p} + M_\mathrm{t}$. The dimension of the space of spin states of both projectile and target remains $(2I_\mathrm{p} + 1)(2I_\mathrm{t} + 1)$, which is a manifestation of the identity

$$\sum_{I=|I_\mathrm{p}-I_\mathrm{t}|}^{I_\mathrm{p}+I_\mathrm{t}} (2I+1) = (2I_\mathrm{p} + 1)(2I_\mathrm{t} + 1). \tag{2.371}$$

From general arguments such as the isotropy of space we can assume that the total angular momentum $\hat{\mathbf{J}}$ of the projectile-target system,

$$\hat{\mathbf{J}} = \hat{\mathbf{L}} + \hat{\mathbf{I}}, \tag{2.372}$$

is conserved. The eigenstates of the total angular momentum are obtained by coupling the eigenfunctions $Y_{l,m}(\theta, \phi)$ of the orbital angular momentum and the spin

states with the appropriate Clebsch–Gordan coefficients,

$$|J, M\rangle = \sum_{m, M_I} \langle l, m; I, M_I | J, M\rangle Y_{l,m}(\theta, \phi)|I, M_I\rangle; \tag{2.373}$$

they are eigenstates of $\hat{\mathbf{J}}^2$ and of $\hat{J}_z$,

$$\begin{aligned} \hat{\mathbf{J}}^2|J, M\rangle &= J(J+1)\hbar^2|J, M\rangle, \\ \hat{J}_z|J, M\rangle &= M\hbar|J, M\rangle, \quad M = -J, -J+1, \ldots, J. \end{aligned} \tag{2.374}$$

The possible values of the total spin I are limited to the range given in (2.369), and for each value J of the total angular momentum, the orbital angular momentum quantum number l can only assume values from $l = |J - I|$ to $l = J + I$. Hence the coupled-channel equations (2.365) can be decomposed into independent blocks labelled by the good quantum numbers J and M, and each block involves only a finite number of coupled radial equations.

For each block of coupled radial equations there are as many linearly independent vectors U of radial channel wave functions $u_{i_s,l,m}$ solving the equations as there are equations in the block. Asymptotically, each radial wave function of a solution is a superposition of the two linearly independent solutions (2.38) of the uncoupled free-particle equation,

$$u_l^{(\mathrm{s})}(kr) \overset{kr\to\infty}{\sim} \sin\left(kr - l\frac{\pi}{2}\right), \qquad u_l^{(\mathrm{c})}(kr) \overset{kr\to\infty}{\sim} \cos\left(kr - l\frac{\pi}{2}\right). \tag{2.375}$$

The coefficients of such superpositions can be obtained e.g. by direct numerical solution of the coupled-channel equations if the potentials are known. They determine the asymptotic form of the radial wave functions for given initial conditions and hence the scattering amplitudes and the observable cross sections.

A possible basis of vectors of solutions $U^{(i_s,l,m)}$ is defined by the following boundary conditions for its component radial wave functions:

$$u^{(i_s,l,m)}_{j_s,l',m'}(kr) \overset{r\to\infty}{\sim} \delta_{i_s,j_s}\delta_{l,l'}\delta_{m,m'}u_l^{(\mathrm{s})}(kr) + K_{i_s,l,m;j_s,l',m'}u_{l'}^{(\mathrm{c})}(kr). \tag{2.376}$$

The coefficients of the cosine terms define the K-matrix or *reactance matrix*, $\mathbf{K} = (K_{i_s,l,m;j_s,l',m'})$. In the trivial case that the coupled channel equations reduce to a single radial equation (2.35), the reactance matrix is simply the tangent of the scattering phase shift δ_l,

$$K \equiv K_l = \tan\delta_l. \tag{2.377}$$

If the potential is real, this phase shift and its tangent are also real. In the many-channel case, the reactance matrix is a hermitian matrix as long as the potential $\hat{V}$ does not contain non-hermitian contributions, which can be used to describe absorptive effects.

We obtain an alternative basis $\Phi^{(i_s,l,m)}$ of vectors of solutions of the coupled-channel equations (2.365) if we choose component radial wave functions which are

asymptotically superpositions not of sine and cosine functions as in (2.376), but of outgoing and incoming radial waves,

$$\begin{aligned}\varphi_l^{(+)}(kr) &\overset{r\to\infty}{\sim} u_l^{(\mathrm{c})}(kr) + \mathrm{i}u_l^{(\mathrm{s})}(kr) \overset{r\to\infty}{\sim} \mathrm{e}^{+\mathrm{i}(kr-l\pi/2)},\\ \varphi_l^{(-)}(kr) &\overset{r\to\infty}{\sim} u_l^{(\mathrm{c})}(kr) - \mathrm{i}u_l^{(\mathrm{s})}(kr) \overset{r\to\infty}{\sim} \mathrm{e}^{-\mathrm{i}(kr-l\pi/2)},\end{aligned} \tag{2.378}$$

$$\varphi^{(i_\mathrm{s},l,m)}_{j_\mathrm{s},l',m'}(r) \overset{r\to\infty}{\sim} \delta_{i_\mathrm{s},j_\mathrm{s}}\delta_{l,l'}\delta_{m,m'}\varphi_l^{(-)}(kr) - S_{i_\mathrm{s},l,m;\,j_\mathrm{s},l',m'}\varphi_{l'}^{(+)}(kr). \tag{2.379}$$

The asymptotic coefficients of the outgoing components $\varphi^{(+)}_{j_\mathrm{s},l'}$ define the *scattering matrix* or *S-matrix*: $\mathbf{S} = (S_{i_\mathrm{s},l,m;\,j_\mathrm{s},l',m'})$.

Since both bases of vectors of solutions, $U^{(i,l,m)}$ and $\Phi^{(i,l,m)}$, with component radial wave functions obeying the boundary conditions (2.376) and (2.379) respectively, span the same space of solutions of the coupled-channel equations, there must be a linear transformation which transforms one basis into the other. This transformation is

$$-\mathrm{i}\left(U^{(i_\mathrm{s},l,m)} + \sum_{j_\mathrm{s},l',m'} S_{i_\mathrm{s},l,m;\,j_\mathrm{s},l',m'}U^{(j_\mathrm{s},l',m')}\right) = \Phi^{(i_\mathrm{s},l,m)}. \tag{2.380}$$

We can see that (2.380) is correct by looking at the asymptotic behaviour of both sides of the equation in the sine–cosine basis (2.376). The coefficients of the sine terms on both sides form the same matrix $-\mathrm{i}(\mathbf{1}+\mathbf{S})$. Requiring that the coefficients of the cosine terms also be the same leads to

$$-\mathrm{i}(\mathbf{1}+\mathbf{S})\mathbf{K} = \mathbf{1} - \mathbf{S}. \tag{2.381}$$

This yields an explicit expression for the S-matrix in terms of $\mathbf{K}$,

$$\mathbf{S} = (\mathbf{1}+\mathrm{i}\mathbf{K})(\mathbf{1}-\mathrm{i}\mathbf{K})^{-1}. \tag{2.382}$$

In the absence of absorptive effects, the S-matrix (2.382) is unitary, because $\mathbf{K}$ is hermitian. In the trivial case that the coupled channel equations reduce to a single radial equation of the form (2.35) for the partial wave l, the S-matrix is simply given by the scattering phase shift δ_l,

$$S \equiv S_l = \frac{1+\mathrm{i}\tan\delta_l}{1-\mathrm{i}\tan\delta_l} = \mathrm{e}^{2\mathrm{i}\delta_l}, \tag{2.383}$$

which agrees with Eq. (2.69) in Sect. 2.3.6.

We can establish a relation connecting the S-matrix to the scattering amplitudes and observable cross sections by recalling the boundary conditions of the channel wave functions for a typical scattering experiment. The full wave function (2.360) describes an incoming wave in the spin channel i_s and the associated channel wave functions have the asymptotic behaviour,

$$\psi_{j_\mathrm{s}}(\mathbf{r}) \overset{r\to\infty}{\sim} \mathrm{e}^{\mathrm{i}kz}\delta_{i_\mathrm{s},j_\mathrm{s}} + \frac{\mathrm{e}^{\mathrm{i}kr}}{r} f_{i_\mathrm{s},j_\mathrm{s}}(\theta,\phi). \tag{2.384}$$

In the partial-waves expansion (2.364) of the total wave function (2.358), we obtain incoming spherical waves only from the plane-wave part of the spin-channel wave function in the entrance channel i_s [cf. (2.43) in Sect. 2.3.3]. A comparison with the spherical waves in (2.378) shows that the solution of the stationary Schrödinger equation obeying the boundary conditions implied by (2.360) is given as the following superposition of the basis vectors $\Phi^{(i_\mathrm{s},l,m=0)}$:

$$U = -\sum_l \frac{\sqrt{\pi(2l+1)}}{k} \mathrm{i}^{l-1} \Phi^{(i_\mathrm{s},l,0)}. \tag{2.385}$$

The vector U defined by (2.385) has the following radial wave functions as components,

$$u_{j_\mathrm{s},l',m'}(r) = -\sum_l \frac{\sqrt{\pi(2l+1)}}{k} \mathrm{i}^{l-1} \varphi^{(i_\mathrm{s},l,0)}_{j_\mathrm{s},l',m'}(r), \tag{2.386}$$

and the $\varphi^{(i_\mathrm{s},l,0)}_{j_\mathrm{s},l',m'}(r)$ have the asymptotic behaviour given in (2.378), (2.379). The spin-channel wave function $\psi_{j_\mathrm{s}}(\mathbf{r})$ in the spin channel j_s is obtained by summing the partial-wave contributions (2.386) according to (2.364),

$$\begin{aligned}\psi_{j_\mathrm{s}}(\mathbf{r}) &= \sum_{l',m'} \frac{u_{j_\mathrm{s},l',m'}(r)}{r} Y_{l',m'}(\theta,\phi) \\ &\overset{r\to\infty}{\sim} \delta_{i_\mathrm{s},j_\mathrm{s}} \mathrm{e}^{\mathrm{i}kz} + \frac{\mathrm{e}^{\mathrm{i}kr}}{r} \sum_{l',m'} Y_{l',m'}(\theta,\phi) \mathrm{i} \sum_l \mathrm{i}^{l-l'} \frac{\sqrt{\pi(2l+1)}}{k} \\ &\quad \times [\delta_{j_\mathrm{s},i_\mathrm{s}} \delta_{l,l'} \delta_{0,m'} - S_{i_\mathrm{s},l,0;\,j_\mathrm{s},l',m'}]. \end{aligned} \tag{2.387}$$

The relation connecting the scattering amplitudes defined by (2.384) with the elements of the S-matrix is thus,

$$f_{i_\mathrm{s},j_\mathrm{s}}(\theta,\phi) = \sum_{l',m'} Y_{l',m'}(\theta,\phi) \sum_l \mathrm{i}^{l-l'-1} \frac{\sqrt{\pi(2l+1)}}{k} [S_{i_\mathrm{s},l,0;\,j_\mathrm{s},l',m'} - \delta_{i_\mathrm{s},j_\mathrm{s}} \delta_{l,l'} \delta_{0,m'}]. \tag{2.388}$$

2.8.2 Spin-$\frac{1}{2}$ Projectile with Spin-Zero Target

The simplest example of the situation discussed in the previous subsection is that of a spin-$\frac{1}{2}$ projectile scattered by a spin-zero target (or vice-versa),

$$I_\mathrm{p} = \frac{1}{2}, \qquad I_\mathrm{t} = 0 \quad \Longrightarrow \quad I = \frac{1}{2}, \qquad M_I = \pm\frac{1}{2}. \tag{2.389}$$

There are two independent spin states labelled by $M_I = +\frac{1}{2}$ and $M_I = -\frac{1}{2}$. To be specific, assume that the interaction potential $\hat{V}$ consists of a local radial potential and a spin–orbit potential

$$\hat{V} = V(r) + V_{\rm so}(r)\hat{\mathbf{L}} \cdot \hat{\mathbf{I}}. \tag{2.390}$$

Since the scalar product $\hat{\mathbf{L}} \cdot \hat{\mathbf{I}}$ can be expressed as

$$\hat{\mathbf{L}} \cdot \hat{\mathbf{I}} = \frac{1}{2}\big(\hat{\mathbf{J}}^2 - \hat{\mathbf{L}}^2 - \hat{\mathbf{I}}^2\big), \quad \text{with} \quad \hat{\mathbf{I}}^2 = \frac{3}{4}\hbar^2, \tag{2.391}$$

the potential $\hat{V}$, which is defined by the matrix elements (2.366) in the (uncoupled) basis of spin and orbital angular momentum states, is diagonal in the coupled basis (2.373) of eigenstates of total angular momentum:

$$\langle J, M; l, I|\hat{V}|J', M'; l', I\rangle = \delta_{J,J'}\delta_{M,M'}\delta_{l,l'}\left[V(r) + \frac{\hbar^2}{2}F(J,l)V_{\rm so}(r)\right]. \tag{2.392}$$

The factor $F(J,l)$ depends on the two possibilities of coupling the spin $I = \frac{1}{2}$ and orbital angular momentum l to total angular momentum J, namely $J = l + \frac{1}{2}$ and $J = l - \frac{1}{2}$,

$$\begin{aligned} F(J,l) &= \frac{2}{\hbar^2}\langle J, M; l, I|\hat{V}|\hat{\mathbf{L}} \cdot \hat{\mathbf{I}}|J, M; l, I\rangle \\ &= J(J+1) - l(l+1) - \frac{3}{4} = \begin{cases} l & \text{for } J = l + \frac{1}{2}, \\ -(l+1) & \text{for } J = l - \frac{1}{2}. \end{cases} \end{aligned} \tag{2.393}$$

The system (2.365) reduces to one single radial equation for each pair of values (l, J) of orbital and total angular momentum quantum numbers.

The S-matrix can be interpreted as the matrix of a "scattering operator" $\hat{S}$ and, due to global rotational invariance, $\hat{S}$ commutes with the total angular momentum. In the present example, the matrix of $\hat{S}$ breaks down into diagonal matrices in the spin spaces corresponding to a given orbital angular momentum quantum number l (and given spin $I = \frac{1}{2}$),

$$S_{J,M,l;J',M',l} = \langle J, M; l, I|\hat{S}|J', M'; l, I\rangle = \delta_{J,J'}\delta_{M,M'}\mathrm{e}^{2\mathrm{i}\delta_l^{(J)}}. \tag{2.394}$$

Here $\delta_l^{(J)}$ is the scattering phase shift determining the asymptotic behaviour of the radial wave function which solves the radial Schrödinger equation for given l and J, i.e. with the radial potential $V(r) + V_{\rm so}(r)F(J,l)$ as defined by Eqs. (2.390), (2.392). The expression for the S-matrix in terms of $\delta_l^{(J)}$ follows as in the spin-free case discussed in Sect. 2.3.6,

$$u_{J,l}(r) \overset{r\to\infty}{\propto} \sin\left(kr - l\frac{\pi}{2} + \delta_l^{(J)}\right) \propto \mathrm{e}^{-\mathrm{i}(kr - l\pi/2)} - \mathrm{e}^{2\mathrm{i}\delta_l^{(J)}}\mathrm{e}^{+\mathrm{i}(kr - l\pi/2)}. \tag{2.395}$$

In order to evaluate the expression (2.388) for the scattering amplitudes, we need the matrix elements of the scattering operator in the uncoupled basis. With $i_s = M_I$ and $j_s = M_I'$, the matrix elements occurring in (2.388) are

$$\begin{aligned} S_{M_I,l,0;M_I',l',m'} &= \langle I, M_I; l, 0|\hat{S}|I, M_I'; l', m'\rangle \\ &= \sum_{J,M}\sum_{J',M'} \langle J, M; l, I|\hat{S}|J', M'; l', I\rangle \\ &\quad \times \langle I, M_I; l, 0|J, M\rangle \langle I, M_I'; l', m'|J', M'\rangle. \end{aligned} \tag{2.396}$$

Since the spin–orbit operator $\hat{\mathbf{I}} \cdot \hat{\mathbf{L}}$ commutes with $\hat{\mathbf{L}}^2$, the S-matrix cannot connect different l-values, so l' must equal l in (2.396). Together with (2.394), Eq. (2.396) reduces to

$$\begin{aligned} S_{M_I,l,0;M_I',l',m'} &= \delta_{l,l'} \sum_{J,M} \mathrm{e}^{2\mathrm{i}\delta_l^{(J)}} \langle I, M_I; l, 0|J, M\rangle \langle I, M_I'; l, m'|J, M\rangle \\ &= \delta_{l,l'} \sum_{J} \mathrm{e}^{2\mathrm{i}\delta_l^{(J)}} \langle I, M_I; l, 0|J, M_I\rangle \langle I, M_I'; l, m'|J, M_I\rangle. \end{aligned} \tag{2.397}$$

The lower line follows from the fact that the first Clebsch–Gordan coefficient $\langle I, M_I; l, 0|J, M\rangle$ vanishes unless $M = M_I$. Hence the component quantum number M in the second Clebsch–Gordan coefficient can also be replaced by M_I. Note that the second coefficient is nonvanishing only when $m' = M_I - M_I'$. For each choice of initial spin state M_I and final spin state M_I' and for each orbital angular momentum quantum number $l > 0$, the expression (2.397) for the S-matrix element is a sum of two contributions, one corresponding to $J = l + \frac{1}{2}$ and one to $J = l - \frac{1}{2}$. (For $l = 0$, J can only be $+\frac{1}{2}$.)

In the present example, the expression (2.388) for the scattering amplitude reduces to,

$$\begin{aligned} f_{M_I,M_I'}(\theta, \phi) &= \sum_l \frac{\sqrt{\pi(2l+1)}}{\mathrm{i}k} Y_{l,m}(\theta, \phi)[S_{M_I,l,0;M_I',l,m} - \delta_{M_I,M_I'}], \\ m &= M_I - M_I'. \end{aligned} \tag{2.398}$$

[The orbital angular momentum quantum numbers l', m' in (2.388) are called l, m in (2.398).]

The relevant Clebsch–Gordan coefficients are listed in Table 2.4. The table lists the values of the second coefficient $\langle \frac{1}{2}, M_I'; l, m|J, M_I\rangle$ in the lower line of Eq. (2.397); the first coefficient is given by replacing M_I' with M_I. The resulting expressions for the scattering amplitudes (2.398) are,

Table 2.4 Clebsch–Gordan coefficient $\langle \frac{1}{2}, M_I'; l, m | J, M_I \rangle$ with $m = M_I - M_I'$

(M_I, M_I')	$(+\frac{1}{2}, +\frac{1}{2})$	$(+\frac{1}{2}, -\frac{1}{2})$	$(-\frac{1}{2}, +\frac{1}{2})$	$(-\frac{1}{2}, -\frac{1}{2})$
$J = l + \frac{1}{2}$	$\sqrt{\frac{l+1}{2l+1}}$	$\sqrt{\frac{l}{2l+1}}$	$\sqrt{\frac{l}{2l+1}}$	$\sqrt{\frac{l+1}{2l+1}}$
$J = l - \frac{1}{2}$	$-\sqrt{\frac{l}{2l+1}}$	$\sqrt{\frac{l+1}{2l+1}}$	$-\sqrt{\frac{l+1}{2l+1}}$	$\sqrt{\frac{l}{2l+1}}$

$$
\begin{aligned}
f_{+\frac{1}{2},+\frac{1}{2}}(\theta) &= \sum_{l=0}^{\infty} \frac{\sqrt{\pi(2l+1)}}{\mathrm{i}k} Y_{l,0}(\theta) \left[\frac{l+1}{2l+1} \mathrm{e}^{2\mathrm{i}\delta_l^{(l+1/2)}} + \frac{l}{2l+1} \mathrm{e}^{2\mathrm{i}\delta_l^{(l-1/2)}} - 1 \right], \\
f_{+\frac{1}{2},-\frac{1}{2}}(\theta,\phi) &= \sum_{l=1}^{\infty} \frac{\sqrt{\pi(2l+1)}}{\mathrm{i}k} Y_{l,1}(\theta,\phi) \frac{\sqrt{l(l+1)}}{2l+1} \left[\mathrm{e}^{2\mathrm{i}\delta_l^{(l+1/2)}} - \mathrm{e}^{2\mathrm{i}\delta_l^{(l-1/2)}} \right], \\
f_{-\frac{1}{2},+\frac{1}{2}}(\theta,\phi) &= \sum_{l=1}^{\infty} \frac{\sqrt{\pi(2l+1)}}{\mathrm{i}k} Y_{l,-1}(\theta,\phi) \frac{\sqrt{l(l+1)}}{2l+1} \left[\mathrm{e}^{2\mathrm{i}\delta_l^{(l+1/2)}} - \mathrm{e}^{2\mathrm{i}\delta_l^{(l-1/2)}} \right], \\
f_{-\frac{1}{2},-\frac{1}{2}}(\theta) &= f_{+\frac{1}{2},+\frac{1}{2}}(\theta).
\end{aligned}
\tag{2.399}
$$

If the effects of the spin–orbit coupling are negligible, then $\delta_l^{(l+1/2)} = \delta_l^{(l-1/2)}$ so the spin-state conserving amplitudes $f_{+\frac{1}{2},+\frac{1}{2}}(\theta)$ and $f_{-\frac{1}{2},-\frac{1}{2}}(\theta)$ have the same form as given by Eqs. (2.44) and (2.47) for the spin-free case, while the *spin-flip amplitudes* $f_{+\frac{1}{2},-\frac{1}{2}}(\theta)$ and $f_{-\frac{1}{2},+\frac{1}{2}}(\theta)$ vanish.

The spin-state conserving amplitudes are independent of the azimuthal angle ϕ and can be written as

$$
f_{+\frac{1}{2},+\frac{1}{2}}(\theta) = f_{-\frac{1}{2},-\frac{1}{2}}(\theta) = f(\theta). \tag{2.400}
$$

The ϕ-dependence of the spin-flip amplitudes is contained solely in the ϕ-dependence of the spherical harmonics and is given by $Y_{l,\pm 1} = \pm \tilde{Y}(\theta) \mathrm{e}^{\pm \mathrm{i}\phi}$, where $\tilde{Y}$ stands for some function of θ. We can thus write the spin-flip amplitudes as

$$
f_{+\frac{1}{2},-\frac{1}{2}}(\theta,\phi) = g(\theta)\mathrm{e}^{+\mathrm{i}\phi}, \qquad f_{-\frac{1}{2},+\frac{1}{2}}(\theta,\phi) = -g(\theta)\mathrm{e}^{-\mathrm{i}\phi}, \tag{2.401}
$$

with a common function $g(\theta)$ for their dependence on the polar angle θ.

The spin state of the projectile-target system can be described by a two-component spinor,

$$
\begin{pmatrix} A \\ B \end{pmatrix} \equiv A \Upsilon_{M_I=+\frac{1}{2}} + B \Upsilon_{M_I=-\frac{1}{2}}. \tag{2.402}
$$

If the incoming plane wave is associated with a given spinor $\binom{A}{B}$, then the outgoing spherical wave will be associated with an angle-dependent spinor given by the spin-dependent scattering amplitudes (2.399),

$$
\psi(\mathbf{r}, M_I) \overset{r\to\infty}{\sim} \mathrm{e}^{\mathrm{i}kz} \begin{pmatrix} A \\ B \end{pmatrix} + \frac{\mathrm{e}^{\mathrm{i}kr}}{r} \begin{pmatrix} Af(\theta) - Bg(\theta)\mathrm{e}^{-\mathrm{i}\phi} \\ Ag(\theta)\mathrm{e}^{+\mathrm{i}\phi} + Bf(\theta) \end{pmatrix}. \tag{2.403}
$$

If we don't measure the spin after the scattering event, then the differential cross section accounting for both spin-state conserving and spin-flipping scattering events is

$$\frac{\mathrm{d}\sigma}{\mathrm{d}\Omega} = \frac{|Af(\theta) - Bg(\theta)\mathrm{e}^{-\mathrm{i}\phi}|^2 + |Ag(\theta)\mathrm{e}^{+\mathrm{i}\phi} + Bf(\theta)|^2}{|A|^2 + |B|^2}$$
$$= \big|f(\theta)\big|^2 + \big|g(\theta)\big|^2 + 2\Im\big[f(\theta)g(\theta)^*\big]\frac{2\Im[AB^*\mathrm{e}^{\mathrm{i}\phi}]}{|A|^2 + |B|^2}. \qquad (2.404)$$

If both A and B are different from zero, the differential cross section (2.404) depends on the azimuthal angle ϕ. The relative importance of the ϕ-dependent contribution is determined by the imaginary part of the product fg^* and is usually expressed with the help of the *Sherman function* $S(\theta)$,

$$S(\theta) = -2\frac{\Im[fg^*]}{|f|^2 + |g|^2} = \mathrm{i}\left[\frac{fg^* - f^*g}{|f|^2 + |g|^2}\right]. \qquad (2.405)$$

It is a speciality of spin-$\frac{1}{2}$ particles, that an arbitrary (pure) spin state is a spin-up state with respect to an appropriately chosen quantization axis. To see this consider an arbitrary normalized spin state $|\Upsilon\rangle = \binom{A}{B}$, $|A|^2 + |B|^2 = 1$. Using the Pauli spin matrices,

$$\hat{\sigma}_x = \begin{pmatrix} 0 & 1 \\ 1 & 0 \end{pmatrix}, \qquad \hat{\sigma}_y = \begin{pmatrix} 0 & -\mathrm{i} \\ \mathrm{i} & 0 \end{pmatrix}, \qquad \hat{\sigma}_z = \begin{pmatrix} 1 & 0 \\ 0 & -1 \end{pmatrix}, \qquad (2.406)$$

we define the three-component *polarization vector*

$$\mathbf{P} = \langle \Upsilon | \hat{\boldsymbol{\sigma}} | \Upsilon \rangle. \qquad (2.407)$$

For the spinor $\binom{A}{B}$ its components are

$$P_x = 2\Re\big[A^*B\big], \qquad P_y = 2\Im\big[A^*B\big], \qquad P_z = |A|^2 - |B|^2, \qquad (2.408)$$

and its length is unity. The projection of the spin operator $\hat{\boldsymbol{\sigma}}$ onto the direction of $\mathbf{P}$ is

$$\hat{\sigma}_P = \mathbf{P} \cdot \hat{\boldsymbol{\sigma}} = P_x\hat{\sigma}_x + P_y\hat{\sigma}_y + P_z\hat{\sigma}_z, \qquad (2.409)$$

and it is easy to show that the spinor $|\Upsilon\rangle = \binom{A}{B}$ is an eigenstate of $\hat{\sigma}_P$ with eigenvalue $+1$.

Equation (2.403) shows that scattering of a spin-$\frac{1}{2}$ particle into the direction (θ, ϕ) transforms the initial spin state $|\Upsilon\rangle \equiv \binom{A}{B}$ of the incoming wave into the new spin state

$$\begin{pmatrix} A' \\ B' \end{pmatrix} = \mathbf{S}\begin{pmatrix} A \\ B \end{pmatrix}, \quad \mathbf{S} = \frac{1}{\sqrt{|f|^2 + |g|^2}}\begin{pmatrix} f(\theta) & -g(\theta)\mathrm{e}^{-\mathrm{i}\phi} \\ g(\theta)\mathrm{e}^{\mathrm{i}\phi} & f(\theta) \end{pmatrix}. \qquad (2.410)$$

The transformation is described by the transformation matrix $\mathbf{S}$, which is in general not unitary and is not to be confused with the S-matrix. The polarization vector $\mathbf{P}'$ of the scattered particle is

$$\mathbf{P}' = \frac{\langle \Upsilon | \mathbf{S}^\dagger \hat{\boldsymbol{\sigma}} \mathbf{S} | \Upsilon \rangle}{\langle \Upsilon | \mathbf{S}^\dagger \mathbf{S} | \Upsilon \rangle}. \tag{2.411}$$

The denominator in (2.411) is needed for correct normalization, because the transformed spinor $\mathbf{S}|\Upsilon\rangle$ is no longer normalized to unity.

2.8.3 Application to Mixed Spin States

As opposed to a *pure state*, which in quantum mechanics is described by a single state vector (or wave function) $|\Upsilon\rangle$, a mixed state is a statistical mixture of different pure states, weighted by real probabilities. A mixed state is described in quantum mechanics by the statistically weighted sum of the projectors onto all contributing quantum mechanical states,

$$\hat{\varrho} = \sum_n w_n |\Upsilon_n\rangle\langle\Upsilon_n|, \quad w_n \geq 0, \qquad \sum_n w_n = 1. \tag{2.412}$$

A pure state corresponds to the special case that one probability w_n is unity while all other probabilities vanish. The operator $\hat{\varrho}$ is the *density operator*; as a matrix in a particular basis it is called the *density matrix*. A completely unpolarized spin-$\frac{1}{2}$ particle is one for which nothing is known about its spin state. With respect to an arbitrary axis of quantization, both spin states $|\Upsilon_+\rangle$ and $|\Upsilon_-\rangle$ are equally probable. The corresponding density operator is

$$\hat{\varrho} = \tfrac{1}{2}|\Upsilon_+\rangle\langle\Upsilon_+| + \tfrac{1}{2}|\Upsilon_-\rangle\langle\Upsilon_-|, \tag{2.413}$$

and the associated density matrix is just $1/2$ times the 2×2 unit matrix.

The expectation value of an observable $\hat{O}$ in a mixed state involves both the uncertainty expressed in the quantum mechanical expectation value and the statistical averaging via the mixed-state probabilities,

$$\langle\langle \hat{O} \rangle\rangle = \mathrm{Tr}[\hat{O}\hat{\varrho}] = \sum_n w_n \langle \Upsilon_n | \hat{O} | \Upsilon_n \rangle. \tag{2.414}$$

A general mixed spin state is neither completely polarized like a pure state, nor completely unpolarized as in (2.413). In the spirit of (2.414) we define the polarization vector for a mixed spin state as

$$\mathbf{P} = \langle\langle \hat{\boldsymbol{\sigma}} \rangle\rangle = \mathrm{Tr}\{\hat{\boldsymbol{\sigma}}\hat{\varrho}\}. \tag{2.415}$$

If we take the direction of $\mathbf{P}$ as the axis of quantization and assume a density operator

$$\hat{\varrho} = w_+ |\Upsilon_+\rangle\langle\Upsilon_+| + w_- |\Upsilon_-\rangle\langle\Upsilon_-|, \quad w_+ + w_- = 1, \tag{2.416}$$

then the component of $\mathbf{P}$ in the direction of this axis is obviously the difference of the probabilities for the spin pointing parallel and antiparallel to $\mathbf{P}$, namely $w_+ - w_-$. This is also the length of the polarization vector, which is smaller than unity for a mixed spin state. The length of the polarization vector serves as definition for the (degree of) polarization. The polarization can vary between zero and unity; it is unity for completely polarized particles (pure spin state) and zero for completely unpolarized particles.

If the incoming spin-$\frac{1}{2}$ projectile is partially polarized with respect to an axis of quantization, which need not be the z-axis, then we describe such a (mixed) spin state by a density operator like (2.416). In order to calculate the differential cross section in such a case, we must first determine the differential cross sections for the two pure states $|\Upsilon_+\rangle$ and $|\Upsilon_-\rangle$ with respect to the axis of quantization according to (2.404) and then incoherently superpose the results with the weights w_+ and w_-.

Scattering into the direction (θ, ϕ) transforms an incoming (pure) spin state $|\Upsilon\rangle$ into the spin state $\mathbf{S}|\Upsilon\rangle$ according to (2.410). Extending this result to mixed states shows that the density operator $\hat{\varrho}$ of the incoming particle is transformed into the density operator

$$\hat{\varrho}' = \frac{\mathbf{S}\hat{\varrho}\mathbf{S}^\dagger}{\mathrm{Tr}\{\mathbf{S}\hat{\varrho}\mathbf{S}^\dagger\}} \tag{2.417}$$

by the scattering process. The denominator in (2.417) ensures correct normalization, $\mathrm{Tr}\{\hat{\varrho}'\} = 1$. With (2.415) we can give a general formula for the polarization vector $\mathbf{P}'$ of the particle scattered into the direction (θ, ϕ),

$$\mathbf{P}' = \mathrm{Tr}\{\hat{\boldsymbol{\sigma}}\hat{\varrho}'\} = \frac{\mathrm{Tr}\{\hat{\boldsymbol{\sigma}}\mathbf{S}\hat{\varrho}\mathbf{S}^\dagger\}}{\mathrm{Tr}\{\mathbf{S}\hat{\varrho}\mathbf{S}^\dagger\}}. \tag{2.418}$$

As an application of the formula (2.418) consider the case that the incoming particle is completely unpolarized. Then $\hat{\varrho}$ is just $1/2$ times the unit matrix and (2.418) simplifies to

$$\mathbf{P}' = \frac{\mathrm{Tr}\{\hat{\boldsymbol{\sigma}}\mathbf{S}\mathbf{S}^\dagger\}}{\mathrm{Tr}\{\mathbf{S}\mathbf{S}^\dagger\}}. \tag{2.419}$$

Inserting the explicit expression (2.410) for the transformation matrix $\mathbf{S}$ yields

$$P'_x = -S(\theta)\sin\phi, \qquad P'_y = S(\theta)\cos\phi, \qquad P'_z = 0 \quad \Longleftrightarrow \quad \mathbf{P}' = S(\theta)\frac{\hat{\mathbf{e}}_z \times \hat{\mathbf{e}}_r}{\sin\theta}, \tag{2.420}$$

where $S(\theta)$ again stands for the Sherman function (2.405). The direction of the polarization vector is perpendicular to the *scattering plane*, which is spanned by the direction of the incoming particle (the z-axis) and the direction of the scattered particle (θ, ϕ). Note that scattered particles can have a finite polarization even if the incoming particles are unpolarized.

In the more general case that the total spin of target and projectile is larger than $\frac{1}{2}$, the coupling of spin and orbital angular momentum is more complicated. Mixed spin

states are then described by a $(2I_\mathrm{p}+1)(2I_\mathrm{t}+1)\times(2I_\mathrm{p}+1)(2I_\mathrm{t}+1)$ density matrix. The appropriate treatment of polarization effects in such more general situations is described in a monograph by Blum on density matrix theory [4].

2.9 When Projectile and Target Are Indistinguishable

If the projectile and the target are exactly identical, e.g. a nucleus, an atom or a molecule in an exactly defined quantum state, then they are indistinguishable within the framework of quantum mechanics. In the centre-of-mass frame of reference, reflecting the distance coordinate $\mathbf{r}$ at the origin, $\mathbf{r}\to-\mathbf{r}$, corresponds to exchanging the position coordinates of projectile and target. The behaviour of the total wave function under such a transformation depends on the symmetry properties of the spin part of the projectile-target wave function. The symmetry properties of the amplitude for identical-particle scattering under reflection thus depend on the spin of the particles, which determines whether they behave as bosons or as fermions.

2.9.1 Spinless Bosons

If target and projectile have vanishing internal angular momentum, $I_\mathrm{p}=I_\mathrm{t}=0$, then interchanging their position coordinates corresponds to interchanging projectile and target; furthermore they behave as bosons, so their wave function is invariant under such an interchange. For the relative motion wave function this implies

$$\psi(-\mathbf{r})=\psi(\mathbf{r}). \tag{2.421}$$

Examples for bosonic particles in nuclear physics are nuclei with an even number of nucleons such as ^{4}He (alpha particles), ^{16}O or ^{24}Mg; examples in atomic physics are atoms or ions with an even total number of nucleons and electrons, e.g. H, ^{4}He, ^{3}He$^+$.

In order to comply with the symmetry requirement (2.421), the scattering solutions of the Schrödinger equation (2.1) should be solved by symmetrized wave functions with the boundary conditions,

$$\begin{aligned}\psi(\mathbf{r}) &\overset{r\to\infty}{\sim} \mathrm{e}^{\mathrm{i}kz}+f(\theta,\phi)\frac{\mathrm{e}^{\mathrm{i}kr}}{r}+\mathrm{e}^{-\mathrm{i}kz}+f(\pi-\theta,\phi+\pi)\frac{\mathrm{e}^{\mathrm{i}kr}}{r}\\ &= \mathrm{e}^{\mathrm{i}kz}+\mathrm{e}^{-\mathrm{i}kz}+f^{(+)}(\theta,\phi)\frac{\mathrm{e}^{\mathrm{i}kr}}{r}.\end{aligned} \tag{2.422}$$

The symmetrized scattering amplitude, which is invariant under reflection at the origin, is related to the scattering amplitude f, as obtained without consideration of symmetry, via

$$f^{(+)}(\theta,\phi)=f(\theta,\pi)+f(\pi-\theta,\phi+\pi). \tag{2.423}$$

Note that $f^{(+)}$ is the realistic, physical scattering amplitude, while the unsymmetrized amplitude f plays the role of a hypothetical quantity which is based on the unphysical neglect of the symmetry requirement. The time-independent stationary wave function (2.422) may seem unusual, since the "incoming plane wave" is effectively a standing wave $2\cos(kz)$. To appreciate that the ansatz (2.422) is meaningful, we should remember that the time-independent treatment of the scattering process is not exact, but a well justified approximation [30]. In a real scattering experiment, the incoming rightward-travelling wave packet reaches the asymptotic regime of large positive z-values at a time when the incoming leftward-travelling wave packet is located mainly at large negative z-values, so the standing wave does not form. The scattered wave, i.e. the outgoing spherical wave is, however, a coherent superposition of the contribution due to the incoming rightward-travelling and the incoming leftward-travelling waves.

The definition of the scattering cross section is obtained by normalizing the outgoing flux from the spherical wave to the current density of the incoming plane wave, see Eqs. (2.4), (2.5) in Sect. 2.1, but in the present case this is not unambiguous. The most common definition is [24, 35, 44]

$$\frac{\mathrm{d}\sigma}{\mathrm{d}\Omega} = \left|f^{(+)}(\theta,\phi)\right|^2 = \left|f(\theta,\phi) + f(\pi-\theta,\phi+\pi)\right|^2, \tag{2.424}$$

which is obtained via the argument that, in a typical scattering experiment, only one of the two incoming directions is actually registered as the incoming current density, so the relevant quantity for normalization remains $|\mathbf{j}_{\mathrm{in}}| = \hbar k/\mu$, even for the symmetrized wave function (2.422). Normalization to the sum of the incoming currents, both from the left and from the right, would lead to a factor $\frac{1}{2}$ on the right-hand side of (2.424),

$$\frac{\mathrm{d}\sigma}{\mathrm{d}\Omega} = \frac{1}{2}\left|f^{(+)}(\theta,\phi)\right|^2 = \frac{1}{2}\left|f(\theta,\phi) + f(\pi-\theta,\phi+\pi)\right|^2. \tag{2.425}$$

With the definition (2.425), the integrated scattering cross section is

$$\sigma = \frac{1}{2}\int \left|f^{(+)}(\theta,\phi)\right|^2 \mathrm{d}\Omega. \tag{2.426}$$

The definition (2.426) agrees with that given in Ref. [35], but there the authors use the definition (2.424) for the differential scattering cross section and argue, that the angle integration should cover only one hemisphere in order "to avoid double counting". This argument does not, however, reflect the situation in a real scattering experiment. Joachain [24] also uses the definition (2.424) for the differential scattering cross section, but he makes a point of noting that the resulting integrated cross section, i.e. (2.426) *without* the $\frac{1}{2}$ on the right-hand side, corresponds to "twice the number of particles removed from the incident beam per unit time and unit incident flux".

With respect to particle conservation as discussed in Sect. 2.1, destructive interference between the outgoing spherical wave and the incoming plane waves in

(2.422) is possible both in the forward and in the backward direction. For the interference contribution to the total flux $\oint \mathbf{j} \cdot \mathrm{d}\mathbf{s}$, Eq. (2.13) is replaced by

$$I_{\text{int}} = -\frac{\hbar}{\mu} 4\pi \left(\Im\big[f^{(+)}(\theta = 0)\big] + \Im\big[f^{(+)}(\theta = \pi)\big] \right) = -\frac{\hbar}{\mu} 8\pi \Im\big[f^{(+)}(\theta = 0)\big]. \tag{2.427}$$

For the symmetric wave function obeying the asymptotic boundary conditions (2.422), particle conservation is expressed by the optical theorem in the form

$$\int \left| f^{(+)}(\theta, \phi) \right|^2 \mathrm{d}\Omega = \frac{8\pi}{k} \Im\big[f^{(+)}(\theta = 0)\big]. \tag{2.428}$$

For radially symmetric potentials, the scattering amplitudes depend only on the polar angle θ, so

$$\left| f^{(+)}(\theta) \right|^2 = \left| f(\theta) + f(\pi - \theta) \right|^2 = \left| f(\theta) \right|^2 + \left| f(\pi - \theta) \right|^2 + 2\Re\big[f^*(\theta) f(\pi - \theta)\big]. \tag{2.429}$$

In the partial-waves expansion (2.44), (2.47) for the scattering amplitude $f(\theta)$,

$$f(\theta) = \sum_{l=0}^{\infty} f_l P_l(\cos\theta), \qquad f_l = \frac{2l+1}{2\mathrm{i}k} \left(\mathrm{e}^{2\mathrm{i}\delta_l} - 1 \right), \tag{2.430}$$

the Legendre polynomials have the property $P_l(\cos(\pi - \theta)) = (-1)^l P_l(\cos\theta)$. In the symmetrized scattering amplitude (2.423), the odd-l contributions drop out while the even-l contributions acquire a factor two,

$$f^{(+)}(\theta) = 2 \sum_{l \text{ even}} f_l P_l(\cos\theta) = \sum_{l \text{ even}} \frac{2l+1}{\mathrm{i}k} \left(\mathrm{e}^{2\mathrm{i}\delta_l} - 1 \right) P_l(\cos\theta). \tag{2.431}$$

For identical spinless bosons as projectile and target, the scattering amplitude with the correct symmetry property, namely $f^{(+)}(\pi - \theta) = f^{(+)}(\theta)$, contains contributions only from even partial waves. The near-threshold behaviour of the s-wave scattering phase shift is still determined by the scattering length a, $\tan\delta_{l=0} \overset{k\to 0}{\sim} -ak$, but Eq. (2.80) describing the near-threshold behaviour of the scattering amplitude and of the scattering cross sections must now be replaced by,

$$\lim_{k\to 0} f^{(+)}(\theta) = 2 f_0 P_0 \sim -2a \quad \Longrightarrow \quad \lim_{k\to 0} \frac{\mathrm{d}\sigma}{\mathrm{d}\Omega} = 2a^2 \quad \text{and} \quad \lim_{k\to 0} \sigma = 8\pi a^2, \tag{2.432}$$

if we use the definitions (2.425) and (2.426) for the scattering cross sections.

Spinless bosons that carry an electric charge necessarily interact via a repulsive Coulomb interaction. The appropriately symmetrized version of the Coulomb scattering amplitude (2.192) is,

$$f_{\text{C}}^{(+)}(\theta) = -\frac{\eta \mathrm{e}^{2\mathrm{i}\sigma_0}}{2k} \left[\frac{\mathrm{e}^{-\mathrm{i}\eta \ln[\sin^2(\theta/2)]}}{\sin^2(\theta/2)} + \frac{\mathrm{e}^{-\mathrm{i}\eta \ln[\cos^2(\theta/2)]}}{\cos^2(\theta/2)} \right], \tag{2.433}$$

and the corresponding differential scattering cross section is

$$\left(\frac{\mathrm{d}\sigma}{\mathrm{d}\Omega}\right)_{\mathrm{C}}^{(+)} = \left(\frac{\eta}{2k}\right)^2 \left[\frac{1}{\sin^4(\theta/2)} + \frac{1}{\cos^4(\theta/2)} + \frac{2\cos(2\eta\ln[\tan(\theta/2)])}{\sin^2(\theta/2)\cos^2(\theta/2)}\right]. \quad (2.434)$$

Equation (2.434) is the *Mott formula* for the scattering of identical charged spinless bosons. It is written here in the usual form *without* the factor $\frac{1}{2}$ in (2.425).

Realistic bosons are composed of an even number of fermions and can generally not be treated as point particles. As an example consider two ^{4}He nuclei, i.e. two alpha particles with mass M_α. The strength C of the repulsive Coulomb potential is

$$C = 4Z_1 Z_2 e^2 = 4 \times 1.4399644\ \text{MeV fm} \approx 5.75996\ \text{MeV fm}, \quad (2.435)$$

in the units generally used in nuclear physics. The other relevant constants for the alpha–alpha system are,

$$\mu = \frac{M_\alpha}{2} \quad \Rightarrow \quad \frac{\hbar^2}{2\mu} = 10.4465\ \text{MeV fm}^2, \qquad a_C = \frac{\hbar^2}{\mu C} = 3.62733\,\text{fm}. \quad (2.436)$$

The properties of alpha–alpha scattering are quite well reproduced for energies from threshold to near 40 MeV in the centre-of-mass system by a local alpha–alpha potential [10],

$$\begin{aligned} V_{\alpha\text{-}\alpha}(r) &= -V_0 \mathrm{e}^{-c_1 r^2} + \mathrm{erf}(c_2 r)\frac{C}{r}, \\ V_0 &= 123\ \text{MeV},\ c_1 = 0.22\ \text{fm}^{-2},\ c_2 = 0.75\ \text{fm}^{-1}. \end{aligned} \quad (2.437)$$

The differential cross section for alpha–alpha scattering at $E = 1$ MeV is shown in Fig. 2.24. At this energy, the Sommerfeld parameter is $\eta = 0.89104$. Naïve superposition of $|f_C(\theta)|^2$ and $|f_C(\pi - \theta)|^2$ gives the "classical" result shown as dotted line. The dashed line shows the Mott formula (2.434). Note that the interference is always constructive around $\theta = \frac{\pi}{2}$. The solid line shows the result

$$\left(\frac{\mathrm{d}\sigma}{\mathrm{d}\Omega}\right)^{(+)} = \left|f_{\mathrm{C}}^{(+)}(\theta) + \tilde{f}^{(+)}(\theta)\right|^2, \quad (2.438)$$

which is obtained for the modified repulsive Coulomb potential (2.437) along the lines described in Sect. 2.5.3. Here $\tilde{f}^{(+)}(\theta) = \tilde{f}(\theta) + \tilde{f}(\pi - \theta)$ is the appropriately symmetrized additional scattering amplitude due to the short-range deviation of the potential (2.437) from the pure Coulomb shape; compare Eqs. (2.213)–(2.217) in Sect. 2.5.2.

If projectile and target are identical bosons with (integer) spin greater than zero, $I_\mathrm{p} = I_\mathrm{t} \geq 1$, then the total spin I of projectile and target can be any integer between zero and $2I_\mathrm{p}$. For $I \geq 1$, the coupling of orbital angular momentum and spin has to be considered, e.g. along the lines of Sect. 2.8.1, and the consequences of the exchange symmetry of the full wave function for the individual spin-channel wave functions are more complicated.

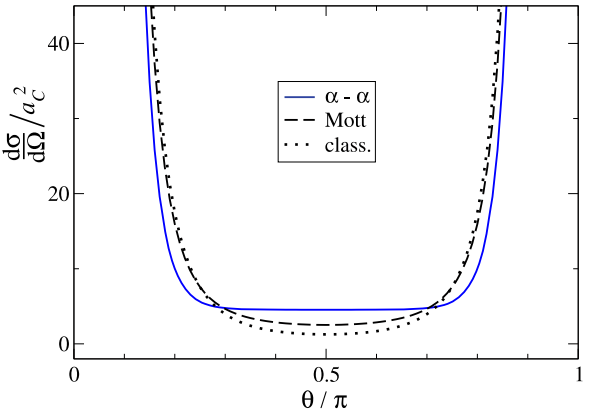

Fig. 2.24 The differential cross section for the scattering of two alpha particles at $E = 1$ MeV in the centre-of-mass system, corresponding to $k = 0.309396$ fm^{-1} and $\eta = 0.89104$. The *solid line* shows the result obtained with the alpha–alpha potential (2.437); the *dashed line* is the Mott formula (2.434) based on the pure Coulomb potential; the *dotted line* is the naïve "classical" result which neglects the interference term in the Mott formula

2.9.2 Spin-$\frac{1}{2}$ Fermions

If projectile and target are identical fermions, then their spin must be an odd multiple of $\frac{1}{2}$, i.e. at least $\frac{1}{2}$. Examples are electrons, nucleons, and atoms or ions with an odd total number of nucleons and electrons such as ^{3}He, ^{4}He$^+$. In the simplest case, $I_\mathrm{p} = I_\mathrm{t} = \frac{1}{2}$, Eq. (2.368) in Sect. 2.8.1 becomes

$$|I, M_I\rangle = \sum_{M_\mathrm{p}=\pm\frac{1}{2}, M_\mathrm{t}=M_I-M_\mathrm{p}} \langle \tfrac{1}{2}, M_\mathrm{p}; \tfrac{1}{2}, M_\mathrm{t} | I, M_I\rangle \Upsilon_{M_\mathrm{p},M_\mathrm{t}}. \tag{2.439}$$

With the appropriate Clebsch–Gordan coefficients, the four coupled spin states are

$$\begin{aligned} |0,0\rangle &= \frac{1}{\sqrt{2}}(\Upsilon_{+\frac{1}{2},-\frac{1}{2}} - \Upsilon_{-\frac{1}{2},+\frac{1}{2}}); \quad \text{(singlet state)} \\ |1,+1\rangle &= \Upsilon_{+\frac{1}{2},+\frac{1}{2}}, \\ |1,0\rangle &= \frac{1}{\sqrt{2}}(\Upsilon_{+\frac{1}{2},-\frac{1}{2}} + \Upsilon_{-\frac{1}{2},+\frac{1}{2}}), \quad \text{(triplet states)} \\ |1,-1\rangle &= \Upsilon_{-\frac{1}{2},-\frac{1}{2}}. \end{aligned} \tag{2.440}$$

The singlet state $I = 0$ is antisymmetric with respect to the exchange of projectile and target, whereas the three triplet states $I = 1$ are symmetric. Since the whole projectile-target wave function must be antisymmetric because we are dealing with fermions, the spatial part of the wave function must have the complementary sym-

metry property, i.e.,

$$\psi(-\mathbf{r}) = \psi(\mathbf{r}) \quad \text{for the singlet state,} \qquad \psi(-\mathbf{r}) = -\psi(\mathbf{r}) \quad \text{for the triplet states.} \tag{2.441}$$

The symmetry requirement (2.441) affects the observable cross section in the scattering of two spin-$\frac{1}{2}$ fermions, even if their interaction does *not* depend on the projectile and target spins. In this case, scattering in the singlet state of projectile and target spin would lead to the symmetrized cross sections (2.425), (2.426) as in the case of spinless bosons,

$$\left(\frac{\mathrm{d}\sigma}{\mathrm{d}\Omega}\right)^{(\mathrm{sing})} = \frac{1}{2}\left|f^{(+)}(\theta,\phi)\right|^2 = \frac{1}{2}\left|f(\theta,\phi) + f(\pi-\theta,\phi+\pi)\right|^2; \tag{2.442}$$

here f is the (hypothetical) scattering amplitude obtained without consideration of symmetry.

On the other hand, scattering in the triplet state of the spins requires a wave function which is antisymmetric in $\mathbf{r}$, i.e., the Schrödinger equation (2.1) should be solved by antisymmetrized wave functions with the boundary conditions,

$$\begin{aligned}\psi(\mathbf{r}) &\overset{r\to\infty}{\sim} \mathrm{e}^{\mathrm{i}kz} + f(\theta,\phi)\frac{\mathrm{e}^{\mathrm{i}kr}}{r} - \mathrm{e}^{-\mathrm{i}kz} - f(\pi-\theta,\phi+\pi)\frac{\mathrm{e}^{\mathrm{i}kr}}{r} \\ &= \mathrm{e}^{\mathrm{i}kz} - \mathrm{e}^{-\mathrm{i}kz} + f^{(-)}(\theta,\phi)\frac{\mathrm{e}^{\mathrm{i}kr}}{r}.\end{aligned} \tag{2.443}$$

The antisymmetrized scattering amplitude, which acquires a factor -1 under reflection at the origin, is related to the (hypothetical) scattering amplitude f obtained without consideration of symmetry via

$$f^{(-)}(\theta,\phi) = f(\theta,\pi) - f(\pi-\theta,\phi+\pi), \tag{2.444}$$

and the differential scattering cross section is

$$\left(\frac{\mathrm{d}\sigma}{\mathrm{d}\Omega}\right)^{(\mathrm{trip})} = \frac{1}{2}\left|f^{(-)}(\theta,\phi)\right|^2 = \frac{1}{2}\left|f(\theta,\phi) - f(\pi-\theta,\phi+\pi)\right|^2; \tag{2.445}$$

For a radially symmetric potential, the scattering amplitudes depend only on θ and not on ϕ, and the even-l contributions fall out of the partial-waves expansion,

$$f^{(-)}(\theta) = 2\sum_{l\ \mathrm{odd}} f_l P_l(\cos\theta) = \sum_{l\ \mathrm{odd}} \frac{2l+1}{\mathrm{i}k}\left(\mathrm{e}^{2\mathrm{i}\delta_l} - 1\right) P_l(\cos\theta). \tag{2.446}$$

A scattering experiment involving two identical spin-$\frac{1}{2}$ fermions in which the spin states are unknown both for the incoming wave and for the outgoing wave, is described according to Sect. 2.8.3 by a density operator which is just one quarter of the unit operator in the four dimensional space of spin states. Under the condition, that the projectile-target interaction does *not depend* on the projectile and target

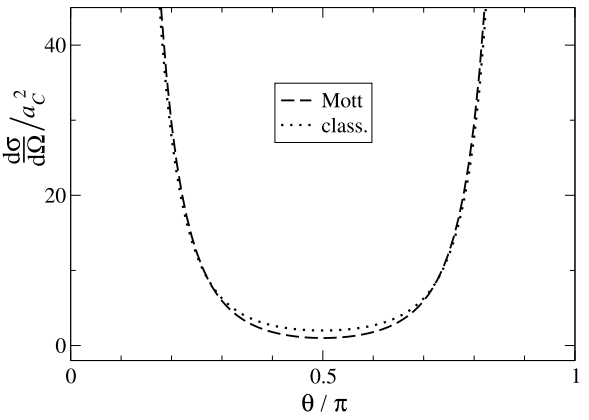

Fig. 2.25 Differential cross section for the scattering of charged spin-$\frac{1}{2}$ fermions as given by (2.450) for $\eta = 1$ (*dashed line*). For electron–electron scattering this corresponds to an energy of near 6.8 eV in the centre-of-mass system. The *dotted line* is the naïve "classical" result which neglects the interference term in the Mott formula

spins, the total spin is conserved and the scattering events can be decomposed into singlet and triplet events as described above. The observed cross section is then the statistical average over the four spin states, each carrying the weight $\frac{1}{4}$. Since the contribution (2.445) is the same for all three triplet states, the observed differential scattering cross section is

$$\frac{\mathrm{d}\sigma}{\mathrm{d}\Omega} = \frac{1}{4}\left(\frac{\mathrm{d}\sigma}{\mathrm{d}\Omega}\right)^{(\mathrm{sing})} + \frac{3}{4}\left(\frac{\mathrm{d}\sigma}{\mathrm{d}\Omega}\right)^{(\mathrm{trip})}. \tag{2.447}$$

If the fermions carry an electric charge, they interact via a repulsive Coulomb interaction. In the singlet state of projectile and particle spin, the scattering amplitude is the symmetrized Coulomb amplitude as already given by (2.433) for charged spinless bosons. In the triplet state, the spatial part of the wave function must be antisymmetric, the relevant antisymmetrized version of the Coulomb scattering amplitude is

$$f_{\mathrm{C}}^{(-)}(\theta) = -\frac{\eta \mathrm{e}^{2\mathrm{i}\sigma_0}}{2k}\left[\frac{\mathrm{e}^{-\mathrm{i}\eta\ln[\sin^2(\theta/2)]}}{\sin^2(\theta/2)} - \frac{\mathrm{e}^{-\mathrm{i}\eta\ln[\cos^2(\theta/2)]}}{\cos^2(\theta/2)}\right], \tag{2.448}$$

and the corresponding differential scattering cross section is,

$$\left(\frac{\mathrm{d}\sigma}{\mathrm{d}\Omega}\right)_{\mathrm{C}}^{(-)} = \left(\frac{\eta}{2k}\right)^2\left[\frac{1}{\sin^4(\theta/2)} + \frac{1}{\cos^4(\theta/2)} - \frac{2\cos(2\eta\ln[\tan(\theta/2)])}{\sin^2(\theta/2)\cos^2(\theta/2)}\right]. \tag{2.449}$$

The differential scattering cross section (2.447) for unpolarized fermions now becomes

$$\left(\frac{\mathrm{d}\sigma}{\mathrm{d}\Omega}\right)_{\mathrm{C}}^{\mathrm{fermion}} = \left(\frac{\eta}{2k}\right)^2\left[\frac{1}{\sin^4(\theta/2)} + \frac{1}{\cos^4(\theta/2)} - \frac{\cos(2\eta\ln[\tan(\theta/2)])}{\sin^2(\theta/2)\cos^2(\theta/2)}\right]. \tag{2.450}$$

This is the *Mott formula* for the scattering of identical charged spin-$\frac{1}{2}$ fermions. To be consistent with common practice, we have *not* included the factor $\frac{1}{2}$ on the right-hand sides of (2.442) and (2.445) in the definition of the Mott scattering cross sections. The Mott cross section for the scattering of identical charged spin-$\frac{1}{2}$ fermions is shown as dashed line in Fig. 2.25 for the case $\eta = 1$. For electron–electron (or positron–positron) scattering a_C is twice the standard Bohr radius a_0, so $\eta = 1$ corresponds to $k = 1/(2a_0)$ and $E = \hbar^2/(4m_{\mathrm{el}}a_0^2) \approx 6.8$ eV. The dotted line in Fig. 2.25 shows the naïve "classical" result which neglects the interference term in the Mott formula. Note that the interference is always destructive around $\theta = \frac{\pi}{2}$ in the case of spin-$\frac{1}{2}$ fermions described by (2.450).

The formulae (2.447) and (2.450) are only valid as long as any dependence on projectile and target spin can be neglected in the projectile-target interaction. If, e.g., spin–orbit coupling is important, then the total spin of target and projectile is no longer conserved and the decomposition (2.447) loses its validity. In this case, the various spin channels may be grouped in eigenspaces of the total angular momentum and the coupled-channel problem can be treated as described in Sect. 2.8.1.

References

1. Abramowitz, M., Stegun, I.A. (eds.): Handbook of Mathematical Functions. Dover, New York (1970)
2. Berry, M.V., Mount, K.E.: Semiclassical approximations in wave mechanics. Rep. Prog. Phys. **35**, 315 (1972)
3. Bethe, H.A.: Theory of the effective range in nuclear scattering. Phys. Rev. **76**, 38 (1949)
4. Blum, K.: Density Matrix Theory and Applications, 2nd edn. Plenum, New York (1996)
5. Boersma, J.: Expansions for Coulomb wave functions. Math. Comput. **23**, 51 (1969)
6. Brackett, F.S., Birge, R.T.: Quantum defect and the new Bohr theory of atomic structure. J. Opt. Sci. Am. Rev. Sci. Instrum. **8**, 213 (1924)
7. Brander, O.: High-energy behaviour of phase shifts for scattering from singular potentials. J. Math. Phys. **22**, 1229 (1980)
8. Breit, G., Condon, E.U., Present, R.D.: Theory of scattering of protons by protons. Phys. Rev. **50**, 825 (1936)
9. Brillouin, L.: La mècanique ondulatoire de Schrödinger: une méthode générale de resolution par approximations successives. C. R. Acad. Sci. **183**, 24 (1926)
10. Buck, B., Friedrich, H., Wheatley, C.: Nucl. Phys. A **275**, 246 (1977)
11. Casimir, H.B.G., Polder, D.: The influence of retardation on the London–van der Waals forces. Phys. Rev. **73**, 360 (1948)
12. Chew, G.F., Goldberger, M.L.: On the analysis of nucleon–nucleon scattering experiments. Phys. Rev. **75**, 1637 (1949)
13. Côté, R., Segev, B., Raizen, M.G.: Retardation effects on quantum reflection from an evanescent-wave atomic mirror. Phys. Rev. A **58**, 3999 (1998)
14. Dalgarno, A., McDowell, M.R.C., Williams, A.: The mobility of ions in unlike gases. Philos. Trans. R. Soc. Lond. Ser. A, Math. Phys. Sci. **250**, 411 (1958)
15. Fermi, E., Marshall, L.: Interference phenomena of slow neutrons. Phys. Rev. **71**, 666 (1947)
16. Friedrich, H.: Theoretical Atomic Physics, 3rd. edn. Springer, Berlin (2006)
17. Friedrich, H., Trost, J.: Phase loss in WKB waves due to reflection by a potential. Phys. Rev. Lett. **26**, 4869 (1996)

18. Friedrich, H., Trost, J.: Working with WKB waves far from the semiclassical limit. Phys. Rep. **397**, 359 (2004)
19. Gamow, G.: Zur Quantentheorie des Atomkerns. Z. Phys. **51**, 204 (1928)
20. Gesztesy, F., Lang, C.B.: On the Abel summability of partial-wave amplitudes for Coulomb-type interactions. J. Math. Phys. **22**, 312 (1981)
21. Gradshteyn, I.S., Ryzhik, I.M.: Table of Integrals, Series, and Products, 5th edn. Academic Press, New York (1994)
22. Hamilton, J., Øverbö, I., Tromborg, B.: Coulomb corrections in non-relativistic scattering. Nucl. Phys. B **60**, 443 (1973)
23. Jeffreys, H.: On certain approximate solutions of linear differential equations of the second order. Proc. Lond. Math. Soc. **23**, 428 (1925)
24. Joachain, C.J.: Quantum Collision Theory. North Holland, Amsterdam (1987)
25. Kamouni, R., Baye, D.: Scattering length and effective range for collisions between light ions within a microscopic model. Nucl. Phys. A **791**, 68 (2007)
26. Kramers, H.A.: Wellenmechanik und halbzählige Quantisierung. Z. Phys. **39**, 828 (1926)
27. Langer, R.E.: On the connection formulas and the solutions of the wave equation. Phys. Rev. **51**, 669 (1937)
28. Levinson, N.: On the uniqueness of the potential in a Schrodinger equation for a given asymptotic phase. Kgl. Danske Videnskab. Selskab, Mat.-Fys. Medd. **25**/9 (1949)
29. Levy, B.R., Keller, J.B.: Low-energy expansion of scattering phase shifts for long-range potentials. J. Math. Phys. **4**, 54 (1963)
30. Messiah, A.: Quantum Mechanics, vol. 1. North Holland, Amsterdam (1961). Chap. 10 Sect. 4
31. Morse, P.M., Feshbach, H.: Methods of Theoretical Physics, Part II. McGraw Hill, New York (1953)
32. Naidon, P., Tiesinga, E., Mitchell, W.F., Julienne, P: Effective-range description of a Bose gas under strong one- or two-dimensional confinement. New J. Phys. **9**, 19 (2007)
33. Newton, R.: Scattering Theory of Waves and Particles. Springer, Berlin (1982)
34. O'Malley, T.F., Spruch, L., Rosenberg, L.: Modification of effective-range theory in the presence of a long-range (r^{-4}) potential. J. Math. Phys. **2**, 491 (1961)
35. Pethick, C.J., Smith, H.: Bose-Einstein Condensation in Dilute Gases, 2nd edn. Cambridge University Press, Cambridge (2008)
36. Ramsauer, C.: Über den Wirkungsquerschnitt der Gasmoleküle gegenüber langsamen Elektronen. Ann. Phys. **64**, 513 (1921)
37. Rosenberg, L.: Levinson–Seaton theorem for potentials with an attractive Coulomb tail. Phys. Rev. A **52**, 3824 (1995)
38. Schrödinger, E.: Quantisierung als Eigenwertproblem. Ann. Phys. **386**, 109 (1926)
39. Schwabl, F.: Quantum Mechanics, 4th edn. Springer, Berlin (2007)
40. Seaton, M.J.: The quantum defect method. Mon. Not. R. Astron. Soc. **118**, 504 (1958)
41. Seaton, M.J.: Quantum defect theory. Rep. Prog. Phys. **46**, 167 (1983)
42. Siegert, A.J.F.: On the derivation of the dispersion formula for nuclear reactions. Phys. Rev. **56**, 750 (1939)
43. Strecok, A.J., Gregory, J.A.: High precision evaluation of the irregular Coulomb wave functions. Math. Comput. **26**, 955 (1972)
44. Taylor, J.R.: Scattering Theory: The Quantum Theory of Nonrelativistic Collisions. Wiley, New York (1972)
45. Townsend, J.S.: Elastic collisions. Proc. R. Soc. Lond. Ser. A, Math. Phys. Sci. **131**, 352 (1931)
46. Townsend, J.S., Bailey, V.A.: The motion of electrons in argon and in hydrogen. Philos. Mag. **44**, 1033 (1922)
47. Trost, J., Friedrich, H.: WKB and exact wavefunctions for inverse power-law potentials. Phys. Lett. A **228**, 127 (1997)
48. van Haeringen, H.: Scattering length and effective range in closed form for the Coulomb plus Yamaguchi potential. Nucl. Phys. A **75**, 355 (1975)

49. Wentzel, G.: Eine Verallgemeinerung der Quantenbedingungen für die Zwecke der Wellenmechanik. Z. Phys. **38**, 518 (1926)
50. Wigner, E.P.: Resonance reactions and anomalous scattering. Phys. Rev. **70**, 15 (1946)
51. Wigner, E.P.: Lower limit for the energy derivative of the scattering phase shift. Phys. Rev. **98**, 145 (1955)
52. Yost, F.L., Wheeler, J.A., Breit, G.: Coulomb wave functions in repulsive fields. Phys. Rev. **49**, 174 (1936)

Chapter 3
Internal Excitation, Inelastic Scattering

When target and/or projectile have internal degrees of freedom beyond the spins discussed in Sect. 2.8, then their internal states can be excited or de-excited by energy transfer from or to the relative-motion degree of freedom. Scattering processes, in which the projectile or target is excited to a quantum state of higher energy, are *inelastic*. A scattering process in which the projectile or target is initially in an excited state and loses energy to the relative-motion degree of freedom are sometimes called "super-elastic". The possibility of exciting or de-exciting internal degrees of freedom can also have observable effects on the cross sections for elastic scattering.

3.1 Coupled-Channel Equations and Scattering Cross Sections

In a straightforward extension of the treatment of internal angular momenta in Sect. 2.8.1, the natural ansatz allowing the consideration of more general internal degrees of freedom of projectile and target is

$$\boldsymbol{\Psi}(\mathbf{r},\xi) = \sum_j \psi_j(\mathbf{r})\Upsilon_j(\xi). \tag{3.1}$$

Here ξ stands for *all* internal degrees of freedom of projectile *and* target, and $\Upsilon_i(\xi)$ are the quantum mechanical wave functions for the respective internal states, ideally eigenstates with eigenvalues E_i of an "internal Hamiltonian" $\hat{H}_\xi$ which acts in the space of internal states,

$$\hat{H}_\xi \Upsilon_i(\xi) = E_i \Upsilon_i(\xi). \tag{3.2}$$

The internal states Υ_i define *channels* for the scattering process, and the wave functions $\psi_i(\mathbf{r})$ are the respective *channel wave functions*. The Schrödinger equation which describes the relative motion of projectile and target and allows for excitation of the interal degrees of freedom is,

$$\left[-\frac{\hbar^2}{2\mu}\Delta + \hat{H}_\xi + \hat{W}(\mathbf{r},\xi)\right]\boldsymbol{\Psi}(\mathbf{r},\xi) = E\boldsymbol{\Psi}(\mathbf{r},\xi). \tag{3.3}$$

H. Friedrich, *Scattering Theory*, DOI 10.1007/978-3-662-48526-2_3

The operator $\hat{W}$ acts on functions of $\mathbf{r}$ and also in the space of internal excitations. Inserting the expansion (3.1) into (3.3) and taking the matrix element with $\langle \Upsilon_i |$ leads to the *coupled-channel equations*

$$-\frac{\hbar^2}{2\mu}\Delta\psi_i(\mathbf{r}) + \sum_j V_{i,j}\psi_j(\mathbf{r}) = (E - E_i)\psi_i(\mathbf{r}). \tag{3.4}$$

The potential-energy term in (3.4) appears as a matrix whose elements $V_{i,j}$ act on functions of the relative distance coordinate $\mathbf{r}$. They are derived from the operator $\hat{W}$ in (3.3) via

$$V_{i,j} = \langle \Upsilon_i | \hat{W} | \Upsilon_j \rangle_\xi. \tag{3.5}$$

The subscript ξ on the matrix element in (3.5) indicates that the integration is over the internal coordinates ξ, but not over the relative-distance coordinate $\mathbf{r}$. The nature of the potentials $V_{i,j}$ is actually quite complex if derived via *ab initio* methods based on a detailed account of the internal structure of projectile and target, see e.g. Ref. [5]. The nature of the projectile-target interaction at large distances is often well known and accurately described by simple local potentials. This is not the case for small distances where projectile and target are close and effects related to details of their internal structure become important. The complications that arise when attempting to describe this close regime on the basis of *ab initio* theories are not the subject of this monograph. For our purposes it is sufficient to think of the $V_{i,j}$ as (not necessarily local) potentials that fall off to zero for large separations of projectile and target. Unless explicitly stated otherwise, this fall-off is assumed to be faster than $1/r^2$.

In the expansion in channels as described by Eqs. (3.1) and (3.2), the channel j is called *open* at a given energy E when $E > E_j$. If $E < E_j$, then the channel j is *closed* and the channel wave function $\psi_j(\mathbf{r})$ necessarily obeys bound-state boundary conditions at large distances. Unbound, scattering states of relative motion of projectile and target can only exist in open channels. The internal energies E_j thus define *channel thresholds* separating the closed, bound regime from the open, unbound regime in the respective channels.

We describe the scattering process with solutions of (3.4) obeying the following boundary conditions,

$$\boldsymbol{\Psi}(\mathbf{r}, \xi) \overset{r\to\infty}{\sim} \mathrm{e}^{\mathrm{i}k_i z}\Upsilon_i(\xi) + \sum_{j \text{ open}} f_{i,j}(\theta, \phi)\frac{\mathrm{e}^{\mathrm{i}k_j r}}{r}\Upsilon_j(\xi). \tag{3.6}$$

The wave number k_j in the open channel j now carries the corresponding subscript, because it is related to the asymptotic kinetic energy $E - E_j$, which can be different in different channels,

$$E - E_j = \frac{\hbar^2 k_j^2}{2\mu} > 0, \quad k_j = \frac{1}{\hbar}\sqrt{2\mu(E - E_j)}. \tag{3.7}$$

In closed channels, the asymptotically available kinetic energy is negative and related to an inverse penetration depth κ_j,

$$E - E_j = -\frac{\hbar^2 \kappa_j^2}{2\mu} < 0, \quad \kappa_j = \frac{1}{\hbar}\sqrt{2\mu(E_j - E)}. \tag{3.8}$$

The asymptotic behaviour (3.6) of the full wave function implies the following boundary conditions for the open-channel wave functions $\psi_j(\mathbf{r})$,

$$\psi_j(\mathbf{r}) \overset{r\to\infty}{\sim} \mathrm{e}^{\mathrm{i}k_i z}\delta_{i,j} + f_{i,j}(\theta,\phi)\frac{\mathrm{e}^{\mathrm{i}k_j r}}{r}, \tag{3.9}$$

while the closed-channel wave functions vanish proportional to $\mathrm{e}^{-\kappa_j r}/r$ asymptotically.

The second term on the right-hand side of (3.6) is a superposition of outgoing spherical waves in various open channels j. The *inelastic scattering amplitude* $f_{i,j}(\theta,\phi)$ describes scattering into the direction (θ,ϕ) accompanied by excitation (or de-excitation) of the internal degrees of freedom from their initial state Υ_i to the final state Υ_j. The current densities, on which the definition of scattering cross sections is based, are proportional to the asymptotic wave number k_i or k_j. For the current density from the outgoing spherical wave in channel j, Eq. (2.4) in Sect. 2.1 is generalized to

$$\mathbf{j}_j(\mathbf{r}) = \frac{\hbar k_j}{\mu}\left|f_{i,j}(\theta,\phi)\right|^2 \frac{\hat{\mathbf{e}}_\mathbf{r}}{r^2} + O\left(\frac{1}{r^3}\right), \tag{3.10}$$

while the incoming current density to which the cross section is normalized is $|\mathbf{j}_i| = \hbar k_i/\mu$. The differential cross section for scattering from the incident channel i to the outgoing channel j is thus,

$$\frac{\mathrm{d}\sigma_{i\to j}}{\mathrm{d}\Omega} = \frac{k_j}{k_i}\left|f_{i,j}(\theta,\phi)\right|^2. \tag{3.11}$$

The cross section for elastic and inelastic scattering in an experiment with incoming flux in the incident channel i is,

$$\sigma = \sum_{j \text{ open}} \sigma_{i\to j}, \quad \sigma_{i\to j} = \int \frac{\mathrm{d}\sigma_{i\to j}}{\mathrm{d}\Omega}\mathrm{d}\Omega = \frac{k_j}{k_i}\int \left|f_{i,j}(\theta,\phi)\right|^2 \mathrm{d}\Omega. \tag{3.12}$$

The current density $\mathbf{j}(\mathbf{r})$ associated with the total wave function (3.1) is appropriately defined as

$$\mathbf{j}(\mathbf{r}) = \Re\left[\left\langle \boldsymbol{\Psi}\middle|\frac{\hat{\mathbf{p}}}{\mu}\middle|\boldsymbol{\Psi}\right\rangle_\xi\right] = \frac{\hbar}{2\mathrm{i}\mu}\sum_j \psi_j^*(\mathbf{r})\nabla\psi_j(\mathbf{r}) + \text{cc.}, \tag{3.13}$$

compare Eq. (2.3) in Sect. 2.1. Channel-mixing contributions to the right-hand side of (3.13) vanish because of the orthogonality of the internal states, $\langle\Upsilon_j|\Upsilon_{j'}\rangle_\xi = \delta_{j,j'}$. If the potential energy operator $\hat{W}$ in the Schrödinger equation (3.3) is hermitian, then the stationary solutions obey the continuity equation in the form

$$\oint \mathbf{j}\cdot\mathrm{d}\mathbf{s} = 0. \tag{3.14}$$

For the surface of a large sphere with radius $r \to \infty$, the contribution of the incoming plane wave in channel i vanishes because of symmetry, as already discussed for elastic scattering in Sect. 2.1. The contribution of the outgoing spherical waves is a generalization of Eq. (2.8) in Sect. 2.1,

$$I_{\text{out}} = \sum_{j \text{ open}} \frac{\hbar k_j}{\mu} \int \left| f_{i,j}(\Omega) \right|^2 \mathrm{d}\Omega = \frac{\hbar k_i}{\mu} \sum_{j \text{ open}} \sigma_{i \to j} = \frac{\hbar k_i}{\mu} \sigma. \tag{3.15}$$

This outgoing flux is compensated by a loss of flux from the incoming plane wave, which is due to destructive interference in the forward direction $\theta = 0$, as described by Eq. (2.13) for the elastic-scattering case. Due to the orthogonality of the internal states Υ_j, the only nonvanishing interference contributions to the total current density (3.13) come from the incident channel i, so the appropriate adaptation of Eq. (2.13) to the present situation is,

$$I_{\text{int}} = -\frac{\hbar}{\mu} 4\pi \Im\big[f_{i,i}(\theta = 0) \big]. \tag{3.16}$$

The optical theorem, which is an expression of particle conservation, now reads

$$\sigma = \frac{4\pi}{k_i} \Im\big[f_{i,i}(\theta = 0) \big]. \tag{3.17}$$

Note that the entire outgoing flux in all channels, both elastic and inelastic, is fed from the destructive forward interference of the incoming plane wave and the outgoing spherical wave in the incident, elastic channel.

3.2 Coupled-Channel Lippmann–Schwinger Equation and Born Approximation

The coupled-channel equations (3.4) can be written, in analogy to (2.15) in Sect. 2.2, as

$$\left(\hat{E} + \frac{\hbar^2}{2\mu} \Delta \right) \Psi = \hat{V} \Psi, \tag{3.18}$$

where Ψ stands for a vector of channel wave functions $\psi_j(\mathbf{r})$, $\hat{V}$ is the operator represented by the matrix of potentials (3.5) and $\hat{E}$ stands for a diagonal matrix with the elements $E - E_j$ corresponding to the asymptotically available energy of relative motion in the respective channels. Equation (3.18) can be transformed into a set of coupled integral equations with the help of the Green's operator $\hat{G}$, which is represented by a diagonal matrix of Green's functions,

$$\hat{G} \equiv \begin{pmatrix} \mathscr{G}_{1,1} & 0 & 0 & \cdots \\ 0 & \mathscr{G}_{2,2} & 0 & \cdots \\ 0 & 0 & \mathscr{G}_{3,3} & \cdots \\ \cdots & \cdots & \cdots & \cdots \end{pmatrix}. \tag{3.19}$$

The Green's operator and the (diagonal) elements of its matrix representation fulfill the defining equations

$$\left[\hat{E} + \frac{\hbar^2}{2\mu}\Delta\right]\hat{G} = \mathbf{1}, \qquad \left[E - E_j + \frac{\hbar^2}{2\mu}\Delta\right]\mathscr{G}_{j,j}(\mathbf{r},\mathbf{r}') = \delta(\mathbf{r}-\mathbf{r}'). \tag{3.20}$$

A formal solution of the multichannel Schrödinger equation (3.18) is

$$\Psi = \Psi^{\mathrm{hom}} + \hat{G}\hat{V}\Psi, \tag{3.21}$$

where Ψ^{hom} is a solution of the "homogeneous" equation, $[\hat{E} + \frac{\hbar^2}{2\mu}\Delta]\Psi^{\mathrm{hom}} = 0$. Equation (3.21) is the Lippmann–Schwinger equation for the multichannel description of the scattering process.

For open channels j with wave number k_j as given in (3.7), the component Green's function is, in analogy to Eqs. (2.17), (2.19) in Sect. 2.2,

$$\mathscr{G}_{j,j}(\mathbf{r},\mathbf{r}') = -\frac{\mu}{2\pi\hbar^2}\frac{\mathrm{e}^{\mathrm{i}k_j|\mathbf{r}-\mathbf{r}'|}}{|\mathbf{r}-\mathbf{r}'|} \overset{|\mathbf{r}|\gg|\mathbf{r}'|}{\sim} -\frac{\mu}{2\pi\hbar^2}\frac{\mathrm{e}^{\mathrm{i}k_j r}}{r}\mathrm{e}^{-\mathrm{i}\mathbf{k}_j\cdot\mathbf{r}'}, \tag{3.22}$$

where $\mathbf{k}_j = k_j\hat{\mathbf{e}}_{\mathbf{r}}$ is the wave vector of length k_j pointing in the direction of $\mathbf{r}$. The corresponding expressions for closed channels are obtained by replacing k_j with $\mathrm{i}\kappa_j$, see Eq. (3.8).

In order to fulfill the boundary conditions (3.9) with the open channel i as the incident channel, Ψ^{hom} in (3.21) is defined to have the following components,

$$\psi_i^{\mathrm{hom}}(\mathbf{r}) = \mathrm{e}^{\mathrm{i}k_i z}, \qquad \psi_j^{\mathrm{hom}}(\mathbf{r}) \equiv 0 \quad \text{for } j \neq i. \tag{3.23}$$

We can write the multichannel Lippmann–Schwinger equation (3.21) explicitly as a set of coupled integral equations for the components of Ψ, i.e. for the channel wave functions $\psi_j(\mathbf{r})$,

$$\psi_j(\mathbf{r}) = \mathrm{e}^{\mathrm{i}k_i z}\delta_{i,j} + \int \mathscr{G}_{j,j}(\mathbf{r},\mathbf{r}')\sum_n V_{j,n}\psi_n(\mathbf{r}')\,\mathrm{d}\mathbf{r}'. \tag{3.24}$$

For the open channels, we can insert the leading asymptotic behaviour of $\mathscr{G}_{j,j}(\mathbf{r},\mathbf{r}')$ for $|\mathbf{r}| \gg |\mathbf{r}'|$ as given by (3.22) and obtain,

$$\psi_j(\mathbf{r}) \overset{r\to\infty}{\sim} \mathrm{e}^{\mathrm{i}k_i z}\delta_{i,j} - \frac{\mu}{2\pi\hbar^2}\frac{\mathrm{e}^{\mathrm{i}k_j r}}{r}\sum_n \int \mathrm{e}^{-\mathrm{i}\mathbf{k}_j\cdot\mathbf{r}'}V_{j,n}\psi_n(\mathbf{r}')\,\mathrm{d}\mathbf{r}'. \tag{3.25}$$

This agrees with the asymptotic behaviour (3.9) of the open-channel wave functions, and the scattering amplitudes are seen to be given by,

$$f_{i,j}(\theta,\phi) = -\frac{\mu}{2\pi\hbar^2}\sum_n \int \mathrm{e}^{-\mathrm{i}\mathbf{k}_j\cdot\mathbf{r}'}V_{j,n}(\mathbf{r}')\psi_n(\mathbf{r}')\,\mathrm{d}\mathbf{r}'. \tag{3.26}$$

The expression on the right-hand side of (3.26) contains the exact channel wave functions ψ_n in all channels n (including the closed channels), so it is not a direct solution of the inelastic scattering problem. An approximate solution can be formulated in the spirit of the Born approximation by replacing the ψ_n in (3.26) by the

components (3.23) of the wave function Ψ^{hom} containing only the incoming plane wave in the incident channel,

$$f_{i,j}^{\text{Born}}(\theta,\phi) = -\frac{\mu}{2\pi\hbar^2}\int \mathrm{e}^{-\mathrm{i}(\mathbf{k}_j - k_i\hat{\mathbf{e}}_z)\cdot\mathbf{r}'} V_{j,i}(\mathbf{r}')\,\mathrm{d}\mathbf{r}'. \tag{3.27}$$

Similar to the expression (2.22) for the elastic-scattering Born amplitude, the right-hand side of (3.27) is essentially the Fourier transform of the relevant interaction, which now is the coupling potential $V_{j,i}$. The Born scattering amplitude $f_{i,j}^{\text{Born}}$ is a function of the conjugate wave number

$$\mathbf{q} = \mathbf{k}_j - k_i\hat{\mathbf{e}}_z = k_j\hat{\mathbf{e}}_r - k_i\hat{\mathbf{e}}_z, \tag{3.28}$$

i.e. of the momentum transfer $\hbar\mathbf{q}$. In contrast to the elastic-scattering case discussed in Sect. 2.2, where the wave number of momentum transfer is connected to the polar scattering angle by the simple relation (2.24), Eq. (3.28) implies a less trivial connection to the polar and azimuthal angles when $k_j \neq k_i$.

3.3 Radial Coupled-Channel Equations

The coupled-channel equations (3.4) can be transformed to a set of coupled ordinary differential equations for radial wave functions via a partial-waves expansion similar to (2.364) in Sect. 2.8.1,

$$\psi_i(\mathbf{r}) = \sum_{l=0}^{\infty}\sum_{m=-l}^{l}\frac{u_{i,l,m}(r)}{r}Y_{l,m}(\theta,\phi). \tag{3.29}$$

The coupled equations for the radial wave functions $u_{i,l,m}(r)$ are now

$$\left[-\frac{\hbar^2}{2\mu}\frac{\mathrm{d}^2}{\mathrm{d}r^2} + \frac{l(l+1)\hbar^2}{2\mu r^2}\right]u_{i,l,m}(r) + \sum_{j,l',m'} V(i,l,m;j,l',m')u_{j,l',m'}(r) = E u_{i,l,m}(r), \tag{3.30}$$

and the matrix of radial potentials is defined via

$$V(i,l,m;j,l',m') = \left\langle \Upsilon_i(\xi)Y_{l,m}(\theta,\phi)\middle|\hat{W}\middle|\Upsilon_j(\xi)Y_{l',m'}(\theta,\phi)\right\rangle_{\xi,\theta,\phi}, \tag{3.31}$$

where the subscripts on the matrix element indicate integration over all internal degrees of freedom ξ as well as over the angles θ and ϕ of the relative distance coordinate $\mathbf{r}$.

The further discussion in this section closely follows the treatment already given for coupled spin channels in elastic scattering in Sect. 2.8.1. However, the internal states $\Upsilon_j(\xi)$ of the projectile-target system are now not just spin multiplets, they also account for internal excitations of projectile and/or target, so there is no limit on the number of channels to be included in the coupled radial equations (3.30). In practice, of course, the choice of channels to be included in a given investigation is guided by physical relevance and feasibility of actual calculations.

An essential generalization of the coupled-channels theory of Sect. 2.8.1 now is, that the wave number k_j depends on the channel index j according to (3.7). This means that the two linearly independent solutions (2.375) of the uncoupled free-particle equations, on which the representation of the complete solutions of the coupled-channel equations is based, contain channel-dependent wave numbers k_j,

$$\begin{aligned} u_l^{(\mathrm{s})}(k_j r) &\overset{k_j r\to\infty}{\sim} \sin\left(k_j r - l\frac{\pi}{2}\right), \\ u_l^{(\mathrm{c})}(k_j r) &\overset{k_j r\to\infty}{\sim} \cos\left(k_j r - l\frac{\pi}{2}\right). \end{aligned} \tag{3.32}$$

As a consequence, the normalization of the regular free-particle wave function,

$$\left\langle u_l^{(\mathrm{s})}(k_j r)\middle| u_l^{(\mathrm{s})}\left(k'_j r\right)\right\rangle = \frac{\pi}{2}\delta\left(k_j - k'_j\right), \tag{3.33}$$

is channel dependent, because $\delta(k_j - k'_j) \neq \delta(k_i - k'_i)$ when $k_j \neq k_i$ [compare Eq. (2.57) in Sect. 2.3.4].

The definitions of the reactance matrix K and the scattering matrix S depend on the normalization of the free-particle basis functions in the respective channels. Inconsistencies due to incompatible normalization properties can be avoided by expanding in terms of the energy-normalized free-particle waves, which carry a factor $\sqrt{2\mu/(\pi\hbar^2 k_j)}$ according to (2.60),

$$\bar{\mathrm{u}}_l^{(\mathrm{s})}(k_j r) = \sqrt{\frac{2\mu}{\pi\hbar^2 k_j}}\, u_l^{(\mathrm{s})}(k_j r), \qquad \bar{\mathrm{u}}_l^{(\mathrm{c})}(k_j r) = \sqrt{\frac{2\mu}{\pi\hbar^2 k_j}}\, u_l^{(\mathrm{c})}(k_j r). \tag{3.34}$$

The normalization of the regular free-particle wave is then independent of the channel,

$$\left\langle \bar{\mathrm{u}}_l^{(\mathrm{s})}(k_j r)\middle| \bar{\mathrm{u}}_l^{(\mathrm{s})}\left(k'_j r\right)\right\rangle = \delta\left(E - E_j - \left(E' - E_j\right)\right) = \delta\left(E - E'\right). \tag{3.35}$$

A solution of the radial coupled-channel equations (3.30) is a vector of radial wave functions, and the number of component wave functions is equal to the number of radial channels included in (3.30). For a given total energy E, there are as many linearly independent vectors of solutions as there are open channels. A basis $U^{(i,l,m)}$ of vectors of solutions can be defined in analogy to (2.376) by the following boundary conditions for the component wave functions $u_{j,l',m'}^{(i,l,m)}$:

$$u_{j,l',m'}^{(i,l,m)}(k_j r) \overset{r\to\infty}{\sim} \delta_{i,j}\delta_{l,l'}\delta_{m,m'}\bar{\mathrm{u}}_l^{(\mathrm{s})}(k_i r) + K_{i,l,m;j,l',m'}\bar{\mathrm{u}}_{l'}^{(\mathrm{c})}(k_j r). \tag{3.36}$$

An alternative basis $\Phi^{(i,l,m)}$ can be constructed with component wave functions obeying boundary conditions analogous to (2.379)

$$\varphi_{j,l',m'}^{(i,l,m)}(r) \overset{r\to\infty}{\sim} \delta_{i,j}\delta_{l,l'}\delta_{m,m'}\varphi_l^{(-)}(k_i r) - S_{i,l,m;j,l',m'}\varphi_{l'}^{(+)}(k_j r); \tag{3.37}$$

the outgoing and incoming free-particle radial waves are now defined by

$$\varphi_l^{(\pm)}(k_j r) \overset{r\to\infty}{\sim} \bar{\mathrm{u}}_l^{(\mathrm{c})}(k_j r) \pm \mathrm{i}\bar{\mathrm{u}}_l^{(\mathrm{s})}(k_j r) \overset{r\to\infty}{\sim} \sqrt{\frac{2\mu}{\pi\hbar^2 k_j}}\,\mathrm{e}^{\pm\mathrm{i}(k_j r - l\pi/2)}. \tag{3.38}$$

Equation (2.380) expressing the solution vectors $\Phi^{(i,l,m)}$ as linear combinations of the basis vectors $U^{(j,l',m')}$ remains valid,

$$-\mathrm{i}\left(U^{(i,l,m)} + \sum_{j,l',m'} S_{i,l,m;\,j,l',m'} U^{(j,l',m')}\right) = \Phi^{(i,l,m)}, \tag{3.39}$$

and the S-matrix defined by (3.37) is related to the K-matrix defined by (3.36) by

$$\mathbf{S} = (\mathbf{1} + \mathrm{i}\mathbf{K})(\mathbf{1} - \mathrm{i}\mathbf{K})^{-1}, \tag{3.40}$$

as in Eq. (2.382) in Sect. 2.8.1.

In order to relate the S-matrix defined by (3.37) with (3.38) to the scattering amplitudes $f_{i,j}$ in (3.9), we now observe that the solution vector obeying the boundary conditions implied by (3.6) is given as the following superposition of the basis vectors $\Phi^{(i,l,0)}$,

$$U = -\pi\hbar \sum_l \sqrt{\frac{2l+1}{2\mu k_i}}\, \mathrm{i}^{l-1} \Phi^{(i,l,0)}. \tag{3.41}$$

In comparison to the right-hand side of (2.385), the right-hand side of (3.41) differs by a factor $\sqrt{\pi\hbar^2 k_i/(2\mu)}$ due to the different definition (3.38) of the component radial wave functions in $\Phi^{(i,l,0)}$. Correspondingly, the component radial wave functions of U as given by (3.41) are

$$u_{j,l',m'}(r) = -\pi\hbar \sum_l \sqrt{\frac{2l+1}{2\mu k_i}}\, \mathrm{i}^{l-1} \varphi^{(i,l,0)}_{j,l',m'}(r), \tag{3.42}$$

and the channel wave functions (3.29) behave asymptotically as

$$\begin{aligned}\psi_j(\mathbf{r}) &= \sum_{l',m'} \frac{u_{j,l',m'}(r)}{r} Y_{l',m'}(\theta,\phi) \\ &\overset{r\to\infty}{\sim} \delta_{i,j} \mathrm{e}^{\mathrm{i}k_i z} + \frac{\mathrm{e}^{\mathrm{i}k_i r}}{r} \sum_{l',m'} Y_{l',m'}(\theta,\phi)\mathrm{i} \sum_l \mathrm{i}^{l-l'} \sqrt{\frac{\pi(2l+1)}{k_i k_j}} \\ &\qquad \times [\delta_{i,j}\delta_{l,l'}\delta_{0,m'} - S_{i,l,0;\,j,l',m'}].\end{aligned} \tag{3.43}$$

Comparison with (3.9) gives

$$f_{i,j}(\theta,\phi) = \sum_{l',m'} Y_{l',m'}(\theta,\phi) \sum_l \mathrm{i}^{l-l'-1} \sqrt{\frac{\pi(2l+1)}{k_i k_j}} [S_{i,l,0;\,j,l',m'} - \delta_{i,j}\delta_{l,l'}\delta_{0,m'}]. \tag{3.44}$$

A procedure for calculating the inelastic scattering amplitudes $f_{i,j}$ from the coupled radial equations (3.30)—with known potentials $V_{i,l,m;\,j,l',m'}$ and for N open channels—can be formulated as follows: Integrate the coupled ordinary differential equations outwards for N linearly independent initial conditions at small r; beyond

the range of the potentials construct linear combinations compatible with the boundary conditions (3.36) or (3.37), determine the S-matrix elements $S_{i_s,l,0;\,j_s,l',m'}$ and apply Eq. (3.44).

Exploiting the orthonormality (2.27) of the spherical harmonics leads to the following expression for the integrated inelastic scattering cross section (3.12),

$$\begin{aligned}\sigma_{i\to j} &= \frac{k_j}{k_i}\int |f_{i,j}|^2\,\mathrm{d}\Omega \\ &= \frac{\pi}{k_i^2}\sum_{l_1,l_2} \mathrm{i}^{l_2-l_1}\sqrt{(2l_1+1)(2l_2+1)} \\ &\quad\times \sum_{l',m'}\left(S^*_{i,l_1,0;\,j,l',m'} - \delta_{i,j}\delta_{l_1,l'}\delta_{0,m'}\right)\left(S_{i,l_2,0;\,j,l',m'} - \delta_{i,j}\delta_{l_2,l'}\delta_{0,m'}\right).\end{aligned} \tag{3.45}$$

The summation index l in (3.44) appears as l_1 (from $f^*_{i,j}$) and l_2 (from $f_{i,j}$) in (3.45). Summing over all outgoing channels j gives

$$\begin{aligned}\sigma &= \sum_{j\ \text{open}} \sigma_{i\to j} \\ &= \frac{\pi}{k_i^2}\sum_{l_1,l_2} \mathrm{i}^{l_2-l_1}\sqrt{(2l_1+1)(2l_2+1)} \\ &\quad\times\left[\left(\sum_{j,l',m'} S^*_{i,l_1,0;\,j,l',m'}S_{i,l_2,0;\,j,l',m'}\right) - S^*_{i,l_1,0;i,l_2,0} - S_{i,l_2,0;i,l_1,0} + \delta_{l_1,l_2}\right] \\ &= \frac{\pi}{k_i^2}\sum_{l_1,l_2} \mathrm{i}^{l_2-l_1}\sqrt{(2l_1+1)(2l_2+1)} \\ &\quad\times\left[\delta_{l_1,l_2} + \left(SS^\dagger\right)_{i,l_2,0;i,l_1,0} - S^*_{i,l_1,0;i,l_2,0} - S_{i,l_2,0;i,l_1,0}\right].\end{aligned} \tag{3.46}$$

On the other hand, the incident-incident scattering amplitude in forward direction $f_{i,i}(\theta=0)$ is, according to (3.44),

$$f_{i,i}(\theta=0) = \sum_{l,l'} \mathrm{i}^{l-l'-1}\,\frac{\sqrt{(2l+1)(2l'+1)}}{2k_i}\,[S_{i,l,0;i,l',0} - \delta_{l,l'}]; \tag{3.47}$$

here we have made use of the relation $Y_{l',m'}(\theta=0) = \delta_{m',0}\sqrt{(2l'+1)/(4\pi)}$, compare Eqs. (2.26) and (2.29) in Sect. 2.3.1. The right-hand side of (3.17) thus has the partial-waves expansion,

$$\begin{aligned}\frac{4\pi}{k_i}\Im\left[f_{i,i}(\theta=0)\right] &= \frac{2\pi}{\mathrm{i}k_i}\left[f_{i,i}(\theta=0) - f^*_{i,i}(\theta=0)\right] \\ &= \frac{\pi}{k_i^2}\sum_{l',l} \mathrm{i}^{l-l'}\sqrt{(2l'+1)(2l+1)}\left[2\delta_{l,l'} - S^*_{i,l',0;i,l,0} - S_{i,l,0;i,l',0}\right].\end{aligned} \tag{3.48}$$

Comparison with (3.46) yields

$$\frac{4\pi}{k_i}\Im\big[f_{i,i}(\theta=0)\big]=\sigma+\frac{\pi}{k_i^2}\sum_{l',l}\mathrm{i}^{l-l'}\sqrt{(2l'+1)(2l+1)}\big[\delta_{l,l'}-\big(SS^\dagger\big)_{i,l,0;i,l',0}\big]. \tag{3.49}$$

If all outgoing flux is accounted for by the channels included in the ansatz (3.1) with (3.29), then the S-matrix is unitary, expressing particle conservation. Unitarity of the S-matrix, $SS^\dagger=\mathbf{1}$, implies $(SS^\dagger)_{i,l,0;i,l',0}=\delta_{l,l'}$, so we recover the optical theorem (3.17).

3.4 Absorption

A complete description of the projectile-target system, including an exact account of the constituents of projectile and target, their mutual interactions and all possibilities of excitation, generally goes beyond the ansatz formulated via Eqs. (3.1) and (3.29). The restriction to a finite, preferably small number of channels in the expansion (3.1) necessarily implies neglecting contributions from a large number of channels, which may be justified by the physical circumstances. When the expansion (3.1) omits open channels, then the outgoing flux in these channels is not registered in the scattering cross section σ, as defined by (3.12). To accommodate such scattering events, and other possible reaction channels not explicitly included in (3.1), we define the *total* cross section σ_{tot} as

$$\sigma_{\mathrm{tot}}=\sigma_{i\to i}+\sum_{j\neq i}\sigma_{i\to j}+\sigma_{\mathrm{abs}}=\sigma+\sigma_{\mathrm{abs}}, \tag{3.50}$$

thus introducing an *absorption cross section* σ_{abs}, which describes the flux loss (per unit time) into unconsidered open channels, normalized to the incoming current density.

As discussed in connection with the optical theorem (3.17), the destructive interference of the incoming plane wave and the outgoing spherical wave in the incident channel is the only source capable of compensating outgoing flux, so particle conservation requires the optical theorem to be formulated as follows,

$$\sigma_{\mathrm{tot}}=\sigma+\sigma_{\mathrm{abs}}=\frac{4\pi}{k_i}\Im\big[f_{i,i}(\theta=0)\big]\quad\Rightarrow\quad\sigma_{\mathrm{abs}}=\frac{4\pi}{k_i}\Im\big[f_{i,i}(\theta=0)\big]-\sigma. \tag{3.51}$$

An expression for σ_{abs} in terms of the S-matrix follows from (3.49),

$$\sigma_{\mathrm{abs}}=\frac{\pi}{k_i^2}\sum_{l',l}\mathrm{i}^{l-l'}\sqrt{(2l'+1)(2l+1)}\big[\delta_{l,l'}-\big(SS^\dagger\big)_{i,l,0;i,l',0}\big], \tag{3.52}$$

and σ_{abs} is nonvanishing only if the S-matrix is not unitary. A non-unitary S-matrix implies that particle number is not conserved within the space defined by the

coupled-channels expansion (3.1). If this ansatz consists of a single channel i with a radially symmetric potential, then

$$S_{i,l,0;i,l',0} = \delta_{l,l'} e^{2i\delta_l} \quad \Rightarrow \quad \sigma_{\text{abs}} = \frac{\pi}{k_i^2} \sum_l (2l+1)\left(1 - \left|e^{2i\delta_l}\right|^2\right), \tag{3.53}$$

compare (2.69) in Sect. 2.3.6. A finite (positive) absorption cross section is obtained if $|e^{2i\delta_l}| < 1$ at least for some partial waves l, and this means that the respective scattering phase shifts δ_l are no longer real, but have a positive imaginary part.

One possibility of generating a non-unitary S-matrix is via a non-hermitian *effective Hamiltonian* acting in the space of channels included in the ansatz (3.1). A single-channel version of a non-hermitian effective Hamiltonian is provided by a complex effective potential $V(\mathbf{r})$. The single-channel Schrödinger equation and its complex conjugate are then,

$$\left(-\frac{\hbar^2}{2\mu}\Delta + V(\mathbf{r})\right)\psi(\mathbf{r}) = E\,\psi(\mathbf{r}), \tag{3.54}$$

$$\left(-\frac{\hbar^2}{2\mu}\Delta + V(\mathbf{r})^*\right)\psi^*(\mathbf{r}) = E\psi^*(\mathbf{r}). \tag{3.55}$$

Multiplying (3.54) by ψ^* and (3.55) by ψ and taking the difference gives

$$-\frac{\hbar^2}{2\mu}\left[\psi^*\Delta\psi - \psi\Delta\psi^*\right] = -i\hbar\nabla\cdot\mathbf{j} = \left(V^* - V\right)|\psi|^2$$

$$\Rightarrow \quad \nabla\cdot\mathbf{j} = \frac{2}{\hbar}\Im\left[V(\mathbf{r})\right]\left|\psi(\mathbf{r})\right|^2. \tag{3.56}$$

A negative imaginary part of the potential $V(\mathbf{r})$ generates a negative divergence of the current density, i.e. a *sink* for particle density.

An alternative method of obtaining a non-unitary S-matrix or complex scattering phase shifts is based on the physical picture that all incoming flux is absorbed at some, typically small, separation of projectile and target. Such a scenario can be realized by requiring the radial wave functions to obey incoming boundary conditions at the appropriate distance. A clean distinction between incoming and outgoing solutions of the Schrödinger equation is given if the semiclassical WKB approximation is justified in the region concerned. This is the case for deep attractive potentials which are ubiquitous in atom-atom scattering, see Sect. 4.1 in Chap. 4.

3.5 Feshbach Resonances

Resonances in general can be understood as "almost bound states", which would be truly bound under a slight modification of the actual circumstances. The *potential* or *shape* resonances discussed in Sect. 2.3.10 are typically trapped by a penetrable potential barrier, and they would be truly-bound states if the penetrability of the barrier were not finite but zero. In a multichannel system, the closed channels can support states which are truly bound in the absence of channel coupling, but which

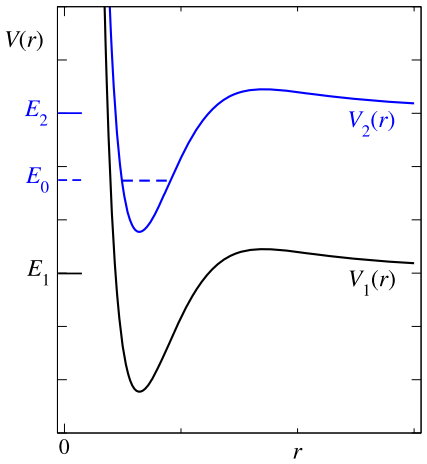

Fig. 3.1 Schematic illustration of a two-channel system. The potential $V_i(r)$ represents the potential in channel i plus the respective internal excitation energy, $V_i(r) = V_{i,i}(r) + E_i$. The uncoupled upper potential V_2 supports one bound state at energy E_0. Due to channel coupling, it appears as a Feshbach resonance in the lower channel $i = 1$, which is open for $E > E_1$

in reality decay due to coupling to open channels. The properties of the continuum states in the open channels show resonant features due to these almost bound states. Resonances in open channels due to the coupling to closed-channel bound states are called *Feshbach resonances* [7, 8]. The study of Feshbach resonances has a long history in nuclear physics [1, 3, 4, 12], as well as in atomic and molecular physics [15, 18, 20].

3.5.1 Single Isolated Feshbach Resonance

The simplest example of a Feshbach resonance is a single bound state in a closed radial channel interacting with the continuum of an open radial channel, as illustrated schematically in Fig. 3.1. The potential $V_i(r)$ represents the potential in channel i plus the respective internal excitation energy which defines the channel threshold, $V_i(r) = V_{i,i}(r) + E_i \overset{r\to\infty}{\to} E_i$. The uncoupled upper potential $V_2(r)$ supports one bound state which appears as a Feshbach resonance in the lower, open channel 1.

Such a system is described by two coupled radial equations,

$$\begin{aligned}\left[-\frac{\hbar^2}{2\mu}\frac{\mathrm{d}^2}{\mathrm{d}r^2} + V_1(r)\right]u_1(r) + V_{1,2}u_2(r) &= Eu_1(r),\\ \left[-\frac{\hbar^2}{2\mu}\frac{\mathrm{d}^2}{\mathrm{d}r^2} + V_2(r)\right]u_2(r) + V_{2,1}u_1(r) &= Eu_2(r).\end{aligned} \tag{3.57}$$

Possible centrifugal potentials for nonvanishing angular momentum in one or both channels are assumed to be incorporated in the potentials V_i. In the absence of channel coupling, channel 2 supports a bound state with radial eigenfunction $u_0(r)$ at energy E_0 between E_1 and E_2,

$$\left[-\frac{\hbar^2}{2\mu}\frac{\mathrm{d}^2}{\mathrm{d}r^2} + V_2(r)\right]u_0(r) = E_0u_0(r), \quad \langle u_0|u_0\rangle = 1, \ E_1 < E_0 < E_2. \tag{3.58}$$

We assume that the closed-channel wave function $u_2(r)$ in (3.57) is restricted to being a multiple of $u_0(r)$. The space of admissible state vectors then consists of the two-component wave functions,

$$U \equiv \begin{pmatrix} u_1(r) \\ A u_0(r) \end{pmatrix}. \tag{3.59}$$

The open-channel component $u_1(r)$ can be any radial wave function obeying the boundary condition $u_1(0) = 0$, while the closed-channel component is fixed, except for an arbitrary constant A.

The coupled-channel Schrödinger equation (3.57) can be solved exactly in the space spanned by the two-component wave functions (3.59). Exploiting (3.58) reduces the lower equation (3.57) to $V_{2,1}(r)u_1(r) = A(E - E_0)u_0(r)$. This cannot, of course, hold in the space of arbitrary closed-channel wave functions, but in the space defined by (3.59) it is only the projection onto u_0 that counts:

$$A(E - E_0) = \langle u_0 | V_{2,1} | u_1 \rangle. \tag{3.60}$$

The upper equation (3.57) can be rewritten as

$$\left[E + \frac{\hbar^2}{2\mu} \frac{\mathrm{d}^2}{\mathrm{d}r^2} - V_1(r) \right] u_1(r) = A V_{1,2} u_0(r), \tag{3.61}$$

and solved with the help of the appropriate radial Green's function $\mathscr{G}(r, r')$, which is defined via

$$\left[E + \frac{\hbar^2}{2\mu} \frac{\mathrm{d}^2}{\mathrm{d}r^2} - V_1(r) \right] \mathscr{G}(r, r') = \delta(r - r') \tag{3.62}$$

and explicitly given by

$$\mathscr{G}(r, r') = -\pi \bar{\mathrm{u}}_1^{(\mathrm{reg})}(r_<) \bar{\mathrm{u}}_1^{(\mathrm{irr})}(r_>). \tag{3.63}$$

As in Eq. (2.63) in Sect. 2.3.5, $r_<$ stands for the smaller and $r_>$ for the larger of the two radial distances r, r'. As a generalization of (2.63), the radial wave functions $\bar{\mathrm{u}}_1^{(\mathrm{reg})}$ and $\bar{\mathrm{u}}_1^{(\mathrm{irr})}$ are solutions of the radial Schrödinger equation *including* the potential V_1 in the open channel, and furthermore they are assumed to be normalized in energy, see Sect. 2.3.4. Their asymptotic behaviour is,

$$\begin{aligned} \bar{\mathrm{u}}_1^{(\mathrm{reg})}(r) &\overset{r\to\infty}{\sim} \sqrt{\frac{2\mu}{\pi\hbar^2 k}} \sin(kr + \delta_{\mathrm{bg}}), \\ \bar{\mathrm{u}}_1^{(\mathrm{irr})}(r) &\overset{r\to\infty}{\sim} \sqrt{\frac{2\mu}{\pi\hbar^2 k}} \cos(kr + \delta_{\mathrm{bg}}), \end{aligned} \tag{3.64}$$

where $k \equiv k_1 = \sqrt{2\mu(E - E_1)}/\hbar$ is the asymptotic wave number in the open channel 1. Here δ_{bg} is the *background phase shift* describing the influence of the potential V_1 on the open-channel wave function in the absence of channel coupling. For nonvanishing angular momentum quantum number l, the arguments of sine and cosine in (3.64) should include the further term $-l\pi/2$.

The solution of (3.58) expressed in terms of the Green's function (3.63) is

$$u_1(r) = \bar{u}_1^{(\mathrm{reg})}(r) + A\int_0^\infty \mathcal{G}(r,r')V_{1,2}(r')u_0(\prime)\,\mathrm{d}r' \overset{r\to\infty}{\sim} \bar{u}_1^{(\mathrm{reg})}(r) - \pi A\langle \bar{u}_1^{(\mathrm{reg})}|V_{1,2}|u_0\rangle \bar{u}_1^{(\mathrm{irr})}(r). \tag{3.65}$$

We write the coefficient in front of $\bar{u}_1^{(\mathrm{irr})}$ as the tangent of an angle,

$$-\pi A\langle \bar{u}_1^{(\mathrm{reg})}|V_{1,2}|u_0\rangle = \tan\delta_{\mathrm{res}}; \tag{3.66}$$

with (3.64), the lower line of (3.65) thus becomes

$$u_1(r) \overset{r\to\infty}{\sim} \sqrt{\frac{2\mu}{\pi\hbar^2 k}}\big[\sin(kr+\delta_{\mathrm{bg}}) + \tan\delta_{\mathrm{res}}\cos(kr+\delta_{\mathrm{bg}})\big] = \frac{1}{\cos(\delta_{\mathrm{res}})}\sqrt{\frac{2\mu}{\pi\hbar^2 k}}\sin(kr+\delta_{\mathrm{bg}}+\delta_{\mathrm{res}}). \tag{3.67}$$

Due to coupling to the bound state in the closed channel 2, the scattering phase shift of the open-channel wave function u_1 acquires an additional, *resonant* contribution δ_{res}, which depends on the amplitude factor A in front of the closed-channel bound state in (3.59). An explicit expression for A is obtained by inserting the upper line of (3.65) for u_1 in (3.60),

$$A(E-E_0) = \langle u_0|V_{2,1}|\bar{u}_1^{(\mathrm{reg})}\rangle + A\langle u_0|V_{2,1}\hat{G}V_{1,2}|u_0\rangle,$$
$$\Longrightarrow \quad A = \frac{\langle u_0|V_{2,1}|\bar{u}_1^{(\mathrm{reg})}\rangle}{E-E_0-\langle u_0|V_{2,1}\hat{G}V_{1,2}|u_0\rangle}. \tag{3.68}$$

The open-channel propagator $\hat{G}$ is the integral operator defined by the kernel $\mathcal{G}(r,r')$, which is given explicitly in Eq. (3.63). Assuming the total Hamiltonian underlying the coupled-channel equations (3.57) to be hermitian implies that the matrix element $\langle u_0|V_{2,1}|\bar{u}_1^{(\mathrm{reg})}\rangle$ is the complex conjugate of $\langle \bar{u}_1^{(\mathrm{reg})}|V_{1,2}|u_0\rangle$, so inserting (3.68) in the expression (3.66) for $\tan\delta_{\mathrm{res}}$ gives

$$\tan\delta_{\mathrm{res}} = -\frac{\pi|\langle u_0|V_{2,1}|\bar{u}_1^{(\mathrm{reg})}\rangle|^2}{E-E_0-\langle u_0|V_{2,1}\hat{G}V_{1,2}|u_0\rangle}. \tag{3.69}$$

The numerator in (3.69) depends on energy via the energy dependence of the regular open-channel wave function $\bar{u}_1^{(\mathrm{reg})}$, and the matrix element in the denominator depends on energy via the energy dependence of the open-channel propagator $\hat{G}$. Assuming that these energy dependences are smooth and weak, we can introduce the (almost) energy-independent parameters

$$E_{\mathrm{R}} = E_0 + \langle u_0|V_{2,1}\hat{G}V_{1,2}|u_0\rangle \tag{3.70}$$

for the position of the resonance, and

$$\Gamma = 2\pi\big|\langle u_0|V_{2,1}|\bar{u}_1^{(\mathrm{reg})}\rangle\big|^2 \tag{3.71}$$

for its width. Equation (3.69) thus simplifies to

$$\tan\delta_{\mathrm{res}} = -\frac{\Gamma/2}{E-E_{\mathrm{R}}}, \tag{3.72}$$

and the dominant energy dependence comes from the pole at E_R. The assumption that the parameters E_R and Γ are essentially energy independent is most readily fulfilled when Γ is small and E_R is sufficiently far from other structures, in particular channel thresholds. The formula (3.72) agrees with the arcus-tangent expression given in Sect. 2.3.10 for the behaviour of scattering phase shifts near potential resonances, compare Eqs. (2.122), (2.128), and its characteristic shape is illustrated in Fig. 2.9.

We wish to choose the normalization of the two-component wave function (3.59) such that the open-channel wave function remains normalized in energy even in the presence of the channel coupling. From the asymptotic form (3.67) of $u_1(r)$, we see that this is achieved by multiplying the two-component wave function by $\cos\delta_{res}$. The thus renormalized two-component wave function has the form

$$\cos\delta_{res}\begin{pmatrix}\bar{u}_1^{(reg)}+\tan\delta_{res}\Delta u_1\\ Au_0(r)\end{pmatrix}=\begin{pmatrix}\cos\delta_{res}\bar{u}_1^{(reg)}+\sin\delta_{res}\Delta u_1\\ \cos\delta_{res}Au_0(r)\end{pmatrix}, \tag{3.73}$$

where Δu_1 is an open-channel contribution which becomes $\bar{u}_1^{(irr)}$ beyond the range of the potentials. The lower component in (3.73) can be rewritten as

$$\cos\delta_{res}Au_0(r)=\frac{\sin\delta_{res}}{\tan\delta_{res}}Au_0(r)=-\frac{\sin\delta_{res}}{\pi\langle\bar{u}_1^{(reg)}|V_{1,2}|u_0\rangle}u_0(r), \tag{3.74}$$

where the expression on the far right of (3.74) is obtained by inserting the left-hand side of (3.66) for $\tan\delta_{res}$. Away from resonance, $\sin\delta_{res}$ is small and $\cos\delta_{res}$ is close to unity, so the open-channel wave function is essentially the regular solution in the uncoupled channel 1, while there is little contribution in the closed channel. At resonance, $\sin\delta_{res}=1$ while $\cos\delta_{res}$ vanishes, so the closed channel features a strong contribution proportional to the reciprocal of the coupling matrix element, while the open-channel wave function is asymptotically proportional to the irregular solution in the uncoupled channel 1, which is shifted by a phase of $\frac{\pi}{2}$ relative to the regular solution.

The width of a Feshbach resonance can be related to a *lifetime* in the framework of time-dependent perturbation theory using Fermi's *Golden Rule*,

$$P_{in\to fin}=\frac{2\pi}{\hbar}\left|\langle\Psi_{in}|\hat{W}|\Psi_{fin}\rangle\right|^2\rho_{fin}(E). \tag{3.75}$$

Here Ψ_{in} and Ψ_{fin} are two eigenstates of an unperturbed Hamiltonian $\hat{H}_0$, but the full Hamiltonian $\hat{H}_0+\hat{W}$ also contains the perturbation $\hat{W}$, so an eigenstate of $\hat{H}_0$ is not stationary, but decays to a superposition involving other eigenstates of $\hat{H}_0$ in the course of time. The quantity $P_{in\to fin}$ describes the transition probability per unit time from the initial eigenstate Ψ_{in} of $\hat{H}_0$ to a final eigenstate Ψ_{fin} of $\hat{H}_0$. The version (3.75) of the Golden Rule applies for final states with a continuous energy spectrum, and $\rho_{fin}(E)$ is the energy-level density of these final states at the energy E, which is conserved during the transition.

The Hamiltonian governing the coupled-channel equations (3.57) can be written as a 2×2 matrix,

$$\hat{H} \equiv \begin{pmatrix} \hat{H}_1 & V_{1,2} \\ V_{2,1} & \hat{H}_2 \end{pmatrix}, \quad \hat{H}_i = -\frac{\hbar^2}{2\mu}\frac{\mathrm{d}^2}{\mathrm{d}r^2} + V_i, \tag{3.76}$$

and decomposed into an unperturbed term $\hat{H}_0$ and a perturbation $\hat{W}$ as follows:

$$\hat{H}_0 = \begin{pmatrix} \hat{H}_1 & 0 \\ 0 & \hat{H}_2 \end{pmatrix}, \qquad \hat{W} = \begin{pmatrix} 0 & V_{1,2} \\ V_{2,1} & 0 \end{pmatrix}. \tag{3.77}$$

The initial eigenstate of $\hat{H}_0$ consists of the uncoupled bound state in the closed channel 2 with no contribution of the open channel 1, and the final state into which it can decay is taken as the regular solution of the open-channel wave function at the appropriate energy:

$$\Psi_{\text{in}} = \begin{pmatrix} 0 \\ u_0 \end{pmatrix}, \qquad \Psi_{\text{fin}} = \begin{pmatrix} \bar{\mathrm{u}}_1^{(\text{reg})} \\ 0 \end{pmatrix}. \tag{3.78}$$

The square of the matrix element in the Golden Rule (3.75) is then

$$\left|\langle \Psi_{\text{in}} | \hat{W} | \Psi_{\text{fin}} \rangle\right|^2 = \left|\langle u_0 | V_{2,1} | \bar{\mathrm{u}}_1^{(\text{reg})} \rangle\right|^2. \tag{3.79}$$

It remains to account for the final-state density ρ_{fin} in (3.75).

For bound states u_n which are normalized to unity and have a discrete but rather dense spectrum of energies E_n, the level density is readily defined as the inverse of $\mathrm{d}E_n/\mathrm{d}n$; e.g. for a particle of mass μ in a one-dimensional box $0 < r < L$,

$$u_n(r) = \sqrt{\frac{2}{L}}\sin(k_n r), \quad k_n = \frac{n\pi}{L}, \qquad E_n = \frac{n^2\pi^2\hbar^2}{2\mu L^2} \quad \Rightarrow \quad \rho_L = \frac{\mu L}{\pi\hbar^2 k_n}. \tag{3.80}$$

As $L \to \infty$, the amplitude of the wave function u_n vanishes while $\rho_L \to \infty$. Any product of a squared matrix element involving u_n with the related level density ρ_L is independent of L,

$$\left|\langle \cdots | \cdots | u_n \rangle\right|^2 \rho_L = \left|\langle \cdots | \cdots | \sin(k_n r) \rangle\right|^2 \times \frac{2}{L}\frac{\mu L}{\pi\hbar^2 k_n} = \frac{2\mu}{\pi\hbar^2 k_n}. \tag{3.81}$$

The L-independence of the expression on the far right of (3.81) allows a smooth transition to infinite L, where the spectrum of energies E, and wave numbers k, is continuous. The correct definition of the energy-level density clearly depends on the choice of normalization of the wave functions $\propto \sin(kr)$, and for wave functions normalized in energy, $\bar{\mathrm{u}}(r) = \sqrt{2\mu/(\pi\hbar^2 k)}\,\sin(kr)$, the appropriate density is $\rho = 1$. This argumentation is also valid beyond the simple box-example. We conclude that for radial wave functions in the continuum which are normalized in energy, i.e. they are asymptotically proportional to $\sqrt{2\mu/(\pi\hbar^2 k)}\sin(kr + \cdots)$ as in (3.64), the appropriate energy-level density is unity.

With $\rho_{\text{fin}}(E) = 1$ and (3.79), the transition rate (3.75) becomes

$$P_{\text{in}\to\text{fin}} = \frac{\Gamma}{\hbar}, \tag{3.82}$$

where Γ is the resonance width as defined by (3.71). Consider the exact time dependent state $\Psi(t)$, which starts as the initial state Ψ_{in} at $t = 0$. The survival probability P_{in} of the initial state is given by $P_{\text{in}} = |\langle\Psi(t)|\Psi_{\text{in}}\rangle|^2$. If the only decay channel is the final state Ψ_{fin}, then

$$\frac{\mathrm{d}P_{\text{in}}}{\mathrm{d}t} = -P_{\text{in}\to\text{fin}}P_{\text{in}} = -\frac{\Gamma}{\hbar}P_{\text{in}} \quad \Longrightarrow \quad P_{\text{in}} = \mathrm{e}^{-t/\tau_{\text{R}}} \quad \text{with } \tau_{\text{R}} = \frac{\hbar}{\Gamma}. \tag{3.83}$$

This relation of the resonance width Γ to its lifetime τ_{R} is the same as Eq. (2.129) in Sect. 2.3.10, where the Γ appears as minus twice the imaginary part of a pole of the S-matrix in the complex energy plane.

As already illustrated in Sect. 2.3.11, a resonant feature in the scattering phase shift leads to observable effects in the scattering cross sections. For a single isolated Feshbach resonance in a partial wave l, the energy dependence of the scattering phase shift δ_l is

$$\delta_l = \delta_{\text{bg}} + \delta_{\text{res}} = \delta_{\text{bg}} - \arctan\left(\frac{\Gamma/2}{E - E_{\text{R}}}\right) \tag{3.84}$$

according to (3.72). The energy dependence of the background phase shift δ_{bg} and of the resonance width Γ are generally weak and smooth and shall be neglected for the time being. The contribution of the partial wave l to the integrated elastic scattering cross section (2.52) is

$$\sigma_{[l]} = \frac{4\pi}{k^2}(2l+1)\sin^2\delta_l = \frac{4\pi}{k^2}(2l+1)\sin^2(\delta_{\text{bg}} + \delta_{\text{res}}). \tag{3.85}$$

Rather than neglecting the background phase shift δ_{bg}, as in the derivation of the Breit–Wigner formula (2.130), we now appreciate that δ_{bg}, which is a property of the potential in the open channel, can be significantly different from zero (mod π). Using the identities

$$\sin^2\delta_l = \frac{1}{1+\cot^2\delta_l}, \qquad \cot(\delta_{\text{bg}} + \delta_{\text{res}}) = \frac{\cot\delta_{\text{bg}}\cot\delta_{\text{res}} - 1}{\cot\delta_{\text{bg}} + \cot\delta_{\text{res}}}, \tag{3.86}$$

we can express $\sin^2\delta_l$ as function of the dimensionless *reduced energy* ε, which is simply the energy relative to the resonance energy, normalized by $\Gamma/2$,

$$\varepsilon = \frac{E - E_{\text{R}}}{\Gamma/2} = -\cot\delta_{\text{res}}, \tag{3.87}$$

$$\sin^2\delta_l = \sin^2\delta_{\text{bg}}\frac{(\varepsilon+q)^2}{1+\varepsilon^2} \quad \text{with } q = -\cot\delta_{\text{bg}}. \tag{3.88}$$

The contribution $\sigma_{[l]}$ of the partial wave l to the scattering cross section σ is thus,

$$\sigma_{[l]} = \frac{4\pi}{k^2}(2l+1)\sin^2\delta_{\text{bg}} \times F(q;\varepsilon). \tag{3.89}$$

This is the result expected in absence of the Feshbach resonance, multiplied by the *Beutler–Fano function*,

$$F(q;\varepsilon) = \frac{(\varepsilon+q)^2}{1+\varepsilon^2}. \tag{3.90}$$

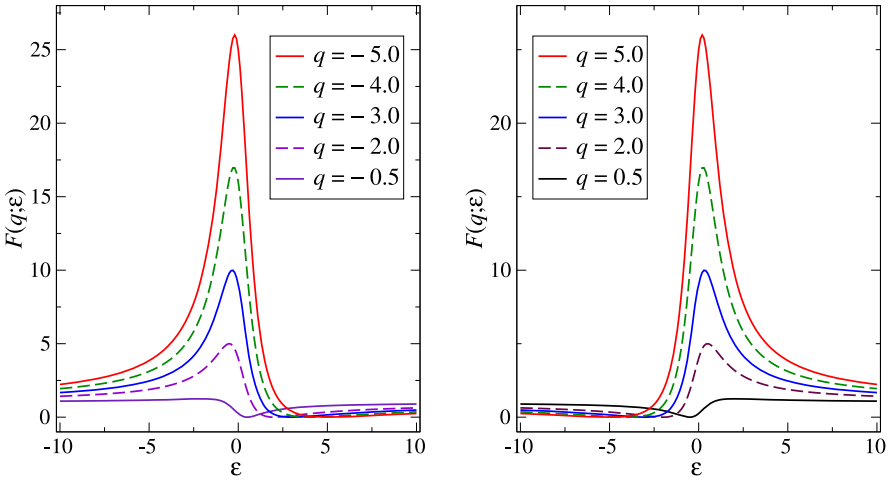

Fig. 3.2 Beutler–Fano function (3.90) for various negative (*left*) and positive (*right*) values of the shape parameter q

The Beutler–Fano function is quite universal and typical for interference phenomena. It is a function of ε and its shape depends on the *shape parameter* q. The Beutler–Fano function has a zero at $\varepsilon = -q$ and, for $q \neq 0$, a maximum with value $1 + q^2$ at $\varepsilon = 1/q$. The function is plotted for various positive and negative shape parameters in Fig. 3.2.

The zero of the Beutler–Fano function, corresponding to a vanishing contribution of the partial wave l to the scattering cross section, can be interpreted as the result of destructive interference between the direct scattering process in the open channel and an indirect process involving the bound state in the closed channel. At the maximum of the Beutler–Fano function, $\sigma_{[l]}$ reaches its maximum value, namely its unitarity limit,

$$F(q;\varepsilon)_{\max} = 1 + q^2 = 1 + \cot^2\delta_{\rm bg} = \frac{1}{\sin^2\delta_{\rm bg}}$$

$$\Rightarrow \quad \sigma_{[l]} = (\sigma_{[l]})_{\max} = \frac{4\pi}{k^2}(2l+1), \tag{3.91}$$

compare Eq. (2.53) in Sect. 2.3.3.

If a resonance is very narrow, $\Gamma \to 0$, then its impact on the scattering cross section becomes negligible, because it is limited to a very small energy range and the magnitude of its influence is bounded by the unitarity limit. Such a restriction does not, however, apply to other observables involving the continuum states of the projectile-target system in the vicinity of a Feshbach resonance.

Consider an observable $\hat{O}$ which might, e.g., be the dipole operator governing the transition amplitude for photoabsorption from some initial state Ψ_a to a final state

Ψ_b in the space of two-channel wave functions (3.59). The strength of the observable signal is typically proportional to the square of a transition matrix element

$$O_{a\to b} = \langle \Psi_a | \hat{O} | \Psi_b \rangle. \tag{3.92}$$

The two-component wave function Ψ_b is of the form (3.73), with the closed-channel component as given in (3.74). Separating the term proportional to $\cos\delta_{\rm res}$ from those proportional to $\sin\delta_{\rm res}$ gives

$$\Psi_b = \cos\delta_{\rm res} \begin{pmatrix} \bar{\mathrm{u}}_1^{(\rm reg)} \\ 0 \end{pmatrix} - \frac{\sin\delta_{\rm res}}{\pi \langle \bar{\mathrm{u}}_1^{(\rm reg)} | V_{1,2} | u_0 \rangle} \begin{pmatrix} \Delta u_1' \\ u_0 \end{pmatrix}; \tag{3.93}$$

here $\Delta u_1'$ is an open-channel contribution which is related to the corresponding contribution Δu_1 in (3.73) by $\Delta u_1' = -\pi \langle \bar{\mathrm{u}}_1^{(\rm reg)} | V_{1,2} | u_0 \rangle \Delta u_1$. The matrix element (3.92) is thus decomposed into two terms proportional to $\cos\delta_{\rm res}$ and $\sin\delta_{\rm res}$, respectively,

$$O_{a\to b} = \cos\delta_{\rm res} \Big\langle \Psi_a \Big| \hat{O} \Big| \begin{pmatrix} \bar{\mathrm{u}}_1^{(\rm reg)} \\ 0 \end{pmatrix} \Big\rangle - \frac{\sin\delta_{\rm res}}{\pi \langle \bar{\mathrm{u}}_1^{(\rm reg)} | V_{1,2} | u_0 \rangle} \Big\langle \Psi_a \Big| \hat{O} \Big| \begin{pmatrix} \Delta u_1' \\ u_0 \end{pmatrix} \Big\rangle. \tag{3.94}$$

The two matrix elements on the right-hand side of (3.94) represent partial transition matrix elements for the transition from the initial state Ψ_a to the components of the final state Ψ_b in the open channel 1 and in the closed channel 2. They can be expected to depend at most weakly on energy and shall be abbreviated as d_1 and d_2 respectively. The expression for the whole transition matrix element (3.94) thus simplifies to

$$O_{a\to b} = d_1 \cos\delta_{\rm res} - \frac{d_2 \sin\delta_{\rm res}}{\pi \langle \bar{\mathrm{u}}_1^{(\rm reg)} | V_{1,2} | u_0 \rangle}, \tag{3.95}$$

and the observable signal is proportional to

$$|O_{a\to b}|^2 = |d_1|^2 \frac{|\varepsilon + q|^2}{1+\varepsilon^2} \quad \text{with} \quad q = \frac{d_2/d_1}{\pi \langle \bar{\mathrm{u}}_1^{(\rm reg)} | V_{1,2} | u_0 \rangle}. \tag{3.96}$$

If q in (3.96) is real, then this is just the Beutler–Fano shape function multiplied onto the result $|d_1|^2$, which is expected in absence of the Feshbach resonance. However, in contrast to the contributions to the scattering cross sections [see (3.89) and (3.91)], there is no bound on magnitude of $|O_{a\to b}|^2$. Very small resonance widths $\Gamma \to 0$ imply very small matrix elements $\langle \bar{\mathrm{u}}_1^{(\rm reg)} | V_{1,2} | u_0 \rangle$ corresponding to very large magnitudes of the shape parameter q. The maximum of the signal corresponding to the maximal value $1+q^2$ of the Beutler–Fano function actually tends to infinity as $\Gamma \to 0$. Even if q is not real, the factor $|\varepsilon+q|^2/(1+\varepsilon^2)$ acquires a large value of order $|q|^2$ for $\varepsilon = 1/|q|$ when $|q|$ is large. All other things remaining constant, $|q|^2 \times \Gamma$ approaches a finite value for $\Gamma \to 0$. For observables other than the scattering cross sections, a vanishing resonance width is compensated by a diverging height of the observable signal.

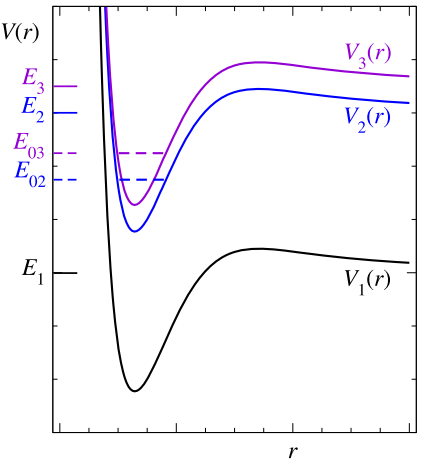

Fig. 3.3 Schematic illustration of a three-channel system. The potential $V_i(r)$ represents the potential in channel i plus the respective internal excitation energy, $V_i(r) = V_{i,i}(r) + E_i$. The uncoupled upper potentials V_2, V_3 each support a bound state at energy E_{02} and E_{03}, respectively. Due to channel coupling, these states appear as Feshbach resonances in the lower channel $i = 1$, which is open for $E > E_1$

3.5.2 *Interfering Resonances*

A straightforward and instructive extension of the case of a single isolated Feshbach resonance is the consideration of two bound states in different closed channels coupling to one open channel, as illustrated in Fig. 3.3. The coupled equations for the three radial channel wave functions are

$$\left[-\frac{\hbar^2}{2\mu}\frac{\mathrm{d}^2}{\mathrm{d}r^2} + V_i\right]u_i(r) \sum_{j\neq i} V_{i,j}u_j(r) = Eu_i(r), \tag{3.97}$$

and the energy is chosen in the interval $E_1 < E < \min\{E_2, E_3\}$ so that channel 1 is open while channels 2 and 3 are closed. The bound state wave functions u_{02} and u_{03} in the closed channels 2 and 3 are, in the absence of channel coupling, solutions of the associated radial equation at the energies E_{02} and E_{03}, respectively, and they are assumed to be normalized to unity,

$$\left[-\frac{\hbar^2}{2\mu}\frac{\mathrm{d}^2}{\mathrm{d}r^2} + V_2\right]u_{02}(r) = E_{02}u_{02}(r), \qquad \left[-\frac{\hbar^2}{2\mu}\frac{\mathrm{d}^2}{\mathrm{d}r^2} + V_3\right]u_{03}(r) = E_{03}u_{03}(r),$$
$$\langle u_{02}|u_{02}\rangle = 1, \qquad \langle u_{03}|u_{03}\rangle = 1. \tag{3.98}$$

Again we assume, that the closed-channel wave functions are restricted to multiples of the respective uncoupled bound-state wave functions, i.e. we now look for solutions of the three-channel problem in the space of three-component wave functions,

$$U \equiv \begin{pmatrix} u_1(r) \\ A_2u_{02}(r) \\ A_3u_{03}(r) \end{pmatrix}. \tag{3.99}$$

Inserting $A_2 u_{02}$ for u_2 and $A_3 u_{03}$ for u_3 in the radial equations (3.97) with $i = 2$ and $i = 3$ and projecting onto $\langle u_{02}|$ and $\langle u_{03}|$ gives, as generalization of (3.60),

$$\begin{aligned} A_2(E - E_{02}) &= \langle u_{02}|V_{2,1}|u_1\rangle + A_3\langle u_{02}|V_{2,3}|u_{03}\rangle, \\ A_3(E - E_{03}) &= \langle u_{03}|V_{3,1}|u_1\rangle + A_2\langle u_{03}|V_{3,2}|u_{02}\rangle. \end{aligned} \tag{3.100}$$

The equation for u_1, i.e. Eq. (3.97) with $i = 1$, can be written as

$$\left[E + \frac{\hbar^2}{2\mu}\frac{\mathrm{d}^2}{\mathrm{d}r^2} - V_1\right] u_1(r) = A_2 V_{1,2} u_{02}(r) + A_3 V_{1,3} u_{03}(r) \tag{3.101}$$

and solved with the help of the Green's function (3.63),

$$\begin{aligned} u_1(r) &= \bar{\mathrm{u}}_1^{(\mathrm{reg})}(r) + \int_0^\infty \mathscr{G}(r, r')\big[A_2 V_{1,2}(r') u_{02}(r') + A_3 V_{1,3}(r') u_{03}(\prime)\big]\mathrm{d}r' \\ &\overset{r\to\infty}{\sim} \bar{\mathrm{u}}_1^{(\mathrm{reg})}(r) - \pi\big[A_2\big\langle\bar{\mathrm{u}}_1^{(\mathrm{reg})}\big|V_{1,2}\big|u_{02}\big\rangle + A_3\big\langle\bar{\mathrm{u}}_1^{(\mathrm{reg})}\big|V_{1,3}\big|u_{03}\big\rangle\big]\bar{\mathrm{u}}_1^{(\mathrm{irr})}(r), \end{aligned} \tag{3.102}$$

so, in place of (3.66), the expression for the resonant contribution to the open-channel phase shift now reads

$$\tan\delta_{\mathrm{res}} = -\pi\big[A_2\big\langle\bar{\mathrm{u}}_1^{(\mathrm{reg})}\big|V_{1,2}\big|u_{02}\big\rangle + A_3\big\langle\bar{\mathrm{u}}_1^{(\mathrm{reg})}\big|V_{1,3}\big|u_{03}\big\rangle\big]. \tag{3.103}$$

Inserting the upper line of (3.102) for u_1 in (3.100) leads to two simultaneous equations for the coefficients A_2 and A_3,

$$\begin{aligned} &A_2\big[E - E_{02} - \langle u_{02}|V_{2,1}\hat{G}V_{1,2}|u_{02}\rangle\big] - A_3\langle u_{02}|V_{2,1}\hat{G}V_{1,3}|u_{03}\rangle \\ &\quad = \big\langle u_{02}\big|V_{2,1}\big|\bar{\mathrm{u}}_1^{(\mathrm{reg})}\big\rangle + A_3\langle u_{02}|V_{2,3}|u_{03}\rangle, \\ &A_3\big[E - E_{03} - \langle u_{03}|V_{3,1}\hat{G}V_{1,3}|u_{03}\rangle\big] - A_2\langle u_{03}|V_{3,1}\hat{G}V_{1,2}|u_{02}\rangle \\ &\quad = \big\langle u_{03}\big|V_{3,1}\big|\bar{\mathrm{u}}_1^{(\mathrm{reg})}\big\rangle + A_2\langle u_{03}|V_{3,2}|u_{02}\rangle. \end{aligned} \tag{3.104}$$

With the abbreviations,

$$\varepsilon_i = E_{0i} + \langle u_{0i}|V_{i,1}\hat{G}V_{1,i}|u_{0i}\rangle, \qquad W_{i,1} = \big\langle u_{0i}\big|V_{i,1}\big|\bar{\mathrm{u}}_1^{(\mathrm{reg})}\big\rangle = W_{1,i}^*, \quad i = 2, 3, \tag{3.105}$$

and

$$W_{2,3} = \langle u_{02}|V_{2,3}|u_{03}\rangle + \langle u_{02}|V_{2,1}\hat{G}V_{1,3}|u_{03}\rangle = W_{3,2}^*, \tag{3.106}$$

the solutions of (3.104) are

$$A_2 = \frac{(E - \varepsilon_3)W_{2,1} + W_{2,3}W_{3,1}}{(E - \varepsilon_2)(E - \varepsilon_3) - |W_{2,3}|^2}, \qquad A_3 = \frac{(E - \varepsilon_2)W_{3,1} + W_{3,2}W_{2,1}}{(E - \varepsilon_2)(E - \varepsilon_3) - |W_{2,3}|^2}, \tag{3.107}$$

so Eq. (3.103) for the resonant contribution to the scattering phase shift becomes

$$\tan\delta_{\mathrm{res}} = -\pi\frac{(E - \varepsilon_3)|W_{2,1}|^2 + W_{1,2}W_{2,3}W_{3,1} + (E - \varepsilon_2)|W_{3,1}|^2 + W_{1,3}W_{3,2}W_{2,1}}{(E - \varepsilon_2)(E - \varepsilon_3) - |W_{2,3}|^2}. \tag{3.108}$$

The matrix element $W_{2,3}$ defined in (3.106) describes the interaction of the closed-channel bound states, both by direct coupling through the term containing $V_{2,3}$, and by indirect coupling via the open channel 1 through the term containing $\hat{G}$. In the absence of this interaction, the resonance energies are $\varepsilon_{2/3}$, as defined in (3.105), and they are shifted from the uncoupled bound-state energies $E_{02/03}$ as in the single-resonance case (3.70). Note that the matrix element $W_{2,3}$ has the dimension of an energy, while the matrix elements $W_{1,2}$, $W_{1,3}$ have the dimension of the square root of an energy; this is due to the fact that the bound-state wave functions u_{0i} are normalized to unity while the continuum wave functions $\bar{u}_1^{(\mathrm{reg})}$ are normalized in energy.

Instead of a single pole as in Eqs. (3.69), (3.72), the right-hand side of (3.108) features two poles, namely the zeros of the denominator

$$D(E) = (E - \varepsilon_2)(E - \varepsilon_3) - |W_{2,3}|^2, \tag{3.109}$$

which lie at

$$E_\pm = \frac{\varepsilon_2 + \varepsilon_3}{2} \pm \sqrt{\left(\frac{\varepsilon_2 - \varepsilon_3}{2}\right)^2 + |W_{2,3}|^2}. \tag{3.110}$$

The interaction of the resonances via the matrix element $W_{2,3}$ leads to a level repulsion of the resonance energies, an effect well known from bound two-level systems.

The widths of the resonances are related to the residue of $\tan\delta_{\mathrm{res}}$ at the respective poles and are explicitly given in terms of the energy derivative of δ_{res} by Eq. (2.132) in Sect. 2.3.10,

$$\Gamma_\pm = 2\left[\left.\frac{\mathrm{d}\delta_{\mathrm{res}}}{\mathrm{d}E}\right|_{E=E_\pm}\right]^{-1}. \tag{3.111}$$

Introducing the abbreviation

$$N(E) = \pi\left[(E - \varepsilon_3)|W_{2,1}|^2 + W_{1,2}W_{2,3}W_{3,1} + (E - \varepsilon_2)|W_{3,1}|^2 + W_{1,3}W_{3,2}W_{2,1}\right] \tag{3.112}$$

for minus the numerator in (3.108) leads to a compact expression for the derivative at the poles, where $D(E) = 0$,

$$\left.\frac{\mathrm{d}\delta_{\mathrm{res}}}{\mathrm{d}E}\right|_{D=0} = \left(1 + \frac{N^2}{D^2}\right)^{-1}\left.\left(\frac{D'N - N'D}{D^2}\right)\right|_{D=0} = \left.\frac{D'}{N}\right|_{E_\pm}. \tag{3.113}$$

Inserting D'/N for the derivative of δ_{res} in (3.111) gives

$$\Gamma_\pm = \pi\left(|W_{2,1}|^2 + |W_{3,1}|^2\right) \pm \pi\,\frac{\frac{1}{2}(\varepsilon_2 - \varepsilon_3)(|W_{2,1}|^2 - |W_{3,1}|^2) + W_{1,2}W_{2,3}W_{3,1} + W_{1,3}W_{3,2}W_{2,1}}{\sqrt{\frac{1}{4}(\varepsilon_2 - \varepsilon_3)^2 + |W_{2,3}|^2}}. \tag{3.114}$$

If the coupling matrix element $W_{3,2}$ vanishes, the resonance energies are $\varepsilon_{2/3}$ and the associated widths are $\Gamma_2 = 2\pi|W_{2,1}|^2$ and $\Gamma_3 = 2\pi|W_{3,1}|^2$. The closed-closed channel coupling not only leads to a level repulsion of the resonance positions, as noted after Eq. (3.110) above, it also affects the resonance widths according to (3.114). The sum of the widths of the two interfering resonances is unaffected,

$$\Gamma_+ + \Gamma_- = 2\pi\left(|W_{2,1}|^2 + |W_{3,1}|^2\right) = \Gamma_2 + \Gamma_3, \tag{3.115}$$

but the distribution of the total width over the two resonances can be strongly affected by the coupling. The extreme situation is that one resonance carries the whole width while the other resonance has exactly vanishing width and corresponds to a *bound state in the continuum*. Such a vanishing width implies an infinite energy derivative of δ_{res} according to (3.111), and it occurs when a zero of the numerator (3.112) coincides with a zero of the denominator (3.109), see Eq. (3.113). The condition for this to happen is:

$$E - \varepsilon_2 = -W_{3,2}W_{2,1}/W_{3,1} \quad \text{and} \quad E - \varepsilon_3 = -W_{2,3}W_{3,1}/W_{2,1}, \tag{3.116}$$

which means that the energies ε_i and matrix elements $W_{i,j}$ fulfill the relations

$$\varepsilon_2 - \varepsilon_3 = W_{3,2}\frac{W_{2,1}}{W_{3,1}} - W_{2,3}\frac{W_{3,1}}{W_{2,1}}. \tag{3.117}$$

If the Hamiltonian governing the coupled-channel equations (3.97) in the space defined by the three-component wave functions (3.99) is not only hermitian but also time-reversal invariant, then its matrix representation can be based on real symmetric matrices. In this case, the right-hand side of (3.117) is real, and the condition can be fulfilled if one (or more) of the parameters involved can be tuned, e.g. by varying the strength of an external field. When a bound state in the continuum is realized at a certain energy, the open-channel phase shift is indeterminate at this energy, because the open-channel wave function obeys bound-state boundary conditions.

Results for a model example are illustrated in Fig. 3.4. In the absence of closed-closed coupling ($W_{2,3} = 0$), there are two Feshbach resonances of different but comparable width, located at $E = 8$ and $E = 10$. A finite coupling matrix element $W_{2,3}$ leads to a repulsion of the resonance positions and a concentration of almost all the width in the lower resonance. In the expression $\sin^2(\delta_{\mathrm{bg}} + \delta_{\mathrm{res}})$, which represents the associated contribution to the scattering cross section, the very narrow resonance at $E \approx 10.8$ is seen as a sharp cut into the Beutler–Fano profile of the broad lower resonance. Note that the strongly asymmetric distribution of the resonance widths as a consequence of the coupling does not necessarily require that the resonances be *overlapping*, i.e. that their separation be smaller than their widths. The two resonant features in the left-hand part of Fig. 3.4 are well separated, regardless of whether or not channel-coupling via $W_{2,3}$ is considered.

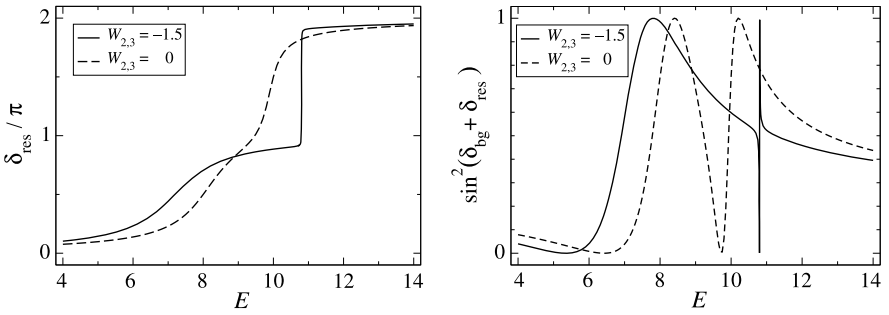

Fig. 3.4 Schematic illustration of the effect of interference of two Feshbach resonances on the scattering phase shift (*left-hand part*) and on the contribution to the scattering cross section (*right-hand part*). The parameter values entering Eq. (3.108) are: $\varepsilon_2 = 8.0$, $\varepsilon_3 = 10.0$, $W_{1,2} = W_{2,1} = 0.5$ and $W_{1,3} = W_{3,1} = 0.3$. The *solid lines* were obtained with a coupling matrix element $W_{2,3} = W_{3,2} = -1.5$ while the *dashed lines* show the results in the absence of coupling, $W_{2,3} = W_{3,2} = 0$. In the *right-hand part*, a background phase shift of $\delta_{bg} = -\pi/6$ is assumed

An approximation to the formula (3.114) can be obtained with Fermi's Golden Rule (3.75), if the two-channel states (3.78) are replaced by appropriate three-channel states and the perturbation $\hat{W}$ is defined accordingly,

$$\Psi_{in}^{(\pm)} = \begin{pmatrix} 0 \\ a_2^{(\pm)} u_{02} \\ a_3^{(\pm)} u_{03} \end{pmatrix}, \qquad \Psi_{fin} = \begin{pmatrix} \bar{u}_1^{(reg)} \\ 0 \\ 0 \end{pmatrix}, \qquad \hat{W} = \begin{pmatrix} 0 & V_{1,2} & V_{1,3} \\ V_{2,1} & 0 & V_{2,3} \\ V_{3,1} & V_{3,2} & 0 \end{pmatrix}. \tag{3.118}$$

The initial states $\Psi_{in}^{(\pm)}$ are the results of diagonalizing the two-level problem defined by the bound states u_{02}, u_{03} and the coupling potential $V_{2,3}$. This yields energy eigenvalues $E_\pm$ as given by (3.110), except that the terms containing the open-channel propagator $\hat{G}$ are missing in the expressions for ε_i and $W_{2,3}$, compare Eqs. (3.105), (3.106). The two-level diagonalization also yields the appropriate superposition amplitudes $a_{2/3}^{(\pm)}$, which are required to obey the usual orthonormality relations. Inserting the objects (3.118) into the Golden Rule (3.75) and taking ρ_{fin} to be unity, as explained in the paragraph containing Eqs. (3.80), (3.81), reproduces the expression (3.114), but again, the energies and matrix elements are missing the contributions from the open-channel Green's operator $\hat{G}$. The non-perturbative derivation of Eqs. (3.108) and (3.114) above shows, that the possible existence of interference-induced exact bound states in the continuum, i.e. of resonances with exactly vanishing width, is not an artefact of the perturbative approach underlying the Golden Rule but is a real feature of systems involving two Feshbach resonances and only one open channel [9]. Such bound states in the continuum have recently been studied also in quantum-billard and quantum-dot systems [13, 14].

3.5.3 Resonances in the Presence of Several Open Channels

The results in Sects. 3.5.1 and 3.5.2 were derived for the case of only one open channel, so all scattering is elastic and its properties are contained in the behaviour of the scattering phase shifts δ_l, i.e. the S-matrix is still simply $\mathrm{e}^{2\mathrm{i}\delta_l}$. This subsection studies resonances, i.e. almost bound states, which can decay into more than one open channel. Whereas the theory for multichannel-scattering as based on coupled radial equations is given in Sects. 3.1–3.3 in a very general form, we now focus on the special features that a resonance causes in the S-matrix.[1]

As discussed in Sect. 2.3.10, the typical arcus-tangent behaviour of the resonant contribution to the scattering phase shift (3.72) can be described by a pole of the S-matrix at the complex energy $E_\mathrm{R} - \mathrm{i}\Gamma/2$,

$$S_l = \mathrm{e}^{2\mathrm{i}\delta_l} = S_\mathrm{bg} S_\mathrm{res} \quad \text{with } S_\mathrm{bg} = \mathrm{e}^{2\mathrm{i}\delta_\mathrm{bg}} \quad \text{and} \quad S_\mathrm{res} = \frac{E - E_\mathrm{R} - \mathrm{i}\Gamma/2}{E - E_\mathrm{R} + \mathrm{i}\Gamma/2}. \tag{3.119}$$

The background part S_bg of the S-matrix is assumed to depend at most weakly on energy, and the resonant part can be written as

$$S_\mathrm{res} = 1 - \frac{\mathrm{i}\Gamma}{E - E_\mathrm{R} + \mathrm{i}\Gamma/2}. \tag{3.120}$$

The coupling of an initial (almost) bound state to the open-channel continuum is manifest in the width Γ, which is given by (3.71) and can be related to the lifetime of the resonance, see the comment following Eq. (3.83). When there are several open channels, the S-matrix is a true matrix. To account for this we extend Eq. (3.120) while retaining its general structure,

$$\mathbf{S}_\mathrm{res} = \mathbf{1} - \frac{\mathrm{i}\mathbf{A}}{E - E_\mathrm{R} + \mathrm{i}\Gamma/2}. \tag{3.121}$$

Here $\mathbf{1}$ is the $N \times N$ unit matrix and $\mathbf{A}$ a general $N \times N$ matrix, N being the number of open (radial) channels.

Assuming that the total S-matrix and the background S-matrix $\mathbf{S}_\mathrm{bg}$ are unitary implies that $\mathbf{S}_\mathrm{res}$ must be unitary,

$$\mathbf{S}_\mathrm{res}\mathbf{S}_\mathrm{res}^\dagger = \mathbf{1}. \tag{3.122}$$

Inserting the right-hand side of (3.121) for $\mathbf{S}_\mathrm{res}$ and its hermitian conjugate for $\mathbf{S}_\mathrm{res}^\dagger$ in (3.122) leads to the following relation,

$$\begin{aligned} &\left(E - E_\mathrm{R} + \mathrm{i}\frac{\Gamma}{2}\right)\mathrm{i}\mathbf{A}^\dagger - \left(E - E_\mathrm{R} - \mathrm{i}\frac{\Gamma}{2}\right)\mathrm{i}\mathbf{A} + \mathbf{A}^\dagger\mathbf{A} = 0 \\ &\quad\Longleftrightarrow\quad (E - E_\mathrm{R})\mathrm{i}\left(\mathbf{A}^\dagger - \mathbf{A}\right) - \frac{\Gamma}{2}\left(\mathbf{A}^\dagger + \mathbf{A}\right) + \mathbf{A}^\dagger\mathbf{A} = 0. \end{aligned} \tag{3.123}$$

[1] The treatment in this subsection is inspired by Chap. 20 of Ref. [17], where further details based on a more stringent mathematical formulation can be found.

If the matrix $\mathbf{A}$ depends at most weakly on energy, then the energy-dependent left-hand side of (3.123) can only vanish if

$$\mathbf{A}^\dagger = \mathbf{A} \quad \text{and} \quad \mathbf{A}^2 = \Gamma\mathbf{A}, \tag{3.124}$$

which implies that the linear operator represented by the matrix

$$\mathbf{B} = \frac{1}{\Gamma}\mathbf{A} \tag{3.125}$$

is a projection operator, $\mathbf{B}^2 = \mathbf{B} = \mathbf{B}^\dagger$. This means that the quotient on the right-hand side of (3.121), which corresponds to $\mathbf{S}_{\rm res} - \mathbf{1}$, projects onto a certain subspace in the space of N-component vectors of radial-channel wave functions.

Picture the resonance as an almost bound state $\Psi_{\rm in}$ of the projectile-target system, which decays due to channel coupling into a final state $\Psi_{\rm fin}$ consisting of a well defined linear combination of open-channel wave functions,

$$\Psi_{\rm in} \longrightarrow \Psi_{\rm fin} = \sum_{i,l,m} \frac{u_{i,l,m}(r)}{r} Y_{l,m}(\theta,\phi)\Upsilon(\xi) \equiv \sum_{\{i\}} \frac{u_{\{i\}}}{r}\Upsilon_{\{i\}}(\xi,\theta,\phi). \tag{3.126}$$

The three quantum numbers i, l, m labelling the radial channels have been compacted to one symbol $\{i\}$ for brevity. If there is no resonant contribution to the scattering process, then the whole S-matrix is given by the background term $\mathbf{S}_{\rm bg}$ alone, $\mathbf{S}_{\rm res}$ is the unit operator and $\mathbf{S}_{\rm res} - \mathbf{1}$ is the null-operator. It is plausible to assume that in the presence of a resonance, the operator $\mathbf{S}_{\rm res} - \mathbf{1}$ filters out the linear combination of channels corresponding to the superposition on the right-hand side of (3.126), i.e. the projector $\mathbf{B}$ defined by (3.125) projects onto a one-dimensional subspace of the N-dimensional space of vectors of outgoing radial waves. This implies that the matrix elements of $\mathbf{B}$ and of $\mathbf{A} = \Gamma\mathbf{B}$ are of the form,

$$\begin{aligned} &\mathrm{B}_{\{i\},\{j\}} = b_{\{i\}} b^*_{\{j\}}, \qquad \sum_{\{i\}} |b_{\{i\}}|^2 = 1, \\ &\mathrm{A}_{\{i\},\{j\}} = \Gamma b_{\{i\}} b^*_{\{j\}} = \gamma_{\{i\}}\gamma^*_{\{j\}}, \qquad \gamma_{\{i\}} = \sqrt{\Gamma} b_{\{i\}}. \end{aligned} \tag{3.127}$$

The expression (3.121) for the resonant part of the S-matrix thus becomes,

$$(\mathbf{S}_{\rm res})_{\{i\},\{j\}} = \delta_{\{i\},\{j\}} - \frac{\mathrm{i}\gamma_{\{i\}}\gamma^*_{\{j\}}}{E - E_{\rm R} + \mathrm{i}\Gamma/2}, \tag{3.128}$$

and the coefficients $\gamma_{\{i\}}$ fulfill the relation,

$$\sum_{\{i\}} |\gamma_{\{i\}}|^2 = \Gamma. \tag{3.129}$$

In the case of only one open channel, the resonance width Γ was given by (3.71) in terms of the square of a transition matrix element, Eq. (3.79). Several open channels can be taken into account by generalizing (3.79) to

$$\left|\langle\Psi_{\rm in}|\hat{W}|\Psi_{\rm fin}\rangle\right|^2 = \sum_{\{i\}} \left|\left\langle\Psi_{\rm in}\middle|\hat{W}\middle|\tfrac{u_{\{i\}}}{r}\Upsilon_{\{i\}}(\xi,\theta,\phi)\right\rangle\right|^2. \tag{3.130}$$

This is consistent with Eq. (3.129) if we relate the coefficients $\gamma_{\{i\}}$ to the matrix elements,

$$\gamma_{\{i\}} = \sqrt{2\pi}\left\langle \Psi_{\text{in}} \middle| \hat{W} \middle| \tfrac{u_{\{i\}}}{r} \Upsilon_{\{i\}}(\xi,\theta,\phi) \right\rangle, \tag{3.131}$$

and call the quantities

$$\Gamma_{\{i\}} = |\gamma_{\{i\}}|^2 = 2\pi \left| \left\langle \Psi_{\text{in}} \middle| \hat{W} \middle| \tfrac{u_{\{i\}}}{r} \Upsilon_{\{i\}}(\xi,\theta,\phi) \right\rangle \right|^2 \tag{3.132}$$

the *partial widths* for the decay of the resonance into the different channels. In the spirit of time-dependent perturbation theory, the partial widths defined in this way are proportional to the respective transition rates into the outgoing channels, so the quotients $\Gamma_{\{i\}}/\Gamma$ define *branching ratios* giving the relative weights of the scattering yields into the various channels.

3.6 Coulombic Potentials, General Theory

3.6.1 Scattering Cross Sections

If projectile and target are charged, then their interaction features a long-range Coulomb potential. It is useful to separate this from the shorter-range potential $\hat{W}$ by writing the Schrödinger equation (3.3) as

$$\left[-\frac{\hbar^2}{2\mu}\Delta + \hat{H}_\xi + \frac{C}{r} + \hat{W}(\mathbf{r},\xi) \right] \boldsymbol{\Psi}(\mathbf{r},\xi) = E\boldsymbol{\Psi}(\mathbf{r},\xi). \tag{3.133}$$

The coupled-channel equations (3.4) now read

$$\left[-\frac{\hbar^2}{2\mu}\Delta + \frac{C}{r} \right] \psi_i(\mathbf{r}) + \sum_j V_{i,j}\psi_j(\mathbf{r}) = (E - E_i)\psi_i(\mathbf{r}), \tag{3.134}$$

and the potentials $V_{i,j}$ are defined as in (3.5). Due to the orthogonality of the Υ_j, the inclusion of the term C/r in the matrix element on the right-hand side of (3.5) gives a nonvanishing contribution only for $j = i$. This contribution is precisely C/r and is included separately in the square bracket on the left-hand side of (3.134), so the potentials $V_{i,j}$ remain of shorter range, i.e. they fall off faster than $1/r^2$ at large distances.

The asymptotic behaviour of the channel wave functions in (3.134) is

$$\begin{aligned} \psi_j(\mathbf{r}) &\overset{r\to\infty}{\sim} \delta_{i,j}\left[\mathrm{e}^{\mathrm{i}[k_i z + \eta_i \ln(k_i[r-z])]} + f_{\mathrm{C},i}(\theta)\frac{\mathrm{e}^{\mathrm{i}(k_i r - \eta_i \ln 2k_i r)}}{r} \right] \\ &\quad + \tilde{f}_{i,j}(\theta,\phi)\frac{\mathrm{e}^{\mathrm{i}(k_j r - \eta_j \ln 2k_j r)}}{r} \\ &= \delta_{i,j}\mathrm{e}^{\mathrm{i}[kz + \eta_i \ln(k_i[r-z])]} + \left[\delta_{i,j} f_{\mathrm{C},i}(\theta) + \tilde{f}_{i,j}(\theta,\phi)\right]\frac{\mathrm{e}^{\mathrm{i}(k_j r - \eta_j \ln 2k_j r)}}{r}, \end{aligned} \tag{3.135}$$

compare Eqs. (2.191), (2.192) and (2.209) in Sect. 2.5. The Sommerfeld parameter $\eta_j = \mu C/(\hbar^2 k_j)$ now carries the channel subscript j, because it depends on the channel wave number k_j, and $f_{\mathrm{C},i}$ is the Coulomb scattering amplitude (2.192) in the incident channel i, i.e., with $k = k_i$ and $\eta = \eta_i$. The *additional* scattering amplitudes $\tilde{f}_{i,j}(\theta,\phi)$ in (3.135) are due to the deviation of the full projectile-target interaction from the pure Coulomb potential, i.e. to the shorter-range potentials $V_{i,j}$.

From (3.135) the differential cross section for elastic scattering, without changing the state Υ_i of the internal degrees of freedom, is

$$\frac{\mathrm{d}\sigma_{i\to i}}{\mathrm{d}\Omega} = \left| f_{\mathrm{C},i}(\theta) + \tilde{f}_{i,i}(\theta,\phi)\right|^2, \tag{3.136}$$

while for inelastic scattering, or for a change to an energetically degenerate internal state $\Upsilon_i \to \Upsilon_j$ with $k_j = k_i$,

$$\frac{\mathrm{d}\sigma_{i\to j}}{\mathrm{d}\Omega} = \frac{k_j}{k_i}\left|\tilde{f}_{i,j}(\theta,\phi)\right|^2, \quad j \neq i. \tag{3.137}$$

3.6.2 Partial-Waves Expansion

In the presence of the long-range Coulomb potential, the radial coupled-channel equations (3.30) are modified to

$$\left[-\frac{\hbar^2}{2\mu}\frac{\mathrm{d}^2}{\mathrm{d}r^2} + \frac{l(l+1)\hbar^2}{2\mu r^2} + \frac{C}{r}\right] u_{i,l,m}(r) + \sum_{j,l',m'} V\big(i,l,m;\, j,l',m'\big) u_{j,l',m'}(r)$$
$$= E u_{i,l,m}(r). \tag{3.138}$$

As in (3.134) the Coulomb potential does not contribute to the channel-coupling potentials, due to the orthogonality of the Υ_j and of the spherical harmonics. The "diagonal" Coulomb contribution is included explicitly in (3.138), and the potentials $V(i,l,m;\, j,l',m')$ are all of shorter range, i.e. they fall off faster than $1/r^2$ at large distances.

The reactance matrix $\tilde{\mathbf{K}}$ and the scattering matrix $\tilde{\mathbf{S}}$ are now defined via the solutions of (3.138) relative to the solutions with the pure Coulomb potential. This means, that the free-particle waves (3.34) are replaced by the (energy-normalized) Coulomb functions,

$$\begin{aligned}
\bar{\mathrm{F}}_l(\eta_j, k_j r) &= \sqrt{\frac{2\mu}{\pi\hbar^2 k_j}} F_l(\eta_j, k_j r) \\
&\overset{r\to\infty}{\sim} \sqrt{\frac{2\mu}{\pi\hbar^2 k_j}} \sin\left(k_j r - \eta_j \ln(2k_j r) - l\frac{\pi}{2} + \sigma_{l,j}\right), \\
\bar{\mathrm{G}}_l(\eta_j, k_j r) &= \sqrt{\frac{2\mu}{\pi\hbar^2 k_j}} G_l(\eta_j, k_j r) \\
&\overset{r\to\infty}{\sim} \sqrt{\frac{2\mu}{\pi\hbar^2 k_j}} \cos\left(k_j r - \eta_j \ln(2k_j r) - l\frac{\pi}{2} + \sigma_{l,j}\right),
\end{aligned} \tag{3.139}$$

compare Eqs. (2.200), (2.202) and (2.237) in Sect. 2.5. Note that the Coulomb phases, $\sigma_{l,j} = \arg[\Gamma(l+1+\mathrm{i}\eta_j)]$, now also depend on the channel j. The sine-cosine based vector $\tilde{U}^{(i,l,m)}$ of solutions of the coupled-channel equations (3.138) is now defined by the component radial wave functions,

$$u^{(i,l,m)}_{j,l',m'}(r) \overset{r\to\infty}{\sim} \delta_{i,j}\delta_{l,l'}\delta_{m,m'}\bar{\mathrm{F}}_l(\eta_j, k_j r) + \tilde{K}_{i,l,m;\,j,l',m'}\bar{\mathrm{G}}_l(\eta_j, k_j r), \tag{3.140}$$

compare (3.36), and the alternative basis $\tilde{\Phi}^{(i,l,m)}$ is constructed in analogy to (3.37),

$$\varphi^{(i,l,m)}_{j,l',m'}(r) \overset{r\to\infty}{\sim} \delta_{i,j}\delta_{l,l'}\delta_{m,m'}\varphi^{(-)}_l(k_i r) - \tilde{S}_{i,l,m;\,j,l',m'}\varphi^{(+)}_{l'}(k_j r), \tag{3.141}$$

with

$$\begin{aligned}
\varphi^{(\pm)}_l(k_j r) &\overset{r\to\infty}{\sim} \bar{\mathrm{G}}_l(\eta_j, k_j r) \pm \mathrm{i}\bar{\mathrm{F}}_l(\eta_j, k_j r) \\
&\overset{r\to\infty}{\sim} \sqrt{\frac{2\mu}{\pi\hbar^2 k_j}} \mathrm{e}^{\pm\mathrm{i}(k_j r - \eta_j \ln(2k_j r) - l\frac{\pi}{2} + \sigma_{l,j})}.
\end{aligned} \tag{3.142}$$

In the presence of a long-range Coulomb interaction, Eqs. (3.140) and (3.141) define the reactance matrix $\tilde{\mathbf{K}}$ and the scattering matrix $\tilde{\mathbf{S}}$ *relative* to the pure-Coulomb scattering situation. The relation (3.39) expressing the vectors of the "incoming-outgoing" basis in terms of the "sine-cosine" basis remains valid, so the identity (3.40) now holds in the form

$$\tilde{\mathbf{S}} = (\mathbf{1} + \mathrm{i}\tilde{\mathbf{K}})(\mathbf{1} - \mathrm{i}\tilde{\mathbf{K}})^{-1}. \tag{3.143}$$

For an explicit evaluation of the elastic and inelastic differential scattering cross sections in the presence of the Coulomb potential, it is necessary to know the *additional* scattering amplitudes $\tilde{f}_{i,j}$ entering Eqs. (3.136) and (3.137). To this end we rewrite the expansion of the pure Coulomb wave (2.207) in partial waves,

$$\psi_{\mathrm{C},i}(\mathbf{r}) = \pi\hbar \sum_{l=0}^{\infty} \sqrt{\frac{2(2l+1)}{\mu k_i}} \mathrm{i}^l \mathrm{e}^{\mathrm{i}\sigma_{l,i}} \frac{\bar{\mathrm{F}}_l(\eta_i, k_i r)}{r} Y_{l,0}(\theta). \tag{3.144}$$

Here $\psi_{\mathrm{C},i}(\mathbf{r})$ is the solution of the pure-Coulomb Schrödinger equation with Sommerfeld parameter η_i and wave number k_i corresponding to the incident channel i; its asymptotic behaviour is given by the content of the big square bracket in the top line of (3.135).

Again we argue that the incoming spherical waves in (3.141) must add up to the inward-travelling contribution from the asymptotic expression for $\bar{\mathrm{F}}_l$ in the pure Coulomb wave (3.144) in the incident channel i. This implies that the solution vector obeying the boundary conditions (3.135) is given by

$$\tilde{U} = -\pi\hbar \sum_l \sqrt{\frac{2l+1}{2\mu k_i}} \mathrm{i}^{l-1} \mathrm{e}^{\mathrm{i}\sigma_{l,i}} \tilde{\boldsymbol{\Phi}}^{(i,l,0)}, \tag{3.145}$$

and its component radial wave functions are

$$u_{j,l',m'}(r) = -\pi\hbar \sum_l \sqrt{\frac{2l+1}{2\mu k_i}} \mathrm{i}^{l-1} \mathrm{e}^{\mathrm{i}\sigma_{l,i}} \varphi^{(i,l,0)}_{j,l',m'}(r). \tag{3.146}$$

The channel wave functions obtained by summing over all the angular momentum components l', m' for a given channel j,

$$\psi_j(\mathbf{r}) = \sum_{l',m'} \frac{u_{j,l',m'}(r)}{r} Y_{l',m'}(\theta,\phi), \tag{3.147}$$

thus have the following asymptotic behaviour:

$$\psi_j(\mathbf{r}) \overset{r\to\infty}{\sim} \delta_{i,j}\psi_{C,i}(r) + \frac{\mathrm{e}^{\mathrm{i}[k_i r - \eta_i \ln(2k_i r)]}}{r} \sum_{l',m'} Y_{l',m'}(\theta,\phi) \sum_{l=0}^{\infty} \mathrm{i}^{l-l'-1} \mathrm{e}^{\mathrm{i}(\sigma_{l,i}+\sigma_{l,j})}$$
$$\times \sqrt{\frac{\pi(2l+1)}{k_i k_j}} [\tilde{S}_{i,l,0;\,j,l',m'} - \delta_{i,j}\delta_{l,l'}\delta_{0,m'}]. \tag{3.148}$$

This agrees with Eq. (3.135), and the *additional* scattering amplitude $\tilde{f}_{i,j}$ due to the shorter ranged potentials $V_{i,j}$ is seen to be given by the elements $\tilde{S}_{i,l,0;\,j,l',m'}$ of the scattering matrix *relative to pure Coulomb scattering* via

$$\tilde{f}_{i,j}(\theta,\phi) = \sum_{l',m';l} Y_{l',m'}(\theta,\phi) \mathrm{i}^{l-l'-1} \mathrm{e}^{\mathrm{i}(\sigma_{l,i}+\sigma_{l,j})}$$
$$\times \sqrt{\frac{\pi(2l+1)}{k_i k_j}} [\tilde{S}_{i,l,0;\,j,l',m'} - \delta_{i,j}\delta_{l,l'}\delta_{0,m'}]. \tag{3.149}$$

Remember that the inelastic differential scattering cross sections are given as the absolute square of the scattering amplitude (3.149) according to (3.137), but that the incident-incident, elastic cross section also involves the pure-Coulomb scattering amplitude $f_{C,i}$ according to (3.136).

3.7 Attractive Coulomb Potentials, Multichannel Quantum-Defect Theory

As already became apparent in Sect. 2.5.4, interactions containing an attractive Coulomb term are special, because they support a quasicontinuum of infinitely many

bound states, whose energy eigenvalues form a Rydberg series and accumulate at threshold, while their appropriately normalized wave functions merge smoothly to the (appropriately normalized) continuum wave functions above threshold. As a prelude to the description of several coupled Coulombic channels let's first consider a single radial channel with a Rydberg series perturbed by a single Feshbach resonance from a second, closed channel.

3.7.1 Perturbed Rydberg Series

As explained in Sect. 2.5.4, bound and continuum states in a modified attractive Coulomb potential can be described by the formulas (2.260), (2.261) and (2.262) of quantum-defect theory, which are repeated here for convenience,

$$\begin{aligned} &\mu^{\mathrm{QD}}(E) + \nu(E) = 0 \pmod 1, \\ &\nu(E) = \begin{cases} -\tilde{\delta}(E)/\pi & \text{for } E > I, \\ \sqrt{\mathscr{R}/(I-E)} & \text{for } E < I. \end{cases} \end{aligned} \tag{3.150}$$

Note that the continuum threshold is now at $E = I$. The quantum-defect function $\mu^{\mathrm{QD}}(E)$ depends smoothly and weakly on energy, in particular near threshold, and it describes the effect of the short-range deviation of the full potential from the pure Coulomb shape. The function $\nu(E)$ has different meanings for energies below and energies above the threshold I.

Below threshold, $\nu(E)$ is a continuous variable, "the continuous effective quantum number". At the energies E_n of the bound states, ν becomes equal to the effective quantum number $\nu(E_n) \equiv \tilde{n} = n - \mu^{\mathrm{QD}}(E_n)$, and Eq. (3.150) is an expression of the Rydberg formula for quantization, compare Eq. (2.252) in Sect. 2.5.4,

$$\mu^{\mathrm{QD}} + \nu = n \quad \Longleftrightarrow \quad E_n = I - \frac{\mathscr{R}}{[n - \mu^{\mathrm{QD}}(E_n)]^2} = I - \frac{\mathscr{R}}{(n-\mu_n)^2}. \tag{3.151}$$

The effective quantum number $\tilde{n}$ differs from the integer quantum number n of the pure Coulomb case by the quantum defect $\mu_n = \mu^{\mathrm{QD}}(E_n)$. The bound states are given as the intersection of $\mu^{\mathrm{QD}}(E)$ with the family of curves $n - \nu(E)$, as illustrated in Fig. 3.5. The solid black line is the almost energy-independent function $\mu^{\mathrm{QD}} \approx 0.7$ and the curves $n - \nu(E)$ are shown as brown lines for values of n ranging from six to fourteen. The corresponding energy levels are shown as vertical black lines at the top edge of the figure.

Above threshold, the effect of the short-range deviation of the full potential from the pure Coulomb shape leads to an additional phase shift $\tilde{\delta}$ in the asymptotic behaviour of the regular solutions of the radial Schrödinger equation, and $\nu(E)$ is proportional to this additional phase shift. The QDT equation (3.150) implies

$$\tilde{\delta}(E) = \pi \mu^{\mathrm{QD}}(E) \pmod \pi. \tag{3.152}$$

In Fig. 3.5, this is expressed in the continuation of the solid black line to the region $E > I$.

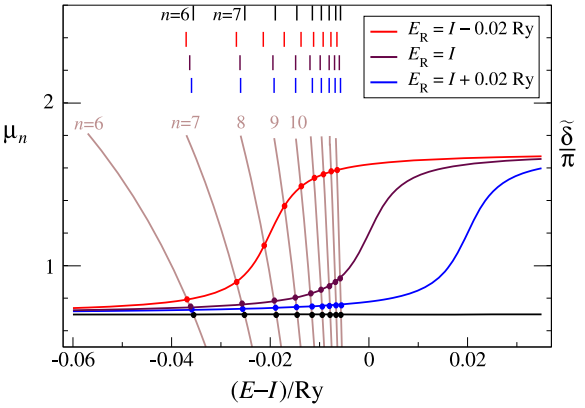

Fig. 3.5 The *solid black line* shows an almost energy-independent quantum-defect function $\mu^{\mathrm{QD}} \approx 0.7$, and the *brown lines* show the family of functions $n - \nu(E)$ with $\nu(E)$ as given in (3.150). Their intersections with μ^{QD} determine the energy eigenvalues E_n of the bound states and their quantum defects μ_n. The *black vertical lines* at the top edge of the figure show the unperturbed energy levels. The effects of a Feshbach resonance with $\Gamma = 0.01\mathscr{R}$ and $E_{\mathrm{R}} = I + 0.02\mathscr{R}$, $E_{\mathrm{R}} = I$ and $E_{\mathrm{R}} = I - 0.02\mathscr{R}$ are shown by the *blue*, *maroon* and *red lines*, which represent the modified quantum-defect function (3.156) for the respective cases. The energy levels of the correspondingly perturbed Rydberg series are shown as *vertical lines* in the same colours in the *upper part* of the figure. For $E_{\mathrm{R}} = I - 0.02\mathscr{R}$ (*red lines*), the perturbation appears as a smooth rise of roughly unity in the quantum defects corresponding to one additional bound state

The power of the QDT equation (3.150) lies in the weak energy dependence of the quantum-defect function and in Seaton's theorem (2.257), which links the bound-state quantum defects to the threshold limit of the additional phase shift $\tilde{\delta}$. Knowledge of this limit implies knowledge of an infinite number of bound-state energies with ever increasing accuracy for $n \to \infty$.

The QDT formula (3.150) can be extended to accommodate the influence of a Feshbach resonance due to an almost bound state in a second, closed channel. In the presence of a Coulomb potential, such a Feshbach resonance manifests itself in much the same way as expressed in Eq. (3.84) in the absence of a Coulomb potential, except that the equation is now formulated for the additional phase shift $\tilde{\delta}$ due to the deviation of the full potential from the pure Coulomb shape:

$$\tilde{\delta} = \tilde{\delta}_{\mathrm{bg}} + \tilde{\delta}_{\mathrm{res}} = \tilde{\delta}_{\mathrm{bg}} - \arctan\left(\frac{\Gamma/2}{E - E_{\mathrm{R}}}\right). \tag{3.153}$$

Here $\tilde{\delta}_{\mathrm{bg}}$ is the background contribution to the additional phase shift, i.e. the additional phase shift as obtained in the absence of the Feshbach resonance. With $\tilde{\delta}_{\mathrm{bg}} = \pi\mu^{\mathrm{QD}}$, we have

$$\tilde{\delta} = \pi\mu^{\mathrm{QD}} - \arctan\left(\frac{\Gamma/2}{E - E_{\mathrm{R}}}\right) \pmod{\pi}. \tag{3.154}$$

By writing $\tilde{\delta}$ as $-\pi\nu$ according to (3.150) we transcribe Eq. (3.154) to

$$\tan\left[\pi\left(\mu^{\mathrm{QD}}+\nu\right)\right]=\frac{\Gamma/2}{E-E_{\mathrm{R}}}. \tag{3.155}$$

The periodicity of the tangent function spares us having to explicitly write "(mod π)" as in (3.154).

The perturbing pole on the right-hand side of (3.155) not only describes the influence of the Feshbach resonance on the additional phase shift $\tilde{\delta}$ above threshold, it also describes the perturbation of the Rydberg series of bound states below threshold, which is due to the coupling to the bound state in the other closed channel. The bound states in the *perturbed Rydberg series* are now given by the intersections of the *modified quantum-defect function*,

$$\mu_{\mathrm{FR}}^{\mathrm{QD}}(E)=\mu^{\mathrm{QD}}-\frac{1}{\pi}\arctan\left(\frac{\Gamma/2}{E-E_{\mathrm{R}}}\right), \tag{3.156}$$

with the family of curves $n-\nu(E)$. Above threshold, $\pi\mu_{\mathrm{FR}}^{\mathrm{QD}}(E)$ corresponds to the additional phase shift $\tilde{\delta}$, including the effect of the perturbing pole, as already expressed in (3.154).

The resonant contributions to the phase shifts and the corresponding perturbations of the bound-state energies in the Rydberg series are illustrated for three different positions E_{R} of the Feshbach resonance in Fig. 3.5. The modified quantum-defect function (3.156) is shown as a coloured solid line for each of the three cases. For $E_{\mathrm{R}}=I+0.02\mathscr{R}$ (blue solid line), the effect of the resonance is manifest mainly above threshold and the shifted bound-state energies (blue vertical lines) are still close to the unperturbed levels (black vertical lines). For $E_{\mathrm{R}}=I$ (maroon lines), the Feshbach resonance straddles the threshold and the threshold limit of the quantum defects is shifted by $\frac{1}{2}$ relative to the unperturbed case. For $E_{\mathrm{R}}=I-0.02\mathscr{R}$ (red lines), the influence of the Feshbach resonance is mainly below threshold. The bound-state spectrum accommodates one additional state, so the energy levels have to move closer together, which is described quantitatively as a rise of the quantum defects by almost unity. At energies above that of the perturber, the energies of the perturbed Rydberg series are again close to the unperturbed levels, but their quantum number is larger by one than in the corresponding unperturbed series.

3.7.2 Two Coupled Coulombic Channels

Now consider the case of two radial channels described by the coupled equations

$$\begin{aligned}\left[-\frac{\mathrm{d}^2}{\mathrm{d}r^2}+V_1(r)-\frac{|C|}{r}\right]u_1(r)+V_{1,2}u_2(r)&=Eu_1(r),\\ \left[-\frac{\mathrm{d}^2}{\mathrm{d}r^2}+V_2(r)-\frac{|C|}{r}\right]u_2(r)+V_{2,1}u_1(r)&=Eu_2(r).\end{aligned} \tag{3.157}$$

The potentials V_i are taken to include the internal excitation E_i which defines the channel threshold, and to include possible centrifugal terms in the case of nonvanishing angular momenta. In systems with attractive Coulomb potentials, the channel thresholds are often ionization thresholds, and it is customary to label them I_i rather than E_i, so $V_i(r) \equiv V_{i,i}(r) + I_i \overset{r\to\infty}{\longrightarrow} I_i$. Radial channels are now labelled simply by i, j rather than $\{i\}$, $\{j\}$ as in Sect. 3.5.3.

In the absence of coupling, each of the two equations (3.157) supports a Rydberg series of bound states below the respective channel threshold I_i,

$$E_{n_1} = I_1 - \frac{\mathscr{R}}{[n_1 - \mu_1^{\mathrm{QD}}(E_{n_1})]^2}, \qquad E_{n_2} = I_2 - \frac{\mathscr{R}}{[n_2 - \mu_2^{\mathrm{QD}}(E_{n_2})]^2}, \tag{3.158}$$

where $\mu_1^{\mathrm{QD}}(E)$ and $\mu_2^{\mathrm{QD}}(E)$ are weakly energy-dependent quantum-defect functions describing the effect of the deviation of the channel potentials in the respective uncoupled channels from a pure Coulomb potential. Above the respective channel thresholds, the continuum-state wave functions are characterized by additional phase shifts $\tilde{\delta}_i$ relative to the pure Coulomb waves. The physical consequences of channel coupling depend on the value of the energy E with respect to the channel thresholds I_i.

We first consider the energy range between the two channel thresholds,

$$I_1 < E < I_2, \tag{3.159}$$

(assuming, without loss of generality, that $I_1 < I_2$). So channel 1 is open while channel 2 is closed, and the properties of the continuum states are characterized by the additional phase shift $\tilde{\delta}_1(E)$ of the open-channel radial wave function relative to the pure Coulomb wave. In the absence of channel coupling, the closed channel 2 supports a Rydberg series of bound states at the energies given by the second equation (3.158). Each of these bound states appears as a Feshbach resonance causing a rise of $\tilde{\delta}_1(E)$ by π, as described by Eqs. (3.154), (3.155) above. This corresponds to a *Rydberg series of Feshbach resonances* [6]. To leading order in the coupling potential, the resonance positions are the energies E_{n_2} of the uncoupled bound states and the widths Γ_{n_2} are given, as in (3.71), by

$$\Gamma_{n_2} = 2\pi \left| \langle u_{n_2} | V_{2,1} | \bar{u}_1^{(\mathrm{reg})} \rangle \right|^2. \tag{3.160}$$

When the open channel describes an electron moving relative to a residual positive ion, the decay of the resonance is an ionization process, and the almost bound state in the closed channel, which defines the Feshbach resonance, is an autoionizing resonance. The Rydberg series of Feshbach resonances then corresponds to Rydberg series of autoionizing resonances.

Towards the series limit $n_2 \to \infty$, the widths (3.160) decrease, because the amplitudes of the bound state wave functions $u_{n_2}(r)$, which are normalized to unity, decrease with n_2 for any given distance r, and the range of r-values contributing significantly to the matrix element in (3.160) is restricted due to the fall-off of $V_{2,1}(r)$ at large distances. The connection to a quantity that remains finite at threshold is achieved by expressing the bound-state wave functions $u_{n_2}(r)$ in terms of the

energy-normalized bound-state wave functions $\bar{u}_{n_2}(r)$, which are defined in analogy to (2.254) in Sect. 2.5.4,

$$\bar{u}_{n_2}(r) = \sqrt{\frac{\tilde{n}_2^3}{2\mathscr{R}}}\, u_{n_2}(r); \tag{3.161}$$

$$\Gamma_{n_2} = \frac{4\pi\mathscr{R}}{\tilde{n}_2^3}\left|\left\langle \bar{u}_{n_2}\middle| V_{2,1}\middle|\bar{u}_1^{(\mathrm{reg})}\right\rangle\right|^2. \tag{3.162}$$

In (3.162) $\tilde{n}_2 = n_2 - \mu_2^{\mathrm{QD}}(E_{n_2})$ is the effective quantum number in channel 2. As $E \to I_2$, $n_2 \to \infty$, the energy-normalized bound-state wave functions $\bar{u}_{n_2}(r)$ converge to a well defined threshold wave function as in (2.255), so the matrix element in (3.162), which is dimensionless, is expected to depend only weakly on energy and to converge to a well defined value in this limit. Note that the widths (3.162) decrease with the cube of the (effective) quantum number $\tilde{n}_2$, as does the separation of successive resonance positions in the Rydberg series of resonances.

The resonance positions E_{n_2} are the zeros of the function

$$T_2(E) = \tan\left[\pi\left(\mu_2^{\mathrm{QD}}(E) + \nu_2(E)\right)\right] \tag{3.163}$$

where $\nu_2(E)$ is the continuous effective quantum number in channel 2,

$$\nu_2(E) = \sqrt{\frac{\mathscr{R}}{I_2 - E}}. \tag{3.164}$$

Expanding $T_2(E)$ around one of its zeros gives

$$T_2(E) \approx (E - E_{n_2})\left.\frac{\mathrm{d}T_2}{\mathrm{d}E}\right|_{E=E_{n_2}} = (E - E_{n_2})\frac{\pi\tilde{n}_2^3}{2\mathscr{R}}. \tag{3.165}$$

Each Feshbach resonance of the Rydberg series is described by a pole term as on the right-hand side of (3.155); using (3.162), (3.163) and (3.165), this pole term can be uniformly written as

$$\frac{\Gamma_{n_2}/2}{E - E_{n_2}} = \frac{\pi^2|\langle \bar{u}_{n_2}|V_{2,1}|\bar{u}_1^{(\mathrm{reg})}\rangle|^2}{\tan[\pi(\mu_2^{\mathrm{QD}}(E) + \nu_2(E))]}. \tag{3.166}$$

Introducing as a weakly energy-dependent parameter the dimensionless quantity

$$|R_{2,1}|^2 = \pi^2\left|\left\langle \bar{u}_{n_2}\middle| V_{2,1}\middle|\bar{u}_1^{(\mathrm{reg})}\right\rangle\right|^2 \tag{3.167}$$

enables us to express the influence of the Rydberg series of Feshbach resonances by the compact equation,

$$\tan\left[\pi\left(\mu_1^{\mathrm{QD}}(E) + \nu_1(E)\right)\right] = \frac{|R_{2,1}|^2}{\tan[\pi(\mu_2^{\mathrm{QD}}(E) + \nu_2(E))]}. \tag{3.168}$$

When $E > E_1$, $\pi\nu_1(E)$ is proportional to the additional phase shift of the open-channel wave function, $\pi\nu_1(E) = -\tilde{\delta}_1(E)$, and (3.168) can be rewritten as

$$\tilde{\delta}_1(E) = \pi\mu_1^{\mathrm{QD}}(E) - \arctan\left\{\frac{|R_{2,1}|^2}{\tan[\pi(\mu_2^{\mathrm{QD}}(E) + \nu_2(E))]}\right\} \quad (\mathrm{mod}\ \pi). \tag{3.169}$$

Equation (3.169) has the same structure as (3.154), i.e. $\tilde{\delta}_1(E) = \pi\mu_{\mathrm{RFR}}^{\mathrm{QD}}(E) (\mathrm{mod}\,\pi)$, with the modified quantum-defect function $\mu_{\mathrm{RFR}}^{\mathrm{QD}}(E)$ now accounting not for a single Feshbach resonance, but for a whole Rydberg series of Feshbach resonances,

$$\mu_{\mathrm{RFR}}^{\mathrm{QD}}(E) = \mu_1^{\mathrm{QD}}(E) - \frac{1}{\pi}\arctan\left\{\frac{|R_{2,1}|^2}{\tan[\pi(\mu_2^{\mathrm{QD}}(E) + \nu_2(E))]}\right\}. \tag{3.170}$$

We now consider the case that both channels are closed,

$$E < I_1 < I_2. \tag{3.171}$$

The steps that led from Eq. (3.155) to Eq. (3.168) are still valid, but $\nu_1(E)$ stands for the continuous effective quantum number in the deeper closed channel 1,

$$\nu_1(E) = \sqrt{\frac{\mathscr{R}}{I_1 - E}}. \tag{3.172}$$

Equation (3.168) now is an equation defining the positions of the energy eigenvalues E_n as the intersections of the family of curves $n - \nu_1(E)$ with the modified quantum-defect function (3.170). This represents a perturbation of the Rydberg series defined by the first equation (3.158) by a whole *Rydberg series of perturbers* located around energies defined by the second equation (3.158). For energies E_{n_2} lying below the lower channel threshold I_1, these perturbers cause a rise in the quantum defects by roughly unity, as in the case $E_{\mathrm{R}} = I - 0.02\mathscr{R}$ illustrated by the red lines in Fig. 3.5. Perturbers with $E_{n_2} > I_1$ are manifest mainly in the continuum as a rise by π in the additional phase shift of the open-channel wave function, as described above, and they compress the bound-state spectrum only slightly. A Feshbach resonance with $E_{n_2} \approx I_1$ straddles the threshold and its influence is distributed evenly on the bound-state and continuum regimes, as illustrated by the maroon lines in Fig. 3.5.

The power of multichannel quantum-defect theory lies in the fact that complex spectra in systems of coupled Coulombic channels can be described with the help of a small number of parameters. These parameters are weakly energy dependent and essentially constant in a sufficiently narrow range of energies, and such a narrow energy range can accommodate a large number of complex spectral features. In the two-channel case, there are three such parameters, μ_1^{QD}, μ_2^{QD} and $|R_{2,1}|^2$. Accurate theoretical or experimental data on a small number of bound or resonant states can be used to determine these parameters, and then further properties of the system, e.g. the positions and widths of infinitely many states in a Rydberg series of autoionizing resonances, follow via the two-channel QDT equation (3.168).

The essential features of two-channel quantum-defect theory are summarized in Fig. 3.6. The black solid line is the modified quantum-defect function (3.170). Below the lower threshold, i.e. for $E < I_1$, its intersections with the family of functions $n - \nu_1(E)$ define energy eigenvalues of the Rydberg series of bound states, which is perturbed by a *Rydberg series of perturbers* due to the coupling to the states in channel 2. With the parameters on which the figure is based, the perturber near

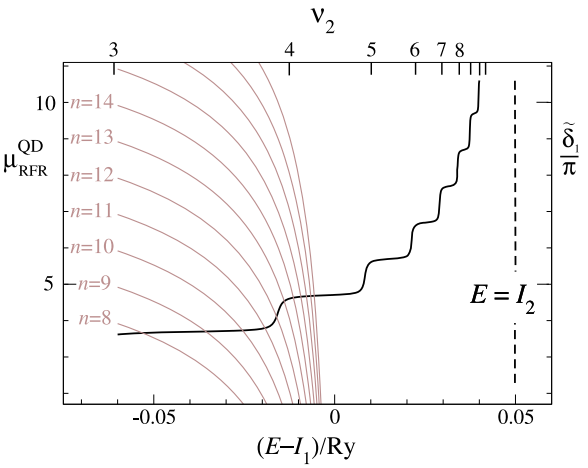

Fig. 3.6 The *black solid line* shows the modified quantum-defect function (3.170). Below the lower chanel threshold I_1, its intersections with the family of functions $n - \nu_1(E)$ (shown as *brown lines*) define the energies of the (perturbed) Rydberg series of bound states. For $I_1 < E < I_2$, $\pi\mu_{\rm RFR}^{\rm QD}(E)$ is the additional phase shift $\tilde{\delta}_1$ of the open-channel wave function, and the rises of $\tilde{\delta}_1$ through π describe a Rydberg series of Feshbach resonances converging to the upper-channel threshold I_2. The figure is based on the energy-independent QDT parameters $\mu_1^{\rm QD} = 0.7$, $\mu_2^{\rm QD} = 0.1$ and $|R_{2,1}|^2 = 0.1$, and the separation of the thresholds is $I_2 - I_1 = 0.05\mathscr{R}$. A scale for the continuous effective quantum number $\nu_2(E)$ as defined by Eq. (3.164) is shown at the top of the figure

$E = I_1 - 0.016\mathscr{R}$ is already the fourth in the series, and its effective quantum number $\tilde{n}_2 = n_2 - \mu_2^{\rm QD}(E_{n_2})$ is $\tilde{n}_2 = 3.9$, corresponding to $n_2 = 4$ and $\mu_2^{\rm QD}(E_{n_2}) = 0.1$. Between the channel thresholds $I_1 < E < I_2$, $\pi\mu_{\rm RFR}^{\rm QD}(E)$ is equal to the additional phase shift $\tilde{\delta}_1$ of the open-channel wave function. The rises of $\tilde{\delta}_1$ by π are manifestations of the Rydberg series of Feshbach resonances converging to the upper-channel threshold I_2. As for the perturbers below I_1, they can be labelled by the quantum number n_2, and their positions E_{n_2} are related to the effective quantum numbers in channel 2 according to the second equation (3.158). At the energy E_{n_2}, the effective quantum number of the perturber or Feshbach resonance corresponds to the continuous effective quantum number (3.164) with respect to the threshold I_2, $\tilde{n}_2 = \nu_2(E_{n_2})$. A scale for the continuous effective quantum number $\nu_2(E)$ is shown at the top of Fig. 3.6.

If the weakly energy-dependent QDT parameters $\mu_1^{\rm QD}$, $\mu_2^{\rm QD}$ and $|R_{2,1}|^2$ are assumed to be constant, then the right-hand side of Eq. (3.170), taken modulo unity, is a periodic function of $\nu_2(E)$ with period unity. If we plot $\mu_{\rm RFR}^{\rm QD} (\mathrm{mod}\, 1)$ not as function of energy but as function of the continuous effective quantum number $\nu_2(E)$, then the whole structure below I_2 in Fig. 3.6 can be accounted for in a reduced plot covering the unit square in the ν_2-$\mu_{\rm RFR}^{\rm QD}$ plane. This is shown as the inner square box in Fig. 3.7. Such a representation of a Rydberg series of perturbers (below I_1) and

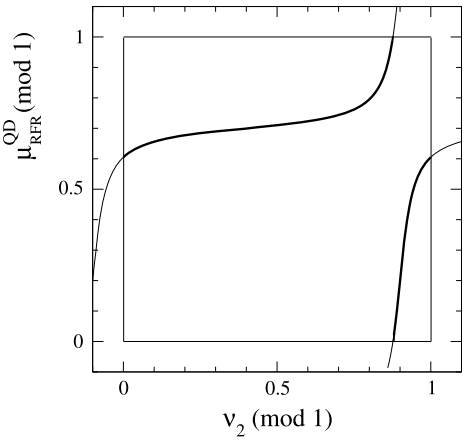

Fig. 3.7 Lu-Fano plot for the QDT parameters $\mu_1^{QD} = 0.7$, $\mu_2^{QD} = 0.1$ and $|R_{2,1}|^2 = 0.1$, with $I_2 - I_1 = 0.05\mathscr{R}$. The *thick solid line* shows the modified quantum-defect function (3.170) (mod 1) as function of the continuous effective quantum number ν_2 with respect to the upper-channel threshold, also taken (mod 1)

Feshbach resonances (above I_1) is called a Lu-Fano plot. The thick solid line contains most of the information of Fig. 3.6. All bound-state quantum defects, (mod 1), lie on this curve as does the additional phase shift $\tilde{\delta}_1$ in units of π. In realistic situations, the QDT parameters are not exactly energy independent, so the quantum defects and additional phase shifts corresponding to the different perturbers in Fig. 3.6, as labelled by the quantum number n_2, will, in Fig. 3.7, lie on curves which are slightly shifted with respect to each other. As $n_2 \to \infty$, these curves converge to a well defined limiting curve [16], because an arbitrarily small energy range near the threshold I_2, where possible variations of the QDT parameters become negligible, accommodates an infinity of perturbers accumulating at I_2.

To conclude this subsection on two coupled Coulombic channels, we focus on the energy range above the upper-channel threshold, where both channels are open,

$$I_1 < I_2 < E. \tag{3.173}$$

In this case, there are, at each energy E, two linearly independent two-component solutions of the coupled radial equations (3.157). One of these solutions can be constructed by continuing the solutions describing the Feshbach resonances converging to the upper threshold I_2 from below to energies above I_2. Near the energies E_{n_2} of the Feshbach resonances, these solutions are given in analogy to (3.73) with (3.74) by

$$\begin{pmatrix} u_1(r) \\ u_2(r) \end{pmatrix} = \begin{pmatrix} \cos\tilde{\delta}_{\rm res}\bar{u}_1^{(\rm reg)}(r) + \sin\tilde{\delta}_{\rm res}\tilde{\Delta}u_1(r) \\ 0 \end{pmatrix} - \frac{\sin\tilde{\delta}_{\rm res}}{\pi\langle\bar{u}_1^{(\rm reg)}|V_{1,2}|u_0\rangle}\begin{pmatrix} 0 \\ u_0(r) \end{pmatrix}, \tag{3.174}$$

where $\tilde{\Delta}u_1(r)$ is an open channel contribution which becomes $\bar{u}_1^{(\rm irr)}(r)$ beyond the range of the short-range deviations of the full potentials from the uncoupled pure Coulomb case. The bound-state wave functions u_0 are actually the wave functions $u_{n_2}(r)$ of the Rydberg series of bound states in the uncoupled closed channel 2.

Beyond the range of the short-range deviations from the uncoupled pure Coulomb case the channel 1 component u_1 is given by

$$u_1(r) = \cos\tilde{\delta}_{\mathrm{res}}\bar{\mathrm{u}}_1^{(\mathrm{reg})}(r) + \sin\tilde{\delta}_{\mathrm{res}}\bar{\mathrm{u}}_1^{(\mathrm{irr})}(r). \tag{3.175}$$

The channel 2 component $u_2(r)$ in (3.174) is

$$u_2(r) = -\frac{\sin\tilde{\delta}_{\mathrm{res}}u_0(r)}{\pi\langle\bar{\mathrm{u}}_1^{(\mathrm{reg})}|V_{1,2}|u_0\rangle} = -\frac{\sin\tilde{\delta}_{\mathrm{res}}\bar{\mathrm{u}}_{n_2}(r)}{\pi\langle\bar{\mathrm{u}}_1^{(\mathrm{reg})}|V_{1,2}|\bar{\mathrm{u}}_{n_2}\rangle}. \tag{3.176}$$

Replacing the bound-state wave functions $u_0(r) \equiv u_{\mathrm{n}_2}(r)$, which are normalized to unity, by the energy-normalized wave functions $\bar{\mathrm{u}}_{n_2}(r)$ does not introduce any further constants, because these wave functions appear both in the numerator and in the denominator of the quotients in (3.176).

The matrix element in the denominator on the far right-hand side of (3.176) depends at most weakly on energy and tends to a constant in the limit $n_2 \to \infty$. By introducing the weakly energy-dependent parameter

$$R_{1,2} = -\pi\langle\bar{\mathrm{u}}_1^{(\mathrm{reg})}\big|V_{1,2}\big|\bar{\mathrm{u}}_{n_2}\rangle, \tag{3.177}$$

Eq. (3.176) can be simplified to

$$u_2(r) = \frac{\sin\tilde{\delta}_{\mathrm{res}}}{R_{1,2}}\bar{\mathrm{u}}_{n_2}(r). \tag{3.178}$$

At the energies E_{n_2} of the resonances, $\sin\tilde{\delta}_{\mathrm{res}} = 1$ and $\cos\tilde{\delta}_{\mathrm{res}} = 0$, so the two-component wave functions solving the coupled channel equations have the properties,

$$u_1(r) \overset{r\to\infty}{\sim} \bar{\mathrm{u}}_1^{(\mathrm{irr})}(r), \qquad u_2(r) = \frac{1}{R_{1,2}}\bar{\mathrm{u}}_{n_2}(r). \tag{3.179}$$

At threshold, the energy-normalized bound-state wave functions of the Rydberg series coverging to I_2 merge into the energy-normalized regular solutions $\bar{\mathrm{u}}_2^{(\mathrm{reg})}(E)$ in the uncoupled channel 2, which is now an open channel. For $n_2 \to \infty$, the Rydberg series of solutions (3.179) merges into two-component solutions with the following asymptotic behaviour above threshold:

$$u_1(r) \overset{r\to\infty}{\sim} \bar{\mathrm{u}}_1^{(\mathrm{irr})}(r), \qquad u_2(r) \overset{r\to\infty}{\sim} \frac{\bar{\mathrm{u}}_2^{(\mathrm{reg})}(r)}{R_{1,2}}; \quad R_{1,2} = -\pi\langle\bar{\mathrm{u}}_1^{(\mathrm{reg})}\big|V_{1,2}\big|\bar{\mathrm{u}}_2^{(\mathrm{reg})}\rangle. \tag{3.180}$$

When both channels are open, there is a linearly independent two-component solution with the asymptotic properties,

$$\upsilon_1(r) \overset{r\to\infty}{\sim} \frac{\bar{\mathrm{u}}_1^{(\mathrm{reg})}(r)}{R_{2,1}}, \qquad \upsilon_2(r) \overset{r\to\infty}{\sim} \bar{\mathrm{u}}_2^{(\mathrm{irr})}(r); \quad R_{2,1} = -\pi\langle\bar{\mathrm{u}}_2^{(\mathrm{reg})}\big|V_{2,1}\big|\bar{\mathrm{u}}_1^{(\mathrm{reg})}\rangle. \tag{3.181}$$

The most general two-component solution of the coupled equations is a superposition of (3.180) and (3.181),

$$A\begin{pmatrix}u_1(r)\\u_2(r)\end{pmatrix}+B\begin{pmatrix}v_1(r)\\v_2(r)\end{pmatrix}\overset{r\to\infty}{\sim}\begin{pmatrix}\frac{B}{R_{2,1}}\bar{u}_1^{(\mathrm{reg})}(r)+A\bar{u}_1^{(\mathrm{irr})}(r)\\ \frac{A}{R_{1,2}}\bar{u}_2^{(\mathrm{reg})}(r)+B\bar{u}_2^{(\mathrm{irr})}(r)\end{pmatrix}. \tag{3.182}$$

The asymptotic phase shift of the wave function $Au_1(r)+Bv_1(r)$ in the open channel 1, relative to the phase of the regular solution $\bar{u}_1(r)$ in the *uncoupled* channel 1 is $\tilde{\delta}_1-\pi\mu_1^{\mathrm{QD}}$. Writing $-\pi\nu_1$ for $\tilde{\delta}_1$ according to (3.150) gives

$$\tilde{\delta}_1-\pi\mu_1^{\mathrm{QD}}=-\pi\left(\nu_1+\mu_1^{\mathrm{QD}}\right). \tag{3.183}$$

Channel 2 is also open, and the asymptotic phase shift of the wave function $Au_2(r)+Bv_2(r)$, relative to the phase of the regular solution $\bar{u}_2(r)$ in the *uncoupled* channel 2 is $\tilde{\delta}_2-\pi\mu_2^{\mathrm{QD}}$. Writing $-\pi\nu_2$ for $\tilde{\delta}_2$ gives

$$\tilde{\delta}_2-\pi\mu_2^{\mathrm{QD}}=-\pi\left(\nu_2+\mu_2^{\mathrm{QD}}\right). \tag{3.184}$$

In the familiar manner, the tangent of the phase (3.183) is the ratio of the coefficients of the irregular and the regular radial wave functions in the superposition constituting the channel 1 component of the right-hand side of (3.182), while the tangent of the phase (3.184) involves the channel 2 component,

$$-\tan\left[\pi\left(\nu_1+\mu_1^{\mathrm{QD}}\right)\right]=\frac{A}{B}R_{2,1},\qquad -\tan\left[\pi\left(\nu_2+\mu_2^{\mathrm{QD}}\right)\right]=\frac{B}{A}R_{1,2}. \tag{3.185}$$

Multiplying the left- and right-hand sides of these two equations gives a result which no longer contains the coefficients A and B,

$$\tan\left[\pi\left(\nu_1+\mu_1^{\mathrm{QD}}\right)\right]\tan\left[\pi\left(\nu_2+\mu_2^{\mathrm{QD}}\right)\right]=R_{2,1}R_{1,2}=|R_{2,1}|^2. \tag{3.186}$$

Equation (3.186) has the same form as Eq. (3.168), which was derived for the case $E<I_2$ where ν_2 stands for the continuous effective quantum number relative to the upper threshold I_2. The definition of the parameters $R_{1,2}$ and $R_{2,1}$ in Eqs. (3.177), (3.180) and (3.181) are consistent with the definition of $|R_{2,1}|^2$ in (3.167), because the energy-normalized bound-state wave functions $\bar{u}_{n_2}$ merge smoothly with the energy-normalized continuum wave functions $\bar{u}_2^{(\mathrm{reg})}$ at the threshold I_2.

Two-channel quantum-defect theory can be summarized for arbitrary energies in one compact equation,

$$\det\begin{pmatrix}\tan[\pi(\nu_1+\mu_1^{\mathrm{QD}})] & R_{1,2}\\ R_{2,1} & \tan[\pi(\nu_2+\mu_2^{\mathrm{QD}})]\end{pmatrix}=0. \tag{3.187}$$

The effects due to the deviation of the full interaction from the uncoupled pure Coulomb case are accounted for via the *quantum-defect parameters*, which depend at most weakly on energy. In (3.187) they are the quantum-defect functions μ_i^{QD} and

the coupling matrix element $R_{2,1} = R^*_{1,2}$. The quantity ν_i has different meanings below and above the respective channel threshold I_i,

$$\nu_i(E) = \begin{cases} \sqrt{\mathscr{R}/(I_i - E)} & \text{for } E < I_i, \\ -\tilde{\delta}_i(E)/\pi & \text{for } E > I_i. \end{cases} \tag{3.188}$$

Below both thresholds, $E < I_1, I_2$, both ν_1 and ν_2 are well defined functions of energy, and Eq. (3.187) represents a quantization condition for the bound-state energies in the perturbed Rydberg series. Between the thresholds, one function ν_i is proportional to the additional phase shift of the open-channel wave function, relative to the uncoupled pure Coulomb case, and Eq. (3.187) represents an explicit equation for this phase shift. When both channels are open, Eq. (3.157) has, for a given energy, a two-dimensional space of two-component solutions, and Eq. (3.187) represents a compatibility equation for the asymptotic phase shifts of the two open-channel wave functions of a given solution.

3.7.3 More than Two Coupled Coulombic Channels

From the formulation (3.187) of quantum-defect theory for two channels, the generalization to an arbitrary finite number N of coupled Coulombic channels seems self-evident:

$$\det \begin{pmatrix} \tan[\pi(\nu_1 + \mu_1^{\mathrm{QD}})] & R_{1,2} & \cdots & R_{1,N} \\ R_{2,1} & \tan[\pi(\nu_2 + \mu_2^{\mathrm{QD}})] & \cdots & R_{2,N} \\ \vdots & \vdots & \ddots & \vdots \\ R_{N,1} & R_{N,2} & \cdots & \tan[\pi(\nu_N + \mu_N^{\mathrm{QD}})] \end{pmatrix} = 0. \tag{3.189}$$

The weakly energy-dependent quantum-defect parameters accounting for the effects due to the deviation of the full interaction from the uncoupled pure Coulomb case now are the N quantum-defect functions μ_i^{QD} and the hermitian $N \times N$ matrix $R_{i,j}$, whose diagonal matrix elements all vanish. The functions ν_i are defined differently below and above the respective channel threshold I_i; this is as already expressed in Eq. (3.188), except that the channel index i counts N channels, not only two. A more rigorous, deductive derivation of the multichannel QDT equation (3.189) is given towards the end of this section.

When all channels are closed, Eq. (3.189) is a quantization rule for the energies of the bound states. They form a Rydberg series which converges to the lowest threshold and is perturbed by $N - 1$ coupled Rydberg series of perturbers. When just one channel, e.g. channel i, is open, Eq. (3.189) is an explicit equation for the additional phase shift $\tilde{\delta}_i = -\pi\nu_i$ of the open-channel wave function. When the number of open channels is N_{open} with $1 < N_{\mathrm{open}} \leq N$, there is an N_{open}-dimensional space of N-component solutions of the coulped radial equations, and Eq. (3.189) is

a compatibility equation for the additional phase shifts of the N_{open} open-channel wave functions of a given solution.

The simplest example for more than two channels is the three-channel case [10, 11, 19]. With the abbreviation

$$T_i = \tan\left[\pi\left(\nu_i + \mu_i^{\text{QD}}\right)\right], \tag{3.190}$$

the multichannel QDT equation (3.189) with $N = 3$ reads,

$$T_1 \det\begin{pmatrix} T_2 & R_{2,3} \\ R_{3,2} & T_3 \end{pmatrix} - R_{1,2} \det\begin{pmatrix} R_{2,1} & R_{2,3} \\ R_{3,1} & T_3 \end{pmatrix} + R_{1,3} \det\begin{pmatrix} R_{2,1} & T_2 \\ R_{3,1} & R_{3,2} \end{pmatrix} = 0. \tag{3.191}$$

Consider energies where only channel 1 is open, while channels 2 and 3 are closed. Then $T_1 = -\tan[\pi(\tilde{\delta}_1(E) - \mu_1^{\text{QD}})]$, while T_2 and T_3 are well-defined functions of energy containing the continuous effective quantum number ν_i with respect to the channel threshold I_i, as given for $E < I_i$ in (3.188). Equation (3.191) is an explicit expression for the "resonant contribution" $\tilde{\delta}_{\text{res}} = \tilde{\delta}_1 - \pi\mu_1^{\text{QD}}$ to the additional phase shift in the open channel 1,

$$\tan\left(\tilde{\delta}_1(E) - \pi\mu_1^{\text{QD}}\right) = -\frac{|R_{1,2}|^2 T_3 + |R_{1,3}|^2 T_2 - R_{1,2}R_{2,3}R_{3,1} - R_{1,3}R_{3,2}R_{2,1}}{T_2 T_3 - |R_{2,3}|^2}. \tag{3.192}$$

If coupling to the open channel 1 is neglected, then the closed channels 2 and 3 support a series of bound states at the energies given by

$$T_2 T_3 = |R_{2,3}|^2, \tag{3.193}$$

which is just the two-channel QDT equation. Assuming without loss of generality that $I_2 < I_3$, this defines a Rydberg series of bound states below I_2, which is distorted by a Rydberg series of perturbers from channel 3, as described in Sect. 3.7.2. Due to their coupling to the open channel 1, these bound states appear as a perturbed Rydberg series of Feshbach resonances, and they are characterized by the poles on the right-hand side of (3.192).

Equation (3.192) has the form

$$\tan\tilde{\delta}_{\text{res}} = -\frac{N(E)}{D(E)}, \tag{3.194}$$

with

$$\begin{aligned} N(E) &= |R_{1,2}|^2 T_3 + |R_{1,3}|^2 T_2 - R_{1,2}R_{2,3}R_{3,1} - R_{1,3}R_{3,2}R_{2,1} \\ D(E) &= T_2 T_3 - |R_{2,3}|^2, \end{aligned} \tag{3.195}$$

similar to Eq. (3.108) in Sect. 3.5.2. The resonance positions are the zeros of $D(E)$, and the energy derivative of $\tilde{\delta}_{\text{res}}$ at resonance is given by

$$\left.\frac{\mathrm{d}\delta_{\text{res}}}{\mathrm{d}E}\right|_{D=0} = \left.\frac{D'}{N}\right|_{D=0}, \tag{3.196}$$

as in (3.113). Neglecting a possible weak energy dependence of the QDT parameters μ_i^{QD} and $R_{i,j}$ gives

$$\frac{\mathrm{d}T_2}{\mathrm{d}E} = \left(1+T_2^2\right)\frac{\pi\nu_2^3}{2\mathscr{R}}, \qquad \frac{\mathrm{d}T_3}{\mathrm{d}E}\left(1+T_3^2\right)\frac{\pi\nu_3^3}{2\mathscr{R}}. \tag{3.197}$$

When $D(E) = 0$ we can insert $|R_{2,3}|^2/T_3$ for T_2, so (3.196) becomes

$$\left.\frac{\mathrm{d}\delta_{\mathrm{res}}}{\mathrm{d}E}\right|_{D=0} = \frac{\pi\nu_2^3}{2\mathscr{R}|R_{1,2}|^2}\frac{T_3^2+|R_{2,3}|^4+(1+T_3^2)|R_{2,3}|^2(\nu_3/\nu_2)^3}{(T_3-R_{2,3}R_{3,1}/R_{2,1})(T_3-R_{3,2}R_{1,3}/R_{1,2})}. \tag{3.198}$$

From Eq. (2.132) in Sect. 2.3.10, which relates the energy derivative of the phase shift to the resonance width Γ, we obtain

$$\Gamma = 2\left[\left.\frac{\mathrm{d}\delta_{\mathrm{res}}}{\mathrm{d}E}\right|_{E_{\mathrm{R}}}\right]^{-1} = \frac{4\mathscr{R}|R_{1,2}|^2}{\pi\nu_2^3}\frac{(T_3-R_{2,3}R_{3,1}/R_{2,1})(T_3-R_{3,2}R_{1,3}/R_{1,2})}{T_3^2+|R_{2,3}|^4+(1+T_3^2)|R_{2,3}|^2(\nu_3/\nu_2)^3}. \tag{3.199}$$

The interpretation of the expression (3.199) as the width of the Feshbach resonance associated with a given pole of $\tan(\tilde{\delta}_1 - \pi\mu_1^{\mathrm{QD}})$ at E_{R} assumes that this width and the widths associated with neighbouring poles are not so large that the resonances overlap strongly.

We had assumed, without loss of generality, that $I_2 < I_3$, so $\nu_3(E)$ remains finite while $\nu_2(E) \to \infty$ as the energy approaches I_2 from below. When the Rydberg series of Feshbach resonances converging to the lower closed-channel threshold I_2 is perturbed by the Rydberg series of resonances from the closed channel with the higher threshold I_3, the resonance positions are perturbed as described by Eq. (3.193), and Eq. (3.199) shows how the perturbations from channel 3 affect the associated resonance widths. The factor

$$\Gamma_0 = \frac{4\mathscr{R}|R_{1,2}|^2}{\pi\nu_2^3} \tag{3.200}$$

describes the widths expected in an unperturbed Rydberg series of Feshbach resonances, compare (3.162) in Sect. 3.7.2, while the following quotient describes the modifications due to the perturbations from channel 3. Towards the lower closed-channel threshold I_2 the ratio $\nu_3(E)/\nu_2(E)$ tends to zero, so the last term in the denominator on the right-hand side of (3.199) becomes negligible. The modified widths can then be written as

$$\Gamma = \frac{4\mathscr{R}|R_{1,2}|^2}{\pi\nu_2^3}\frac{|\varepsilon+p|^2}{1+\varepsilon^2}, \tag{3.201}$$

with

$$\varepsilon = \frac{T_3}{|R_{2,3}|^2}, \qquad p = -\frac{R_{3,1}}{R_{3,2}R_{2,1}}. \tag{3.202}$$

If the matrix $R_{i,j}$ is not only hermitian, but real and symmetric, which is the case if the quantum mechanics defined by the coupled-channel equations (3.138) is time-reversal invariant, then the parameter p is real and Eq. (3.201) represents the unperturbed widths (3.200) multiplied by a Beutler–Fano function, compare Eq. (3.90) in

Sect. 3.5.1. The shape parameter is p, and the role of the reduced energy is played by the quantity ε as defined in (3.202). It varies from $-\infty$ to $+\infty$ during each period of the tangent defining $T_3(E)$ according to (3.190), and it passes through zero at each energy of the Rydberg series of bound states in the uncoupled closed channel 3. In each such period corresponding to one perturber from the closed channel 3, there is a point of maximum width when $\varepsilon = 1/p$ and a point of vanishing width when $\varepsilon = -p$. If this point of vanishing width coincides with the position of a resonance in the perturbed series, as given by (3.193), then there actually is a resonance of vanishing width, i.e., a bound state in the continuum. The condition for this to occur is,

$$T_3 = \frac{R_{2,3}R_{3,1}}{R_{2,1}}, \qquad T_2 = \frac{|R_{2,3}|^2}{T_3} = \frac{R_{3,2}R_{2,1}}{R_{3,1}}. \tag{3.203}$$

If Eq. (3.201) is not a good description of resonance widths in the perturbed series, either because the resonances overlap too strongly or because it is not justified to neglect the term containing $(\nu_3/\nu_2)^3$ in the denominator on the right-hand side of (3.199), there nevertheless always is a bound state in the continuum when the conditions (3.203) are fulfilled. This is because the zeros of numerator and denominator on the right-hand side of (3.194) vanish simultaneously, compare discussion around Eq. (3.116) in Sect. 3.5.2.

The MQDT parameters can be derived by *ab initio* methods, at least in principle, but empirical methods based on fitting to a moderate number of experimentally or theoretically obtained benchmarks have proven very effective. Multichannel quantum-defect theory has been successfully used in a wide range of applications involving complex spectra in atomic systems [2].

Because of its general importance, we now derive Eq. (3.189) in a more rigorous, deductive way. Consider a system of N coupled Coulombic channels at an energy for which all channels are open. In the absence of coupling, the radial equation for a given channel j has a regular solution $\bar{\mathrm{u}}_j^{(\mathrm{reg})}(r)$, which we assume to be normalized in energy, and an irregular solution $\bar{\mathrm{u}}_j^{(\mathrm{irr})}(r)$, which is asymptotically shifted by a phase of $\frac{\pi}{2}$ relative to the regular solution. From (3.139) their asymptotic behaviour is,

$$\begin{aligned}
\bar{\mathrm{u}}_j^{(\mathrm{reg})}(r) &\overset{r\to\infty}{\sim} \sqrt{\frac{2\mu}{\pi\hbar^2 k_j}}\,\sin\!\left(k_j r - \eta_j \ln(2k_j r) - l_j\frac{\pi}{2} + \sigma_{l_j,j} + \pi\mu_j^{\mathrm{QD}}\right),\\
\bar{\mathrm{u}}_j^{(\mathrm{irr})}(r) &\overset{r\to\infty}{\sim} \sqrt{\frac{2\mu}{\pi\hbar^2 k_j}}\,\cos\!\left(k_j r - \eta_j \ln(2k_j r) - l_j\frac{\pi}{2} + \sigma_{l_j,j} + \pi\mu_j^{\mathrm{QD}}\right).
\end{aligned} \tag{3.204}$$

Here $\pi\mu_j^{\mathrm{QD}}$ represents the background phase shift due to the "diagonal" potential and l_j is the orbital angular momentum quantum number in the uncoupled channel j.

There is an N-dimensional space of N-component solutions of the coupled radial equations and a basis of this space can be defined by the N solutions $U^{(i)}$ whose components are characterized by the following asymptotic behaviour:

$$u_j^{(i)}(r) \overset{r\to\infty}{\sim} \delta_{i,j}\bar{\mathrm{u}}_j^{(\mathrm{reg})}(r) + (1-\delta_{i,j})R_{i,j}\bar{\mathrm{u}}_j^{(\mathrm{irr})}(r). \tag{3.205}$$

The most general solution of the coupled radial equations is a superposition

$$U = \sum_{i=1}^{N} Z_i U^{(i)} \tag{3.206}$$

of these basis solutions, defined by the N coefficients Z_i. The asymptotic behaviour of the j-th component of the solution (3.206) is

$$u_j(r) = \sum_{i=1}^{N} Z_i\, u_j^{(i)}(r) \overset{r\to\infty}{\sim} Z_j\bar{\mathrm{u}}_j^{(\mathrm{reg})}(r) + \left(\sum_{i\neq j} Z_i R_{i,j}\right)\bar{\mathrm{u}}_j^{(\mathrm{irr})}(r). \tag{3.207}$$

The asymptotic phase shift of the wave function in the open channel j relative to the background phase shift already contained in the definition of $\bar{\mathrm{u}}_j^{(\mathrm{reg})}(r)$ is $\tilde{\delta}_j - \pi\mu_j^{\mathrm{QD}} = -\pi(\nu_j + \mu_j^{\mathrm{QD}})$, and the tangent of this relative phase shift is the ratio of the coefficients of $\bar{\mathrm{u}}_j^{(\mathrm{irr})}(r)$ and $\bar{\mathrm{u}}_j^{(\mathrm{reg})}(r)$ in (3.207),

$$\begin{aligned} &\tan\left[\pi\left(\nu_j + \mu_j^{\mathrm{QD}}\right)\right] = -\frac{1}{Z_j}\sum_{i\neq j} Z_i R_{i,j} \\ &\quad\Longleftrightarrow\quad \tan\left[\pi\left(\nu_j + \mu_j^{\mathrm{QD}}\right)\right]Z_j + \sum_{i\neq j} Z_i R_{i,j} = 0. \end{aligned} \tag{3.208}$$

The formulation on the right-hand side of Eq. (3.208) exposes the nature of the equations for the tangents of the relative phase shifts as a homogeneous system of linear equations for the coefficients Z_j. The matrix defining the system is precisely the matrix appearing on the left-hand side of (3.189), and the condition that the determinant of this matrix should vanish is just the condition for the existence of nontrivial solutions.

When some of the N channels are closed, the dimension of the space of N-component solutions of the coupled radial equations (3.138) is equal to the number N_{open} of open channels, $N_{\mathrm{open}} < N$. The radial wave functions in the open channels behave asymptotically as given by (3.207), but in a closed channel k the radial wave function $u_k(r)$ must obey bound-state boundary conditions. At distances beyond the range of the short-range potentials $V_{i,j}$, $u_k(r)$ is proportional to the appropriate Whittaker function,

$$u_k(r) \propto W_{|\eta_k|,l_k+\frac{1}{2}}(2\kappa_k r) \overset{\kappa_k r\to\infty}{\propto} (2\kappa_k r)^{|\eta_k|}\mathrm{e}^{-\kappa_k r}, \tag{3.209}$$

compare Eq. (2.245) in Sect. 2.5.4. Sufficiently close to the respective threshold I_k, the bound-state wave function $u_k(r)$ has a finite but large number of oscillations, which are shifted by a phase $\tilde{\delta}$ with respect to the bound states of similar

energy in the pure Coulomb potential. These shifts are related to the effective quantum number $\tilde{n}_k$ by $\tilde{\delta} = -\pi\tilde{n}_k (\mathrm{mod}\,\pi)$, as discussed in Sect. 2.5.4 in connection with Eq. (2.256). At the bound state energy corresponding to the inverse penetration depth κ_k in channel k, the effective quantum number $\tilde{n}_k$ is equal to the modulus $|\eta_k|$ of the Sommerfeld parameter in channel k, compare Eq. (2.252), so the phase $\tilde{\delta}$ is not arbitrary but must fulfill the relation

$$\tilde{\delta} = -\pi\tilde{n}_k = -\pi\sqrt{\frac{\mathscr{R}}{I_k - E}} \equiv -\pi\,\nu_k(E) \pmod{\pi}. \tag{3.210}$$

In each of the $N - N_{\mathrm{open}}$ closed channels k, $E < I_k$, the quantity $\nu_k(E)$ stands for a well defined function of energy, and the multichannel QDT equation (3.189) represents a compatibility equation for the N_{open} additional phase shifts $\tilde{\delta}_i$ in the open-channel wave functions of a given N-component solution of the coupled radial equations (3.138).

The open-channel part of the matrix $R_{i,j}$ and the open-channel quantum-defect functions μ_i^{QD} can be related to the reactance matrix $\tilde{\mathbf{K}}$, as defined via (3.140) in Sect. 3.6.2. This also establishes a relation to the scattering matrix $\tilde{\mathbf{S}}$, which is related to $\tilde{\mathbf{K}}$ via (3.143).

In order to relate the parameters of multichannel quantum-defect theory to the reactance matrix, we express the radial basis functions (3.204) in terms of the energy-normalized regular Coulomb functions $\bar{\mathrm{F}}_j$ and the corresponding irregular Coulomb functions $\bar{\mathrm{G}}_j$,

$$\begin{aligned} \bar{\mathrm{u}}_j^{(\mathrm{reg})}(r) &\overset{r\to\infty}{\sim} \cos\bigl(\pi\mu_j^{(\mathrm{QD})}\bigr)\bar{\mathrm{F}}_j + \sin\bigl(\pi\mu_j^{(\mathrm{QD})}\bigr)\bar{\mathrm{G}}_j \\ \bar{\mathrm{u}}_j^{(\mathrm{irr})}(r) &\overset{r\to\infty}{\sim} \cos\bigl(\pi\mu_j^{(\mathrm{QD})}\bigr)\bar{\mathrm{G}}_j - \sin\bigl(\pi\mu_j^{(\mathrm{QD})}\bigr)\bar{\mathrm{F}}_j. \end{aligned} \tag{3.211}$$

For easier readability we suppress all subscripts except for the channel label j, which actually stands for $\{j\} \equiv j, l', m'$, see comment after Eq. (3.157).

With the abbreviations μ_j^{C} for $\cos(\pi\mu_j^{(\mathrm{QD})})$ and μ_j^{S} for $\sin(\pi\mu_j^{(\mathrm{QD})})$ the asymptotic behaviour of the j-th component (3.207) of the general solution (3.206) is

$$\begin{aligned} u_j(r) &\overset{r\to\infty}{\sim} \bigl[\mu_j^{\mathrm{C}}\bar{\mathrm{F}}_j + \mu_j^{\mathrm{S}}\bar{\mathrm{G}}_j\bigr]Z_j + \bigl[\mu_j^{\mathrm{C}}\bar{\mathrm{G}}_j - \mu_j^{\mathrm{S}}\bar{\mathrm{F}}_j\bigr]\sum_{i\neq j} Z_i R_{i,j} \\ &= \left[\mu_j^{\mathrm{C}} Z_j - \mu_j^{\mathrm{S}}\sum_{i\neq j} Z_i R_{i,j}\right]\bar{\mathrm{F}}_j + \left[\mu_j^{\mathrm{S}} Z_j + \mu_j^{\mathrm{C}}\sum_{i\neq j} Z_i R_{i,j}\right]\bar{\mathrm{G}}_j. \end{aligned} \tag{3.212}$$

With the appropriate choice of coefficients Z_i, the solution (3.206) with the components (3.212) corresponds to a basis solution $\tilde{U}^{(k)}$, whose components are characterized by the asymptotic behaviour (3.140),

$$u_j^{(k)}(r) \overset{r\to\infty}{\sim} \delta_{k,j}\bar{\mathrm{F}}_j + \tilde{K}_{k,j}\bar{\mathrm{G}}_j. \tag{3.213}$$

The label "k" in (3.213) corresponds to "i, l, m" in (3.140) and the label "j" in (3.213) to "j, l', m'" in (3.140).

For each of the N linearly independent N-component solutions $\tilde{U}^{(k)}$, the coefficients of $\bar{\mathrm{F}}_j$ and $\bar{\mathrm{G}}_j$ in (3.213) must agree with the corresponding coefficients in (3.212), as generated by the N numbers $Z_i^{(k)}$,

$$\mu_j^{\mathrm{C}} Z_j^{(k)} - \mu_j^{\mathrm{S}} \sum_{i \neq j} Z_i^{(k)} R_{i,j} = \delta_{k,j}, \qquad \mu_j^{\mathrm{S}} Z_j^{(k)} + \mu_j^{\mathrm{C}} \sum_{i \neq j} Z_i^{(k)} R_{i,j} = \tilde{K}_{k,j}. \quad (3.214)$$

We introduce the notations $\boldsymbol{\mu}^{\mathrm{C}}$ and $\boldsymbol{\mu}^{\mathrm{S}}$ for the diagonal $N \times N$ matrices with the elements μ_i^{C} and with the elements μ_i^{S}, respectively, $\mathbf{R}$ for the matrix with the off-diagonal elements $R_{i,j}$ and zeros on the diagonal, and $\mathbf{Z}$ for the matrix in which each row consists of the coefficients $Z_i^{(k)}$ defining one of the N-component solutions $\tilde{U}^{(k)}$. The equations (3.214) can then be written in matrix form,

$$\mathbf{Z}\big(\boldsymbol{\mu}^{\mathrm{C}} - \mathbf{R}\boldsymbol{\mu}^{\mathrm{S}}\big) = \mathbf{1}, \qquad \mathbf{Z}\big(\boldsymbol{\mu}^{\mathrm{S}} + \mathbf{R}\boldsymbol{\mu}^{\mathrm{C}}\big) = \tilde{\mathbf{K}}. \quad (3.215)$$

Elimination of $\mathbf{Z}$ leads to an explicit relation between the matrix $\mathbf{R}$ and the reactance matrix $\tilde{\mathbf{K}}$,

$$\tilde{\mathbf{K}} = \big(\boldsymbol{\mu}^{\mathrm{C}} - \mathbf{R}\boldsymbol{\mu}^{\mathrm{S}}\big)^{-1}\big(\boldsymbol{\mu}^{\mathrm{S}} + \mathbf{R}\boldsymbol{\mu}^{\mathrm{C}}\big). \quad (3.216)$$

The essential difference in the definition (3.205) of the matrix elements $R_{i,j}$ and the definition (3.140) for the elements $\tilde{K}_{i,j}$ of the reactance matrix is, that the effect of short-range deviations from the pure Coulomb potentials in the uncoupled equations is, in (3.205), already accounted for by the respective additional background phase shifts $\pi\mu_i^{\mathrm{QD}}$ in the definition (3.204) of the regular and irregular reference wave functions. For this reason, the matrix $\mathbf{R}$ is called the *phase-shifted reactance matrix*. In the absence of channel coupling, the matrix $\mathbf{R}$ vanishes and $\tilde{\mathbf{K}}$ is a diagonal matrix with $\tilde{K}_{i,i} = \sin(\pi\mu_i^{(\mathrm{QD})})/\cos(\pi\mu_i^{(\mathrm{QD})}) = \tan(\pi\mu_i^{(\mathrm{QD})})$. If we neglect the background phase shifts, $\pi\mu_i^{\mathrm{QD}} = 0$, then $\boldsymbol{\mu}^{\mathrm{C}}$ becomes the unit matrix while $\boldsymbol{\mu}^{\mathrm{S}}$ vanishes, so $\tilde{\mathbf{K}} = \mathbf{R}$.

References

1. Amos, K., von Dortmans, P.J., Geramb, H.V., Karataglidis, S., Raynal, J.: Nucleon-nucleus scattering: a microscopic nonrelativistic approach. Adv. Nucl. Phys. **25**, 275 (2000)
2. Aymar, M., Greene, C.H., LucKoenig, E.: Multichannel Rydberg spectroscopy of complex atoms. Rev. Mod. Phys. **68**, 1015 (1996)
3. Auerbach, N., Zevelinsky, V.: Doorway states in nuclear reactions as a manifestation of the "super-radiant" mechanism. Nucl. Phys. A **781**, 67 (2007)
4. Auerbach, N., Zevelinsky, V.: Super-radiant dynamics, doorways and resonances in nuclei and other open mesoscopic systems. Rep. Prog. Phys. **74**, 106301 (2011)
5. Barrett, R.F., Robson, B.A., Tobocman, W.: Calculable methods for many-body scattering. Rev. Mod. Phys. **55**, 155 (1983)
6. Burke, P.G., Taylor, A.J.: The excitation of He^+ by electron impact. J. Phys. B **2**, 44 (1969)
7. Feshbach, H.: Unified theory of nuclear reactions. Ann. Phys. **5**, 357 (1958)
8. Feshbach, H.: Unified theory of nuclear reactions II. Ann. Phys. **19**, 287 (1962)
9. Friedrich, H., Wintgen, D.: Interfering resonances and bound states in the continuum. Phys. Rev. A **32**, 3231 (1985)

10. Gounand, F., Gallagher, T.F., Sandner, W., Safinya, K.A., Kachru, R.: Interaction between two Rydberg series of autoionizing levels in barium. Phys. Rev. A **27**, 1925 (1983)
11. Giusti-Suzor, A., Lefebvre-Brion, H.: Theoretical study of complex resonances near ionization thresholds: application to the N_2 photoionization spectrum. Phys. Rev. A **30**, 3057 (1984)
12. Lejeune, A., Mahaux, C.: Wave functions near resonance and R-matrix expansion. Nucl. Phys. A **145**, 613 (1970)
13. Sadreev, A.F., Bulgakov, E.N., Rotter, I.: Bound states in the continuum in open quantum billiards with a variable shape. Phys. Rev. B **73**, 235342 (2006)
14. Solis, B., Ladrón de Guevara, M.L., Orellana, P.A.: Friedel phase discontinuity and bound states in the continuum in quantum dot systems. Phys. Lett. A **372**, 4736 (2008)
15. Silva, R.E.F., Rivière, P., Martin, F.: Autoionizing decay of H_2 doubly excited states by using xuv-pump–infrared-probe schemes with trains of attosecond pulses. Phys. Rev. A **85**, 063414 (2012)
16. Starace, A.: Absolute line strengths by analysis of Lu–Fano plots with application to excited state transitions in neon. J. Phys. B **6**, 76 (1973)
17. Taylor, J.R.: Scattering Theory: the Quantum Theory of Nonrelativistic Collisions. Wiley, New York (1972)
18. Taylor, H.S., Nazaroff, G.V., Golebiewski, A.: Qualitative aspects of resonances in electron–atom and electron–molecule scattering, excitation, and reactions. J. Chem. Phys. **45**, 2872 (1966)
19. Wintgen, D., Friedrich, H.: Perturbed Rydberg series of autoionizing resonances. Phys. Rev. A **35**, 1628 (1987)
20. Wang, H.W., Lu, X., Sun, X.M., Cai, Z.T., Feng, D.C.: New calculation method on the lifetime of the reactive scattering resonance states. Chem. Phys. Lett. **443**, 369 (2007)

Chapter 4
Special Topics

4.1 Deep Potentials Falling off Faster than $1/r^2$ Asymptotically

As already discussed in Chap. 2, the characteristic features of scattering by a potential, in particular at near-threshold energies, depend crucially on whether its fall-off at large distances is faster or slower than $1/r^2$. In contrast to long-range Coulombic potentials, which support infinite Rydberg series of bound states if the Coulombic tail is attractive, potentials falling off faster than $1/r^2$ support at most a finite number of bound states. A special situation arises if the potential falls off faster than $1/r^2$, while being so deep that the number of bound states is very large. In this case, there is a range of energies around threshold, excluding the immediate near-threshold regime, where semiclassical approximations are quite accurate and able to describe the systematics of scattering phase shifts and bound-state energy progressions. In the immediate near-threshold regime, however, quantum mechanical effects, as typically expressed in Wigner's threshold law, are dominant. An accurate treatment of deep potentials falling off faster than $1/r^2$ must include a reliable account of this extreme quantum regime in the immediate vicinity of the threshold.

Since the transition between the semiclassical regime away from threshold and the extreme quantum regime at threshold is most easily demonstrated for the bound states below threshold, we start with the theory of near-threshold quantization in Sect. 4.1.1. Above-threshold continuum states are treated in the subsequent subsections on quantum reflection (Sect. 4.1.2) and scattering (Sect. 4.1.3). The treatment in Sects. 4.1.1 to 4.1.3 is restricted to the case of vanishing angular momentum. The implications of nonvanishing angular momentum are explained in Sect. 4.1.4.

4.1.1 Near-Threshold Quantization

Consider a potential $V(r)$ which falls off faster than $1/r^2$ at large distances and is so deeply attractive at small distances that it supports a large, albeit finite number

H. Friedrich, *Scattering Theory*, DOI 10.1007/978-3-662-48526-2_4

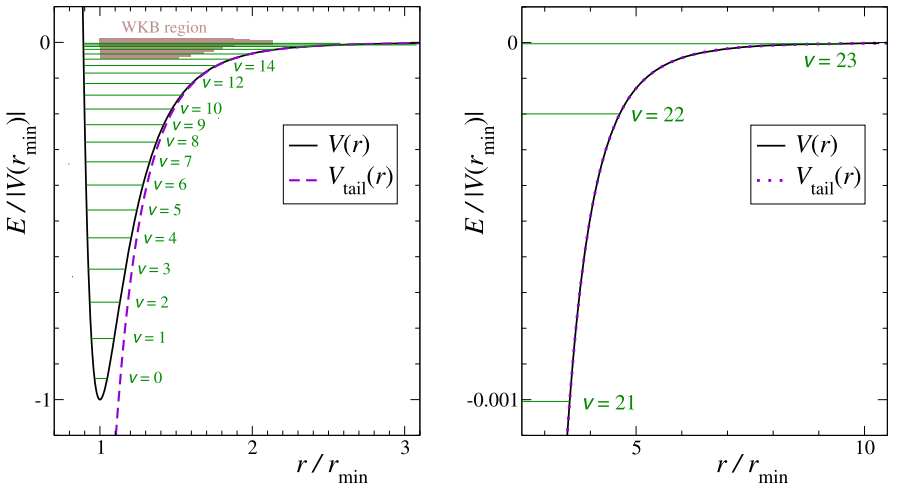

Fig. 4.1 Deep potential falling off faster than $1/r^2$ at large distances. The example is actually the Lennard–Jones potential (2.298) with $B_{\mathrm{LJ}} = 10^4$, which supports 24 bound states, $\upsilon = 0, 1, 2, \ldots, 23$. The brown shaded area in the left-hand panel schematically indicates where the WKB approximation is accurate at near-threshold energies

of bound states. An example with 24 bound states is shown in Fig. 4.1. Since such potentials typically describe the interatomic interaction in diatomic molecules, we adopt the molecular physics notation and use the letter "υ" for "vibrational" to label the bound states. The potential in Fig. 4.1 actually corresponds to the Lennard–Jones potential (2.298) already discussed in Sect. 2.6.5, and the dimensionless parameter B_{LJ}, which is defined by Eq. (2.299) and determines the quantum mechanical properties of the potential, is $B_{\mathrm{LJ}} = 10^4$ in the present case. The theory below is, however, very general and does not rely on any special properties of the potential, except that it should be deep and fall off faster than $1/r^2$ at large distances.

In the bound-state regime, the total energy is negative and related to the asymptotic inverse penetration depth κ by

$$E = -\frac{\hbar^2\kappa^2}{2\mu}. \tag{4.1}$$

Since the potential is deep, a total energy near threshold implies that the kinetic energy is large in a region of r-values between the inner classical turning point $r_{\mathrm{in}}(E)$ and the outer classical turning point $r_{\mathrm{out}}(E)$. This justifies the assumption, that there is a "WKB region" between $r_{\mathrm{in}}(E)$ and $r_{\mathrm{out}}(E)$, where the condition formulated as Eq. (2.141) in Sect. 2.4.1 is well fulfilled, so the solution of the radial Schrödinger equation is accurately given by the WKB representation,

$$u(r) \propto \frac{1}{\sqrt{p(E;r)}} \cos\left[\frac{1}{\hbar}\int_{r_{\mathrm{in}}(E)}^{r} p\big(E;r'\big)\mathrm{d}r' - \frac{\phi_{\mathrm{in}}(E)}{2}\right]. \tag{4.2}$$

For vanishing angular momentum, the local classical momentum (2.136) is

$$p(E;r) = \sqrt{2\mu\big[E - V(r)\big]}; \tag{4.3}$$

it is real and positive in the classically allowed region $V(r) < E$. The phase $\phi_{\rm in}(E)$ is the reflection phase at the classical turning point $r_{\rm in}(E)$, as introduced in Sect. 2.4.2, see Eq. (2.145). Reflection phases are chosen to be $\frac{\pi}{2}$ in conventional WKB theory [11, 55], but allowing them to depend on energy makes it possible to use WKB wave functions to derive results which are highly accurate, or even exact, far away from the semiclassical limit [35]. The condition that the right-hand side of (4.2) accurately represents the exact wave function $u(r)$ for r-values in the WKB region defines $\phi_{\rm in}(E)$.

An alternative and equally valid WKB representation of $u(r)$ is obtained by choosing the outer classical turning point $r_{\rm out}(E)$ as point of reference:

$$u(r) \propto \frac{1}{\sqrt{p(E;r)}} \cos\left[\frac{1}{\hbar}\int_r^{r_{\rm out}(E)} p\big(E;r'\big)\mathrm{d}r' - \frac{\phi_{\rm out}(E)}{2}\right], \tag{4.4}$$

and $\phi_{\rm out}(E)$ is the reflection phase at $r_{\rm out}(E)$. Compatibility of (4.2) and (4.4) requires that the argument of the cosines be equal modulo π, up to a sign, for all r-values in the WKB region. This leads to a quantization condition for the bound-state energies E_υ:

$$\frac{1}{\hbar}\int_{r_{\rm in}(E_\upsilon)}^{r_{\rm out}(E_\upsilon)} p(E_\upsilon;r)\mathrm{d}r = \upsilon\pi + \frac{\phi_{\rm in}(E_\upsilon)}{2} + \frac{\phi_{\rm out}(E_\upsilon)}{2}, \quad \upsilon \text{ integer.} \tag{4.5}$$

If we take both reflection phases to be equal to $\frac{\pi}{2}$, then the right-hand side of (4.5) becomes $(\upsilon + \frac{1}{2})\pi$, as in the conventional Bohr-Sommerfeld quantization rule [55].

At threshold, $E = 0$, the condition (4.5) with integer υ is fulfilled only if there is a bound state exactly at threshold. For the general case, we write

$$\frac{1}{\hbar}\int_{r_{\rm in}(0)}^{\infty} p(E=0;r)\mathrm{d}r = \upsilon_{\rm D}\pi + \frac{\phi_{\rm in}(0)}{2} + \frac{\phi_{\rm out}(0)}{2}, \tag{4.6}$$

where $\upsilon_{\rm D}$ is the *threshold quantum number*, which is in general non-integer. The present theory is especially suited for the description of diatomic molecules or molecular ions, where the bound-to-continuum threshold is the dissociation threshold, hence the subscript "D".

Subtracting Eq. (4.5) from (4.6) yields the *quantization rule*,

$$\upsilon_{\rm D} - \upsilon = F(E_\upsilon), \tag{4.7}$$

with the *quantization function* $F(E)$ given by

$$F(E) = \frac{1}{\pi\hbar}\left[\int_{r_{\rm in}(0)}^{\infty} p(0;r)\mathrm{d}r - \int_{r_{\rm in}(E)}^{r_{\rm out}(E)} p(E;r)\mathrm{d}r\right] - \frac{\phi_{\rm in}(0)-\phi_{\rm in}(E)}{2\pi} - \frac{\phi_{\rm out}(0)-\phi_{\rm out}(E)}{2\pi}. \tag{4.8}$$

By definition, $F(E)$ vanishes at threshold,

$$F(E=0) = 0. \tag{4.9}$$

Since the bound-state energies form a discrete finite set, it is always possible to find a smooth function $F(E)$ with (4.9) such that (4.7) is fulfilled at all bound-state energies E_υ. The explicit expression (4.8) is trivially valid, if we allow appropriate values of $\phi_{\rm in}(E)$ and $\phi_{\rm out}(E)$. If, at a given energy E, there is a WKB region between the inner and outer classical turning points where the WKB approximation is sufficiently accurate, then the reflection phases $\phi_{\rm in}(E)$ and $\phi_{\rm out}(E)$ can be determined precisely via (4.2) and (4.4), respectively.

The leading near-threshold energy dependence of the quantization function (4.8) is a property of the large-distance behaviour of the potential. To be specific, we assume that the potential is accurately given at large distances by a reference potential, the "tail potential" $V_{\rm tail}(r)$,

$$V(r) \overset{r \text{ large}}{\sim} V_{\rm tail}(r). \tag{4.10}$$

As reference potential, $V_{\rm tail}(r)$ is defined for all $r > 0$, but it only represents the true interaction for large distances. The phrase "r large" over the "$\sim$" sign in (4.10) has been chosen deliberately in order to emphasize that, in general, it is not just the leading asymptotic behaviour of $V(r)$ that is important. The radial Schrödinger equation with the reference potential $V_{\rm tail}(r)$ alone and vanishing angular momentum reads

$$-\frac{\hbar^2}{2\mu}\frac{\mathrm{d}^2u}{\mathrm{d}r^2} + V_{\rm tail}(r)u(r) = Eu(r). \tag{4.11}$$

Being an approximation to the full potential at large distances, the reference potential $V_{\rm tail}(r)$ falls off faster than $1/r^2$ for $r \to \infty$. At small distances, the full interaction is not well described by the reference potential $V_{\rm tail}(r)$, and its precise form is usually not well known anyhow. In the following we choose $V_{\rm tail}(r)$ such that it diverges to $-\infty$ more rapidly than $-1/r^2$ for $r \to 0$. This has the advantage that the WKB representations of the solutions of (4.11), at any energy E, become increasingly accurate for decreasing r and are, in fact, exact in the limit $r \to 0$. This can be confirmed by verifying that the quantality function (2.139) vanishes for $r \to 0$ when the potential is more singular than $1/r^2$ in this limit.

As for the repulsive inverse-power potentials discussed in Sect. 2.4.2, the proximity to the semiclassical or anticlassical limits can be estimated via the value of a typical classically defined action in units of $\hbar$. Such a classical action is provided by

the product of the momentum-like quantity $\hbar\kappa$ and the outer classical turning point $r_{\rm out}(E)$, which is the same for the full interaction and for the reference potential $V_{\rm tail}(r)$ at near-threshold energies and diverges to infinity at threshold,

$$r_{\rm out}(E) \overset{\kappa\to 0}{\longrightarrow} \infty. \tag{4.12}$$

The typical action $\hbar\kappa r_{\rm out}(E)$ in units of $\hbar$ is thus $\kappa r_{\rm out}(E)$, a quantity that has been called the "reduced classical turning point" [85]. With $r^2 V_{\rm tail}(r) \overset{r\to\infty}{\longrightarrow} 0$ it follows from (4.12) that

$$\begin{aligned} \big|V_{\rm tail}\big(r_{\rm out}(E)\big)\big| r_{\rm out}(E)^2 = \frac{\hbar^2\kappa^2}{2\mu} r_{\rm out}(E)^2 \overset{\kappa\to 0}{\longrightarrow} 0 \\ \Longrightarrow \quad \kappa r_{\rm out}(E) \overset{\kappa\to 0}{\longrightarrow} 0. \end{aligned} \tag{4.13}$$

The threshold $E = 0$ represents the anticlassical or extreme quantum limit of the Schrödinger equation (4.11). For the singular attractive reference potential $V_{\rm tail}(r)$, the outer classical turning point moves towards the origin for $E \to -\infty$,

$$r_{\rm out}(E) \overset{\kappa\to\infty}{\longrightarrow} 0, \tag{4.14}$$

and with $r^2 V_{\rm tail}(r) \overset{r\to 0}{\longrightarrow} -\infty$ it follows that

$$\big|V_{\rm tail}\big(r_{\rm out}(E)\big)\big| r_{\rm out}(E)^2 = \frac{\hbar^2\kappa^2}{2\mu} r_{\rm out}(E)^2 \overset{\kappa\to\infty}{\longrightarrow} \infty \quad \Longrightarrow \quad \kappa r_{\rm out}(E) \overset{\kappa\to\infty}{\longrightarrow} \infty. \tag{4.15}$$

The semiclassical limit of the Schrödinger equation (4.11) is at $\kappa \to \infty$, i.e. for large binding energies. How close the semiclassical limit is approached in a realistic potential well depends on its depth.

The quantization function (4.8) contains a contribution $F_{\rm tail}(E)$, which is determined solely by the reference potential $V_{\rm tail}(r)$,

$$\begin{aligned} F_{\rm tail}(E) = \lim_{r_{\rm in}\to 0} \frac{1}{\pi\hbar}\left[\int_{r_{\rm in}}^{r_{\rm out}(0)} p_{\rm tail}(0;r)\mathrm{d}r - \int_{r_{\rm in}}^{r_{\rm out}(E)} p_{\rm tail}(E;r)\mathrm{d}r\right] \\ - \frac{\phi_{\rm out}(0) - \phi_{\rm out}(E)}{2\pi}, \end{aligned} \tag{4.16}$$

where $p_{\rm tail}$ is the local classical momentum defined with $V_{\rm tail}(r)$,

$$p_{\rm tail}(E;r) = \sqrt{2\mu\big[E - V_{\rm tail}(r)\big]}. \tag{4.17}$$

As the inner classical turning point $r_{\rm in}$ tends to zero, the action integrals in (4.16) actually diverge, but their difference remains well defined in the limit. The tail part (4.16) of the quantization function contains no contribution from the inner reflection phases, because the wave functions become independent of energy for $r \to 0$ so the difference $\phi_{\rm in}(0) - \phi_{\rm in}(E)$ vanishes for $r_{\rm in} \to 0$.

In addition to the tail contribution $F_{\text{tail}}(E)$, the quantization function contains a contribution $F_{\text{sr}}(E)$ arising from the deviation of the full interaction from the reference potential $V_{\text{tail}}(r)$ at small distances:

$$F(E) = F_{\text{tail}}(E) + F_{\text{sr}}(E). \tag{4.18}$$

Since the full quantization function $F(E)$ vanishes at threshold according to (4.9), and since $F_{\text{tail}}(E = 0)$ is obviously zero, the same must hold for $F_{\text{sr}}(E = 0)$. Furthermore, $F_{\text{sr}}(E)$ is defined in the short-range region of the potential, where the bound-to-continuum threshold is not an outstanding value of the energy, so it must be a smooth function of energy near threshold. Hence we can write

$$F_{\text{sr}}(E) \overset{\kappa \to 0}{\sim} \gamma_{\text{sr}} E + O\left(E^2\right), \tag{4.19}$$

where γ_{sr} is a constant with the dimension of an inverse energy.

As will be seen in the following, the leading near-threshold behaviour of $F_{\text{tail}}(E)$ is of lower order than E, so this is also the leading near-threshold behaviour of the full quantization function $F(E)$. The short-range contribution $F_{\text{sr}}(E)$ is of higher order, namely $O(E)$, and its magnitude depends on how accurately the reference potential $V_{\text{tail}}(r)$ describes the full interaction at finite distances. Its influence is small if $V_{\text{tail}}(r)$ is a good approximation of the full interaction down to distances where the WKB representation, on which the definition of $F_{\text{tail}}(E)$ is based, accurately describes the solutions of Eq. (4.11). Since the WKB approximation breaks down at the outer classical turning point $r_{\text{out}}(E)$, this implies that the reference potential be a good approximation of the full interaction down to distances somewhat smaller than $r_{\text{out}}(E)$.

If the quantization function is known accurately for a reasonable range of near-threshold energies, then a small number of energy eigenvalues in this range can be used to complement the spectrum and extrapolate to the dissociation threshold. This can, for example, make it possible to reliably predict the energy of the dissociation threshold from the relative separations of a few observed energy levels some distance away from threshold.

With the quantization function decomposed into a tail contribution and a short-range part as in (4.18), and with the ansatz (4.19) for the short-range part, the quantization rule (4.7) can be rewritten as

$$\upsilon + F_{\text{tail}}(E_\upsilon) = \upsilon_{\text{D}} - F_{\text{sr}}(E) \overset{E \to 0}{\sim} \upsilon_{\text{D}} - \gamma_{\text{sr}} E_\upsilon. \tag{4.20}$$

As expressed on the far right of (4.20), the effects of the short-range deviation of the full interaction from the reference potential $V_{\text{tail}}(r)$ are contained in two parameters, the threshold quantum number υ_{D} and the short-range correction coefficient γ_{sr}; the next term is of order E^2. According to (4.20), a plot of $\upsilon + F_{\text{tail}}(E_\upsilon)$ against E_υ should approach a straight-line behaviour towards threshold; υ_{D} and γ_{sr} can be deduced from the interception of this line with the ordinate and the gradient of the line, respectively.

The decomposition (4.18) of the full quantization function into a tail contribution and a short-range part and the representation (4.20) of the quantization rule are always valid. There is *no* semiclassical approximation involved, even though the tail contribution $F_{\rm tail}(E)$ to the quantization function is expressed in tems of WKB wave functions. For the short-range correction term to be small, however, the deviation of the full interaction from the reference potential $V_{\rm tail}(r)$ should be restricted to sufficiently small distances, at which the WKB representations of the solutions of Eq. (4.11) are accurate.

The near-threshold behaviour of $F_{\rm tail}(E)$ is crucially determined by the near-threshold energy dependence of the outer reflection phase. This can be derived under very general conditions, as described in detail in [76] and summarized below.

The solution of (4.11) obeying bound state boundary conditions,

$$u^{(\kappa)}(r) \overset{r\to\infty}{\sim} \mathrm{e}^{-\kappa r}, \tag{4.21}$$

is accurately the represented for $r \to 0$ by the WKB expression

$$u^{(\kappa)}(r) \overset{r\to 0}{\sim} \frac{\mathscr{D}(\kappa)}{\sqrt{p_{\rm tail}(E;r)}} \cos\left(\frac{1}{\hbar}\int_r^{r_{\rm out}(E)} p_{\rm tail}\big(E;r'\big)\mathrm{d}r' - \frac{\phi_{\rm out}(E)}{2}\right). \tag{4.22}$$

Guided by the derivation of the effective-range expansion in Sect. 2.3.8, we introduce two wave functions $u^{(\kappa)}(r)$ and $u^{(0)}(r)$ which solve Eq. (4.11) at the energies $E = -\hbar^2\kappa^2/(2\mu)$ and $E = 0$, respectively. We also introduce two solutions $w^{(\kappa)}$ and $w^{(0)}$, which have the same large-r boundary conditions, but are solutions of the free equation, without $V_{\rm tail}(r)$,

$$\begin{aligned} &w^{(\kappa)}(r) = \mathrm{e}^{-\kappa r}, \qquad w^{(0)}(r) \equiv 1, \\ &u^{(\kappa)}(r) \overset{r\to\infty}{\sim} w^{(\kappa)}(r), \qquad u^{(0)}(r) \overset{r\to\infty}{\sim} w^{(0)}(r). \end{aligned} \tag{4.23}$$

From the radial Schrödinger equation we obtain

$$\int_{r_l}^{r_u} \big(u^{(\kappa)}u^{(0)\prime\prime} - u^{(\kappa)\prime\prime}u^{(0)}\big)\mathrm{d}r = \big[u^{(\kappa)}u^{(0)\prime} - u^{(\kappa)\prime}u^{(0)}\big]_{r_l}^{r_u} = -\kappa^2 \int_{r_l}^{r_u} u^{(\kappa)}u^{(0)}\mathrm{d}r \tag{4.24}$$

for arbitrary lower and upper integration limits r_l and r_u. The contribution of the upper integration limit r_u to the square bracket in the middle part of (4.24) vanishes in the limit $r_u \to \infty$, because of the exponential decay of $u^{(\kappa)}(r)$ at large r. The contribution from the lower integration limit r_l follows from the WKB representation of the wave function (4.22) and its derivative,

$$\begin{aligned} u^{(\kappa)\prime}(r) = \frac{\mathscr{D}(\kappa)}{\sqrt{p_{\rm tail}(E;r)}}\Bigg[&-\frac{1}{2}\frac{p'_{\rm tail}(E;r)}{p_{\rm tail}(E;r)} \cos\left(\frac{1}{\hbar}\int_r^{r_{\rm out}(E)} p_{\rm tail}\big(E;r'\big)\mathrm{d}r' - \frac{\phi_{\rm out}(E)}{2}\right) \\ &+ \frac{p_{\rm tail}(E;r)}{\hbar} \sin\left(\frac{1}{\hbar}\int_r^{r_{\rm out}(E)} p_{\rm tail}\big(E;r'\big)\mathrm{d}r' - \frac{\phi_{\rm out}(E}{2}\right)\Bigg]. \end{aligned} \tag{4.25}$$

Equations (4.22) and (4.25) also apply for $u^{(0)}$ if we insert $E = 0$. Since $V_{\text{tail}}(r)$ is more singular than $-1/r^2$ at the origin, $1/p_{\text{tail}}(E;r)$ vanishes faster than r, and the contributions from the cosine in (4.25) to the products $u^{(\kappa)}u^{(0)\prime}$ and $u^{(\kappa)\prime}u^{(0)}$ in (4.24) vanish for $r_l \to 0$. With the abbreviations

$$S_{\text{tail}}(E) = \int_{r_l}^{r_{\text{out}}(E)} p_{\text{tail}}(E;r)\mathrm{d}r, \qquad I_\kappa = \frac{S_{\text{tail}}(E)}{\hbar} - \frac{\phi_{\text{out}}(E)}{2} \tag{4.26}$$

we obtain from (4.22) and (4.25)

$$\left[u^{(\kappa)}u^{(0)\prime} - u^{(\kappa)\prime}u^{(0)}\right]_{r_l\to 0} = \frac{\mathscr{D}(\kappa)\mathscr{D}(0)}{\hbar}\sin(I_0 - I_\kappa)\Big|_{r_l\to 0} = -\kappa^2\int_0^\infty u^{(\kappa)}u^{(0)}\mathrm{d}r. \tag{4.27}$$

For the free-particle solutions we obtain

$$\left[w^{(\kappa)}w^{(0)\prime} - w^{(\kappa)\prime}w^{(0)}\right]_{r_l}^{r_u} = -\kappa^2\int_{r_l}^{r_u} w^{(\kappa)}w^{(0)}\mathrm{d}r. \tag{4.28}$$

Again, the contributions from r_u vanish for $r_u \to \infty$ while the contribution from r_l is

$$\left[w^{(\kappa)}w^{(0)\prime} - w^{(\kappa)\prime}w^{(0)}\right]_{r_l\to 0} = \kappa = -\kappa^2\int_0^\infty w^{(\kappa)}w^{(0)}\mathrm{d}r. \tag{4.29}$$

Combining (4.27) and (4.29) gives

$$\begin{aligned}
&\frac{\mathscr{D}(\kappa)\mathscr{D}(0)}{\hbar}\sin(I_0 - I_\kappa)\\
&= \frac{\mathscr{D}(\kappa)\mathscr{D}(0)}{\hbar}\sin\left(\frac{S_{\text{tail}}(0) - S_{\text{tail}}(E)}{\hbar} - \frac{\phi_{\text{out}}(0) - \phi_{\text{out}}(E)}{2}\right)\\
&= \kappa + \kappa^2\int_0^\infty \left[u^{(\kappa)}(r)u^{(0)}(r) - w^{(\kappa)}(r)w^{(0)}(r)\right]\mathrm{d}r.
\end{aligned} \tag{4.30}$$

Resolving for $\phi_{\text{out}}(E)$ gives

$$\frac{\phi_{\text{out}}(E)}{2} = \frac{\phi_{\text{out}}(0)}{2} - \frac{S_{\text{tail}}(0) - S_{\text{tail}}(E)}{\hbar} + \arcsin\left[\frac{\kappa - \rho(E)\kappa^2}{\mathscr{D}(0)\mathscr{D}(\kappa)/\hbar}\right], \tag{4.31}$$

with the length $\rho(E)$ defined by

$$\rho(E) = \int_0^\infty \left[w^{(\kappa)}(r)w^{(0)}(r) - u^{(\kappa)}(r)u^{(0)}(r)\right]\mathrm{d}r. \tag{4.32}$$

The action integrals $S_{\text{tail}}(0)$ and $S_{\text{tail}}(E)$ diverge as the lower integration limit tends to zero, but the difference $S_{\text{tail}}(0) - S_{\text{tail}}(E)$ tends to a well defined value in this limit.

In order to account correctly for the contributions of order κ^2 in the arcsin term in (4.31), it is necessary to know the zero-energy limit of $\rho(E)$,

$$\rho(0) = \int_0^\infty \left[\left(w^{(0)}(r)\right)^2 - \left(u^{(0)}(r)\right)^2\right] \mathrm{d}r \stackrel{\text{def}}{=} \rho_{\text{eff}}, \tag{4.33}$$

as well as the behaviour of $\mathscr{D}(\kappa)$ up to first order in κ. This can be obtained, as described in [35], on the basis of the two linearly independent threshold ($E = 0$) solutions $u_0^{(0)}(r)$ and $u_1^{(0)}(r)$ of the Schrödinger equation (4.11) which are defined by the following large-r boundary conditions,

$$u_0^{(0)}(r) \overset{r\to\infty}{\sim} 1, \qquad u_1^{(0)}(r) \overset{r\to\infty}{\sim} r. \tag{4.34}$$

For $r \to 0$, these wave functions can be written as WKB waves,

$$u_{0,1}^{(0)}(r) \overset{r\to 0}{\sim} \frac{D_{0,1}}{\sqrt{p_{\text{tail}}(0;r)}} \cos\left(\frac{1}{\hbar}\int_r^\infty p_{\text{tail}}(0;r')\mathrm{d}r' - \frac{\phi_{0,1}}{2}\right), \tag{4.35}$$

which exactly defines the amplitudes $D_{0,1}$ and the phases $\phi_{0,1}$. The amplitude D_0 is the threshold value $\mathscr{D}(0)$ of the amplitude defined in (4.22), and ϕ_0 is the threshold value of the outer reflection phase $\phi_{\text{out}}(E)$. For small but nonvanishing values of κ, the solution $u^{(\kappa)}(r)$ obeying the bound-state boundary condition (4.21) is given, up to and including the first order in κ, by

$$u^{(\kappa)}(r) \overset{\kappa r\to 0}{\sim} u_0^{(0)}(r) - \kappa u_1^{(0)}(r) \overset{r\to\infty}{\sim} 1 - \kappa r. \tag{4.36}$$

The WKB representation of the wave function (4.36), which is valid for small r and exact in the limit $r \to 0$, follows via (4.35),

$$\begin{aligned} u^{(\kappa)}(r) &\overset{r\to 0}{\sim} \frac{D_0}{\sqrt{p_{\text{tail}}(0;r)}}\left[\cos\left(\frac{S_{\text{tail}}(0)}{\hbar} - \frac{\phi_0}{2}\right) - \frac{D_1}{D_0}\kappa\cos\left(\frac{S_{\text{tail}}(0)}{\hbar} - \frac{\phi_1}{2}\right)\right] \\ &= \frac{D_0}{\sqrt{p_{\text{tail}}(0;r)}}\left[1 - \frac{D_1}{D_0}\kappa\cos\left(\frac{\phi_0-\phi_1}{2}\right)\right] \\ &\quad \times \cos\left(\frac{S_{\text{tail}}(0)}{\hbar} - \frac{\phi_1}{2} - \frac{D_1}{D_0}\kappa\sin\left(\frac{\phi_0-\phi_1}{2}\right)\right) + O\left(\kappa^2\right). \end{aligned} \tag{4.37}$$

Comparing amplitude and phase of the right-hand sides of (4.22) and (4.37) gives

$$\mathscr{D}(\kappa) = D_0\left[1 - \frac{D_1}{D_0}\kappa\cos\left(\frac{\phi_0-\phi_1}{2}\right)\right] + O\left(\kappa^2\right), \tag{4.38}$$

$$\frac{\phi_{\text{out}}(E)}{2} = \frac{\phi_0}{2} - \frac{S_{\text{tail}}(0) - S_{\text{tail}}(E)}{\hbar} + b\kappa + O\left(\kappa^2\right), \tag{4.39}$$

with the length b in (4.39) defined as

$$b = \frac{D_1}{D_0}\sin\left(\frac{\phi_0-\phi_1}{2}\right). \tag{4.40}$$

Expanding the arcsin term on the right-hand side of (4.31) gives the near-threshold expansion of the outer reflection phase up to and including second order in κ as

$$\frac{\phi_{\text{out}}(E)}{2} \overset{\kappa\to 0}{\sim} \frac{\phi_{\text{out}}(0)}{2} - \frac{S_{\text{tail}}(0) - S_{\text{tail}}(E)}{\hbar} + b\kappa - \frac{(d\kappa)^2}{2}; \tag{4.41}$$

the length d is defined by

$$\frac{d^2}{2} = b(\rho_{\text{eff}} - \bar{a}) \quad \text{with} \quad \bar{a} = \frac{D_1}{D_0}\cos\left(\frac{\phi_0 - \phi_1}{2}\right) = b\cot\left(\frac{\phi_0 - \phi_1}{2}\right). \tag{4.42}$$

In deriving (4.41) we compared the linear terms in (4.31) and (4.39) to deduce $\hbar/\mathscr{D}(0)^2 = b$.

Away from threshold, $\kappa \to \infty$, the outer reflection phase approaches its semiclassical limit $\frac{\pi}{2}$. A measure for the proximity to the semiclassical limit is given by the reduced classical turning point $\kappa r_{\text{out}}(E)$, see discussion involving Eqs. (4.12) to (4.15) above, so it is reasonable to assume that the leading high-κ behaviour of the outer reflection phase is given by

$$\phi_{\text{out}}(E) \overset{\kappa\to\infty}{\sim} \frac{\pi}{2} + \frac{D}{\kappa r_{\text{out}}(E)}, \tag{4.43}$$

with some dimensionless constant D characteristic for the reference potential $V_{\text{tail}}(r)$.

A remarkable feature of the near-threshold expansion (4.41) of the outer reflection phase is, that the term containing the difference of the action integrals exactly cancels the corresponding contribution to the quantization function, as represented by the big square bracket in the expression (4.16). The near-threshold behaviour of $F_{\text{tail}}(E)$ is thus given by

$$F_{\text{tail}}(E) \overset{\kappa\to 0}{\sim} \frac{b\kappa}{\pi} - \frac{(d\kappa)^2}{2\pi}. \tag{4.44}$$

The leading term on the right-hand side of (4.44), linear in κ, is reminiscent of Wigner's threshold law for s-waves. Since the short-range correction $F_{\text{sr}}(E)$ is of order E at threshold, this term also represents the leading energy dependence of the full quantization function $F(E)$:

$$F(E) \overset{\kappa\to 0}{\sim} \frac{b\kappa}{\pi}, \tag{4.45}$$

which is universally valid for all potentials falling off faster than $1/r^2$ at large distances. The second term on the right-hand side of (4.44), quadratic in κ, is only well defined for reference potentials falling off faster than $1/r^3$, see the paragraph after Eq. (4.53) below.

For a potential $V(r)$ falling off faster than $1/r^3$ at large distances, the s-wave scattering length a diverges when the threshold quantum number υ_{D} is an integer, i.e. when there is an s-wave bound state exactly at threshold, see Eq. (2.88) in

Sect. 2.3.8. The derivation above enables us to formulate an explicit relation connecting the scattering length a with the threshold quantum number υ_{D}.

The asymptotic behaviour of the regular solution $u(r)$ of the Schrödinger equation with the full potential $V(r)$ is, according to Eqs. (2.83) and (4.34),

$$u(r) \overset{r\to\infty}{\propto} 1 - \frac{r}{a} \quad \Longrightarrow \quad u(r) \overset{r \text{ large}}{\propto} u_0^{(0)}(r) - \frac{1}{a} u_1^{(0)}(r). \tag{4.46}$$

The phrase "r large" refers to distances which are large enough for the full potential to be well approximated by $V_{\mathrm{tail}}(r)$ and at the same time small enough for the WKB representations (4.35) to be accurate representations of $u_0^{(0)}(r)$ and $u_1^{(0)}(r)$. For such values of r,

$$\begin{aligned} u(r) &\propto \frac{D_1}{\sqrt{p(0;r)}} \cos\left(\frac{1}{\hbar}\int_r^\infty p\big(0;r'\big)\mathrm{d}r' - \frac{\phi_1}{2}\right) \\ &\quad - \frac{aD_0}{\sqrt{p(0;r)}} \cos\left(\frac{1}{\hbar}\int_r^\infty p\big(0;r'\big)\mathrm{d}r' - \frac{\phi_0}{2}\right) \\ &\propto \frac{1}{\sqrt{p(0;r)}} \cos\left(\frac{1}{\hbar}\int_r^\infty p\big(0;r'\big)\mathrm{d}r' - \frac{\phi_+}{4} - \eta\right), \end{aligned} \tag{4.47}$$

with the angles $\phi_\pm$ and η given by

$$\phi_\pm = \phi_0 \pm \phi_1, \qquad \tan\eta = \frac{a + D_1/D_0}{a - D_1/D_0} \tan\left(\frac{\phi_-}{4}\right). \tag{4.48}$$

Taking the inner classical turning point as reference gives

$$u(r) \propto \frac{1}{\sqrt{p(0;r)}} \cos\left(\frac{1}{\hbar}\int_{r_{\mathrm{in}}(0)}^r p\big(0;r'\big)\mathrm{d}r' - \frac{\phi_{\mathrm{in}}(0)}{2}\right), \tag{4.49}$$

and compatibility of (4.47) and (4.49) implies

$$\frac{1}{\hbar}\int_{r_{\mathrm{in}}(0)}^\infty p(0;r)\mathrm{d}r = \frac{\phi_{\mathrm{in}}(0)}{2} + \eta + \frac{\phi_+}{4} \pmod{\pi}. \tag{4.50}$$

Comparison with (4.6) gives

$$\eta = \upsilon_{\mathrm{D}}\pi + \frac{\phi_-}{4} \pmod{\pi}. \tag{4.51}$$

Resolving the second equation (4.48) for a and inserting (4.51) for η yields

$$\begin{aligned} a &= \frac{D_1}{D_0} \frac{\tan(\upsilon_{\mathrm{D}}\pi + \frac{\phi_-}{4}) + \tan(\frac{\phi_-}{4})}{\tan(\upsilon_{\mathrm{D}}\pi + \frac{\phi_-}{4}) - \tan(\frac{\phi_-}{4})} \\ &= \frac{D_1}{D_0} \sin\left(\frac{\phi_-}{2}\right)\left[\frac{1}{\tan(\frac{\phi_-}{2})} + \frac{1}{\tan(\upsilon_{\mathrm{D}}\pi)}\right]. \end{aligned} \tag{4.52}$$

In terms of the parameters b and $\bar{a}$ as defined in Eqs. (4.40) and (4.42), this relation simplifies to

$$a = \bar{a} + \frac{b}{\tan(\upsilon_D \pi)} = \bar{a} + \frac{b}{\tan(\Delta_D \pi)}, \quad \Delta_D = \upsilon_D - \lfloor \upsilon_D \rfloor. \tag{4.53}$$

Equation (4.53) is very fundamental, giving an explicit relation between the s-wave scattering length a and the threshold quantum number υ_D. Because of the periodicity of the tangent, it is actually only the *remainder* Δ_D that counts. The remainder can assume values between zero and unity and quantifies the proximity of the most weakly bound state to threshold. A value of Δ_D very close to zero indicates a bound state very close to threshold, while a value very close to unity indicates that the potential just fails to support a further bound state.

Equation (4.53) enables a physical interpretation of the parameters entering the derivation of the expression (4.44) for the near-threshold behaviour of the tail contribution $F_{\text{tail}}(E)$ of the quantization function. In an ensemble of potentials characterized by evenly distributed values of the remainder Δ_D, the values of the scattering length will be evenly distributed around the mean value $\bar{a}$, hence $\bar{a}$ is called the *mean scattering length*, a term first introduced by Gribakin and Flambaum in [36]. We call the length b, which determines the leading term in the near-threshold behaviour (4.44) of the quantization function and the second term on the right-hand side of (4.53), the *threshold length*. The definition (4.33) of ρ_{eff} resembles, except for a factor two, the definition (2.103) of the effective range r_{eff} in Sect. 2.3.8, and we call it the *subthreshold effective range*. Note however, that the wave functions $u^{(0)}$ and $w^{(0)}$ that enter in the definition of ρ_{eff} remain bounded for $r \to \infty$, according to (4.23), so the expression (4.33) gives a well defined value for ρ_{eff} for any reference potential falling off faster than $1/r^3$ at large distances. The length d, which defines the next-to-leading term in the near-threshold behaviour (4.44) of the quantization function, is related to the mean scattering length $\bar{a}$, the threshold length b and the subthreshold effective range ρ_{eff} via the first equation (4.42). We use the term *effective length* for the parameter d.

The relation (4.53) makes it possible to extend Eq. (2.88), which relates the asymptotic inverse penetration depth κ_b of a bound state very near threshold to the scattering length, to the next order in $1/\kappa_b$. With the quantization rule (4.7) we can rewrite (4.53) as

$$a = \bar{a} + \frac{b}{\tan[\pi F(E_b)]} = \bar{a} + \frac{b}{\tan[\pi (F_{\text{tail}}(E_b) + F_{\text{sr}}(E_b))]}, \tag{4.54}$$

where $E_b = -\hbar^2 \kappa_b^2/(2\mu)$ is the energy of the very weakly bound state. Replacing $F_{\text{sr}}(E_b)$ by its leading term $\gamma_{\text{sr}} E_b$ according to (4.19) and using the leading two terms of the Taylor expansion of the tangent yields [76]

$$a = \frac{1}{\kappa_b} + \rho_{\text{eff}} + \pi \frac{\hbar^2 \gamma_{\text{sr}}}{2\mu b} + O(\kappa_b). \tag{4.55}$$

It is interesting to observe, that the next-to-leading term in the expansion (4.55), i.e. the term of order κ_b^0, is *not* the mean scattering length $\bar{a}$, as one might guess from Eq. (4.53) [36], but the subthreshold effective range ρ_{eff}, *plus* a contribution which comes from short-range effects and is proportional to the constant γ_{sr}. In this light, one might ask what sense it makes to extend the near-threshold expansion (4.44) of $F_{\text{tail}}(E)$ up to second order in κ, when short-range effects bring in a term of the same order. The answer lies in the observation, that the length scales associated with the potential tail are generally very large, so that both ρ_{eff} and b are much larger than typical length scales associated with γ_{sr}. The dimensionless ratio $\pi\gamma_{\text{sr}}\hbar^2/(2\mu b\rho_{\text{eff}})$ of the third term on the right-hand side of (4.55) to the second term is thus usually very small, see also Example 1 below. Furthermore, a clean identification of the tail function $F_{\text{tail}}(E)$ over the whole range of energies from threshold to $-\infty$ is a prerequisite for the identification of the short-range correction $F_{\text{sr}}(E)$ due to the deviation of the full interaction from the reference potential at small distances.

At energies far from threshold, $\kappa \to \infty$, the outer reflection phase approaches its semiclassical limit according to (4.43), so the leading high-κ behaviour of $F_{\text{tail}}(E)$ is,

$$F_{\text{tail}}(E) \overset{\kappa\to\infty}{\sim} \frac{S_{\text{tail}}(0) - S_{\text{tail}}(E)}{\pi\hbar} - \left(\frac{\phi_0}{2\pi} - \frac{1}{4}\right) + \frac{D/(2\pi)}{\kappa r_{\text{out}}(E)}. \tag{4.56}$$

The zero-energy value ϕ_0 of the outer reflection phase, the lengths defining its low-κ expansion (4.41), i.e. b, $\bar{a}$, ρ_{eff} and d, and the parameter D in (4.43), (4.56) are *tail parameters*; they are properties of the reference potential $V_{\text{tail}}(r)$ alone. For a reference potential V_{tail} for which the Schrödinger equation (4.11) has analytically known solutions at threshold, $E = 0$, the tail parameters can be derived analytically. The exact behaviour of $F_{\text{tail}}(E)$ in between the near-threshold regime and the high-κ, semiclassical regime is generally not known analytically, but it can be calculated numerically by a straightforward evaluation of Eq. (4.16).

The application of the theory described in this section is particularly elegant for potentials with a large-distance behaviour that is well described by a single-power tail,

$$V_{\text{tail}}(r) \equiv V_\alpha^{\text{att}}(r) = -\frac{C_\alpha}{r^\alpha} = -\frac{\hbar^2}{2\mu}\frac{(\beta_\alpha)^{\alpha-2}}{r^\alpha}, \quad C_\alpha > 0,\ \alpha > 2. \tag{4.57}$$

As for the repulsive inverse-power potentials (2.160) discussed in Sect. 2.4.2, the potential strength coefficient C_α in (4.57) is expressed in terms of the characteristic quantum length

$$\beta_\alpha = \left(\frac{2\mu C_\alpha}{\hbar^2}\right)^{1/(\alpha-2)}, \tag{4.58}$$

which does not exist in classical mechanics. The beauty of single-power reference potentials (4.57) is that the properties of the solution of the Schrödinger equation (4.11) depend only on the dimensionless product $\kappa\beta_\alpha$ and not on energy and potential strength independently, see Appendix A.2. For example, the reduced classical

Table 4.1 Numerical values of tail parameters for single-power reference potentials (4.57), as given analytically in (4.61). The last row contains the values of the dimensionless parameter B_o governing the exponential fall-off of the modulus of the amplitude for quantum reflection according to (4.93) in Sect. 4.1.2

α	3	4	5	6	7	$\alpha \to \infty$
ϕ_0	$\frac{3}{2}\pi$	π	$\frac{5}{6}\pi$	$\frac{6}{8}\pi$	$\frac{7}{10}\pi$	$(\frac{1}{2}+\frac{1}{\alpha-2})\pi$
b/β_α	$\frac{3}{2}$	1	0.6313422	0.4779888	0.3915136	$\frac{1}{\alpha-2}\pi$
$\bar{a}/\beta_\alpha$	–	0	0.3645056	0.4779888	0.5388722	1
$\rho_{\text{eff}}/\beta_\alpha$	–	$\frac{\pi}{3}$	0.7584176	0.6973664	0.6826794	1
d/β_α	–	$\sqrt{\frac{2\pi}{3}}$	0.7052564	0.4579521	0.3355665	$\frac{6.43}{(\alpha-2)^{3/2}}$
D	0.8095502	0.5462620	0.4554443	0.4089698	0.3806186	$\frac{1}{12}\pi$
B_o	2.24050	1.69443	1.35149	1.12025	0.95450	$\frac{2}{\alpha}\pi$

turning point is given by

$$\kappa r_{\text{out}}(E) = (\kappa\beta_\alpha)^{1-2/\alpha}, \tag{4.59}$$

and the difference of the action integrals appearing in (4.16), (4.56) is

$$\begin{aligned}\lim_{r_{\text{in}}\to 0}\frac{1}{\pi\hbar}\left[\int_{r_{\text{in}}}^{\infty} p_{\text{tail}}(0;r)\mathrm{d}r - \int_{r_{\text{in}}}^{r_{\text{out}}(E)} p_{\text{tail}}(E;r)\mathrm{d}r\right]\\ = \frac{(\kappa\beta_\alpha)^{1-2/\alpha}}{(\alpha-2)\sqrt{\pi}}\frac{\Gamma(\frac{1}{2}+\frac{1}{\alpha})}{\Gamma(1+\frac{1}{\alpha})}.\end{aligned} \tag{4.60}$$

The tail parameters $\phi_{\text{out}}(0) \equiv \phi_0$, b, $\bar{a}$, ρ_{eff} and d defining the low-κ expansion (4.41) of the outer reflection phase, and the parameter D in (4.43) are explicitly given for inverse-power tails (4.57) by [35, 76],

$$\begin{aligned}&\phi_0 = \left(\nu+\frac{1}{2}\right)\pi, \qquad \frac{b}{\beta_\alpha} = \nu^{2\nu}\frac{\Gamma(1-\nu)}{\Gamma(1+\nu)}\sin(\pi\nu),\\ &\frac{\bar{a}}{\beta_\alpha} = \nu^{2\nu}\frac{\Gamma(1-\nu)}{\Gamma(1+\nu)}\cos(\pi\nu),\\ &\frac{\rho_{\text{eff}}}{\beta_\alpha} = \frac{\pi(2\nu)^{2\nu}\nu\Gamma(\frac{1}{2}+2\nu)}{\sin(\pi\nu)\Gamma(\frac{1}{2}+\nu)\Gamma(1+3\nu)}, \qquad D = \frac{\sqrt{\pi}}{12}\frac{\alpha+1}{\alpha}\frac{\Gamma(\frac{1}{2}-\frac{1}{\alpha})}{\Gamma(1-\frac{1}{\alpha})},\end{aligned} \tag{4.61}$$

with the abbreviation $\nu = 1/(\alpha-2)$. The expression for d follows from those for b, $\bar{a}$ and ρ_{eff} via (4.42). Numerical values are given in Table 4.1.

The behaviour of the outer reflection phase $\phi_{\text{out}}(E)$ is illustrated in Fig. 4.2 for powers $\alpha = 3, \ldots, 7$. The abscissa is linear in $\kappa r_{\text{out}} = (\kappa\beta_\alpha)^{1-2/\alpha}$, so the initial decrease is linear in the plot, compare (4.39) and (4.60). In contrast to the reflection phases for repulsive inverse-power potentials shown in Fig. 2.16 in Sect. 2.4.2, the threshold values ϕ_0 depend on the power α as given in the first equation (4.61).

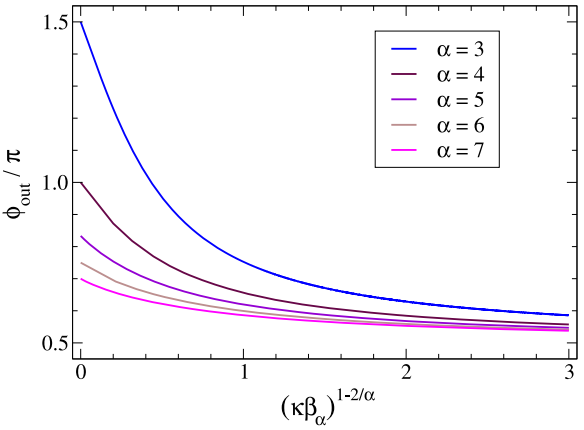

Fig. 4.2 Outer reflection phase ϕ_{out} for attractive inverse-power potentials (4.57) as function of the reduced classical turning point $\kappa r_{\text{out}} = (\kappa\beta_\alpha)^{1-2/\alpha}$. (Adapted from [85])

For a given power $\alpha > 2$, one quantization function $F_{\text{tail}}(E) \equiv F_\alpha(\kappa\beta_\alpha)$ applies for all potential strengths. An expression for $F_\alpha(\kappa\beta_\alpha)$ which is accurate all the way from threshold to the semiclassical limit of large κ, can be obtained by interpolating between the near-threshold expression (4.44) and the high-κ limit (4.56). With (4.59) and (4.60), the high-κ limit of $F_\alpha(\kappa\beta_\alpha)$ is,

$$F_\alpha(E) \overset{\kappa\to\infty}{\sim} \frac{(\kappa\beta_\alpha)^{1-2/\alpha}}{(\alpha-2)\sqrt{\pi}} \frac{\Gamma(\frac{1}{2}+\frac{1}{\alpha})}{\Gamma(1+\frac{1}{\alpha})} - \frac{1}{2(\alpha-2)} + \frac{D/(2\pi)}{(\kappa\beta_\alpha)^{1-2/\alpha}}. \tag{4.62}$$

For $\alpha = 6$, an analytical expression involving one dimensionless fitting parameter B was derived in [76],

$$F_{\alpha=6}(E) = \frac{2b\kappa - (d\kappa)^2}{2\pi[1+(\kappa B)^4]} + \frac{(\kappa B)^4}{1+(\kappa B)^4}\left[-\frac{1}{8} + \frac{D}{2\pi(\kappa\beta_6)^{2/3}} + \frac{\Gamma(\frac{2}{3})(\kappa\beta_6)^{2/3}}{4\sqrt{\pi}\,\Gamma(\frac{7}{6})}\right]. \tag{4.63}$$

All other parameters appearing in (4.63) are as given in Eq. (4.61) and Table 4.1 for $\alpha = 6$. With the value $B = 0.9363\beta_6$, the expression (4.63) reproduces the exact values, calculated by evaluating Eq. (4.16) numerically, to within an accuracy near 10^{-4} or better in the whole range from threshold to the high-κ limit [76].

For $\alpha = 4$, a more sophisticated treatment of the semiclassical, high-κ limit is needed to achieve a comparable accuracy on the basis of a small number of fitting parameters. An extension of the high-κ expansion (4.43) of the outer reflection phase to higher inverse powers of the reduced classical turning point $(\kappa\beta_4)^{1/2}$,

$$\phi_{\text{out}}(E) \overset{\kappa\beta_4\to\infty}{\sim} \frac{\pi}{2} + \sum_{j=1,3,5,7} \frac{D^{(j)}}{(\kappa\beta_4)^{j/2}}, \tag{4.64}$$

Table 4.2 Coefficients $D^{(j)}$ in the high-κ expansion (4.64) of the outer reflection phase for a $-1/r^4$ reference potential

$D^{(1)}$	$D^{(3)}$	$D^{(5)}$	$D^{(7)}$
$\frac{5\sqrt{\pi}}{48}\Gamma(\frac{1}{4})/\Gamma(\frac{3}{4})$	$-\frac{35\sqrt{\pi}}{384}\Gamma(\frac{3}{4})/\Gamma(\frac{1}{4})$	$\frac{475\sqrt{\pi}}{3584}\Gamma(\frac{5}{4})/\Gamma(-\frac{1}{4})$	$-\frac{63305\sqrt{\pi}}{221184}\Gamma(\frac{7}{4})/\Gamma(-\frac{3}{4})$
0.5462620	−0.0546027	−0.0434388	0.0964461

Table 4.3 Coefficients c_i, d_i in the expression (4.66) for $F_{\alpha=3}(E)$

i	c_i	d_i	i	c_i	d_i
1	8.198894514574	7.367727350550	5	185.465618264420	242.028021052411
2	38.229531850326	32.492317936470	6	141.484936909078	250.115055730896
3	85.724646494548	85.380005002970	7	60.927524697423	63.749260455229
4	147.081920247084	169.428485967491	8	56.372265754601	112.744531509202

leads to the following analytical expression based on two fitting parameters, the lengths B_6 and B_7,

$$F_{\alpha=4}(E) = \frac{[2b\kappa - (d\kappa)^2]/(2\pi)}{1+(\kappa B_6)^6+(\kappa B_7)^7} + \frac{(\kappa B_6)^6+(\kappa B_7)^7}{1+(\kappa B_6)^6+(\kappa B_7)^7} \times \left[-\frac{1}{4} + \frac{\Gamma(\frac{3}{4})}{\Gamma(\frac{5}{4})}\frac{(\kappa\beta_4)^{1/2}}{2\sqrt{\pi}} + \frac{D^{(1)}/(2\pi)}{(\kappa\beta_4)^{1/2}} + \frac{D^{(3)}/(2\pi)}{(\kappa\beta_4)^{3/2}} + \frac{D^{(5)}/(2\pi)}{(\kappa\beta_4)^{5/2}} + \frac{D^{(7)}/(2\pi)}{(\kappa\beta_4)^{7/2}}\right]. \tag{4.65}$$

The coefficients $D^{(j)}$, which determine the expansion (4.64), are given analytically and numerically in Table 4.2. With $B_6 = 1.622576\beta_4$ and $B_7 = 1.338059\beta_4$ for the fitted lengths, the expression (4.65) reproduces the exact values, calculated by evaluating Eq. (4.16) numerically, to within an accuracy near 10^{-4} or better in the whole range from threshold to the high-κ limit [77].

For $\alpha = 3$, it turned out to be more practical [62] to approximate $F_{\alpha=3}(E)$ by a rational function of the reduced classical turning point $(\kappa\beta_3)^{1/3}$,

$$F_{\alpha=3}(E) = \frac{\Gamma(\frac{5}{6})}{\sqrt{\pi}\,\Gamma(\frac{4}{3})}(\kappa\beta_3)^{1/3} + \frac{3+\sum_{i=1}^{i_{\max}} c_i(\kappa\beta_3)^{i/3}}{4+\sum_{i=1}^{i_{\max}} d_i(\kappa\beta_3)^{i/3}} - \frac{3}{4}. \tag{4.66}$$

With expansions up to $i_{\max} = 8$ in the numerator and the denominator of the second term on the right-hand side of (4.66), the formula is able to reproduce the exact quantization function, calculated by evaluating Eq. (4.16) numerically, to within an accuracy near $5\cdot 10^{-8}$ or better in the whole range from threshold to the high-κ limit [62]. The coefficients c_i and d_i with which this is achieved are listed in Table 4.3.

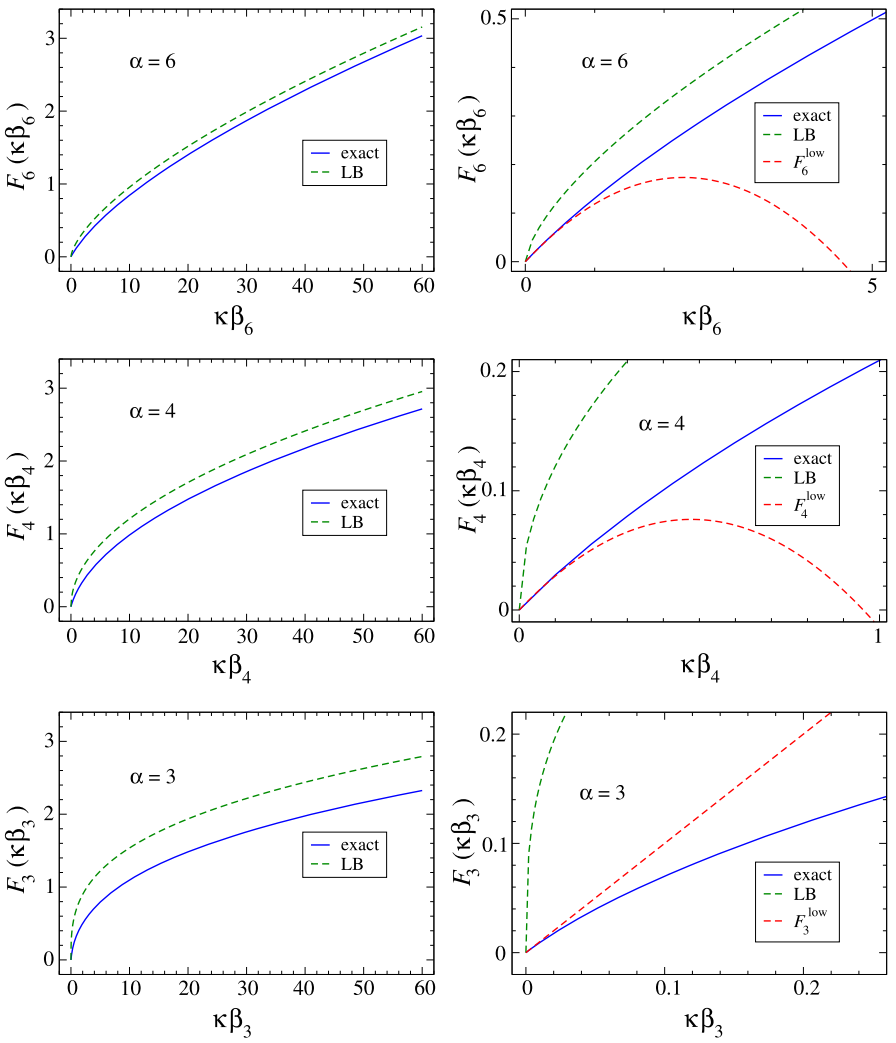

Fig. 4.3 Tail contribution $F_{\rm tail}(E) \equiv F_\alpha(\kappa\beta_\alpha)$ to the quantization function for single-power reference potentials (4.57). The *solid blue lines* are the exact results, which are accurately given by the expressions (4.63), (4.65) and (4.66) for $\alpha = 6, 4$ and 3, respectively. The *dashed green lines* show the LeRoy–Bernstein functions [52, 84], and the *dashed red lines* in the three panels on the right-hand side show the low-energy expansion (4.44) including both terms, linear and quadratic in $\kappa\beta_\alpha$ for $\alpha = 6$ and $\alpha = 4$ and only the leading linear term for $\alpha = 3$

The quantization functions (4.16) for the single-power tails (4.57) are shown for the cases $\alpha = 6, 4$ and 3 in Fig. 4.3 as functions of $\kappa\beta_\alpha$. The solid blue lines show exact functions, which are accurately approximated by the expressions (4.63), (4.65) and (4.66) all the way from threshold to the high-κ limit. The dashed green lines show the LeRoy–Bernstein functions $F_\alpha^{\rm LB}(E)$ [52, 84], which are obtained

by ignoring the contribution from the outer reflection phase in (4.16). The LeRoy–Bernstein function is given explicitly by the first term on the right-hand side of (4.62). It is wrong at threshold, because it misses the energy-dependence (4.41) cancelling the contribution from the action integrals, and it is also wrong in the high-κ, semiclassical limit, because it misses the contribution

$$\frac{\phi_{\text{out}}(0)}{2\pi} - \frac{\pi/2}{2\pi} = \frac{1}{2(\alpha-2)}. \tag{4.67}$$

This leads to significant errors when extrapolating from bound-state energies to threshold, e.g. in order to determine the value of the dissociation threshold or of the scattering length from spectroscopic energies [62, 76, 77].

The dashed red lines in the three right-hand panels in Fig. 4.3 show the low-energy expansion (4.44) of $F_\alpha(E)$, including both terms, linear and quadratic in $\kappa\beta_\alpha$ for $\alpha = 6$ and $\alpha = 4$ and only the leading linear term for $\alpha = 3$. They allow us to estimate the extent of the near-threshold quantum regime. From the quantization rule (4.7) it is clear, that the value of $F(E_\upsilon)$ lies between zero and unity for the highest bound state with quantum number $\upsilon_{\max} = \lfloor \upsilon_{\text{D}} \rfloor$, between one and two for the second-highest bound state with quantum number $\upsilon_{\max} - 1$, etc. The range covered in the left-hand panels of Fig. 4.3 thus only accommodates the highest three bound states of a potential with the respective single-power tail. The enlargements in the right-hand part of the figure show that the near-threshold linear behaviour of the quantization function is restricted to a very small energy range indeed; in the majority of cases, it does not even contain the highest bound state, and the second-highest bound state is definitely beyond the range of validity of the near-threshold expansion (4.44), even when the second term, quadratic in κ, is included in the examples $\alpha = 6$ and $\alpha = 4$. The range of validity of near-threshold, effective-range type expansions is *tiny*. Nevertheless, an accurate description of this near-threshold quantum regime and a reliable interpolation to the large-κ semiclassical regime are paramount to a practicable application of the quantization-function concept in realistic situations.

4.1.1.1 Example 1. The Lennard–Jones Potential

We consider again the Lennard–Jones potential,

$$V_{\text{LJ}}(r) = \mathscr{E}\left[\left(\frac{r_{\min}}{r}\right)^{12} - 2\left(\frac{r_{\min}}{r}\right)^{6}\right], \tag{4.68}$$

which was already discussed in Sect. 2.6.5. The quantum mechanical properties of this potential are determined by the parameter $B_{\text{LJ}} = \mathscr{E} 2\mu r_{\min}^2/\hbar^2$, see (2.299). The natural definition of the reference potential $V_{\text{tail}}(r)$ in this case is

$$V_{\text{tail}}(r) \equiv V_6^{\text{att}}(r) = -2\mathscr{E}\frac{(r_{\min})^6}{r^6} = -\frac{\hbar^2}{2\mu}\frac{(\beta_6)^4}{r^6} \quad \text{with } \beta_6 = r_{\min}(2B_{\text{LJ}})^{1/4}. \tag{4.69}$$

Table 4.4 Energies in units of $\mathscr{E}$ of the highest twelve bound states in the Lennard–Jones potential (4.68) with $B_{\rm LJ} = 10^4$ [72]

υ	E_υ	υ	E_υ	υ	E_υ
12	−0.115225890999	16	−0.031813309316	20	−0.003047136244
13	−0.087766914229	17	−0.020586161356	21	−0.001052747695
14	−0.064982730497	18	−0.012350373216	22	−0.000198340301
15	−0.046469911358	19	−0.006657024344	23	−0.000002696883

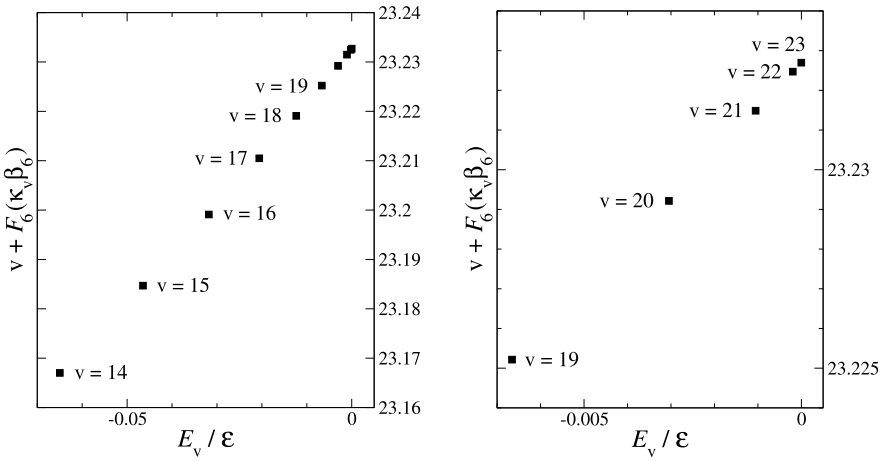

Fig. 4.4 Plot of $\upsilon + F_6(\kappa_\upsilon \beta_6)$ against energy for the highest ten bound states in the Lennard–Jones potential (4.68) with $B_{\rm LJ} = 10^4$. The energies are as listed in Table 4.4 and the quantization function $F_6(\kappa\beta_6)$ is as given by Eq. (4.63)

For $B_{\rm LJ} = 10^4$ we have $\beta_6 = 10 \times 2^{1/4} r_{\rm min}$, and the potential supports 24 bound states, $\upsilon = 0, 1, \ldots, 23$. This is actually the potential illustrated in Fig. 4.1. It was used by Paulsson et al. [72] to discuss the accuracy of higher-order WKB approximations. The energies of the highest twelve bound states are listed in Table 4.4.

According to (4.20), a plot of $\upsilon + F_6(\kappa_\upsilon \beta_6)$ against E_υ should approach a straight-line behaviour towards threshold, κ_υ being the asymptotic inverse penetration depth at the energy E_υ. This is illustrated impressively in Fig. 4.4. The solid squares represent the highest ten bound states in the left-hand part and the highest five bound states in the right-hand part. The x-coordinate of each square is its energy eigenvalue E_υ (in units of $\mathscr{E}$), and the y-coordinate is $\upsilon + F_6(\kappa_\upsilon \beta_6)$, where $F_6(\kappa\beta_6)$ is the quantization function (4.63), and β_6 is as given in (4.69).

The fact that the linear behaviour in Fig. 4.4 reaches from threshold down to several states below threshold shows that the quantization rule based on Eq. (4.63) is reliable over this large energy range. To demonstrate this more quantitatively, Table 4.5 lists the values of the threshold quantum number $\upsilon_{\rm D}$ and the short-range correction parameter $\gamma_{\rm sr}$ as obtained by fitting a straight line through two succes-

Table 4.5 Values of the threshold quantum number υ_D and the short-range correction parameter γ_{sr} [in units of $\mathscr{E}^{-1}$] as obtained by fitting a straight line through two successive bound states, υ and $\upsilon + 1$, according to (4.20), see Fig. 4.4. Also listed are the values of the scattering length a [in units of r_{min}] as obtained via (4.53) with the respective values of υ_D

υ	υ_D	$\gamma_{sr}\mathscr{E}$	a/r_{min}	υ	υ_D	$\gamma_{sr}\mathscr{E}$	a/r_{min}
13	23.227230	−0.926599	12.2461	18	23.232378	−1.075980	12.0355
14	23.229053	−0.954646	12.1706	19	23.232591	−1.107941	12.0270
15	23.230401	−0.983664	12.1155	20	23.232685	−1.138876	12.0232
16	23.231354	−1.013615	12.0768	21	23.232699	−1.151726	12.0227
17	23.231988	−1.044432	12.0512	22	23.232700	−1.159540	12.0226

sive points, υ and $\upsilon + 1$. The values both of υ_D and of γ_{sr} converge rapidly and smoothly with increasing quantum number υ. The value of the threshold quantum number obtained by extrapolating from the sixth- and fifth-highest states ($\upsilon = 18$ and $\upsilon = 19$) already lies within 0.0004 of the value extrapolated via the highest two states, $\upsilon_D = 23.23270$. This is also reflected in the similarly rapid and smooth convergence of the values of the scattering length a, as derived from the respective values of the threshold quantum number υ_D and the tail parameters $\bar{a}$ and b according to (4.53). In the present case of a $1/r^6$ reference potential, $\bar{a}$ and b are identical and both approximately equal to $0.478\beta_6$, see Table 4.1. With β_6 as given in (4.69), we have $\bar{a} = b \approx 5.684 r_{min}$ in the present case. The well converged value of the scattering length, as obtained with the highest two states, is already predicted to within 0.1% when extrapolating from the sixth- and fifth-highest states ($\upsilon = 18$ and $\upsilon = 19$).

Note that the magnitude of the short-range correction coefficient γ_{sr} is of the order of $1/\mathscr{E}$, where $\mathscr{E}$ is the depth of the potential. Characteristic energies associated with the potential tail are typically of the order

$$E_{\beta_6} = \frac{\hbar^2}{2\mu(\beta_6)^2}. \tag{4.70}$$

In the present example, $E_{\beta_6} \approx 0.7 \times 10^{-6}\mathscr{E}$, so the short-range correction coefficient γ_{sr} is near to six powers of ten smaller than typical inverse energies associated with the scale set by the reference potential $V_6(r)$. This justifies carrying the near-threshold expansions of the outer reflection phase (4.41) and the quantization function (4.44) to second order in κ, even though the short-range corrections come in at the same order.

The results above show, that the quantization function (4.63) for a $1/r^6$ reference potential accurately accounts for the level progression of the high-lying bound states in the deep Lennard–Jones potential (4.68), with the large value of B_{LJ} allowing the full potential to support 24 bound states. With only two parameters, υ_D and γ_{sr}, to account for all short-range effects, an accurate extrapolation to threshold, e.g. to deduce the value of the scattering length, is possible from several states below threshold. Such a clean separation of short-range effects from the influence of the

Table 4.6 Energy eigenvalues (in atomic units) relative to the dissociation threshold of the highest ten bound states in the $L = 0$, $1s\sigma_g$ series of the H_2^+ molecular ion according to Hilico et al. [45]

υ	E_υ	υ	E_υ	υ	E_υ	υ	E_υ
10	−0.021970529704	13	−0.009458409007	16	−0.001967933877	18	−0.000109592359
11	−0.017272525961	14	−0.006373841570	17	−0.000709200873	19	$-3.39093933 \cdot 10^{-6}$
12	−0.013097363811	15	−0.003867245551				

potential tail is possible, when the distances at which the full interaction deviates significantly from the reference potential $V_{\text{tail}}(r)$ are small compared to characteristic length scales of $V_{\text{tail}}(r)$. In the present example, it was sufficient to take the leading single-power term of the potential as reference potential, because the deviation of $V(r)$ from $V_{\text{tail}}(r)$ is only given by the repulsive $1/r^{12}$ contribution, which is of very short range. In more realistic cases, a more sophisticated choice of reference potential may be needed to describe a range of near-threshold energies containing more than one or two bound states. This is demonstrated as Example 2 for the H_2^+ molecular ion below.

4.1.1.2 Example 2. The H_2^+ Molecular Ion

The H_2^+ ion, consisting of a proton and a neutral hydrogen atom, is one of the most fundamental molecular systems. Since its properties have been thoroughly examined in experiments and *ab initio* calculations, the system is ideally suited for testing and demonstrating the strengths and possible weaknesses of a theory focussing on the role of the potential tail, as done recently in Ref. [50].

Highly accurate energy eigenvalues of bound states of H_2^+ have been calculated by Hilico et al. [45]; the energies of the highest ten $L = 0$, $1s\sigma_g$ bound states are listed in Table 4.6.

The p-H potential at large distances can be decomposed into a polarisation term $V_{\text{pol}}(r)$, and an exchange term $V_{\text{ex}}(r)$ which is responsible for the energy splitting of the states with gerade and with ungerade parity [55]. The present example focusses on the $1s\sigma_g$ configuration, where the polarisation term is attractive,

$$V_{1s\sigma_g}(r) = V_{\text{pol}}(r) - V_{\text{ex}}(r). \tag{4.71}$$

The expansion of $V_{\text{pol}}(r)$ and $V_{\text{ex}}(r)$ for large internuclear separations r was given to a large number of terms in 1968 by Damburg and Propin [27]. Leading terms, in atomic units, are

$$V_{\text{pol}}^{\text{DP}}(r) = -\frac{9}{4r^4} - \frac{15}{2r^6} - \frac{213}{4r^7}, \qquad V_{\text{ex}}^{\text{DP}}(r) = 2re^{-r-1}\left(1 + \frac{1}{2r} - \frac{25}{8r^2}\right). \tag{4.72}$$

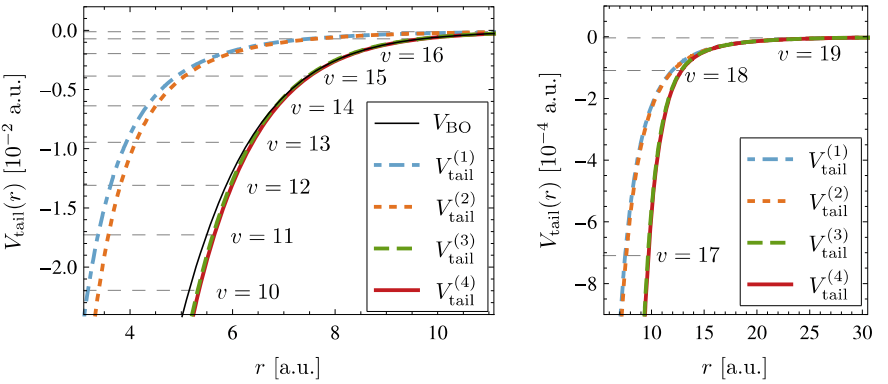

Fig. 4.5 Reference potentials $V_{\rm tail}^{(1)}(r)$ [Eq. (4.73)], $V_{\rm tail}^{(2)}(r)$ [Eq. (4.74)], $V_{\rm tail}^{(3)}(r)$ [Eq. (4.75)] and $V_{\rm tail}^{(4)}(r)$ [Eq. (4.76)] in an energy range encompassing the highest ten bound states in the $L = 0$, $1s\sigma_g$ configuration, see Table 4.6. The corresponding energy levels are shown as *horizontal dashed lines*. The potential $V_{\rm BO}(r)$ corresponds to the minimal electronic energy at internuclear separation r; this should be a good approximation to the full interaction for the range of r-values in the figure. (From [50])

Including only the leading asymptotic term of the polarisation potential to define the reference potential gives a single-power tail (4.57) with $\alpha = 4$,

$$V_{\rm tail}^{(1)}(r) = -\frac{9}{4r^4} \equiv -\frac{\hbar^2}{2\mu}\frac{(\beta_4)^2}{r^4}. \tag{4.73}$$

With the reduced mass $\mu = 918.32627$ a.u. this translates into a quantum length $\beta_4 = 64.2843$ a.u.

The reference potential (4.73) is shown in Fig. 4.5 (dot-dashed blue line) together with the potential $V_{\rm BO}(r)$ (solid black line), which represents the electronic ground-state energy at each internuclear separation r [71] and should be a good approximation to the full interaction in the range of distances in the figure. The energies of the highest ten bound states, as listed in Table 4.6, are shown as horizontal dashed lines in the figure. The single-power reference potential (4.73) is clearly far too weak for distances less than about 12 a.u., while the outer classical turning point lies in this range at the energies E_υ of all states with $\upsilon \leq 17$. Since the dominance of $F_{\rm tail}(E)$ over short-range corrections requires the reference potential to be an accurate approximation of the full interaction down to distances somewhat smaller than the outer classical turning point, the usefulness of the single-power tail (4.73) is expected to be limited to a very narrow range of near-threshold energies, encompassing at most the highest one or two levels.

In order to understand how the choice of reference potential affects the separation of short-range and tail effects, the authors of Ref. [50] investigated three further versions for $V_{\rm tail}(r)$:

$$V_{\rm tail}^{(2)}(r) = -\frac{9}{4r^4} - \frac{15}{2r^6}, \tag{4.74}$$

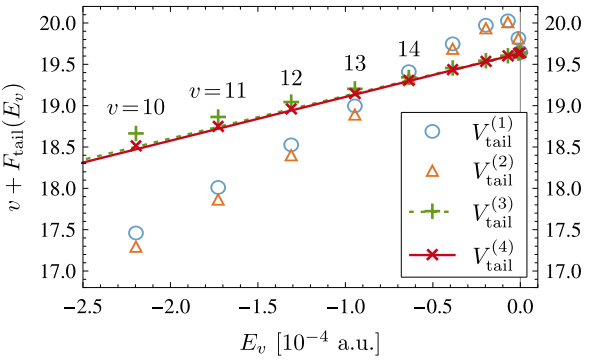

Fig. 4.6 Plots of $\upsilon + F_{\rm tail}(E_\upsilon)$ against E_υ with the quantization function $F_{\rm tail}(E)$ defined via (4.16), (4.17) on the basis of the definitions (4.73)–(4.76) of $V_{\rm tail}$. The *straight dashed green* and *solid red lines* are fitted according to (4.20) through the highest two states, $\upsilon = 18$ and $\upsilon = 19$, with $F_{\rm tail}(E)$ based on $V_{\rm tail}^{(3)}$ and $V_{\rm tail}^{(4)}$, respectively. (Adapted from [50])

Table 4.7 Values $\upsilon + F_{\rm tail}(E_\upsilon)$ at the energies given in Table 4.6 for the quantization functions based on the definitions (4.73), (4.74), (4.75) and (4.76) of $V_{\rm tail}(r)$

υ	$V_{\rm tail}^{(1)}$	$V_{\rm tail}^{(2)}$	$V_{\rm tail}^{(3)}$	$V_{\rm tail}^{(4)}$	υ	$V_{\rm tail}^{(1)}$	$V_{\rm tail}^{(2)}$	$V_{\rm tail}^{(3)}$	$V_{\rm tail}^{(4)}$
10	17.4612	17.2870	18.6570	18.5089	15	19.7486	19.6804	19.4491	19.4310
11	18.0115	17.8571	18.8562	18.7444	16	19.9740	19.9285	19.5374	19.5304
12	18.5268	18.3929	19.0367	18.9557	17	20.0268	20.0028	19.5976	19.5968
13	18.9980	18.8853	19.1968	19.1416	18	19.8143	19.8073	19.6291	19.6287
14	19.4120	19.3213	19.3349	19.3007	19	19.6468	19.6467	19.6346	19.6343

$$V_{\rm tail}^{(3)}(r) = -\frac{9}{4r^4} - 2r\mathrm{e}^{-r-1}, \tag{4.75}$$

$$V_{\rm tail}^{(4)}(r) = -\frac{9}{4r^4} - \frac{15}{2r^6} - \frac{213}{4r^7} - 2r\mathrm{e}^{-r-1}\left(1 + \frac{1}{2r} - \frac{25}{8r^2}\right). \tag{4.76}$$

These further reference potentials are shown as dotted orange $[V_{\rm tail}^{(2)}(r)]$, dashed green $[V_{\rm tail}^{(3)}(r)]$ and solid red lines $[V_{\rm tail}^{(4)}(r)]$ in Fig. 4.5. The addition of the next-order dispersion term $-15/(2r^6)$, which defines $V_{\rm tail}^{(2)}(r)$, is not a significant improvement over $V_{\rm tail}^{(1)}(r)$, but $V_{\rm tail}^{(3)}(r)$ and $V_{\rm tail}^{(4)}(r)$, which include a contribution from the polarization potential, offer a far better representation of the full potential in the whole range $r > 5$ a.u.

The quality with which the reference potentials $V_{\rm tail}^{(i)}(r)$ approximate the full potential is reflected in the accuracy with which a plot of $\upsilon + F_{\rm tail}(E_\upsilon)$ against E_υ yields a straight line with a small gradient according to (4.20). The plots are shown in Fig. 4.6, and the numerical values on which they are based are listed in Table 4.7.

Table 4.8 For the definitions (4.73)–(4.76) of the reference potential, the table lists the values of the threshold quantum number υ_D and the short-range correction coefficient γ_{sr} as obtained by fitting a straight line through the highest two states $\upsilon = 18$ and $\upsilon = 19$ according to (4.20), together with the tail parameters $\bar{a}$, b and ϕ_0. The last column shows the value obtained for the scattering length according to (4.53)

V_{tail}	υ_D	γ_{sr} [a.u.]	$\bar{a}$ [a.u.]	b [a.u.]	ϕ_0	a [a.u.]
$V_{tail}^{(1)}$	19.6414	1577.3	0	64.28	π	−30.60
$V_{tail}^{(2)}$	19.6410	1517.4	$O(10^{-15})$	64.27	3.14396	−30.49
$V_{tail}^{(3)}$	19.6348	−51.57	−2.49	63.09	3.07548	−30.93
$V_{tail}^{(4)}$	19.6345	−52.91	−2.38	63.12	3.06881	−30.77

As already seen in Fig. 4.5, the potential tails $V_{tail}^{(1)}(r)$ and $V_{tail}^{(2)}(r)$ are only a fair approximation of the full potential for distances larger than about 12 a.u. The energy levels for which the outer classical turning point lies in this range are the highest state $\upsilon = 19$ and the second-highest state $\upsilon = 18$, only. Correspondingly, the behaviour of $\upsilon + F_{tail}(E_\upsilon)$ for $\upsilon \leq 17$ and for $\upsilon \geq 18$ cannot, not even approximately, be reconciled to one straight line, see blue circles and red triangles in Fig. 4.6. In contrast the points based on $V_{tail}^{(3)}(r)$ show a much smoother energy dependence, while for $V_{tail}^{(4)}(r)$ the behaviour of $\upsilon + F_{tail}(E_\upsilon)$ is quite close to linear down to $\upsilon = 10$.

Table 4.8 lists the values of the threshold quantum number υ_D and the short-range correction coefficient γ_{sr} as obtained by fitting a straight line through the last two states $\upsilon = 18$ and $\upsilon = 19$ according to (4.20) for the various choices of reference potential. Also listed are the tail parameters $\bar{a}$ (mean scattering length), b (threshold length) and ϕ_0 (threshold value of the outer reflection phase). The last column shows the respective values of the scattering length a that follow via (4.53). Although the choice of reference potential strongly influences the energy range over which the tail contribution to the quantization function governs the energy progression of the near-threshold bound states, the extrapolation to $E = 0$ yields a very stable value of the threshold quantum number υ_D, which turns out to be quite insensitive to the choice of $V_{tail}(r)$. This puts rather tight bounds on the value of the scattering length, which follows via (4.53) and is seen to lie in the range between −31 and −30.5 a.u. Interestingly, this range does not include the value $a = -29.3$ a.u., which was derived in [16] by solving the appropriate Faddeev equations for the three-body *ppe* system. Two of the authors of Ref. [45], who obtained the energy eigenvalues in Table 4.6, were also coauthors of Ref. [16]. It seems that the scattering length given there is not quite consistent with the progression of near-threshold energy levels given in [45]. The same applies to the value $a = -28.8$ a.u., which was obtained in Ref. [13] by calculating p-H scattering cross sections down to very low energies.

Figure 4.7 shows the scattering length derived via (4.53), with the threshold quantum number υ_D obtained by fitting a straight line through two bound states υ and $\upsilon + 1$ according to (4.20), as function of the quantum number υ. For the reference potentials (4.73) and (4.74), the predictions are outside the range of the figure

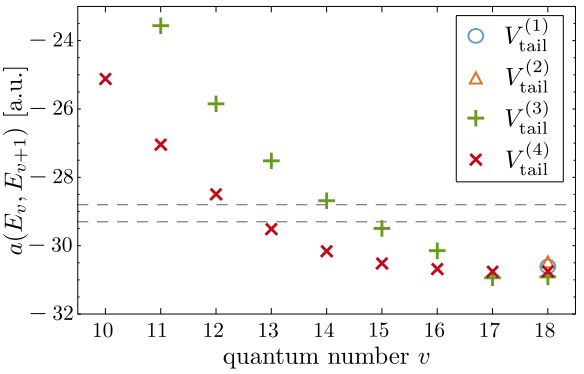

Fig. 4.7 Scattering length a according to (4.53) with $\upsilon_{\rm D}$ obtained by fitting a straight line through the points υ and $\upsilon+1$ in Fig. 4.6 according to (4.20). The *blue circle* and the *red triangle* at $\upsilon = 18$ are based on $V_{\rm tail}^{(1)}(r)$ and $V_{\rm tail}^{(2)}(r)$. The *upright green* and *diagonal red crosses* are based on $V_{\rm tail}^{(3)}(r)$ and $V_{\rm tail}^{(4)}(r)$, respectively. The *dashed horizontal lines* show the values $a = -29.3$ a.u. and $a = -28.8$ a.u. given in [16] and [13]. (Adapted from[50])

for $\upsilon \leq 17$. With the more sophisticated choices (4.75) and (4.76) of reference potential, a rapid and smooth convergence with υ is observed, similar to the case of the Lennard–Jones potential, see Table 4.5. With the reference potential $V_{\rm tail}^{(4)}(r)$, the scattering length obtained from the fifth and fourth highest state ($\upsilon = 15$ and $\upsilon = 16$) already lies within 0.3 a.u. of the value obtained with the highest two states.

This example shows, how a sufficiently sophisticated choice of reference potential can substantially increase the energy range over which the progression of near-threshold energy levels can be understood as a property of $V_{\rm tail}(r)$. The "bad news" is, that any choice of $V_{\rm tail}(r)$ beyond the single-power form (4.57) destroys the universality of the quantization function. Whereas the quantization function $F_\alpha(\kappa\beta_\alpha)$ for a single-power tail caters for all values of the potential strength, expressed through the quantum length β_α, adding any further term to the definition of $V_{\rm tail}(r)$ only makes sense in an application to a specific system. For any reference potential containing two or more terms, however, the quantization function will depend on the ratios of the strengths of the various terms. These ratios are most likely to be unique to a particular system, so the quantization function derived for a given system will be applicable to this special case only.

4.1.2 Quantum Reflection

Above threshold, the radial Schrödinger equation with a reference potential $V_{\rm tail}(r)$ is still of the form (4.11), but the energy is now positive,

$$E = \frac{\hbar^2 k^2}{2\mu}, \tag{4.77}$$

and its spectrum continuous. We assume again, that the reference potential $V_{\text{tail}}(r)$ is attractive, falls off faster than $1/r^2$ at large distances and is more singular than $-1/r^2$ at small distances. Proximity to the semiclassical or anticlassical limits can, as for energies below threshold, be estimated by the value of a typical classical action in units of $\hbar$, see discussion involving Eqs. (4.12) to (4.15) above. At positive energies, there is no outer classical turning point, but a classically defined characteristic distance can be identified as the distance r_E at which the value of the potential is equal to minus the absolute value of the energy E:

$$V_{\text{tail}}(r_E) = -|E|. \tag{4.78}$$

The distance r_E is the classical turning point in the potential $-V_{\text{tail}}(r)$ at energy $|E|$. A typical classical action is now provided the product of r_E and the asymptotic momentum $\hbar k$, corresponding in units of $\hbar$ to kr_E. Thus kr_E is a generalization of the concept of the reduced classical turning point introduced in Sect. 4.1.1. For the singular attractive potential $V_{\text{tail}}(r)$, the high-energy limit $k \to \infty$ implies $kr_E \to \infty$ and corresponds to the semiclassical limit of the Schrödinger equation (4.11), while the threshold limit $k \to 0$ implies $kr_E \to 0$ and corresponds to the anticlassical limit.

The local classical momentum $p_{\text{tail}}(E; r) = \sqrt{2\mu[E - V_{\text{tail}}(r)]}$ is real and positive for all distances $0 < r < \infty$. At distances noticeably smaller than r_E, as defined in (4.78), $p_{\text{tail}}(E; r)$ is dominated by the contribution from $V_{\text{tail}}(r)$ and becomes independent of energy. The quantality function (2.139) becomes insensitive to the energy and vanishes for $r \to 0$, so the WKB representations of the solutions of (4.11) become exact in the limit $r \to 0$. This implies that the solutions of (4.11) can, for any energy E, be unambiguously decomposed into incoming and outgoing radial waves at small distances. At distances much larger than r_E, the potential $V_{\text{tail}}(r)$ is only a small correction to the dominant, constant part $\hbar k$ of $p_{\text{tail}}(E; r)$, and the Schrödinger equation (4.11) becomes that for free-particle motion. For $r \gg r_E$, the wave function essentially describes free-particle motion and can also be decomposed into incoming and outgoing waves. In between the near-origin regime $r \to 0$ and the large-distance regime $r \gg r_E$, there is a *nonclassical region* of the reference potential $V_{\text{tail}}(r)$, with distances of the order of the generalized reduced classical turning point r_E, where the condition (2.141) is not well fulfilled—at least at low energies. Even though there is no potential barrier and no classical turning point, incoming waves can be partially reflected in this nonclassical region of coordinate space, so that only a fraction of the incoming radial wave penetrates through to the near-origin regime. Such classically forbidden reflection is a purely quantum mechanical phenomenon and is called *quantum reflection*; it is the counterpart of classically forbidden transmission through a potential barrier—called tunnelling.

For each energy E, i.e. for each wave number k, there are two linearly independent solutions of Eq. (4.11), and the physically relevant linear combination of these two solutions is chosen by defining appropriate boundary conditions at small distances. For ordinary scattering problems, this boundary condition is chosen to ensure that the regular solution of the radial Schrödinger equation with the full interaction matches to the solution of (4.11) at large distances. Other choices are,

however, possible. Choosing incoming boundary conditions at $r \to 0$,

$$u(r) \overset{r\to 0}{\sim} \frac{T}{\sqrt{p_{\text{tail}}(E;r)}} \exp\left(-\frac{\mathrm{i}}{\hbar}\int_{r_0}^{r} p_{\text{tail}}\big(E;r'\big)\mathrm{d}r'\right), \tag{4.79}$$

corresponds to assuming that all incoming flux which is transmitted through the nonclassical region of the potential tail to small distances is absorbed. Note that, for sufficiently small r, the upper integration limit r is smaller than the lower integration limit r_0 in the integral in (4.79), so the integral itself is negative. Writing the argument of the WKB wave function as upper limit in the action integral has the advantage, that wave functions containing $\exp(-\frac{\mathrm{i}}{\hbar}\int^r \cdots)$ are easily identified as inward-travelling waves, whereas wave functions containing $\exp(+\frac{\mathrm{i}}{\hbar}\int^r \cdots)$ are outward-travelling waves.

Starting with the incoming boundary conditions (4.79), the Schrödinger equation (4.11) can be integrated outwards, which yields a well defined solution that can be decomposed into incoming and outgoing radial waves at large distances,

$$u(r) \overset{r\to\infty}{\sim} \frac{1}{\sqrt{\hbar k}}\big(\mathrm{e}^{-\mathrm{i}kr} + R\mathrm{e}^{+\mathrm{i}kr}\big). \tag{4.80}$$

Since the potential $V_{\text{tail}}(r)$ is strongly r-dependent for $r \to 0$, the right-hand side of (4.79) necessarily contains the prefactor $1/\sqrt{p_{\text{tail}}(E;r)}$. The factor $1/\sqrt{\hbar k}$ on the right-hand side of (4.80) is included for consistency. The transmission coefficient T in (4.79) can be chosen such that there is no further proportionality constant in front of the incoming wave in (4.80). The phase of T also depends on the choice of the lower integration limit r_0 in the action integral. Equation (4.80) defines the *quantum reflection amplitude* R. Comparing Eq. (4.80) with Eqs. (2.68) and (2.69) in Sect. 2.3.6 shows that the reflection amplitude R can be interpreted as minus the s-wave S-matrix,

$$R \equiv -S_{l=0} = -\mathrm{e}^{2\mathrm{i}\boldsymbol{\delta}_0}, \tag{4.81}$$

with an s-wave scattering phase shift $\boldsymbol{\delta}_0$. Incoming boundary conditions imply absorption, so the S-matrix is no longer unitary, which is expressed through a complex phase shift $\boldsymbol{\delta}_0$.

The immediate near-threshold behaviour of the quantum reflection amplitude can be easily derived [35] on the basis of the two threshold ($E = 0$) solutions $u_0^{(0)}(r)$ and $u_1^{(0)}(r)$ of the radial Schrödinger equation (4.11), which are defined by their asymptotic behaviour (4.34). From their small-r behaviour (4.35), it follows that the linear combination

$$\begin{aligned} u(r) \;&=\; \frac{\mathrm{e}^{\mathrm{i}\phi_0/2}}{D_1}u_1^{(0)}(r) - \frac{\mathrm{e}^{\mathrm{i}\phi_1/2}}{D_0}u_0^{(0)}(r) \\ &\overset{r\to 0}{\propto} \frac{1}{\sqrt{p_{\text{tail}}(0;r)}} \exp\left(-\frac{\mathrm{i}}{\hbar}\int_{\infty}^{r} p_{\text{tail}}\big(0;r'\big)\mathrm{d}r'\right) \end{aligned} \tag{4.82}$$

obeys incoming boundary conditions for $r \to 0$. At large distances, the superposition (4.82) behaves as

$$u(r) \overset{r\to\infty}{\sim} -\frac{\mathrm{e}^{\mathrm{i}\phi_1/2}}{D_0} + \frac{\mathrm{e}^{\mathrm{i}\phi_0/2}}{D_1} r, \tag{4.83}$$

which is to be compared with

$$\frac{1}{\sqrt{\hbar k}}\left(\mathrm{e}^{-\mathrm{i}kr} + R\mathrm{e}^{+\mathrm{i}kr}\right) \overset{kr\to 0}{\propto} 1 + R - \mathrm{i}k(1-R)r. \tag{4.84}$$

Since the ratio of the constant term and the coefficient of r must be the same in (4.83) and (4.84), we obtain

$$\frac{D_0}{D_1}\mathrm{e}^{\mathrm{i}(\phi_0-\phi_1)/2} = \frac{\mathrm{i}k(1-R)}{1+R} \quad \Longrightarrow \quad R \overset{k\to 0}{\sim} -\frac{1 - \mathrm{i}k\mathrm{e}^{-\mathrm{i}(\phi_0-\phi_1)/2} D_1/D_0}{1 + \mathrm{i}k\mathrm{e}^{-\mathrm{i}(\phi_0-\phi_1)/2} D_1/D_0}, \tag{4.85}$$

and, with the threshold length b and mean scattering length $\bar{a}$ as defined in (4.40), (4.42),

$$R \overset{k\to 0}{\sim} -\left[1 - 2k\frac{D_1}{D_0}\left[\sin\left(\frac{\phi_0-\phi_1}{2}\right) + \mathrm{i}\cos\left(\frac{\phi_0-\phi_1}{2}\right)\right]\right] = -\big[1 - 2\mathrm{i}(\bar{a} - \mathrm{i}b)k\big]. \tag{4.86}$$

Expressing R in terms of the complex phase shift $\boldsymbol{\delta}_0$ according to (4.81) reveals the following near-threshold behaviour of $\boldsymbol{\delta}_0$,

$$\boldsymbol{\delta}_0 \overset{k\to 0}{\sim} -(\bar{a} - \mathrm{i}b)k = -\mathscr{A}k. \tag{4.87}$$

Thus the mean scattering length $\bar{a}$ and the threshold length b, introduced in Sect. 4.1.1 as tail parameters of a singular reference potential $V_{\mathrm{tail}}(r)$, appear as the real part and minus the imaginary part of the *complex scattering length* [3, 88, 89],

$$\mathscr{A} = \bar{a} - \mathrm{i}b, \tag{4.88}$$

which describes the leading near-threshold behaviour of the quantum reflection amplitude. The mean scattering length is well defined only for potentials falling off faster than $1/r^3$ at large distances, but the threshold length b is well defined for potentials falling off faster than $1/r^2$. The leading near-threshold behaviour of the modulus of the quantum reflection amplitude is determined by the threshold length b,

$$|R| \overset{k\to 0}{\sim} 1 - 2bk + O\big(k^2\big) = \mathrm{e}^{-2bk} + O\big(k^2\big). \tag{4.89}$$

Note that the probability $|R|^2$ for quantum reflection approaches unity at threshold, so quantum reflection always becomes dominant at sufficiently low energies.

The effective-range expansion, described for the phase shifts of ordinary scattering in Sect. 2.3.8, can be adapted for the complex phase shifts of quantum reflection,

as described in Ref. [3]. Equation (2.103) becomes

$$k\cot\delta_0 \overset{k\to 0}{\sim} -\frac{1}{\bar{a}-\mathrm{i}b}+\frac{1}{2}\mathscr{R}_{\mathrm{eff}}k^2, \quad \mathscr{R}_{\mathrm{eff}}=2\int_0^\infty \left(\left[w^{(0)}(r)\right]^2-\left[u^{(0)}(r)\right]^2\right)\mathrm{d}r, \tag{4.90}$$

but the radial wave function $u^{(0)}(r)$ is now defined as the solution of (4.11) which obeys incoming boundary conditions for $r\to 0$ and the following boundary conditions for large r:

$$u^{(0)}(r) \overset{r\to\infty}{\sim} 1-\frac{r}{\bar{a}-\mathrm{i}b}. \tag{4.91}$$

The wave function $w^{(0)}(r)$ in (4.90) assumes the form (4.91) in the whole range of r-values, from the origin to infinity,

$$w^{(0)}(r)=1-\frac{r}{\bar{a}-\mathrm{i}b}. \tag{4.92}$$

The parameter $\mathscr{R}_{\mathrm{eff}}$ in (4.90) is the complex effective range. As for the real effective range in ordinary scattering, it is well defined for potentials $V_{\mathrm{tail}}(r)$ falling off faster than $1/r^5$ at large distances.

At high energies corresponding to the semiclassical limit of the Schrödinger equation (4.11), the probability for the classically forbidden process of quantum reflection vanishes. For an infinitely differentiable potential $V_{\mathrm{tail}}(r)$, the probability generally decreases exponentially with an exponent proportional to a typical classical action in units of $\hbar$, e.g. to the generalized reduced classical turning point kr_E introduced above,

$$|R| \overset{k\to\infty}{\propto} \mathrm{e}^{-B_{\mathrm{o}}kr_E}, \tag{4.93}$$

with some dimensionless constant B_{o}.

For an attractive single-power tail (4.57), the generalized reduced classical turning point is given by

$$kr_E=(k\beta_\alpha)^{1-2/\alpha}, \tag{4.94}$$

and the quantum reflection amplitude depends only on $k\beta_\alpha$. The exponent on the right-hand side of (4.93) describing the high-energy behaviour of $|R|$ is $B_{\mathrm{o}}kr_E=B_{\mathrm{o}}(k\beta_\alpha)^{1-2/\alpha}$ in this case; the coefficients B_{o} were derived in [33] and are given in the last row of Table 4.1 in Sect. 4.1.1. Plots of $\ln|R|$, as function both of $k\beta_\alpha$ and of $(k\beta_\alpha)^{1-2/\alpha}$, are shown in Fig. 4.8. The linear initial fall-off of the various curves in the left-hand part of the figure is in agreement with (4.89), and the gradients $-2b/\beta_\alpha$ reflect the respective threshold lengths b as already given in Eq. (4.61) and Table 4.1. In the right-hand part of the figure, the fall-off at large values of $(k\beta_\alpha)^{1-2/\alpha}$ is in agreement with (4.93); the straight dashed lines show $-B_{\mathrm{o}}(k\beta_\alpha)^{1-2/\alpha}$ with the values B_{o} as given in the bottom row of Table 4.1. With increasing power α, the exponent $B_{\mathrm{o}}(k\beta_\alpha)^{1-2/\alpha}$ describing the high-energy behaviour of $|R|$ approaches the exponent $-2bk$ describing its low-energy behaviour, see the corresponding entries in

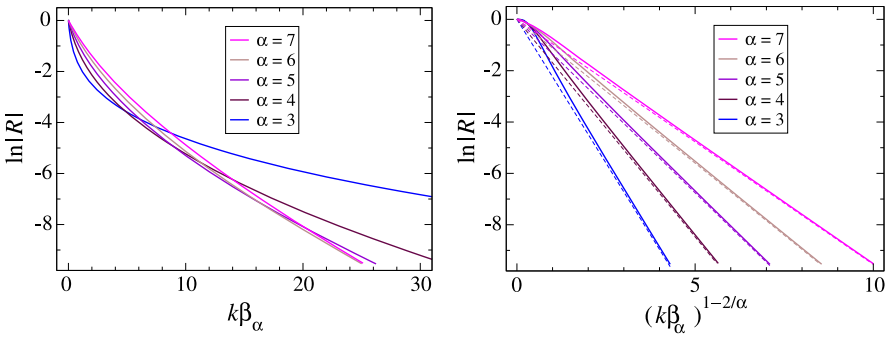

Fig. 4.8 Logarithmic plot of the modulus $|R|$ of the quantum reflection amplitude for attractive inverse-power potentials (4.57) for $\alpha = 3, \ldots, 7$ as functions of $k\beta_\alpha$ (*left-hand part*) and of $(k\beta_\alpha)^{1-2/\alpha}$ (*right-hand part*). The *straight dashed lines* in the right-hand part show the functions $-B_o(k\beta_\alpha)^{1-2/\alpha}$ with the coefficients B_o given in the bottom row of Table 4.1. (Adapted from [33])

the last column of Table 4.1. Thus the low- and high-energy behaviour of $|R|$ merges into a single exponential form for single-power tails (4.57) with large power α,

$$|R| \overset{\alpha\to\infty}{\sim} \mathrm{e}^{-2\pi k\beta_\alpha/\alpha} \tag{4.95}$$

for all energies.

The tail parameters of attractive single-power tails (4.57) can be related in a very elegant way to corresponding parameters of the repulsive inverse-power potentials (2.160) discussed in Sect. 2.4. To see this, observe that the repulsive inverse-power potential (2.160) becomes the attractive inverse-power potential (4.57) by an appropriate transformation of the quantum length β_α. With $\nu = 1/(\alpha - 2)$:

$$\beta_\alpha \to \beta_\alpha^{-\mathrm{i}\pi\nu} \quad \Longrightarrow \quad \frac{(\beta_\alpha)^{\alpha-2}}{r^\alpha} \to -\frac{(\beta_\alpha)^{\alpha-2}}{r^\alpha}. \tag{4.96}$$

The same transformation, $\beta_\alpha \to \beta_\alpha^{-\mathrm{i}\pi\nu}$, transforms the purely imaginary local classical momentum under the repulsive inverse-power potential to a real local classical momentum in the attractive inverse-power potential. The radial wave function which is exactly equal to its WKB representation in the limit $r \to 0$ for inverse-power tails with $\alpha > 2$, is transformed from the regular solution which vanishes monotonically for $r \to 0$ in the repulsive case to the oscillating solution obeying incoming boundary conditions in the attractive case. All properties which depend on the quantum length β_α carry over from the repulsive to the attractive case via the transformation (4.96). The scattering length, which is given by (2.181) for the repulsive inverse-power potential (2.160), transforms according to

$$a = \nu^{2\nu}\frac{\Gamma(1-\nu)}{\Gamma(1+\nu)}\beta_\alpha \quad \longrightarrow \quad \nu^{2\nu}\frac{\Gamma(1-\nu)}{\Gamma(1+\nu)}\beta_\alpha\big[\cos(\pi\nu) - \mathrm{i}\sin(\pi\nu)\big] = \bar{a} - \mathrm{i}b \tag{4.97}$$

to the complex scattering length $\mathscr{A} = \bar{a} - \mathrm{i}b$; the expressions following for the mean scattering length $\bar{a}$ and the threshold length b according to (4.97) are those already given in (4.61) . Similarly, the complex effective range $\mathscr{R}_{\mathrm{eff}}$ appearing in (4.90) is, for attractive single-power potentials (4.57) with $\alpha > 5$, just $\mathrm{e}^{-\mathrm{i}\pi\nu}$ times the real effective range r_{eff} of the corresponding repulsive inverse-power potential (4.57) with the same quantum length β_α [3]. The straightforward relationship between repulsive and attractive inverse-power potentials makes it possible to adapt the extensive results on the near-threshold behaviour of phase shifts which were derived in [22] for repulsive inverse-power potentials to the description of quantum reflection by attractive inverse-power potentials.

4.1.2.1 Observation of Quantum Reflection

Quantum reflection is observable in collisions of ultracold atoms with surfaces. At *large* distances, the projectile interacts with a plane surface via electrostatic van der Waals forces, which are modified at *very large* distances due to retardation [19]. Such "Casimir-Polder potentials" have all the properties assumed for the reference potential $V_{\mathrm{tail}}(r)$ in this section. Due to translational invariance parallel to the surface, the motion normal to the surface is decoupled from the parallel motion, and it is governed by a one-dimensional Schrödinger equation equivalent to the s-wave radial equation of scattering in three-dimensional space. Very low normal velocities can be achieved with grazing incidence of very slow projectiles. Atoms which are transmitted through the nonclassical region of the potential are accelerated towards the surface and are likely to transfer at least some small fraction of their kinetic energy to the surface, which leads to trapping of the atom at the surface if its total energy falls below zero. Such "sticking" is classically expected to become dominant at very low velocities, but early experiments with liquid helium surfaces indicated a suppression of sticking probabilities towards threshold, which was confirmed in quantum mechanical calculations [10, 12]. The quenched sticking probabilities are due to quantum reflection in the potential tail, whereby only a fraction of the incident atoms actually penetrates through to the deep attractive part of the atom-surface potential [18, 90]. Quantitative measurements of quantum reflection probabilities for ultracold atoms scattering off solid surfaces have since been performed by several groups, e.g. [21, 74, 78], and the growing activity in the field of ultracold atoms and molecules has drawn particular attention to this phenomenon [15, 20, 26, 32, 60, 61, 70, 91].

The van der Waals interaction between a neutral atom and a plane conducting or dielectric surface is $-C_3/r^3$, but at very large distances it becomes equal to $-C_4/r^4$ due to retardation effects [19]. The quotient of the strength coefficients in the limiting cases has the dimension of a length,

$$L = \frac{C_4}{C_3}; \tag{4.98}$$

it roughly defines a transition range separating the nonretarded van der Waals regime $r \ll L$ from the highly retarded regime $r \gg L$. At very small distances of a few atomic units or so, the atom-surface potential is rather complicated, but this "close region" is not important when considering quantum reflection with incoming boundary conditions. Beyond the close region, the singular, attractive atom-surface potential can be written as

$$V_{\rm tail}(r) = -\frac{C_3}{r^3}\mathrm{v}\left(\frac{r}{L}\right), \qquad \lim_{x\to 0}\mathrm{v}(x) = 1, \qquad \lim_{x\to\infty}\mathrm{v}(x) = \frac{1}{x}. \tag{4.99}$$

The *shape function* $\mathrm{v}(x)$ interpolates between the $-C_3/r^3$ behaviour for $r \ll L$ and the $-C_4/r^4$ behaviour for $r \gg L$.

In order to explain the quantum reflection probabilities that he observed in his pioneering experiments involving metastable neon atoms and solid surfaces, Shimizu [78] modelled the atom-surface potential with a very simple shape function,

$$\mathrm{v}_1(x) = \frac{1}{1+x} \quad \Longrightarrow \quad V_{\rm tail}(r) = -\frac{\hbar^2}{2\mu}\left[\frac{r^3}{\beta_3} + \frac{r^4}{(\beta_4)^2}\right]^{-1}. \tag{4.100}$$

The lengths β_3 and β_4 are the quantum lengths for the single-power forms (4.57), which the potential (4.99) approaches in the limits $r \to 0$ and $r \to \infty$, respectively. An alternative interpolation is guided by the exact potential for a hydrogen atom interacting with a perfectly conducting surface, which was calculated numerically in [57]. For this we define the shape function

$$\mathrm{v}_{\rm H}(r) = \frac{1+\xi x}{1+x+\xi x^2}, \quad \xi = 0.31608. \tag{4.101}$$

With the shape function (4.101) and the coefficients C_3, C_4 appropriate for the case of a hydrogen atom in front of a conducting surface,

$$C_3 = \frac{1}{12}\langle\psi_0|r^2|\psi_0\rangle = \frac{1}{4}\ \text{a.u.}, \qquad C_4 = \frac{3}{8\pi}\frac{\alpha_{\rm d}(0)}{\alpha_{\rm fs}} \approx 73.61\ \text{a.u.} \tag{4.102}$$

the potential (4.99) reproduces the values of the hydrogen-surface potential tabulated in [57] to within 0.6 % in the whole range of r-values. In (4.102), ψ_0 stands for the hydrogen atom's ground-state wave function, $\alpha_{\rm d}(0) = \frac{9}{2}$ a.u. is its static dipole polarizability and $\alpha_{\rm fs}$ is the dimensionless fine structure constant. The parameter ξ in (4.101) is not a fit parameter, but is determined by the condition that the universal next-to-leading term in the small-distance expansion of the potential of a Z-electron atom in front of a conducting wall [9],

$$V_Z(r) \overset{r\to 0}{\sim} \frac{C_3}{r^3} + \frac{Z\alpha_{\rm fs}}{4\pi r^2}, \tag{4.103}$$

is given correctly by the formula (4.101) for the hydrogen case $Z = 1$. This leads to $\xi = 1 - \alpha_{\rm fs}C_4/[4\pi(C_3)^2]$.

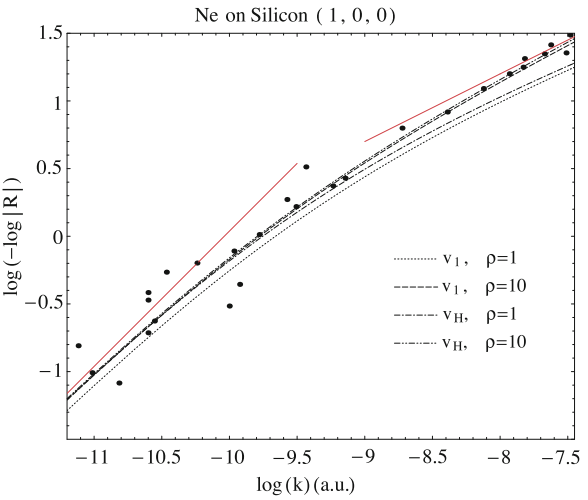

Fig. 4.9 Modulus of the quantum reflection amplitude, as observed in the scattering of metastable neon atoms off a silicon surface [78]. The figure shows $\ln(-\ln|R|)$ as function of $\ln(k)$ (natural logarithms) with k measured in atomic units, i.e. in units of the inverse Bohr radius. The curves show the results obtained by numerically solving the Schrödinger equation (4.11) with potentials (4.99) constructed with the shape functions v_1 and v_H. The quantum length β_4 associated with the strength C_4 of the potential in the highly retarded limit is $\beta_4 = 11400$ a.u. in all cases. For the $-C_3/r^3$ van der Waals limit of the potential, the quantum length is $\beta_3 = 11400$ a.u. for $\rho = 1$ and $\beta_3 = 114000$ a.u. for $\rho = 10$. The *straight red line* in the *bottom left* corner shows the behaviour $\ln|R| \sim -2\beta_4 k$ expected in the low-k regime. The *straight red line* in the *top right* corner shows the behaviour $\ln|R| \propto -\sqrt{\beta_4 k}$ expected in the high-k regime for a single-power $1/r^4$ potential. (From [33])

As shown in [33], which part of the atom-wall potential dominantly influences quantum reflection depends on the ratio $\rho = \beta_3/\beta_4$ of the quantum lengths characterizing the single-power limits at small and large distances. For $\rho < 1$, the energy dependence of $|R|$ is largely determined by the nonretarded van der Waals part of the potential; for $\rho > 1$, the retarded $-C_4/r^4$ part is dominant. Thus the smaller of the two quantum lengths is the one belonging to the dominant term. This observation may be counter-intuitive, but it is understandable when looking at the expression for the atom-wall potential that is given on the far right of (4.100).

The transition from the leading linear behaviour (4.89) of $|R|$ near threshold to the high-k behaviour (4.93) can be exposed by studying $\ln(-\ln|R|)$ as a function of $\ln k$,

$$|R| = \mathrm{e}^{-Bk^C} \quad \Longrightarrow \quad \ln\bigl(-\ln|R|\bigr) = \ln(B) + C\ln(k). \tag{4.104}$$

A plot of $\ln(-\ln|R|)$ against $\ln(k)$ is shown in Fig. 4.9 for the quantum reflection of metastable neon atoms by a silicon surface, as studied by Shimizu in [78]. The dots are the experimental data and the curves are the results obtained by numerically solving the Schrödinger equation (4.11) with potentials (4.99) constructed with the

shape functions v_l and v_H. The quantum length corresponding to the highly retarded $-C_4/r^4$ part of the potential was $\beta_4 = 11400$ a.u. in all four cases. The value of β_3 was chosen to be equal to β_4, corresponding to $\rho = 1$, or to be ten times larger, corresponding to $\rho = 10$. The straight red line in the bottom left of the figure has unit gradient, corresponding to the universal near-threshold behaviour (4.89). The results obtained with all potentials in Fig. 4.9 approach such behaviour in the low-k limit, and the data are consistent, albeit with a very large scatter. Towards large k, the gradients of the curves in Fig. 4.9 decrease gradually. The experimental points are well fitted by the two curves with $\rho = 10$, i.e. with $\beta_3 = 114000$ a.u. They are essentially the same for both shape functions, (4.100) and (4.101), and they are also independent of β_3 as long as β_3 is significantly larger than β_4. Essentially the same result is obtained with a single-power $-1/r^4$ potential with the appropriate quantum length $\beta_4 = 11400$ a.u. The straight red line in the top right corner of the figure shows the large-k behaviour expected in this case according to (4.93), with $B_o k r_E = B_o(k\beta_4)^{1/2}$; its gradient is $\frac{1}{2}$. In contrast, the large-k behaviour of the two curves with $\rho = 1$ is closer to the expectation of a $-1/r^3$ potential, where the asymptotic gradient is $\frac{1}{3}$. One expects the nonretarded $-1/r^3$ part of the potential at moderate distances to have increasing influence at higher energies, but at the energies where this happens, the quantum reflection yields are very small.

As already pointed out by Shimizu in [78], the highly retarded part of the neon-surface interaction is essentially responsible for quantum reflection observed in the experiment. Also for other atom-wall systems, involving e.g. bosonic alkali atoms, hydrogen or metastable helium, the crucial parameter β_3/β_4 is generally significantly larger than unity [33, 35]. Quantum reflection is well described on the basis of the highly retarded, single-power $-1/r^4$ potential in all these cases.

It is also worth noting, that all characteristic lengths, including the transition length (4.98) are very large, typically several hundreds or thousands of atomic units (Bohr radii) [33, 35]. Quantum reflection is generated at really large atom-surface distances. The same applies for the quantum reflection of ultracold molecules, as was impressively demonstrated in a recent experiment by Zhao et al. who scattered helium dimers off a solid diffraction grating at very low energies corresponding to normal incident velocities near 10 cm/s, translating to a kinetic energy near 0.6 neV ($\approx 2 \times 10^{-11}$ a.u.) in the normal direction. The very fragile helium dimer, with a binding energy of only 4×10^{-8} a.u. and a bond length of almost 100 a.u. (Bohr radii), is expected to fragment while being accelerated under the influence of the attractive molecule-surface potential with a well depth near 2×10^{-4} a.u. However, a noticeable fraction of the incident dimers is spared this fate due to quantum reflection, which occurs "tens of nanometers above the actual surface where the $\cdots$ forces are still too feeble to break up even the fragile He_2 bond" [91].

4.1.2.2 Nonplanar Surfaces

For atoms scattering off an absorbing sphere, the radius of the sphere enters as a further length in the problem. As shown in [4], the nonclassical region of the

potential tail moves to smaller r-values when the radius of the sphere is decreased, but the transition region between nonretarded van der Waals regime and the highly retarded regime is essentially independent of this radius and roughly the same as for an atom in front of a plane surface. The sensitivity of quantum reflection to the nonretarded part of the atom-surface potential thus becomes increasingly noticeable for smaller spheres.

It is interesting to consider the threshold limits of the cross sections for elastic scattering and for absorption of atoms interacting with an absorbing sphere. The electrostatic van der Waals potential is proportional to $1/r^6$, but at very large distances the atom-sphere potential is proportional to $1/r^7$ due to retardation effects [19]. Towards threshold, the scattering amplitude is dominated by the s-wave ($l = 0$), and the complex scattering phase shift is determined by the complex scattering length. With Eq. (2.47) in Sect. 2.3.3 and Eqs. (4.87), (4.88) above,

$$f(\theta) \overset{k\to 0}{\sim} \frac{1}{k}\boldsymbol{\delta}_0 \overset{k\to 0}{\sim} -\bar{a} + \mathrm{i}b. \tag{4.105}$$

The elastic scattering cross section $|f(\theta)|^2$ remains finite, the square of the real scattering length in the nonabsorbing case is simply replaced by the absolute square of the complex scattering length in the presence of absorption,

$$\frac{\mathrm{d}\sigma_{\mathrm{el}}}{\mathrm{d}\Omega} \overset{k\to 0}{\sim} |\mathscr{A}|^2 = \bar{a}^2 + b^2, \quad \sigma_{\mathrm{el}} \overset{k\to 0}{\sim} 4\pi\left(\bar{a}^2 + b^2\right). \tag{4.106}$$

In contrast, the absorption cross section, as given by Eq. (3.53) in Sect. 3.4, behaves as follows towards threshold:

$$\sigma_{\mathrm{abs}} \overset{k\to 0}{\sim} \frac{\pi}{k^2}\left(1 - \left|\mathrm{e}^{2\mathrm{i}\boldsymbol{\delta}_0}\right|^2\right) \overset{k\to 0}{\sim} \frac{\pi}{k^2}\left(1 - |1 - 2kb - 2\mathrm{i}\bar{a}k|^2\right) \overset{k\to 0}{\sim} \frac{4\pi b}{k}. \tag{4.107}$$

This is consistent with the optical theorem (3.17), according to which

$$\sigma_{\mathrm{tot}} = \frac{4\pi}{k}\Im\left[f(\theta = 0)\right] \overset{k\to 0}{\sim} \frac{4\pi}{k}\Im[-\bar{a} + \mathrm{i}b]; \tag{4.108}$$

the total cross section $\sigma_{\mathrm{tot}} = \sigma_{\mathrm{el}} + \sigma_{\mathrm{abs}}$ is dominated towards threshold by the diverging contribution of the absorption cross section (4.107).

The absorption cross section, which is related to the probability for transmission through the nonclassical region of the potential tail, can be used to calculate the rate for a reaction that occurs when projectile and target meet [24]. Since this involves an average over the product of σ_{abs} and the asymptotic relative velocity $\hbar k/\mu$, reaction rates following from absorption cross sections that diverge as in (4.107) tend to finite limits at threshold.

For an atom interacting with a conducting cylinder, the nonclassical region of the potential tail is not so sensitive to the radius of the cylinder. As in the case of the plane wall, the highly retarded part of the atom-cylinder potential is important for

quantum reflection by a conducting cylinder with realistic dimensions. The nonretarded part of the interaction is more likely to play a role for dielectric cylinders [30]. Note that for a cylinder, the atom-surface interaction is much more complicated than for a plane or spherical surface. Furthermore, due to translational invariance along the direction parallel to the cylinder axis, the scattering problem is actually two-dimensional, and quantum mechanical scattering theory in two dimensions is somewhat more subtle than in the one- and three-dimensional cases, in particular near threshold. A detailed description of scattering theory in two spatial dimensions is given later in Sect. 4.3.

4.1.3 Elastic Scattering

Near-threshold quantization, discussed in Sect. 4.1.1, involved matching the regular solution of the radial Schrödinger equation with the full potential to a solution of the radial Schrödinger equation (4.11) obeying bound-state boundary conditions. The potential in (4.11) is the attractive reference potential $V_{\text{tail}}(r)$, which is more singular than $1/r^2$ at small distances, is a good approximation of the full potential at large distances and falls off faster than $1/r^2$ for $r \to \infty$. The influence of the potential tail was contained in one single quantization function (4.16), constructed at each energy E with the help of the small-r behaviour of the asymptotically bound solution of (4.11), which is accurately given by its WKB representation for $r \to 0$.

At positive energies, there are two linearly independent physically meaningful solutions of (4.11) for each energy E, and the small-r behaviour of each solution is determined by an amplitude and a phase, e.g. in the WKB representation of this solution for $r \to 0$. One overall normalization constant is always arbitrary, so the quantum mechanical properties of the reference potential are manifest not in one tail function, as in subthreshold quantization, but in three tail functions at positive energies. In the previous subsection on quantum reflection, the two linearly independent solutions of (4.11) were the incoming and outgoing radial waves $\mathrm{e}^{\pm \mathrm{i}kr}/\sqrt{\hbar k}$, and three appropriate tail functions are the modulus and phase of the quantum reflection amplitude R and the phase of the transmission amplitude T, the modulus of T being already determined by flux conservation, $|R|^2 + |T|^2 = 1$.

An alternative choice of two linearly independent solutions of (4.11) is provided by the wave functions obeying the following large-r boundary conditions [65]:

$$u_{\text{s}}(r) \overset{r\to\infty}{\sim} \sin(kr), \qquad u_{\text{c}}(r) \overset{r\to\infty}{\sim} \cos(kr). \tag{4.109}$$

Beyond the short-range deviations of the full interaction from the reference potential $V_{\text{tail}}(r)$, the regular solution $u_{\text{reg}}(r)$ of the full problem is a superposition of the two solutions of (4.11),

$$u_{\text{reg}}(r) \overset{r \text{ large}}{\propto} \cos\delta_0 u_{\text{s}}(r) + \sin\delta_0 u_{\text{c}}(r). \tag{4.110}$$

The properties of the reference potential $V_{\rm tail}(r)$ are contained in the amplitudes and phases of the WKB representations of $u_{\rm s}(r)$ and $u_{\rm s}(r)$ for $r \to 0$, where these representation become exact. The explicit expressions for the WKB representations contain the lower integration limit in the action integrals as point of reference. In the presence of a classical turning point, this turning point is a natural choice, but for the singular, attractive reference potential $V_{\rm tail}(r)$, there is no classical turning point at positive energy. One conspicuous point is the distance r_E at which the potential $V(r_E)$ is equal to minus the energy E, see Eq. (4.78) in Sect. 4.1.2; it lies in the heart of the nonclassical region of $V_{\rm tail}(r)$. With this choice, the WKB representations of the two solutions of (4.11) defined by the boundary conditions (4.109) can be written as

$$\begin{aligned} u_{\rm s}(r) &\overset{r\to 0}{\sim} \frac{A_{\rm s}}{\sqrt{p_{\rm tail}(E;r)}} \sin\!\left(\frac{1}{\hbar}\int_{r_E}^{r} p_{\rm tail}\big(E;r'\big)\mathrm{d}r' - \phi_{\rm s}\right), \\ u_{\rm c}(r) &\overset{r\to 0}{\sim} \frac{A_{\rm c}}{\sqrt{p_{\rm tail}(E;r)}} \cos\!\left(\frac{1}{\hbar}\int_{r_E}^{r} p_{\rm tail}\big(E;r'\big)\mathrm{d}r' - \phi_{\rm c}\right), \end{aligned} \tag{4.111}$$

with the local classical momentum $p_{\rm tail}(E;r) = \sqrt{2\mu[E - V_{\rm tail}(r)]}$, which is real and positive in the whole range $0 < r < \infty$. Equation (4.111) defines the amplitudes $A_{\rm s,c}$ which are real and taken to be positive, and the phases $\phi_{\rm s,c}$, which are real. These amplitudes and phases are tail functions determined entirely by the reference potential $V_{\rm tail}(r)$. They are functions of energy, but for simplicity in notation this is not explicitly written in the formulae below. Note that the lower limit r_E of the integrals in (4.111) is larger than the upper limit r when $r \to 0$.

At distances r which are small enough for the WKB representations (4.111) of $u_{\rm s}(r)$ and $u_{\rm c}(r)$ to be valid, and at the same time large enough so that the reference potential $V_{\rm tail}(r)$ is a good approximation of the full interaction, the regular solution (4.110) behaves as

$$u_{\rm reg}(r) \propto \frac{1}{\sqrt{p_{\rm tail}(E;r)}} \sin\!\left(\frac{1}{\hbar}\int_{r_E}^{r} p_{\rm tail}\big(E;r'\big)\mathrm{d}r' - \phi_{\rm sr}(E)\right). \tag{4.112}$$

The position r in (4.112) lies beyond the short-range deviations of the full interaction from the reference potential $V_{\rm tail}(r)$, and the inner boundary condition $u_{\rm reg}(0) = 0$ is carried over in terms of the phase $\phi_{\rm sr}(E)$. From (4.110) and (4.111) it follows, that $\phi_{\rm sr}(E)$ is related to the scattering phase shift δ_0 by

$$\tan\delta_0 = \frac{A_{\rm s}}{A_{\rm c}} \frac{\sin(\phi_{\rm s} - \phi_{\rm sr}(E))}{\cos(\phi_{\rm c} - \phi_{\rm sr}(E))}. \tag{4.113}$$

The choice of the reference point r_E in (4.112) may seem unconventional, but it allows the WKB expression to be written in terms of $p_{\rm tail}(E;r')$ rather than $p(E;r')$, which is defined in (4.3) and involves the full interaction. A more conventional WKB representation for $u_{\rm reg}(r)$ is,

$$u_{\rm reg}(r) \propto \frac{1}{\sqrt{p(E;r)}} \cos\!\left(\frac{1}{\hbar}\int_{r_{\rm in}(E)}^{r} p\big(E;r'\big)\mathrm{d}r' - \frac{\phi_{\rm in}(E)}{2}\right), \tag{4.114}$$

which defines the inner reflection phase $\phi_{\rm in}(E)$, compare Eq. (4.2) in Sect. 4.1.1. For distances r beyond the short-range deviations of the full interaction from the reference potential $V_{\rm tail}(r)$, $p_{\rm tail}(E;r)$ and $p(E;r)$ are essentially equal, so the factors in front of the sine in (4.112) and cosine (4.114) are the same. Equating the sine and cosine parts relates $\phi_{\rm in}(E)$ to $\phi_{\rm sr}(E)$:

$$\begin{aligned}\phi_{\rm sr}(E) &= \frac{\phi_{\rm in}(E)}{2} - \frac{\pi}{2} - \frac{1}{\hbar}\int_{r_{\rm in}(E)}^{r} p\big(E;r'\big)\mathrm{d}r' - \frac{1}{\hbar}\int_{r}^{r_E} p_{\rm tail}\big(E;r'\big)\mathrm{d}r' \\ &= \frac{\phi_{\rm in}(E)}{2} - \frac{\pi}{2} - \frac{1}{\hbar}\int_{r_{\rm in}(E)}^{r_E} p\big(E;r'\big)\mathrm{d}r'. \end{aligned} \tag{4.115}$$

Since the range of integration in the second integral in the top line of (4.115) is beyond the short-range deviations, the momentum $p_{\rm tail}(E;r')$ can be replaced by $p(E;r')$ in this integral, which leads to the expression in the bottom line. With the quantization condition at threshold, Eq. (4.6) in Sect. 4.1.1, the phase $\phi_{\rm sr}(E)$ can be related to the threshold quantum number $\upsilon_{\rm D}$,

$$\begin{aligned}\phi_{\rm sr}(E) = -\upsilon_{\rm D}\pi - \frac{\phi_{\rm out}(0)}{2} - \frac{\pi}{2} - \frac{\phi_{\rm in}(0)-\phi_{\rm in}(E)}{2} \\ + \frac{1}{\hbar}\int_{r_E}^{\infty} p(0;r)\mathrm{d}r + \frac{1}{\hbar}\int_{r_{\rm in}(0)}^{r_E} p(0;r)\mathrm{d}r - \frac{1}{\hbar}\int_{r_{\rm in}(E)}^{r_E} p(E;r)\mathrm{d}r.\end{aligned} \tag{4.116}$$

The difference $\phi_{\rm in}(0) - \phi_{\rm in}(E)$ of the inner reflection phases in (4.116) is a smooth function of energy and vanishes at $E = 0$. The leading near-threshold energy dependence of the right-hand side of (4.116) comes from the difference of action integrals in the lower line. Replacing the momenta $p(0;r)$ and $p(E:r)$ in the second and third integrals, i.e. in those with upper limit r_E, by $p_{\rm tail}(0;r)$ and $p_{\rm tail}(E:r)$ introduces an error of order E at most. This is because the difference between p and $p_{\rm tail}$ is limited to short distances and hence a smooth function of E, while the difference of the two integrals clearly vanishes at $E = 0$. In the first integral, covering the range r_E to infinity, $p(0;r)$ can be replaced by $p_{\rm tail}(0;r)$, because r is always beyond the range of the short-range deviations. With the abbreviation

$$\xi = \frac{1}{\hbar}\int_{r_E}^{\infty} p_{\rm tail}(0;r)\mathrm{d}r + \frac{1}{\hbar}\int_{0}^{r_E}\big[p_{\rm tail}(0;r) - p_{\rm tail}(E;r)\big]\mathrm{d}r - \frac{\phi_{\rm out}(0)}{2} - \frac{\pi}{2}, \tag{4.117}$$

we can rewrite Eq. (4.116) as

$$\phi_{\rm sr}(E) = -\upsilon_{\rm D}\pi + \xi + \pi f_{\rm sr}(E), \tag{4.118}$$

where $f_{\rm sr}(E)$ is a smooth function of energy which vanishes at threshold and accounts for all residual short-range effects. The expression (4.113) thus becomes

$$\tan\delta_0 = \frac{A_{\rm s}}{A_{\rm c}}\frac{\sin([\upsilon_{\rm D} - f_{\rm sr}(E)]\pi - \xi + \phi_{\rm s})}{\cos([\upsilon_{\rm D} - f_{\rm sr}(E)]\pi - \xi + \phi_{\rm c})}. \tag{4.119}$$

The influence of the reference potential $V_{\rm tail}(r)$ on the low-energy behaviour of the scattering phase shift δ_0 is expressed through the three tail functions, $A_{\rm s}/A_{\rm c}$, $\phi_{\rm s}$ and $\phi_{\rm c}$. The auxiliary tail function ξ defined in (4.117) is needed to compensate the effects of choosing the lower integration limit in the action integrals to be r_E rather than some energy independent value. Such a choice would introduce an unnecessary element of arbitrariness in the formulation.

Towards threshold, the solutions $u_{\rm s}(r)$ and $u_{\rm c}(r)$ of (4.11), defined by their asymptotic behaviour (4.109), approach the threshold solutions $u_1^{(0)}(r)$ and $u_0^{(0)}(r)$, which were introduced in Sect. 4.1.1 and are defined by the asymptotic behaviour (4.34),

$$u_{\rm s}(r) \overset{k\to 0}{\sim} k u_1^{(0)}(r), \qquad u_{\rm c}(r) \overset{k\to 0}{\sim} u_0^{(0)}(r). \tag{4.120}$$

Consequently, the threshold limits of the tail functions can be expressed in terms of the amplitudes $D_{0,1}$ and phases $\phi_{0,1}$ defining the WKB representations (4.35) of $u_1^{(0)}(r)$ and $u_0^{(0)}(r)$, and the threshold value of ξ follows from (4.117):

$$\begin{aligned} &\frac{A_{\rm s}}{A_{\rm c}} \overset{k\to 0}{\sim} k\frac{D_1}{D_0}, \qquad \phi_{\rm s} \overset{k\to 0}{\longrightarrow} -\frac{\pi}{2} - \frac{\phi_1}{2}, \qquad \phi_{\rm c} \overset{k\to 0}{\longrightarrow} -\frac{\phi_0}{2}, \\ &\xi \overset{k\to 0}{\longrightarrow} -\frac{\pi}{2} - \frac{\phi_0}{2}. \end{aligned} \tag{4.121}$$

With $f_{\rm sr}(E=0)=0$, the near-threshold limit of Eq. (4.119) is seen to be

$$\tan\delta_0 \overset{k\to 0}{\sim} -k\frac{D_1}{D_0}\left[\cos\left(\frac{\phi_0-\phi_1}{2}\right) + \frac{\sin(\frac{\phi_0-\phi_1}{2})}{\tan(\upsilon_{\rm D}\pi)}\right] = -k\left(\bar{a} + \frac{b}{\tan(\upsilon_{\rm D}\pi)}\right). \tag{4.122}$$

The threshold length b and the mean scattering length $\bar{a}$ are as already defined in (4.40) and (4.42) in Sect. 4.1.1, so Eq. (4.122) is consistent with the expression (4.53) for the scattering length a. Remember that a finite value for the mean scattering length $\bar{a}$ exists only for reference potentials $V_{\rm tail}(r)$ falling off faster than $1/r^3$ at large distances.

As mentioned at the beginning of this subsection, the parameters of quantum reflection by the nonclassical part the reference potential $V_{\rm tail}(r)$ can also serve as appropriate tail functions to describe the influence of $V_{\rm tail}(r)$ on the scattering phase shifts [66]. To see this, consider the solution $u_{\rm inc}(r)$ of (4.11) which obeys incoming boundary conditions for $r\to 0$ and behaves as (4.80) for $r\to\infty$. In terms of the solutions $u_{\rm s}(r)$ and $u_{\rm s}(r)$, with the asymptotic behaviour (4.109) we have

$$u_{\rm inc}(r) = -\frac{\rm i}{\sqrt{\hbar k}}(1-R)u_{\rm s}(r) + \frac{1}{\sqrt{\hbar k}}(1+R)u_{\rm c}(r). \tag{4.123}$$

From (4.111) the small-r behaviour of this wave function is

$$u_{\mathrm{inc}}(r) \overset{r\to 0}{\sim} \frac{\mathrm{e}^{-\mathrm{i}I}}{2\sqrt{\hbar k p_{\mathrm{tail}}(E;r)}}\left[(1-R)A_{\mathrm{s}}\mathrm{e}^{\mathrm{i}\phi_{\mathrm{s}}}+(1+R)A_{\mathrm{c}}\mathrm{e}^{\mathrm{i}\phi_{\mathrm{c}}}\right] + \frac{\mathrm{e}^{+\mathrm{i}I}}{2\sqrt{\hbar k p_{\mathrm{tail}}(E;r)}}\left[(1+R)A_{\mathrm{c}}\mathrm{e}^{-\mathrm{i}\phi_{\mathrm{c}}}-(1-R)A_{\mathrm{s}}\mathrm{e}^{-\mathrm{i}\phi_{\mathrm{s}}}\right], \quad (4.124)$$

with $I=\frac{1}{\hbar}\int_{r_E}^{r} p_{\mathrm{tail}}(E;r')\mathrm{d}r'$. Since $u_{\mathrm{inc}}(r)$ is required to obey incoming boundary conditions for $r\to 0$, the content of the square bracket in the lower line of (4.124) must vanish,

$$(1+R)A_{\mathrm{c}}\mathrm{e}^{-\mathrm{i}\phi_{\mathrm{c}}}=(1-R)A_{\mathrm{s}}\mathrm{e}^{-\mathrm{i}\phi_{\mathrm{s}}}. \quad (4.125)$$

The quotient $A_{\mathrm{s}}/A_{\mathrm{c}}$ of the real and positive amplitudes defined by (4.111) is thus related to the quantum reflection amplitude R by

$$\frac{A_{\mathrm{s}}}{A_{\mathrm{c}}}=\left|\frac{1+R}{1-R}\right|. \quad (4.126)$$

The phase of the square bracket on the right-hand side of the upper line of (4.124) can be deduced by exploiting (4.125) to replace either $(1-R)A_{\mathrm{s}}$ by $(1+R)A_{\mathrm{c}}\mathrm{e}^{\mathrm{i}(\phi_{\mathrm{c}}-\phi_{\mathrm{s}})}$ or $(1+R)A_{\mathrm{c}}$ by $(1-R)A_{\mathrm{s}}\mathrm{e}^{\mathrm{i}(\phi_{\mathrm{s}}-\phi_{\mathrm{c}})}$. This phase represents the argument of the transmission coefficient T as defined by (4.79), provided that the lower limit r_0 in the action integral is taken as r_E. With this definition of T,

$$\arg T=\phi_{\mathrm{s}}+\arg(1+R)=\phi_{\mathrm{c}}+\arg(1-R). \quad (4.127)$$

In terms of the amplitudes for reflection by and transmission through the nonclassical region of the reference potential $V_{\mathrm{tail}}(r)$, Eq. (4.119) reads

$$\tan\delta_0=\left|\frac{1+R}{1-R}\right|\frac{\sin([\upsilon_{\mathrm{D}}-f_{\mathrm{sr}}(E)]\pi-\xi+\arg T-\arg(1+R))}{\cos([\upsilon_{\mathrm{D}}-f_{\mathrm{sr}}(E)]\pi-\xi+\arg T-\arg(1-R))}. \quad (4.128)$$

Equation (4.119) and its rephrased version (4.128) transparently expose how the energy dependence of the scattering phase shift δ_0 is influenced by the reference potential $V_{\mathrm{tail}}(r)$. As for near-threshold quantization discussed in Sect. 4.1.1, the threshold quantum number υ_{D}, more precisely the remainder $\Delta_{\mathrm{D}}=\upsilon_{\mathrm{D}}-\lfloor\upsilon_{\mathrm{D}}\rfloor$, crucially determines the leading energy dependence of δ_0.

For reference potentials $V_{\mathrm{tail}}(r)$ falling off faster than $1/r^3$ at large distances, the leading proportionality of $\tan\delta_0$ to k comes from the prefactor (4.126) in front of the quotient of sine and cosine, and the actual value of the scattering length a depends sensitively on Δ_{D}, as seen in Eq. (4.122) and in Eq. (4.53) in Sect. 4.1.1. The scattering length a and the remainder Δ_{D} are interchangeable parameters; each one characterizes how near the most weakly bound state is to threshold.

For potentials falling off as $-1/r^3$ asymptotically, there is no finite scattering length, and the threshold quantum number's remainder Δ_{D} assumes the role of the critical parameter determining the near-threshold beahaviour of the s-wave phase shift δ_0. In 2013, Müller [67] derived the exact analytical expression for the leading

behaviour of δ_0 up to and including all terms of order k^2,

$$\tan\delta_0 = -\left[\ln(k\beta_3) + \frac{\pi}{\tan(\pi\Delta_D)} + 3\gamma_E + \ln 2 - \frac{3}{2}\right](k\beta_3) + \pi\left[\ln(k\beta_3) + \frac{\pi}{\tan(\pi\Delta_D)} + 3\gamma_E + \ln 2 - \frac{19}{12}\right](k\beta_3)^2 + O\big(k^3\big). \quad (4.129)$$

In (4.129), $\gamma_E = 0.577\cdots$ is Euler's constant (see Appendix B.3) and β_3 is the quantum length corresponding to the leading asymptotic term $-C_3/r^3$ according to (4.58).

At large energies, for which the quantum reflection amplitude is close to zero, the prefactor in (4.119), (4.128) is essentially unity and the arguments of sine and cosine in the quotient are essentially the same and equal to δ_0 itself,

$$\delta_0 \overset{k\to\infty}{\sim} \big[\upsilon_D - f_{sr}(E)\big]\pi - \xi + \phi_s = \big[\upsilon_D - f_{sr}(E)\big]\pi - \xi + \arg T. \quad (4.130)$$

In this semiclassical regime, the threshold quantum number υ_D affects the scattering phase shift only as an additive constant. Further effects due to the short-range deviation of the full interaction from the reference potential $V_{tail}(r)$ enter via the correction term $f_{sr}(E)$, which is a smooth function of energy, in particular at threshold, and vanishes at $E = 0$:

$$f_{sr}(E) = \gamma_{sr}E + O\big(E^2\big). \quad (4.131)$$

Again, the description above is particularly useful for single-power tails (4.57), for which the tail properties depend not on energy and potential strength independently, but only on the dimensionless product $k\beta_\alpha$ of the wave number k and the quantum length β_α. The point of reference in units of β_α is $r_E/\beta_\alpha = (k\beta_\alpha)^{-2/\alpha}$ according to (4.94), and the auxiliary function (4.117) is given by [65]

$$\xi = -\left(\frac{3}{4} + \frac{\nu}{2}\right)\pi + 2\nu\eta_\alpha(k\beta_\alpha)^{1-2/\alpha}, \quad \text{with } \nu = \frac{1}{\alpha-2} \quad \text{and} \quad (4.132)$$

$$\eta_\alpha = \sqrt{2} - \frac{\alpha}{\alpha+2}\,{}_2F_1\left(\frac{1}{2}, \frac{1}{2} + \frac{1}{\alpha}; \frac{3}{2} + \frac{1}{\alpha}; -1\right); \quad (4.133)$$

${}_2F_1$ stands for the hypergeometric function defined by Eq. (B.52) in Appendix B.5. The leading near-threshold behaviour of the tail functions A_s/A_c, ϕ_s and ϕ_c is, for any $\alpha > 3$ [65],

$$\frac{A_s}{A_c} \overset{k\to 0}{\sim} \nu^{2\nu}\frac{\Gamma(1-\nu)}{\Gamma(1+\nu)}k\beta_\alpha = k\sqrt{\bar{a}^2 + b^2}, \quad (4.134)$$

$$\phi_{s/c} \overset{k\to 0}{\sim} \left(-\frac{1}{2} \pm \frac{\nu - \frac{1}{2}}{2}\right)\pi + 2\nu\eta_\alpha(k\beta_\alpha)^{1-2/\alpha}. \quad (4.135)$$

The leading near-threshold behaviour of $\tan\delta_0$ is as given in (4.122), with $\bar{a}$ and b as given in Eq. (4.61) and Table 4.1 in Sect. 4.1.1. In the semiclassical limit of large k, the prefactor (4.126) approaches unity exponentially, compare Eq. (4.93),

Table 4.9 Numerical values of dimensionless parameters η_α and ρ_α as defined in Eqs. (4.133) and (4.136), respectively

α	3	4	5	6	7	$\alpha \to \infty$
η_α	0.908797	0.847213	0.802904	0.769516	0.743463	0.532840
ρ_α	0.769516	0.847213	0.885769	0.908797	0.924102	1

and

$$\phi_{\mathrm{s/c}} \overset{k\to\infty}{\sim} -\rho_\alpha (k\beta_\alpha)^{1-2/\alpha}, \quad \rho_\alpha = \sqrt{2} - \frac{\alpha/2}{\alpha-1} {}_2F_1\left(\frac{1}{2}, 1-\frac{1}{\alpha}; 2-\frac{1}{\alpha}; -1\right), \quad \alpha > 2. \tag{4.136}$$

The high-k behaviour of the phase shift is thus

$$\delta_0 \overset{k\to\infty}{\sim} \left(\upsilon_{\mathrm{D}} - f_{\mathrm{sr}}(E) + \frac{3}{4} + \frac{\nu}{2}\right)\pi - (\rho_\alpha + 2\nu\eta_\alpha)(k\beta_\alpha)^{1-2/\alpha}, \tag{4.137}$$

as already given in [31]. Numerical values of the dimensionless parameters η_α and ρ_α are listed in Table 4.9

For a single power tail (4.57), the quantum length β_α can be related to an energy E_{β_α},

$$E_{\beta_\alpha} = \frac{\hbar^2}{2\mu\beta_\alpha^2}, \tag{4.138}$$

which defines a scale separating the extreme quantum region immediately near threshold from the regime of somewhat larger energies, where the influence of the reference potential can be described semiclassically. (See also Eq. (4.70) in Sect. 4.1.1.) For $E \ll E_{\beta_\alpha}$ corresponding to $k\beta_\alpha \ll 1$, the near-threshold expansions (4.134), (4.135) apply and the phase shift may be expressed via the scattering length according to (4.122); for $\alpha = 3$ the near-threshold expansion of the phase shift is expressed via the remainder Δ_{D} according to (4.129). As the energy increases beyond E_{β_α} corresponding to $k\beta_\alpha$ growing beyond unity, the semiclassical expression (4.137) becomes increasingly accurate.

As specific examples consider single-power reference potentials (4.57) with $\alpha = 6$ and $\alpha = 4$. The auxiliary function (4.117) is given according to (4.132) in these cases by

$$\xi = -\frac{7}{8}\pi + \frac{1}{2}\eta_6 (k\beta_6)^{2/3} \quad \text{for } \alpha = 6 \quad \text{and} \tag{4.139}$$

$$\xi = -\pi + \frac{1}{2}\eta_4 (k\beta_4)^{1/2} \quad \text{for } \alpha = 4. \tag{4.140}$$

The tail functions $A_{\mathrm{s}}/A_{\mathrm{c}}$, ϕ_{s} and ϕ_{c} are shown for both powers in Fig. 4.10.

The scattering phase shifts that follow via (4.119) are shown for various values of the remainder Δ_{D} in Fig. 4.11. The leading linear behaviour near threshold, which is in accordance with Wigner's threshold law, is restricted to the extreme quantum regime $k\beta_\alpha \ll 1$ corresponding to $E \ll E_{\beta_\alpha}$. The scattering length a depends sensi-

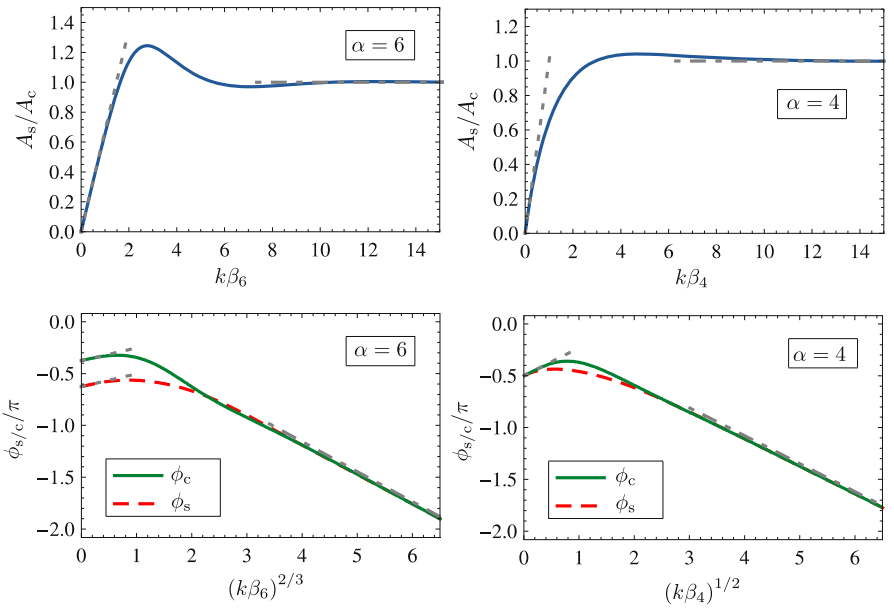

Fig. 4.10 Tail functions for a single-power reference potential (4.57) with $\alpha = 6$ (*left-hand panels*) and $\alpha = 4$ (*right-hand panels*). The *upper panels* show the ratios A_s/A_c of the amplitudes defined by the WKB representations (4.111) of the wave functions $u_s(r)$ and $u_c(r)$ in the limit $r \to 0$, as functions of $k\beta_\alpha$; the *lower panels* show the phases ϕ_s and ϕ_c as functions of $(k\beta_\alpha)^{1-2/\alpha}$. The straight *grey dashed lines* show the low-energy limits (4.134), (4.135). The straight *grey dot-dashed lines* show the high-energy limit: unity for A_s/A_c and Eq. (4.136) for $\phi_{s/c}$. (From [65])

tively on the remainder Δ_D according to (4.53) and for large $|a|$, the linear regime is restricted even further by the condition $k|a| < 1$. The dot-dashed lines in Fig. 4.11 show the cases of vanishing scattering length, which are achieved with $\Delta_D = \frac{3}{4}$ for $\alpha = 6$ and $\Delta_D = \frac{1}{2}$ for $\alpha = 4$. In these cases, the versions (2.103) or (2.286) of the effective-range expansion don't work, but the corresponding expansions for $\tan\delta_0$, e.g. (2.104) for potentials falling off faster than $1/r^5$ at large distances, are applicable. See Sects. 2.3.8 and 2.6.3 in Chap. 2.

Since the quantum lengths β_α are very large in realistic systems, typically hundreds or even many thousands of atomic units (Bohr radii), the truly quantum mechanical near-threshold regime $k\beta_\alpha \ll 1$ is tiny, as already observed for near-threshold quantization in Sect. 4.1.1. In contrast to the bound regime below threshold however, the energy spectrum above threshold is continuous and any ever so small range of energies near threshold accommodates physically meaningful wave functions.

The phase shifts shown in Fig. 4.11 were obtained via (4.119) without considering possible short-range corrections due to the deviation of the full interaction from the reference potential $V_{tail}(r)$ at small distances, i.e. assuming $f_{sr} \equiv 0$. The characteristic length scale for such short-range corrections is typically of the order of a few atomic units (Bohr radii), associated with a characteristic energy much larger

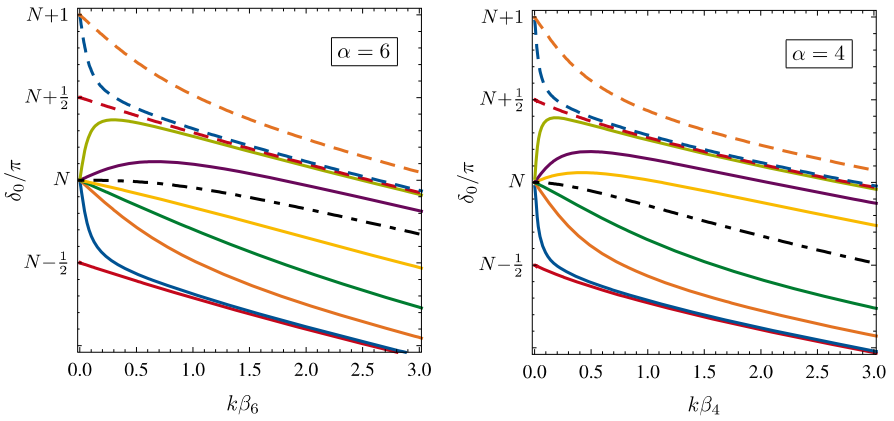

Fig. 4.11 s-wave phase shifts as given by (4.119) for a potential with a single-power tail (4.57) for various values of the remainder Δ_{D}. The additional short-range correction given through $f_{\mathrm{sr}}(E)$ is taken to be zero. The *solid lines* show the results obtained with $\Delta_{\mathrm{D}} = 0, 0.01, 0.1, 0.5, 0.99$ (from bottom to top). For the lowest three values of Δ_{D}, the plots are repeated (as *dashed lines*) with a shift of π, which would correspond to one additional bound state in a potential well. The *dot-dashed lines* show the respective phase shift for the value of Δ_{D} for which the scattering length vanishes, $\Delta_{\mathrm{D}} = \frac{3}{4}$ for $\alpha = 6$ and $\Delta_{\mathrm{D}} = \frac{1}{2}$ for $\alpha = 4$. (Adapted from [65])

than E_{β_α}. In the energy range covered in Fig. 4.11, the effect of the short-range correction term f_{sr} in (4.119) is negligibly small in a sufficiently deep Lennard–Jones type potential where the potential tail is well described by the single-power form (4.57) [65].

Consider again the Lennard–Jones potential (4.68) with $B_{\mathrm{LJ}} = 10^4$, which was studied as Example 1 in Sect. 4.1.1. The short-range correction function $f_{\mathrm{sr}}(E)$ was derived from the exact numerically calculated phase shifts by resolving Eq. (4.119), and $\upsilon_{\mathrm{D}} - f_{\mathrm{sr}}(E)$ is shown as the solid curve in the right-hand part ($E > 0$) of Fig. 4.12. The left-hand part ($E < 0$) of the figure repeats the plot in the right-hand part of Fig. 4.4, where $\upsilon + F_6(\kappa_\upsilon \beta_6)$ is plotted as function of energy for the highest five bound states $\upsilon = 19, \ldots, 23$. Note that the energy is now given in the units of E_{β_6} as defined in (4.70). It is related to the depth $\mathscr{E}$ of the Lennard–Jones potential by $E_{\beta_6}/\mathscr{E} = (B_{\mathrm{LJ}})^{-3/2}/\sqrt{2}$, which in the present case means $E_{\beta_6} \approx 0.7 \times 10^{-6}\mathscr{E}$. According to the quantization rule (4.7) and the decomposition (4.18), the squares in the left-hand part of Fig. 4.12 lie on the curve $\upsilon_{\mathrm{D}} - F_{\mathrm{sr}}(E)$, where $F_{\mathrm{sr}}(E)$ is the short-range correction to the quantization function. This curve clearly merges smoothly into the function $f_{\mathrm{sr}}(E)$ accounting for the analogous short-range correction above threshold. So the short-range correction coefficient γ_{sr}, defined by (4.19) in the subthreshold regime and by (4.131) on the scattering side of the threshold, is seen to be the same in both cases. The dashed horizontal line in Fig. 4.12 indicates the value $\upsilon_{\mathrm{D}} = 23.2327$ of the threshold quantum number and the other dashed line shows the linear function $\upsilon_{\mathrm{D}} - \gamma_{\mathrm{sr}} E$, with $\gamma_{\mathrm{sr}} = -1.16/\mathscr{E} = -8.2 \times 10^{-7}/E_{\beta_6}$, compare Table 4.5 in Sect. 4.1.1.

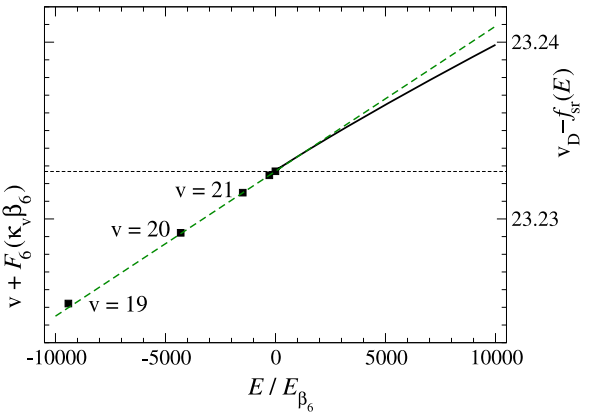

Fig. 4.12 For the Lennard–Jones potential (4.68) with $B_{LJ} = 10^4$, the left-hand part ($E < 0$) shows $\upsilon + F_6(\kappa_\upsilon \beta_6)$ as function of energy for the highest five bound states $\upsilon = 19, \ldots, 23$ (*solid squares*). The right-hand part ($E > 0$) shows $\upsilon_D - f_{sr}(E)$, derived from the exact numerically calculated phase shifts by resolving Eq. (4.119). The *dashed horizontal line* indicates the value $\upsilon_D = 23.2327$ of the threshold quantum number; the other *dashed line* shows the linear function $\upsilon_D - \gamma_{sr} E$, with $\gamma_{sr} = -1.16/\mathscr{E} = -8.2 \times 10^{-7}/E_{\beta_6}$, compare Table 4.5

4.1.4 Nonvanishing Angular Momentum

For nonvanishing angular momentum quantum number l, the radial Schrödinger equation (4.11) with the reference potential $V_{tail}(r)$ becomes

$$-\frac{\hbar^2}{2\mu}\frac{d^2u}{dr^2} + V_{tail}^{(l)}(r)u(r) = Eu(r), \quad V_{tail}^{(l)}(r) = V_{tail}(r) + \frac{l(l+1)\hbar^2}{2\mu r^2}. \tag{4.141}$$

Since $V_{tail}(r)$ is more singular than $1/r^2$ at small distances, its influence becomes increasingly dominant for $r \to 0$, and the influence of the centrifugal potential in (4.141) becomes negligible in this limit. At large distances, however, the centrifugal term dominates over $V_{tail}(r)$, which falls off faster than $1/r^2$, and this gives rise to a centrifugal barrier separating the regime of free-particle motion at large distances from the region of WKB validity for $r \to 0$. For a sufficiently deep full interaction, there still is a region of r-values where r is large enough for the full interaction to be accurately represented by the reference potential $V_{tail}(r)$ and at the same time small enough for the WKB representations of the solutions of (4.141) to be sufficiently accurate.

As example, Fig. 4.13 shows the tail of the potential already featured in Fig. 4.1 together with the effective potential, which includes the centrifugal potential, in this case for angular momentum quantum number $l = 8$. The procedure outlined in the previous three subsections can also be applied in the case of nonvanishing angular momentum. In the bound state regime, the outer classical turning point $r_{out}(E)$ does not go to infinity for $E \to 0$, but assumes a finite value $r_{E=0}$ corresponding to the inner base point of the centrifugal barrier. With this in mind, the tail contribution

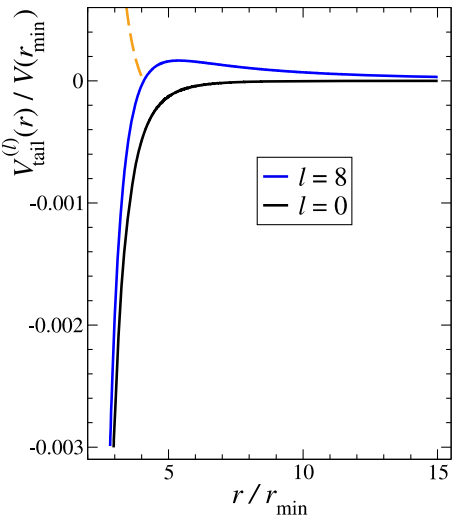

Fig. 4.13 Tail of the deep potential already featured in Fig. 4.1 (*solid black line*), together with the effective potential $V_{\rm tail}^{(l)}(r)$ as defined in (4.141), for angular momentum quantum number $l = 8$ (*solid blue line*). The *dashed orange line* shows the location of the reference point r_E which is defined for positive energies by (4.149)

$F_{\rm tail}(E)$ to the quantization function is still defined by Eq. (4.16) in Sect. 4.1.1, but the local classical momentum $p_{\rm tail}(r')$ in the action integrals is now replaced by

$$p_{\rm tail}^{(l)}(r') = \sqrt{2\mu\big[E - V_{\rm tail}^{(l)}(r')\big]}. \tag{4.142}$$

For small noninteger values of l in the range $-\frac{1}{2} < l < +\frac{1}{2}$, the leading near-threshold behaviour of $F_{\rm tail}(E)$ was derived in [59] for single power tails (4.57),[1]

$$F_\alpha^{(l)}(\kappa\beta_\alpha) \overset{\kappa\to 0}{\sim} \frac{\pi\,\nu(0)^{2\nu(l)}}{\sin[(l+\frac{1}{2})\pi](l+\frac{1}{2})\nu(l)[\Gamma(l+\frac{1}{2})\Gamma(\nu(l))]^2}\left(\frac{\kappa\beta_\alpha}{2}\right)^{2l+1} + O\big((\kappa\beta_\alpha)^{4l+2}\big) + O(E), \quad -\frac{1}{2} < l < +\frac{1}{2}; \tag{4.143}$$

here $\nu(l)$ is a generalization of $\nu \equiv \nu(0)$ as defined in (4.132),

$$\nu(l) = \frac{2l+1}{\alpha - 2}. \tag{4.144}$$

At the upper end of the interval given in (4.143), i.e., $l = \frac{1}{2}$, the energy dependence $(\kappa\beta_\alpha)^{2l+1}$ is already of order E. For all higher l-values, in particular for all positive integers, the leading energy dependence of the tail contribution to the quantization function $F_{\rm tail}^{(l)}(E)$ is of order E. A separation of tail effects from the influence of

[1] Noninteger values of l are not merely of academic interest. They can describe the effects of inverse-square potentials of other origin than the centrifugal term. In two-dimensional scattering described in Sect. 4.3, the radial Schrödinger equation with integer angular momentum quantum number m resembles that of the 3D case when $l = |m| - \frac{1}{2}$.

short-range deviations of the full interaction from the reference potential $V_{\text{tail}}(r)$ is still possible for $l > 0$. As in Figs. 4.4 and 4.6 in Sect. 4.1.1, a plot of $\upsilon + F_{\text{tail}}^{(l)}(E_\upsilon)$ against E_υ approaches a straight-line behaviour towards threshold, from which the parameters $\upsilon_{\text{D}}(l)$ and γ_{sr} can be extracted. For inverse-power tails (4.57), the threshold quantum number $\upsilon_{\text{D}}(l)$ for nonvanishing l is related to the threshold quantum number $\upsilon_{\text{D}}(0)$ by [35, 59],

$$\upsilon_{\text{D}}(l) = \upsilon_{\text{D}}(0) - \frac{l}{\alpha - 2}. \tag{4.145}$$

This relation has been used by Lemeshko and Friedrich [53, 54] to estimate the number of ro-vibrational bound states in diatomic molecules and molecular ions.

Turning to "quantum reflection", the imposition of incoming boundary conditions on the solutions of (4.141) remains meaningful for $l > 0$; it describes the absorption of all inward travelling flux which manages to penetrate the nonclassical region of the effective reference potential $V_{\text{tail}}^{(l)}(r)$. For energies below the maximum of the centrifugal barrier, the term "quantum reflection" is inappropriate, because reflection is classically allowed whereas transmission is classically forbidden. The leading near-threshold behaviour of the transmission (tunnelling) probabilities P_{T} was calculated in [58] for centrifugal barriers consisting of a single-power tail (4.57) plus the centrifugal potential, i.e., for the potential $V_{\text{tail}}^{(l)}(r)$ in (4.141),

$$P_{\text{T}} \overset{k\to 0}{\sim} \frac{4\pi^2 \nu(0)^{2\nu(l)} (k\beta_\alpha/2)^{2l+1}}{(l+\frac{1}{2})\nu(l)[\Gamma(l+\frac{1}{2})\Gamma(\nu(l))]^2}, \tag{4.146}$$

wherefrom the behaviour of the modulus of the reflection amplitude follows via

$$|R| = \sqrt{1 - P_{\text{T}}} \overset{P_{\text{T}}\to 0}{\sim} 1 - \frac{1}{2} P_{\text{T}}. \tag{4.147}$$

Note that the penetrability of the centrifugal barrier is always proportional to k^{2l+1} near threshold, and only the proportionality constant depends on the power in the reference potential $V_{\text{tail}}(r)$. In contrast to similar formulas for the near-threshold behaviour of the phases of the transmission and reflection amplitudes, the proportionality of P_{T} and of $1 - |R|$ to k^{2l+1} is not restricted by a relation like $2l + 3 < \alpha$, compare Sect. 2.6 in Chap. 2. All quantities based on the tunnelling probability through a centrifugal barrier obey Wigner's threshold law.

For ordinary scattering, the procedure described in Sect. 4.1.3 can easily be extended to the case of nonvanishing angular momentum quantum number l. For $l \neq 0$, the two linearly independent solutions of (4.141) are chosen to be those behaving asymptotically as

$$\begin{aligned} u_{\text{s}}^{(l)}(r) &\overset{r\to\infty}{\sim} kr j_l(kr) \overset{r\to\infty}{\sim} \sin\left(kr - l\frac{\pi}{2}\right), \\ u_{\text{c}}^{(l)}(r) &\overset{r\to\infty}{\sim} -kr y_l(kr) \overset{r\to\infty}{\sim} \cos\left(kr - l\frac{\pi}{2}\right). \end{aligned} \tag{4.148}$$

The amplitudes $A_{\mathrm{s,c}}$ and phases $\phi_{\mathrm{s,c}}$ are defined via the WKB representations of these wave functions for $r \to 0$, as in (4.111) for the case $l = 0$, but the local classical momentum p_{tail} is replaced by $p_{\mathrm{tail}}^{(l)}$ given by (4.142). The point of reference r_E is now chosen as the classical turning point of $-V_{\mathrm{tail}}^{(l)}(r)$,

$$V_{\mathrm{tail}}^{(l)}(r_E) = V_{\mathrm{tail}}(r_E) + \frac{l(l+1)\hbar^2}{2\mu(r_E)^2} = -E < 0. \tag{4.149}$$

The dashed orange line in Fig. 4.13 shows the location of reference point r_E for each positive energy E. At threshold, $r_E \equiv r_0$ coincides with the inner base point of the centrifugal barrier, which is also the limit of the outer classical turning point $r_{\mathrm{out}}(E)$ when the threshold is approached from below. The auxiliary tail function (4.117) is, for $l > 0$, defined by

$$\xi^{(l)} = \frac{1}{\hbar}\int_{r_E}^{r_0} p_{\mathrm{tail}}^{(l)}(0;r)\mathrm{d}r + \frac{1}{\hbar}\int_0^{r_E}\left[p_{\mathrm{tail}}^{(l)}(0;r) - p_{\mathrm{tail}}^{(l)}(E;r)\right]\mathrm{d}r - \frac{\phi_{\mathrm{out}}(0)}{2} - \frac{\pi}{2}. \tag{4.150}$$

The theory described above, including nonvanishing angular momenta, has been shown to work well in a realistic application to near-threshold bound and continuum states of the $^{88}Sr_2$ molecule in Ref. [49].

4.1.5 Summary

For a deep potential with an attractive tail falling off faster than $1/r^2$ at large distances, tail effects and short-range effects are most effectively identified by defining a reference potential $V_{\mathrm{tail}}(r)$, which describes the full interaction accurately at large distances and tends to $-\infty$ more rapidly than $-1/r^2$ at small distances. The influence of the reference potential is contained in a few tail functions, which are functions of energy that are determined solely by $V_{\mathrm{tail}}(r)$. They are related to the amplitudes and phases in the WKB representation of exact solutions of the Schrödinger equation, with $V_{\mathrm{tail}}(r)$, in the limit $r \to 0$. Since the WKB approximation is exact for $r \to 0$ in this case, referring to the WKB representation does *not* imply a semiclassical approximation.

The near-threshold bound state energies and scattering phase shifts are significantly influenced by the threshold quantum number υ_{D}, or rather by its remainder $\Delta_{\mathrm{D}} = \upsilon_{\mathrm{D}} - \lfloor \upsilon_{\mathrm{D}} \rfloor$, which is a property of the full interaction and tells us how close this is to supporting a bound state exactly at threshold. Further effects of the short-range deviation of the full interaction from $V_{\mathrm{tail}}(r)$ enter via a smooth function of energy which vanishes at threshold. We called it $F_{\mathrm{sr}}(E)$ below threshold and $f_{\mathrm{sr}}(E)$ above threshold, but both functions merge smoothly with a common gradient at $E = 0$:

$$F_{\mathrm{sr}}(E) = \gamma_{\mathrm{sr}}E + O\left(E^2\right) \quad \text{for } E < 0, \qquad f_{\mathrm{sr}}(E) = \gamma_{\mathrm{sr}}E + O\left(E^2\right) \quad \text{for } E > 0. \tag{4.151}$$

The short-range correction (4.151) vanishes in the limit that the range of the deviations of the full interaction from the reference potential $V_{\mathrm{tail}}(r)$ is small compared to the characteristic length scales of $V_{\mathrm{tail}}(r)$.

The positions of the near-threshold energy levels are determined by the quantization rule (4.7), which can be written as (4.20) when the quantization function is written as a sum of $F_{\mathrm{tail}}(E)$ and the short-range correction $F_{\mathrm{sr}}(E)$. The contribution $F_{\mathrm{tail}}(E)$ is a tail function depending only on the properties of the reference potential $V_{\mathrm{tail}}(r)$. The immediate near-threshold behaviour of the quantization function $F(E)$ and of the quantization rule (4.7) is universal for all potentials falling off faster than $1/r^2$ at large distances,

$$F(E) \overset{\kappa\to 0}{\sim} \frac{b\kappa}{\pi} + O(E), \qquad \upsilon_{\mathrm{D}} - \upsilon \overset{\kappa_\upsilon\to 0}{\sim} \frac{b\kappa_\upsilon}{\pi} + O(E), \tag{4.152}$$

where b is the threshold length. It is a property of $V_{\mathrm{tail}}(r)$ alone and is defined by Eq. (4.40).

At above-threshold energies, the s-wave scattering phase shift is given by (4.119) or, alternatively, by (4.128). In Eq. (4.119) the ratio $A_{\mathrm{s}}/A_{\mathrm{c}}$, the angles ϕ_{s}, and ϕ_{c}, as well as the auxiliary function ξ are tail functions depending only on the reference potential $V_{\mathrm{tail}}(r)$. The same holds for the quantum reflection amplitude R, the phase of the transmission amplitude T and the same auxiliary function ξ in the alternative formulation (4.128).

The immediate near-threshold behaviour of the phase shift depends sensitively on the remainder $\Delta_{\mathrm{D}} = \upsilon_{\mathrm{D}} - \lfloor \upsilon_{\mathrm{D}} \rfloor$. For potentials falling off faster than $1/r^3$ at large distances, we have $\tan\delta_0 \overset{k\to 0}{\sim} -ka$ and the scattering length a is related to the remainder Δ_{D} by (4.53), i.e.

$$a = \bar{a} + \frac{b}{\tan(\Delta_{\mathrm{D}}\pi)}, \tag{4.153}$$

where $\bar{a}$ is the mean scattering length defined in Eq. (4.42). The relation (4.153) follows from the immediate near-threshold behavior (4.121) of the tail functions occurring in (4.119). For potentials falling off as $-1/r^3$ asymptotically, the near-threshold behaviour of the tail functions yields the behaviour (4.129).

The mean scattering length $\bar{a}$ and the threshold length b together make up the complex scattering length $\mathscr{A}$ which determines the leading near-threshold behaviour of the amplitude R for quantum reflection by the reference potential $V_{\mathrm{tail}}(r)$,

$$R = -\mathrm{e}^{2\mathrm{i}\delta_0}, \quad \delta_0 \overset{k\to 0}{\sim} -k\mathscr{A}, \quad \mathscr{A} = \bar{a} - \mathrm{i}b. \tag{4.154}$$

Note that the leading near-threshold behaviour of the modulus $|R|$ of the quantum reflection amplitude is determined according to (4.89) by the threshold length b alone

$$|R| \overset{k\to 0}{\sim} 1 - 2bk + O\big(k^2\big) = \mathrm{e}^{-2bk} + O\big(k^2\big). \tag{4.155}$$

The semiclassical limit is approached away from threshold, both for positive and negative energies, i.e. for large $|E|$. The behaviour of the scattering phase shift is given in the high-k limit by Eq. (4.130), and the influence of the threshold quantum number reduces to a simple additive constant in this limit.

The theory described in this section is particularly elegant for potential tails that are well described by a single-power reference potential (4.57). In this case, all tail functions depend only on $\kappa\beta_\alpha$ (below threshold) or $k\beta_\alpha$ (above threshold). The transition between the immediate near-threshold quantum regime and the semiclassical regime away from threshold occurs when $\kappa\beta_\alpha$ or $k\beta_\alpha$ is of the order of unity. The range of the quantum regime is tiny when compared with typical potential depths, because the length scale of the reference potential is very large (in atomic units) for typical atomic or molecular interactions, see e.g. Table 1 in Ref. [17].

4.1.6 Relation to Other Approaches

Deep potentials typically occurring in atomic and molecular physics have been studied by many researchers over the years. Inspired by the success of quantum-defect theory for Coulombic potentials, i.e. modified Coulomb potentials with short-range deviations from the pure $1/r$ behaviour, Greene et al. [41, 43] and Giusti [42] formulated an adaptation of quantum-defect theory to more general situations, in particular to potentials falling off faster than $1/r^2$ at large distances. This approach was applied to elastic and inelastic scattering by several authors [37, 39, 40, 44, 63, 64]. The description of scattering in these references is essentially equivalent to the theory described in the previous five subsections in that it attempts to separate the effects due to the singular reference potential from the short-range effects due to the deviation of the full interaction from the reference potential at small distances. For a compact review of this line of work see the description beginning on p. 4962 of Ref. [75]. Although the applications of this "generalized quantum-defect theory" have been very successful, the use of the language of quantum-defect theory in connection with potentials falling off faster than $1/r^2$ at large distances has been and remains unfortunate.

The term "quantum defect" was introduced for systems described by modified Coulomb potentials to account for the shift of energy levels relative to the levels in a pure Coulomb potential, which serves as reference potential. Above the ionization threshold, the quantum-defect function describes the additional phase shift, relative to the phase of the regular wave functions in the reference potential, the pure Coulomb potential, see Sect. 2.5.4 in Chap. 2 and Sect. 3.7 in Chap. 3.

For potentials falling off faster than $1/r^2$ at large distances, the reference potentials generally in use are too singular to supply a reference spectrum of bound states or a definite phase of scattering states, relative to which a "defect" or additional phase shift could be defined. Other marked differences are the number of bound states, which is infinite for Coulombic potentials and finite for potentials falling off faster than $1/r^2$ at large distances, and the semiclassical limit, which is at $E \to 0$ for Coulombic potentials and $|E| \to \infty$ for potentials falling off faster than $1/r^2$.

Samuel Johnson once wrote: "Language is the dress of thought" [47]. For the treatment of potentials which fall off faster than $1/r^2$ at large distances, the language of quantum-defect theory is more of a disguise. Interpreting potentials that fall off faster than $1/r^2$ as a generalization of Coulombic potentials tends to obscure the fundamental differences between these two types of interaction. This is potentially confusing and can promote misconceptions. One example is provided by the observation made by Gao in 1999, that for single-power potential tails proportional to $-1/r^6$ or to $-1/r^3$ conventional WKB quantization leads to poorer results towards the dissociation threshold [38]. Although the failure of conventional WKB quantization at threshold was long well known [72], the observation in Ref. [38] was celebrated as sensational evidence for the "breakdown" of Bohr's correspondence principle, according to which the behaviour of a quantized system is expected to become increasingly (semi-)classical as the quantum number tends to infinity. This alledged breakdown of Bohr's correspondence principle was spotlighted in two key media, *Physical Review Focus* [73] and *Nature*'s "News" [6]. Apart from the fact that the limit of infinite quantum number cannot be reached in a system with a finite number of bound states, it was textbook knowledge at the time, that for homogeneous potential tails proportional to $1/r^\alpha$, the semiclassical limit is for $|E| \to \infty$ when $\alpha > 2$, and this means $E \to -\infty$ in the bound-state regime, see e.g. discussion involving Eqs. (5.153)–(5.156) in [34]. "Large quantum numbers" means not large υ, but large $\upsilon_\mathrm{D} - \upsilon$, and the semiclassical limit is approached not towards threshold but towards increasing binding energy, at least as far as the finite depth of any realistic potential well permits. Deep potentials falling off faster than $1/r^2$ at large distances thus show conformity with Bohr's correspondence principle and not its breakdown. Appropriate refutations of Ref. [38] were published in 2001 [8, 29]. In order to avoid accidents such as the one documented by Refs. [6, 38, 73], it is important to have a proper appreciation of the differences between potentials with a Coulombic tail and those falling off faster than $1/r^2$ at large distances.

A further difference to Coulombic potentials is, that realistic atomic potentials falling off faster than $1/r^2$ are often not so well represented at large distance by the leading asymptotic inverse-power term alone, at least not in an energy range encompassing more than one or two of the most weakly bound states. The universality of the theory for single-power reference potentials (4.57), where the universal tail functions depending on $\kappa\beta_\alpha$ below and on $k\beta_\alpha$ above threshold apply to all potentials with a given power α, regardless of strength, is lost when a more sophisticated reference potential is used. The tail functions must then be calculated independently for each specific system, and the question arises, whether it may not be worthwhile to simply solve the radial Schrödinger equation directly to obtain bound-state energies and scattering phase shifts.

A pragmatic approach to describe near-threshold states of deep potentials is based on defining a (analytical) model potential $V_\mathrm{mod}(r)$, which is a good approximation of the potential tail at large distances, where it is well known, and is non-singular at small distances, where the exact interaction is often not so well known. Being regular at the origin, the model potential supports a finite number of bound states below threshold and well defined scattering states above threshold. The lesser

known short-range part of the potential can be equipped with a small number of model parameters to be fitted in order to reproduce known benchmarks of problem under investigation, e.g. bound-state energy levels and the scattering length. For the bound and continuum states in a relatively narrow energy range around threshold, the behaviour of the wave functions at short distances is essentially independent of energy, and their behaviour at large distances can be obtained by solving the radial Schrödinger equation. Near-threshold effects depending on the potential tail can be described accurately in this way, because the model potential accurately represents the exact interaction at large distances. This approach is very flexible and easily extended to multi-channel scattering situations. It has been followed successfully in recent years, in particular by Tiemann and collaborators [28, 56, 79, 80, 82, 83].

4.2 Near-Threshold Feshbach Resonances

4.2.1 Motivation

The successful preparation of Bose–Einstein condensates of dilute atomic gases in 1995 [2, 25] gave a tremendous boost to the field of ultracold atoms and molecules. A new book series of annual reviews on the subject was launched in 2013 [69].

In a first approximation, a condensate of N indistinguishable bosonic particles is described by a completely symmetric many-body wave function, in which each individual boson occupies the same single-particle quantum state, $\psi_N(\mathbf{r})$. In a mean-field treatment of the interparticle interactions, this single-particle wave function is determined via the Gross–Pitaevskii equation, also called the "nonlinear Schrödinger equation". With the assumption that the mutual two-body interaction of the bosons is of short range [46], this equation can be approximately written as [23]

$$\left(-\frac{\hbar^2}{2M}\Delta + W(\mathbf{r}) + \frac{4\pi\hbar^2}{M}a\left|\psi_N(\mathbf{r})\right|^2\right)\psi_N(\mathbf{r}) = \mu_{\mathrm{cp}}\psi_N(\mathbf{r}), \tag{4.156}$$

where M is the mass of each boson, $W(\mathbf{r})$ is an external confining potential and μ_{cp} is the chemical potential which corresponds to the energy of the single-particle ground state. In this approximate version of the Gross–Pitaevskii equation, the two-particle interaction between the bosons (e.g. bosonic alkali atoms) is accounted for by the scattering length a in the term which contains $|\psi_N(\mathbf{r})|^2$ and makes the equation nonlinear. Clearly, the magnitude and the sign of the scattering length have a dominating influence of the solution of (4.156) and on whether or not a Bose–Einstein condensate can form at all.

As discussed on several occasions in this book, the scattering length depends sensitively on how close the highest bound state in a potential well is to the continuum threshold, which in an atom-atom system is the dissociation threshold, see e.g. Eq. (2.88) in Sect. 2.3.8 and Eq. (4.55) in Sect. 4.1.1; it acquires large positive values for bound states very close to threshold and large negative values if the potential

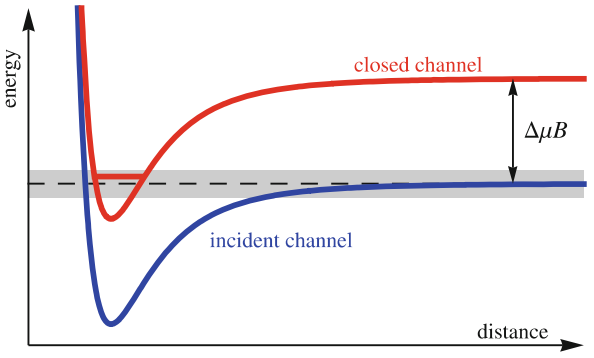

Fig. 4.14 Schematic illustration of atom–atom potentials in a two-channel situation. The closed channel (*red curve*) acquires a shift $\Delta\mu B$ relative to the lower, the "incident" channel (*blue curve*) due to different effect of a magnetic field of strength B. The closed channel supports a bound state close to the threshold of the incident channel

just fails to support a further bound state, see e.g. Fig. 2.5 in Sect. 2.3.8. As shown below, this general behaviour of the scattering length also holds when the weakly or almost bound state involved originates from an inelastic channel, i.e., when there is a Feshbach resonance at an energy very near to the threshold of the elastic channel. In diatomic systems, elastic and inelastic channels can have different magnetic properties (e.g. magnetic moments of the individual atoms), so the bound and continuum states in the elastic and in inelastic channels can acquire different shifts in the presence of an external magnetic field. This makes it possible to tune the position of a Feshbach resonance relative to the threshold of the elastic channel by varying the strength of the external field, and thus offers a practical way of manipulating and controlling Bose–Einstein condensates through the corresponding variations of the scattering length. A comprehensive review on Feshbach resonances as a tool to control the interaction in gases of ultracold atoms was published in 2010 by Chin et al. [14].

Consider the two-channel situation illustrated schematically in Fig. 4.14. In the presence of an external magnetic field of strength B, the channel thresholds are shifted by $\Delta\mu B$ due to the difference $\Delta\mu$ in the relevant magnetic moments. The upper channel is closed for energies near the threshold of the lower channel, which we call "incident channel" for want of a better word. In the absence of channel coupling, the closed channel supports a bound state at an energy E_0 near the threshold of the incident channel, and the coupling of this state to the incident-channel wave functions appears as a Feshbach resonance in the incident channel.

Close to the threshold of the incident channel, which we take to be at $E = 0$, the behaviour of the incident-channel phase shift δ is determined by the scattering length a: $\delta \overset{k\to 0}{\sim} -ak$. As the position of the Feshbach resonance is tuned to pass the threshold of the incident channel, a pole singularity of the scattering length is observed at a given strength B_0 of the magnetic field. This is generally empirically parametrized as [14, 68]

$$a = a_{\mathrm{bg}}\left(1 + \frac{\Delta B}{B - B_0}\right), \tag{4.157}$$

where a_{bg} is the background scattering length for the incident channel in the absence of channel coupling. It has become customary in the cold-atoms community to use

the term "magnetic Feshbach resonance" to describe such a pole in the scattering length. This can be confusing to anyone with a broader education in scattering theory, because Feshbach resonances are a much more general phenomenon and not restricted to energies near a threshold.

The empirical formula (4.157) satisfactorily describes the pole of the scattering length that occurs when a Feshbach resonance crosses the threshold of the incident channel, but it does not reveal the physical origin of the parameters involved nor their interdependencies. The theory described in the next two subsections aims to provide a physically motivated parametrization of a Feshbach resonance near threshold which transparently reveals its influence on scattering properties and on the bound-state spectrum.

4.2.2 Threshold-Insensitive Parametrization of a Feshbach Resonance

The influence of a single isolated Feshbach resonance on the scattering phase shift of the incident channel was given in Sect. 3.5.1 in Chap. 3,

$$\delta = \delta_{\mathrm{bg}} + \delta_{\mathrm{res}}, \qquad \tan\delta_{\mathrm{res}} = -\frac{\Gamma/2}{E - E_{\mathrm{R}}}, \tag{4.158}$$

where δ_{bg} is the background phase shift due to the potential in the uncoupled incident channel and δ_{res} is the resonant phase shift due to coupling to the bound state in the closed channel. The parameters E_{R} and Γ are given by

$$E_{\mathrm{R}} = E_0 + \langle u_{\mathrm{c}}|V_{\mathrm{c,i}}\hat{G}V_{\mathrm{i,c}}|u_{\mathrm{c}}\rangle, \qquad \Gamma = 2\pi\left|\langle u_{\mathrm{c}}|V_{\mathrm{c,i}}|\bar{u}_{\mathrm{i}}^{(\mathrm{reg})}\rangle\right|^2, \tag{4.159}$$

where u_{c} is the wave function of the bound state in the uncoupled closed channel, $V_{\mathrm{c,i}}$ and $V_{\mathrm{i,c}}$ are the channel-coupling potentials, $\bar{u}_{\mathrm{i}}^{(\mathrm{reg})}(r)$ is the energy-normalized regular wave function in the uncoupled incident channel and the operator $\hat{G}$ is the propagator (Green's operator) in the uncoupled incident channel; its kernel is the Green's function

$$\mathscr{G}(r, r') = -\pi\bar{u}_{\mathrm{i}}^{(\mathrm{reg})}(r_<)\bar{u}_{\mathrm{i}}^{(\mathrm{irr})}(r_>). \tag{4.160}$$

The pole of $\tan\delta_{\mathrm{res}}$ defines the resonance energy, i.e. the position E_{R} of the resonance, which differs from the bound-state energy E_0 in the uncoupled closed channel by a shift given by the matrix element containing the incident-channel propagator. When E_{R} is far from the incident-channel threshold and the channel coupling is not too strong, the energy dependence of Γ is weak and its value at $E = E_{\mathrm{R}}$ defines the width of the resonance. This straightforward interpretation breaks down towards the incident-channel threshold. The matrix element describing the shift between E_0 and E_{R} goes smoothly through a constant value at threshold, but the energy dependence of the parameter Γ poses a more serious problem.

The behaviour of $\bar{u}_i^{(\mathrm{reg})}(r)$ is, beyond the range of the incident-channel potential, given by

$$\bar{u}_i^{(\mathrm{reg})}(r) = \sqrt{\frac{2\mu}{\pi\hbar^2 k}}\sin\bigl[k(r+\delta_{\mathrm{bg}}/k)\bigr] \overset{k\to 0}{\sim} \sqrt{\frac{2\mu k}{\pi\hbar^2}}(r-a_{\mathrm{bg}}), \tag{4.161}$$

compare (3.64) in Sect. 3.5.1. Remember that the near-threshold behaviour of the phase shift δ_{bg} in the uncoupled incident channel is $\delta_{\mathrm{bg}} \overset{k\to 0}{\sim} -a_{\mathrm{bg}}k$. From (4.161) it follows, that $\bar{u}_i^{(\mathrm{reg})}(r)$ can be written as

$$\bar{u}_i^{(\mathrm{reg})}(r) = \sqrt{\frac{2\mu k}{\pi\hbar^2}}\tilde{u}_i^{(\mathrm{reg})}(r) \quad \text{with} \quad \tilde{u}_i^{(\mathrm{reg})}(r) \overset{r\to\infty,k\to 0}{\sim} (r-a_{\mathrm{bg}}). \tag{4.162}$$

The irregular radial wave $\bar{u}_i^{(\mathrm{irr})}(r)$ behaves, beyond the range of the incident-channel potential, as

$$\bar{u}_i^{(\mathrm{irr})}(r) = \sqrt{\frac{2\mu}{\pi\hbar^2 k}}\cos\bigl[k(r+\delta_{\mathrm{bg}}/k)\bigr] \overset{k\to 0}{\sim} \sqrt{\frac{2\mu}{\pi\hbar^2 k}}\cos\bigl[k(r-a_{\mathrm{bg}})\bigr], \tag{4.163}$$

and can thus be written as

$$\bar{u}_i^{(\mathrm{irr})}(r) = \sqrt{\frac{2\mu}{\pi\hbar^2 k}}\tilde{u}_i^{(\mathrm{irr})}(r) \quad \text{with} \quad \tilde{u}_i^{(\mathrm{irr})}(r) \overset{r\to\infty,k\to 0}{\longrightarrow} 1; \tag{4.164}$$

the wave function $\tilde{u}_i^{(\mathrm{irr})}(r)$ converges to a k-independent function of r at threshold. In a product of $\bar{u}_i^{(\mathrm{reg})}(r)$ and $\bar{u}_i^{(\mathrm{irr})}(r)$, the near-threshold dependencies on k cancel, so the Green's function (4.160) and the matrix element defining the energy shift in the first equation (4.159) tend to finite limits at threshold. On the other hand, the parameter Γ as defined in (4.159) vanishes proportional to k, which makes Eq. (4.158) less easy to interpret near threshold.

This problem can be solved by formulating a threshold-insensitive description of the Feshbach resonance, which is possible when the incident-channel is deep in the spirit of Sect. 4.1 and well described at large distances by a singular reference potential $V_{\mathrm{tail}}(r)$ [81]. If channel-coupling effects are of sufficiently short range, then the regular wave function in the incident channel can be written in the form (4.112) in a range of r-values, which are large enough so that the wave function already contains the effects due to the deviation of the full interaction, including channel coupling, from the uncoupled reference potential $V_{\mathrm{tail}}(r)$, and at the same time small enough for the WKB representation of the wave in the reference potential $V_{\mathrm{tail}}(r)$ to be sufficiently accurate. As elaborated in Ref. [81], the effect of the Feshbach resonance on the phase of the regular wave under the influence of $V_{\mathrm{tail}}(r)$ can be obtained in a way similar to the derivation of (4.158) and (4.159) above, except that the (energy-normalized) continuum wave functions of the incident channel are replaced by incident-channel wave functions $u_i^{(\mathrm{reg})}(r)$ which, in the range

of r-values referred to above, have the form (4.112) with the phase $\phi_{\rm sr}$ given by (4.118),

$$u_{\rm i}^{\rm (reg)}(r) = \sqrt{\frac{2\mu}{\pi\hbar}} \frac{1}{\sqrt{p_{\rm tail}(E;r)}} \sin\left(\frac{1}{\hbar}\int_{r_E}^{r} p_{\rm tail}\big(E;r'\big){\rm d}r' - \phi_{\rm sr}(E)\right). \tag{4.165}$$

[Remember that, in the range of r-values considered here, the upper limit r of the integral in (4.165) is smaller than the lower limit r_E.] The effect of channel coupling on the incident-channel wave is the same as in the standard treatment leading to Eqs. (4.158) and (4.159). The regular solution acquires an additional resonant phase

$$\phi_{\rm sr}(E) \longrightarrow \phi_{\rm sr}(E) + \arctan\left(\frac{\bar{\Gamma}/2}{E - E_{\rm R}}\right), \tag{4.166}$$

and the width $\bar{\Gamma}$ is given by

$$\bar{\Gamma} = 2\pi \left|\langle u_{\rm c}|V_{\rm c,i}|u_{\rm i}^{\rm (reg)}\rangle\right|^2, \tag{4.167}$$

where the wave function $u_{\rm i}^{\rm (reg)}(r)$ is as defined in connection with Eq. (4.165). As long as the range of r-values, where both the bound-state wave function $u_{\rm c}(r)$ in the uncoupled closed channel and the coupling potential $V_{\rm c,i}$ are significantly non-vanishing, is small, the matrix element in (4.167) is essentially independent of energy in the near-threshold regime, because the regular wave function, which behaves as (4.165) at small distances, only becomes sensitive to the threshold at large distances. The width $\bar{\Gamma}$ defined by (4.167) is thus threshold-insensitive. At energies far above the incident-channel threshold, the wave function (4.165) becomes equal to the energy-normalized regular wave function $\bar{\rm u}_{\rm i}^{\rm (reg)}(r)$ for all moderate and large distances, so

$$\Gamma \overset{E\ \text{large}}{\longrightarrow} \bar{\Gamma}. \tag{4.168}$$

With the appropriate choice of the irregular radial wave function $u_{\rm i}^{\rm (irr)}(r)$, to replace $\bar{\rm u}_{\rm i}^{\rm (irr)}(r)$ in (4.160), the product of $u_{\rm i}^{\rm (reg)}$ and $u_{\rm i}^{\rm (irr)}$ converges to a well-defined function at $E = 0$. The matrix element defining the small shift between the position $E_{\rm R}$ of the Feshbach resonance and the energy E_0 of the bound state in the uncoupled closed channel is threshold-insensitive.

The determination of the scattering phase shift in the incident channel follows as already described in Sect. 4.1.3 after Eq. (4.112). The result is

$$\tan\delta = \frac{A_{\rm s}}{A_{\rm c}} \frac{\sin([\Delta_{\rm D} - f_{\rm sr}(E)]\pi + \bar{\delta}_{\rm res} - \xi + \phi_{\rm s})}{\cos([\Delta_{\rm D} - f_{\rm sr}(E)]\pi + \bar{\delta}_{\rm res} - \xi + \phi_{\rm c})}, \tag{4.169}$$

with the threshold-insensitive resonant phase shift,

$$\bar{\delta}_{\rm res} = -\arctan\left(\frac{\bar{\Gamma}/2}{E - E_{\rm R}}\right). \tag{4.170}$$

In (4.169), $\Delta_\mathrm{D} = \upsilon_\mathrm{D} - \lfloor \upsilon_\mathrm{D} \rfloor$ is the noninteger remainder of the threshold quantum number υ_D, and the functions $A_\mathrm{s}/A_\mathrm{c}$, ϕ_s and ϕ_c as well as the auxiliary function ξ are tail functions depending only on the reference potential $V_\mathrm{tail}(r)$ in the incident channel, as defined through Eqs. (4.109), (4.111) and (4.117) in Sect. 4.1.3; $f_\mathrm{sr}(E)$ is a smooth function of E which vanishes at threshold and accounts for residual corrections due to the deviation of the full interaction in the uncoupled incident channel from the reference potential at small distances.

Since the resonance is a short-range effect, it makes sense to amalgamate the threshold-insensitive resonant phase and the uncoupled, single-channel remainder Δ_D to an "extended remainder",

$$\bar{\Delta}_\mathrm{D}(E) = \Delta_\mathrm{D} - \frac{1}{\pi} \arctan\left(\frac{\bar{\Gamma}/2}{E - E_\mathrm{R}} \right). \tag{4.171}$$

With the definition (4.171) of the extended remainder the formula (4.169) becomes,

$$\tan\delta = \frac{A_\mathrm{s}}{A_\mathrm{c}} \frac{\sin([\bar{\Delta}_\mathrm{D}(E) - f_\mathrm{sr}(E)]\pi - \xi + \phi_\mathrm{s})}{\cos([\bar{\Delta}_\mathrm{D}(E) - f_\mathrm{sr}(E)]\pi - \xi + \phi_\mathrm{c})}. \tag{4.172}$$

At energies sufficiently far above the incident-channel threshold, the ratio $A_\mathrm{s}/A_\mathrm{c}$ tends to unity and the phases ϕ_s and ϕ_c become equal. Hence the arguments of sine and cosine in the quotient on the right-hand side of (4.172) become the same and equal to the phase δ on the left-hand side, but instead of Eq. (4.130) in Sect. 4.1.3 we now have

$$\delta \overset{E \text{ large}}{\approx} \left[\bar{\Delta}_\mathrm{D}(E) - f_\mathrm{sr}(E)\right]\pi - \xi + \phi_\mathrm{s} = \delta_\mathrm{bg} + \delta_\mathrm{res} \quad \text{with}$$
$$\delta_\mathrm{bg} = \left[\Delta_\mathrm{D} - f_\mathrm{sr}(E)\right]\pi - \xi + \phi_\mathrm{s} \quad \text{and} \quad \delta_\mathrm{res} = -\arctan\left(\frac{\bar{\Gamma}/2}{E - E_\mathrm{R}} \right); \tag{4.173}$$

this is consistent with Eqs. (4.158), (4.168) above.

4.2.3 *Influence on the Scattering Length*

We now assume, that the potential falls off faster than $1/r^3$ asymptotically, so that a well defined scattering length exists. Towards threshold, an additive decomposition of the scattering phase shift δ into a background contribution and a resonant term, as in (4.173), is no longer possible. The behaviour $A_\mathrm{s}/A_\mathrm{c} \overset{k\to 0}{\propto} k$, as given in the first equation (4.121) in Sect. 4.1.3, ensures the behaviour $\delta \overset{k\to 0}{\sim} -ak$ for the scattering phase shift, and the value of the scattering length is obtained by the same steps that led to the far right-hand side of (4.122),

$$\tan\delta \overset{k\to 0}{\sim} -k\left(\bar{a} + \frac{b}{\tan(\bar{\upsilon}_\mathrm{D}(E=0)\pi)} \right) = -k\left(\bar{a} + \frac{b}{\tan(\bar{\Delta}_\mathrm{D}(E=0)\pi)} \right). \tag{4.174}$$

The essential difference between Eqs. (4.174) and (4.122) is that, in place of the threshold quantum number υ_D, Eq. (4.174) contains the threshold value of the "extended threshold quantum number",

$$\bar{\upsilon}_D(E) = \upsilon_D - \frac{1}{\pi}\arctan\left(\frac{\bar{\Gamma}/2}{E - E_R}\right), \tag{4.175}$$

or, equivalently, the extended remainder (4.171). Equation (4.174) shows that, even in the presence of a near-threshold Feshbach resonance, the phase shift $\delta(k)$ is nailed down to be an integer multiple of π at threshold, which precludes the existence of a resonance feature of finite width in the scattering phase shift straddling the threshold, as observed for the additional phase shifts in potentials with an attractive Coulombic tail, see Fig. 3.5 in Sect. 3.7.1.

The scattering length following from (4.174) is the term in the big round brackets on the right-hand sides,

$$a = \bar{a} + \frac{b}{\tan[\bar{\Delta}_D(E=0)\pi]} = \bar{a} + \frac{b}{\tan[\Delta_D\pi + \arctan(\bar{\Gamma}/(2E_R))]}. \tag{4.176}$$

In the absence of channel coupling, the incident-channel phase shift is the background phase shift δ_{bg}, and its leading near-threshold behaviour is $\delta_{bg} \overset{k\to 0}{\sim} -a_{bg}k$, which defines the background scattering length a_{bg}. It is related to the single-channel remainder, i.e. the remainder Δ_D in the uncoupled incident channel by (4.53),

$$a_{bg} = \bar{a} + \frac{b}{\tan(\Delta_D\pi)} \quad \Longrightarrow \quad \Delta_D\pi = \arctan\left(\frac{b}{a_{bg} - \bar{a}}\right). \tag{4.177}$$

Inserting the expression on the far right of (4.177) for $\Delta_D\pi$ in (4.176) gives

$$a = \left[a_{bg} + \frac{\bar{\Gamma}/2}{E_R}\left(\bar{a}\frac{a_{bg} - \bar{a}}{b} - b\right)\right]\left[1 + \frac{\bar{\Gamma}/2}{E_R}\left(\frac{a_{bg} - \bar{a}}{b}\right)\right]^{-1}. \tag{4.178}$$

Equation (4.178) is a universally valid formula for the scattering length a as function of the position E_R of a Feshbach resonance, which may be tuned, e.g. as a function of the strength of an external field, from values above threshold, $E_R > 0$, to values below threshold $E_R < 0$. On the right-hand side of (4.178), a_{bg} is the background scattering length due to the potential in the uncoupled incident channel and $\bar{\Gamma}$ is the threshold-insensitive width (4.167). The lengths $\bar{a}$ and b are the mean scattering length and the threshold length of the singular reference potential $V_{tail}(r)$; they are properties of the $V_{tail}(r)$ only and independent of the position and width of the Feshbach resonance. For a given reference potential describing the large-distance behaviour of the potential in the incident channel, the value of the scattering length depends on two quantities with a clear physical interpretation: the background scattering length a_{bg} and the ratio of the threshold-insensitive width $\bar{\Gamma}$ to the position E_R of the Feshbach resonance relative to the threshold.

If the distance E_R of the Feshbach resonance from threshold is much larger than its width, then the scattering length a is barely affected by the channel coupling,

$$\frac{\bar{\Gamma}}{E_R} \to 0 \quad \Longrightarrow \quad a \to a_{bg}. \tag{4.179}$$

If the uncoupled incident channel supports a bound state exactly at threshold, then $|a_{bg}| \to \infty$. From (4.178) we deduce,

$$|a_{bg}| \to \infty \quad \Longrightarrow \quad a = \bar{a} + b\frac{E_R}{\bar{\Gamma}/2}. \tag{4.180}$$

In this case, the scattering length a is a linear function of E_R and there is no pole.

For $|a_{bg}| < \infty$, the pole of the scattering length, which is customarily called *the* (magnetic) Feshbach resonance in the cold-atoms community, generally occurs for a nonvanishing value of E_R:

$$|a| \to \infty \quad \text{for } E_R = E_{Rpole}, \quad E_{Rpole} = \frac{\bar{\Gamma}}{2}\frac{(\bar{a} - a_{bg})}{b} = -\frac{\bar{\Gamma}/2}{\tan(\Delta_D \pi)}. \tag{4.181}$$

Whether the value of E_{Rpole} is above or below threshold depends on the sign of $\bar{a} - a_{bg}$, which in turn depends on whether the (single-channel) remainder Δ_D is smaller or larger than $\frac{1}{2}$. If the background scattering length a_{bg} is smaller than the mean scattering length of the reference potential $V_{tail}(r)$, then $\tan(\Delta_D \pi)$ is negative, corresponding to $\frac{1}{2} < \Delta_D < 1$, and $E_{Rpole} > 0$; if $a_{bg} > \bar{a}$, then $\tan(\Delta_D \pi)$ is positive, corresponding to $0 < \Delta_D < \frac{1}{2}$, and $E_{Rpole} < 0$.

A plot of the scattering length (4.178) as function of a_{bg} and $E_R/(\bar{\Gamma}/2)$ is shown in Fig. 4.15 for an inverse-power tail (4.57) with $\alpha = 6$. Dark red areas indicate large positive, dark blue areas large negative values. The white diagonal shows the position of the pole of a as given by (4.181). It crosses the vertical axis $a_{bg} = 0$ at $E_R/(\bar{\Gamma}/2) = 1$, because the two tail parameters $\bar{a}$ and b are equal in this case, compare Eq. (4.61) and Table 4.1 in Sect. 4.1.1.

4.2.4 Influence on the Bound-State Spectrum

The derivation of Eq. (4.169) was based on the influence of the Feshbach resonance on the regular incident-channel wave function (4.165), and this influence consists of an additional resonant phase in the argument of the sine on the right-hand side, see (4.166). The distances r where the representation (4.165) of the regular radial wave function is valid lie in the WKB regime where the potential is deep and where the wave functions are insensitive to the position of the threshold. The derivation can thus be continued to the bound-state regime at negative energies, which leads to a simple modification of the quantization rule (4.7)

$$\upsilon_D - \frac{1}{\pi}\arctan\left(\frac{\bar{\Gamma}/2}{E_\upsilon - E_R}\right) - \upsilon = F(E_\upsilon), \tag{4.182}$$

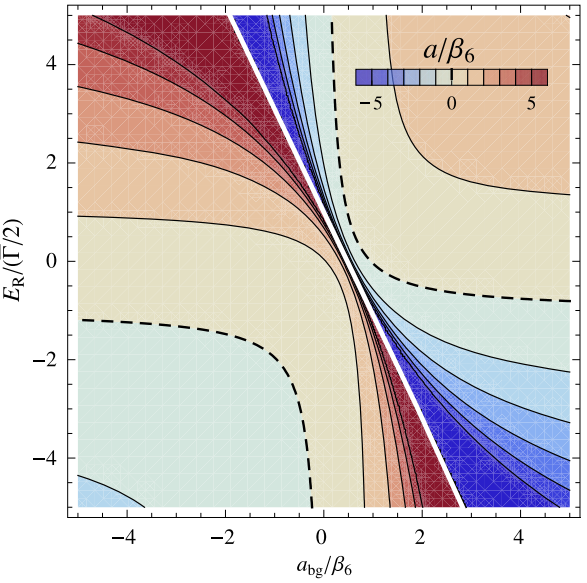

Fig. 4.15 For a single-power reference potential (4.57) with $\alpha = 6$, the figure shows values of the scattering length a given by Eq. (4.178) as function of the background scattering length a_{bg} (in units of β_6) and the position E_R of a Feshbach resonance (in units of half its threshold-insensitive width, i.e. of $\bar{\Gamma}/2$). *Dark red areas* indicate large positive, *dark blue areas* large negative values. The white diagonal shows the pole E_{Rpole} as given by (4.181). Vanishing values of a occur along the *dashed lines*. (From [81])

i.e., the threshold quantum number υ_D is simply replaced by the extended threshold quantum number (4.175),

$$\bar{\upsilon}_D(E_\upsilon) - \upsilon = F(E_\upsilon) = F_{tail}(E_\upsilon) + F_{sr}(E_\upsilon), \tag{4.183}$$

where the expression on the far-right contains the decomposition (4.18) of the quantization function $F(E)$ into the tail contribution $F_{tail}(E)$, as defined by (4.16) in Sect. 4.1.1, and the short-range correction $F_{sr}(E)$, which is a smooth function of energy and vanishes at $E = 0$. Since the quantization functions in (4.183) vanish for $E_\upsilon = 0$, the condition for the existence of a bound state exactly at threshold is now, that the threshold value of the extended threshold quantum number $\bar{\upsilon}_D(E = 0)$ be an integer, i.e. that the threshold value of the extended remainder be zero:

$$\bar{\Delta}_D(E = 0) = \Delta_D + \frac{1}{\pi}\arctan\left(\frac{\bar{\Gamma}/2}{E_R}\right) = 0. \tag{4.184}$$

[Remember that the branch of the arcus-tangent is chosen such that $\arctan(1/x)$ varies smoothly from zero to $-\pi$ as x varies from $-\infty$ to ∞.]

If the position E_R of the Feshbach resonance lies somewhat above threshold, then its influence on the bound-state spectrum is small. If it lies below threshold, $E_R < 0$, then the quantization rule (4.183) produces one additional bound state, an *intruder* or *perturber state* in the vicinity of E_R, compared to the "unperturbed" spectrum of the uncoupled incident channel. [We keep the term "incident" channel at subthreshold energies, even though there can be no genuine incident waves when the channel is closed.]

The exact position of the intruder state, i.e. of the perturber, depends on the position and width of the Feshbach "resonance" and on the unperturbed spectrum.

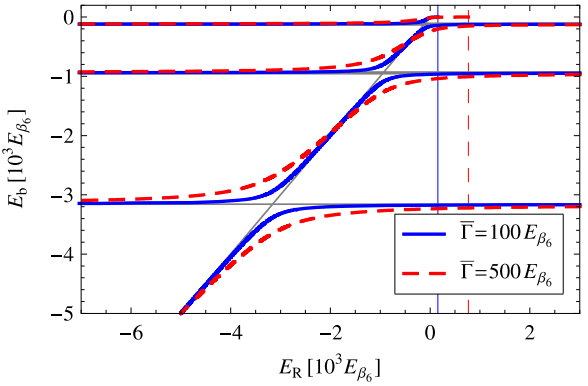

Fig. 4.16 For a deep incident-channel potential with a single-power tail (4.57) with $\alpha = 6$ and a remainder $\Delta_D = 0.9$, the highest three bound-state energies following from (4.182) are shown as functions of the position E_R of a Feshbach resonance. The *solid blue* (*dashed red*) *lines* correspond to a threshold-insensitive width $\bar{\Gamma} = 100E_{\beta_6}$ ($\bar{\Gamma} = 500E_{\beta_6}$). The short-range correction term $F_{sr}(E)$ is neglected. The unit of energy is $E_{\beta_6} = \hbar^2/[2\mu(\beta_6)^2]$. The *straight horizontal lines* show the unperturbed bound-state energies and the *straight diagonal line* corresponds to $E_b = E_R$. The *straight vertical lines* indicate the respective values of E_R at which the scattering length diverges according to (4.181). (Adapted from [81])

Near the threshold of a deep incident-channel potential, the unperturbed spectrum is essentially determined by the singular reference potential $V_{tail}(r)$ and the remainder Δ_D, as discussed in Sect. 4.1.1. Figure 4.16 shows the dependence on E_R of the energies of the highest three states, as given by Eq. (4.182), in a deep potential with an inverse-power tail (4.57) with $\alpha = 6$ for a value $\Delta_D = 0.9$ of the (single-channel) remainder. The straight horizontal lines in Fig. 4.16 show the unperturbed bound-state energies; the solid blue and dashed red lines show the perturbed bound-state energies corresponding, respectively, to the values $\bar{\Gamma} = 100E_{\beta_6}$ and $\bar{\Gamma} = 500E_{\beta_6}$ of the threshold-insensitive width. The short-range correction $F_{sr}(E)$ is neglected here.

Without channel coupling, the spectrum would consist of the unperturbed levels in the incident channel (straight horizontal lines in Fig. 4.16) plus the intruder at $E_b = E_R$ (straight diagonal line in Fig. 4.16). Channel coupling leads to avoided crossings between the unperturbed levels and the intruder state. The value of E_R for which the least bound state is exactly at threshold defines the position E_{Rpole} of the pole of the scattering length as given by (4.181). The straight vertical lines in Fig. 4.16 indicate the values of E_R at which this pole occurs for the respective choice of $\bar{\Gamma}$. According to (4.181), the pole occurs at $E_R = -\bar{\Gamma}/[2\tan(0.9\pi)] \approx 1.54 \times \bar{\Gamma}$ in the present case(s).

The bound state at threshold is a two-component wave function with contributions from the incident channel and the closed channel. Its composition can be understood in a physically appealing way as a consequence of level repulsion between the Feshbach resonance at E_R, which comes from the closed-channel bound state, and a weakly bound incident-channel state just below threshold or a state just

above threshold, which is only marginally unbound. A small value of the single-channel remainder Δ_D implies that the uncoupled incident channel supports a bound state close to threshold, which can be pushed to threshold by level repulsion from a lower-lying Feshbach resonance. A single-channel remainder Δ_D close to unity suggests a marginally unbound state just above threshold, which can be pushed down to threshold from a higher-lying Feshbach resonance; this is the situation depicted in Fig. 4.16. In both cases, the bound state at threshold is close to the uncoupled incident channel wave function with a small contribution due to coupling from the closed channel. If Δ_D is close to $\frac{1}{2}$, then the uncoupled incident channel is as far as possible from supporting a bound state at threshold. The two-channel wave function of the bound state at threshold is then strongly influenced by the Feshbach resonance from the closed-channel and it occurs at a value E_{Rpole} close to zero. If Δ_D is a little below $\frac{1}{2}$, then $E_{\mathrm{Rpole}} < 0$; a Feshbach resonance just below threshold is pushed up to threshold by the highest bound state of the incident channel. When Δ_D is a little above $\frac{1}{2}$, a Feshbach resonance just above threshold is pushed down by coupling to the incident channel; $E_{\mathrm{Rpole}} > 0$ in this case.

A relation connecting the scattering length as given by (4.176) with the asymptotic inverse penetration length κ_b of a bound state very near threshold can be found, as in the derivation of Eq. (4.55) in Sect. 4.1.1, by exploiting Eqs. (4.182)–(4.184). The low-energy expansion of the quantization function (multiplied by π) gives,

$$\pi F(E_b) \overset{\kappa_b \to 0}{\sim} b\kappa_b - \frac{1}{2}(d\kappa_b)^2 + \pi\gamma_{sr}E_b. \tag{4.185}$$

From (4.182) we have

$$\Delta_D\pi = \pi F(E_b) + \arctan\left(\frac{\bar{\Gamma}/2}{E_b - E_R}\right) \pmod{\pi}; \tag{4.186}$$

inserting this expression for $\Delta_D\pi$ in the argument of the tangent on the far right-hand side of (4.176) leads to

$$a \overset{\kappa_b \to 0}{\sim} \frac{1}{\kappa_b} + \rho_{\mathrm{eff}} + \frac{\hbar^2}{2\mu b}\left[\pi\gamma_{sr} - \frac{\bar{\Gamma}/2}{E_R^2 + (\bar{\Gamma}/2)^2}\right] + O(\kappa_b). \tag{4.187}$$

Equation (4.187) shows that the leading universal result already formulated as Eq. (2.88) in Sect. 2.3.8, namely $a \overset{\kappa_b \to 0}{\sim} 1/\kappa_b + O(\kappa_b^0)$, also holds when the near-threshold bound state is generated by the coupling of the incident channel to a near-threshold Feshbach resonance. A different result given at the end of Sect. 4.1.3 in the third edition of Ref. [34] is incorrect.

4.2.5 Relation to the Empirical Formula (4.157)

In a typical experiment involving a Feshbach resonance whose position is tuned past an incident channel's threshold, the quintessential observation is the pole of the scat-

tering length, which occurs when the energy E_R of the Feshbach resonance assumes the value E_{Rpole}, as given in (4.181). Expressing E_R as $E_{Rpole} + E_R - E_{Rpole}$ and exploiting (4.177) and (4.181), we can rewrite Eq. (4.176) as

$$a = a_{bg} - \frac{b}{\sin^2(\Delta_D \pi)} \frac{\bar{\Gamma}/2}{E_R - E_{Rpole}}. \tag{4.188}$$

In order to connect to the empirical formula (4.157), let's assume that the energy E_R of the Feshbach resonance depends linearly on the strength B of an external magnetic (or other) field,

$$E_R = E_{Rpole} + \Delta\mu(B - B_0), \tag{4.189}$$

where B_0 is the field strength of the pole and $\Delta\mu$ is a constant with physical dimension energy per field strength. This choice of notation is consistent with the label $\Delta\mu B$ for the variable energy in Fig. 4.14. As function of the field strength B, the scattering length (4.188) is

$$a = a_{bg} - \frac{b}{\sin^2(\Delta_D \pi)} \frac{\bar{\Gamma}/2}{\Delta\mu(B - B_0)} = a_{bg}\left[1 - \frac{b/a_{bg}}{\sin^2(\Delta_D \pi)} \frac{\bar{\Gamma}/2}{\Delta\mu(B - B_0)}\right], \tag{4.190}$$

so the width ΔB, introduced as an empirical parameter in (4.157), is explicitly given as

$$\Delta B = -\frac{b}{a_{bg}} \frac{1}{\sin^2(\Delta_D \pi)} \frac{\bar{\Gamma}}{2\Delta\mu}. \tag{4.191}$$

Expressing $\sin^2(\Delta_D \pi)$ in terms of a_{bg} according to (4.177) gives an expression for ΔB in terms of a_{bg} and the tail parameters $\bar{a}$ and b:

$$\Delta B = -\frac{\bar{\Gamma}}{2\Delta\mu} \frac{1}{b}\left[\frac{\bar{a}^2 + b^2}{a_{bg}} - 2\bar{a} + a_{bg}\right]. \tag{4.192}$$

Equations (4.191), (4.192) show that the width ΔB of a "magnetic Feshbach resonance", as observed in a typical experiment, reflects not only the strength of the coupling between the bound state in the closed channel and the incident-chanel wave functions, which is expressed in the threshold-insensitive width $\bar{\Gamma}$. It also depends sensitively on the properties of the uncoupled incident channel, as expressed in the background phase shift a_{bg}. If the uncoupled incident channel supports a bound state (or if there is a virtual state) very near threshold, a_{bg} becomes very large and the empirical formula (4.157) is no longer applicable, as discussed in connection with Eq. (4.180) above. Another interesting situation is $a_{bg} \to 0$, corresponding to little or no interaction in the absence of channel coupling. In this case, the width ΔB as defined via (4.157) diverges, and a more appropriate empirical formula would be,

$$a = a_{bg} + \frac{\Delta_B}{B - B_0} \quad \text{with} \quad \Delta_B \equiv a_{bg}\Delta B = -\frac{\bar{\Gamma}}{2\Delta\mu} \frac{1}{b}\left(\bar{a}^2 + b^2 - 2a_{bg}\bar{a} + a_{bg}^2\right). \tag{4.193}$$

The width Δ_B defined in this way has the physical dimension of a length times field strength. In the limit of vanishing background phase shift, $a_{\rm bg} \to 0$, it converges to a finite value determined by the threshold-insensitive width $\bar{\Gamma}$ of the Feshbach resonance and the tail parameters $\bar{a}$ and b.

4.3 Quantum Description of Scattering in Two Spatial Dimensions

Two-dimensional scattering problems arise naturally when the motion of projectile and target is restricted to a plane, e.g. a surface separating two bulk media. A scattering problem can also become effectively two-dimensional, if a three-dimensional configuration is translationally invariant in one direction. This is the case for a projectile scattering off a cylindrically symmetric target, e.g., an atom or molecule scattering off a cylindrical wire or nanotube. The motion of the projectile is free in the direction parallel to the cylinder axis, and we are left with a two-dimensional scattering problem in a plane perpendicular to the cylinder axis. Essential features of the two-dimensional scattering problem were illuminated by Lapidus [51], Verhaar et al. [87] and Adhikari [1] some decades ago. The recent intense activity in physics involving ultracold atoms and their interaction with nanostructures such as cylindrical nanotubes has lead to a renewed interest in this subject, in particular in the low-energy, near-threshold regime [5, 30, 48, 86].

As in Sect. 1.4 in Chap. 1 we assume that the 2D scattering process occurs in the y–z plane, where the scattering angle θ varies between $-\pi$ and π, see Fig. 4.17. As in Chap. 2, the quantum mechanical description of the scattering process is based on the Schrödinger equation

$$\left[-\frac{\hbar^2}{2\mu}\Delta + V(\mathbf{r})\right]\psi(\mathbf{r}) = E\psi(\mathbf{r}), \tag{4.194}$$

but $\mathbf{r}$ now stands for the two-component displacement vector in the y–z plane, and Δ is the 2D-Laplacian.

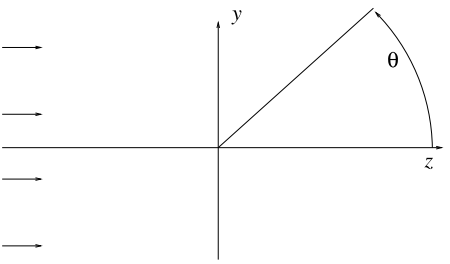

Fig. 4.17 Two-dimensional scattering in the y–z plane. The z-axis shows in the direction of incidence, and the scattering angle θ varies between $-\pi$ and π

4.3.1 Scattering Amplitude and Scattering Cross Section

We look for solutions of (4.194) with the following boundary conditions,

$$\psi(\mathbf{r}) \overset{r\to\infty}{\sim} \mathrm{e}^{\mathrm{i}kz} + f(\theta)\frac{\mathrm{e}^{\mathrm{i}kr}}{\sqrt{r}}. \tag{4.195}$$

Essential differences to the three-dimensional case (2.2) are, that the outgoing spherical wave becomes an outgoing circular wave whose amplitude decreases proportional to $1/\sqrt{r}$ instead of to $1/r$, and that the physical dimension of the scattering amplitude $f(\theta)$ is the square root of a length in the two-dimensional case. The current density $\mathbf{j}_{\mathrm{out}}(\mathbf{r})$ associated with the outgoing circular wave is

$$\mathbf{j}_{\mathrm{out}}(\mathbf{r}) = \frac{\hbar k}{\mu}\left|f(\theta)\right|^2\frac{\hat{\mathbf{e}}_{\mathbf{r}}}{r} + O\left(\frac{1}{r^{3/2}}\right), \tag{4.196}$$

while the incoming current density associated with the "plane wave" $\mathrm{e}^{\mathrm{i}kz}$ in (4.195) can again be written as $\mathbf{j}_{\mathrm{in}} = \hat{\mathbf{e}}_z\hbar k/\mu$. The surface element of a large sphere in the three-dimensional case, $r^2\mathrm{d}\Omega$, is now replaced by the arc-element of a large circle, $r\mathrm{d}\theta$, and the differential scattering cross section is defined by the flux scattered into this arc, $\mathbf{j}_{\mathrm{out}}(\mathbf{r})\cdot\hat{\mathbf{e}}_{\mathbf{r}}r\mathrm{d}\theta$, normalized to the incoming current density $|\mathbf{j}_{\mathrm{in}}| = \hbar k/\mu$,

$$\mathrm{d}\lambda = \left|f(\theta)\right|^2\mathrm{d}\theta, \qquad \frac{\mathrm{d}\lambda}{\mathrm{d}\theta} = \left|f(\theta)\right|^2. \tag{4.197}$$

The integrated scattering cross section is

$$\lambda = \int_{-\pi}^{\pi}\frac{\mathrm{d}\lambda}{\mathrm{d}\theta}\mathrm{d}\theta = \int_{-\pi}^{\pi}\left|f(\theta)\right|^2\mathrm{d}\theta. \tag{4.198}$$

Note that the differential and the integrated scattering cross sections have the physical dimension of a length. The differential cross section can be interpreted as the length perpendicular to the direction of incidence from which the incoming particles are scattered into the differential arc defined by $\mathrm{d}\theta$, while the integrated cross section corresponds to the length from which particles are scattered at all.

Particle conservation implies that the total flux through a circle, $\int_{-\pi}^{\pi}\mathbf{j}\cdot\hat{\mathbf{e}}_{\mathbf{r}}r\mathrm{d}\theta$ should vanish for large radius r. The contribution from the incoming wave $\mathrm{e}^{\mathrm{i}kz}$ vanishes on symmetry grounds, while the contribution from the outgoing circular wave is:

$$I_{\mathrm{out}} = \lim_{r\to\infty}\int_{-\pi}^{\pi}\mathbf{j}_{\mathrm{out}}(\mathbf{r})\cdot\hat{\mathbf{e}}_{\mathbf{r}}r\mathrm{d}\theta = \frac{\hbar k}{\mu}\int_{-\pi}^{\pi}\left|f(\theta)\right|^2\mathrm{d}\theta = \frac{\hbar k}{\mu}\lambda. \tag{4.199}$$

The contribution $\mathbf{j}_{\mathrm{int}}(\mathbf{r})$ of the interference of incoming "plane" and outgoing circular wave to the current density is,

$$\mathbf{j}_{\mathrm{int}}(\mathbf{r}) = \frac{\hbar k}{2\mu}f(\theta)\frac{\mathrm{e}^{\mathrm{i}k(r-z)}}{\sqrt{r}}(\hat{\mathbf{e}}_{\mathbf{r}} + \hat{\mathbf{e}}_z) + \mathrm{cc} + \cdots, \tag{4.200}$$

so the interference contribution to the flux through a circle of large radius r is

$$\mathbf{j}_{\text{int}}(\mathbf{r}) \cdot \hat{\mathbf{e}}_{\mathbf{r}} r \mathrm{d}\theta = \frac{\hbar k}{2\mu} f(\theta) \mathrm{e}^{\mathrm{i}kr(1-\cos\theta)} \sqrt{r}(1+\cos\theta) + \text{cc}. \tag{4.201}$$

The integral over the right-hand side of (4.201) can be evaluated by the method of stationary phase, since the integrand contributes only around $\cos\theta = 1$ for $r \to \infty$. This gives

$$I_{\text{int}} = \int_{-\pi}^{\pi} \mathbf{j}_{\text{int}}(\mathbf{r}) \cdot \hat{\mathbf{e}}_{\mathbf{r}} r \mathrm{d}\theta = 2\frac{\hbar k}{\mu} \sqrt{\frac{\pi}{k}} \big[\Re\big\{ f(\theta=0) \big\} - \Im\big\{ f(\theta=0) \big\} \big]. \tag{4.202}$$

Particle conservation requires $I_{\text{out}} + I_{\text{int}} = 0$, so with (4.199) we obtain the *optical theorem for scattering in two-dimensional space*,

$$\lambda = 2\sqrt{\frac{\pi}{k}} \big[\Im\big\{ f(\theta=0) \big\} - \Re\big\{ f(\theta=0) \big\} \big]. \tag{4.203}$$

4.3.2 Lippmann–Schwinger Equation and Born Approximation

Adapting the treatment of Sect. 2.2 to the case of two spatial dimensions leads to the Lippmann–Schwinger equation

$$\psi(\mathbf{r}) = \mathrm{e}^{\mathrm{i}kz} + \int \mathscr{G}_{\text{2D}}(\mathbf{r}, \mathbf{r}') V(\mathbf{r}') \psi(\mathbf{r}') \mathrm{d}\mathbf{r}', \tag{4.204}$$

which looks just like the corresponding equation (2.18) in 3D, except that the free-particle Green's function $\mathscr{G}_{\text{2D}}(\mathbf{r}, \mathbf{r}')$, defined by the 2D version of Eq. (2.16), is

$$\mathscr{G}_{\text{2D}}(\mathbf{r}, \mathbf{r}') = \frac{\mathrm{i}\mu}{2\hbar^2} H_0^{(1)}\big(k|\mathbf{r}-\mathbf{r}'|\big) \overset{k|\mathbf{r}-\mathbf{r}'|\to\infty}{\sim} \frac{\mathrm{i}\mu}{2\hbar^2} \mathrm{e}^{-\mathrm{i}\pi/4} \sqrt{\frac{2}{\pi k|\mathbf{r}-\mathbf{r}'|}} \mathrm{e}^{\mathrm{i}k|\mathbf{r}-\mathbf{r}'|}. \tag{4.205}$$

Here $H_0^{(1)}$ stands for the zero-order Hankel function of the first kind, see Eqs. (B.32) and (B.33) in Appendix B.4. In the asymptotic region $|\mathbf{r}| \gg |\mathbf{r}|'$ the Green's function in (4.204) can be replaced by

$$\mathscr{G}_{\text{2D}}(\mathbf{r}, \mathbf{r}') = \frac{\mu \mathrm{e}^{\mathrm{i}\pi/4}}{\hbar^2 \sqrt{2\pi k}} \frac{\mathrm{e}^{\mathrm{i}kr}}{\sqrt{r}} \left[\mathrm{e}^{-\mathrm{i}\mathbf{k}_{\mathbf{r}} \cdot \mathbf{r}'} + O\left(\frac{r'}{r}\right) \right]. \tag{4.206}$$

This is the 2D version of (2.19); $\mathbf{k}_{\mathbf{r}}$ again stands for $k\hat{\mathbf{e}}_{\mathbf{r}}$, but $\hat{\mathbf{e}}_{\mathbf{r}}$ is now the radial unit vector in the y–z plane. Inserting (4.206) in (4.204) gives the asymptotic form (4.195) with

$$f(\theta) = \frac{\mu \mathrm{e}^{\mathrm{i}\pi/4}}{\hbar^2 \sqrt{2\pi k}} \int \mathrm{e}^{-\mathrm{i}\mathbf{k}_{\mathbf{r}} \cdot \mathbf{r}'} V(\mathbf{r}') \psi(\mathbf{r}') \mathrm{d}\mathbf{r}'. \tag{4.207}$$

The Born approximation is defined by replacing the exact solution $\psi(\mathbf{r}')$ in the integrand in (4.207) by the incoming "plane" wave $\mathrm{e}^{\mathrm{i}kz'} = \mathrm{e}^{\mathrm{i}(k\hat{\mathbf{e}}_z)\cdot\mathbf{r}'}$,

$$f^{\mathrm{Born}}(\theta) = \frac{\mu \mathrm{e}^{\mathrm{i}\pi/4}}{\hbar^2\sqrt{2\pi k}} \int \mathrm{d}\mathbf{r}' \mathrm{e}^{-\mathrm{i}\mathbf{k}_\mathbf{r}\cdot\mathbf{r}'} V(\mathbf{r}') \mathrm{e}^{\mathrm{i}kz'} = \frac{\mu \mathrm{e}^{\mathrm{i}\pi/4}}{\hbar^2\sqrt{2\pi k}} \int \mathrm{d}\mathbf{r}' \mathrm{e}^{-\mathrm{i}\mathbf{q}\cdot\mathbf{r}'} V(\mathbf{r}'), \tag{4.208}$$

where $\hbar\mathbf{q}$ is the momentum transferred from the incoming wave travelling in the direction of $\hat{\mathbf{e}}_z$ to the outgoing wave travelling in the direction of $\hat{\mathbf{e}}_\mathbf{r}$,

$$\mathbf{q} = k(\hat{\mathbf{e}}_\mathbf{r} - \hat{\mathbf{e}}_z), \qquad q = |\mathbf{q}| = 2k\sin(\theta/2). \tag{4.209}$$

For a radially symmetric potential $V(\mathbf{r}) = V(r)$, Eq. (4.208) can be simplified via an expansion of the exponential $\mathrm{e}^{-\mathrm{i}\mathbf{q}\cdot\mathbf{r}'}$ in polar variables [compare (4.219) below],

$$f^{\mathrm{Born}}(\theta) = \frac{\mu \mathrm{e}^{\mathrm{i}\pi/4}}{\hbar^2\sqrt{2\pi k}} 2\pi \int_0^\infty V(r) J_0\big(2kr\sin(\theta/2)\big) r\,\mathrm{d}r. \tag{4.210}$$

4.3.3 Partial-Waves Expansion and Scattering Phase Shifts

For planar motion in the y–z plane, there is only one relevant component of angular momentum, namely $\hat{L} = y\hat{p}_z - z\hat{p}_y$, and in terms of the angle θ,

$$\hat{L} = \frac{\hbar}{\mathrm{i}} \frac{\partial}{\partial\theta}. \tag{4.211}$$

The eigenfunctions of $\hat{L}$ are $\mathrm{e}^{\mathrm{i}m\theta}$ with $m = 0, \pm1, \pm2, \ldots$, and the corresponding eigenvalues are $m\hbar$. Any wave function $\Psi(\mathbf{r}) \equiv \Psi(r,\theta)$ can be expanded in the complete basis of eigenfunctions of $\hat{L}$,

$$\Psi(\mathbf{r}) = \sum_{m=-\infty}^{\infty} \frac{u_m(r)}{\sqrt{r}} \mathrm{e}^{\mathrm{i}m\theta}. \tag{4.212}$$

From the polar representation of the Laplacian in 2D, we can write the kinetic energy operator in (4.194) as,

$$-\frac{\hbar^2}{2\mu}\Delta = -\frac{\hbar^2}{2\mu}\left(\frac{\partial^2}{\partial r^2} + \frac{1}{r}\frac{\partial}{\partial r}\right) + \frac{\hat{L}^2}{2\mu r^2}. \tag{4.213}$$

We assume a radially symmetric potential, $V(\mathbf{r}) = V(r)$. Inserting the expansion (4.212) into the Schrödinger equation (4.194) then gives, with the help of (4.213), an uncoupled set of radial equations for the radial wave functions $u_m(r)$,

$$\left[-\frac{\hbar^2}{2\mu}\frac{\mathrm{d}^2}{\mathrm{d}r^2} + \frac{(m^2 - \frac{1}{4})\hbar^2}{2\mu r^2} + V(r)\right] u_m(r) = E u_m(r). \tag{4.214}$$

The 2D radial Schrödinger equation looks similar to the 3D radial Schrödinger equation (2.35) in Sect. 2.3.2. In fact, Eqs. (4.214) and (2.35) are identical, if we equate $|m| - \frac{1}{2}$ with the 3D angular momentum quantum number l:

$$l \equiv |m| - \frac{1}{2}. \tag{4.215}$$

Many results derived for the 3D radial waves in Sect. 2.3 can be carried over to the 2D radial waves simply via (4.215), but integer values of m imply half-integer values of l, so the results of Sect. 2.3.2 have to be checked to see whether they hold in these cases. This is particularly important for s-waves in 2D ($m = 0$), which correspond to $l = -\frac{1}{2}$.

For the free-particle case $V(r) \equiv 0$, two linearly independent solutions of the radial equation (4.214) are

$$u_m^{(\mathrm{s})}(kr) = \sqrt{\frac{\pi}{2}kr}\, J_{|m|}(kr), \qquad u_m^{(\mathrm{c})}(kr) = -\sqrt{\frac{\pi}{2}kr}\, Y_{|m|}(kr), \tag{4.216}$$

where $J_{|m|}$ and $Y_{|m|}$ stand for the *ordinary Bessel functions* of the first and second kind, respectively [see Appendix B.4]. Their asymptotic behaviour is given by[2]

$$\begin{aligned} u_m^{(\mathrm{s})}(kr) &\overset{kr\to\infty}{\sim} \sin\left[kr - \left(|m| - \frac{1}{2}\right)\frac{\pi}{2}\right], \\ u_m^{(\mathrm{c})}(kr) &\overset{kr\to\infty}{\sim} \cos\left[kr - \left(|m| - \frac{1}{2}\right)\frac{\pi}{2}\right]. \end{aligned} \tag{4.217}$$

The influence of a potential $V(r)$ is manifest in the asymptotic phase shifts δ_m of the regular solutions of the radial Schrödinger equation (4.214). When $V(r)$ falls off faster than $1/r^2$ at large distances the effective potential in (4.214) is dominated by the centrifugal term at large distances, and the regular solution can be taken to be a superposition of the two radial free-particle wave functions (4.216) obeying (4.217),

$$u_m(r) \overset{r\to\infty}{\propto} A u_m^{(\mathrm{s})}(kr) + B u_m^{(\mathrm{c})}(kr) \overset{r\to\infty}{\propto} \sin\left[kr - \left(|m| - \frac{1}{2}\right)\frac{\pi}{2} + \delta_m\right], \tag{4.218}$$

with $\tan\delta_m = B/A$.

In order to relate the scattering phase shifts to the scattering amplitude, we first expand the incoming "plane" wave of (4.195) in partial waves,

$$\mathrm{e}^{\mathrm{i}kz} = \sum_{m=-\infty}^{\infty} \mathrm{i}^m J_m(kr)\mathrm{e}^{\mathrm{i}m\theta} \overset{kr\to\infty}{\sim} \sum_{m=-\infty}^{\infty} \frac{1}{\sqrt{2\pi \mathrm{i}kr}}\left(\mathrm{e}^{\mathrm{i}kr} + (-1)^m \mathrm{i}\mathrm{e}^{-\mathrm{i}kr}\right). \tag{4.219}$$

[2] Due to the m-independent term $\frac{\pi}{4}$ appearing in the arguments both of $u_m^{(\mathrm{s})}(kr)$ and of $u_m^{(\mathrm{c})}(kr)$ in (4.217), there is no *a priori* preference for the assignment of an asymptotic "sine-" or "cosine-like" behaviour. The present nomenclature is chosen to make the connection to the 3D case as transparent as possible.

The appropriate partial-waves expansion for the scattering amplitude is

$$f(\theta) = \sum_{m=-\infty}^{\infty} f_m \mathrm{e}^{\mathrm{i}m\theta}, \tag{4.220}$$

and the constant coefficients f_m are the partial-wave scattering amplitudes. Expressing the sum of "plane" and circular wave in the form (4.212) gives an explicit expression for the asymptotic behaviour of the radial wave functions,

$$\begin{aligned} u_m(r) &\overset{r\to\infty}{\sim} \frac{1}{\sqrt{2\pi\mathrm{i}k}}\left[(1+\sqrt{2\pi\mathrm{i}k}\,f_m)\mathrm{e}^{\mathrm{i}kr} + \mathrm{i}(-1)^m \mathrm{e}^{-\mathrm{i}kr}\right] \\ &= \frac{\mathrm{i}(-1)^m}{\sqrt{2\pi\mathrm{i}k}}\left[\mathrm{e}^{-\mathrm{i}kr} - \mathrm{i}(-1)^m(1+\sqrt{2\pi\mathrm{i}k}\,f_m)\mathrm{e}^{\mathrm{i}kr}\right]. \end{aligned} \tag{4.221}$$

We can rewrite the asymptotic form of the regular solution (4.218) as

$$\begin{aligned} u_m(r) &\overset{r\to\infty}{\propto} \sin\left[kr - \left(|m| - \frac{1}{2}\right)\frac{\pi}{2} + \delta_m\right] \\ &\propto \mathrm{e}^{-\mathrm{i}[kr-(|m|-\frac{1}{2})\frac{\pi}{2}+\delta_m]}\mathrm{e}^{-\mathrm{i}\delta_m} - \mathrm{e}^{\mathrm{i}[kr-(|m|-\frac{1}{2})\frac{\pi}{2}+\delta_m]}\mathrm{e}^{+\mathrm{i}\delta_m} \\ &\propto \mathrm{e}^{-\mathrm{i}kr} - \mathrm{e}^{-\mathrm{i}(|m|-\frac{1}{2})\pi}\mathrm{e}^{\mathrm{i}kr}\mathrm{e}^{2\mathrm{i}\delta_m}. \end{aligned} \tag{4.222}$$

Comparing the lower lines of Eqs. (4.221) and (4.222) gives

$$\mathrm{e}^{2\mathrm{i}\delta_m} = 1 + \sqrt{2\pi\mathrm{i}k}\,f_m, \quad f_m = \frac{1}{\sqrt{2\pi\mathrm{i}k}}\left(\mathrm{e}^{2\mathrm{i}\delta_m} - 1\right) = \sqrt{\frac{2\mathrm{i}}{\pi k}}\mathrm{e}^{\mathrm{i}\delta_m}\sin\delta_m. \tag{4.223}$$

Equation (4.223) can be used to express the scattering cross sections in terms of the scattering phase shifts,

$$\begin{aligned} \frac{\mathrm{d}\lambda}{\mathrm{d}\theta} &= \left|f(\theta)\right|^2 = \sum_{m,m'} f_m^* f_{m'} \mathrm{e}^{\mathrm{i}(m'-m)\theta} \\ &= \frac{2}{\pi k}\sum_{m,m'} \mathrm{e}^{\mathrm{i}(\delta_{m'}-\delta_m)}\sin\delta_{m'}\sin\delta_m \mathrm{e}^{\mathrm{i}(m'-m)\theta}, \end{aligned} \tag{4.224}$$

$$\lambda = \int_{-\pi}^{\pi}\left|f(\theta)\right|^2 \mathrm{d}\theta = 2\pi\sum_{m=-\infty}^{\infty}\left|f_m\right|^2 = \frac{4}{k}\sum_{m=-\infty}^{\infty}\sin^2\delta_m. \tag{4.225}$$

The scattering amplitude in forward direction is

$$f(\theta=0)=\sum_{m=-\infty}^{\infty} f_m=\sqrt{\frac{2\mathrm{i}}{\pi k}}\sum_{m=-\infty}^{\infty}\mathrm{e}^{\mathrm{i}\delta_m}\sin\delta_m$$

$$=\sqrt{\frac{2}{\pi k}}\sum_{m=-\infty}^{\infty}\sin\delta_m\mathrm{e}^{\mathrm{i}(\delta_m+\pi/4)},\quad\text{hence}\tag{4.226}$$

$$\Im\{f(0)\}-\Re\{f(0)\}=\frac{2}{\sqrt{\pi k}}\sum_{m=-\infty}^{\infty}\sin^2\delta_m=\frac{1}{2}\sqrt{\frac{k}{\pi}}\lambda,\tag{4.227}$$

which again yields the optical theorem (4.203).

4.3.4 Near-Threshold Behaviour of the Scattering Phase Shifts

The leading near-threshold behaviour of the phase shifts can be derived from the small-argument behaviour of the free-particle solutions (4.216),

$$u_m^{(\mathrm{s})}(kr)\overset{kr\to0}{\sim}\frac{\sqrt{\pi}}{\Gamma(|m|+1)}\left(\frac{kr}{2}\right)^{\frac{1}{2}+|m|},\tag{4.228}$$

$$u_m^{(\mathrm{c})}(kr)\overset{kr\to0}{\sim}\frac{\Gamma(|m|)}{\sqrt{\pi}}\left(\frac{kr}{2}\right)^{\frac{1}{2}-|m|}\quad\text{for } m\neq0.\tag{4.229}$$

The case $m=0$ is special, because the two powers of r appearing in (4.228) and (4.229), namely $\frac{1}{2}+|m|$ and $\frac{1}{2}-|m|$ are equal in this case. We focus first on the case $m\neq0$; the special case of s-waves in 2D is treated in Sect. 4.3.5 below.

At distances r beyond the range of the potential, the radial wave function $u_m(r)$ is a superposition of the free-particle wave functions (4.216); towards threshold, $k\to0$, the product kr tends to zero so we can make use of the small-argument expressions (4.228), (4.229),

$$u_m(r)\overset{kr\to0}{\propto}u_m^{(\mathrm{s})}(kr)+\tan\delta_m u_m^{(\mathrm{c})}(kr)$$

$$\sim\frac{\sqrt{\pi}}{\Gamma(|m|+1)}\left(\frac{k}{2}\right)^{\frac{1}{2}+|m|}\left[r^{|m|+\frac{1}{2}}+\tan\delta_m\left(\frac{k}{2}\right)^{-2|m|}\frac{\Gamma(|m|)\Gamma(|m|+1)}{\pi r^{|m|-\frac{1}{2}}}\right].\tag{4.230}$$

Directly at threshold, the radial Schrödinger equation (4.214) has a regular solution $u_m^{(0)}(r)$ which is defined up to a constant by the boundary condition $u_m^{(0)}(0)=0$ and is a function of r only. The wave function (4.230) must become proportional to this k-independent solution for $k\to0$, so in the second term in the square bracket in the

lower line of Eq. (4.230), the k-dependence of $\tan\delta_m$ must compensate the factor $(k/2)^{-2|m|}$, $\tan\delta \overset{k\to 0}{\propto} k^{2|m|}$. More explicitly,

$$\tan\delta_m \overset{k\to 0}{\sim} \mp\frac{\pi}{\Gamma(|m|)\Gamma(|m|+1)}\left(\frac{a_m k}{2}\right)^{2|m|}. \tag{4.231}$$

The characteristic length a_m appearing on the right-hand side of (4.231) is the *scattering length* in the partial wave $m \neq 0$. Equation (4.231) is essentially identical to Eq. (2.77) in Sect. 2.3.8 if we replace $|m|$ by $l + \frac{1}{2}$, except that the power $2|m|$ in (4.231) is always even for integer m, so the possibility of having positive or negative values on the right-hand side has to be explicitly included via the $\mp$ sign.

As in the 3D case, the threshold behaviour (4.231) is only valid in all partial waves if the potential $V(r)$ in the radial Schrödinger equation (4.214) falls off faster than any power of $1/r$ at large distances. For potentials falling off as $1/r^\alpha$, the considerations of Sect. 2.6 can be carried over to the 2D case, remembering that l now stands for $|m| - \frac{1}{2}$. In particular, the condition for the validity of Eq. (4.231) now reads $2|m| < \alpha - 2$. For $2|m| > \alpha - 2$, Eq. (2.274) in Sect. 2.6.1 is applicable, provided $l + \frac{1}{2}$ is replaced by $|m|$. The special case treated in Sect. 2.6.2 becomes the special case $2|m| = \alpha - 2$, and the (marginally) leading term of the near-threshold behaviour of $\tan\delta_m$ is given by Eq. (2.280).

4.3.5 The Case $m = 0$, s-Waves in Two Dimensions

The case of s-waves in two dimensions is special, because the radial Schrödinger equation (4.214) now reads

$$\left[-\frac{\hbar^2}{2\mu}\frac{\mathrm{d}^2}{\mathrm{d}r^2} - \frac{1}{4}\frac{\hbar^2}{2\mu r^2} + V(r)\right]u_{m=0}(r) = E u_{m=0}(r), \tag{4.232}$$

and the centrifugal potential is *attractive*. In the language of Sect. 2.7 on potentials with inverse-square tails, the 2D s-wave radial equation (4.232) corresponds to the "critically attractive case" treated in Sects. 2.7.1.3 and 2.7.2.3. This degree of attractivity of an inverse-square potential marks the boundary to the "over-critically attractive" case. If the factor $\frac{1}{4}$ in front of the inverse-square term in (4.232) were replaced by $\frac{1}{4} + \varepsilon$ with an ever so small positive ε, then the radial Schrödinger equation (4.232) would support an infinite dipole series of bound states, as described in Sect. 2.7.2.2.

The free-particle solutions, for $V(r) \equiv 0$ in (4.232), are

$$u^{(\mathrm{s})}_{m=0}(r) = \sqrt{\frac{\pi}{2}kr}\,J_0(kr), \qquad u^{(\mathrm{s})}_{m=0}(r) = -\sqrt{\frac{\pi}{2}kr}\,Y_0(kr), \tag{4.233}$$

compare (2.330) in Sect. 2.7.1.3 and (4.216). Their small-argument behaviour is

$$u^{(\mathrm{s})}_{m=0}(kr) \overset{kr\to 0}{\sim} \sqrt{\frac{\pi}{2}kr}, \qquad u^{(\mathrm{c})}_{m=0}(kr) \overset{kr\to 0}{\sim} -\sqrt{\frac{2}{\pi}kr}\left[\ln\left(\frac{kr}{2}\right) + \gamma_{\mathrm{E}} + O\big((kr)^2\big)\right]; \tag{4.234}$$

compare (2.332) in Sect. 2.7.1.3. Beyond the range of the interaction potential $V(r)$, the regular solution of the radial Schrödinger equation (4.232) is a superposition of the free-particle waves (4.233), and its asymptotic behaviour is,[3]

$$u_{m=0}(r) \overset{r\to\infty}{\propto} \sqrt{kr}\big[J_0(kr) - \tan\delta_{m=0} Y_0(kr)\big] \overset{kr\to\infty}{\propto} \sin\left(kr + \frac{\pi}{4} + \delta_{m=0}\right). \tag{4.235}$$

The leading near-threshold behaviour of the s-wave scattering phase shift is as already derived in Eq. (2.350),

$$\cot\delta_{m=0} \overset{k\to 0}{\sim} \frac{2}{\pi}\left(\ln\left(\frac{ka}{2}\right) + \gamma_{\mathrm{E}}\right). \tag{4.236}$$

Equation (4.236) defines the scattering length a for s-waves in two dimensions. In the limit $k \to 0$, the wave function (4.235) converges to a k-independent limit $u^{(0)}_{m=0}$,

$$u_{m=0}(r) \overset{k\to 0}{\propto} u^{(0)}_{m=0}(r) \overset{r\to\infty}{\propto} -\sqrt{r}\ln\left(\frac{r}{a}\right). \tag{4.237}$$

The wave function on the far right of (4.237) has exactly one node (beyond $r = 0$), and this node lies at $r = a$. For a potential falling off as $1/r^\alpha$ at large distances, a well-defined scattering length in the partial wave m exists as long as $2|m| < \alpha - 2$. For $m = 0$, this condition is fulfilled for all $\alpha > 2$. The scattering length a defined according to Eqs. (4.236), (4.237) is well defined for all interaction potentials which fall off faster than $1/r^2$ at large distances.

It is worthwhile to reflect a little on the remarkable situation of s-waves in 2D. At threshold, the regular free-particle wave is proportional to $\sqrt{r}$, corresponding to r^{l+1} when $l = -\frac{1}{2}$. The "irregular" solution, which we might expect to be proportional to r^{-l}, is actually proportional to $\sqrt{r}\ln r$, which seems only marginally less regular than the regular wave. An arbitrary superposition of these two free-particle waves can be written as

$$u(r) \propto A\sqrt{r} - \sqrt{r}\ln r = -\sqrt{r}\ln\left(\frac{r}{\mathrm{e}^A}\right), \tag{4.238}$$

which is just the form on the right-hand side of (4.237), with the scattering length given by $a = \mathrm{e}^A$. In two-dimensional scattering, the scattering length is never negative.

[3] Since $m = 0$ corresponds to $l = -\frac{1}{2}$, the phase shift $\tilde{\delta}$ in Sect. 2.7.2.3 is actually *the* scattering phase shift $\delta_{m=0}$ in the present case, see Eq. (2.341).

The leading near-threshold behaviour of the s-wave phase shift (4.236) was already given in Ref. [87], together with the next term of the effective-range expansion in two dimensions,

$$\cot\delta_{m=0} \overset{k\to 0}{\sim} \frac{2}{\pi}\left[\ln\left(\frac{ka}{2}\right) + \gamma_{\mathrm{E}} + \frac{(kr_{\mathrm{eff}})^2}{2}\right]; \tag{4.239}$$

the effective range in 2D is defined by

$$r_{\mathrm{eff}}^2 = 2\int_0^\infty \left(\left[w^{(0)}(r)\right]^2 - \left[u^{(0)}(r)\right]^2\right)\mathrm{d}r, \tag{4.240}$$

see also [5]. Here $u^{(0)}(r)$ is the regular solution, at threshold, of (4.232), which behaves as the right-hand side of (4.237) asymptotically, and $w^{(0)}(r)$ is the free-particle solution which has this form for all r,

$$w^{(0)}(r) = -\sqrt{r}\ln\left(\frac{r}{a}\right), \qquad u^{(0)}(r) \overset{r\to\infty}{\sim} -\sqrt{r}\ln\left(\frac{r}{a}\right). \tag{4.241}$$

In contrast to the similar-looking definition of the effective range in 3D, see Eq. (2.103) in Sect. 2.3.8, the right-hand side of (4.240) has the physical dimension of a length squared. Note that r_{eff}^2 defined in this way can be negative. The integral on the right-hand side of (4.240) converges to a well defined limit for interaction potentials falling off faster than $1/r^4$ at large distances [5].

The leading near-threshold behaviour of the scattering cross sections is, naturally, dominated by the contribution from the s-wave. From (4.220), (4.223) and (4.236) we obtain

$$f(\theta) \overset{k\to 0}{\sim} f_0 \overset{k\to 0}{\sim} \frac{\sqrt{\pi\,\mathrm{i}/(2k)}}{\ln(\frac{ka}{2}) + \gamma_{\mathrm{E}}}, \tag{4.242}$$

so

$$\frac{\mathrm{d}\lambda}{\mathrm{d}\theta} \overset{k\to 0}{\sim} \frac{\pi/(2k)}{|\ln(\frac{ka}{2}) + \gamma_{\mathrm{E}}|^2} \quad \text{and} \quad \lambda \overset{k\to 0}{\sim} \frac{\pi^2/k}{|\ln(\frac{ka}{2}) + \gamma_{\mathrm{E}}|^2}. \tag{4.243}$$

The quantum mechanical scattering cross sections in two dimensions diverge at threshold. This divergence is essentially as $1/k$, moderated marginally by the logarithmic factor. Note that the expressions in (4.242) and (4.243), where the leading behaviour contains the logarithm in the expression $\ln(ka/2) + \gamma_{\mathrm{E}}$, are only meaningful when $ka/2$ is so small, that $\ln(ka/2) < -\gamma_{\mathrm{E}}$, i.e., for

$$ka < 2\exp(-\gamma_{\mathrm{E}}). \tag{4.244}$$

For a reference potential $V_{\mathrm{tail}}(r)$, which is attractive and more singular than $1/r^2$ at short distances, and falls off faster than $1/r^2$ at large distances, the radial Schrödinger equation

$$\left[-\frac{\hbar^2}{2\mu}\frac{\mathrm{d}^2}{\mathrm{d}r^2} - \frac{1}{4}\frac{\hbar^2}{2\mu r^2} + V_{\mathrm{tail}}(r)\right]u_{m=0}(r) = E u_{m=0}(r) \tag{4.245}$$

can be solved with incoming boundary conditions, which describes absorption in the close region $r \to 0$. At large distances, the radial wave function still has the form given in the bottom line of (4.222), but the phase shift is now complex. With $m = 0$,

$$u(r) \overset{r\to\infty}{\propto} \mathrm{e}^{-\mathrm{i}kr} - \mathrm{i}\mathrm{e}^{2\mathrm{i}\delta}\mathrm{e}^{\mathrm{i}kr} \propto \mathrm{e}^{-\mathrm{i}(kr+\frac{\pi}{4})} - \mathrm{e}^{2\mathrm{i}\delta}\mathrm{e}^{\mathrm{i}(kr+\frac{\pi}{4})}. \tag{4.246}$$

The right-hand side(s) of (4.246) represent an incoming radial wave together with an outgoing radial wave, which is generated by *quantum reflection* in the nonclassical part of coordinate space. Defining the coefficient of $\mathrm{e}^{\mathrm{i}(kr+\pi/4)}$ as the quantum reflection amplitude gives

$$R = -\mathrm{e}^{2\mathrm{i}\delta}, \tag{4.247}$$

similar to Eq. (4.81) for s-waves in 3D.

The leading near-threshold behaviour of the complex phase shift $\boldsymbol{\delta}$ is given by a formula similar to (4.236), except that the real scattering length a is replaced by a complex scattering length $\mathscr{A}$, which is defined through the zero-energy solution $u^{(0)}(r)$ of (4.245) obeying incoming boundary conditions for $r \to 0$:

$$u^{(0)}(r) \overset{r\to\infty}{\propto} -\sqrt{r}\ln\left(\frac{r}{\mathscr{A}}\right) = -\sqrt{r}\ln\left(\frac{r}{|\mathscr{A}|}\right) + \sqrt{r}\mathrm{i}\arg(\mathscr{A}). \tag{4.248}$$

For the complex phase shift $\boldsymbol{\delta}$ we have

$$\cot\boldsymbol{\delta} \overset{k\to 0}{\sim} \frac{2}{\pi}\left[\ln\left(\frac{k\mathscr{A}}{2}\right) + \gamma_{\mathrm{E}}\right], \tag{4.249}$$

which, for the quantum reflection amplitude (4.247), implies

$$R \overset{k\to 0}{\sim} -1 - \frac{\mathrm{i}\pi}{\ln(\frac{k\mathscr{A}}{2}) + \gamma_{\mathrm{E}} + \mathrm{i}(\arg(\mathscr{A}) - \frac{\pi}{2})}. \tag{4.250}$$

The results (4.249) and (4.250) are derived in Ref. [5], where further terms up to and including $O(k^2)$ are also given. (Note that the quantum reflection amplitude in [5] is i times the amplitude R defined above.)

For *near-threshold quantization* in a deep potential which is well described at large distances by the singular reference potential $V_{\mathrm{tail}}(r)$, the quantization rule $\upsilon_{\mathrm{D}} - \upsilon = F(E)$ is determined by the quantization function $F(E)$, and the universal near-threshold behaviour of this quantization function for s-states in 2D is

$$F(E) \overset{\kappa\to 0}{\sim} \frac{1}{\pi}\arctan\left(\frac{\arg\mathscr{A}}{\ln(\frac{k|\mathscr{A}|}{2}) + \gamma_{\mathrm{E}}}\right) + O\big(\kappa^2\big). \tag{4.251}$$

The complex scattering length $\mathscr{A}$ is as defined in (4.248), and it is a property of the reference potential $V_{\mathrm{tail}}(r)$. The relation connecting the threshold quantum number υ_{D} with the scattering length a reads

$$a = |\mathscr{A}|\exp\left(-\frac{\arg(\mathscr{A})}{\tan(\upsilon_{\mathrm{D}}\pi)}\right), \tag{4.252}$$

so, for a bound-sate energy $E_\mathrm{b} = -\hbar^2\kappa_\mathrm{b}^2/(2\mu)$ very close to threshold,

$$a \overset{\kappa_\mathrm{b}\to 0}{\sim} \frac{2\exp(-\gamma_\mathrm{E})}{\kappa_\mathrm{b}} + O(\kappa_\mathrm{b}). \tag{4.253}$$

For further details, see Ref. [5].

4.3.6 Rutherford Scattering in Two Dimensions

An instructive example showing interesting differences to the well-studied case of scattering in 3D is the case of Rutherford scattering in two dimensions, which was first treated comprehensively by Barton [7]. The potential is

$$V(\mathbf{r}) = \frac{C}{r}. \tag{4.254}$$

This could be the interaction between two point particles whose motion is restricted to a two-dimensional plane embedded in three-dimensional space. It is worth remembering, however, that the Coulomb interaction in a genuinely two-dimensional space does not have this r-dependence. In terms of the scaled coordinate $\boldsymbol{\rho} = k\mathbf{r}$, the Schrödinger equation reads

$$\left[-\Delta_{\boldsymbol{\rho}} + \frac{2\eta}{\rho}\right]\psi = \psi, \tag{4.255}$$

where η is the Sommerfeld parameter

$$\eta = \frac{\mu C}{\hbar^2 k}. \tag{4.256}$$

As in Sect. 2.5.1, we introduce the quantum mechanical length a_C, which does not exist in classical mechanics,

$$a_C = \frac{1}{|\eta|k} = \frac{\hbar^2}{\mu|C|}, \quad |\eta| = \frac{1}{a_C k}. \tag{4.257}$$

For an attractive potential, $C < 0$ in (4.254), a_C is the usual Bohr radius.

As in the 3D case, the Schrödinger equation (4.255) has analytical solutions in 2D as well. Equations (2.190), (2.191) and (2.192) in Sect. 2.5.1 are replaced in 2D by

$$\psi_\mathrm{C}(\mathbf{r}) = \mathrm{e}^{-\frac{\pi}{2}\eta}\frac{\Gamma(\frac{1}{2}+\mathrm{i}\eta)}{\Gamma(\frac{1}{2})}\mathrm{e}^{\mathrm{i}kz}F\left(-\mathrm{i}\eta, \frac{1}{2}; \mathrm{i}k[r-z]\right), \tag{4.258}$$

$$\psi_\mathrm{C}(\mathbf{r}) = \mathrm{e}^{\mathrm{i}[kz+\eta\ln(k[r-z])]}\left[1 + O\left(\frac{1}{k[r-z]}\right)\right] + f_\mathrm{C}(\theta)\frac{\mathrm{e}^{\mathrm{i}(kr-\eta\ln 2kr)}}{\sqrt{r}}\left[1 + O\left(\frac{1}{k[r-z]}\right)\right] \tag{4.259}$$

and

$$f_{\mathrm{C}}(\theta) = -\frac{\eta \mathrm{e}^{\mathrm{i}\pi/4}}{\sqrt{2k\sin^2(\theta/2)}} \frac{\Gamma(\frac{1}{2}+\mathrm{i}\eta)}{\Gamma(1-\mathrm{i}\eta)} \mathrm{e}^{-\mathrm{i}\eta \ln[\sin^2(\theta/2)]}, \tag{4.260}$$

respectively. The function F in (4.258) again denotes the confluent hypergeometric function, see Appendix B.5. With the identities

$$\left|\Gamma\left(\frac{1}{2}+\mathrm{i}\eta\right)\right|^2 = \frac{\pi}{\cosh(\pi\eta)}, \qquad \left|\Gamma(1-\mathrm{i}\eta)\right|^2 = \frac{\pi\eta}{\sinh(\pi\eta)}, \tag{4.261}$$

we obtain the differential cross section for Rutherford scattering in two dimensions,

$$\frac{\mathrm{d}\lambda}{\mathrm{d}\theta} = \left|f_{\mathrm{C}}(\theta)\right|^2 = \frac{\eta\tan(\pi\eta)}{2k\sin^2(\theta/2)} = \frac{|C|}{4E}\frac{\tanh(\pi|\eta|)}{\sin^2(\theta/2)} = \left(\frac{\mathrm{d}\lambda}{\mathrm{d}\theta}\right)_{\mathrm{Ruth}}^{\mathrm{qm}}. \tag{4.262}$$

In contrast to the 3D case, the quantum mechanical result (4.262) does *not* agree with the classical Rutherford cross section in two dimensions,

$$\left(\frac{\mathrm{d}\lambda}{\mathrm{d}\theta}\right)_{\mathrm{Ruth}}^{\mathrm{class}} = \frac{|C|}{4E}\frac{1}{\sin^2(\theta/2)}, \tag{4.263}$$

see Eq. (1.55) in Sect. 1.4. On the other hand, evaluating Eq. (4.210) gives the corresponding result in Born approximation,

$$\left(\frac{\mathrm{d}\lambda}{\mathrm{d}\theta}\right)_{\mathrm{Ruth}}^{\mathrm{Born}} = \left(\frac{\mu C}{\hbar^2}\right)^2 \frac{\pi}{2k^3\sin^2(\theta/2)} = \frac{|C|}{4E}\frac{\pi|\eta|}{\sin^2(\theta/2)}. \tag{4.264}$$

In terms of the quantum mechanical length a_C (the "Bohr radius") defined in (4.257),

$$\left(\frac{\mathrm{d}\lambda}{\mathrm{d}\theta}\right)_{\mathrm{Ruth}}^{\mathrm{qm}} = \frac{a_C/2}{(a_C k)^2}\frac{\tanh[\pi/(a_C k)]}{\sin^2(\theta/2)}, \tag{4.265}$$

$$\left(\frac{\mathrm{d}\lambda}{\mathrm{d}\theta}\right)_{\mathrm{Ruth}}^{\mathrm{class}} = \frac{a_C/2}{(a_C k)^2}\frac{1}{\sin^2(\theta/2)}, \qquad \left(\frac{\mathrm{d}\lambda}{\mathrm{d}\theta}\right)_{\mathrm{Ruth}}^{\mathrm{Born}} = \frac{a_C/2}{(a_C k)^2}\frac{\pi/(a_C k)}{\sin^2(\theta/2)}. \tag{4.266}$$

Comparing Eqs. (4.265) and (4.266) shows that the coincidence of Rutherford scattering in 3D, namely that classical mechanics, the Born approximation and the full quantum mechanical treatment all yield the same result (1.42) for the differential scattering cross section [see also (2.194) and (2.196) in Sect. 2.5.1], is lifted in two spatial dimensions. The angular dependence, $\mathrm{d}\lambda/\mathrm{d}\theta \propto 1/\sin^2(\theta/2)$, is the same in all three cases, but the energy-dependent prefactors of the classical cross section and of the Born approximation differ from the exact quantum mechanical result. This is illustrated in Fig. 4.18, where the respective differential cross sections, multiplied by $\sin^2(\theta/2)$, are plotted as a functions of the dimensionless product $ka_C = 1/|\eta|$.

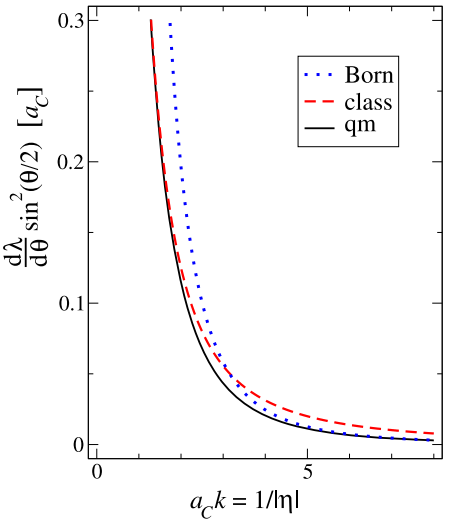

Fig. 4.18 Rutherford scattering in two spatial dimensions. The *solid black line* shows the exact quantum mechanical differential cross section (4.265) [in units of the "Bohr radius" a_C] multiplied by $\sin^2(\theta/2)$ as function of the dimensionless product $a_C k = 1/|\eta|$. The *dashed red line* and the *dotted blue line* show the corresponding classical result and the result of the Born approximation (4.266)

Both the classical cross section and the Born approximation overestimate the exact quantum mechanical cross sections (4.262), (4.265). As already observed by Barton [7], the Born approximation becomes accurate in the high-energy limit, whereas the classical result becomes exact in the low-energy limit,

$$\left(\frac{d\lambda}{d\theta}\right)^{\text{Born}}_{\text{Ruth}} \overset{k\to\infty}{\sim} \left(\frac{d\lambda}{d\theta}\right)^{\text{qm}}_{\text{Ruth}}, \qquad \left(\frac{d\lambda}{d\theta}\right)^{\text{class}}_{\text{Ruth}} \overset{k\to 0}{\sim} \left(\frac{d\lambda}{d\theta}\right)^{\text{qm}}_{\text{Ruth}}. \tag{4.267}$$

The example is a nice illustration of the fact that, for homogeneous potentials of degree -1, i.e., of the Coulomb type, the classical limit is at the threshold $E = 0$, and the classical treatment becomes increasingly inaccurate for large values of $|E|$. This is well accepted for bound states at negative energies, where $E \to 0$ corresponds to the limit of infinite quantum numbers, but it is not so widely appreciated for the regime of positive energies.

References

1. Adhikari, S.K.: Quantum scattering in two dimensions. Am. J. Phys. **54**, 362 (1986)
2. Anderson, M.H., Ensher, J.R., Matthews, M.R., Wieman, C.E., Cornell, E.A.: Observation of Bose–Einstein condensation in a dilute atomic vapor. Science **269**, 198 (1995)
3. Arnecke, F., Friedrich, H., Madroñero, J.: Effective-range expansion for quantum reflection amplitudes. Phys. Rev. A **74**, 062702 (2006)
4. Arnecke, F., Friedrich, H., Madroñero, J.: Scattering of ultracold atoms by absorbing nanospheres. Phys. Rev. A **75**, 042903 (2007)
5. Arnecke, F., Friedrich, H., Raab, P.: Near-threshold scattering, quantum reflection, and quantization in two dimensions. Phys. Rev. A **78**, 052711 (2008)
6. Ball, P.: Lost correspondence. Nature (1999). doi:10.1038/news991202-2, http://www.nature.com/news/1999/991126/full/news991202-2.html

7. Barton, G.: Rutherford scattering in two dimensions. Am. J. Phys. **51**, 420 (1982)
8. Boisseau, C., Audouard, E., Vigué, J.: Comment on "Breakdown of Bohr's correspondence principle". Phys. Rev. Lett. **86**, 2694 (2001)
9. Barton, G.: Frequency shifts near an interface: inadequacy of two-level atomic models. J. Phys. B **7**, 2134 (1974)
10. Böheim, J., Brenig, W., Stutzki, J.: On the low energy limit of reflection and sticking coefficients in atom-surface scattering II: Long range forces. Z. Phys. B **48**, 43 (1982). Erratum: Z. Phys. B **49**, 362 (1983)
11. Berry, M.V., Mount, K.E.: Semiclassical approximations in wave mechanics. Rep. Prog. Phys. **35**, 315 (1972)
12. Brenig, W.: Low-energy limit of reflection and sticking coefficients in atom surface scattering: 1. Short-range forces. Z. Phys. B **36**, 227 (1980)
13. Bodo, E., Zhang, P., Dalgarno, A.: Ultra-cold ion–atom collisions: near resonant charge exchange. New J. Phys. **10**, 033024 (2008)
14. Chin, C., Grimm, R., Julienne, P., Tiesinga, E.: Feshbach resonances in ultracold gase. Rev. Mod. Phys. **82**, 1225 (2010)
15. Côté, R., Heller, E.J., Dalgarno, A.: Quantum suppression of cold atomic collisions. Phys. Rev. A **53**, 234 (1996)
16. Carbonell, J., Lasauskas, R., Delande, D., Hilico, L., Kiliç, S.: A new vibrational level of the H_2^+ molecular ion. Europhys. Lett. **64**, 316 (2003)
17. Crubellier, A., Luc-Koenig, E.: Threshold effects in the photoassociation of cold atoms: R-6 model in the Milne formalism. J. Phys. B **39**, 1417 (2006)
18. Clougherty, D.P., Kohn, W.: Quantum theory of sticking. Phys. Rev. B **46**, 4921 (1992)
19. Casimir, H.B.G., Polder, D.: The influence of retardation on the London–van der Waals forces. Phys. Rev. **73**, 360 (1948)
20. Côté, R., Segev, B.: Quantum reflection engineering: the bichromatic evanescent-wave mirror. Phys. Rev. A **67**, 041604(R) (2003)
21. Druzhinina, V., DeKieviet, M.: Experimental observation of quantum reflection far from threshold. Phys. Rev. Lett. **91**, 193202 (2003)
22. Del Giudice, E., Galzenati, E.: On singular potential scattering I. Nuovo Cimento **38**, 435 (1965)
23. Dalfovo, F., Giorgini, S., Guilleumas, M., Pitaevskii, L., Stringari, S.: Collective and single-particle excitations of a trapped Bose gas. Phys. Rev. A **56**, 3840 (1997)
24. Dickinson, A.S.: Quantum reflection model for ionization rate coefficients in cold metastable helium collisions. J. Phys. B **40**, F237 (2007)
25. Davis, K.B., Mewes, M.-O., Andrews, M.R., van Druten, N.J., Durfee, D.S., Kurn, D.M., Ketterle, W.: Bose–Einstein condensation in a gas of sodium atoms. Phys. Rev. Lett. **75**, 3969 (1995)
26. Dashevskaya, E.I., Maergoiz, A.I., Troe, J., Litvin, I., Nikitin, E.E.: Low-temperature behavior of capture rate constants for inverse power potentials. J. Chem. Phys. **118**, 7313 (2003)
27. Damburg, R.J., Propin, R.K.: On asymptotic expansions of electronic terms of the molecular ion H_2^+. J. Phys. B **1**, 681 (1968)
28. Docenko, O., Tamanis, M., Zaharova, J., Ferber, R., Pashov, A., Knöckel, H., Tiemann, E.: The coupling of the $X^1\Sigma^+$ and $a^3\Sigma^+$ states of the atom pair Na + Cs and modelling cold collisions. J. Phys. B **39**, S929 (2006)
29. Eltschka, C., Friedrich, H., Moritz, M.J.: Comment on "Breakdown of Bohr's correspondence principle". Phys. Rev. Lett. **86**, 2693 (2001)
30. Fink, M., Eiglsperger, J., Madroñero, J., Friedrich, H.: Influence of retardation in the scattering of ultracold atoms by conducting nanowires. Phys. Rev. A **85**, 040702(R) (2012); Fink, M.: Scattering and Absorption of Ultracold Atoms by Nanotubes. Doctoral thesis, Technical University Munich (2013): http://mediatum.ub.tum.de/doc/1141600/1141600.pdf
31. Flambaum, V.V., Gribakin, G., Harabati, C.: Analytical calculation of cold-atom scattering. Phys. Rev. A **59**, 1998 (1999)

32. Friedrich, H., Jurisch, A.: Quantum reflection times for attractive potential tails. Phys. Rev. Lett. **92**, 103202 (2004)
33. Friedrich, H., Jacoby, G., Meister, C.G.: Quantum reflection by Casimir van der Waals potential tails. Phys. Rev. A **65**, 032902 (2002)
34. Friedrich, H.: Theoretical Atomic Physics, 2nd edn. Springer, Berlin (1998). 3rd. Ed. 2006
35. Friedrich, H., Trost, J.: Working with WKB waves far from the semiclassical limit. Phys. Rep. **397**, 359 (2004)
36. Gribakin, G.F., Flambaum, V.V.: Calculation of the scattering length in atomic collisions using the semiclassical approximation. Phys. Rev. A **48**, 546 (1993)
37. Gao, B.: Quantum-defect theory of atomic collisions and molecular vibration spectra. Phys. Rev. A **58**, 4222 (1998)
38. Gao, B.: Breakdown of Bohr's correspondence principle. Phys. Rev. Lett. **83**, 4225 (1999)
39. Gao, B.: General form of the quantum-defect theory for $-1/r^{\alpha}$ type of potentials with $\alpha > 2$. Phys. Rev. A **78**, 012702 (2008)
40. Gao, B.: Universal properties in ultracold ion–atom interactions. Phys. Rev. Lett. **104**, 231201 (2010)
41. Greene, C., Fano, U., Strinati, G.: General form of quantum defect theory. Phys. Rev. A **19**, 1485 (1979)
42. Giusti, A.: A multichannel quantum defect approach to dissociative recombination. J. Phys. B **13**, 3867 (1980)
43. Greene, C.H., Rau, A.R.P.: General form of the quantum-defect theory. II. Phys. Rev. A **26**, 2441 (1982)
44. Gao, B., Tiesinga, E., Williams, C.J., Julienne, P.S.: Multichannel quantum-defect theory for slow atomic collisions. Phys. Rev. A **72**, 042719 (2005)
45. Hilico, L., Billy, N., Grémaud, B., Delande, D.: Ab initio calculation of the $J = 0$ and $J = 1$ states of the H_2^+, D_2^+ and HD^+ molecular ions. Eur. Phys. J. D **12**, 449 (2000)
46. Huang, K., Yang, C.N.: Quantum-mechanical many-body problem with hard-sphere interaction. Phys. Rev. A **105**, 767 (1957)
47. Johnson, S.: Life of Abraham Cowley. In: Lonsdale, R. (ed.) The Lives of the Most Eminent English Poets. Oxford University Press, Oxford (2006). (First published 1781)
48. Khuri, N.N., Martin, A., Richard, J.-M., Wu, T.T.: Low-energy potential scattering in two and three dimensions. J. Math. Phys. **50**, 072105 (2009)
49. Kaiser, A., Müller, T.-O., Friedrich, H.: Influence of higher-order dispersion coefficients on near-threshold bound and continuum states: application to $^{88}Sr_2$. J. Chem. Phys. **135**, 214302 (2011)
50. Kaiser, A., Müller, T.-O., Friedrich, H.: Quantisation rule for highly excited vibrational states of H_2^+. Mol. Phys. **111**, 878 (2013)
51. Lapidus, I.R.: Quantum-mechanical scattering in two dimensions. Am. J. Phys. **50**, 45 (1982)
52. LeRoy, R.J., Bernstein, R.B.: Dissociation energy and long-range potential of diatomic molecules from vibrational spacings of higher levels. J. Chem. Phys. **52**, 3869 (1970)
53. Lemeshko, M., Friedrich, B.: Rotational and rotationless states of weakly bound molecules. Phys. Rev. A **79**, 050501 (2009)
54. Lemeshko, M., Friedrich, B.: Rotational structure of weakly bound molecular ions. J. At. Mol. Sci. **1**, 39 (2010)
55. Landau, L.D., Lifschitz, E.M.: Quantenmechanik. Theoretische Physik, vol. 3, p. 81. Akademie-Verlag, Berlin (1965)
56. Laue, T., Tiesinga, E., Samuelis, C., Knöckel, H., Tiemann, E.: Magnetic-field imaging of weakly bound levels of the ground-state Na_2 dimer. Phys. Rev. A **65**, 023412 (2002)
57. Marinescu, M., Dalgarno, A., Babb, J.F.: Retarded long-range potentials for the alkali-metal atoms and a perfectly conducting wall. Phys. Rev. A **55**, 1530 (1997)
58. Moritz, M.J., Eltschka, C., Friedrich, H.: Threshold properties of attractive and repulsive inverse-square potentials. Phys. Rev. A **63**, 042101 (2001)
59. Moritz, M.J., Eltschka, C., Friedrich, H.: Near-threshold quantization and level densities for potential wells with weak inverse-square tail. Phys. Rev. A **64**, 022101 (2001)

60. Madroñero, J., Friedrich, H.: Influence of realistic atom wall potentials in quantum reflection traps. Phys. Rev. A **75**, 022902 (2007)
61. Mody, A., Haggerty, M., Doyle, J.M., Heller, E.J.: No-sticking effect and quantum reflection in ultracold collisions. Phys. Rev. B **64**, 085418 (2001)
62. Müller, T.-O., Friedrich, H.: Near-threshold quantization for potentials with inverse-cube tails. Phys. Rev. **83**, 022701 (2011)
63. Mies, F.: A multichannel quantum defect analysis of diatomic predissociation and inelastic atomic scattering. J. Chem. Phys. **80**, 2514 (1984)
64. Mies, F., Julienne, P.S.: A multichannel quantum defect analysis of two-state couplings in diatomic molecules. J. Chem. Phys. **80**, 2526 (1984)
65. Müller, T.-O., Kaiser, A., Friedrich, H.: s-Wave scattering for deep potentials with attractive tails falling off faster than $-1/r^2$. Phys. Rev. **84**, 032701 (2011)
66. Müller, T.-O., Kaiser, A., Friedrich, H.: Addendum to "s-Wave scattering for deep potentials with attractive tails falling off faster than $-1/r^2$". Phys. Rev. **84**, 054702 (2011)
67. Müller, T.-O.: Threshold law far attractive inverse-cube interactions. Phys. Rev. Lett. **110**, 260401 (2013)
68. Moerdijk, A.J., Verhaar, B.J., Axelsson, A.: Resonances in ultracold collisions of ^{6}Li, ^{7}Li, and ^{23}Na. Phys. Rev. A **51**, 4852 (1995)
69. Madison, K.W., Wang, Y., Rey, A.M., Bongs, K. (eds.): Annual Review of Cold Atoms and Molecules, vol. 1. World Scientific, Singapore (2013)
70. Oberst, H., Kouznetsov, D., Shimizu, K., Fujita, J., Shimizu, F.: Fresnel diffraction mirror for an atomic wave. Phys. Rev. Lett. **94**, 013203 (2005)
71. Peek, J.M.: Eigenparameters for the $1s\sigma g$ and $2p\sigma u$ orbitals of H_2^+. J. Chem. Phys. **43**, 3004 (1965)
72. Paulsson, R., Karlsson, F., LeRoy, R.J.: Reliability of high-order phase integral eigenvalues for single and double minimum potentials. J. Chem. Phys. **79**, 4346 (1983)
73. Phys. Rev. Focus: Apply quantum principle with caution, http://prlo.aps.org/story/v4/st26 (1999)
74. Pasquini, T., Shin, Y., Sanner, C., Saba, M., Schirotzek, A., Pritchard, D.E., Ketterle, W.: Quantum reflection from a solid surface at normal incidence. Phys. Rev. Lett. **93**, 223201 (2004)
75. Quémener, G., Julienne, P.S.: Ultracold molecules under control. Chem. Rev. **112**, 4949 (2012)
76. Raab, P., Friedrich, H.: Quantization function for deep potentials with attractive tails. Phys. Rev. A **78**, 022707 (2008)
77. Raab, P., Friedrich, H.: Quantization function for potentials with $-1/r^4$ tails. Phys. Rev. A **80**, 052705 (2009)
78. Shimizu, F.: Specular reflection of very slow metastable neon atoms from a solid surface. Phys. Rev. Lett. **86**, 987 (2001)
79. Stein, A., Knöckel, H., Tiemann, E.: Fourier-transform spectroscopy of Sr_2 and revised ground-state potential. Phys. Rev. A **78**, 042508 (2008)
80. Steinke, M., Knöckel, H., Tiemann, E.: (X)1 $^1\Sigma^+$ state of LiNa studied by Fourier-transform spectroscopy. Phys. Rev. A **85**, 042720 (2012)
81. Schwarz, F., Müller, T.-O., Friedrich, H.: Near-threshold Feshbach resonances in interatomic collisions and spectra. Phys. Rev. A **85**, 052703 (2012)
82. Schuster, T., Scelle, R., Trautmann, A., Knoop, S., Oberthaler, M.K., Haverhals, M.M., Goosen, M.R., Kokkelmans, S.J.J.M.F., Tiemann, E.: Feshbach spectroscopy and scattering properties of ultracold Li + Na mixtures. Phys. Rev. A **85**, 042721 (2012)
83. Samuelis, C., Tiesinga, E., Laue, T., Elbs, M., Knöckel, H., Tiemann, E.: Cold atomic collisions studied by molecular spectroscopy. Phys. Rev. A **63**, 012710 (2000)
84. Stwalley, W.: The dissociation energy of the hydrogen molecule using long-range forces. Chem. Phys. Lett. **6**, 241 (1970)
85. Trost, J., Eltschka, C., Friedrich, H.: Quantisation in molecular potentials. J. Phys. B **31**, 361 (1998)

86. Ticknor, C.: Two-dimensional dipolar scattering. Phys. Rev. A **80**, 052702 (2009)
87. Verhaar, B.J., van den Eijnde, P.H.W., Voermans, M.A., Schaffrath, M.M.J.: Scattering length and effective range in two dimensions: application to adsorbed hydrogen atoms. J. Phys. A **17**, 595 (1984)
88. Voronin, A.Y., Froelich, P.: Quantum reflection of ultracold antihydrogen from a solid surface. J. Phys. B **38**, L301 (2005)
89. Voronin, A.Y., Froelich, P., Zygelman, B.: Interaction of ultracold antihydrogen with a conducting wall. Phys. Rev. A **72**, 062903 (2005)
90. Yu, I.A., Doyle, J.M., Sandberg, J.C., Cesar, C.L., Kleppner, D., Greytak, T.J.: Evidence for universal quantum reflection of hydrogen from liquid ^{4}He. Phys. Rev. Lett. **71**, 1589 (1993)
91. Zhao, B.S., Meijer, G., Schöllkopf, W.: Quantum reflection of He_2 several nanometers above a grating surface. Science **331**, 892 (2011)

Appendix A
Scaling

A.1 Classical Mechanics

The dynamics of a conservative classical system obeys significant scaling relations when the potential is a homogeneous function of the coordinates. A function $U(x_1, \ldots, x_f)$ is said to be *homogeneous of degree* d when there exists a real number $d \neq 0$ such that

$$U(\xi x_1, \ldots, \xi x_f) = \xi^d U(x_1, \ldots, x_f) \quad \text{for any } \xi \in (0, \infty). \tag{A.1}$$

For example, harmonic potentials are homogeneous of degree $d = 2$, Coulomb potentials (without short-range deviations from the $1/r$-dependence) are homogeneous of degree $d = -1$, single-power potentials, such as (1.25) in Chap. 1, (2.160) in Chap. 2 or (4.57) in Chap. 4, are homogeneous of degree $d = -\alpha$.

Consider a system with f degrees of freedom and mass parameters $m_i, i = 1, \ldots, f$ governed by a potential $U(\bar{x}_1, \ldots, \bar{x}_f) = \bar{F} V(\bar{x}_1, \ldots, \bar{x}_f)$, where V is a given function which is homogeneous of degree d and $\bar{x}_1, \ldots, \bar{x}_f$ are the spatial coordinates in a given reference frame. The coefficient $\bar{F} \neq 0$ is included explicitly as strength parameter of the potential. The evolution as function of the time $\bar{t}$ is determined by Newton's equations [1]

$$m_i \frac{\mathrm{d}^2 \bar{x}_i}{\mathrm{d}\bar{t}^2} = -\bar{F} \frac{\partial}{\partial \bar{x}_i} V(\bar{x}_1, \ldots, \bar{x}_f), \quad i = 1, \ldots, f. \tag{A.2}$$

Solutions of (A.2) are classical trajectories $\bar{x}_1(\bar{t}), \ldots, \bar{x}_f(\bar{t})$, which are uniquely determined by the initial conditions $\bar{x}_i(\bar{t}_0), \dot{\bar{x}}_i(\bar{t}_0)$ at some initial time $\bar{t}_0$. Along a given trajectory $\bar{x}_i(\bar{t})$, the total energy is

$$\bar{E} = \sum_{i=1}^{f} \frac{m_i}{2} \frac{\mathrm{d}^2 \bar{x}_i}{\mathrm{d}\bar{t}^2} + \bar{F} V\big(\bar{x}_1(\bar{t}), \ldots, \bar{x}_f(\bar{t})\big), \tag{A.3}$$

and it is a conserved quantity.

H. Friedrich, *Scattering Theory*, DOI 10.1007/978-3-662-48526-2

For a given reference trajectory $\bar{x}_i(\bar{t})$, which solves the equations (A.2) at energy $\bar{E}$ and field strength $\bar{F}$, we look for "mechanically similar" trajectories, which are related to the reference trajectory by a simple stretching or compressing of the coordinates in space and time,

$$x_i = \xi \bar{x}_i, \quad i = 1, \ldots, f, \quad \xi > 0; \qquad t = \tau \bar{t}, \quad \tau > 0. \tag{A.4}$$

In terms of the "stretched variables" x_i, t, Eq. (A.2) reads,

$$\frac{\tau^2}{\xi} m_i \frac{\mathrm{d}^2 x_i}{\mathrm{d}t^2} = -\xi^{1-d} \bar{F} \frac{\partial}{\partial x_i} V(x_1, \ldots, x_f), \quad i = 1, \ldots, f. \tag{A.5}$$

Newton's equations of motion for trajectories $x_i(t)$ in the potential $FV(x_1, \ldots, x_f)$, with a new potential strength F, $F/\bar{F} > 0$, are:

$$m_i \frac{\mathrm{d}^2 x_i}{\mathrm{d}t^2} = -F \frac{\partial}{\partial x_i} V(x_1, \ldots, x_f), \quad i = 1, \ldots, f. \tag{A.6}$$

Equation (A.5) is equivalent to Eq. (A.6) if the stretching factors in the space and time variables fulfill the following relations:

$$\frac{\tau^2}{\xi} = \xi^{1-d} \frac{\bar{F}}{F}. \tag{A.7}$$

For a fixed potential strength, $F = \bar{F}$, and $d = -1$, as in the Kepler–Coulomb potential, the relation (A.7) for the stretching coefficients becomes $\tau^2 = \xi^3$, which is known as Kepler's third law.

The conserved energy of the "stretched trajectory" $x_i(t)$ at the new field strength F is

$$E = \sum_{i=1}^{f} \frac{m_i}{2} \frac{\mathrm{d}^2 x_i}{t^2} + FV\big(x_1(t), \ldots, x_f(t)\big) = \frac{\xi^2}{\tau^2} \bar{E} = \xi^d \frac{F}{\bar{F}} \bar{E}. \tag{A.8}$$

The trajectories at nonvanishing energy E and field strength F can be assigned to four similarity classes depending on whether E and F are positive or negative. Within each similarity class, the solutions of Newton's equations (A.6) at any energy E and any field strength F can be related to a reference solution at energy $\bar{E}$ and field strength $\bar{F}$ by the similarity transformation (A.4) with coefficients fulfilling (A.7). For $\bar{E} = 0$, trajectories at field strength $\bar{F}$ are transformed via (A.4), (A.7) to trajectories at field strength F, and the new energy E vanishes automatically according to (A.8).

Resolving (A.7) and (A.8) for the stretching coefficients gives

$$\xi = \left(\frac{E}{\bar{E}} \frac{\bar{F}}{F}\right)^{1/d}, \quad \tau = \left(\frac{E}{\bar{E}}\right)^{\frac{1}{d}-\frac{1}{2}} \left(\frac{\bar{F}}{F}\right)^{\frac{1}{d}} = \xi \sqrt{\frac{\bar{E}}{E}}. \tag{A.9}$$

From the first equation (A.9) it follows, that

$$\xi^d \frac{F}{E} = \frac{\bar{F}}{\bar{E}}. \tag{A.10}$$

Since the right-hand side of (A.10) does not depend on the choice of the stretching coefficient ξ, nor on the potential strength F, the left-hand side must be invariant under all stretching transformations upholding mechanical similarity. The qualitative properties of the dynamics depends not on potential strength F and energy E independently, but only on the combination $\xi^d F/E$, where ξ is a measure for the linear dimensions of the trajectories in the appropriate set of mechanically similar trajectories, e.g. the impact parameter in the trajectories of a scattering problem.

A.2 Quantum Mechanics

In quantum mechanics, the equation of motion for the system whose classical correspondent is given by (A.6) is the time-dependent Schrödinger equation

$$-\sum_{i=1}^{f} \frac{\hbar^2}{2m_i} \frac{\partial^2 \Psi}{\partial x_i^2} + FV(x_1, \ldots, x_f)\Psi(x_1, \ldots, x_f; t) = \mathrm{i}\hbar \frac{\partial \Psi}{\partial t}, \tag{A.11}$$

and stationary solutions for a given energy E obey the time-independent Schrödinger equation

$$-\sum_{i=1}^{f} \frac{\hbar^2}{2m_i} \frac{\partial^2 \psi}{\partial x_i^2} + FV(x_1, \ldots, x_f)\psi(x_1, \ldots, x_f) = E\psi(x_1, \ldots, x_f). \tag{A.12}$$

In the transition to quantum mechanics, the classical coordinates x_i and canonically conjugate momenta $p_j = m_j \mathrm{d}x_j/\mathrm{d}t$ become operators which fulfill the canonical commutation relations,

$$[x_i, p_j] = \mathrm{i}\hbar. \tag{A.13}$$

The similarity transformation (A.4), when fulfilling the conditions (A.7), (A.9), connects a classical trajectory for energy E and field strength F with a mechanically similar reference trajectory at energy $\bar{E}$ and field strength $\bar{F}$. This transformation is *not* a canonical transformation [1]. As a consequence, if the physical system at energy E and field strength F is described by the coordinates x_i and momenta p_j obeying the canonical commutation relations (A.13), then the coordinates $\bar{x}_i$ and $\bar{p}_j$ of the reference system obey the modified commutation relations,

$$[\bar{x}_i, \bar{p}_j] = \frac{\tau}{\xi^2}[x_i, p_j] = \mathrm{i}\bar{\hbar}, \quad \bar{\hbar} = \frac{\tau}{\xi^2}\hbar = \left(\frac{\bar{E}}{E}\right)^{\frac{1}{2}+\frac{1}{d}} \left(\frac{F}{\bar{F}}\right)^{\frac{1}{d}} \hbar, \tag{A.14}$$

i.e., Planck's constant $\hbar$ is replaced by an *effective Planck's constant* $\bar{\hbar}$ in the reference system. For $d = -2$, the energy factor in (A.14) is unity, and $\bar{\hbar}$ depends only on the ratio of the potential strengths.

The term "semiclassical limit" is often formulated as "$\hbar \to 0$", which is, of course, not to be taken literally, because $\hbar$ is a *constant*. What is meant is, that typical classical actions of the classical motion are large compared to $\hbar$. For homogeneous potentials, a clean and precise definition of the semiclassical limit can be given on the basis of Eq. (A.14).

In the canonical system at energy E and potential strength F, described by the coordinates $x_1, \ldots, x_f$ and momenta $p_1, \ldots, p_f$, we wish to know how the variation of E and F affects the proximity to the semiclassical limit. To this end, we compare with the reference system at fixed energy $\bar{E}$ and fixed field strength $\bar{F}$, described by the coordinates $\bar{x}_1, \ldots, \bar{x}_f$ and momenta $\bar{p}_1, \ldots, \bar{p}_f$. The classical dynamics of the system of interest, at energy E and field strength F, is equivalent to the classical dynamics of the reference system and the respective classical trajectories are connected via the similarity transformation (A.4), (A.7). For the quantum mechanics of the reference system to be equivalent to the quantum mechanics of the system of interest, however, the relevant coordinates $\bar{x}_i$ and momenta $\bar{p}_j$ must obey the *noncanonical* commutation relations (A.14), with the effective Planck's constant $\bar{\hbar}$ replacing $\hbar$. The semiclassical limit now clearly corresponds to the case $\bar{\hbar} \to 0$. Which limits of energy and field strength correspond to the semiclassical limit depends on the degree d of homogeneity of the potential, as summarized below:

$$\begin{aligned}
0 < d: &\quad F \to 0 && \text{or} && |E| \to \infty \\
-2 < d < 0: &\quad |F| \to \infty && \text{or} && E \to 0 \\
d = -2: &\quad |F| \to \infty && \text{and} && E \quad \text{arbitrary} \\
d < -2: &\quad |F| \to \infty && \text{or} && |E| \to \infty .
\end{aligned}$$

The opposite limits of field strength and/or energy define the anticlassical or extreme quantum limit of the Schrödinger equation. For given field strength F it lies at $E \to 0$ for $d < -2$ or $d > 0$, but for $-2 < d < 0$ (e.g. Coulomb potentials), the anticlassical limit is for $|E| \to \infty$. This is as shown for repulsive inverse-power potentials in Sect. 2.4.2, see Table 2.1.

Single-power potentials

$$V(r) = \frac{C_\alpha}{r^\alpha} = \pm \frac{\hbar^2}{2\mu} \frac{(\beta_\alpha)^{\alpha-2}}{r^\alpha}, \tag{A.15}$$

are homogeneous of order $d = -\alpha$. The occurrence of Planck's constant $\hbar$ introduces a natural length scale which does not exist in classical mechanics:

$$\beta_\alpha = \left(\frac{2\mu |C_\alpha|}{\hbar^2} \right)^{1/(\alpha-2)}, \quad \alpha \neq 2. \tag{A.16}$$

The radial Schrödinger equation for energy $E = \hbar^2 k^2/(2\mu)$ in partial wave l reads,

$$-\frac{\mathrm{d}^2 u}{\mathrm{d}r^2} + \left(\frac{l(l+1)}{r^2} \pm \frac{(\beta_\alpha)^{\alpha-2}}{r^\alpha}\right) u(r) = k^2 u(r). \tag{A.17}$$

Introducing the dimensionless coordinate $\rho = r/\beta_\alpha$ leads to

$$-\frac{\mathrm{d}^2 u}{\mathrm{d}\rho^2} + \left(\frac{l(l+1)}{\rho^2} \pm \frac{1}{\rho^\alpha}\right) u(r) = (k\beta_\alpha)^2 u(\rho). \tag{A.18}$$

Equation (A.18) shows, that the quantum mechanical properties of the single-power potential (A.15) depend not on energy E and potential strength C_α independently, but only on the dimensionless product $k\beta_\alpha$. For negative energies, $E = -\hbar^2\kappa^2/(2\mu) < 0$, the right-hand side of (A.17) is replaced by $-\kappa^2 u(r)$ and the right-hand side of (A.18) by $-(\kappa\beta_\alpha)^2 u(\rho)$; the quantum mechanical properties depend only on the dimensionless product $\kappa\beta_\alpha$.

For inverse-square potentials,

$$V(r) = \pm\frac{\hbar^2}{2\mu}\frac{\gamma}{r^2} \tag{A.19}$$

the strength coefficient γ is dimensionless and there is no natural definition for a quantum length. With the scaled coordinate $\rho = kr$ ($\rho = \kappa r$) the appropriately scaled radial Schrödinger equation in the partial wave l reads

$$-\frac{\mathrm{d}^2 u}{\mathrm{d}\rho^2} + \left(\frac{l(l+1)}{\rho^2} \pm \frac{\gamma}{\rho^2}\right) u(r) = \pm u(\rho), \tag{A.20}$$

which is free of any energy scale. A solution at one positive (negative) energy is, by simple rescaling, also a solution at any other positive (negative) energy.

References

1. Landau, L.D., Lifshitz, E.M.: Course of Theoretical Physics, Vol. 1 Mechanics, (3rd ed.). Butterworth-Heinemann (1976)

Appendix B
Special Functions

B.1 Legendre Polynomials, Spherical Harmonics

A compact description of various sets of orthogonal polynomials, including Legendre polynomials, is given in Hochstrasser's Chapter [2] of the "Handbook of Mathematical Functions". The lth Legendre polynomial $P_l(x)$ is a polynomial of degree l in x,

$$P_l(x) = \frac{1}{2^l l!}\frac{\mathrm{d}^l}{\mathrm{d}x^l}\left(x^2-1\right)^l, \quad l = 0, 1, \ldots. \tag{B.1}$$

It has l zeros in the interval between -1 and $+1$; for even (odd) l, $P_l(x)$ is an even (odd) function of x. The *associated Legendre functions* $P_{l,m}(x)$, $|x| \le 1$, are products of $(1-x^2)^{m/2}$ with polynomials of degree $l-m$ ($m = 0, \ldots, l$),

$$P_{l,m}(x) = \left(1-x^2\right)^{m/2}\frac{\mathrm{d}^m}{\mathrm{d}x^m}P_l(x). \tag{B.2}$$

The spherical harmonics $Y_{l,m}(\theta,\phi)$ are products of $\mathrm{e}^{\mathrm{i}m\phi}$ with polynomials of degree $|m|$ in $\sin\theta$ and of degree $l-|m|$ in $\cos\theta$; the θ-dependence is given by the associated Legendre functions (B.2) as functions of $x = \cos\theta$. For $m \ge 0, 0 \le \theta \le \pi$ we have

$$\begin{aligned} Y_{l,m}(\theta,\phi) &= (-1)^m\left[\frac{(2l+1)}{4\pi}\frac{(l-m)!}{(l+m)!}\right]^{1/2}P_{l,m}(\cos\theta)\mathrm{e}^{\mathrm{i}m\phi} \\ &= (-1)^m\left[\frac{(2l+1)}{4\pi}\frac{(l-m)!}{(l+m)!}\right]^{1/2}\sin^m\theta\frac{\mathrm{d}^m}{\mathrm{d}(\cos\theta)^m}P_l(\cos\theta)\mathrm{e}^{\mathrm{i}m\phi}. \end{aligned} \tag{B.3}$$

The spherical harmonics for negative azimuthal quantum numbers m are obtained via

$$Y_{l,-m}(\theta,\phi) = (-1)^m\left(Y_{l,m}(\theta,\phi)\right)^*. \tag{B.4}$$

H. Friedrich, *Scattering Theory*, DOI 10.1007/978-3-662-48526-2

B.2 Error Function

The error function $\mathrm{erf}(x)$ is an antisymmetric function defined by

$$\mathrm{erf}(x) = \frac{2}{\sqrt{\pi}} \int_0^x \mathrm{e}^{-t^2} \mathrm{d}t. \tag{B.5}$$

Its small-argument behaviour is

$$\mathrm{erf}(x) \overset{x\to 0}{\sim} \frac{2}{\sqrt{\pi}} \left(x - \frac{x^3}{3} \right). \tag{B.6}$$

For real argument x, $\mathrm{erf}(x)$ increases monotonically to unity with increasing x, and it approaches unity as

$$\mathrm{erf}(x) \overset{x\to\infty}{\sim} 1 - \frac{\mathrm{e}^{-x^2}}{x\sqrt{\pi}} \left(1 - \frac{1}{2x^2} \right). \tag{B.7}$$

B.3 Gamma Function

The gamma function $\Gamma(z)$ is defined by

$$\Gamma(z+1) = \int_0^\infty t^z \mathrm{e}^{-t} \mathrm{d}t \tag{B.8}$$

and has the property

$$\Gamma(z+1) = z\Gamma(z). \tag{B.9}$$

For nonnegative integers $z = n$ we have $\Gamma(n+1) = n!$. For half-integral z we can derive $\Gamma(z)$ recursively from the value $\Gamma(\frac{1}{2}) = \sqrt{\pi}$ via (B.9). Furthermore,

$$\Gamma\left(\frac{z+1}{2} \right) \Gamma\left(\frac{z}{2} \right) = \frac{\sqrt{\pi}}{2^{z-1}} \Gamma(z). \tag{B.10}$$

The small-z behaviour of $\Gamma(z)$ is,

$$\frac{1}{\Gamma(z)} = \frac{z}{\Gamma(z+1)} = z + \gamma_\mathrm{E} z^2 + O\left(z^3\right), \tag{B.11}$$

where $\gamma_\mathrm{E} = 0.5772156649\ldots$ is Euler's constant, see (B.30) below.

The argument z may be complex, and: $\Gamma(z^*) = [\Gamma(z)]^*$.

Useful product formulae are,

$$\Gamma(\mathrm{i}y)\Gamma(-\mathrm{i}y) = \left|\Gamma(\mathrm{i}y)\right|^2 = \frac{\pi}{y \sinh(\pi y)}, \tag{B.12}$$

$$\Gamma(1+\mathrm{i}y)\Gamma(1-\mathrm{i}y) = \left|\Gamma(1+\mathrm{i}y)\right|^2 = \frac{\pi y}{\sinh(\pi y)}, \tag{B.13}$$

$$\Gamma\left(\frac{1}{2}+\mathrm{i}y\right)\Gamma\left(\frac{1}{2}-\mathrm{i}y\right) = \left|\Gamma\left(\frac{1}{2}+\mathrm{i}y\right)\right|^2 = \frac{\pi}{\cosh(\pi y)}, \tag{B.14}$$

$$\Gamma\left(\frac{1}{4}+\mathrm{i}y\right)\Gamma\left(\frac{3}{4}-\mathrm{i}y\right) = \frac{\pi\sqrt{2}}{\cosh(\pi y)+\mathrm{i}\sinh(\pi y)}. \tag{B.15}$$

The right-hand sides of these formulae also apply if y is not real, e.g. for $y = \mathrm{i}x$, (B.13) becomes

$$\Gamma(1+x)\Gamma(1-x) = \frac{\pi x}{\sin(\pi x)}. \tag{B.16}$$

For large arguments we have *Stirling's formula*,

$$\Gamma(z) \overset{z\to\infty}{\sim} \mathrm{e}^{-z} z^{z-1/2}\sqrt{2\pi}\left[1+\frac{1}{12z}+\frac{1}{288z^2}+O\left(\frac{1}{z^3}\right)\right]. \tag{B.17}$$

From (B.13) it follows that $|\Gamma(1+\mathrm{i}y)| = \sqrt{\pi y/\sinh(\pi y)}$. By induction we can conclude,

$$\left|\Gamma(1+l+\mathrm{i}y)\right| = \left(\prod_{n=1}^{l}|n+\mathrm{i}y|\right)\sqrt{\frac{\pi y}{\sinh(\pi y)}} \overset{|y|\to\infty}{\sim} \sqrt{2\pi}\,\mathrm{e}^{-\frac{\pi}{2}|y|}|y|^{l+1/2}. \tag{B.18}$$

B.4 Bessel Functions

In many special cases describing realistic situations, the radial Schrödinger equation has analytical solutions in the form of Bessel functions, which makes these special functions particularly important. An excellent review of the definitions and properties of Bessel functions is contained in Olver's chapter [4] in the "Handbook of Mathematical Functions". Although the title of that chapter is "Bessel Functions of Integer Order", most results apply also for noninteger and even for complex orders.

The defining differential equation for (ordinary) Bessel functions of order ν is:

$$z^2\frac{\mathrm{d}^2\mathscr{C}_\nu}{\mathrm{d}z^2} + z\frac{\mathrm{d}\mathscr{C}_\nu}{\mathrm{d}z} - \left(\nu^2 - z^2\right)\mathscr{C}_\nu = 0. \tag{B.19}$$

The connection to the radial Schrödinger equation is achieved via the transformation $u(z) = \sqrt{z}\mathscr{C}_\nu(z)$, which leads to the following differential equation for $u(z)$,

$$-\frac{\mathrm{d}^2u}{\mathrm{d}z^2} + \frac{\nu^2-\frac{1}{4}}{z^2}u = u. \tag{B.20}$$

Multiplying Eq. (B.20) by $\hbar^2/2\mu$ and writing kr for z yields the radial Schrödinger equations (2.35) and (4.214) in the free-particle case $V(r) \equiv 0$, with

$$\begin{aligned} &\nu^2 - \frac{1}{4} = l(l+1) \Rightarrow \nu^2 = \left(l + \frac{1}{2}\right)^2 \quad \text{in 3D (Eq. (2.35))}, \\ &\nu^2 = m^2 \quad \text{in 2D (Eq. (4.214))}. \end{aligned} \tag{B.21}$$

Equation (B.20) has two linearly independent solutions, which can be defined by their boundary conditions for $z \to 0$ or for $z \to \infty$. The (ordinary) "Bessel function of the first kind" $J_\nu(z)$ has a series expansion

$$J_\nu(z) = \left(\frac{z}{2}\right)^\nu \sum_{k=0}^{\infty} \frac{(-\frac{1}{4}z^2)^k}{k!\Gamma(\nu + k + 1)} \tag{B.22}$$

and obeys the following boundary conditions,

$$J_\nu(z) \overset{z\to 0}{\sim} \frac{(z/2)^\nu}{\Gamma(\nu+1)}\left[1 - \frac{(z/2)^2}{\nu+1} + O\left(\left(\frac{z}{2}\right)^4\right)\right], \tag{B.23}$$

$$\sqrt{\frac{\pi}{2}z}J_\nu(z) \overset{|z|\to\infty}{\sim} \sin\left(z - \frac{(\nu - \frac{1}{2})\pi}{2}\right) + O\left(\frac{1}{|z|}\right). \tag{B.24}$$

When the order ν is an integer, $\nu = n$,

$$J_{-n}(z) = (-1)^n J_n(z). \tag{B.25}$$

When ν is not an integer, $J_\nu(z)$ and $J_{-\nu}(z)$ are linearly independent.

The ordinary Bessel function with maximal phase difference to $J_\nu(z)$ for large z is the "Bessel function of the second kind" $Y_\nu(z)$, which is defined for noninteger order ν by

$$Y_\nu(z) = \frac{J_\nu(z)\cos(\nu\pi) - J_{-\nu}(z)}{\sin(\nu\pi)}, \tag{B.26}$$

and for integer order n by $Y_n(z) \overset{\text{def}}{=} \lim_{\nu\to n} Y_\nu(z)$. The large-$z$ behaviour of $Y_\nu(z)$ is

$$\sqrt{\frac{\pi}{2}z}Y_\nu(z) \overset{|z|\to\infty}{\sim} -\cos\left(z - \frac{(\nu - \frac{1}{2})\pi}{2}\right) + O\left(\frac{1}{|z|}\right). \tag{B.27}$$

The low-argument behaviour of $Y_\nu(z)$ can be derived for noninteger order ν from (B.23) and (B.26):

$$\begin{aligned} Y_\nu(z) \overset{z\to 0}{\sim} &-\left(\frac{z}{2}\right)^{-\nu} \frac{\Gamma(1+\nu)}{\nu\pi}\left[1 - \frac{(z/2)^2}{1-\nu} + O\left(\left(\frac{z}{2}\right)^4\right)\right] \\ &+ \cot(\nu\pi)\frac{(z/2)^\nu}{\Gamma(1+\nu)}\left[1 - \frac{(z/2)^2}{1+\nu} + O\left(\left(\frac{z}{2}\right)^4\right)\right]. \end{aligned} \tag{B.28}$$

For integer order, $\nu = n$, the expansion of $Y_n(z)$ in z involves logarithmic terms. For $\nu = 0$ we have

$$Y_0(z) \overset{z\to 0}{\sim} \frac{2}{\pi}\left[\ln\left(\frac{z}{2}\right) + \gamma_{\mathrm{E}}\right] J_0(z) + \frac{2}{\pi}\left(\frac{z}{2}\right)^2 + O\left(\left(\frac{z}{2}\right)^4\right). \tag{B.29}$$

The square bracket in (B.29) contains Euler's constant,

$$\gamma_{\mathrm{E}} = -\left.\frac{\mathrm{d}\Gamma}{\mathrm{d}z}\right|_{z=1} \approx 0.577256649\ldots \tag{B.30}$$

For $\nu = n \geq 1$, the leading term in the expansion of $Y_n(z)$ is $-\frac{1}{\pi}(n-1)!(z/2)^{-n}$, in agreement with the leading term in (B.28); each further term contains an additional factor $(z/2)^2$, as long as the combined exponent of $z/2$ remains smaller than n. At order $(z/2)^n$ the expansion contains a logarithmic contribution $\frac{2}{\pi}\ln(\frac{1}{2}z)J_n(z)$ (see Eq. (9.1.11) in [4]). Similar to (B.25) for the J_n, we have

$$Y_{-n}(z) = (-1)^n Y_n(z) \tag{B.31}$$

for integer order n.

The Bessel functions of the first and second kind, which are real-valued for real argument z, can be combined with complex coefficients to define the Bessel functions of the third kind or "Hankel functions":

$$H_\nu^{(1)}(z) = J_\nu(z) + \mathrm{i}Y_\nu(z), \qquad H_\nu^{(2)}(z) = J_\nu(z) - \mathrm{i}Y_\nu(z). \tag{B.32}$$

Their large-z behaviour follows from (B.24), (B.27),

$$\begin{aligned} \sqrt{\frac{\pi}{2}z}H_\nu^{(1)}(z) &\overset{|z|\to\infty}{\sim} \mathrm{e}^{\mathrm{i}(z-\frac{1}{2}\nu-\frac{\pi}{4})}, \\ \sqrt{\frac{\pi}{2}z}H_\nu^{(2)}(z) &\overset{|z|\to\infty}{\sim} \mathrm{e}^{-\mathrm{i}(z-\frac{1}{2}\nu-\frac{\pi}{4})}. \end{aligned} \tag{B.33}$$

For free-particle motion in 3D, the order of the Bessel functions solving the radial Schrödinger equation is half integer, $\nu = l + \frac{1}{2}$. The corresponding *spherical Bessel functions* are denoted by lower-case letters and are defined as,

$$j_l(z) = \sqrt{\frac{\pi}{2z}}J_{l+\frac{1}{2}}(z), \qquad y_l(z) = \sqrt{\frac{\pi}{2z}}Y_{l+\frac{1}{2}}(z), \tag{B.34}$$

$$h_l^{(1)}(z) = \sqrt{\frac{\pi}{2z}}H_{l+\frac{1}{2}}^{(1)}(z), \qquad h_l^{(2)}(z) = \sqrt{\frac{\pi}{2z}}H_{l+\frac{1}{2}}^{(2)}(z). \tag{B.35}$$

The real regular and irregular radial free-particle wave functions are the solutions of (B.20) with $z = kr$, i.e. $krj_l(kr)$ and $-kry_l(kr)$, as given in (2.38) in Sect. 2.3.3.

The corresponding "spherical Hankel functions" give the linear combinations corresponding to incoming or outgoing spherical waves,

$$krh_l^{(1)}(kr) \overset{kr\to\infty}{\sim} -\mathrm{i}\mathrm{e}^{\mathrm{i}(kr-l\frac{\pi}{2})}, \qquad krh_l^{(2)}(kr) \overset{kr\to\infty}{\sim} \mathrm{i}\mathrm{e}^{-\mathrm{i}(kr-l\frac{\pi}{2})}. \tag{B.36}$$

According to Eq. (9.1.53) in Ref. [4], the differential equation

$$-\frac{\mathrm{d}^2u}{\mathrm{d}z^2} + \left(\frac{l(l+1)}{z^2} - \frac{1}{z^\alpha}\right)u(z) = 0 \tag{B.37}$$

is solved by functions of the form

$$u(z) = \sqrt{z}\mathscr{C}_{\nu(l)}\left(\frac{2}{\alpha-2}z^{1-\alpha/2}\right), \quad \text{with } \nu(l) = \frac{2l+1}{\alpha-2}. \tag{B.38}$$

If we interpret the dimensionless argument z as r/β, Eq. (B.37) is just the radial wave equation (2.266) at threshold in the partial wave l for the single-power potential $V_\alpha(r)$, as defined in (2.264), with $C_\alpha < 0$. The solutions (B.38) are of the form given in (2.267), (2.268) in Sect. 2.6.1.

The *modified Bessel functions* are solutions of the differential equation

$$z^2\frac{\mathrm{d}^2\mathscr{Z}_\nu}{\mathrm{d}z^2} + z\frac{\mathrm{d}\mathscr{Z}_\nu}{\mathrm{d}z} - \left(\nu^2+z^2\right)\mathscr{Z}_\nu = 0. \tag{B.39}$$

As for the ordinary Bessel functions, the connection to the radial Schrödinger equation is achieved via the transformation $u(z) = \sqrt{z}\mathscr{Z}_\nu(z)$, which leads to the following differential equation for $u(z)$,

$$-\frac{\mathrm{d}^2u}{\mathrm{d}z^2} + \frac{\nu^2-\frac{1}{4}}{z^2}u = -u. \tag{B.40}$$

Multiplying Eq. (B.40) by $\hbar^2/(2\mu)$ and writing κr for z again yields the radial Schrödinger equations (2.35) and (4.214), in the free-particle case $V(r) \equiv 0$, but now for negative energy $E = -\hbar^2\kappa^2/(2\mu) < 0$. The order parameter ν is again related the angular momentum quantum numbers in 3D and in 2D by Eq. (B.21).

The modified Bessel function $I_\nu(z)$ of order ν solves Eq. (B.39) and is related to the ordinary Bessel function of the first kind by,

$$\mathrm{i}^\nu I_\nu(z) = J_\nu(\mathrm{i}z), \quad (-\pi < \arg z \le \pi/2). \tag{B.41}$$

Its behaviour for small $|z|$ is, as for J_ν,

$$I_\nu(z) \overset{z\to0}{=} \frac{(\frac{1}{2}z)^\nu}{\Gamma(\nu+1)}, \quad (\nu \neq -1, -2, -3, \ldots). \tag{B.42}$$

For $|z| \to \infty$ the asymptotic form of I_ν is

$$I_\nu(z) \overset{|z|\to\infty}{=} \frac{\mathrm{e}^z}{\sqrt{2\pi z}}, \quad \left(\left|\arg(z)\right| < \pi/2\right). \tag{B.43}$$

For noninteger values of ν the modified Bessel functions $I_\nu(z)$ and $I_{-\nu}(z)$ defined by (B.41), (B.22) are linearly independent, and there is a linear combination

$$K_\nu(z) = \frac{\pi}{2}\frac{I_{-\nu}(z) - I_\nu(z)}{\sin(\nu\pi)}, \tag{B.44}$$

which vanishes asymptotically,

$$K_\nu(z) \overset{|z|\to\infty}{=} \sqrt{\frac{\pi}{2z}}\mathrm{e}^{-z}, \quad (|\arg z| < 3\pi/2). \tag{B.45}$$

For integer order n, $K_n(z) \overset{\text{def}}{=} \lim_{\nu\to n} K_\nu(z)$.

The *Airy functions* are essentially Bessel functions of order $1/3$,

$$\begin{aligned} \mathrm{Ai}(z) &= \frac{1}{3}\sqrt{z}\big[I_{-1/3}(\zeta) - I_{1/3}(\zeta)\big] = \frac{1}{\pi}\sqrt{\frac{z}{3}}K_{1/3}(\zeta), \\ \mathrm{Bi}(z) &= \sqrt{\frac{z}{3}}\big[I_{-1/3}(\zeta) + I_{1/3}(\zeta)\big], \quad \text{where } \zeta = \frac{2}{3}z^{3/2}. \end{aligned} \tag{B.46}$$

For large $|z|$,

$$\begin{aligned} &2\sqrt{\pi}\,\mathrm{Ai}(z) \overset{|z|\to\infty}{\sim} z^{-1/4}\mathrm{e}^{-\zeta}, \quad \big(|\arg(z)| < \pi\big), \\ &\sqrt{\pi}\,\mathrm{Ai}(-z) \overset{|z|\to\infty}{\sim} z^{-1/4}\cos\left(\zeta - \frac{\pi}{4}\right), \quad \left(\big|\arg(z)\big| < \frac{2\pi}{3}\right). \end{aligned} \tag{B.47}$$

The Airy functions are solutions of the differential equation

$$\frac{\mathrm{d}^2 w}{\mathrm{d}z^2} - zw(z) = 0, \tag{B.48}$$

which has the structure of a Schrödinger equation with a linear potential, see Eqs. (2.146) and (2.147) in Sect. 2.4.2.

B.5 Confluent Hypergeometric Functions, Coulomb Functions, Whittaker's Function

The confluent hypergeometric function, also called "degenerate hypergeometric function", is defined according to Chap. 13 in [1] and Sect. 9.2 in [3] as

$$F(a,b;z) = \sum_{n=0}^{\infty}\frac{\Gamma(a+n)}{\Gamma(a)}\frac{\Gamma(b)}{\Gamma(b+n)}\frac{z^n}{n!}. \tag{B.49}$$

It is a solution of the equation

$$z\frac{\mathrm{d}^2\mathscr{C}}{\mathrm{d}z^2}+(b-z)\frac{\mathrm{d}\mathscr{C}}{\mathrm{d}z}=a\mathscr{C}(z). \tag{B.50}$$

Alternative notations for $F(a,b;z)$ are: ${}_1F_1(a,b;z)$, $M(a,b;z)$, $\Phi(a,b;z)$.

A linearly independent solution of (B.50), sometimes also called confluent hypergeometric function, is

$$\begin{aligned} U(a,b;z)=&\frac{\Gamma(1-b)}{\Gamma(a-b+1)}F(a,b;z)\\ &+\frac{\Gamma(b-1)}{\Gamma(a)}z^{1-b}F(a-b+1,2-b;z). \end{aligned} \tag{B.51}$$

An alternative notation for $U(a,b;z)$ is $\Psi(a,b;z)$.

The Gaussian hypergeometric series, also called the hypergeometric function, is defined by

$${}_2F_1(a,b;c,z)=\sum_{n=0}^{\infty}\frac{\Gamma(a+n)}{\Gamma(a)}\frac{\Gamma(b+n)}{\Gamma(b)}\frac{\Gamma(c)}{\Gamma(c+n)}\frac{z^n}{n!}. \tag{B.52}$$

The confluent hypergeometric functions (B.49), (B.51) are important in the context of Coulomb potentials, because they occur as components in solutions of relevant Schrödinger equations, see, e.g. Eq. (2.190) in Sect. 2.5.1 and Eq. (4.258) in Sect. 4.3.6. An important special case is the radial Schrödinger equation for motion in a pure Coulomb potential at energy $E=\hbar^2k^2/(2\mu)$, characterized by the Sommerfeld parameter η [Eq. (2.198) in Sect. 2.5.1],

$$\left[-\frac{\mathrm{d}^2}{\mathrm{d}\rho^2}+\frac{l(l+1)}{\rho^2}+\frac{2\eta}{\rho}\right]u_l(\rho)=u_l(\rho). \tag{B.53}$$

Two linearly independent solutions are the regular Coulomb function $F_l(\rho,\eta)$, as defined in Eq. (2.199) in Sect. 2.5.1, and the irregular Coulomb function $G_l(\rho,\eta)$, as defined in Eq. (2.203).

Whittaker's equation,

$$\frac{\mathrm{d}^2\mathscr{C}}{\mathrm{d}z^2}-\left[\frac{m^2-\frac{1}{4}}{z^2}-\frac{\lambda}{z}\right]\mathscr{C}(z)=\frac{1}{4}\mathscr{C}(z), \tag{B.54}$$

acquires the form of the radial Schrödinger equation for an attractive pure Coulomb potential at negative energy $E=-\hbar^2\kappa^2/(2\mu)$ if we write $(l+\frac{1}{2})^2$ for m^2 and replace z by $2\rho\equiv 2\kappa r$ and λ by $-\eta=|\eta|\equiv 1/(a_C\kappa)$, a_C being the Bohr radius:

$$\left[-\frac{\mathrm{d}^2}{\mathrm{d}\rho^2}+\frac{l(l+1)}{\rho^2}-\frac{2|\eta|}{\rho}\right]u_l(\rho)=-u_l(\rho). \tag{B.55}$$

Two solutions of (B.55) are

$$M_{|\eta|,l+\frac{1}{2}}(2\rho) = (2\rho)^{l+1}\mathrm{e}^{-\rho}F\big(l+1-|\eta|, 2l+2; 2\rho\big), \tag{B.56}$$

$$M_{|\eta|,-l-\frac{1}{2}}(2\rho) = (2\rho)^{-l}\mathrm{e}^{-\rho}F\big(-l-|\eta|, -2l; 2\rho\big). \tag{B.57}$$

The linear combination of (B.56) and (B.57) which vanishes for large ρ is Whittaker's function,

$$W_{|\eta|,l+\frac{1}{2}}(2\rho) = \frac{\Gamma(-2l-1)}{\Gamma(-l-|\eta|)}M_{|\eta|,l+\frac{1}{2}}(2\rho) + \frac{\Gamma(2l+1)}{\Gamma(l+1-|\eta|)}M_{|\eta|,-l-\frac{1}{2}}(2\rho), \tag{B.58}$$

$$W_{|\eta|,l+\frac{1}{2}}(2\rho) \overset{\rho\to\infty}{\sim} \mathrm{e}^{-\rho}(2\rho)^{|\eta|}\left[1+O\left(\frac{1}{\rho}\right)\right]. \tag{B.59}$$

At least one gamma function in (B.58) is ill-defined for integer l, but the expression for $W_{|\eta|,l+\frac{1}{2}}(2\rho)$ is well defined when taking the limit as l approaches its integer value. For integer nonnegative l, $W_{|\eta|,l+\frac{1}{2}}(2\rho)$ vanishes as $\rho \to 0$ when $|\eta|$ is an integer larger than l; in this case $W_{|\eta|,l+\frac{1}{2}}(2\rho)$ is a regular normalizable solution of (B.55).

References

1. Abramowitz, M., Stegun, I.A. (Eds.): Handbook of Mathematical Functions, Dover Publications, New York, 1970.
2. Hochstrasser, U.W.: Orthogonal Polynomials, Chap. 22 in [1].
3. Gradshteyn, I.S., Ryzhik, I.M.: Table of Integrals, Series, and Products. Academic Press, New York (1980).
4. Olver, F.W.J.: Bessel Functions of Integer Order, Chap. 9 in [1].

Index

H. Friedrich, *Scattering Theory*, DOI 10.1007/978-3-662-48526-2